frontiers | Research Topics

Advances in genetics and molecular breeding of ornamental plants

Edited by
Shunli Wang, Byoung Ryong Jeong, Pejman Azadi and Daqiu Zhao

Published in
Frontiers in Plant Science

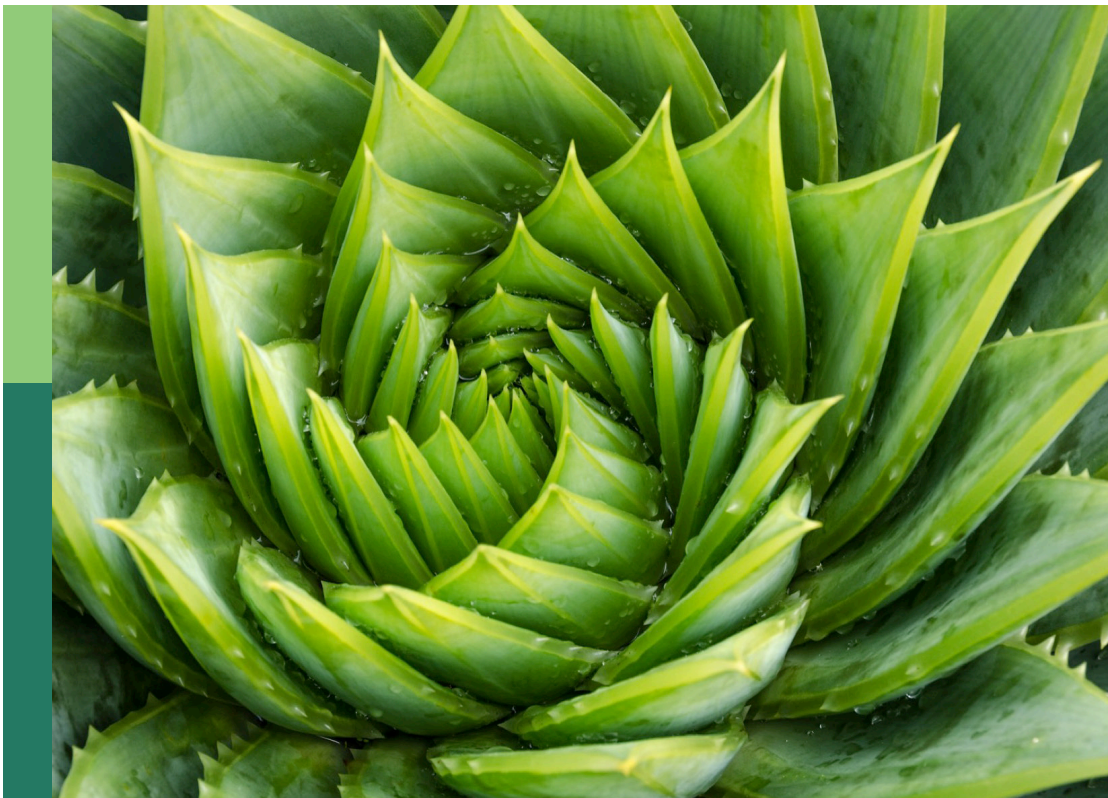

ISSN 1664-8714
ISBN 978-2-83251-937-0
DOI 10.3389/978-2-83251-937-0

About Frontiers

Frontiers is more than just an open access publisher of scholarly articles: it is a pioneering approach to the world of academia, radically improving the way scholarly research is managed. The grand vision of Frontiers is a world where all people have an equal opportunity to seek, share and generate knowledge. Frontiers provides immediate and permanent online open access to all its publications, but this alone is not enough to realize our grand goals.

Frontiers journal series

The Frontiers journal series is a multi-tier and interdisciplinary set of open-access, online journals, promising a paradigm shift from the current review, selection and dissemination processes in academic publishing. All Frontiers journals are driven by researchers for researchers; therefore, they constitute a service to the scholarly community. At the same time, the *Frontiers journal series* operates on a revolutionary invention, the tiered publishing system, initially addressing specific communities of scholars, and gradually climbing up to broader public understanding, thus serving the interests of the lay society, too.

Dedication to quality

Each Frontiers article is a landmark of the highest quality, thanks to genuinely collaborative interactions between authors and review editors, who include some of the world's best academicians. Research must be certified by peers before entering a stream of knowledge that may eventually reach the public - and shape society; therefore, Frontiers only applies the most rigorous and unbiased reviews. Frontiers revolutionizes research publishing by freely delivering the most outstanding research, evaluated with no bias from both the academic and social point of view. By applying the most advanced information technologies, Frontiers is catapulting scholarly publishing into a new generation.

What are Frontiers Research Topics?

Frontiers Research Topics are very popular trademarks of the *Frontiers journals series*: they are collections of at least ten articles, all centered on a particular subject. With their unique mix of varied contributions from Original Research to Review Articles, Frontiers Research Topics unify the most influential researchers, the latest key findings and historical advances in a hot research area.

Find out more on how to host your own Frontiers Research Topic or contribute to one as an author by contacting the Frontiers editorial office: frontiersin.org/about/contact

Advances in genetics and molecular breeding of ornamental plants

Topic editors

Shunli Wang — Chinese Academy of Agricultural Sciences (CAAS), China
Byoung Ryong Jeong — Gyeongsang National University, Republic of Korea
Pejman Azadi — Agricultural Biotechnology Research Institute of Iran, Iran
Daqiu Zhao — Yangzhou University, China

Citation

Wang, S., Jeong, B. R., Azadi, P., Zhao, D., eds. (2023). *Advances in genetics and molecular breeding of ornamental plants*. Lausanne: Frontiers Media SA.
doi: 10.3389/978-2-83251-937-0

Table of contents

frontiers | Frontiers in Plant Science

ORIGINAL RESEARCH
published: 12 May 2022
doi: 10.3389/fpls.2022.903674

Genetic Diversity Study on Geographical Populations of the Multipurpose Species *Elsholtzia stauntonii* Using Transferable Microsatellite Markers

Chenxing Zhang[1,2,3], Chunfeng Jia[4], Xinru Liu[1,2,3], Hanqing Zhao[1,2,3], Lu Hou[1,2,3], Meng Li[1,2,3], Binbin Cui[4] and Yingyue Li[1,2,3]**

[1] National Engineering Research Center of Tree Breeding and Ecological Restoration, College of Biological Sciences and Technology, Beijing Forestry University, Beijing, China, [2] Key Laboratory of Genetics and Breeding in Forest Trees and Ornamental Plants, Ministry of Education, College of Biological Sciences and Technology, Beijing Forestry University, Beijing, China, [3] The Tree and Ornamental Plant Breeding and Biotechnology Laboratory of National Forestry and Grassland Administration, Beijing Forestry University, Beijing, China, [4] College of Biochemistry and Environmental Engineering, Baoding University, Baoding, China

OPEN ACCESS

Edited by:
Shunli Wang,
Chinese Academy of Agricultural Sciences (CAAS), China

Reviewed by:
Sezai Ercisli,
Atatürk University, Turkey
Zhang Qingyu,
Northwest A&F University, China

***Correspondence:**
Yingyue Li
yingyueli@bjfu.edu.cn
Binbin Cui
cbb0508@163.com

Specialty section:
This article was submitted to Plant Breeding, a section of the journal Frontiers in Plant Science

Received: 24 March 2022
Accepted: 21 April 2022
Published: 12 May 2022

Citation:
Zhang C, Jia C, Liu X, Zhao H, Hou L, Li M, Cui B and Li Y (2022) Genetic Diversity Study on Geographical Populations of the Multipurpose Species Elsholtzia stauntonii Using Transferable Microsatellite Markers. Front. Plant Sci. 13:903674. doi: 10.3389/fpls.2022.903674

Elsholtzia stauntonii Benth. (Lamiaceae) is an economically important ornamental, medicinal and aromatic plant species. To meet the increasing market demand for *E. stauntonii*, it is necessary to assess genetic diversity within the species to accelerate the process of genetic improvement. Analysis of the transferability of simple sequence repeat (SSR) markers from related species or genera is a fast and economical method to evaluate diversity, and can ensure the availability of molecular markers in crops with limited genomic resources. In this study, the cross-genera transferability of 497 SSR markers selected from other members of the Lamiaceae (*Salvia* L., *Perilla* L., *Mentha* L., *Hyptis* Jacq., *Leonurus* L., *Pogostemon* Desf., *Rosmarinus* L., and *Scutella* L.) to *E. stauntonii* was 9.05% (45 primers). Among the 45 transferable markers, 10 markers revealed relatively high polymorphism in *E. stauntonii*. The genetic variation among 825 individuals from 18 natural populations of *E. stauntonii* in Hebei Province of China was analyzed using the 10 polymorphic SSR markers. On the basis of the SSR data, the average number of alleles (N_A), expected heterozygosity (H_E), and Shannon's information index (I) of the 10 primers pairs were 7.000, 0.478, and 0.688, respectively. Lower gene flow (N_m = 1.252) and high genetic differentiation (F_{st} = 0.181) were detected in the populations. Analysis of molecular variance (AMOVA) revealed that most of the variation (81.47%) was within the populations. Integrating the results of STRUCTURE, UPGMA (Unweighted Pair Group Method with Arithmetic Mean) clustering, and principal coordinate analysis, the 825 samples were grouped into two clusters associated with geographical provenance (southwestern and northeastern regions), which was consistent with the results of a Mantel test (r = 0.56, $p < 0.001$).

Overall, SSR markers developed in related genera were effective to study the genetic structure and genetic diversity in geographical populations of *E. stauntonii*. The results provide a theoretical basis for conservation of genetic resources, genetic improvement, and construction of a core collection for *E. stauntonii*.

Keywords: cross-transferability, *Elsholtzia stauntonii* Benth., simple sequence repeat (SSR) markers, genetic diversity, population structure

INTRODUCTION

Plants provide the fundamental support system for life on Earth and plant diversity is a key property of ecosystems (Moreira et al., 2016). Lamiaceae, with more than 7,000 species around the world, is a large family of flowering plants and an important part of plant diversity (Harley et al., 2004). Some species of the family have been commercially exploited worldwide (e.g., *Lavandula angustifolia*) (Pistelli et al., 2017), while many others are known locally for their ornamental, biological, and medicinal properties (e.g., *Hedeoma patens*) (Leyva-Lopez et al., 2016). *Elsholtzia stauntonii* Benth., a perennial deciduous subshrub of the Lamiaceae family, is widely distributed in China, especially in Hebei Province (Editorial committee of the Flora of China, and Chinese Academy of Sciences, 1977). *Elsholtzia stauntonii* is aromatic and its essential oils show insecticidal activity against certain pests of stored products (Lv et al., 2012). Consequently, *E. stauntonii* is used in novel biological insecticides (Liang et al., 2021). With its dense flowers, late flowering and bright colors, *E. stauntonii* is a popular bedding plant cultivated in public gardens and a wild nectar plant (Tian et al., 2007). Its branches and leaves are also used as a traditional Chinese medicinal material for treating common colds, toothache, and digestive system diseases (Zheng et al., 1999; Pekhova et al., 2020). Furthermore, the species is of ecological importance owing to its strong tolerance of drought and barren environments (Si and Peng, 2017). Previous studies on *E. stauntonii* have mainly focused on its morphological traits (Zhou et al., 2016), cultivation and propagation (Zhou et al., 2014), and extraction and identification of volatile oils (Guo et al., 2012; Xing et al., 2019). Little information is available on the genome and genetic diversity of this species. Studies of genetic diversity have been performed on many Lamiaceae species to clarify the genetic relationships among species (Bahadirli and Ayanoglu, 2020) and to identify molecular markers associated with agronomic traits for marker-assisted breeding (Lim et al., 2021). Therefore, with recognition of the value of this important but neglected species, it is crucial to evaluate the genetic variation in *E. stauntonii*.

Understanding the genetic diversity and structure of germplasm resources is a prerequisite for formulating effective breeding and conservation strategies (Gepts, 2006; Engelhardt et al., 2014; Vanavermaete et al., 2021). In recent years, with advances in molecular biological technologies, molecular marker-based analysis of genetic variation has avoided the limitations of morphological and biochemical indicators that are readily affected by environmental factors, and are more accurate for evaluation of population genetic parameters (Agarwal et al., 2008; Nadeem et al., 2018). Among the various types of molecular markers, microsatellites (or simple sequence repeats; SSRs) have become the preferred choice because of their high degree of reproducibility, ability to identify high levels of genetic polymorphism, codominant inheritance, and abundance in plant genomes (Powell et al., 1996; Grover and Sharma, 2016; Jose et al., 2018). Currently, SSR markers have been widely used in assessments of population genetic diversity (Gadissa et al., 2018), cultivar identification (Pinto et al., 2018; Sulu et al., 2020), and association mapping (Yang et al., 2020) as effective tools to describe genetic variation in plants. Using available genomic or expressed sequence tag databases (Vieira et al., 2016), a large number of SSR markers have been developed in Lamiaceae species, such as *Scutellaria baicalensis* (Zhang et al., 2014), *Perilla frutescens* (Ha et al., 2021), and *Salvia splendens* (Jiao et al., 2020). However, owing to the lack of genetic information, to date no SSR markers are available for evaluation of the genetic diversity within *E. stauntonii*, which limits its breeding and commercial development.

An alternative approach to overcome the time-consuming and costly development of SSR primers for target species is to exploit the transferability of SSR primers between related species or genera (Peakall et al., 1998; Pan et al., 2018). The transfer of SSR markers has been successful in many cases, as documented among Lamiaceae species (Karaca et al., 2013), from *Gossypium hirsutum* and *Corchorus olitorius* to Malvaceae species (Satya et al., 2016), among *Allium* species and among members of the Alliaceae (Barboza et al., 2018), and from *Ricinus communis* to Euphorbiaceae species (Dharajiya et al., 2020).

In this study, cross-genera amplification of SSR markers in Lamiaceae species was used to enrich the genetic database of *E. stauntonii*. On this basis, the genetic diversity and population structure of 825 *E. stauntonii* individuals sampled from 18 regions in Hebei Province, China, which is an important center in the distribution range of the species, were successfully evaluated using 10 highly polymorphic cross-transferable SSR markers. The results provide insight into the genetic resources of *E. stauntonii*, and represent a foundation for the effective management and genetic improvement of the species.

MATERIALS AND METHODS

Plant Materials

A field survey of extant *E. stauntonii* populations in Hebei Province, China was conducted from July to September 2020. Samples of 825 mature and disease-free individuals were randomly collected from 18 populations in the natural distribution area; the sample size per population ranged from 43 to 50 individuals (**Table 1**). To ensure sufficient geographical representation of the samples, the distance between sampled

TABLE 1 | Location and sampling site characteristics of 18 *Elsholtzia stauntonii* geographical populations (825 individuals).

Population name	Sample size	Location	Latitude (N)/Longitude (E)	Altitude (m)
HS	50	Shexian, Handan	N:36°36′/E:113°52′	880
XW	44	Wangnaocun, Xingtai	N:36°54′/E:114°4′	540
XM	47	Malingguan, Xingtai	N:37°20/E:113°57′	900
SZ	46	Zanhuangxian, Shijiazhuang	N:37°39′/E:114°23′	969
SP	48	Pingshanxian, Shijiazhuang	N:38°15′/E:114°11′	1,200
BF	46	Fupingxian, Baoding	N:38°53′/E:114°1′	1,200
BZ	46	Zoumayizhen, Baoding	N:39°8′/E:114°36′	915
ZQ	46	Qiaomaichuancun, Zhangjiakou	N:40°2′/E:115°16′	1,200
ZF	47	Feihuyu, Zhangjiakou	N:39°43′/E:114°38′	1,200
BL	43	Laishuixian, Baoding	N:39°23′/E:115°46′	984
BY	47	Yixian, Baoding	N:39°14′/E:114°58′	975
ZC	46	Chichengxian, Zhangjiakou	N:40°58′/E:115°57′	1,000
CF	43	Fengningxian, Chengde	N:41°46′/E:116°20′	1,100
CY	47	Yunwushan, Chengde	N:41°9′/E:116°45′	800
CL	43	Longhuaxian, Chengde	N:41°22′/E:117°48′	800
CX	46	Xinglongxian, Chengde	N:40°25′/E:117°30′	700
CC	46	Chengdexian, Chengde	N:40°46′/E:118°10′	800
QD	44	Dushan, Qinhuangdao	N:40°29′/E:118°48′	700

individuals was more than 50 m. The GPS coordinates were recorded for each population. The altitude of all sampled populations ranged from 540 to 1,200 m, with an average altitude of 937 m. Fresh leaves were desiccated in silica gel and stored at –20°C until use.

DNA Extraction and Genotyping With Simple Sequence Repeats Markers

Total genomic DNA of all samples was extracted using a Plant Genomic DNA Kit (Tiangen Biotech, Beijing, China). The DNA quality was evaluated by 1.0% agarose gel electrophoresis. DNA quantification was conducted with a NanoDrop 2000 spectrophotometer (Thermo Fisher Scientific, Wilmington, DE, United States) and the DNA concentration was adjusted to 20 ng/μL.

In total, 497 SSR markers from eight genera of Lamiaceae were used to perform cross-amplification tests on 16 randomly selected *E. stauntonii* samples from different populations (**Table 2**). Primers were synthesized by RuiBiotech (Beijing, China). To allow fluorescent labeling, the universal M13 sequence was added to the 5′ end of all forward primers. The PCR mixture was prepared in accordance with the method of Zhang et al. (2015) with modifications. Briefly, the PCR mixture (20 μl) contained 10 μl of 2 × Taq PCR Mix, 2 μl (40 ng) genomic DNA, 4 μl (4 pmol) fluorescent-dye-labeled M13 primer, and 4 μl (4 pmol) mixed complementary forward and reverse primers. The temperature profile used was as follows: an initial step of 5 min at 94°C, followed by 35 cycles of 30 s at 94°C, 30 s at 54°C, and 1 min at 72°C, then eight cycles of 30 s at 94°C, 30 s at 53°C, and 30 s at 72°C, and a final step of 10 min at 72°C. Capillary electrophoresis of the PCR products was performed using an ABI 3730xl DNA Analyzer (Tiangen Biotech, Beijing, China). GeneMarker version 2.2.0 software (Holland and Parson, 2011) was used to analyze the fragment size of the products and determine whether the primers detected polymorphisms.

TABLE 2 | SSR markers from eight genera in the Lamiaceae used to evaluate cross-genera transferability to *Elsholtzia stauntonii*.

Genera used for cross amplification	Number of SSR markers tested	References
Salvia L.	297	Radosavljević et al., 2011, 2012; Jiao et al., 2020; Krak et al., 2020
Perilla L.	128	Kwon et al., 2005; Sa et al., 2015, 2018, 2019; Ma et al., 2017; Wang et al., 2017; Park et al., 2019; Ha et al., 2021
Mentha L.	25	Vining et al., 2019
Hyptis Jacq.	15	Blank et al., 2014
Rosmarinus L.	12	Segarra-Moragues and Gleiser, 2009
Scutellaria L.	10	Zhang et al., 2014
Pogostemon Desf.	6	Sandes et al., 2013
Leonurus L.	4	Ren, 2012

Data Analysis

The SSR markers that successfully amplified single and specific bands within the expected product size range were considered to be transferable. The percentage transferability for each donor genus was calculated as (number of SSRs transferred/total number of SSRs screened) × 100. Similarly, the percentage transferability of SSR markers classified by repeat motifs (di-/tri-/tetra-/penta-/hexa-/complex-nucleotide) was estimated. Population diversity and population structure of *E. stauntonii* were assessed based on the transferred microsatellite loci.

For each SSR locus, important indices of genetic diversity were calculated using GenAlEx version 6.5 (Peakall and Smouse, 2012) and Microsatellite-Toolkit (Park, 2001) software. The indices comprised number of alleles (N_A), number of effective alleles (N_E), Shannon's information index (I), observed heterozygosity (H_O), expected heterozygosity (H_E), inbreeding coefficient (F_{is}), gene flow (N_m), and genetic differentiation index (F_{st}). The polymorphic information content (PIC) value and Hardy–Weinberg equilibrium (HWE) for the loci were calculated using PowerMarker version 3.25 (Liu and Muse, 2005).

Analysis of molecular variance (AMOVA) was conducted using Arlequin version 3.5 (Excoffier and Lischer, 2010) to estimate the variance components of genetic variation among and within populations. Bayesian analysis was performed to evaluate the population genetic structure and detect the most likely number of population genetic clusters of *E. stauntonii* using STRUCTURE version 2.3.4 (Pritchard et al., 2000). For each simulated value of *K* (range from 1 to 18), 15 independent runs were performed with a burn-in period of 200,000 iterations followed by 1,000,000 Markov chain Monte Carlo repetitions. The ΔK method (Evanno et al., 2005) was implemented in the Structure Harvester (Earl and VonHoldt, 2012) program based on the STRUCTURE results to determine the optimum *K* value. The percentage membership of each individual in every cluster (*Q* value) was determined; an individual with a *Q* value higher than 0.80 was considered to have a single genetic component (a pure individual). Nei's genetic distance (DA) (Nei et al., 1983) among the 825 individuals and 18 populations was calculated using PowerMarker version 3.25 (Liu and Muse, 2005). To explore the genetic relationships among all samples, the DA matrix was used to construct a dendrogram by hierarchical clustering with the unweighted pair group method with arithmetic mean (UPGMA) using PowerMarker version 3.25 (Liu and Muse, 2005). The dendrograms were visualized, manipulated, and annotated with the Interactive Tree of Life online tool (Letunic and Bork, 2007). Based on the standardized covariance of genetic distance, a principal coordinate analysis (PCoA) was conducted with GenAlEx version 6.5 (Peakall and Smouse, 2012). A clustering heatmap was prepared with Microsoft Excel based on the pairwise Nei's genetic distance between populations and the F_{st} values.

The geographic distance between the sampling locations was calculated with Geographic Distance Matrix Generator version 1.2.3 software[1]. The Mantel test was performed to analyze the correlation between geographic and genetic distance of different populations using the "ggpubr[2]" and "ggplot2" (Ginestet, 2011) packages in R version 4.1.1 (Ihaka and Gentleman, 1996). The map was created using the "sf" (Pebesma, 2018), "ggplot2" (Ginestet, 2011), and "ggspatial[3]" packages in R version 4.1.1.

RESULTS

Transferability of Simple Sequence Repeats Markers

Of the 497 SSRs mined, 45 primers (9.05%) successfully amplified genomic DNA of *E. stauntonii* and produced PCR products of the expected size (**Supplementary Table 1**). Transferability of the SSR markers varied among eight genera of Lamiaceae: 26.67% of the SSR markers of *Hyptis* Jacq., 25.00% of *Leonurus* L., 16.67% of *Pogostemon* Desf., 13.28% of *Perilla* L., 8.33% of *Rosmarinus* L., 6.73% of *Salvia* L., and 4.00% of *Mentha* L. were transferable to *E. stauntonii*, whereas no SSR marker was transferable from *Scutellaria* L. (**Figure 1**). The transferability of SSR markers based on simple di-/tri-nucleotide repeat motifs (7.89–9.65%) was

[1]http://biodiversityinformatics.amnh.org/opensource/gdmg/index.php

[2]https://cran.r-project.org/package=ggpubr

[3]https://cran.r-project.org/package=ggspatial

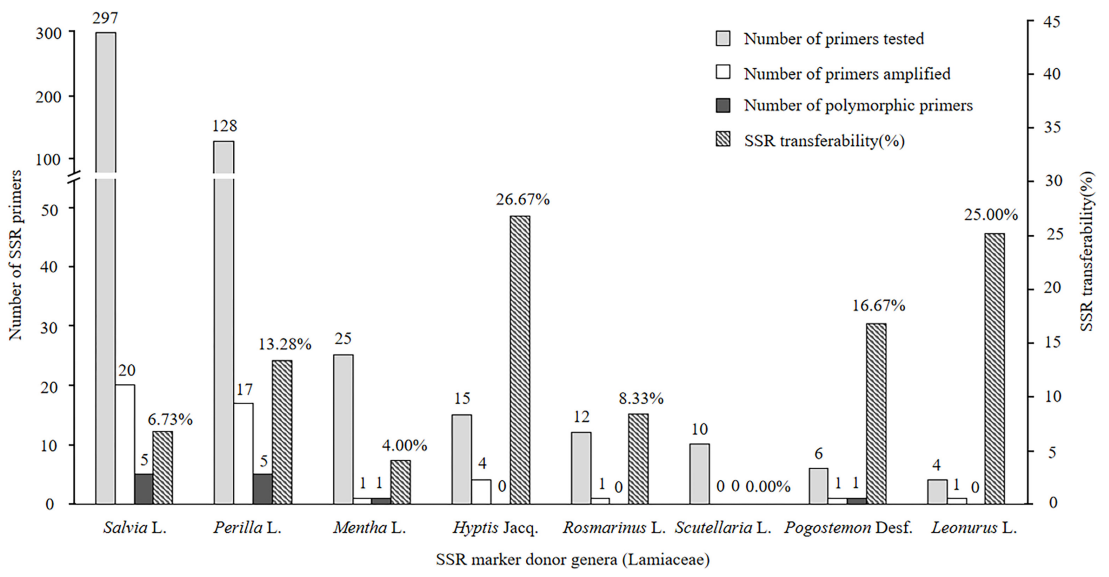

FIGURE 1 | Confamiliar transferability of SSR markers to *Elsholtzia stauntonii* from other genera of Lamiaceae.

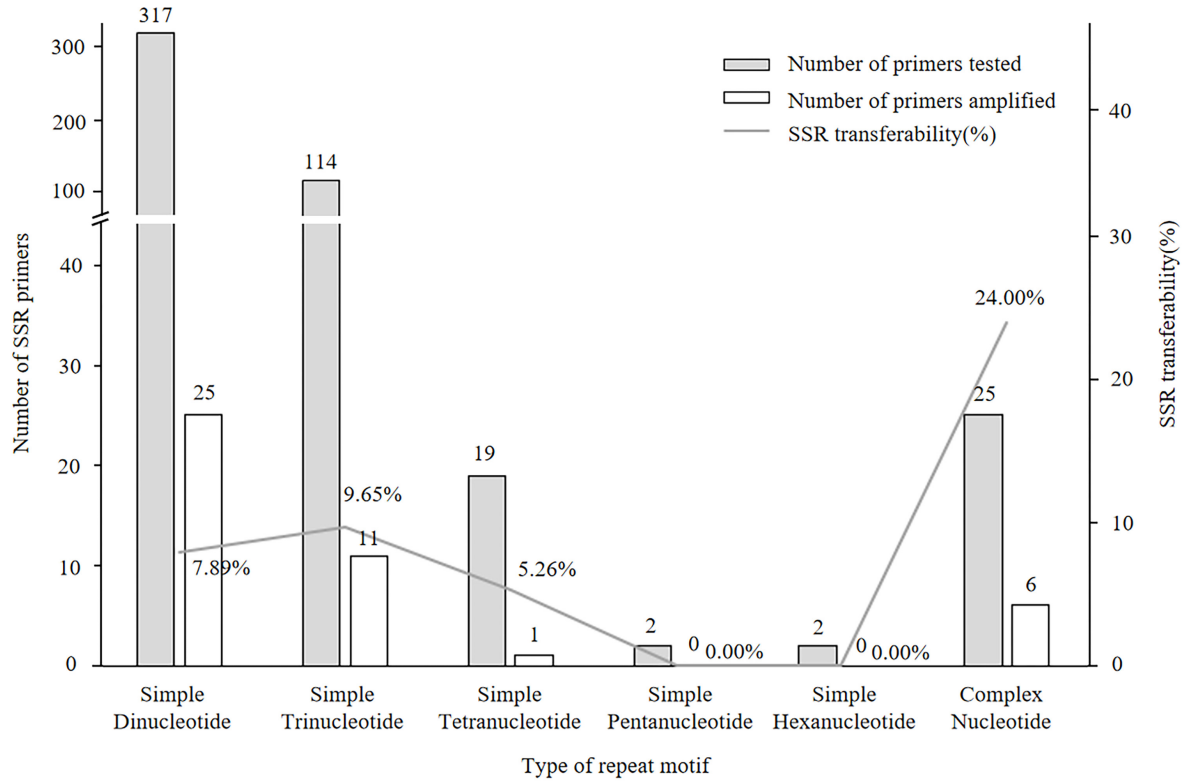

FIGURE 2 | Transferability of SSR markers to *Elsholtzia stauntonii* based on SSR repeat motif length. The repeat motif of eighteen SSRs was not available.

TABLE 3 | Characterization of 10 polymorphic SSR primer pairs.

SSR primer	Primer sequence (5′ to 3′)	Repeat motif	Allele size (bp)	N_A	H_O	H_E	PIC	F_{is}	HWE
KNUPF15[a]	F:CCACACGTAAACCTCATAAACC R:TTATCTCTAAAGAAATCGGGCA	$(CT)_{16}$	168–186	10	0.611	0.750	0.708	0.185	***
KNUPF67[b]	F:ATTGATTCTCTATCAACCTGGC R:CTCATCATCGGATCAACCTAGT	$(GCT)_7$	189–201	4	0.194	0.264	0.230	0.265	***
ssps251[c]	F:GACGCTCAAATGGTGAATCC R:ACGCTGATCTGGAAAGATGG	$(TC)_{11}$	231–277	24	0.469	0.879	0.868	0.466	***
ssps321[c]	F:ACGTGAACACACACCACCAT R:ACAGCATCAGCAACAGCAAC	$(GCT)_{10}$	220–235	8	0.336	0.425	0.390	0.209	***
ssps344[c]	F:CCTTCACCTGGGATGGAGTA R:GCCCTTTCAACCAAAACAAA	$(CT)_{10}$	177–235	2	0.241	0.214	0.191	−0.126	***
ssps512[c]	F:GGCTCCTCGTTTTATGGTGA R:GCATTAGTTGATGCCGAGGT	$(GA)_{11}$	163–195	3	0.236	0.499	0.376	0.527	***
ssps711[c]	F:CCGACGTGAACATACACCAC R:TTATGCAGCAGCAGGTTTTG	$(GCT)_{10}$	335–350	6	0.327	0.414	0.379	0.210	***
Pca6[d]	F: ACAAAGGGTTGACGATTG R:GTGATGAAACTGTCTCTCCTG	$(TG)_4$ (TC) $(TG)_5$ $(AG)_4$.$(TGTT)_3$	232–248	9	0.391	0.584	0.545	0.330	***
GBPF203[e]	F:GTTTTGTTGCAGCTCGATTT R:TGGGTTTGGAAAGTATTGATG	$(GA)_5$ (TAA) $(AG)_{26}$	132–162	2	0.439	0.352	0.290	−0.247	***
C3787[f]	F:GAGAGTACGGCGAGTAATTG R:TATCAACGTGAAGGAGACTTG	$(ATTT)_4$	145–157	2	0.356	0.396	0.317	0.101	**
Mean				7.000	0.360	0.478	0.429	0.192	–

*N_A, number of alleles; H_O, observed heterozygosity; H_E, expected heterozygosity; PIC, polymorphic information content; F_{is}, inbreeding coefficient; HWE, Hardy–Weinberg equilibrium; **$p < 0.01$; ***$p < 0.001$. [a,b,c,d,e,f], Previously published microsatellite markers ([a]: Sa et al., 2018; [b]: Sa et al., 2019; [c]: Jiao et al., 2020; [d]: Sandes et al., 2013; [e]: Sa et al., 2015; [f]: Vining et al., 2019).*

higher than that based on tetra-/penta-/hexa-nucleotide repeat motifs (**Figure 2**). The SSR markers based on complex (simple imperfect, compound perfect/imperfect) nucleotide repeats also showed high transferability (24.00%).

Polymorphism Analysis Based on Transferable Simple Sequence Repeats Markers

Among the 45 transferable SSR markers, 35 markers were monomorphic (33 primers) or showed very low levels of polymorphism (two primers) based on capillary electrophoresis results (**Supplementary Table 1**). Ten (2.01%) primer pairs showed higher polymorphism and were used for analysis of genetic diversity in *E. stauntonii* (**Table 3**).

In total, 70 alleles were amplified by the 10 polymorphic SSR markers among 825 *E. stauntonii* individuals, with a mean of 7.000 observed alleles per locus, and ranging in length from 132 to 350 bp (**Table 3**). The number of alleles per marker varied from 2 (ssps344, GBPF203, and C3787) to 24 (ssps251). Among the 10 markers, the observed heterozygosity (H_O) of eight markers was lower than the expected heterozygosity (H_E), and the average inbreeding coefficient (F_{is}) was positive. The PIC values ranged from 0.191 to 0.868, with a mean of 0.429. Eight SSR markers showed moderate or high polymorphism levels (PIC $>$ 0.25) and two markers (ssps344 and KNUPF67) showed low polymorphism levels (PIC $<$ 0.25) among the tested *E. stauntonii* populations. All SSR genotyping data for the 10 loci showed strongly significant deviation from the HWE ($p < 0.01$) (**Table 3**).

Population Genetic Diversity and Differentiation

In general, the difference in genetic diversity among the 18 geographical populations of *E. stauntonii* was observed (**Table 4**). The genetic diversity indices N_A and N_E of individual populations ranged from 2.400 (XW) to 3.900 (XM), and from 1.406 (ZQ) to 2.532 (CX), with means of 3.267 and 1.971, respectively. The average H_O and H_E were 0.359 and 0.388, ranging from 0.253 (XW) to 0.478 (CX), and from 0.260 (ZQ) to 0.506 (CX), respectively. The I value ranged from 0.450 (ZQ) to 0.887 (CX), with an average of 0.688. The highest level of genetic diversity was detected in CX, whereas XW and ZQ showed the lowest genetic diversity (**Table 4**).

The average F_{st}, a measure of the degree of genetic differentiation among populations, was 0.181 and the average N_m was 1.252 (**Table 4**). These results were consistent with those of AMOVA, which revealed that 18.53% of the genetic variation occurred among the populations and 81.47% was present within the populations (**Table 5**).

The pairwise F_{st} ranged from 0.020 (between populations CY and ZC) to 0.199 (between populations CX and ZQ) (**Figure 3**). The pairwise Nei's genetic distance ranged from 0.034 to 0.359, with the highest value (0.359) between the CX and ZQ populations and the second highest (0.328) between the CX and XW populations (**Figure 3**). In general, populations that were geographically closer had lower genetic distances (SZ–XM, 52.43 km, 0.034), whereas higher genetic distances were observed for populations that were farther apart (CX–XW, 490.81 km, 0.328). Mantel test results revealed a strongly significant correlation between genetic and geographic distance among the 18 natural populations ($r = 0.56$, $p < 0.001$) (**Figure 4**).

TABLE 4 | Genetic diversity for 10 polymorphic SSR markers in 18 natural populations of *Elsholtzia stauntonii* (total of 825 individuals).

Population	N_A	N_E	I	H_O	H_E	F_{st}	N_m
HS	2.600	1.674	0.520	0.263	0.311		
XW	2.400	1.545	0.477	0.253	0.284		
XM	3.900	2.331	0.699	0.351	0.361		
SZ	3.700	2.030	0.675	0.291	0.358		
SP	3.600	1.969	0.704	0.419	0.393		
BF	3.600	2.066	0.691	0.324	0.353		
BZ	3.600	2.205	0.745	0.377	0.405		
ZQ	2.600	1.406	0.450	0.273	0.260		
ZF	3.700	1.943	0.757	0.417	0.415		
BL	3.100	1.888	0.695	0.416	0.406		
BY	3.300	2.275	0.790	0.438	0.444		
ZC	3.700	2.005	0.775	0.372	0.447		
CF	3.200	1.726	0.624	0.319	0.352		
CY	3.200	2.227	0.848	0.409	0.497		
CL	3.500	1.816	0.608	0.291	0.317		
CX	3.500	2.532	0.887	0.478	0.506		
CC	2.800	2.065	0.782	0.430	0.478		
QD	2.800	1.771	0.664	0.348	0.401		
Mean	3.267	1.971	0.688	0.359	0.388	0.181	1.252

N_E, number of effective alleles; I, Shannon's Information Index; F_{st}, genetic differentiation index; N_m, gene flow.

Genetic Relationship and Population Structure

To determine the genetic structure of *E. stauntonii* populations, the co-ancestral relationship among populations was analyzed based on a Bayesian assignment model. The *Q* value of 680 individuals, accounting for 82.42% of the total samples, was greater than 0.8, indicating that most individuals had a relatively simple genetic background (**Supplementary Table 2**). STRUCTURE analysis revealed a distinct peak for ΔK at $K = 2$, indicating that the *E. stauntonii* samples could be grouped into two major clusters; these two subpopulations roughly corresponded to the southwestern and northeastern regions of Hebei Province (**Figures 5A,B**, **6**). The four populations (ZQ, ZF, BY, and BL) situated at the junction of the two regions contained abundant genetic variation and the lineages were obviously mixed (**Figure 6**). These populations contained genetic information of dual origins, with an average assignment of 49.7% to Cluster I (red) and 50.3% to Cluster II (green), whereas the other populations were relatively independent (**Figure 6** and **Supplementary Table 3**).

The UPGMA dendrogram grouped the 18 *E. stauntonii* populations into three major clusters. The populations XW, HS, XM, and SZ formed one cluster, the populations BF, SP, BZ, BL, BY, ZF, and ZQ formed a separate cluster, and the

TABLE 5 | Analysis of molecular variance (AMOVA) for 825 *Elsholtzia stauntonii* individuals clustered in 18 populations.

Source of variation	Degrees of freedom	Sum of squares	Percentage of variation (%)	*P*-value
Among populations	17	727.551	18.53%	<0.001
Within populations	807	3178.441	81.47%	<0.001
Total	824	3905.992	100.00%	

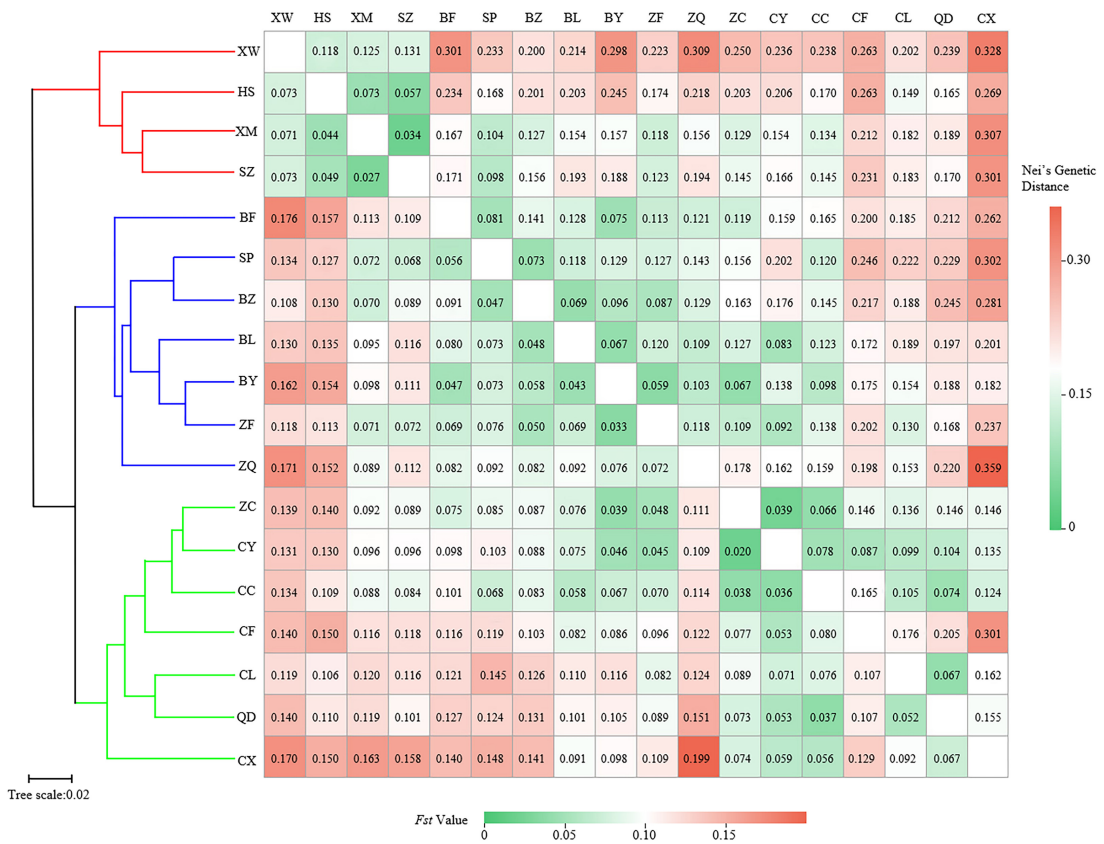

FIGURE 3 | Clustering heatmap of pairwise genetic differentiation index (F_{st}) (values below the diagonal), and pairwise Nei's genetic distance (values above the diagonal) among 18 populations of *Elsholtzia stauntonii*.

remaining populations (ZC, CY, CC, CF, CL, QD, and CX) formed a third group (**Figure 3**). However, the UPGMA tree of 825 individuals contained clusters of individuals from different populations and the samples were grouped into two major clades (**Figure 7A**). Consistent with the population dendrogram, the individuals of seven populations (ZC, CY, CC, CF, CL, QD, and CX) in the northeastern region were merged into a cluster and showed a broadly mixed ancestry, whereas the majority of individuals from the 11 populations in the southwestern region were grouped in the same cluster. In general, genetic proximity was observed between neighboring populations, whereas few genotypes shared an ancestry with individuals in geographically distant populations (**Figure 7A**).

Principal coordinate analysis was performed to visualize the multidimensional relationships among individuals based on genetic distance (**Figure 7B**). The closer they were on the PCoA graph, the less genetically differentiated they were, such as the HS, XM and SZ populations. Principal coordinates (PC) 1 and 2 explained 25.51% and 23.83% of the variance, respectively, and a combined 49.34% of the total variation. The PCoA analysis separated the populations into two clusters, which further confirmed the presence of genetic structure among *E. stauntonii* populations (**Figure 7B**).

DISCUSSION

Cross-Genera Transferability of Microsatellite Markers

Cross-taxa transferability enables the development of microsatellite markers, based on markers from related species, at low cost (Kalia et al., 2011; Bernardes et al., 2021). In the present study, the transferability observed (9.05%) was similar to the average of approximately 10% reported in cross-genera

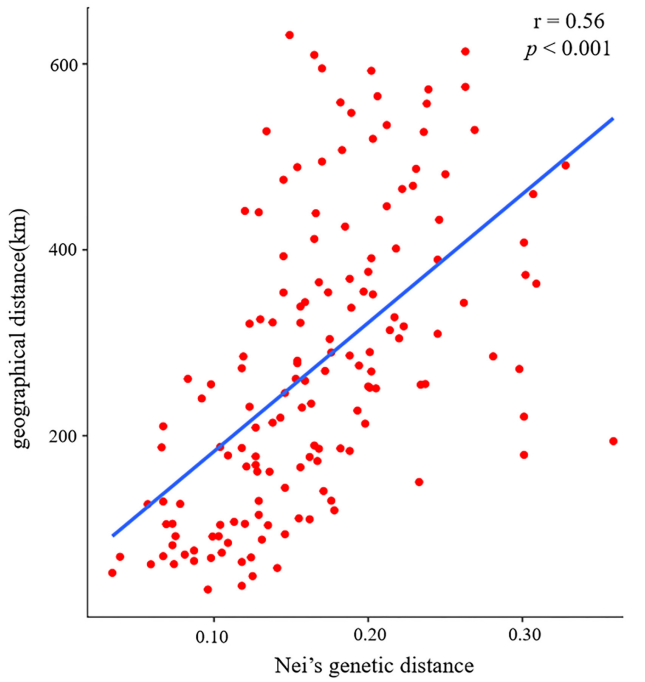

FIGURE 4 | Mantel test results of the correlation between Nei's genetic distance and geographical distance among 18 populations of *Elsholtzia stauntonii*.

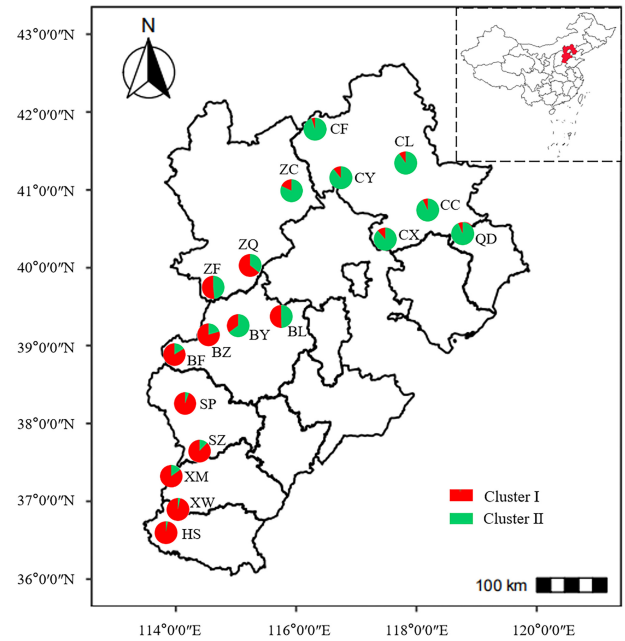

FIGURE 6 | Geographical distribution of 18 populations of *Elsholtzia stauntonii* and lineage contribution to gene pools. The pie diagram was drawn based on the results of STRUCTURE analysis with $K = 2$ and represents the average proportion of cluster membership of all individuals in each population.

transferability studies of eudicots between 1997 and mid-2006 (Barbará et al., 2007). However, the percentage transferability determined here was lower than the cross-genera amplification percentage observed in some families, such as Bignoniaceae (40.58%) (Kalia et al., 2020) and Cactaceae (35.16%) (Bombonato et al., 2019), and much lower than that between species within the same genus (Miranda et al., 2020; Pern et al., 2020; Li et al., 2021).

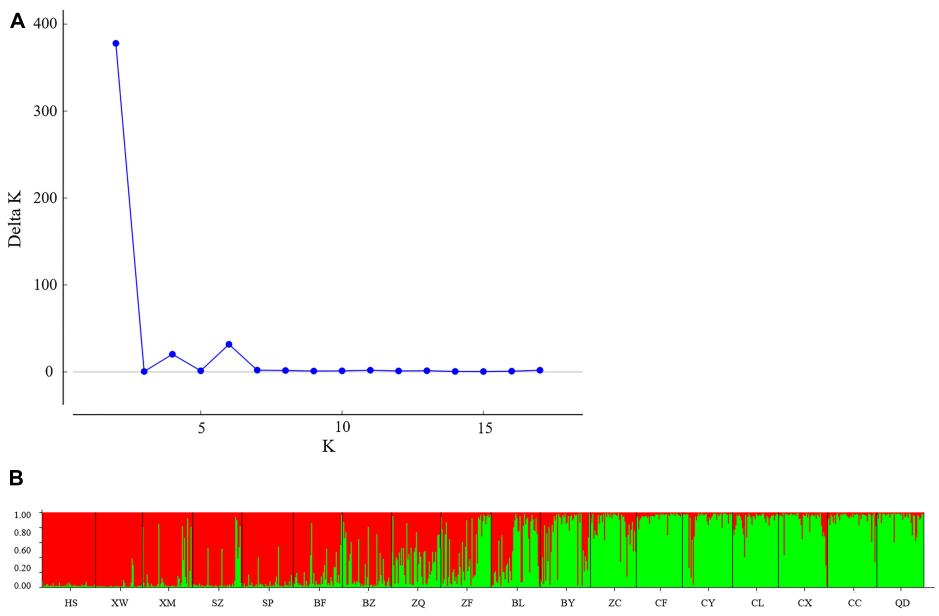

FIGURE 5 | Population structure of 825 *Elsholtzia stauntonii* individuals based on 10 SSR markers. **(A)** Delta *K* values from STRUCTURE analysis of the *E. stauntonii* individuals. **(B)** Histogram from STRUCTURE analysis for the model with $K = 2$.

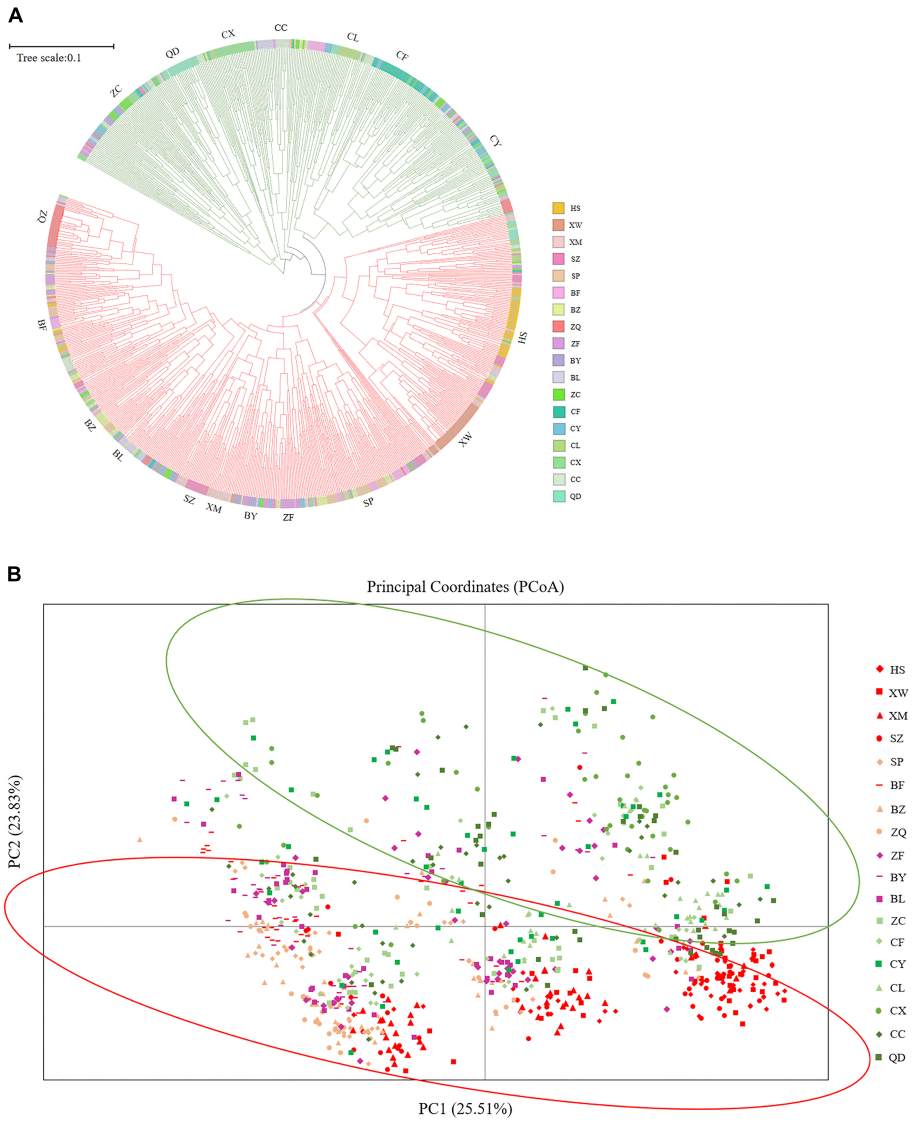

FIGURE 7 | (A) UPGMA tree constructed based on Nei's genetic distance of 825 *Elsholtzia stauntonii* individuals. **(B)** Principal coordinate analysis (PCoA) of 825 individuals from 18 populations.

The transferability of SSR markers between species or genera is determined by the conservation of DNA sequences and the stability of primer binding sites in flanking regions of SSRs during evolution (Ellegren, 2000; Saeed et al., 2016). A higher cross-taxa amplification percentage of SSR markers is expected between species with a close phylogenetic relationship, especially when both donor and target species are congeneric (Lesser et al., 2012; Karaca et al., 2013; Bharti et al., 2018). Therefore, it was speculated that *E. stauntonii* might have a relatively distant genetic relationship with its donor species (Jarne and Lagoda, 1996; Li et al., 2017). Nevertheless, although the primary contributing factor is phylogenetic proximity, transferability may also be influenced by other factors, such as the size and complexity of the relevant genome and whether the microsatellite is sited within a coding region (Oliveira et al., 2006).

The SSR transferability is also affected by the base repeat type of SSR core units (Gao et al., 2013). In general, SSR markers with a trinucleotide repeat motif show higher transferability than those with dinucleotide-type repeat motifs (Ellis and Burke, 2007; Harijan et al., 2017). A similar trend in heterologous SSR marker transferability has been reported for Euphorbiaceae, with the transfer rate of simple trinucleotide repeats being 11.44% higher than that of dinucleotide repeats (Dharajiya et al., 2020). One reason might be that the selection of frameshift mutations limits the fixation of microsatellites whose motif lengths are not divisible by three (e.g., di-/tetra-/pentanucleotide repeats), whereas fixation of mutant microsatellite whose motif lengths are divisible by three (tri-/hexanucleotide repeats) is not affected by differential selection pressures in coding and non-coding regions (Metzgar et al., 2000; Dutta et al., 2011;

Shivakumar et al., 2017). Moreover, microsatellites based on a complex nucleotide sequence show a lower mutation rate and higher transferability than simple repeats (Jin et al., 1996; Kalia et al., 2020). Given that more than 63% of the SSR markers used in the present study were di-nucleotide motif repeats, this may be an additional reason for the low transferability. Regardless, the 10 polymorphic transferable SSR markers identified in this study could be used to accelerate analysis of the genetic diversity of *E. stauntonii* and related species.

Genetic Diversity and Population Structure Analysis

All 10 transferable SSR primers used in the present study deviated significantly from the HWE ($p < 0.01$), which might reflect that the samples were collected from natural populations affected by complex environmental factors and human activities (Wang and Shete, 2012; Peng et al., 2021). The investigation found that *E. stauntonii* mainly resided beside rivers and valleys at lower altitudes, and its living environment was easily disturbed by tourism, grazing, and farmland planting. The mean PIC was 0.429, indicating that the genetic diversity of *E. stauntonii* germplasm in Hebei Province was generally moderate ($0.25 < PIC < 0.5$) (Botstein et al., 1980), which was lower than that reported for *Scutellaria baicalensis* (0.72) (Qi et al., 2015) and *Perilla frutescens* (0.582) (Park et al., 2019). The genetic diversity possessed by a species is determined by its evolutionary and ecological history (Aboukhalid et al., 2017). For *E. stauntonii*, the wide original geographic distribution theoretically contributes to the high level of genetic diversity detected. The moderate genetic diversity observed in this study might be limited by the number of markers, the test method, or the regions of sample collection (Budak et al., 2004; Serrote et al., 2020). Furthermore, it is generally accepted that markers of high transferability are less polymorphic among closely related species (Ni et al., 2015).

Genetic variation of a population can be measured by the number of alleles and heterozygosity (Huang et al., 2020; Savić et al., 2021). The mean N_A (7.000) and N_E (1.971) observed in the present study were slightly higher than the values (6.45 and 1.67, respectively) for 12 *Plectranthus edulis* populations evaluated using 20 SSR markers (Gadissa et al., 2018), but lower than the values reported for *Salvia splendens* (N_A = 11.829, N_E = 3.261) (Jiao et al., 2020) and *Juglans nigra* (N_A = 9.99, N_E = 7.51) (Schneider et al., 2019). Compared with previous studies on Lamiaceae species, *E. stauntonii* (H_O = 0.360) has higher genetic diversity than *Salvia fruticosa* (H_O = 0.307) (Radosavljević et al., 2015) and *Hedeoma piperita* (H_O = 0.3) (Herrera-Arroyo et al., 2020), but a higher level of genetic diversity has been observed in *Rosmarinus officinalis* (H_O = 0.63) (Segarra-Moragues et al., 2015). These results also indicated that the tested *E. stauntonii* samples showed moderate genetic diversity. The observed heterozygosity in the present study was lower than the expected heterozygosity (H_E = 0.478), indicating that the number of heterozygotes was lower than the predicted value (García-Arias et al., 2018). The average inbreeding coefficient (F_{is} = 0.192) in the population was positive and high, which similarly suggested there was an overabundance of homozygotes (Liu et al., 2019; Bairu et al., 2021). The reproductive characteristics of species might be an important factor in heterozygote deficiency in populations; for example, the combination of hermaphroditic flowers and profuse flowering of *E. stauntonii* may lead to improved levels of inbreeding which can reduce the genetic diversity of this widely distributed species (Zigene et al., 2021).

Genetic differentiation is an important index of the genetic structure of populations within a species (Wang, 2020). In the current study, gene flow of *E. stauntonii* (N_m = 1.252) was moderately low, lower than that reported for *Eragrostis tef* (N_m = 4.742) (Tadesse et al., 2021) and *Mucuna pruriens* (N_m = 7.48) (Lepcha and Sathyanarayana, 2021), but it was consistent with the high genetic differentiation (F_{st} = 0.181) (Balloux and Lugon-Moulin, 2002). The low gene flow, which might be caused by the small sampling range and habitat fragmentation, increased the within-population genetic variation and promoted population differentiation (Young et al., 1996; Li et al., 2014; Peng et al., 2021). Notably, among the 18 populations, the greatest genetic differentiation was observed between the CX and ZQ populations, which may be considered as potential parents for hybrid breeding. Furthermore, AMOVA revealed that the variation among *E. stauntonii* populations (18.53%) was higher than that of many other plant species, such as *Origanum vulgare* subsp. *hirtum* (8%) (Alekseeva et al., 2021) and *Allium sativum* L. (12.29%) (Poljuha et al., 2021), suggesting that disruption of gene flow between the populations played a role in determining the genetic differentiation of populations. Similarly, the results of the Mantel test ($r = 0.56$, $p < 0.001$) showed that increase in geographic distance reduced gene flow. Therefore, geographic distance may be the principal factor for genetic differentiation in *E. stauntonii*.

In the UPGMA clustering analysis, a certain deviation was observed in the clustering of individuals and of populations, which might be due to the high degree of gene exchange between populations. Overall, the clustering results observed with STRUCTURE, PCoA, and UPGMA were essentially similar, indicating that there might be two gene pools of *E. stauntonii*. Examination of the topography and geomorphology in Hebei Province indicated that the genetic structure of *E. stauntonii* was delimited according to geographical location and topographic barriers: one genealogical lineage each was located near the Taihang Mountains and the Yanshan Mountains. Previous studies have shown that geographical barriers play a crucial role in preventing plant dispersal (Fan et al., 2013; Zhao and Gong, 2015; Zeng et al., 2018), for example, the Tanaka Line in southwest China has a marked effect on the divergence and evolution of plant species (Ju et al., 2018). In this study, populations ZQ and CX on both sides of the mountain ranges presented the greatest F_{st} and genetic distance values, although their geographic distance was relatively close (194.14 km apart from each other), which also indicated the role of geographical barriers in genetic differentiation. The Taihang and Yanshan mountains may be responsible for maintaining the major southwest–northeast split of *E. stauntonii* populations by hindering animal-mediated gene

exchange. Thus, natural adaptation and geographical barriers may explain the differentiation of the two regions. Moreover, in the present analyses, each group was more or less intermingled with lineages of the other group, indicating that there was a certain level of gene flow between the populations, which has also been reported in *Tectona grandis* (Balakrishnan et al., 2021). The levels of genetic admixture differed substantially from population to population and seemed to be associated with the geographic location of the population, which indicated that interbreeding was an ongoing process, especially for the ZF, ZQ, BY, and BL populations (Mangaravite et al., 2016). These four populations had relatively high gene introgression, indicating that these populations had relatively rich genetic backgrounds and might be potential centers of diversification in this species. From the perspective of cultivar development and conservation, these populations may be valuable because they may contain novel alleles.

CONCLUSION

In this study, SSR markers from seven genera of Lamiaceae were transferable to *E. stauntonii*. Analysis based on 10 transferable SSR markers showed that, although the genetic diversity in 18 geographical populations of *E. stauntonii* was slightly lower than that of certain other species in the Lamiaceae, the genetic diversity was generally rich and the populations showed a high degree of genetic differentiation. STRUCTURE, PCoA, and UPGMA clustering analyses of all individuals resolved two genetic clusters, which might reflect geographical barriers to gene flow. By screening the study materials with superior traits and rich genetic variation, some individuals in the present experiment are expected to be utilized in the future improvement programmes of *E. stauntonii* to meet the increasing demand from the floriculture, essential oil, pharmaceutical, and other industries. The information obtained from the analysis of genetic diversity and population structure provides a foundation for the conservation, management, and utilization of *E. stauntonii*.

DATA AVAILABILITY STATEMENT

The original contributions presented in the study are included in the article/**Supplementary Material**, further inquiries can be directed to the corresponding authors.

AUTHOR CONTRIBUTIONS

YL and BC conceived and designed the experiments and obtained the funding. CZ, XL, and HZ conducted the experiments. CJ and BC contributed to the investigation. CZ, LH, and ML collected and analyzed the data. CZ wrote the manuscript. YL provided suggestions and comments for the manuscript. All authors read and approved the final manuscript.

FUNDING

This work was financially supported by the Key Research and Development Program of Hebei Province (20326332D).

SUPPLEMENTARY MATERIAL

The Supplementary Material for this article can be found online at: https://www.frontiersin.org/articles/10.3389/fpls.2022.903674/full#supplementary-material

REFERENCES

Aboukhalid, K., Machon, N., Lambourdiere, J., Abdelkrim, J., Bakha, M., Douaik, A., et al. (2017). Analysis of genetic diversity and population structure of the endangered *Origanum compactum* from Morocco, using SSR markers: implication for conservation. *Biol. Conserv.* 212, 172–182. doi: 10.1016/j.biocon.2017.05.030

Agarwal, M., Shrivastava, N., and Padh, H. (2008). Advances in molecular marker techniques and their applications in plant sciences. *Plant Cell Rep.* 27, 617–631. doi: 10.1007/s00299-008-0507-z

Alekseeva, M., Zagorcheva, T., Rusanova, M., Rusanov, K., and Atanassov, I. (2021). Genetic and flower volatile diversity in natural populations of *Origanum vulgare* subsp. hirtum (Link) Ietsw. in Bulgaria: toward the development of a core collection. *Front. Plant Sci.* 12:679063. doi: 10.3389/fpls.2021.679063

Bahadirli, N. P., and Ayanoglu, F. (2020). Genetic diversity of *Salvia* species from Turkey assessed by microsatellite markers. *J. Appl. Res. Med. Aromat. Plants* 20:100281. doi: 10.1016/j.jarmap.2020.100281

Bairu, M. W., Amelework, A. B., and Coetzer, W. G. (2021). Genetic diversity and population structure of six South African *Acacia mearnsii* breeding populations based on SSR markers. *J. Plant Res.* 134, 1243–1252. doi: 10.1007/s10265-021-01331-2

Balakrishnan, S., Dev, S. A., Sakthi, A. R., Vikashini, B., Bhasker, T. R., Magesh, N. S., et al. (2021). Gene-ecological zonation and population genetic structure of *Tectona grandis* L.f. in India revealed by genome-wide SSR markers. *Tree Genet. Genomes* 17:33. doi: 10.1007/s11295-021-01514-x

Balloux, F., and Lugon-Moulin, N. (2002). The estimation of population differentiation with microsatellite markers. *Mol. Ecol.* 11, 155–165. doi: 10.1046/j.0962-1083.2001.01436.x

Barbará, T., Palma-Silva, C., Paggi, G. M., Bered, F., Fay, M. F., and Lexer, C. (2007). Cross-species transfer of nuclear microsatellite markers: potential and limitations. *Mol. Ecol.* 16, 3759–3767. doi: 10.1111/j.1365-294X.2007.03439.x

Barboza, K., Beretta, V., Kozub, P. C., Salinas, C., Morgenfeld, M. M., Galmarini, C. R., et al. (2018). Microsatellite analysis and marker development in garlic: distribution in EST sequence, genetic diversity analysis, and marker transferability across *Alliaceae*. *Mol. Genet. Genomics* 293, 1091–1106. doi: 10.1007/s00438-018-1442-5

Bernardes, V., Murakami, D. M., Bizão, N., Souza, T. N., Silva, M. J., and Telles, M. P. C. (2021). Transferability and characterization of microsatellite markers from *Byrsonima cydoniifolia* A. Juss. (*MALPIGHIACEAE*) in seven related taxa from Cerrado biome reveal genetic relationships. *Mol. Biol. Rep.* 48, 4039–4046. doi: 10.1007/s11033-021-06411-z

Bharti, R., Kumar, S., and Parekh, M. J. (2018). Development of genomic simple sequence repeat (gSSR) markers in cumin and their application in diversity analyses and cross-transferability. *Ind. Crops Prod.* 111, 158–164. doi: 10.1016/j.indcrop.2017.10.018

Blank, A. F., Jesus, A. S., Santos, C. P., Grando, C., Pinheiro, J. B., Zucchi, M. I., et al. (2014). Development and characterization of novel microsatellite markers in *Hyptis pectinate* (*Lamiaceae*). *Genet. Mol. Res.* 13, 10173–10176. doi: 10.4238/2014.december.4.11

Bombonato, J. R., Bonatelli, I. A. S., Silva, R. G. A., Moraes, E. M., Zappi, D. C., Taylor, N. P., et al. (2019). Cross-genera SSR transferability in cacti revealed by a case study using Cereus (*Cereeae*, *Cactaceae*). *Genet. Mol. Biol.* 42, 87–94. doi: 10.1590/1678-4685-GMB-2017-0293

Botstein, D., White, R. L., Skolnick, M., and Davis, R. W. (1980). Construction of a genetic linkage map in man using restriction fragment length polymorphisms. *Am. J. Hum. Genet.* 32, 314–331.

Budak, H., Shearman, R. C., Parmaksiz, I., and Dweikat, I. (2004). Comparative analysis of seeded and vegetative biotype buffalograsses based on phylogenetic relationship using ISSRs, SSRs, RAPDs, and SRAPs. *Theor. Appl. Genet.* 109, 280–288. doi: 10.1007/s00122-004-1630-z

Dharajiya, D. T., Shah, A., Galvadiya, B. P., Patel, M. P., Srivastava, R., Pagi, N. K., et al. (2020). Genome-wide microsatellite markers in castor (*Ricinus communis* L.): identification, development, characterization, and transferability in *Euphorbiaceae*. *Ind. Crops Prod.* 151:112461. doi: 10.1016/j.indcrop.2020.112461

Dutta, S., Kumawat, G., Singh, B. P., Gupta, D. K., Singh, S., Dogra, V., et al. (2011). Development of genic-SSR markers by deep transcriptome sequencing in pigeonpea [*Cajanus cajan* (L.) Millspaugh]. *BMC Plant Biol.* 11:17. doi: 10.1186/1471-2229-11-17

Earl, D. A., and VonHoldt, B. M. (2012). STRUCTURE HARVESTER: a website and program for visualizing STRUCTURE output and implementing the Evanno method. *Conserv. Genet. Resour.* 4, 359–361. doi: 10.1007/s12686-011-9548-7

Editorial committee of the Flora of China, and Chinese Academy of Sciences (1977). "*Elsholtzia*(*Lamiaceae*)," in *Flora of China*, Vol. 66, eds Z. Y. Wu and X. W. Li (Beijing: Science Press). 304–348.

Ellegren, H. (2000). Microsatellite mutations in the germline: implications for evolutionary inference. *Trends Genet.* 16, 551–558. doi: 10.1016/S0168-9525(00)02139-9

Ellis, J. R., and Burke, J. M. (2007). EST-SSRs as a resource for population genetic analyses. *Heredity* 99, 125–132. doi: 10.1038/sj.hdy.6801001

Engelhardt, K. A. M., Lloyd, M. W., and Neel, M. C. (2014). Effects of genetic diversity on conservation and restoration potential at individual, population, and regional scales. *Biol. Conserv.* 179, 6–16. doi: 10.1016/j.biocon.2014.08.011

Evanno, G., Regnaut, S., and Goudet, J. (2005). Detecting the number of clusters of individuals using the software STRUCTURE: a simulation study. *Mol. Ecol.* 14, 2611–2620. doi: 10.1111/j.1365-294X.2005.02553.x

Excoffier, L., and Lischer, H. E. L. (2010). Arlequin suite ver 3.5: a new series of programs to perform population genetics analyses under Linux and Windows. *Mol. Ecol. Resour.* 10, 564–567. doi: 10.1111/j.1755-0998.2010.02847.x

Fan, D. M., Yue, J. P., Nie, Z. L., Li, Z. M., Comes, H. P., and Sun, H. (2013). Phylogeography of *Sophora davidii* (*Leguminosae*) across the 'Tanaka-Kaiyong Line', an important phytogeographic boundary in Southwest China. *Mol. Ecol.* 22, 4270–4288. doi: 10.1111/mec.12388

Gadissa, F., Tesfaye, K., Dagne, K., and Geleta, M. (2018). Genetic diversity and population structure analyses of *Plectranthus edulis* (Vatke) Agnew collections from diverse agro-ecologies in Ethiopia using newly developed EST-SSRs marker system. *BMC Genet.* 19:92. doi: 10.1186/s12863-018-0682-z

Gao, C. H., Ren, X. D., Mason, A. S., Li, J., Wang, W., Xiao, M. L., et al. (2013). Revisiting an important component of plant genomes: microsatellites. *Funct. Plant Biol.* 40, 645–661. doi: 10.1071/FP12325

García-Arias, F. L., Osorio-Guarín, J. A., and Zarantes, V. M. N. (2018). Association study reveals novel genes related to yield and quality of fruit in cape gooseberry (*Physalis peruviana* L.). *Front. Plant Sci.* 9:362. doi: 10.3389/fpls.2018.00362

Gepts, P. (2006). Plant genetic resources conservation and utilization. *Crop Sci.* 46, 2278–2292. doi: 10.2135/cropsci2006.03.0169gas

Ginestet, C. (2011). Ggplot2: elegant graphics for data analysis. *J. R. Stat. Soc. A Stat.* 174, 245–245. doi: 10.1111/j.1467-985X.2010.00676_9.x

Grover, A., and Sharma, P. C. (2016). Development and use of molecular markers: past and present. *Crit. Rev. Biotechnol.* 36, 290–302. doi: 10.3109/07388551.2014.959891

Guo, Z. Q., Liu, Z. Z., Wang, X. H., Liu, W. R., Jiang, R., Cheng, R. Y., et al. (2012). Elsholtzia: phytochemistry and biological activities. *Chem. Cent. J.* 6:147. doi: 10.1186/1752-153X-6-147

Ha, Y. J., Sa, K. J., and Lee, J. K. (2021). Identifying SSR markers associated with seed characteristics in Perilla (*Perilla frutescens* L.). *Physiol. Mol. Biol. Plants* 27, 93–105. doi: 10.1007/s12298-021-00933-3

Harijan, Y., Nishanth, G. K., Katageri, I. S., and Khadi, B. M. (2017). Transferability of heterologous SSR markers to cotton genotypes. *Electron. J. Plant Breed.* 8, 379–384. doi: 10.5958/0975-928X.2017.00057.6

Harley, R. M., Atkins, S., Budantsev, A. L., Cantino, P. D., Conn, B. J., Grayer, R., et al. (2004). "Labiatae," in *Families and Genera of Vascular Plants*, Vol. 7, eds K. Kubitzki and J. W. Kadereit (Berlin: Springer). 167–275.

Herrera-Arroyo, M. L., Rico, Y., and Bedolla-García, B. Y. (2020). Morphotype divergence and genetic diversity of Hedeoma piperita Benth. in western Mexico. *Mol. Biol. Rep.* 47, 8925–8934. doi: 10.1007/s11033-020-05946-x

Holland, M. M., and Parson, W. (2011). GeneMarker® HID: a reliable software tool for the analyses of forensic STR data. *J. Forensic Sci.* 56, 29–35. doi: 10.1111/j.1556-4029.2010.01565.x

Huang, C. J., Chu, F. H., Huang, Y. S., Hung, Y. M., Tseng, Y. H., Pu, C. E., et al. (2020). Development and technical application of SSR-based individual identification system for *Chamaecyparis taiwanensis* against illegal logging convictions. *Sci. Rep.* 10:22095. doi: 10.1038/s41598-020-79061-z

Ihaka, R., and Gentleman, R. (1996). R: a language for data analyses and graphics. *J. Comput. Graph. Stat.* 5, 299–314. doi: 10.1080/10618600.1996.10474713

Jarne, P., and Lagoda, P. J. (1996). Microsatellites, from molecules to populations and back. *Trends Ecol. Evol.* 11, 424–429. doi: 10.1016/0169-5347(96)10049-5

Jiao, S. Q., Dong, A. X., Shi, T. L., Liu, H., Porth, I., Xin, H. B., et al. (2020). Development of a large gene-associated SSR marker set and in-depth genetic characterization in scarlet sage. *Front. Genet.* 11:504. doi: 10.3389/fgene.2020.00504

Jin, L., Macaubas, C., Hallmayer, J., Kimura, A., and Mignot, E. (1996). Mutation rate varies among alleles at a microsatellite locus: phylogenetic evidence. *Proc. Natl. Acad. Sci. U.S.A.* 93, 15285–15288. doi: 10.1073/pnas.93.26.15285

Jose, A. G., Concepción, M., and Francisco, M. (2018). Trends in plant research using molecular markers. *Planta* 247, 543–557. doi: 10.1007/s00425-017-2829-y

Ju, M. M., Fu, Y., Zhao, G. F., He, C. Z., Li, Z. H., and Tian, B. (2018). Effects of the Tanaka Line on the genetic structure of *Bombax ceiba* (Malvaceae) in dry-hot valley areas of southwest China. *Ecol. Evol.* 8, 3599–3608. doi: 10.1002/ece3.3888

Kalia, R. K., Chhajer, S., and Pathak, R. (2020). Cross genera transferability of microsatellite markers from other members of family Bignoniaceae to *Tecomella undulata* (Sm.) Seem. *Acta Physiol. Plant.* 42:151. doi: 10.1007/s11738-020-03138-5

Kalia, R. K., Rai, M. K., Kalia, S., Singh, R., and Dhawan, A. K. (2011). Microsatellite markers: an overview of the recent progress in plants. *Euphytica* 177, 309–334. doi: 10.1007/s10681-010-0286-9

Karaca, M., Ince, A. G., Aydin, A., and Ay, S. T. (2013). Cross-genera transferable e-microsatellite markers for 12 genera of the *Lamiaceae* family. *J. Sci. Food Agric.* 93, 1869–1879. doi: 10.1002/jsfa.5982

Krak, K., Vit, P., Douda, J., and Mandak, B. (2020). Development of 18 microsatellite markers for *Salvia pratensis*. *Appl. Plant Sci.* 8, e11316. doi: 10.1002/aps3.11316

Kwon, S. J., Lee, J. K., Kim, N. S., Yu, J. W., Dixit, A., Cho, E. G., et al. (2005). Isolation and characterization of microsatellite markers in *Perilla frutescens* Brit. *Mol. Ecol. Notes* 5, 455–457. doi: 10.1111/j.1471-8286.2005.00901.x

Lepcha, P., and Sathyanarayana, N. (2021). Variability for seed-based economic traits and genetic diversity analysis in Mucuna pruriens population of northeast India. *Agric. Res.* 1–11. doi: 10.1007/s40003-021-00568-6

Lesser, M. R., Parchman, T. L., and Buerkle, C. A. (2012). Cross-species transferability of SSR loci developed from transciptome sequencing in lodgepole pine. *Mol. Ecol. Resour.* 12, 448–455. doi: 10.1111/j.1755-0998.2011.03102.x

Letunic, I., and Bork, P. (2007). Interactive Tree of Life (iTOL): an online tool for phylogenetic tree display and annotation. *Bioinformatics* 23, 127–128. doi: 10.1093/bioinformatics/btl529

Leyva-Lopez, N., Nair, V., Bang, W. Y., Cisneros-Zevallos, L., and Heredia, J. B. (2016). Protective role of terpenes and polyphenols from three species of Oregano (*Lippia graveolens*, *Lippia palmeri* and *Hedeoma patens*) on the suppression of lipopolysaccharide-induced inflammation in RAW 264.7 macrophage cells. *J. Ethnopharmacol.* 187, 302–312. doi: 10.1016/j.jep.2016.04.051

Li, C. H., Zheng, Y. Q., Liu, Y., Lin, F. R., and Huang, P. (2021). Development of genomic SSR for the subtropical hardwood tree *Dalbergia* hupeana and assessment of their transferability to other related species. *Forests* 12, 804–804. doi: 10.3390/f12060804

Li, K. Q., Chen, L., Feng, Y. H., Yao, J. X., Li, B., Xu, M., et al. (2014). High genetic diversity but limited gene flow among remnant and fragmented natural populations of *Liriodendron* chinense Sarg. *Biochem. Syst. Ecol.* 54, 230–236. doi: 10.1016/j.bse.2014.01.019

Li, P., Qi, Z. C., Liu, L. X., Ohi-Toma, T., Lee, J., Hsieh, T. H., et al. (2017). Molecular phylogenetics and biogeography of the mint tribe Elsholtzieae (*Nepetoideae*, *Lamiaceae*), with an emphasis on its diversification in East Asia. *Sci. Rep.* 7:2057. doi: 10.1038/s41598-017-02157-6

Liang, J. Y., Ning, A. Q., Lu, P. Y., An, Y., Wang, Z. L., Zhang, J., et al. (2021). Biological activities and synergistic effects of *Elsholtzia*stauntonii essential oil from flowers and leaves and their major constituents against *Tribolium castaneum*. *Eur. Food Res. Technol.* 247, 2609–2619. doi: 10.1007/s00217-021-03829-4

Lim, S. E., Sa, K. J., and Lee, J. K. (2021). Bulk segregant analysis identifies SSR markers associated with leaf and seed related traits in Perilla crop (*Perilla frutescens* L.). *Genes Genom.* 43, 323–332. doi: 10.1007/s13258-021-01056-5

Liu, K., and Muse, S. V. (2005). PowerMarker: an integrated analyses environment for genetic marker analyses. *Bioinformatics* 21, 2128–2129. doi: 10.1093/bioinformatics/bti282

Liu, Y. L., Geng, Y. P., Song, M. L., Zhang, P. F., Hou, J. L., and Wang, W. Q. (2019). Genetic structure and diversity of glycyrrhiza populations based on transcriptome SSR markers. *Plant Mole. Biol. Rep.* 37, 401–412. doi: 10.1007/s11105-019-01165-2

Lv, J. H., Su, X. H., and Zhong, J. J. (2012). Fumigant activity of *Elsholtzia stauntonii* extract against Lasioderma serricorne. *S. Afr. J. Sci.* 108, 77–79. doi: 10.4102/sajs.v108i7/8.556

Ma, S. J., Sa, K. J., Hong, T. K., and Lee, J. K. (2017). Genetic diversity and population structure analysis in *Perilla frutescens* from Northern areas of China based on simple sequence repeats. *Genet. Mol. Res.* 16:16039746. doi: 10.4238/gmr16039746

Mangaravite, E., Vinson, C. C., Rody, H. V. S., Carniello, M. A., Silva, R. S., and Oliveira, L. O. (2016). Contemporary patterns of genetic diversity of *Cedrela fissilis* offer insight into the shaping of seasonal forests in eastern South America. *Am. J. Bot.* 103, 307–316. doi: 10.3732/ajb.1500370

Metzgar, D., Bytof, J., and Wills, C. (2000). Selection against frameshift mutations limits microsatellite expansion in coding DNA. *Genome Res.* 10, 72–80. doi: 10.1101/gr.10.1.72

Miranda, K. M. C., Guimarães, R. A., Silva, M. J., Oliveira, P. R. O., Ribeiro, T. G., Mendes, T. P., et al. (2020). Cross-amplification and characterization of microsatellite markers in species of Manihot Mill. (*Euphorbiaceae*) endemic to the Brazilian Cerrado. *Acta Bot. Bras.* 34, 772–777. doi: 10.1590/0102-33062019abb0374

Moreira, X., Abdala-Roberts, L., Rasmann, S., Castagneyrol, B., and Mooney, K. A. (2016). Plant diversity effects on insect herbivores and their natural enemies: current thinking, recent findings, and future directions. *Curr. Opin. Insect Sci.* 14, 1–7. doi: 10.1016/j.cois.2015.10.003

Nadeem, M. A., Nawaz, M. A., Shahid, M. Q., Dogan, Y., Comertpay, G., Yildiz, M., et al. (2018). DNA molecular markers in plant breeding: current status and recent advancements in genomic selection and genome editing. *Biotechnol. Biotechnol. Equip.* 32, 261–285. doi: 10.1080/13102818.2017.1400401

Nei, M., Tajima, F., and Tateno, Y. (1983). Accuracy of estimated phylogenetic trees from molecular data. *J. Mol. Evol.* 19, 153–170. doi: 10.1007/BF01840887

Ni, Z. X., Bai, T. D., Cai, H., Chen, S. F., and Xu, L. (2015). The Transferability of *Pinus massoniana* SSR in other *Pinus* species. *Mol. Plant Breed.* 13, 2811–2817. doi: 10.13271/j.mpb.013.002811

Oliveira, E. J., Pádua, J. G., Zucchi, M. I., Vencovsky, R., and Vieira, M. L. C. (2006). Origin, evolution and genome distribution of microsatellites. *Genet. Mol. Biol.* 29, 294–307. doi: 10.1590/S1415-47572006000200018

Pan, L., Huang, T., Yang, Z., Tang, L., Cheng, Y., Wang, J., et al. (2018). EST-SSR marker characterization based on RNA-sequencing of Lolium multiflorum and cross transferability to related species. *Mol. Breed.* 38:80. doi: 10.1007/s11032-018-0775-4

Park, D. H., Sa, K. J., Lim, S. E., Ma, S. J., and Lee, J. K. (2019). Genetic diversity and population structure of *Perilla frutescens* collected from Korea and China based on simple sequence repeats (SSRs). *Genes Genom.* 41, 1329–1340. doi: 10.1007/s13258-019-00860-4

Park, S. D. E. (2001). *Trypanotolerance in West African Cattle and the Population Genetic Effects of Selection*. Dissertation's thesis. Dublin: University of Dublin.

Peakall, R., Gilmore, S., Keys, W., Morgante, M., and Rafalski, A. (1998). Cross-species amplification of soybean (*Glycine max*) simple sequence repeats (SSRs) within the genus and other legume genera: implications for the transferability of SSRs in plants. *Mol. Biol. Evol.* 15, 1275–1287. doi: 10.1093/oxfordjournals.molbev.a025856

Peakall, R., and Smouse, P. E. (2012). GenAlEx 6.5: genetic analysis in Excel. population genetic software for teaching and research—an update. *Bioinformatics* 28, 2537–2539. doi: 10.1093/bioinformatics/bts460

Pebesma, E. (2018). Simple features for R: standardized support for spatial vector data. *R J.* 10, 439–446. doi: 10.32614/RJ-2018-009

Pekhova, O. A., Timasheva, L. A., Danilova, I. L., and Belova, I. V. (2020). Accumulation of biologically active substances in plants of *Elsholtzia*stauntonii Benth. grown in the foothill zone of the Crimea. *Agrar. Bullet. Urals.* 11, 76–84. doi: 10.32417/1997-4868-2020-202-11-76-84

Peng, J. Y., Shi, C., Wang, D. W., Li, S. Z., Zhao, X. L., Duan, A. N., et al. (2021). Genetic diversity and population structure of the medicinal plant *Docynia delavayi* (Franch.) Schneid revealed by transcriptome-based SSR markers. *J. Appl. Res. Med. Aromat. Plants* 21:100294. doi: 10.1016/j.jarmap.2021.100294

Pern, Y. C., Lee, S. Y., Ng, W. L., and Mohamed, R. (2020). Cross-amplification of microsatellite markers across agarwood-producing species of the Aquilarieae tribe (*Thymelaeaceae*). *3 Biotech* 10:103. doi: 10.1007/s13205-020-2072-2

Pinto, M. V., Poornima, H. S., Sivaprasad, V., and Naik, V. G. (2018). A new set of mulberry-specific SSR markers for application in cultivar identification and DUS testing. *J. Genet.* 97, e31–e37. doi: 10.1007/s12041-018-0900-5

Pistelli, L., Najar, B., Giovanelli, S., Lorenzini, L., Tavarini, S., and Angelini, L. G. (2017). Agronomic and phytochemical evaluation of lavandin and lavender cultivars cultivated in the Tyrrhenian area of Tuscany (Italy). *Ind. Crops Prod.* 109, 37–44. doi: 10.1016/j.indcrop.2017.07.041

Poljuha, D., Franić, M., Kralj, I., Weber, T., Šatović, Z., Ban, D., et al. (2021). Genetic diversity and structure analysis of Croatian garlic collection assessed by SSR markers. *Folia Hortic.* 33, 157–171. doi: 10.2478/fhort-2021-0011

Powell, W., Morgante, M., Andre, C., Hanafey, M., Vogel, J., Tingey, S., et al. (1996). The comparison of RFLP, RAPD, AFLP and SSR (microsatellite) markers for germplasm analysis. *Mol. Breed.* 2, 225–238. doi: 10.1016/j.scienta.2011.06.015

Pritchard, J. K., Stephens, M., and Donnelly, P. (2000). Inference of population structure using multilocus genotype data. *Genetics* 155, 945–959. doi: 10.1093/genetics/155.2.945

Qi, L. J., Long, P., Jiang, C., Yuan, Y., and Huang, L. Q. (2015). Development of microsatellites and genetic diversity analysis of *Scutellaria baicalensis* Georgi using genomic-SSR markers. *Acta Pharm. Sin.* 50, 500–505. doi: 10.16438/j.0513-4870.2015.04.002

Radosavljević, I., Jakse, J., Javornik, B., Satovic, Z., and Liber, Z. (2011). New microsatellite markers for *Salvia officinalis* (*Lamiaceae*) and cross-amplification in closely related species. *Am. J. Bot.* 98, e316–e318. doi: 10.3732/ajb.1000462

Radosavljević, I., Satovic, Z., Jakse, J., Javornik, B., Greguraš, D., Jug-Dujaković, M., et al. (2012). Development of new microsatellite markers for *Salvia officinalis* L. and its potential use in conservation-genetic studies of narrow sndemic *Salvia* brachyodon Vandas. *Int. J. Mol. Sci.* 13, 12082–12093. doi: 10.3390/ijms130912082

Radosavljević, I., Satovic, Z., and Liber, Z. (2015). Causes and consequences of contrasting genetic structure in sympatrically growing and closely related species. *AoB Plants* 7:106. doi: 10.1093/aobpla/plv106

Ren, P. (2012). *The research on genetic diversity of Leonurus japonicus germplasm resources in Henan province. [master's thesis]*. Zhengzhou (HN): Henan Agricultural University.

Sa, K. J., Choi, I. Y., Park, K. C., and Lee, J. K. (2018). Genetic diversity and population structure among accessions of *Perilla frutescens* (L.) Britton in East Asia using new developed microsatellite markers. *Genes Genom.* 40, 1319–1329. doi: 10.1007/s13258-018-0727-8

Sa, K. J., Choi, I. Y., Ueno, M., and Lee, J. K. (2015). Genetic diversity and population structure in cultivated and weedy types of Perilla in East Asia and other countries as revealed by SSR marker. *Hortic. Environ. Biotechnol.* 56, 524–534. doi: 10.1007/s13580-015-0039-8

Sa, K. J., Lim, S. E., Choi, I. Y., Park, K. C., and Lee, J. K. (2019). Development and characterization of new microsatellite markers for *Perilla frutescens* (L.) Britton. *Am. J. Plant Sci.* 10, 1623–1630. doi: 10.4236/ajps.2019.109115

Saeed, A. F., Wang, R. Z., and Wang, S. H. (2016). Microsatellites in pursuit of microbial genome evolution. *Front. Microbiol.* 6:1462. doi: 10.3389/fmicb.2015.01462

Sandes, S. S., Pinheiro, J. B., Zucchi, M. I., Monteiro, M., Arrigoni-Blank, M. F., and Blank, A. F. (2013). Development and characterization of microsatellite primers in *Pogostemon cablin* (*Lamiaceae*). *Genet. Mol. Res.* 12, 2837–2840. doi: 10.4238/2013.August.8.4

Satya, P., Paswan, P. K., Ghosh, S., Majumdar, S., and Ali, N. (2016). Confamiliar transferability of simple sequence repeat (SSR) markers from cotton (*Gossypium hirsutum* L.) and jute (*Corchorus olitorius* L.) to twenty two Malvaceous species. *3 Biotech* 6:65. doi: 10.1007/s13205-016-0392-z

Savić, A., Pipan, B., Vasić, M., and Meglič, V. (2021). Genetic diversity of common bean (*Phaseolus vulgaris* L.) germplasm from Serbia, as revealed by single sequence repeats (SSR). *Sci. Hortic.* 288:110405. doi: 10.1016/j.scienta.2021.110405

Schneider, S. J., Hwang, A. Y., Land, S. D., Chen, L. L., Thomas, A. L., and Hwang, C. F. (2019). Genetic diversity of ten black walnut (*Juglans nigra* L.) cultivars and construction of a mapping population. *Tree Genet. Genomes* 15:62. doi: 10.1007/s11295-019-1369-y

Segarra-Moragues, J. G., and Gleiser, G. (2009). Isolation and characterisation of di and tri nucleotide microsatellite loci in *Rosmarinus officinalis* (*Lamiaceae*), using enriched genomic libraries. *Conserv. Genet.* 10, 571–575. doi: 10.1007/s10592-008-9572-7

Segarra-Moragues, J. G., Marco, Y. C., Castellanos, M. C., Molina, M. J., and García-Fayos, P. (2015). Ecological and historical determinants of population genetic structure and diversity in the Mediterranean shrub *Rosmarinus officinalis* (*Lamiaceae*). *Bot. J. Linn. Soc.* 180, 50–63. doi: 10.1111/boj.12353

Serrote, C. M. L., Reiniger, L. R. S., Silva, K. B., Rabaiolli, S. M. D., and Stefanel, C. M. (2020). Determining the polymorphism information content of a molecular marker. *Gene* 726:144175. doi: 10.1016/j.gene.2019.144175

Shivakumar, M. S., Ramesh, S., Mohan Rao, A., Udaykumar, H. R., and Keerthi, C. M. (2017). Cross legume species/genera transferability of SSR markers and their utility in assessing transferability of SSR markers and their utility in assessing polymorphism among advanced breeding lines in Dolichos bean (*Lablab purpureus* L.). *Int. J. Curr. Microbiol. App. Sci.* 6, 656–668. doi: 10.20546/ijcmas.2017.608.083

Si, S. X., and Peng, Z. F. (2017). Introduction and domestication and application of *Elsholtzia stauntonii* in the middle and lower reaches of the Yellow River Plain. *J. Anhui Agri. Sci.* 45:214. doi: 10.13989/j.cnki.0517-6611.2017.04.053

Sulu, G., Kacar, Y. A., Polat, I., Kitapci, A., Turgutoglu, E., Simsek, O., et al. (2020). Identification of genetic diversity among mutant lemon and mandarin varieties using different molecular markers. *Turk. J. Agric. For.* 44, 465–478. doi: 10.3906/tar-1909-67

Tadesse, M., Kebede, M., and Girma, D. (2021). Genetic diversity of Tef [*Eragrostis tef* (Zucc.) Trotter] as revealed by microsatellite markers. *Int. J. Genomics* 2021:6672397. doi: 10.1155/2021/6672397

Tian, Y. L., Li, J. Q., Wang, W. H., Shi, A. P., and Wang, H. L. (2007). The germplasm resource and ornamental character of the *Lamiaceae* in Beijing. *J. Beijing Univ. Agric.* 22, 41–43. doi: 10.13473/j.cnki.issn.1002-3186.2007.03.006

Vanavermaete, D., Fostier, J., Maenhout, S., and De Baets, B. (2021). Deep scoping: a breeding strategy to preserve, reintroduce and exploit genetic variation. *Theor. Appl. Genet.* 134, 3845–3861. doi: 10.1007/s00122-021-03932-w

Vieira, M. L. C., Santini, L., Diniz, A. L., and Munhoz, C. D. F. (2016). Microsatellite markers: what they mean and why they are so useful. *Genet. Mol. Biol.* 39, 312–328. doi: 10.1590/1678-4685-GMB-2016-0027

Vining, K. J., Pandelova, I., Hummer, K., Bassil, N., Contreras, R., Neill, K., et al. (2019). Genetic diversity survey of *Mentha aquatica* L. and *Mentha suaveolens* Ehrh., mint crop ancestors. *Genet. Resour. Crop Evol.* 66, 825–845. doi: 10.1007/s10722-019-00750-4

Wang, J., and Shete, S. (2012). Testing departure from Hardy-Weinberg proportions. *Methods Mol. Biol.* 850, 77–102. doi: 10.1007/978-1-61779-555-8_6

Wang, S. Q. (2020). Genetic diversity and population structure of the endangered species *Paeonia* decomposita endemic to China and implications for its conservation. *BMC Plant Biol.* 20:510. doi: 10.1186/s12870-020-02682-z

Wang, X. P., Wen, H., Shang, Z. W., Yang, S., Xu, J., and Shen, Q. (2017). Genetic relationship and genetic diversity of 13 *Perilla frutescens* varieties based on SSR markers. *Guizhou Agri. Sci.* 45, 103–106.

Xing, X. Q., Li, M. D., Gong, Y. M., Niu, B., Hao, N., Tian, Y. L., et al. (2019). Comparative analysis of volatile components in essential oil of *Elsholtzia*stauntonii and different organs. *South Chin. Agri.* 13, 150–155. doi: 10.19415/j.cnki.1673-890x.2019.02.077

Yang, Y. Y., He, R. Q., Zheng, J., Hu, Z. H., Wu, J., and Leng, P. S. (2020). Development of EST-SSR markers and association mapping with floral traits in Syringa oblata. *BMC Plant Biol.* 20:436. doi: 10.1186/s12870-020-02652-5

Young, A., Boyle, T., and Brown, T. (1996). The population genetic consequences of habitat fragmentation for plants. *Trends Ecol. Evol.* 11, 413–418. doi: 10.1016/0169-5347(96)10045-8

Zeng, Y. F., Zhang, J. G., Abuduhamiti, B., Wang, W. T., and Jia, Z. Q. (2018). Phylogeographic patterns of the desert poplar in Northwest China shaped by both geology and climatic oscillations. *BMC Ecol. Evol.* 18:75. doi: 10.1186/s12862-018-1194-1

Zhang, W. J., Yuan, Q. J., Jiang, D., Zhang, Y. Q., and Huang, L. Q. (2014). Development and characterisation of microsatellite markers for the medicinal plant *Scutellaria baicalensis* (*Lamiaceae*). *Biochem. Syst. Ecol.* 54, 267–271. doi: 10.1016/j.bse.2014.01.005

Zhang, Z. Y., Cui, B. B., Mao, J. F., Pang, X. M., and Li, Y. Y. (2015). Novel polymorphic EST-derived microsatellite markers for the red-listed five needle pine, *Pinus* dabeshanensis. *Conserv. Genet. Resour.* 7, 191–192. doi: 10.1007/s12686-014-0329-y

Zhao, Y. J., and Gong, X. (2015). Genetic divergence and phylogeographic history of two closely related species (*Leucomeris decora* and *Nouelia insignis*) across the' Tanaka Line' in southwest China. *BMC Evol. Biol.* 15:134. doi: 10.1186/s12862-015-0374-5

Zheng, S., Kang, S., Shen, Y., and Sun, L. (1999). Three new c-methylated flavones from *Elsholtzia*stauntonii. *Planta Med.* 65, 173–175. doi: 10.1055/s-2006-960459

Zhou, X. M., Li, B. Y., and Wang, Y. J. (2014). Cultivation and management of *Elsholtzia*stauntonii. *Chin. Flowers Hortic.* 24, 40–41.

Zhou, X. M., Liu, H. C., and Li, B. Y. (2016). Type and distribution of trichomes on the leaf epidermis of *Elsholtzia stautonii* and the secreting process of the glandular trichomes. *Acta Hortic. Sin.* 43, 1555–1565. doi: 10.16420/j.issn.0513-353x.2016-0154

Zigene, Z. D., Asfaw, B. T., and Bitima, T. D. (2021). Analysis of genetic diversity in rosemary (*Salvia* rosemarinus Schleid.) using SSR molecular marker for its management and sustainable use in Ethiopian genebank. *Genet. Resour. Crop Evol.* 68, 279–293. doi: 10.1007/s10722-020-00984-7

Conflict of Interest: The authors declare that the research was conducted in the absence of any commercial or financial relationships that could be construed as a potential conflict of interest.

Publisher's Note: All claims expressed in this article are solely those of the authors and do not necessarily represent those of their affiliated organizations, or those of the publisher, the editors and the reviewers. Any product that may be evaluated in this article, or claim that may be made by its manufacturer, is not guaranteed or endorsed by the publisher.

frontiers | Frontiers in Plant Science

TYPE Original Research
PUBLISHED 03 August 2022
DOI 10.3389/fpls.2022.955590

OPEN ACCESS

EDITED BY
Daqiu Zhao,
Yangzhou University, China

REVIEWED BY
Antje Feller,
University of Tübingen, Germany
Zhaoyu Gu,
China Agricultural University, China

*CORRESPONDENCE
Long Li
lilong1949@126.com

SPECIALTY SECTION
This article was submitted to Plant Breeding, a section of the journal Frontiers in Plant Science

RECEIVED 28 May 2022
ACCEPTED 08 July 2022
PUBLISHED 03 August 2022

CITATION
Shi Q, Yuan M, Wang S, Luo X, Luo S, Fu Y, Li X, Zhang Y and Li L (2022) *PrMYB5* activates anthocyanin biosynthetic *PrDFR* to promote the distinct pigmentation pattern in the petal of *Paeonia rockii*. *Front. Plant Sci.* 13:955590. doi: 10.3389/fpls.2022.955590

PrMYB5 activates anthocyanin biosynthetic *PrDFR* to promote the distinct pigmentation pattern in the petal of *Paeonia rockii*

Qianqian Shi[1], Meng Yuan[1], Shu Wang[1], Xiaoning Luo[1], Sha Luo[1], Yaqi Fu[1], Xiang Li[1], Yanlong Zhang[1] and Long Li[2,3]*

[1]College of Landscape Architecture and Art, Northwest A&F University, Yangling, China, [2]Co-Innovation Center for Sustainable Forestry in Southern China, Nanjing Forestry University, Nanjing, China, [3]Bamboo Research Institute, Nanjing Forestry University, Nanjing, China

Paeonia rockii is well-known for its distinctive large dark-purple spot at the white petal base and has been considered to be the main genetic source of spotted tree peony cultivars. In this study, the petal base and petal background of *Paeonia ostii* (pure white petals without any spot), *P. rockii*, and other three tree peony cultivars were sampled at four blooming stages from the small bell-like bud stage to the initial blooming stage. There is a distinct difference between the pigmentation processes of spots and petal backgrounds; the spot pigmentation was about 10 days earlier than the petal background. Moreover, the cyanin and peonidin type anthocyanin accumulation at the petal base mainly contributed to the petal spot formation. Then, we identified a C1 subgroup R2R3-MYB transcription factor, *PrMYB5*, predominantly transcribing at the petal base. This is extremely consistent with *PrDFR* and *PrANS* expression, the contents of anthocyanins, and spot formation. Furthermore, *PrMYB5* could bind to and activate the promoter of *PrDFR* in yeast one-hybrid and dual-luciferase assays, which was further verified in overexpression of *PrMYB5* in tobacco and *PrMYB5*-silenced petals of *P. rockii* by comparing the color change, anthocyanin contents, and gene expression. In summary, these results shed light on the mechanism of petal spot formation in *P. rockii* and speed up the molecular breeding process of tree peony cultivars with novel spot pigmentation patterns.

KEYWORDS

***Paeonia rockii*, *PrMYB5*, *PrDFR*, anthocyanin biosynthesis, petal spot**

Introduction

Petal spot is a kind of regular variegated pattern of flower color, which exists in angiosperm, such as *Nomocharis meleagrina*, *Torenia fournieri*, *Sparaxia elegans*, *Dendrobium nobile*, and *Paeonia suffruticosa* (Gao et al., 2015; Zhang et al., 2015; Shi et al., 2017; Su et al., 2017; Gu et al., 2019). It not only imparts ornamental and commercial values but also affects the preferences of pollinators and promotes the success

of pollination (Davies et al., 2012; Glover et al., 2013), so the molecular mechanism of petal spot formation has always been a research hotspot.

The formation of petal spots is determined by the specific spatiotemporal transcription of genes in the anthocyanin biosynthesis pathway (ABP), resulting in specific anthocyanins accumulation in defined petal regions (Suzuki et al., 2016). In ABP, chalcone synthase (*CHS*), chalcone isomerase (*CHI*), flavanoid 3'-hydroxylase (*F3'H*), flavanone 3-hydroxylase (*F3H*), dihydroflavonol 4-reductase (*DFR*), anthocyanidin synthase (*ANS*), and flavonoid glucosyltransferase (*UFGT*) are mainly controlled by MYB transcription factor (TF), basic helix–loop–helix (bHLH), and WD40 protein in different plants (Cao et al., 2020; Yan et al., 2021). To date, the spatio-temporal regulation mechanisms involved in petal spot formation have been explored in many ornamental plants, including *Antirrhinum* spp., *Petunia hybrid*, *Lilium* spp., *Mimulus* spp., *Clarkia gracilis*, and *Phalaenopsis* spp. (Schwinn et al., 2006; Albert et al., 2011; Shang et al., 2011; Yamagishi, 2011, 2020; Yamagishi et al., 2010; Glover et al., 2013; Yuan et al., 2014; Hsu et al., 2015; Martins et al., 2017). In the same way, *CgMYB1* activated *CgDFR2* and *CgANS* to produce petal spots in *C. gracilis* (Martins et al., 2017). However, the specific regulation mechanism of petal spot is rarely studied in woody ornamental plants, especially wild tree peony species.

Tree peony is one of the most famous traditional flowers in China and is popular all over the world for its large, colorful, and distinct flowers. At present, there are more than 2,000 cultivars worldwide with various petal pigmentation patterns, such as spots, stripes, and more complex designs (Zhou et al., 2014). *Paeonia rockii* is the most important wild tree peony species in Northwest China and has a large dark-purple spot at the white petal base, which has been confirmed as a main genetic source of spot pigmentation in tree peony (Wang et al., 2000; Shi et al., 2017). *Paeonia ostii* has pure white petals without any spots, and other tree peony cultivars of *P. suffruticosa,* "Lanhudie" (LHD), "Mochi Jinhui" (MCJH), and {High Noon" (HN), possess different degrees of purple spots on differentially colored petal backgrounds, which can be considered as the control group for the spot pigmentation study of *P. rockii*. Therefore, it is urgent to explore the molecular mechanism of petal spot pigmentation of *P. rockii* to accelerate the molecular breeding process of a variegated tree peony in China. Previous research demonstrated that the spot formation at the petal base of tree peony was primarily attributed to the spatial biosynthesis of cyanidin (Cy) and peonidin (Pn) anthocyanins (Zhang et al., 2015; Shi et al., 2017). The anthocyanin structural genes and anthocyanin regulatory MYBs have been identified in tree peony cultivars, including *PsMYB114L, PsMYB12L*, *PsMYB12*, *PsMYB111*, *PsMYB4*, *PsMYB57*, and *PsMYB58* (Gu et al., 2019; Zhang et al., 2019, 2020a,b; Luo et al., 2021). Among them, *PsMYB12* directly activated the expression of *PsCHS* by forming an MBW regulatory complex with bHLH and WD40 proteins, which were specific to the petal blotch in tree peony cultivar "Qing Hai Hu Yin Bo" (Gu et al., 2019). However, whether and how other MYBs regulated the petal spot formation in *P. rockii* are almost unknown.

Previously comparative transcriptome analyses of *P. rockii* and *P. ostii* flowers suggested that *CHS*, *DFR*, *ANS*, glutathione S-transferase (*GST*), and two R2R3-MYB TFs might be related to petal spot formation in *P. rockii* (Shi et al., 2017). In the present study, we investigated one anthocyanin regulatory R2R3-MYB TF *PrMYB5* in *P. rockii* and analyzed the expression patterns at different parts of petals during flower opening of *P. rockii, P. ostii,* and other three tree peony cultivars. Furthermore, we conducted gene overexpression in tobacco plants, virus-induced gene silencing (VIGS), and RNA *in situ* hybridization to verify that *PrMYB5* can individually regulate the distinct petal pigmentation in *P. rockii* by activating *PrDFR* expression, resulting in anthocyanin accumulation. The results aim to provide valuable resources and theoretical supports for molecular breeding of variegation cultivars in tree peony and supply references for the studies on the spot formation mechanism in other woody plants.

Materials and methods

Sample preparation

The plants of *P. rockii*, *P. ostii*, and three tree peony cultivars *P. suffruticosa,* "Lanhudie," "Mochi Jinhui," and "High Noon," were grown in the germplasm repository of the Northwest A&F University, Shaanxi, China. Petal backgrounds and petal bases at four different blooming stages were sampled separately from March to April, 2018 (Figure 1). The four blooming stages include: stage 1 (S1): a small bell-like bud stage when the petals are mainly yellow-green; stage 2 (S2): a large bell-like bud stage when the petal bases turn obvious color with the yellow-green background; stage 3 (S3): a bell-like bud extending stage when spots get bigger and darker; and stage 4 (S4): an initiating blooming stage when spots are completely formed (Figure 1). Tobacco plants (*Nicotiana tabacum* L. cv. K326) were grown in a conservatory under 16 h/8 h light photoperiod at 25°C. The color indices (L^*, a^*, b^*, C, and h) were measured in the fresh petals at four stages using a colorimeter (CR-400, Konica Minolta, Osaka, Japan). The other materials were immediately frozen in liquid nitrogen and then stored at −80°C.

HPLC analysis

Flavonoids were detected in tree peony petals and tobacco petals using the high-performance liquid chromatography (HPLC) method, as previously reported (Luo et al., 2021). First, each sample was ground into powder in liquid nitrogen. Then,

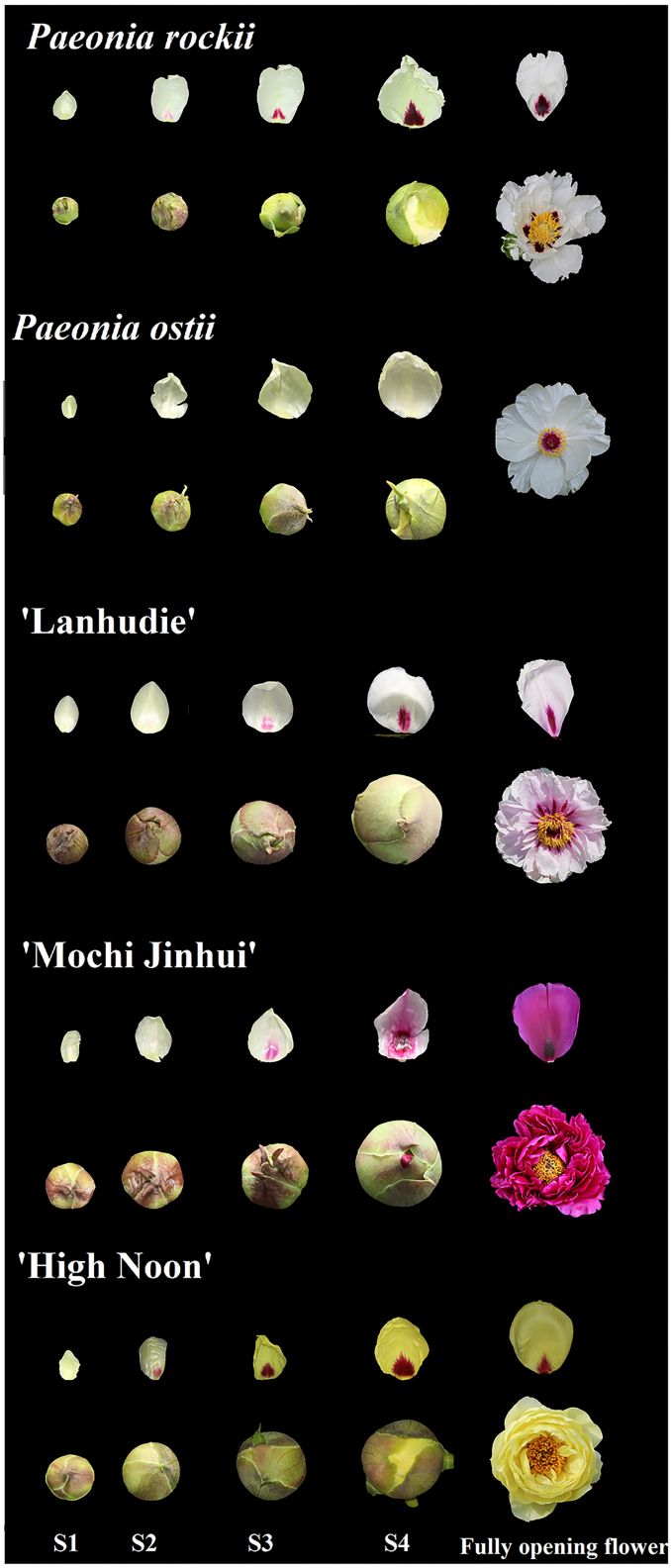

FIGURE 1
Flower phenotypes of *Paeonia rockii, P. ostii, P. suffruticosa* "Lanhudie," "Mochi Jinhui," and "High Noon" at four different opening stages. S1: stage 1, small bell-like bud stage when the petals were mainly yellow-green; S2: stage 2, large bell-like bud stage when the petal bases turn obvious color with the yellow-green background; S3: stage 3, bell-like bud extending stage when spots get bigger and darker; S4: stage 4, initiating blooming stage when spots are completely formed.

1 mg of petal powder was extracted with 2 ml methanol-formic acid (99:1, V/V) at 4°C for 24 h in the dark. After ultrasonic-assisted extraction for 30 min and centrifugation at 10,000 rpm for 10 min, liquid supernatant was gathered and filtered using a 0.22 μm nylon microporous membrane. Flavonoid analysis was done as follows: eluent A: 0.04% formic acid; eluent B: acetonitrile. Elution procedure: 1–40 min: 5–40% B; 40–45 min, 40–100% B; 45–55 min, 100%B; 55–60 min, 100–5% B. Flow rate: 0.5 mL •min^{-1}, column temperature: 40°C, injection volume: 10 μL. We used Cy3G, Cy3G5G, Pg3G, Pg3G5G, Pn3G, Pn3G5G, Ap, Ch, Is, Km, Lu, and Qu from the Shanghai Yuanye Bio-Technology Co., Ltd (Shanghai, China) as standards. All assays were conducted with three biological replicates.

Isolation of full-length CDNA, sequence alignment, and phylogenetic tree analysis

Total RNA was extracted from 100 mg petal base of *P. rockii* at S4 using the Quick RNA Isolation Kit (Bioteke Corporation, Beijing, China). After RNA purity and integrity were checked, full-length cDNAs of *PrMYB5* were cloned using the SMARTer RACE 5'/3' Kit (TAKARA Corporation, Beijing, China) according to the manufacturer's protocols. The primers are listed in Supplementary Table 1.

The multiple sequence alignment and phylogenetic tree of PrMYB5 and some anthocyanin biosynthesis and spot formation related R2R3-MYB proteins from tree peony and other plants were performed using the DNAMAN6.0.3.99 software and the MEGA 6.0 software using the neighbor-joining method, respectively.

Subcellular localization

The *PrMYB5* ORF was cloned into the pC2300-GFP vector with the *KpnI*and *SalI* restriction sites using In-Fusion Cloning and then transformed into the onion epidermal cells through particle bombardment experiment. After onion tissues were cultured at 25°C for 24 h in the dark, we used a laser confocal microscope (Leica TCS SP2) to observe the fluorescence. All primers are listed in Supplementary Table 1.

RNA *in situ* hybridization

RNA *in situ* hybridization was conducted according to the previously reported method (Li et al., 2018). The stage 4 petal background and petal base of *P. rockii* were fixed in 4% paraformaldehyde at 4°C for 24 h. After being dehydrated through a graded ethanol series and then embedded in paraffin, the petals were sectioned into 10 μm thick and followed by dewaxing with xylene, rehydrating through an ethanol series, pretreating with proteinase K (1μg mL^{-1}) in 1×PBS at 37°C for 30 min, prehybriding and hybriding followed previous protocols: two times of 1× SSC at 45°C for 20 min and two times of 0.5× SSC at 42°C for 15 min (Hsu et al., 2015; Li et al., 2018). The antisense and sense probes of *PrMYB5* were synthesized using gene-specific primers with T7 and SP6 RNA polymerase-binding sites, which are shown in Supplementary Table 1.

qRT-PCR analysis

Total RNAs were extracted and reverse transcribed into first-strand cDNA for real-time quantitative PCR (qRT-PCR) using the PrimeScript^{TM} RT Master MIX reverse transcription kit (TaKaRa, Beijing, China). qRT-PCR was conducted using SYBR$^{®}$ Premix Ex Taq^{TM} II (Perfect Real Time) Kit (TaKaRa, Beijing, China) on a Bio-Rad CFX96^{TM} Real-Time system (Bio-Rad, Hercules, CA, USA) according to the reaction conditions mentioned previously (Luo et al., 2021). The transcription levels of genes were normalized to the *PsUbiquitin* expression level and calibrated to the expression level in *P. ostii* petal background at S1. Three biological replicates and technical replicates were performed for each reaction. All primers are listed in Supplementary Table 1.

Interaction network analysis

Based on the transcripts of *PrMYB5* and the structural genes and flavonoid components, a network was established using the R package (https:// www. r- project.org) with a coefficient of $R \geq 0.5$ or $R \leq -0.5$. The hub genes were determined to be co-expressed genes with strong interconnections. Finally, the network was visualized using Cytoscape (v.3.1.0; Shannon et al., 2013).

Generation of PrMYB5-overexpressing tobacco plants

The ORF of *PrMYB5* was cloned into the pCAMBIA1300 vector, and the constructs were transformed into tobacco using the previously described method (Horsch and Klee, 1986). After T0 generation transgenic tobacco was obtained, we screened overexpressed-*PrMYB5* transgenic lines (OE-PrMYB5) using PCR and collected seeds until the T2 generation OE-PrMYB5 plants were obtained. Finally, three T2 generation OE-PrMYB5 lines were selected to detect color indices, quantify flavonoid levels, and qRT-PCR verification as described above. All primers are listed in Supplementary Table 1.

Transient silencing of *PrMYB5* in petals of *P. rockii* by virus-induced gene silencing (VIGS)

According to the previous VIGS approach (Luo et al., 2022), about 200 bp fragment at the 3' end of *PrMYB5* ORF was cloned into the TRV2 vector digested with KpnI and XhoI. The TRV2-*PrMYB5* construct, TRV1, and TRV2 empty vectors were transferred into *Agrobacterium* strain GV3101. Then, the mixtures with *Agrobacterium* containing TRV1 and that containing TRV2, TRV2-*PrMYB5* at a ratio of 1:1 were cultured for 4 h at 25°C in the dark, and then infected fresh petal discs with 1.2 cm diameter from the center of petal background and petal base of *P. rockii* at S4 through vacuum infiltration (Luo et al., 2022). After vacuuming for 2 days, petal discs were washed with deionized water and collected for further analysis. All primers are listed in Supplementary Table 1.

Cloning and sequence analysis of *PrDFR* and *PrANS* promoter region

The promoters of *PrDFR* and *PrANS* were cloned from the S4 petal genomic DNA of *P. rockii* using the Genome Walking Kit (TAKARA, Beijing, China). Based on the mRNA sequences of *PrDFR* and *PrANS*, three reverse primers, SP1, SP2, and SP3, were used in three rounds of PCR for *PrDFR* and *PrANS* promoters cloning, respectively (Supplementary Table 1). The forward primer was AP4 in all PCR reactions, which was supplied in the kit. *cis*-elements analysis was detected using the online software PlantCARE (http://bioinformatics.psb.ugent.be/webtools/plantcare/html/; Lescot et al., 2002).

Yeast one-hybrid assay (Y1H)

First, the *PrMYB5* ORF was inserted into the pGADT7 vector (*SmaI* and *SacI* restriction sites) to obtain pGADT7-*PrMYB5*. The *PrDFRpro* and *PrANSpro* were cloned into the pHIS2 vector with *EcoR I* and *Sac I* restriction sites. Then, all constructs co-transformed pairwise into yeast strain AfHY187 according to the lithium acetate method (Zhang et al., 2018). All primers used in Y1H are shown in Supplementary Table 1.

Dual-luciferase assays

The *PrDFRpro* and *PrANSpro* were cloned into the pGreenII 0800-LUC vector between *Sal I* and *Hind III* restriction sites to obtain *PrANSpro*-pGreenII 0800-LUC and *PrDFRpro*-pGreenII 0800-LUC constructs, respectively. In the meantime, the ORF of *PrMYB5* was inserted into the pGreenII 62-SK vector using *BamH I* and *EcoR I* restriction sites to obtain the *PrMYB5*-pGreenII 62-SK construct. All primers are listed in Supplementary Table 1. After transforming into *Agrobacterium* strain GV3101, the mixtures of cultures (*PrMYB5*-SK+*PrANS*-0800, *PrMYB5*-SK+*PrDFR*-0800) were infiltrated into *N. benthamiana* leaves with needleless syringes (Zhang et al., 2018). After 72 h infiltration, firefly luciferase (LUC) and renilla luciferase (REN) were assayed. The LUC to REN ratio was calculated to measure the binding activity of *PrMYB5* to the promoters. Each combination was conducted in three biological replicates and three technical replicates.

Results

Petal spot pigmentation during flower opening

Petal basal spots began to emerge at the small bell-like bud stage (S1) when petals were not colored and fully formed until the blooming stage (S4). However, petals began to color from the bell-like bud extending stage (S3) after 10 days (Figure 1). The same phenomenon also appeared in other tree peony cultivars with different petal spot patterns (Figure 1).

Then, the color indices of petal tissues of *P. rockii* (PR), *P. ostii* (PO), "Lanhudie" (LHD), "Mochi Jinhui" (MCJH), and "High Noon" (HN) were measured at S1–S4 (Supplementary Figure 1). According to the Royal Horticultural Society Color Chart (RHSCC), the background color of PR at S1–S4 was the same as that of PO petals. The petal base colors of PR and PO were green at S1, and then the petal base color of PR varied greatly from green to dark purple at S2–S4 (Supplementary Table 2). At the petal bases of PR, a^* (redness) value raised gradually from S1 to S4, while b^* (yellowness) value decreased; the L^* (lightness) values peaked at S2, and then subsequently declined from S3 to S4 (Supplementary Figure 1A); h (hue angle) and C^* (chroma) decreased from S1 to S3, and then increased at S4; h-value at S4 was $\sim 0^\circ$ (360°), consistent with the dark-purple color (Supplementary Figure 1A). However, color indices of petal bases in PO changed slightly during flower opening, which were similar to those of petal background in PO and PR (Supplementary Figure 1B). Furthermore, the color of petal spots at the S4 stage in LHD, MCJH, and HN were moderate purplish-red, dark purple, and strong red, respectively (Supplementary Table 2). Similarly, L^* and b^* values declined, and conversely, a^* value increased from S1 to S4 at the petal base of LHD, MCJH, and HN (Supplementary Figures 1C–E). The values of h and C^* were all consistent with their petal base colors (Supplementary Figures 1C–E).

Significant differences in flavonoid compositions and contents were measured in petal backgrounds and bases of PR, PO, LHD, MCJH, and HN during petal spot

formation (Figure 2). Generally, flavones and flavonols were predominantly accumulated at the petal background of white and yellow flowers, including kaempferol (Km), apigenin (Ap), isorhamnetin (Is), luteolin (Lu), and chrysoeriol (Ch), which also occurred at petal bases at S1. Anthocyanins were abundantly accumulated from S2 and reached the highest peak at S4. For pink and purple flowers, the anthocyanin accumulation in petal spots was relatively higher than that of petal backgrounds. During dark-purple petal spot formation in PR and MCJH, peonidin 3, 5-*O*-glucoside (Pn3G5G), cyanidin 3, 5-*O*-glucoside (Cy3G5G), and cyanidin 3-*O*-glucoside (Cy3G) were the dominated anthocyanins and most abundant at S4. In addition, Pn3G5G and Cy3G were considered as the major anthocyanins and accumulated more and more abundantly during petal spots formation of LHD, whereas peonidin 3-*O*-glucoside (Pn3G) and Pn3G5G in HN. In contrast, flavonoids were accumulated similarly in petal bases with petal background in PO and PR (Figure 2).

Identification and RNA *in situ* hybridization of *PrMYB5* in *P. rockii* petal

In our previous flower transcriptome database of *P. rockii* (Shi et al., 2017), an R2R3-MYB TF related to anthocyanin regulation named *PrMYB5* (Genbank accession number: c117848) was obtained. *PrMYB5* contained an 828 bp open reading frame (ORF), encoding a protein of 275 amino acids (Supplementary Figure 2A). PrMYB5 contained highly conserved R2 and R3 domains at the N-terminus, indicating that it belonged to the typical R2R3-MYB family. Meanwhile, phylogenetic analysis showed PrMYB5 in the same clade as petal spot formation regulated MYBs, including OgMYB1 and PeMYB11, full-red pigmentation regulatory PeMYB2, venation pattern regulatory PeMYB12, and anthocyanin-promoting MYBs, such as *Zea mays* C1 (ZmC1), ZmPL, PsMYB12L, and PsMYB114L (Supplementary Figure 2B). Furthermore, we detected the fluorescence PrMYB5-GFP (green fluorescent protein) fusion protein in the nucleus of *Allium cepa* cell protoplasts, suggesting that PrMYB5 is a nuclear-localized TF in regulating petal spot formation (Supplementary Figure 2C).

RNA *in situ* hybridization in the petal background and petal base of *P. rockii* at S4 showed that PrMYB5 expressed more highly on the adaxial surface than on the abaxial surface of the petal base (Figure 3A). On the contrary, no expression of *PrMYB5* was detected in the epidermal cells of the petal background (Figure 3D). These results were consistent with the transverse section phenotypes (Figures 3C,F). As a negative control, hybridization with sense probes was conducted (Figures 3B,E). Therefore, *PrMYB5* showed distinct expression patterns in the petal background and petal base of *P. rockii*.

Expression analyses of *PrMYB5* and structural genes in anthocyanin biosynthetic pathway

To further identify the function of *PrMYB5* associated with the petal spot formation, we analyzed the expression patterns of *PrMYB5* and four key structural genes (*PrCHS*, *PrF3′H*, *PrDFR*, and *PrANS*) that have been screened in our previous study (Shi et al., 2017). The expression levels of *PrMYB5* at the petal spot increased first and then decreased and peaked at S3 in PR, which were significantly higher than those at the petal background of *P. rockii* all the time. Compared to PR, *PrMYB5* is hardly expressed in all petals of PO (Figure 4A). In addition, the expression levels of *PrMYB5* in LHD, MCJH, and HN increased continuously from S1 to S4 (Figure 4A), and the transcript of *PrMYB5* at the petal base exhibited higher abundance than that at the petal background. In general, the expression level of *PrMYB5* increased dramatically with the spot formation in spotted species and cultivars. Especially, it is expressed in the highest abundance in the petal base of MCJH with darker petal spot (Figure 4A).

The transcripts of *PrCHS* and *PrF3'H* in petal background were higher than those at petal spot except for *PrCHS* in LHD and MCJH, whereas they displayed higher expression levels at petal base than petal background in PO (Figures 4B,C). However, *PrDFR* showed a gradually increasing expression trend at the petal bases of PR, LHD, MCJH, and HN from S1 to S4, which is similar with those of *PrANS* (Figures 4D,E). Especially, the expression levels of *PrDFR* were significantly more abundant at petal bases than those of *PrANS* from S1 to S4 in PR and MCJH. The interaction network based on flavonoid accumulation and gene expression profiles revealed that *PrMYB5* was positively correlated with *PrDFR* and *PrANS*, directly associating with Pn3G5G and Cy3G5G (Supplementary Figure 3).

Overexpression of *PrMYB5* in tobacco

To characterize *PrMYB5* function in anthocyanin biosynthesis, we overexpressed *PrMYB5* in tobacco plants and obtained three *PrMYB5* transgenic lines (OE-*PrMYB5* 1–3) (Figure 5). The petals of OE-*PrMYB5* displayed deeper red color compared with wild-type plants, while the sepals, stamens, pistils, and leaves of transgenic lines had no obvious difference (Figure 5A). All OE lines displayed higher transcripts than WT (Figure 5A). Consistently, L^* and b^* values of corollas in all OE-*PrMYB5* were observably lower than those in wild-type, whereas a^* value was higher in all OE-*PrMYB5* (Figure 5B). Furthermore, the corollas of three OE-*PrMYB5* lines accumulated more Pg3G, Pn3G5G, Pn3G, Cy3G5G, and Cy3G than those of wild-type (Figure 5C), but not obviously different from other flavonoid components (Figure 5C). The

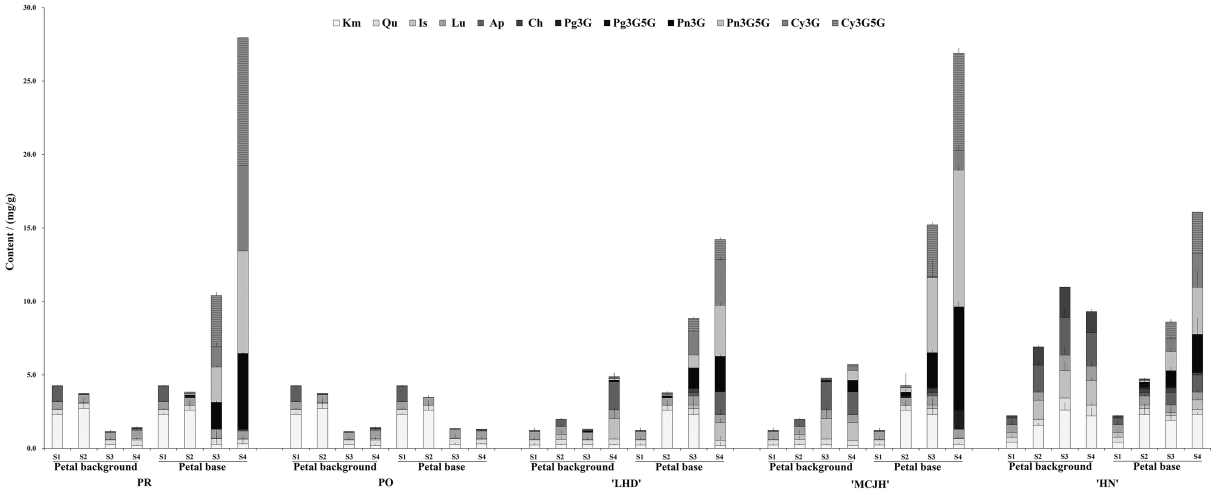

FIGURE 2
The contents of flavonoids in petal background and base of *P. rockii* (PR), *P. ostii* (PO), and three tree peony cultivars "Lanhudie" (LHD), "Mochi Jinhui" (MCJH), and "High Noon" (HN) during petal spot formation. S1–S4 represent four different blooming stages. Cy3G, cyanidin 3-O-glucoside; Cy3G5G, cyanidin 3, 5-O-glucoside; Pg3G, pelargonidin 3-O-glucoside; Pg3G5G, pelargonidin 3, 5-O-glucoside; Pn3G, peonidin 3-O-glucoside; Pn3G5G, peonidin 3, 5-O-glucoside; Km, kaempferol; Qu, quercetin; Lu, luteolin; Is, isorhamnetin; Ap, apigenin; Ch, chrysoeriol.

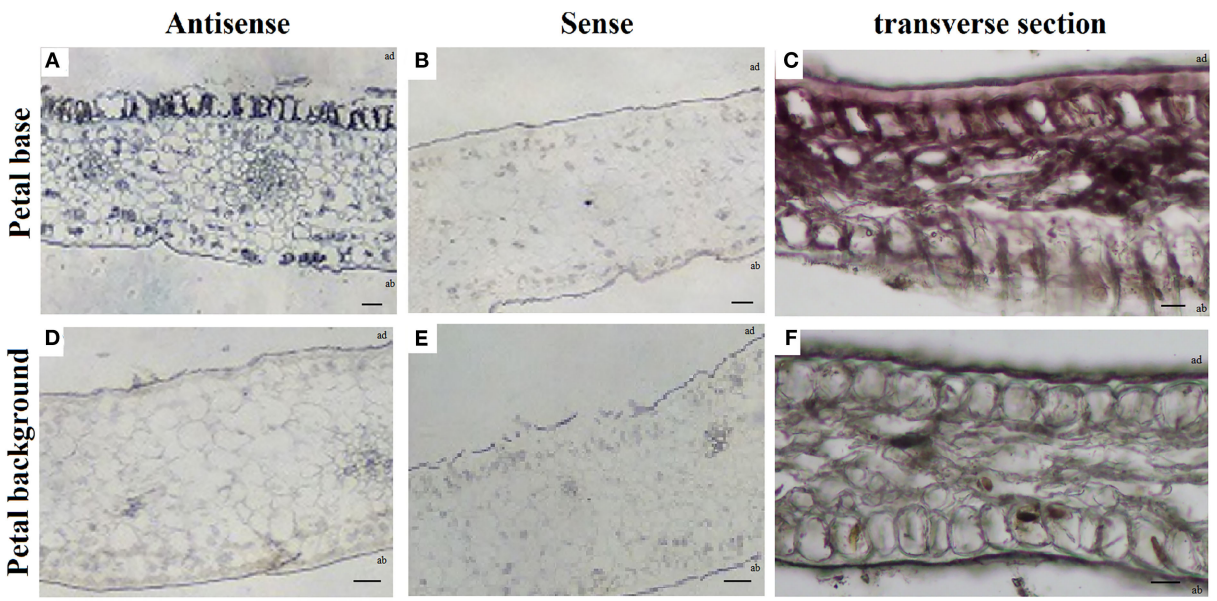

FIGURE 3
RNA *in situ* hybridization of *PrMYB5* transcripts in the stage 4 petals of *P. rockii*. **(A,B)** Transverse sections of the petal base of *P. rockii* were hybridized with antisense or sense RNA probes of *PrMYB5*. **(C)** Transverse section of the petal base of *P. rockii*. **(D,E)** Transverse sections of the petal background of *P. rockii* were hybridized with antisense or sense RNA probes of *PrMYB5*. **(F)** Transverse sections of the petal background of *P. rockii*. ab indicates Abaxial surface; ad indicates Adaxial surfaces. Bars = 100 mm.

above results indicate that *PrMYB5* could significantly promote anthocyanin biosynthesis in tobacco.

The transcript of *PrMYB5* was 70-fold higher in petals of OE-*PrMYB5* than that in wild type, and those in leaves were also 26-fold more abundant (Figure 5D). Correspondingly, four structural genes were also upregulated in the petals of three OE-*PrMYB5* lines. Particularly, *NtDFR* and *NtANS* exhibited the most significant high transcripts in petals of three transgenic lines. The bHLH TF *NtAn1*, stimulating the anthocyanin biosynthesis in tobacco, upregulated in the petals of all three

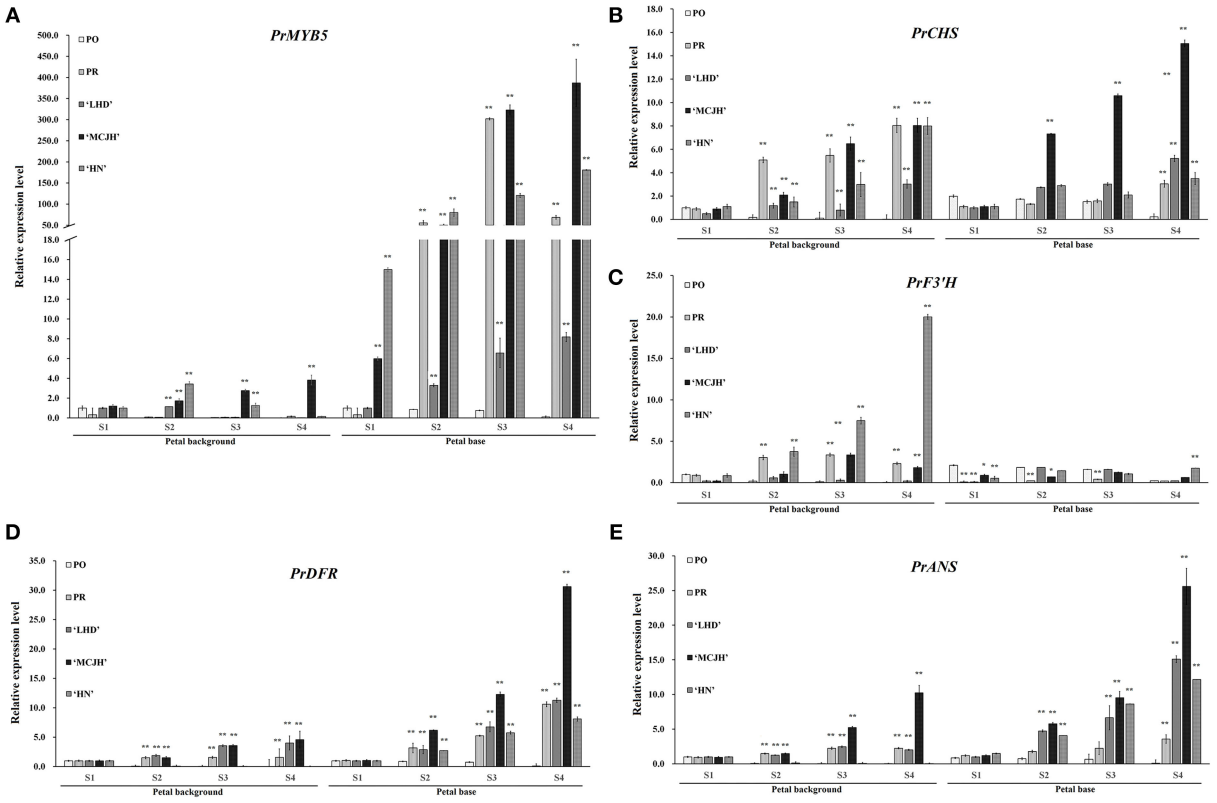

FIGURE 4
The expression profiles of *PrMYB5* and four related structural genes in *P. rockii* (PR), *P. ostii* (PO), and three tree peony cultivars "Lanhudie" (LHD), "Mochi Jinhui" (MCJH) and "High Noon" (HN) using qRT-PCR. The expression profiles of *PrMYB5* **(A)**, *PrCHS* **(B)**, *PrF3'H* **(C)**, *PrDFR* **(D)**, and *PrANS* **(E)** in all samples. S1–S4 represent four different blooming stages.

transgenic lines. In short, *PrMYB5* acted as a positive TF to activate anthocyanin accumulation in the petals.

Transient silencing of *PrMYB5* in *P. rockii* petal

After VIGS were conducted in petal discs of *P. rockii*, the colors of all *PrMYB5*-silenced petal base discs were visibly lighter than those of the blank-control and empty vector control (Figures 6A,B). The changes of flavonoid contents were mainly concentrated in down-accumulation of Km and Lu in *PrMYB5*-silenced petal background discs (Figure 6C), and the contents of Cy3G, Cy3G5G, Pn3G, and Pn3G5G observably decreased in *PrMYB5*-silenced petal base discs (Figure 6D). Correspondingly, *PrMYB5* is down-regulated in *PrMYB5*-silenced petal background discs and base discs, accompanied by decreased expression levels of *PrCHS*, *PrDFR*, and *PrANS* (Figures 6E,F). It is noteworthy that *PrDFR* was significantly downregulated in *PrMYB5*-silenced petal base discs, indicating the direct positive regulatory relationship between *PrMYB5* and *PrDFR* contributing to petal spot formation.

Regulatory relationship between *PrMYB5* and *PrANS* / *PrDFR* promoters

To verify whether *PrMYB5 is* regulating *PrDFR* and *PrANS*, we cloned the promoter sequences of *PrDFR* (*PrDFRpro*) and *PrANS* (*PrANSpro*), with the length of 1,067 and 1,021 bp, respectively (Supplementary Figure 5). *PrDFRpro* included one MYB-binding site (5'-CAAC(A/G) G-3'), four MYB sites (5'-(T/C) AACC (A/G)-3'), two MYC sites (CA(A/T) (T/G) TG), and four G-box (5'-CACGT(T/G)-3'), while *PrANSpro* had two MYB sites, two MYC sites, and two G-box (5'-CACGT (T/G)-3') (Figure 7A), suggesting a potential regulatory relationship among *PrMYB5*, *PrDFR*, and *PrANS*.

To further verify whether *PrMYB5* activated *PrDFR* or *PrANS*, we first performed yeast one-hybrid (Y1H) assays (Figure 7B). Compared with the corresponding control groups, the yeast cells co-transformed with *PrMYB5*::pGADT7+*PrDFRpro*::pHIS2 and *PrMYB5*::pGADT7+*PrANSpro*::pHIS2 could grow normally on SD/-His/-Leu/-Trp selective medium with 2.5 mM 3-AT and 10 mM 3-AT, respectively (Figure 7B). Then, a dual-luciferase assay was conducted. The relative luciferase level

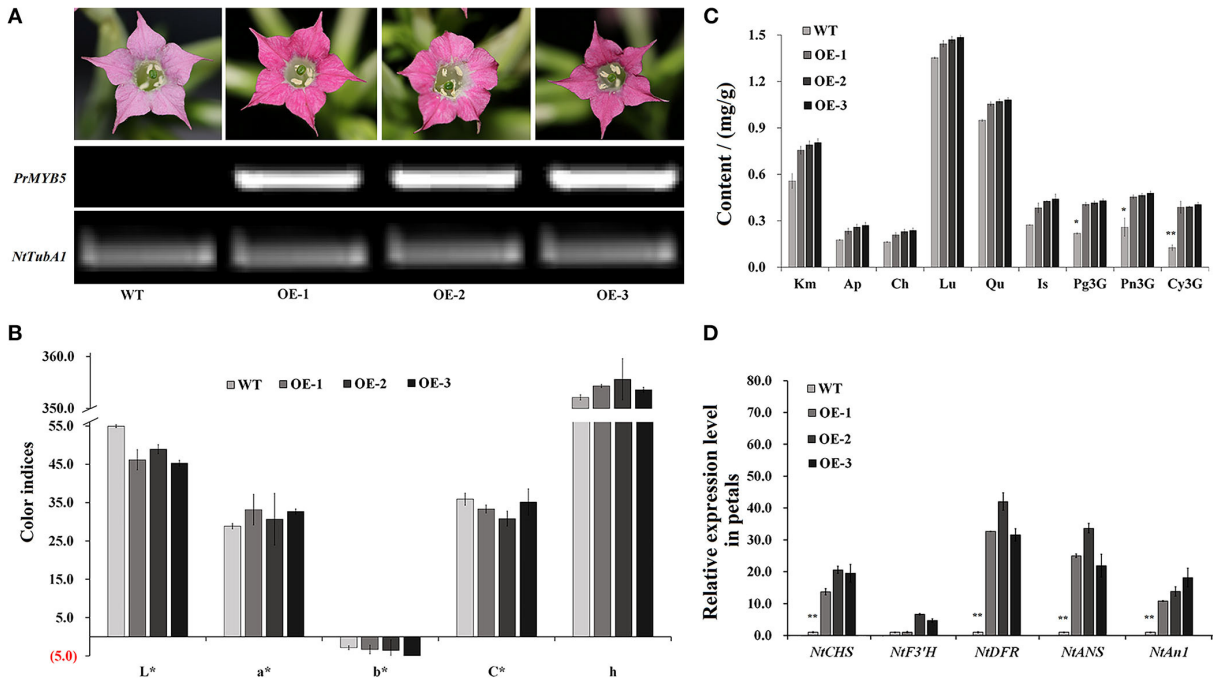

FIGURE 5
Overexpression of *PrMYB5* promotes the accumulation of anthocyanins in tobacco. **(A)** Flower phenotypes of OE-lines (OE-1, 2, and 3) and wild-type (WT) petals, and their corresponding *PrMYB5* transcription levels. *NtTubA1* was used as an endogenous control. **(B)** The color indices in OE-lines and wild-type petals. *L** represents the lightness. *a** represents the redness. *b** represents the yellowness. *C** represents chroma. *h* represents the hue angle. **(C)** The contents of pigments in OE-lines and wild-type petals. **(D)** Expression profiles of *PrMYB5* and structural genes in OE-lines petals by qRT-PCR. *Indicates significant differences at $P < 0.05$; **indicates relatively significant differences at $P < 0.01$.

of *PrMYB5*::SK+*PrDFR*::LUC was more than 3-folds than the control (SK+*PrDFR*::LUC), while no obvious enhancement was found in *PrMYB5*::SK+*PrANS*::LUC. Taken together, *PrMYB5* preferred directly activating the *PrDFR* promoter, promoting Cy- and Pn- anthocyanin at the petal base of *P. rockii* (Figure 7C).

Discussion

The spot at the petal base of *P. rockii* mainly contributes to various spot patterns of tree peony (Wang et al., 2000; Shi et al., 2017). Pigmentation at the petal base begins much earlier than petal background pigmentation in tree peony (Figure 1, Supplementary Table 2), which is similar to those in snapdragons and lilies (Shang et al., 2011; Yamagishi et al., 2014). That is, petal spot pigmentation and petal background pigmentation may be independent.

Cy-based anthocyanins were the major cause of dark-purple spot, while Pn-based anthocyanins were for a vivid purple-red spot in tree peony (Shi et al., 2017; Gu et al., 2019). As expected, Cy3G, Cy3G5G, and Pn3G5G were the dominant anthocyanins in the dark-purple petal spot of PR and MCJH, whereas Pn3G5G and Cy3G in purplish red petal spots of LHD, and Pn3G5G and Pn3G in vivid red petal spots of HN (Figure 2). Whether the flower color is white, yellow, pink, or purplish red, the contents of anthocyanins were markedly higher in the petal spots, while flavones and flavonols accumulated at little different levels. Similar results have been found for petal spot formation in *Viola* × *wittrockiana* Gams. and *C. gracilis* (Martins et al., 2013; Li et al., 2014).

The biosynthesis of distinct Cy and Pn types of anthocyanins is regulated by structural genes and TFs (Suzuki et al., 2016). Among them, DFR and ANS catalyze the dihydroflavonols into the corresponding anthocyanins. Although they were expressed both in the red and purple colored petal areas, the expression levels of *PrDFR* in petal spot were observably different from those in the colored petal background, positively correlating with the accumulation of Pn3G5G and Cy3G5G (Figure 4; Supplementary Figure 3). Similar results in *C. gracilis*, *Oncidium* Gower Ramsey, and *Viola* × *wittrockiana*. Gams. showed that the different expression of *DFR* genes in petal spot activated anthocyanin production resulting in spot pattern (Chiou and Yeh, 2008; Martins et al., 2013; Li et al., 2014). Thus, the differences in anthocyanin accumulation between petal background and spot may be explained by the special spatial and temporal expression of *PrDFR*.

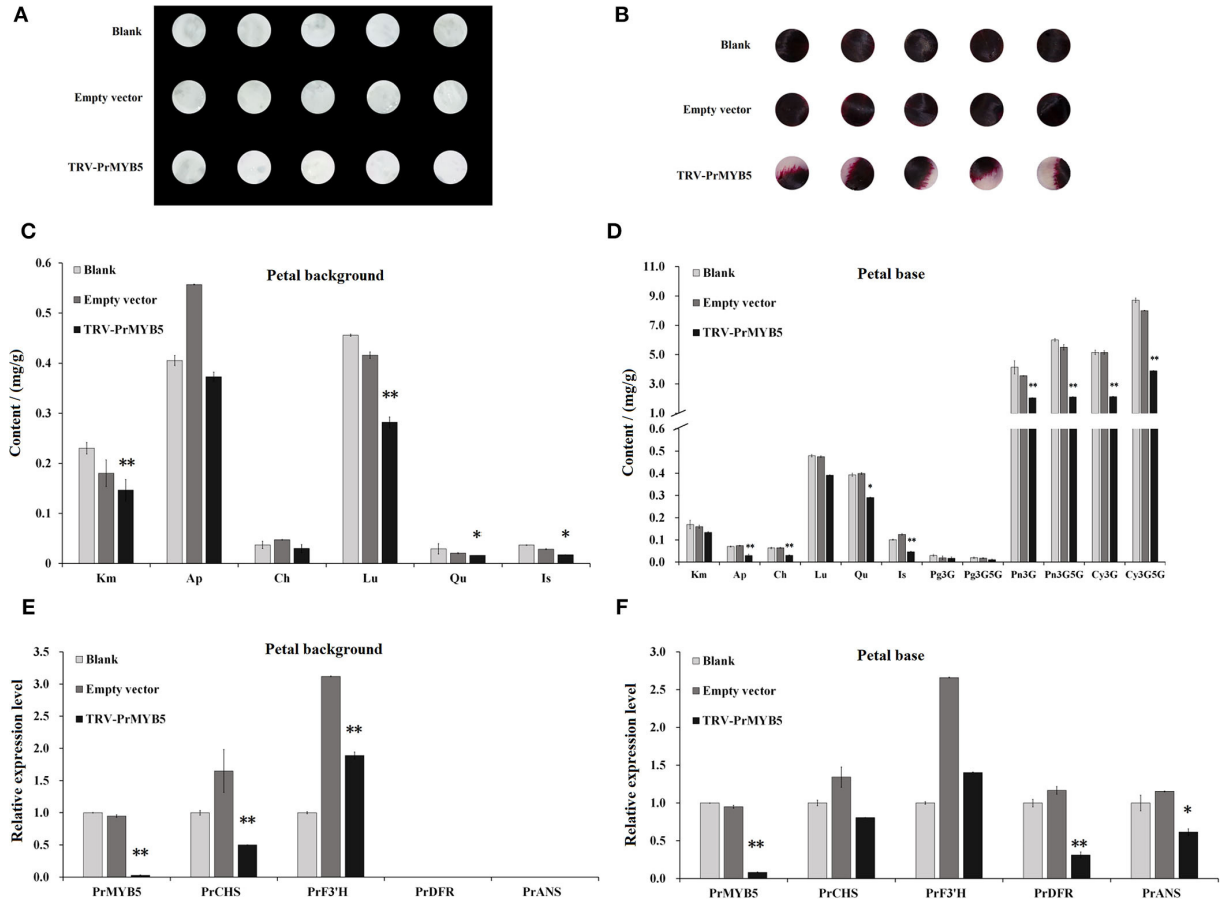

FIGURE 6
Transient silencing of *PrMYB5* in *P. rockii* petals using virus gene silencing (VIGS). Phenotypes of petal background disc **(A,B)**. The flavonoids accumulation in the petal background disc **(C)** and petal base disc **(D)**. The expression levels of *PrMYB5* and structural genes in petal background disc **(E)** and petal base disc **(F)**. *Indicates significant differences at $P < 0.05$; **indicates relatively significant differences at $P < 0.01$).

Among the TFs involved in anthocyanin biosynthesis, R2R3-MYB TFs play major roles in determining spot formation (Hsu et al., 2015). In this study, the R2R3-MYB anthocyanin regulator, *PrMYB5* was grouped in the same clade with OgMYB1, PeMYB11, ZmC1, ZmPL, and PsMYB12L (Supplementary Figure 2B), of which ZmC1, ZmPL, OgMYB1, and PeMYB11 belong to C1 subgroup of R2R3-MYBs, which is involved in upregulating anthocyanin biosynthesis (Jiang et al., 2004; Kranz et al., 2010; Stracke et al., 2010). In addition, *OgMYB1* was critical for the mosaic red pigmentation in the lip crest of *Oncidium* spp. (Chiou and Yeh, 2008), and *PeMYB11* was responsive to the red spots in the callus of the lip in *Phalaenopsis* spp. (Hsu et al., 2015). *PrMYB5* participating in the petal spot formation was further verified using *in situ* hybridization (Figure 3). In particular, *PrMYB5* showed a more abundant transcript at petal spots and upregulated gradually with the formation of spots at the petal base (Figure 4). In other plants, R2R3-MYBs in the C1 subgroup can regulate all structural genes in the flavonoid biosynthesis pathway, including *CHS*, *CHI*, *F3H*, *DFR*, and *ANS* (Chiu et al., 2010; Petroni and Tonelli, 2011; Liu et al., 2016; Schwinn et al., 2016), through binding MYB-binding sites or MYB sites' *cis*-elements with their promoters (Allan et al., 2008; Liu et al., 2016). Notably, a highly clear association existed among *PrMYB5*, *PrDFR,* and *PrANS* transcriptions during petal coloration and spot formation (Figure 4). In addition, Y1H and dual-luciferase assays revealed that *PrMYB5* had a significant activation effect on the *PrDFR* promoter. It has been reported that *McMYB10* can promote *McDFR1* expression and increase anthocyanins accumulation in *Malus* crabapple (Tian et al., 2017). *MdMYB10* and *MdMYB1* can promote the accumulation of anthocyanins in apple peels through binding to the *DFR* promoter (Fornale et al., 2014). Overexpression of *PrMYB5* in tobacco made petals appear deeper red, consisting with the increased Pg3G, Pn3G5G, Pn3G, Cy3G5G, and Cy3G levels and significantly upregulated *NtDFR* expression in petals of transgenic tobacco lines (Figures 5B–D). On the other hand, the reduction of Cy3G, Cy3G5G, Pn3G, and Pn3G5G caused by *PrMYB5* silencing in

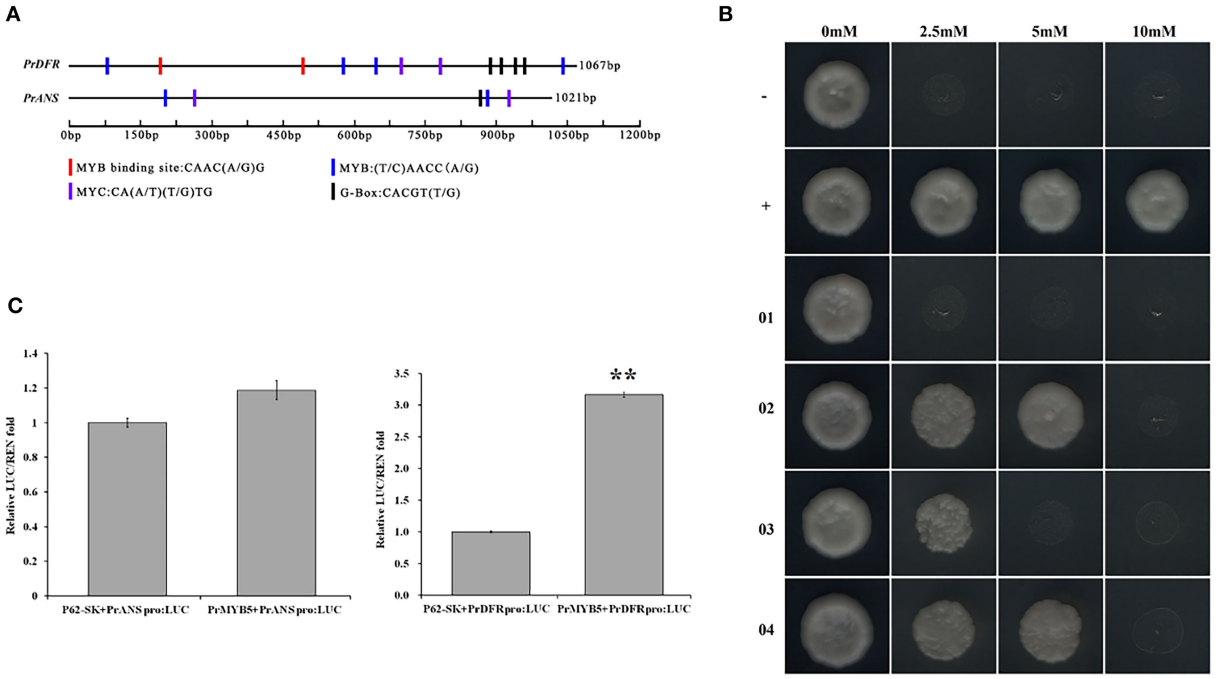

FIGURE 7
Transcriptional activity analysis of PrMYB5 against the promoters of *PrDFR* and *PrANS*. **(A)** Schematic overview of *PrDFR* and *PrANS* promoters. The lengths, MYB binding sites, MYB sites, MYC sites, and G-box sites are marked with black solid lines and colored rectangles, respectively. **(B)** Recombinant yeast on the SD medium without His, Leu, and Trp with 0 mM, 2.5 mM, 5 mM, and 10 mM indicate the SD medium without His, Leu, and Trp with 3-AT at concentrations of 0, 2.5, 5, and 10 mM, respectively. -, a negative control (pGADT7+p53::pHis2); +, a positive control (pGADT7::53+p53::pHis2); 01, pGADT7+*PrDFR*::pHis2; 02, *PrMYB5*::pGADT7+*PrDFR*::pHis2; 03, pGADT7+*PrANS*::pHis2; 04, *PrMYB5*::pGADT7+*PrANS*::pHis2. **(C)** Dual-luciferase assay in tobacco leaves. **Indicates relatively significant differences at $P < 0.01$.

petal spots of *P. rockii* was consistent with the downregulation of *PrCHS*, *PrDFR*, and *PrANS*, particularly *PrDFR* (Figure 6), indicating that *PrMYB5* probably played a key role in petal spot formation of *P. rockii* through promoting *PrDFR* abundant expression at the petal base. Likewise, *LhMYB18* activated the promoter of the DFR gene in tobacco plants (Yamagishi, 2018), and *CgMYB1* activates *CgDFR2* to produce petal spots in *C. gracilis* (Martins et al., 2017).

Conclusion

In summary, we compared the distinct pigmentation processes between petal bases and petal backgrounds of *P. rockii* and other tree peony cultivars, and further demonstrated that the petal spot formation was mainly attributed to the spatiotemporal transcription of *PrMYB5* activating *PrDFR* promoters, which was associated with the Cy and Pn type anthocyanin accumulation at the petal base. However, the complex and exact regulation mechanism of *PrMYB5* on petal spot formation requires to further research. These results not only provide a reference for further exploring the molecular mechanism of novel spot pigmentation patterns in *P. rockii*, but also lay the theoretical foundation for molecular breeding of novel spotted tree peony cultivars.

Data availability statement

The datasets presented in this study can be found in online repositories. The names of the repository/repositories and accession number(s) can be found in the article/Supplementary material.

Author contributions

QS and LL designed this research, performed data analysis, and wrote the manuscript. MY and SW performed the experiments and data analysis. XLu assisted in bioinformatics analyses. SL, YF, and XLi helped in the preparation of plant material. YZ provided some supervision of the study. All authors read and approved the final manuscript.

Funding

This work was supported by the National Natural Science Foundation of China (Grant No. 31800599), the Natural

Science Foundation of Shannxi Province, China (Grant No. 2017JQ3024), and the National Key R&D Program of China (Grant No. 2019YFD1001505).

Acknowledgments

We thank YZ for field and laboratory support.

Conflict of interest

The authors declare that the research was conducted in the absence of any commercial or financial relationships that could be construed as a potential conflict of interest.

Publisher's note

Supplementary material

The Supplementary Material for this article can be found online at: https://www.frontiersin.org/articles/10.3389/fpls.2022.955590/full#supplementary-material

References

Albert, N. W., Lewis, D. H., Zhang, H., Schwinn, K., Jameson, P., and Davies, K. (2011). Members of an R2R3-MYB transcription factor family in Petunia are developmentally and environmentally regulated to control complex floral and vegetative pigmentation patterning. *Plant J.* 65, 771–784. doi: 10.1111/j.1365-313X.2010.04465.x

Allan, A. C., Hellens, R. P., and Laing, W. A. (2008). MYB transcription factors that colour our fruit. *Trends Plant Sci.* 13, 99–102. doi: 10.1016/j.tplants.2007.11.012

Cao, Y., Li, K., Li, Y., Zhao, X., and Wang, L. (2020). MYB transcription factors as regulators of secondary metabolism in plants. *Biology* 9, 61. doi: 10.3390/biology9030061

Chiou, C. Y., and Yeh, K. W. (2008). Differential expression of MYB gene (*OgMYB1*) determines color patterning in floral tissue of *Oncidium Gower* Ramsey. *Plant Mol. Biol.* 66, 379–388. doi: 10.1007/s11103-007-9275-3

Chiu, L., Zhou, X., Burke, S., Wu, X., Prior, R. L., and Li, L. (2010). The purple cauliflower arises from activation of a MYB transcription factor. *Plant Physiol.* 154, 1470–1480. doi: 10.1104/pp.110.164160

Davies, K. M., Albert, N. W., and Schwinn, K. E. (2012). From landing lights to mimicry: the molecular regulation of flower colouration and mechanisms for pigmentation patterning. *Funct. Plant Biol.* 39, 619–638. doi: 10.1071/FP12195

Fornale, S., Lopez, E., Salazarhenao, J. E., Fernanadeznohales, P., Rigau, J., and Caparrosruiz, D. (2014). AtMYB7, a new player in the regulation of UV-Sunscreens in *Arabidopsis thaliana*. *Plant Cell Physiol.* 55, 507–516. doi: 10.1093/pcp/pct187

Gao, Y., Harris, A., and and He, X. (2015). Morphological and ecological divergence of *Lilium* and *Nomocharis* within the hengduan Mountains and Qinghai-Tibetan Plateau may result from habitat specialization and hybridization. *BMC Evol. Biol.* 15, 147–168. doi: 10.1186/s12862-015-0405-2

Glover, B. J., Walker,. R. H., Moyroud, E., and Brockington, S. F. (2013). How to spot a flower. *New Phytol.* 197, 687–689. doi: 10.1111/nph.12112

Gu, Z., Zhu, J., Hao, Q., Yuan, Y., Duan, Y., Men, S., et al. (2019). A novel R2R3-MYB transcription factor contributes to petal blotch formation by regulating organ-specific expression of *PsCHS* in tree peony (*Paeonia suffruticosa*). *Plant Cell Physiol.* 60, 599–611. doi: 10.1093/pcp/pcy232

Horsch, R., and Klee, H. (1986). Rapid assay of foreign gene expression in leaf discs transformed by *Agrobacterium tumefaciens*: role of T-DNA borders in the transfer process. *Proc. Natl. Acad. Sci. U. S. A.* 83, 4428–4432. doi: 10.1073/pnas.83.12.4428

Hsu, C. C., Chen, Y. Y., Tsai, W. C., Chen, W. H., and Chen, H. H. (2015). Three R2R3-MYB transcription factors regulate distinct floral pigmentation patterning in *Phalaenopsis* spp. *Plant Physiol.* 168, 175. doi: 10.1104/pp.114.254599

Jiang, C., Gu, X., and Peterson, T. (2004). Identification of conserved gene structures and carboxy-terminal motifs in the Myb gene family of *Arabidopsis* and *Oryza sativa* L. ssp. indica. *Genome Biol.* 5, R46. doi: 10.1186/gb-2004-5-7-r46

Kranz, H. D., Denekamp, M., Greco, R., Jin, H., Leyva, A., Messner, R. C., et al. (2010). Towards functional characterization of the members of the R2R3-MYB gene family from *Arabidopsis thaliana*. *Plant J.* 16, 263–276. doi: 10.1046/j.1365-313x.1998.00278.x

Lescot, M., Déhais, P., Thijs, G., Marchal, K., Moreau, Y., Van, D. P., et al. (2002). Plantcare, a database of plant cis-acting regulatory elements and a portal to tools for in silico analysis of promoter sequences. *Nucl. Acids Res.* 30, 325–327. doi: 10.1093/nar/30.1.325

Li, L., Cheng, Z., Ma, Y., Bai, Q., Li, X., and Gao, J. (2018). The association of hormone signaling genes, transcription, and changes in *shoot* anatomy during moso bamboo growth. *Plant Biotechnol. J.* 16, 72–85. doi: 10.1111/pbi.12750

Li, Q., Wang, J., Sun, H. Y., and Shang, X. F. (2014). Lower color patterning in pansy (*Violawittrockiana* Gams.) is caused by the differential expression of three genes from the anthocyanin pathway in acyanic and cyanic flower areas. *Plant Physiol. Bioch.* 84, 134–141. doi: 10.1016/j.plaphy.2014.09.012

Liu, C., Long, J., Zhu, K., Liu, L., Yang, W., Zhang, H., et al. (2016). Characterization of a citrus R2R3-MYB transcription factor that regulates the flavonol and hydroxycinnamic acid biosynthesis. *Sci. Rep.* 6, 25352. doi: 10.1038/srep25352

Luo, X. N., Luo, S., Fu, Y. Q., Kong, C., Wang, K., Sun, D. Y., et al. (2022). Genome-wide identification and comparative profiling of microRNAs reveal flavonoid biosynthesis in two contrasting flower color cultivars of tree peony. *Front. Plant Sci.* 2021:797799. doi: 10.3389/fpls.2021.797799

Luo, X. N., Sun, D. Y., Wang, S., Luo, S., Fu, Y. Q., Niu, L. X., et al. (2021). Integrating full-length transcriptomics and metabolomics reveals the regulatory mechanisms underlying yellow pigmentation in tree peony (*Paeonia suffruticosa* Andr.) flower. *Hortic. Res.* 8, 235. doi: 10.1038/s41438-021-00666-0

Martins, T. R., Berg, J. J., Blinka, S., Rausher, M. D., and Baum, D. A. (2013). Precise spatial-temporal regulation of the anthocyanin biosynthetic pathway leads to petal spot formation in *Clarkia gracilis* (Onagraceae). *New Phytol.* 197, 958–969. doi: 10.1111/nph.12062

Martins, T. R., Jiang, P., and Rausher, M. D. (2017). How petals change their spots: cis-regulatory re-wiring in *Clarkia* (Onagraceae). *New Phytol.* 216, 510–518. doi: 10.1111/nph.14163

Petroni, K., and Tonelli, C. (2011). Recent advances on the regulation of anthocyanin synthesis in reproductive organs. *Plant Sci.* 181, 219–229. doi: 10.1016/j.plantsci.2011.05.009

Schwinn, K., Ngo, H., Kenel, F., Brummell, D. A., Albert, N. W., Mccallum, J. A., et al. (2016). The onion (*Allium cepa* L.) R2R3-MYB gene MYB1 regulates anthocyanin biosynthesis. *Front. Plant Sci.* 7, 1865. doi: 10.3389/fpls.2016.01865

Schwinn, K., Venail, J., Shang, Y., Mackay, S., Alm, V., Betelli, E., et al. (2006). A small family of MYB-regulatory genes controls floral pigmentation intensity and patterning in the genus *Antirrhinum*. *Plant Cell* 18, 831–851. doi: 10.1105/tpc.105.039255

Shang, Y. J., Venail, J., Mackay, S., Bailcy, P., Schwinn, K., Jamcson, P., et al. (2011). The molecular basis for venation patterning of pigmentation and its effect on pollinator attraction in flowers of *Antirrhinum*. *New Phytol.* 189, 602–615. doi: 10.1111/j.1469-8137.2010.03498.x

Shannon, P., Markiel, A., Ozier, O., Baliga, N. S., Wang, J. T., Ramage, D., et al. (2013). Cytoscape: a software environment for integrated models of biomolecular interaction networks. *Genome Res.* 13, 2498–2504. doi: 10.1101/gr.1239303

Shi, Q., Li, L., Zhang, X., Luo, J. R., Li, X., Zhai, L. J., et al. (2017). Biochemical and comparative transcriptomic analyses identify candidate genes related to variegation formation in *Paeonia rockii*. *Molecules* 22, 1364. doi: 10.3390/molecules22081364

Stracke, R., ishihara, H. G., Barsch, A., Mehrten, F., Niehaus, K., and Weisshaar, B. (2010). Different regulation of closely related R2R3-MYB transcription factors controls flavonol accumulation in different parts of the *Arabidopsis thaliana* seedling. *Plant J.* 50, 660–677. doi: 10.1111/j.1365-313X.2007.03078.x

Su, S., Xiao, W., Guo, W., Yao, X., Xiao, J., Ye, Z., et al. (2017). The CYCLOIDEA-RADIALIS module regulates petal shape and pigmentation, leading to bilateral corolla symmetry in *Torenia fournieri* (Linderniaceae). *New Phytol.* 215, 1582–1593. doi: 10.1111/nph.14673

Suzuki, K., Suzuki, T., Nakatsuka, T., Dohra, H., Yamagishi, M., Matsuyama, K., et al. (2016). RNA-seq-based evaluation of bicolor tepal pigmentation in Asiatic hybrid lilies (*Lilium* spp.). *BMC Genom.* 17, 61. doi: 10.1186/s12864-016-2995-5

Tian, J., Chen, M. C., Zhang, J., Li, K. T., Song, T. T., Zhang, X., et al. (2017). Characteristics of dihydroflavonol 4-reductase gene promoters from different leaf colored *Malus crabapple* cultivars. *Hortic. Res.* 4, 17070. doi: 10.1038/hortres.2017.70

Wang, L., Hashimoto, F., Shiraishi, A., Shimizu, K., Aoki, N., and Sakata, Y. (2000). Petal coloration and pigmentation of tree peony cultivars of Xibei (the Northwest of China). *J. Japanese Soc. Hortic. Sci.* 69, 233.

Yamagishi, M. (2011). Oriental hybrid lily Sorbonne homologue of *LhMYB12* regulates anthocyanin biosynthesis in flower tepals and tepal spots. *Mol. Breeding* 28, 381–389. doi: 10.1007/s11032-010-9490-5

Yamagishi, M. (2018). Involvement of a LhMYB18 transcription factor in large anthocyanin spot formation on the flower tepals of the Asiatic hybrid lily (*Lilium* spp.) cultivar "Grand Cru". *Mol. Breeding* 38, 60. doi: 10.1007/s11032-018-0806-1

Yamagishi, M. (2020). MYB19LONG is involved in brushmark pattern development in Asiatic hybrid lily (*Lilium* spp.) flowers. *Sci. Hortic.* 272, 109570. doi: 10.1016/j.scienta.2020.109570

Yamagishi, M., Shimoyamada, Y., Nakatsuka, T., and Masuda, K. (2010). Two R2R3-MYB genes, homologs of Petunia *AN2*, regulate anthocyanin biosynthesis in flower Tepals, tepal spots and leaves of Asiatic hybrid lily. *Plant Cell Physiol* 51:463–474. doi: 10.1093/pcp/pcq011

Yamagishi, M., Toda, S., and Tasaki, K. (2014). The novel allele of the LhMYB12 gene is involved in splatter-type spot formation on the flower tepals of *Asiatic hybrid* lilies (*Lilium* spp.). *New Phytol.* 201, 1009–1020. doi: 10.1111/nph.12572

Yan, H., Pei, X., Zhang, H., Li, X., Zhang, X., Zhao, M., et al. (2021). MYB-mediated regulation of anthocyanin biosynthesis. *Int. J. Mol. Sci.* 22, 3103. doi: 10.3390/ijms22063103

Yuan, Y. W., Sagawa, J. M., Frost, L., Vela, J. P., and Bradshaw, H. D. (2014). Transcriptional control of floral anthocyanin pigmentation in monkeyflower (*Mimulus*). *New Phytol.* 204, 1013–1027. doi: 10.1111/nph.12968

Zhang, X. P., Xu, Z. D., Yu, X. Y., Zhao, L. Y., Zhao, M. Y., Han, X., et al. (2019). Identification of two novel R2R3-MYB transcription factors, PsMYB114L and PsMYb12L, related to anthocyanin biosynthesis in *Paeonia suffruticosa*. *Int. J. Mol. Sci.* 20, 1055. doi: 10.3390/ijms20051055

Zhang, Y., Cheng, Y., Xu, S., Ma, H., Han, J., and Zhang, Y. (2020a). Tree peony variegated flowers show a small insertion in the F3'H gene of the acyamic flower parts. *BMC Plant Biol.* 20, 211. doi: 10.1186/s12870-020-02428-x

Zhang, Y., Cheng, Y., Ya, H., Xu, S., and Han, J. (2015). Transcriptome sequencing of purple petal spot region in tree peony reveals differentially expressed anthocyanin structural genes. *Trends Plant Sci.* 6, 964. doi: 10.3389/fpls.2015.00964

Zhang, Y., Xu, S., Cheng, Y., Wang, J., Wang, X., Liu, R., et al. (2020b). Functional identification of PsMYB57 involved in anthocyanin regulation of tree peony. *BMC Genet.* 21, 124. doi: 10.1186/s12863-020-00930-7

Zhang, Y., Yin, X., Xiao, Y., Zhang, Z., Li, S., Liu, X., et al. (2018). An ETHYLENE RESPONSE FACTOR-MYB transcription complex regulates furaneol biosynthesis by activating QUINONE OXIDOREDUCTASE expression in strawberry. *Plant Physiol.* 178, 189. doi: 10.1104/pp.18.00598

Zhou, S., Zou, X., Zhou, Z., Liu, J., Xu, C., Yu, J., et al. (2014). Multiple species of wild tree peonies gave rise to the 'king of flowers', *Paeonia suffruticosa* Andrews. *Proc. Biol. Sci.* 281, 1687–1694. doi: 10.1098/rspb.2014.1687

frontiers | Frontiers in Plant Science

TYPE Original Research
PUBLISHED 14 September 2022
DOI 10.3389/fpls.2022.1003635

OPEN ACCESS

EDITED BY
Shunli Wang,
Chinese Academy of Agricultural Sciences (CAAS), China

REVIEWED BY
Bo Hong,
Hefei Institute of Physical Science, China
SiLan Dai,
Beijing Forestry University, China

*CORRESPONDENCE
Jiafu Jiang
jiangjiafu@njau.edu.cn

†These authors have contributed equally to this work

SPECIALTY SECTION
This article was submitted to Plant Breeding, a section of the journal Frontiers in Plant Science

RECEIVED 26 July 2022
ACCEPTED 17 August 2022
PUBLISHED 14 September 2022

CITATION
Shi Z, Han X, Wang G, Qiu J, Zhou L-j, Chen S, Fang W, Chen F and Jiang J (2022) Transcriptome analysis reveals chrysanthemum flower discoloration under high-temperature stress. *Front. Plant Sci.* 13:1003635. doi: 10.3389/fpls.2022.1003635

Transcriptome analysis reveals chrysanthemum flower discoloration under high-temperature stress

Zhenjie Shi†, Xiaoying Han†, Guohui Wang†, Jing Qiu, Li-jie Zhou, Sumei Chen, Weimin Fang, Fadi Chen and Jiafu Jiang*

Sanya Institute of Nanjing Agricultural University, State Key Laboratory of Crop Genetics and Germplasm Enhancement, Key Laboratory of Landscaping, Ministry of Agriculture and Rural Affairs, Key Laboratory of Biology of Ornamental Plants in East China, National Forestry and Grassland Administration, College of Horticulture, Nanjing Agricultural University, Nanjing, China

Temperature is an important environmental factor affecting plant anthocyanin synthesis. High temperatures are associated with decreased anthocyanin pigmentation in chrysanthemum. To reveal the effects of high temperature on anthocyanin biosynthesis in chrysanthemum, ray florets of the heat-sensitive cultivar "Nannong Ziyunying" (ZYY) were subjected to RNA sequencing. A total of 18,286 unigenes were differentially expressed between the control and treatment groups. Functional annotation and enrichment analyses of these unigenes revealed that the heat shock response and flavonoid pathways were significantly enriched, suggesting that the expression of these genes in response to high temperature is associated with the fading of chrysanthemum flower color. In addition, genes related to anthocyanin synthesis and heat shock response were differentially expressed under high-temperature stress. Finally, to further investigate the molecular mechanism of discoloration under high-temperature stress and facilitate the use of marker-assisted breeding for developing novel heat-tolerant cultivars, these results were used to mine candidate genes by analyzing changes in their transcription levels in chrysanthemum.

KEYWORDS

chrysanthemum, anthocyanin biosynthesis, high temperature, flower discoloration, RNA-Seq

Introduction

With the intensification of global warming, high-temperature stress has become a major environmental factor limiting the normal growth and development of plants. Elevated temperatures affect a series of physiological, biochemical, and developmental processes in plants, such as photosynthesis and respiration, pollen activity, membrane stability, and enzyme activity, which in turn affect yield and quality (Atkin and Tjoelker, 2003; Nagar et al., 2015; Dusenge et al., 2019; Zhu et al., 2021). Temperature tolerance varies greatly among different plants. For instance, the rise in global temperatures

has produced little effect on plants native to the tropics and subtropics; meanwhile, chrysanthemum is a cold-tolerant but heat-labile ornamental plant that is greatly affected by high temperatures (Gins et al., 2019). In general, high-temperature stress leads to delay in flowering, fading of flower color, and variation in flower type in chrysanthemums. Among these, flower color is one of the most important ornamental characteristics, and anthocyanins are the key component for flower color. Temperature-mediated regulation of flower color and the flavonoid pathway has been extensively studied (Nozaki and Fukai, 2008; Van Der Ploeg and Heuvelink, 2015). However, only a few studies have explored the regulation of chrysanthemum discoloration under high-temperature stress.

Anthocyanins are naturally synthesized water-soluble pigments present in various plant tissues and organs, such as roots, stems, leaves, flowers, fruits, and seeds. The anthocyanin synthetic pathway, or the phenylalanine pathway, is divided into three stages (Figure 1) (Winkel-Shirley, 2002). The first stage involves a phenylalanine precursor, which is oxidized by phenylalanine ammonia lyase (PAL), cinnamate 4-hydroxylase (C4H), and 4-coumaroyl CoA enzyme (4CL) to produce 4-coumaroyl-CoA. At the second stage, 4-coumaroyl-CoA is catalyzed by chalcone synthase (CHS) to produce chalcone, which is isomerized by chalcone isomerase (CHI) to form colorless trihydroxyflavonol. Finally, flavanone 3-hydroxylase (F3H), flavonoid-3',5'-hydroxylase (F3'5'H), and flavonoid-3'-hydroxylase (F3'H) catalyze the formation of colorless dihydroflavonols. At the third stage, colorless dihydroflavonols are further reduced to leucoanthocyanidins by dihydroflavonol 4-reductase (DFR) and then converted to anthocyanins by anthocyanin synthase (ANS) (Hichri et al., 2011; Zhang et al., 2016). Subsequently, glycosyltransferase (GT), methyltransferase (MT), and acyltransferase (AT) catalyze the formation of cornflower (cyanidin, Cy), geranium (pelargonidin, Pg), and delphinium (delphinidin, Dp) pigments (Caputi et al., 2012; Zhao et al., 2012; Bontpart et al., 2015). Of note, chrysanthemums lack the delphinium synthetic pathway; thus, there are no blue chrysanthemums in nature (Noda et al., 2017). Structural genes encoding *CHS*, *CHI*, *DFR*, *F3H*, *ANS*, and *3GT* involved in anthocyanin synthesis have been verified in several species (Shi et al., 2015; Sun et al., 2016; Li et al., 2020).

In recent years, several transcription factors involved in anthocyanin biosynthesis have been elucidated. For instance, MYB, bHLH, WD40, MADS-box and bZIP transcription factors are related to flower color. Structural genes involved in flavonoid pathways are primarily regulated by the conserved MYB–bHLH–WD40 (MBW) complex (Nabavi et al., 2020), which directly regulate flavonoid metabolism in plants through the transcriptional activation or repression of related structural genes. Among these, the transcription factor R2R3–MYB, which is the core component of the MBW protein complex, is mainly responsible for regulating flavonoid metabolism in plants (Xu et al., 2015). The MADS box proteins are a large family of transcription factors (TF) that control various developmental processes, not only the MADS box gene family has been involved in floral organogenesis according to the ABCDE model. However, MADS box TFs also regulate anthocyanin biosynthesis (Li et al., 2016; Qi et al., 2022). Further, bZIP transcription factors are involved in many signaling pathways, such as light signaling, environmental stress responses, and biological processes of plant growth and development (Chinnusamy et al., 2004; Golldack et al., 2014; An et al., 2019). HY5 is an important bZIP transcription involved in anthocyanin synthesis. It affects anthocyanin synthesis and metabolism by regulating the promoter activity of anthocyanin synthetic structural genes, including *CHS*, *CHI*, *F3H*, *F3'H*, *DFR*, and *ANS* (Zhang et al., 2011). Additionally, anthocyanin biosynthesis is affected by environmental factors, such as light and temperature. Temperature is crucial for anthocyanin metabolism. As such, the red color of maple leaves fades from the cooler northern regions to the warmer southern regions of the United States. This is because higher temperatures improve respiration, promote sugar consumption, and inhibit anthocyanin accumulation, leading to leaf color fading in plants (Deal et al., 1990). Furthermore, temperature affects the transcriptional expression of various genes in plants. Anthocyanin accumulation in marigold leaves is related to temperature, and accumulated temperatures are negatively correlated with marigold anthocyanin content (Armitage and Carlson, 1981). Under low temperatures, anthocyanin synthesis-related genes are induced and activated, elevating anthocyanin content in plants. In apple fruit, GT activity is significantly increased at low temperatures, increasing anthocyanin content beyond the normal value (Ubi et al., 2006). However, under high temperature, genes related to anthocyanin synthesis are inhibited, thereby reducing anthocyanin content (Islam et al., 2005). In plum fruits, over 60–70% anthocyanins are degraded under high temperature (Niu et al., 2017). Recently, a novel atypical subgroup 7 (SG7) R2R3–MYB transcription factor, CmMYB012, was discovered in chrysanthemum, which blocks anthocyanin biosynthesis by inhibiting *CmCHS*, *CmDFR*, *CmANS*, and *CmUFGT* expression under high-temperature stress (Zhou et al., 2021). Chrysanthemums can grow normally at 18–25°C; above 32°C, however, growth and development are delayed. In the temperature-sensitive chrysanthemum cultivars "Nannong Sichengdian," "Nannong Ziyunying," and "Nannong Zizhu," flower color fades and ornamental quality declines under heat stress (Qiu, 2018). Abiotic stresses affect anthocyanin synthesis through several pathways. To date, the molecular mechanisms of chrysanthemum anthocyanin synthesis and flower discoloration in high-temperature environments remain unclear and warrant further exploration.

When plants are subjected to high-temperature stress, a series of heat shock response (HSR) pathways are activated, including the antioxidant protection system, thermoprotectant synthesis, membrane lipid peroxidation, heat

shock protein expression, hormone regulation and signaling, and transcriptional regulation (Hasanuzzaman et al., 2013). Heat shock transcription factors (HSFs) and heat shock proteins (HSPs) play central roles in high-temperature stress response and acquired thermotolerance in plants (Zhang et al., 2015). HSFs act as key regulators of heat stress response. Specifically, they serve as transcriptional activators of HSPs, which are the terminal components of signal transduction pathways and mediate the expression of HSPs (Qu et al., 2013). HsfA1s are key transcriptional regulators in HSR (Ohama et al., 2017). Moreover, HSPs play pivotal roles in heat tolerance and are essential for the normal growth and development of plants under high temperatures. HSPs function as molecular chaperones and are classified into five families based on their molecular weight: HSP100, HSP90, HSP70, HSP60, and small HSPs (sHSPs) (Whitley et al., 1999; Tsan and Gao, 2004). Ca^{2+} and reactive oxygen species (ROS) are involved in signaling pathways that connect heat stress sensors and transcriptional regulators (Kotak et al., 2007). As one of the first signals in HSR, Ca^{2+} influx increases the strength of response (Liu et al., 2005). This alters plasma membrane (PM) fluidity, which in turn regulates cyclic nucleotide-gated calcium channels (CNGCs), allowing Ca^{2+} to enter the cytoplasm. CNGCs activate HSR by regulating the transition of cAMP and cGMP. As a Ca^{2+} signaling transmitter, CaM3 interacts with phosphorylated genes in response to heat stress (Finka et al., 2012; Tunc-Ozdemir et al., 2013). Additionally, nitric oxide (NO) has been reported to improve plant heat tolerance. In particular, NO acts as a signal upstream of CAM3 under heat stress (Rai et al., 2020). Furthermore, oxidative stress induced by HSR acts as secondary stress, which mediates ROS generation and causes molecular and cellular damage (Qu et al., 2013). The generated ROS are sensed by HSFs, which activate mitogen-activated protein kinase (MAPK) signaling, ultimately leading to the synthesis of antioxidant enzymes (SOD, POD, APX, CAT, and GPX) (Martindale and Holbrook, 2002). The MAPK cascade is an important signal transduction pathway in plants, being closely related to growth, development, and stress response (Kumar et al., 2020).

Here, using RNA sequencing (RNA-Seq), we found that anthocyanin synthesis-related genes, including *CHS*, *CHI*, *DFR*, *F3H*, *ANS*, *3GT*, and *F3'H*, were significantly downregulated by heat in the temperature-sensitive cultivar "Nannong Ziyunying." Moreover, MYB, bHLH, WD40, and bZIP transcription factors that regulate flavonoid metabolism and genes related to heat stress response-related processes, such as Ca^{2+} signaling, MAPK cascade, HSF and HSP function, and ROS generation, were differentially expressed between heat-treated and untreated plants. Overall, the present study aimed to explore molecular mechanisms underlying anthocyanin synthesis under high-temperature stress.

Materials and methods

Plant material and growth conditions

The cut-flower chrysanthemum cultivars "Nanong Ziyunying" and "Nannong Zizhu" were obtained from the China Chrysanthemum Germplasm Resources Preservation Center of Nanjing Agricultural University. Cuttings were rooted in trays for 15 days, transplanted into pots, grown for a month at a suitable temperature (day/night = 24°C/18°C), and cultured under a 16/8 h light/dark cycle and 70% relative humidity until the bud period. Thereafter, two groups of plants were transferred to separate light incubators with different environments: control group (CK) (8/16 h light/dark cycle with day and night temperature of 22°C) and high-temperature treatment group (8/16 h light/dark cycle with day/night temperatures of 38°C/22°C). Both groups of plants were watered every 5 days during the treatment period. The two cultivars with different treatments were sampled at the bud, early bloom, and bloom stages at the same period. Three biological and three technical replicates were collected for each sample and stored in liquid nitrogen for subsequent high-throughput sequencing assays.

Determination of anthocyanin type and content

Determination of anthocyanin type

Qualitative analysis was performed to determine the anthocyanin type in high-temperature-treated cultivars. Briefly, the ray florets of "Nannong Ziyunying" and "Nannong Zizhu" were collected; each fresh sample weighed approximately 0.1 g. Then, 5 mL of petroleum ether, 5 mL of 10% hydrochloric acid, and 5 mL of 30% ammonia water were added to the samples. Subsequently, the samples were rapidly ground to a slurry, and the supernatant was collected after centrifugation (at 5,000 rpm for 10 min) for analysis. The type of anthocyanin component was determined based on color change.

Determination of anthocyanin content

Anthocyanin content of high-temperature-treated cultivars was determined as follows. At the flowering stage, ray florets of both cultivars from different treatment groups were collected. Next, 0.2 g of each sample was weighed and cryogenically ground to a powder. Then, 5 mL of solvent (methanol:water:formic acid:trifluoroacetic acid = 70:27:2:1) was added to each sample, and the extracts were shaken thoroughly. After 24 h, the samples were centrifuged (at 5,000 rpm for 10 min), and the supernatant was collected for analysis. Absorbance was measured at 530 and 657 nm using a

spectrophotometer (Puana/T6 New Century). Each sample was analyzed three times.

Anthocyanin content was calculated according to the following formula:

$$\text{Anthocyanin content} = \text{OD}/\text{ g·FW}$$
$$\Delta\text{OD} = \text{OD}_{530} - 1/4\text{OD}_{657}$$

Total RNA extraction, library construction, and RNA-Seq

Total RNA was extracted using RNA isoPlus (TaKaRa, Japan). The quality of extracted RNA was determined using agarose gel electrophoresis, and RNA quality and concentration were confirmed using a spectrophotometer (ND-1,000; NanoDrop, Wilmington, DE). High-throughput sequencing was performed using the BGISEQ-500 platform.

The basic steps and data processing methods for transcriptome sequencing were as follows. First, total RNA was processed for mRNA enrichment and rRNA depletion. DNA/RNA hybrid strands were selectively digested using RNase H, the remaining DNA probe was digested with DNase I, and desired RNA was obtained after purification. Next, RNA was fragmented in a specific buffer and then reverse transcribed with N6 random primers to synthesize double-stranded DNA; ends of the DNA fragments were blunted, modified, and PCR-amplified with specific primers. The obtained PCR products were thermally denatured into single strands and circularized with bridge primers to obtain a single-stranded circular DNA library for sequencing. Finally, high-quality clean reads were obtained after filtering the raw reads. Clean reads were assembled using Trinity and TGICL to remove redundancy and splicing, and the final unigenes were obtained by matching with the reference genome. Functional annotation and simple sequence repeat (SSR) detection of unigenes, simultaneous calculation of differentially expressed genes (DEGs) for each sample, and in-depth cluster and functional enrichment analyses were performed as described below.

DEG analysis, gene function annotation, GO and KEGG enrichment

BLAST (https://blast.ncbi.nlm.nih.gov/Blast.cgi) was used to search the assembled unigenes against the NCBI NR (non-redundant protein sequences), Pfam (protein families), Swiss-Prot (a manually annotated and reviewed protein sequences), Kyoto Encyclopedia of Genes and Genomes (KEGG), Cluster of Orthologous Groups (COG), NCBI NT (nucleotide sequences), Gene Ontology (GO), and Eukaryotic Orthologous Groups (KOG) functional databases. The GO functions of all unigenes were classified using WEGO. According to the KEGG annotation information, metabolic pathways of the unigenes were explored. DEGs were detected using the PossionDis method. The Q-value was used to correct for the significant *p*-values obtained in original hypothesis tests. To minimize the false-positive rate, a Q-value<0.01 and $|\log_2$ fold change$|>1$ were set as the thresholds for filtering DEGs. A $\log_2$ fold change>0 indicated an upregulated gene; otherwise, it was considered downregulated.

Quantitative real-time PCR

Light Cycler 480 was used for qRT-PCR on DEGs to verify the reliability of the transcriptomic data. The specific primers used for qRT-PCR were designed using Primer Premier 5 (Table 1). Three technical and three biological replicates were set for each test sample. The reactions were performed using SYBR Premix Ex Taq^{TM} (TaKaRa, Japan) according to the manufacturer's instructions. *CmEF1α* was selected as the reference gene. Relative gene expression was assessed using the $2^{-\Delta\Delta CT}$ method.

Results

Phenotypic analysis of "Nannong Ziyunying" and "Nannong Zizhu" under high-temperature stress

The chrysanthemum cultivars "Nannong Ziyunying" and "Nannong Zizhu" were easily affected, and their flower color changed under high-temperature stress. We analyzed the anthocyanin types of the two cultivars and found that the pigments were anthocyanins and flavonoids but not carotenoids (Figure 2A). Thus, we hypothesized that temperature affects anthocyanin synthesis during flowering in "Nannong Ziyunying" and "Nannong Zizhu" subjected to heat stress. In addition, the flower color of both cultivars faded following high-temperature treatment (Figure 2B). To explore the correlation between flower color and anthocyanin content, we measured anthocyanin content in treated and untreated fresh ray florets. The total anthocyanin content in the control and treatment groups was, respectively 27.89 and 10.19 $\text{OD}\cdot\text{g}^{-1}\cdot\text{FW}$ for "Nanong Ziyunying" and respectively, 3.16 and 0.38 $\text{OD}\cdot\text{g}^{-1}\cdot\text{FW}$ for "Nannong Zizhu." Thus, in both cultivars, the total anthocyanin content of ray florets was significantly reduced after high-temperature treatment (Figure 2C).

Transcriptome analysis after high-temperature treatment

The heat-sensitive cultivar "Nanong Ziyunying" was selected as the material for transcriptome analysis. Fresh ray florets were

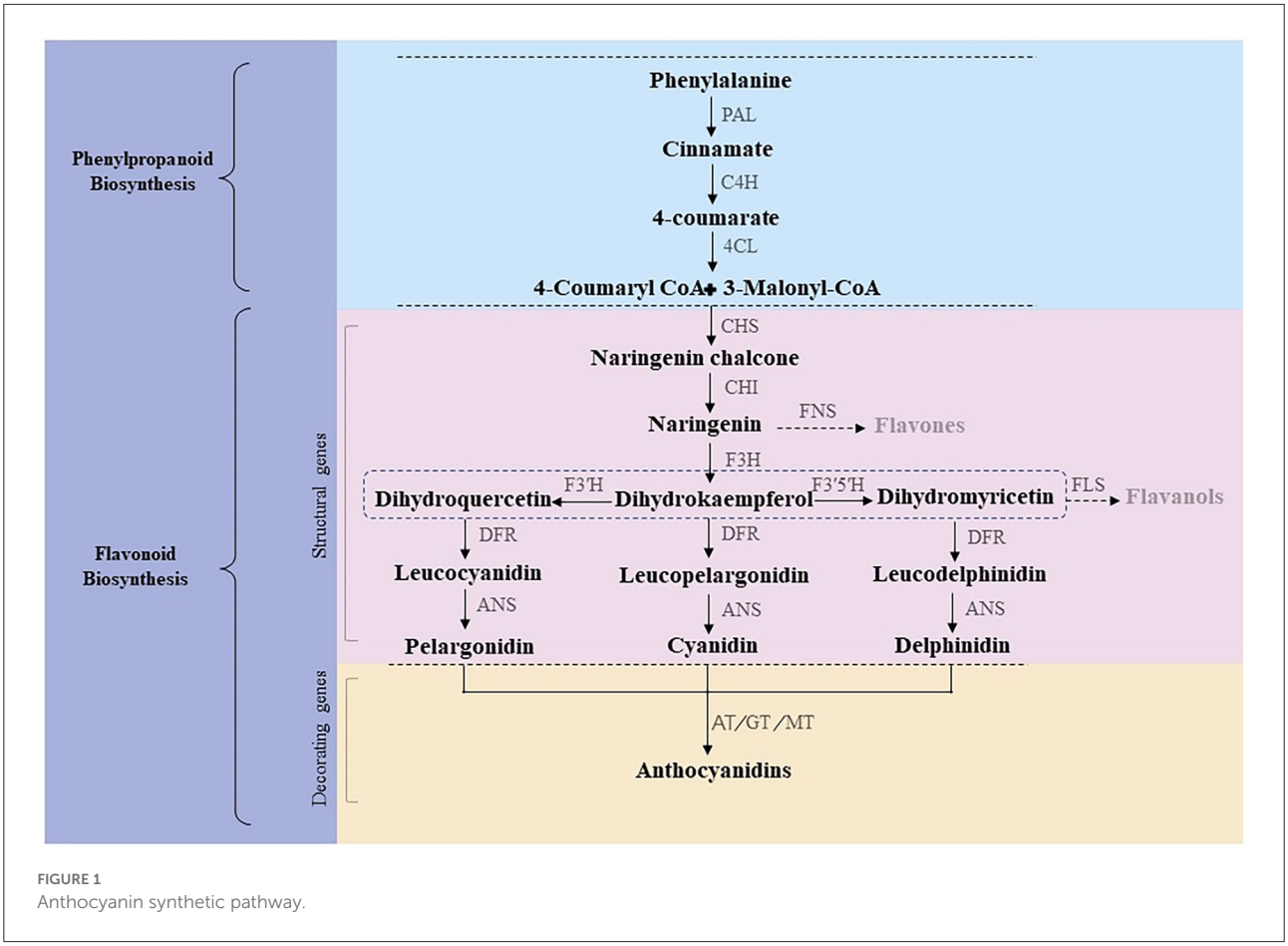

FIGURE 1
Anthocyanin synthetic pathway.

TABLE 1 Primers used in the study.

Primer name	Sequence (5'-3')
qCmCHS-F	ATCATCCAATGATGGTGCCATATAGGC
qCmCHS-R	GACCGCTACACCTCCTAATTGTGTACT
qCmCHI-F	ATACCTGAAGCACCAATCGCAGT
qCmCHI-R	ATTTTCCTCTAGTTGAAAAAGCC
qCmF3H-F	CCAACATTCATCATTCATCTCCCCAGA
qCmF3H-R	ACTTGACAACAACCACTTTCAGGGAGG
qCmDFR-F	CGGAGAAAGCAGCATGGAAA
qCmDFR-R	GGGAACGAGGGACTGATAAATG
qCmANS-F	ATCAACTACTACCCAAAATGCCC
qCmANS-R	CCTAACCTTCTCCTTATTCACAA
qCm3GT-F	GGAGAAATGGAAGATAAACCGAA
qCm3GT-R	CGCCGAATAAAGGAAATCCTAAG
qCmEF1α-F	GTACCCTGGGCACCACAAGT
qCmEF1α-R	CTACCAACGGCCTGCAAATC
qCmHY5-F	GGCTGACAAAGAAAACAAACGGT
qCmHY5-R	CGTTTTGCAGTGTGGACAAACGC

subjected to high-temperature and normal conditions, and high-quality RNA was extracted. Three biological replicates were used per treatment group. The control groups were designated ZYY-1, ZYY-2, and ZYY-3, and the high-temperature treatment groups were designated H-ZYY-1, H-ZYY-2, and H-ZYY-3. After sequencing, raw data were filtered and processed for statistical analysis (Table 2). Overall, the six databases contained a low proportion of low-quality bases (quality<20) and the sequencing quality was good (Figure 3).

A total data of 38.93 GB of data were generated from the BGISEQ-500 platform. After assembly and de-redundancy, 151,614 unigenes were obtained. The total length, average length, N50, and GC content were 154,407,019 bp, 1,018 bp, 1,561, and 39.36%, respectively (Table 3). The obtained unigenes were annotated against the seven functional databases using BLAST, and respectively 93,977 (NR: 61.98%), 56,053 (NT: 36.97%), 63,543 (Swiss-Prot: 41.91%), 72,078 (KOG: 47.54%), 69,096 (KEGG: 45.57%), 73,203 (GO: 48.28%), and 63,728 (Pfam: 42.03%) unigenes were functionally annotated. The transdecoder detected 72,964 coding sequences and 20,880 SSRs

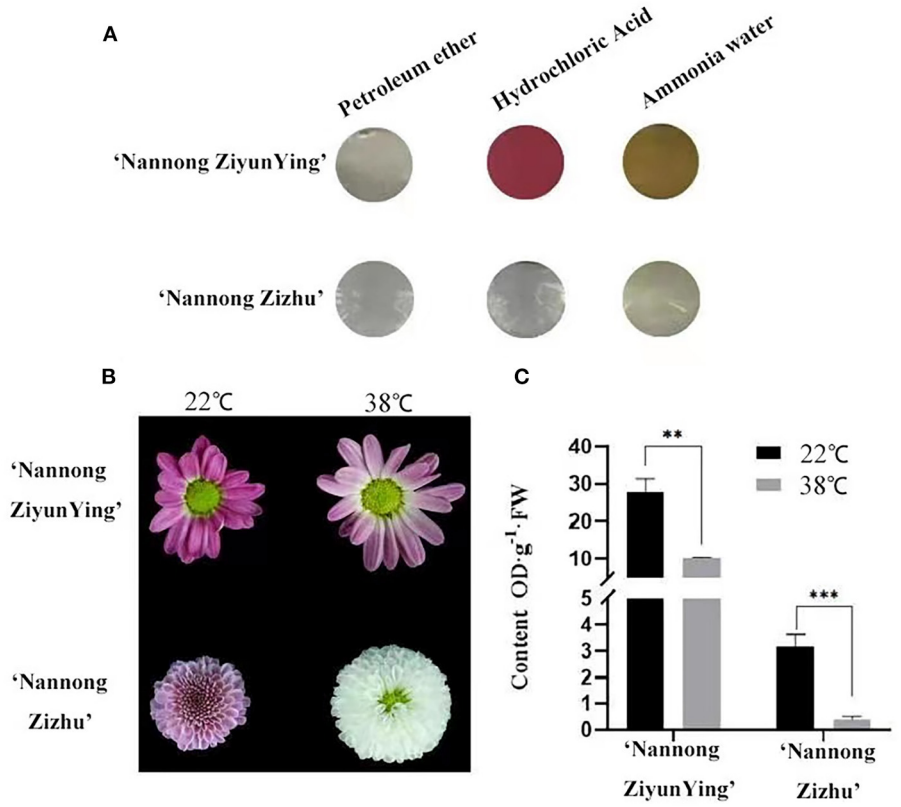

FIGURE 2
Qualitative analysis of anthocyanin types and content in two cut chrysanthemum cultivars. **(A)** Calibration of anthocyanin components. **(B)** Comparison of high-temperature-treated and untreated flower color phenotypes. **(C)** Anthocyanin content of high-temperature treated and untreated cultivars. Error bars represent standard deviations from three biological replicates. Values are presented as mean ± SE ($n = 3$). **Significant at $P < 0.01$ and ***extremely significant at $P < 0.001$, as determined by Student's *t*-test.

distributed in 17,391 unigenes and predicted 2,742 unigenes encoding transcription factors.

Analysis of DEGs and functional enrichment after high temperature treatment

As shown in Figure 4, Venn diagrams of transcripts illustrated 6,841 co-expressed genes, 4,657 ZYY-specific, and 4638 H-ZYY-specific genes between the control (ZYY) and treated (H-ZYY) groups (Figure 4A). Analysis of transcriptome data revealed 18,286 DEGs between ZYY and H-ZYY, of which 14,331 unigenes were downregulated and 3,955 were upregulated in the treatment group (Figure 4B). Additionally, hierarchical clustering of DEGs was observed between ZYY (ZYY-1, ZYY-2, and ZYY-3) and H-ZYY (H-ZYY-1, H-ZYY-2, and H-ZYY-3) (Figure 4C).

The functional classification of GO annotations mainly included three categories, namely "molecular function" "cellular component" and "biological processes" corresponding to respectively, 15, 15, and 9 specific functions (Figure 5A). Among these, respectively 5,447 and 5,415 unigenes annotated to "molecular function" mainly focused on "catalytic activity" and "binding." Moreover, 3,341 unigenes annotated to "biological processes" mainly focused on "cellular and metabolic processes." Among unigenes annotated to "cell components," 3,355, 3,241, 3,550, and 3,374 focused on "cell" "cell part" "membrane" and "membrane part," respectively. Gene-related KEGG pathways were divided into five branches: "cellular processes" "environmental information processing" "genetic information processing" "metabolism" and "organismal systems" (Figure 5B). Most of the unigenes were functionally annotated to "metabolic pathways" which were divided into 11 sub-categories, with 2,224 genes in the global and overview maps and 847 genes in the carbohydrate metabolism category. In addition, unigenes classified into "genetic information processing" pathways were divided into four sub-categories focusing on "translation" and "folding, sorting, and degradation," with respectively, 1,015 and 757 genes.

TABLE 2 Filtered read quality statistics.

Sample	Total raw reads (M)	Total clean reads (M)	Total clean bases (Gb)	Clean reads Q20 (%)	Clean reads Q30 (%)	Clean read ratio (%)
ZYY-1	69.96	67.1	6.71	98.22	92.16	95.9
ZYY-2	67.47	64.28	6.43	98.18	92.1	95.28
ZYY-3	67.47	64.31	6.43	98.15	91.94	95.33
H-ZYY-1	67.47	64.38	6.44	98.22	92.2	95.42
H-ZYY-2	67.47	64.57	6.46	98.17	92.02	95.71
H-ZYY-3	67.47	64.57	6.46	98.19	92.06	95.71

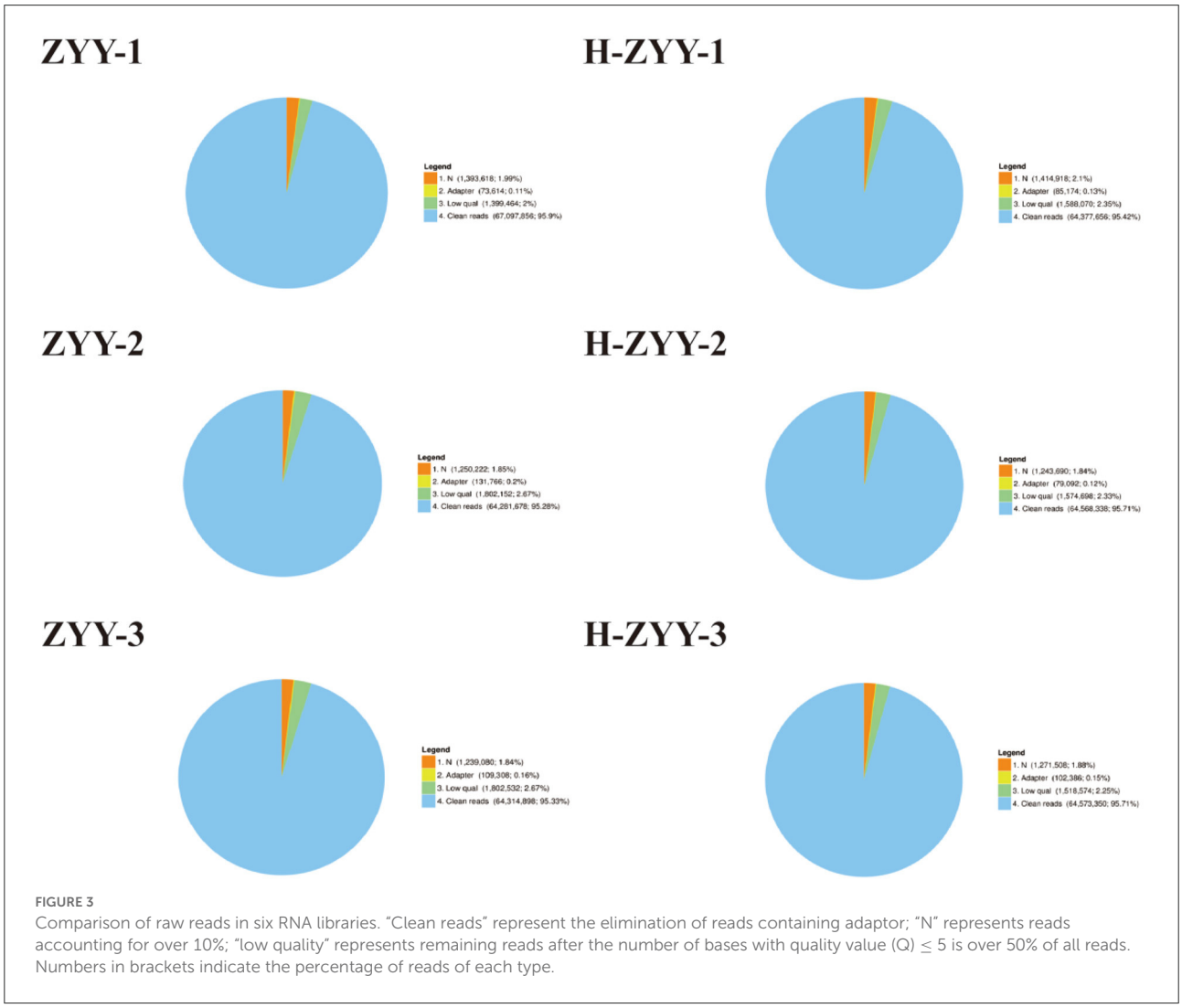

FIGURE 3
Comparison of raw reads in six RNA libraries. "Clean reads" represent the elimination of reads containing adaptor; "N" represents reads accounting for over 10%; "low quality" represents remaining reads after the number of bases with quality value (Q) ≤ 5 is over 50% of all reads. Numbers in brackets indicate the percentage of reads of each type.

Functional enrichment analysis revealed abundant unigenes in "RNA transport" "spliceosome" and "plant MPAK signaling" pathways. Of the 416, 408, and 306 DEGs, 63 were enriched in "flavonoid biosynthesis" which is associated with flower color (Figure 5C).

RNA-Seq database mining of DEGs in response to high-temperature treatment

DEGs between the ZYY and H-ZYY groups were compared with the gene function annotation information, and the

TABLE 3 Unigene quality index statistics.

Sample	Total number	Total length	Mean length	N50	N70	N90	GC (%)
ZYY-1	98,773	77,777,880	787	1,176	718	337	39.58
ZYY-2	92,109	72,159,678	783	1,170	716	336	39.7
ZYY-3	97,167	75,886,636	780	1,163	712	334	39.59
H-ZYY-1	82,749	70,451,968	851	1,257	799	376	39.84
H-ZYY-2	82,070	69787,861	850	1264	794	374	39.9
H-ZYY-3	83,300	70,866,818	850	1,263	793	375	39.82
All-unigene	151,614	154,407,019	1,018	1,561	1,012	463	39.36

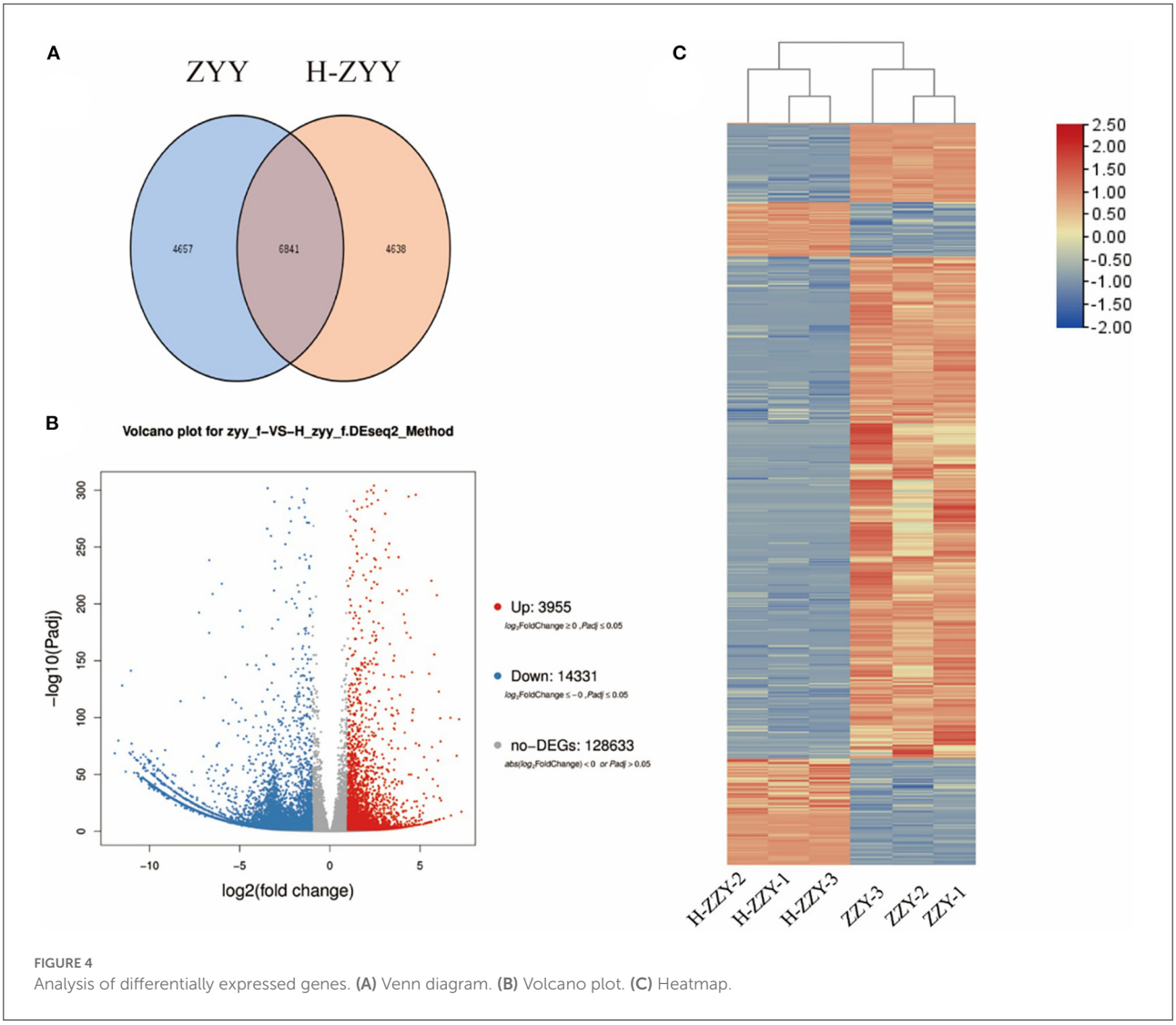

FIGURE 4
Analysis of differentially expressed genes. **(A)** Venn diagram. **(B)** Volcano plot. **(C)** Heatmap.

transcription factors and genes potentially involved in response to high-temperature treatment were extracted from the transcriptome database. Since the flower color of "Nannong Ziyunying" changed after high-temperature treatment, we performed differential analysis of genes related to flower color metabolism. The structural genes *CHS* (Unigene47149_All), *CHI* (CL16685.Contig2_All), *DFR* (Unigene32692_All), *F3H* (CL14465.Contig9_All), *ANS* (CL12615.Contig3_All), *3GT*

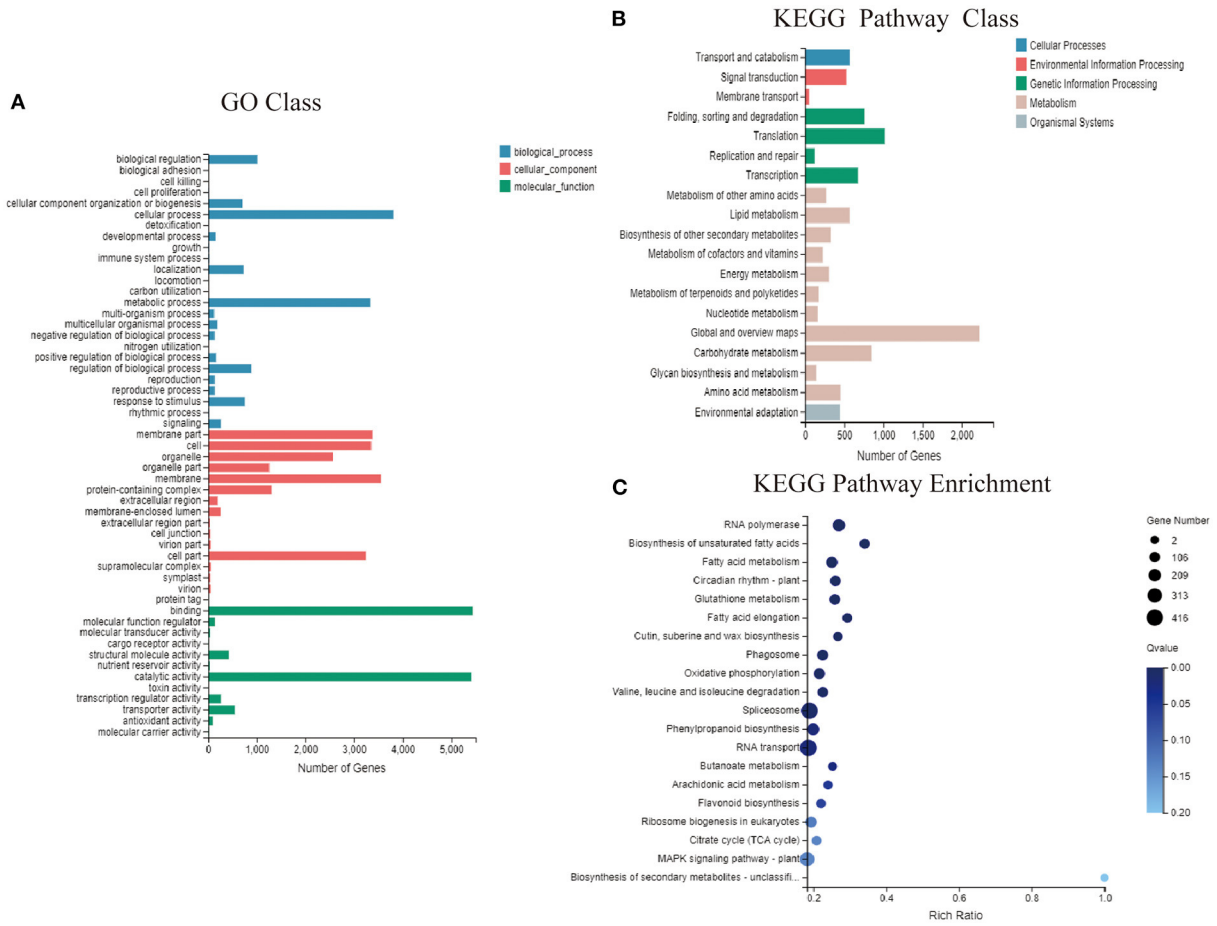

FIGURE 5
GO and KEGG functional enrichment analysis. **(A)** Functional distribution of GO annotations. **(B)** KEGG function distribution statistics. **(C)** KEGG function-enriched bubble chart.

(CL10945.Contig1_All), and *F3'H* (CL3093Contig1_All) were downregulated (Figure 6A). The MBW transcription factors, which are associated with flower color, were analyzed. Of these, nine MYB transcription factors; the bHLH transcription factor *AN1* (Unigene43198_All); and three WD40 transcription factors, namely *TTG1* (CL5816.Contig5_All), *COP1* (Unigene24944_All), and *SPA4* (CL5840.Contig2_All), were downregulated (Figure 6B). The expression levels of MADS-box transcription factors also changed in the two phenotypes of ray florets after high-temperature treatment. Among them, the expression of *AGL31* (CL2420.Contig3_All), *MADS15* (CL16766.Contig1_All), and *MADS25* (Unigene38459_All) etc., were upregulated, while *CMB1-like* (Unigene34995_All), *AGL15* (Unigene19595_All), *AGL3* (Unigene40538_All), *SOC1* (Unigene31972_All), *FLC* (Unigene24171_All), *AGL15* (Unigene26731_All), and *MADS8* (Unigene52611_All), were significantly downregulated (Figure 6G). Furthermore, signaling molecules, such as Ca^{2+} and ROS, accumulate in plants in response to high-temperature stress. Ca^{2+} is one of the primary and essential signals for heat shock response, and it activates MAPK to transmit signals to the nucleus (Ohama et al., 2017). Our analysis revealed that *MAPKKK17* (CL6043.Contig2_All), *MAPKKK5* (Unigene19893_All), the MAPK kinase substrate protein At1g80180 (Unigene2236_All), and *MAPKKK18* (Unigene47170_All) in the MAPK cascade were upregulated following high-temperature treatment. Likewise, the intracellular Ca^{2+} signaling pathway genes *CAM3* (CL12903.Contig2_All), *CCAMK* (Unigene26523_All), *SCAMP4* (Unigene40171_All), and *CNGC2* (CL4349.Contig1_Al) were upregulated, whereas *CDKA*-1 (Unigene41169_All) and *TDR4* (CL12077.Contig2_All) were downregulated (Figure 6C) after high-temperature treatment. Stress induces ROS production via both enzymatic and non-enzymatic pathways and is associated with multiple stages of plant development and growth. Our analysis revealed that several genes encoding

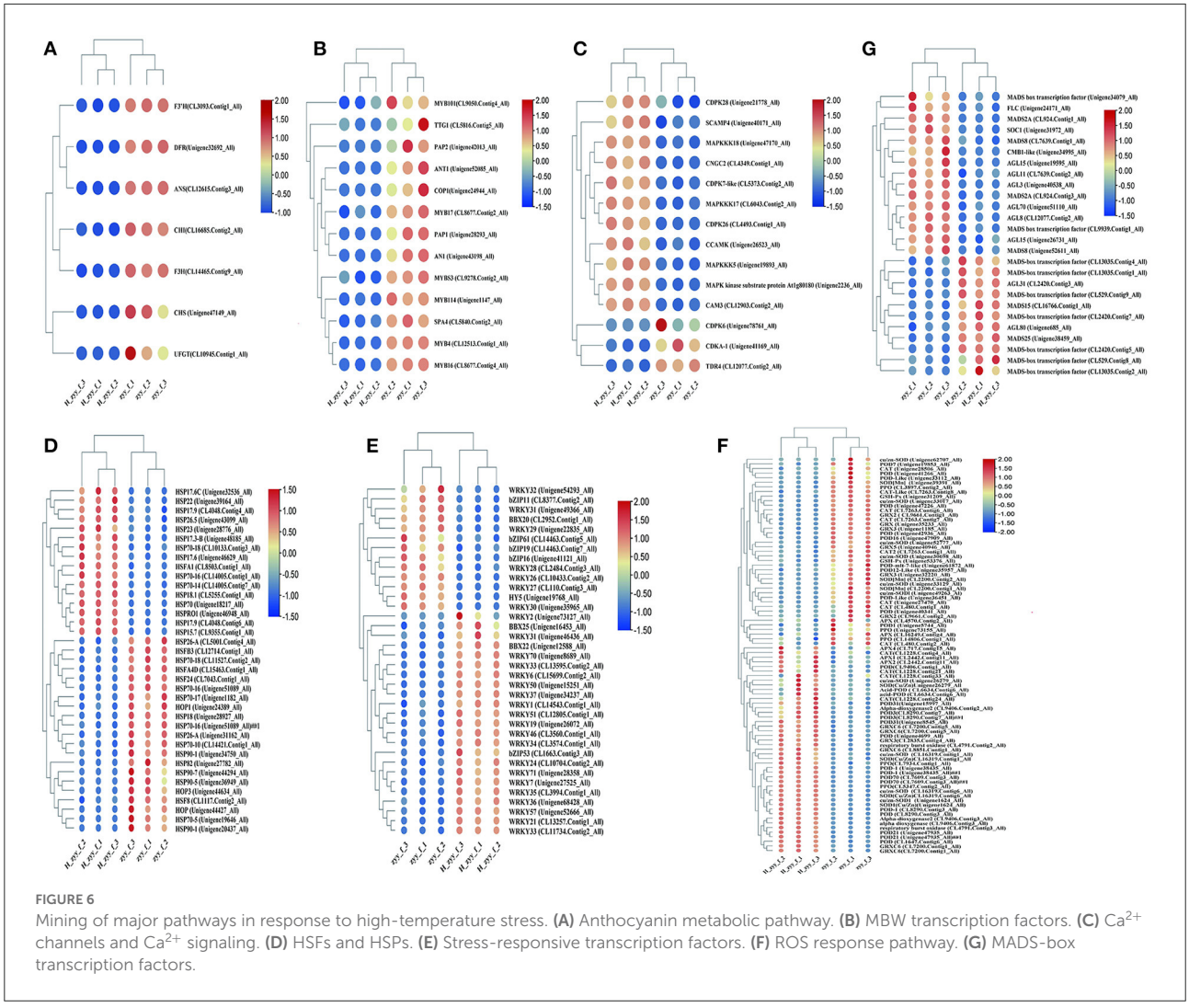

FIGURE 6
Mining of major pathways in response to high-temperature stress. **(A)** Anthocyanin metabolic pathway. **(B)** MBW transcription factors. **(C)** Ca^{2+} channels and Ca^{2+} signaling. **(D)** HSFs and HSPs. **(E)** Stress-responsive transcription factors. **(F)** ROS response pathway. **(G)** MADS-box transcription factors.

antioxidant enzymes, such as *SOD[Mn]* (CL2200.Contig2_All), *Cu/Zn-SOD* (Unigene49263_Al), POD (Unigene40341_All), *POD-like* (Unigene36451_All), *POD16* (Unigene47909_All), *POD7* (Unigene19853_All), *CAT* (Unigene27470_All), *CAT2* (CL7263.Contig1_All), *APX* (CL16249.Contig4_All), *PPO* (CL3897.Contig2_All), *GRX2* (CL9661.Contig1_All), and *GRX3* (Unigene32220_All) were downregulated under high-temperature stress. However, *Cu/zn-SOD* (CL16319.Contig1_All), *POD31* (Unigene8545_All), *POD3* (CL8290.Contig7_All), *POD-1* (Unigene38435_All), *PPO* (CL7934.Contig1_All), CAT (CL1228.Contig24_All), *GRXC6* (CL7200.Contig1_All), *APX2* (CL2442.Contig11_All) were upregulated, indicating heat enhanced ROS metabolism (Figure 6F).

HSFs and HSPs are involved in various biological processes, particularly in response to heat stress. Specifically, the heat shock transcription factor (Hsf) *HsfA1* (CL8503.Contig1_All) was upregulated, while *HSF8* (CL1117.Contig2_All), *HSFB3* (CL12714.Contig1_All), *HSFA4D* (CL15463.Contig1_All), and *HSF24* (CL7043.Contig1_All) were downregulated. In addition, 16 HSPs were upregulated and 16 were downregulated after high-temperature treatment. Among these, *HSP70* (Unigene18217_All) was significantly upregulated, whereas *HSP90* (Unigene31147_All) was significantly downregulated (Figure 6D). In addition to HSFs and HSPs, transcription factors, such as B-box (BBX), bZIP, DREB, and WRKY, were differentially expressed. In particular, the BBX transcription factors *BBX22* (Unigene12588_All) and *BBX25* (Unigene16453_All) were upregulated, while *BBX20* (CL2952.Contig1_All) was downregulated. Among bZIP transcription factors, *bZIP53* (CL1663.Contig3_All), *bZIP61* (CL14463.Contig5_All), *bZIP19* (CL14463.Contig7_All), *bZIP11* (CL8377.Contig2_All), and *bZIP16* (Unigene41121_All) were upregulated, while *HY5* (Unigene19768_All) was significantly downregulated. DREB is an important stress-responsive transcription factor in

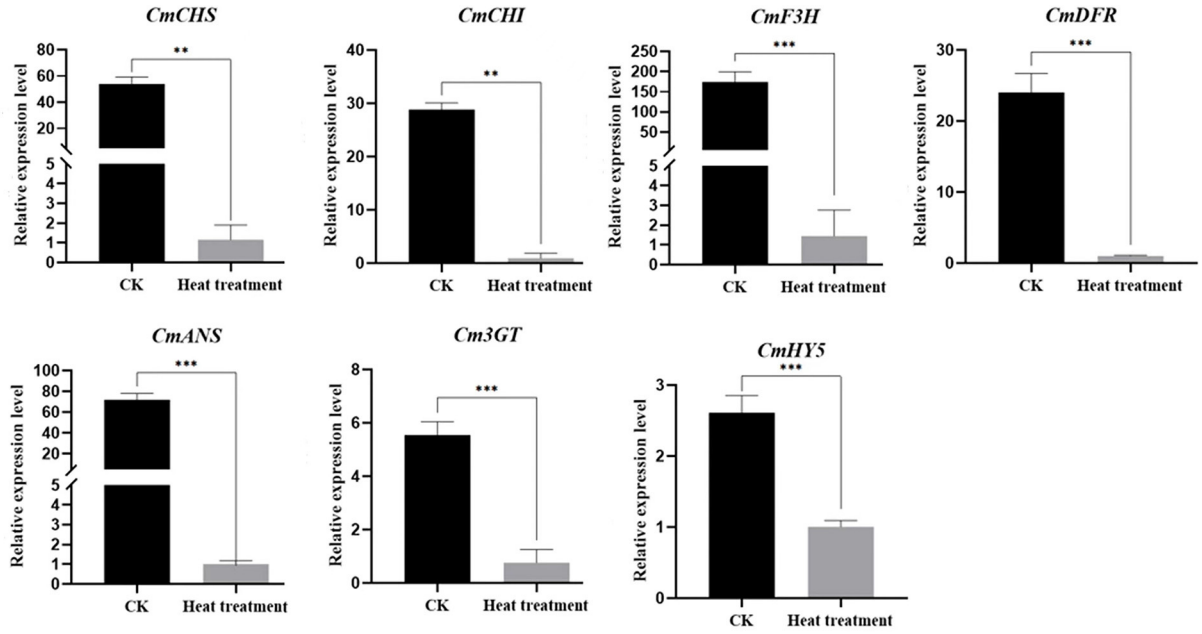

FIGURE 7
Verification of the relative expression of anthocyanin metabolism gene following high-temperature treatment. Values are presented as mean ± SE ($n = 3$). **Significant at $P < 0.01$ and ***significant at $P < 0.001$, as determined by Student's *t*-test.

plants, which can specifically bind *cis*-acting DRE/CRT elements to induce the expression of stress tolerance genes (Luo et al., 2015). Our analysis revealed that *DREB3* (CL11734.Contig2_All), *DREB1F* (CL3574.Contig1_All), *DREB1A* (CL3994.Contig1_All), *DREB1B* (Unigene68428_All), and *DREB1D* (Unigene34237_All) were upregulated in response to high temperature. In addition, 22 WRKY transcription factors were differentially expressed, of which 15 were upregulated and 7 were downregulated. Specifically, *WRKY2* (Unigene73127_All) was significantly upregulated, while *WRKY3* (CL110.Contig3_All) was significantly downregulated (Figure 6E).

qRT-PCR validation of flower color-related DEGs

To validate the expression of differential genes in the RNA-Seq database, we selected seven DEGs, namely *CmCHS*, *CmCHI*, *CmDFR*, *CmF3H*, *CmANS*, *Cm3GT*, and *CmHY5*, which are structural anthocyanin synthetic genes and transcription factors, for qRT-PCR analysis. The results of qRT-PCR were consistent with those of RNA-Seq, and all seven genes were significantly downregulated after high-temperature treatment (Figure 7).

Discussion

How does chrysanthemum respond to high-temperature stress?

Through transcriptome analysis, changes in flower color following high-temperature treatment of the heat-sensitive cultivar "Nannong Ziyunying" at the molecular level were revealed. Our analysis revealed that *HsfA1* (CL8503.Contig1_All) was significantly upregulated after high-temperature treatment. HsfA1 is a key regulator of response to high-temperature stress (El-Shershaby et al., 2019). For instance, in tomato, HsfA1 serves a unique function of regulating plant thermotolerance as a major transcription factor in response to heat stress, and *hsfa1* mutants exhibit a heat-sensitive phenotype (Mishra et al., 2002). In addition, *HSP70* (Unigene18217_All) expression was significantly upregulated after high-temperature treatment. HSP70 is the main and highly conserved protein activated by stress (Usman et al., 2017), and the role of HSP70 in relation to heat tolerance has been reported in several crops, such as soybean (*Glycine max*) (Ortiz and Cardemil, 2001), wheat (*Triticum aestivum*) (Duan et al., 2011), chili pepper (*Capsicum annuum*) (Usman et al., 2015), chrysanthemum (*Chrysanthemum morifolium* Ramat) (Song et al., 2014), and creeping bentgrass (*Agrostis palustris*) (Ye et al., 2012). The same results were obtained in our experiments,

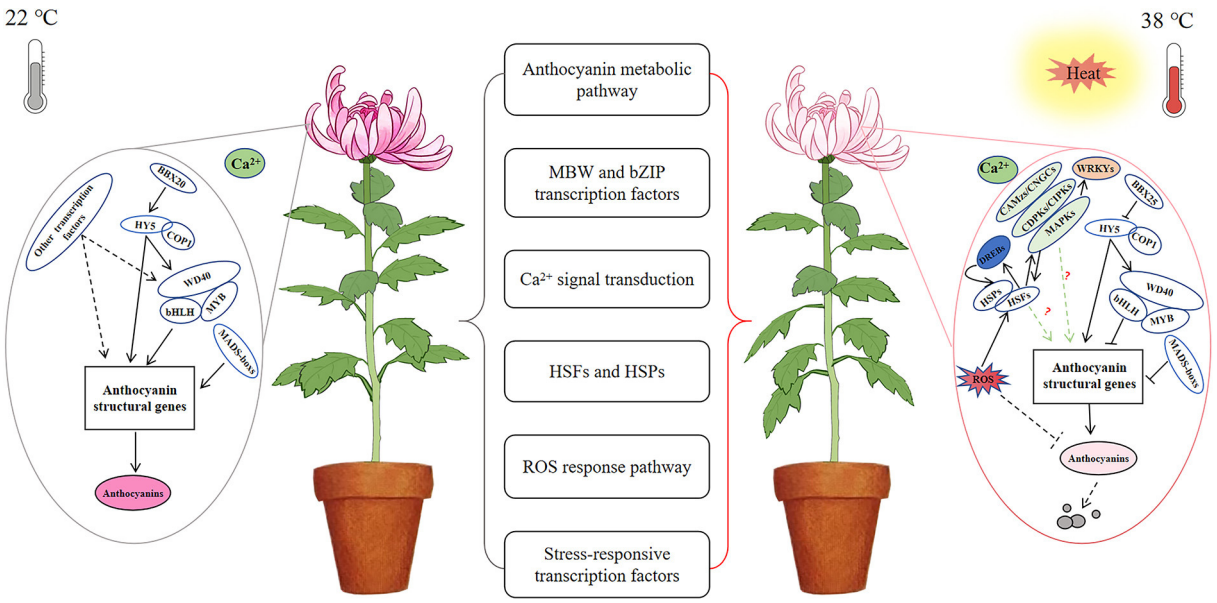

FIGURE 8
A possible regulatory network of chrysanthemum flower color under high temperature stress. Anthocyanin biosynthesis was normal at 22°C; anthocyanin biosynthesis was inhibited and accelerated degradation under high temperature stress at 38°C.

indicating that HSFs and HSPs respond to high-temperature stress in chrysanthemum.

In addition, high-temperature stress promotes the fluidity of cell membrane, which is related to Ca^{2+} channels in the cell membrane structure. Genes involved in Ca^{2+} signaling are activated under high-temperature stress, and heat shock signals are transmitted from the outside to inside of cells through CNGCs, which are implicated in the regulation of Ca^{2+} signaling (Finka et al., 2012). In particular, CNGC2 and CNGC4 are associated with high-temperature stress response (Gao et al., 2012). Our analysis revealed that *CNGC2* (CL4349.Contig1_All) was upregulated after high-temperature treatment, suggesting that Ca^{2+} signaling is activated under heat stress in chrysanthemum. In the Ca^{2+} signaling pathway, Ca^{2+} ions combine with calmodulin (CaM) to promote the activity of calcium-dependent protein kinases (CDPKs) and MAPKs, which transmit heat stress signals to the nucleus and regulate the expression of thermostable genes (Awasthi et al., 2015). According to our transcriptomic data, MAPKs (Unigene2236_All) and CAM3 (CL12903.Contig2_All) were upregulated after high-temperature treatment. In addition, high-temperature stress induces ROS production and accumulation in plants, promoting antioxidant enzyme activity. In the present study, the expression levels of *SOD*, *POD*, *CAT*, *GRX*, *PPO*, and *APX* were significantly altered (Figure 6F). Increased activity of these antioxidant enzymes is beneficial for scavenging different types of ROS [e.g., singlet oxygen ($^1O_2$), superoxide (O_2^-), hydrogen peroxide (H_2O_2), and hydroxyl radicals (OH^-)] generated by high-temperature stress and enhancing the heat tolerance of plants (Medina et al., 2021). In addition, polyphenol oxidase (PPO) and peroxidase (POD) have been implicated in the anthocyanin degradation pathway for regulating flower and fruit color (Oren-Shamir, 2009; Zhang et al., 2019). ROS metabolism, similar to Ca^{2+} signaling pathway, mediates heat response and regulates immune activity in plants. Furthermore, ROS promote the expression of heat shock transcription factors; however, excess ROS accumulation leads to the generation of large amounts of NO, which induces the expression of CaM3 and promotes the transcription of downstream HsfA1 and related HSP genes (Ohama et al., 2017; Zhu et al., 2021). Furthermore, NO possesses ROS scavenging activity, and it has been reported to improve the antioxidant and thermal tolerance of *Arabidopsis* (Wang et al., 2014) and chrysanthemum (Yang et al., 2011). Typically, when plants are subjected to high-temperature stress, a series of transcriptional regulatory cascades are activated to respond to heat shock. HSF and HSP expression, Ca^{2+} signaling activation, and ROS production are the three major regulatory networks involved in HSR (Ohama et al., 2017). Our analysis of transcriptomic data revealed that genes and enzymes associated with these three pathways produced a transcriptional regulatory response in chrysanthemum; therefore, these components may also be the major regulators of HSR in chrysanthemum. However, the precise responses of these pathways to high temperature and mechanisms underlying the regulation of flower color in chrysanthemum remain unclear.

What is the link between anthocyanin synthesis and high temperature stress?

Anthocyanin biosynthesis is regulated by an array of enzymes. Genes encoding these enzymes, namely *CHS*, *CHI*, *DFR*, *F3H*, *ANS*, *3GT*, and *F3'H*, are called structural genes related to anthocyanin metabolism (Willits et al., 2005; Zhang et al., 2014). Our transcriptome analysis revealed that the expression of anthocyanin synthesis-related genes was significantly downregulated (Figures 6A, 7), consistent with qRT-PCR results, and the total anthocyanin content also decreased under high-temperature stress. In addition, *CmHY5* (Unigene19768_All), a bZIP transcription factor, was significantly downregulated. HY5 is known to regulate flower color in apples, and its association with BBXs, COP1, and MYBs has been demonstrated in rice (Luo et al., 2018), *Arabidopsis* (Gangappa et al., 2013), and apple (Liu et al., 2019). Here, we used qRT-PCR to verify HY5 downregulation and to further investigate the molecular mechanism underlying the regulation of flower color under high-temperature stress. In plants, structural genes involved in anthocyanin biosynthesis are primarily regulated by a class of conserved MBW complexes (Jin et al., 2016; Goswami et al., 2018). Among these, the MYB and bHLH transcription factors play major regulatory roles. Specifically, the MBW protein complex directly regulates anthocyanin content in plants by activating or inhibiting the transcription of structural genes related to anthocyanin synthesis (Nabavi et al., 2020). In our analysis, eight MYB transcription factors were downregulated (Figure 6B). These results are consistent with reports that high-temperature stress inhibited the expression of *MdMYB4*, *MdMYB16*, *MdMYB17*, and *MdMYB114* and affected the synthesis of anthocyanin in apples (Lin-Wang et al., 2011). *MpMYBS3* is highly expressed in response to low-temperature signals (Dou et al., 2016), and our analysis showed that *CmMYBS3* (CL9278.Contig2_All) was downregulated under high-temperature stress; hence, CmMYBS3 may be involved in high-temperature stress response. *PpMYB114* promotes the expression of *PpUFGT* involved in anthocyanin metabolism (Ni et al., 2019). In the present study, *CmMYB114* (Unigene1147_All) and *Cm3GT* (CL8501.Contig3_All) were downregulated after high-temperature treatment, indicating that a similar regulatory network may exist in chrysanthemum. In *Petunia hybrida*, *PhPAP1* positively regulated the anthocyanin structural gene *PhCHS*, and the overexpression of *PhPAP1* and *PhCHS* led to abundant anthocyanin accumulation after 12 h of UV-A irradiation (Matoušek et al., 2006). Moreover, in the ethylene-insensitive *Arabidopsis* mutant *ein2-1*, abundant sucrose-induced anthocyanins were accumulated at high temperature through elevated PAP1 transcription (Kwon et al., 2011). These results are consistent with *CmPAP1* (Unigene28293_All) downregulation after high-temperature treatment in our experiment. In chrysanthemum, a large amount of ethylene may be synthesized under high-temperature stress, which downregulates downstream *CmPAP1* expression and hinders anthocyanin accumulation. Furthermore, PAP1 and PAP2 can bind the COP1/SPA complex and positively control anthocyanin accumulation in *Arabidopsis* (Maier et al., 2013). Our data showed that PAP2 (Unigene42013_Al), COP1 (Unigene24944_All), and SPA4 (CL5840.Contig2_All) were downregulated, indicating a similar regulatory mechanism in chrysanthemum. ANT1 can form a complex with EGL3, GL3, and TTG1 to positively regulate anthocyanin metabolism (Petroni and Tonelli, 2011), which is consistent observation that ANT1 (Unigene52085_All) was downregulated in chrysanthemum at high temperature.

Furthermore, bHLH transcription factors affect flower color. In particular, PhAN1 can interact with MYB and WD to positively regulate anthocyanin synthesis and activate various signaling pathways through interaction with MYB transcription factors (Quattrocchio et al., 2006; Petroni and Tonelli, 2011). In *Arabidopsis thaliana*, the WD protein TTG1 acts in concert with the GL3, EGL3, or TT8 proteins as well as the R2R3–MYB transcription factors PAP1, PAP2, MYB113, and MYB114 (Zhang et al., 2003; Zimmermann et al., 2004; Gonzalez et al., 2008). In *Freesia hybrida* Klatt, FhTTG1 encodes the WD40 protein, which forms the MBW complex and regulates anthocyanin or procyanidin biosynthesis, the specificity of which depends, in part, on the interacting proteins (Yamagishi et al., 2010; Verweij et al., 2016; Qi et al., 2022). Our data showed that the bHLH transcription factor AN1 (Unigene52085_All) and the WD40 protein TTG1 (CL5816.Contig5_All) were downregulated; these proteins may interact with MYB transcription factors to form the MBW complex and reduce anthocyanin synthesis under high-temperature stress. In addition, MADS-box transcription factors have been found to be involved in anthocyanin biosynthesis in a variety of plants, such as apple (Onik et al., 2018), strawberry (Lu et al., 2018), and sweet cherry (Qi et al., 2020). Recently, studies have shown that ScAG and ScAGL11 as negative regulators of anthocyanin biosynthesis in *Senecio cruentus* ray florets, which influence bicolor pattern formation (Qi et al., 2022). In our results, *CMB1-like* (Unigene34995_All), *AGL15* (Unigene19595_All), *AGL3* (Unigene40538_All), and *SOC1* (Unigene31972_All) were significantly downregulated after high temperature stress. It is speculated that MADS-box transcription factors are involved in anthocyanin biosynthesis in chrysanthemum, but the specific molecular mechanism needs to be further studied.

In summary, chrysanthemum response to high temperature may involve the following three pathways: (1) extracellular Ca^{2+} influx promotes Ca^{2+} channels and signaling responses, which in turn promotes the expression of downstream MAPKs and transmits the high-temperature signal to the nucleus; (2) ROS production and accumulation of leads to a series of complex heat stress response pathways, such

as HSF and HSP synthesis and NO accumulation, which in turn activates the plant's own immune stress response; and (3) structural genes involved in anthocyanin synthesis are downregulated, thereby inhibiting anthocyanin production and leading to flower discoloration under high temperature in chrysanthemum. These structural genes are regulated by different MBW protein complexes and other transcription factors that affect anthocyanin biosynthetic pathways in plants. However, although we assessed the expression of genes related to plant response to high temperature and anthocyanin metabolism through transcriptome analysis, response to heat stress and regulation of anthocyanin metabolism in plants involve complex regulatory networks. The links among these genes and their respective molecular functions remain clear and warrant further exploration.

Conclusion

The discoloration phenotype of chrysanthemums under high-temperature stress is directly related to the inhibition of anthocyanin synthesis. However, multiple pathways may be involved in response to high-temperature stress, indicating the presence of a complex molecular regulatory network involving anthocyanin metabolism in chrysanthemums (Figure 8). Overall, our preliminary transcriptomic analysis revealed the regulation of flower color, as affected by high-temperature stress, although the precise molecular mechanism should be further studied.

Data availability statement

The datasets generated for this study can be found in the NCBI sequence reads archive (SRA) database under BioProject No. PRJNA859415.

Author contributions

JJ designed the experiments. XH and JQ performed the experiments. ZS and XH analyzed the data. ZS, XH, and GW wrote the manuscript. L-jZ, SC, WF, and FC discussed the results and commented on the manuscript. L-jZ and ZS provided the funds. All authors contributed to the article and approved the submitted version.

Funding

This work was financially supported by the Hainan Provincial Natural Science Foundation of China (322QN340), the special research fund for doctoral students of Sanya Yazhou Bay Science and Technology City (HSPHDSRF-2022-07-002), and the Guiding Fund Key Projects for Sanya Institute of Nanjing Agricultural University (NAUSY-ZD03).

Conflict of interest

The authors declare that the research was conducted in the absence of any commercial or financial relationships that could be construed as a potential conflict of interest.

Publisher's note

All claims expressed in this article are solely those of the authors and do not necessarily represent those of their affiliated organizations, or those of the publisher, the editors and the reviewers. Any product that may be evaluated in this article, or claim that may be made by its manufacturer, is not guaranteed or endorsed by the publisher.

References

An, J. P., Wang, X. F., Zhang, X. W., Bi, S. Q., You, C. X., and Hao, Y. J. (2019). MdBBX22 regulates UV-B-induced anthocyanin biosynthesis through regulating the function of MdHY5 and is targeted by MdBT2 for 26S proteasome-mediated degradation. *Plant Biotechnol. J.* 17, 2231. doi: 10.1111/pbi.13196

Armitage, A., and Carlson, W. (1981). The effect of quantum flux density, day and night temperature and phosphorus and potassium status on anthocyanin and chlorophyll content in marigold leaves [Tagetes patula]. *J. Am. Soc. Horticultural Sci.* 106, 639–642. doi: 10.21273/JASHS.106.5.639

Atkin, O. K., and Tjoelker, M. G. (2003). Thermal acclimation and the dynamic response of plant respiration to temperature. *Trends Plant Sci.* 8, 343–351. doi: 10.1016/S1360-1385(03)00136-5

Awasthi, R., Bhandari, K., and Nayyar, H. (2015). Temperature stress and redox homeostasis in agricultural crops. *Front. Environ. Sci.* 3, 11. doi: 10.3389/fenvs.2015.00011

Bontpart, T., Cheynier, V., Ageorges, A., and Terrier, N. (2015). BAHD or SCPL acyltransferase? What a dilemma for acylation in the world of plant phenolic compounds. *New Phytol.* 208, 695–707. doi: 10.1111/nph.13498

Caputi, L., Malnoy, M., Goremykin, V., Nikiforova, S., and Martens, S. (2012). A genome-wide phylogenetic reconstruction of family 1 UDP-glycosyltransferases revealed the expansion of the family during the adaptation of plants to life on land. *Plant J.* 69, 1030–1042. doi: 10.1111/j.1365-313X.2011.04853.x

Chinnusamy, V., Schumaker, K., and Zhu, J. K. (2004). Molecular genetic perspectives on cross-talk and specificity in abiotic stress signalling in plants. *J. Exp. Bot.* 55, 225–236. doi: 10.1093/jxb/erh005

Deal, D., Raulston, J., and Hinesley, L. (1990). Leaf color retention, dark respiration, and growth of red-leafed Japanese maples under high night temperatures. *J. Am. Soc. Hortic. Sci.* 115, 135–140. doi: 10.21273/JASHS.115.1.135

Dou, T. X., Hu, C. H., Sun, X. X., Shao, X. H., Wu, J H., Ding, L. J., et al. (2016). MpMYBS3 as a crucial transcription factor of cold signaling confers the cold tolerance of banana. *PCTOC.* 125, 93–106. doi: 10.1007/s11240-015-0932-y

Duan, Y. H., Guo, J., Ding, K., Wang, S. J., Zhang, H., Dai, X. W., et al. (2011). Characterization of a wheat HSP70 gene and its expression in response to stripe rust infection and abiotic stresses. *Mol. Biol. Rpt.* 38, 301–307. doi: 10.1007/s11033-010-0108-0

Dusenge, M. E., Duarte, A. G., and Way, D. A. (2019). Plant carbon metabolism and climate change: elevated CO 2 and temperature impacts on photosynthesis, photorespiration and respiration. *New Phytol.* 221, 32–49. doi: 10.1111/nph.15283

El-Shershaby, A., Ullrich, S., Simm, S., Scharf, K.-D., Schleiff, E., and Fragkostefanakis, S. (2019). Functional diversification of tomato HsfA1 factors is based on DNA binding domain properties. *Gene* 714, 143985. doi: 10.1016/j.gene.2019.143985

Finka, A., Cuendet, A. F. H., Maathuis, F. J., Saidi, Y., and Goloubinoff, P. (2012). Plasma membrane cyclic nucleotide gated calcium channels control land plant thermal sensing and acquired thermotolerance. *Plant Cell* 24, 3333–3348. doi: 10.1105/tpc.112.095844

Gangappa, S. N., Crocco, C. D., Johansson, H., Datta, S., Hettiarachchi, C., Holm, M., et al. (2013). The Arabidopsis B-BOX protein BBX25 interacts with HY5, negatively regulating BBX22 expression to suppress seedling photomorphogenesis. *The Plant Cell.* 25, 1243–1257. doi: 10.1105/tpc.113.109751

Gao, F., Han, X., Wu, J., Zheng, S., Shang, Z., Sun, D., et al. (2012). A heat-activated calcium-permeable channel–arabidopsis cyclic nucleotide-gated ion channel 6–is involved in heat shock responses. *Plant J.* 70, 1056–1069. doi: 10.1111/j.1365-313X.2012.04969.x

Gins, M., Gins, V., Kononkov, P., Baikov, A., Pivovarov, V., Fotev, Y. V., et al. (2019). The effect of low positive temperature on the content of low-molecular weight antioxidants in the organs of a vegetable chrysanthemum. *Russ. Agric. Sci.* 45, 434–438. doi: 10.3103/S1068367419050070

Golldack, D., Li, C., Mohan, H., and Probst, N. (2014). Tolerance to drought and salt stress in plants: unraveling the signaling networks. *Front. Plant Sci.* 5, 151. doi: 10.3389/fpls.2014.00151

Gonzalez, A., Zhao, M., Leavitt, J. M., and Lloyd, A. M. (2008). Regulation of the anthocyanin biosynthetic pathway by the TTG1/bHLH/Myb transcriptional complex in arabidopsis seedlings. *Plant J.* 53, 814–827. doi: 10.1111/j.1365-313X.2007.03373.x

Goswami, G., Nath, U. K., Park, J.-I., Hossain, M. R., Biswas, M. K., Kim, H.-T., et al. (2018). Transcriptional regulation of anthocyanin biosynthesis in a high-anthocyanin resynthesized Brassica napus cultivar. *J. Biol. Res. Thessaloniki* 25, 1–15. doi: 10.1186/s40709-018-0090-6

Hasanuzzaman, M., Nahar, K., Alam, M. M., Roychowdhury, R., and Fujita, M. (2013). Physiological, biochemical, and molecular mechanisms of heat stress tolerance in plants. *Int. J. Mol. Sci.* 14, 9643–9684. doi: 10.3390/ijms14059643

Hichri, I., Barrieu, F., Bogs, J., Kappel, C., Delrot, S., and Lauvergeat, V. (2011). Recent advances in the transcriptional regulation of the flavonoid biosynthetic pathway. *J. Exp. Bot.* 62, 2465–2483. doi: 10.1093/jxb/erq442

Islam, M. S., Jalaluddin, M., Garner, J. O., Yoshimoto, M., and Yamakawa, O. (2005). Artificial shading and temperature influence on anthocyanin compositions in sweetpotato leaves. *HortScience* 40, 176–180. doi: 10.21273/HORTSCI.40.1.176

Jin, X., Huang, H., Wang, L., Sun, Y., and Dai, S. (2016). Transcriptomics and metabolite analysis reveals the molecular mechanism of anthocyanin biosynthesis branch pathway in different Senecio cruentus cultivars. *Front. Plant Sci.* 7, 1307. doi: 10.3389/fpls.2016.01307

Kotak, S., Larkindale, J., Lee, U., von Koskull-Döring, P., Vierling, E., and Scharf, K.-D. (2007). Complexity of the heat stress response in plants. *Curr. Opin. Plant Biol.* 10, 310–316. doi: 10.1016/j.pbi.2007.04.011

Kumar, R. R., Arora, K., Goswami, S., Sakhare, A., Singh, B., Chinnusamy, V., et al. (2020). MAPK enzymes: a ROS activated signaling sensors involved in modulating heat stress response, tolerance and grain stability of wheat under heat stress. *3 Biotech* 10, 1–11. doi: 10.1007/s13205-020-02377-0

Kwon, Y., Oh, J. E., Noh, H., Hong, S.-W., Bhoo, S. H., and Lee, H. (2011). The ethylene signaling pathway has a negative impact on sucrose-induced anthocyanin accumulation in arabidopsis. *J. Plant Res.* 124, 193–200. doi: 10.1007/s10265-010-0354-1

Li, C., Wang, Y., Xu, L., Nie, S., Chen, Y., Liang, D., et al. (2016). Genome-wide characterization of the MADS-box gene family in radish (*Raphanus sativus L.*) and assessment of its roles in flowering and floral organogenesis. *Front. Plant Sci.* 7, 1390. doi: 10.3389/fpls.2016.01390

Li, L., Ye, J., Li, H., and Shi, Q. (2020). Characterization of metabolites and transcripts involved in flower pigmentation in primula vulgaris. *Front. Plant Sci.* 11, 572517. doi: 10.3389/fpls.2020.572517

Lin-Wang, K., Micheletti, D., Palmer, J., Volz, R., Lozano, L., Espley, R., et al. (2011). High temperature reduces apple fruit colour via modulation of the anthocyanin regulatory complex. *Plant Cell Environ.* 34, 1176–1190. doi: 10.1111/j.1365-3040.2011.02316.x

Liu, H.T., Sun, D.Y., and Zhou, R.G. (2005). Ca2+ and AtCaM3 are involved in the expression of heat shock protein gene in arabidopsis. *Plant Cell Environ.* 28, 1276–1284. doi: 10.1111/j.1365-3040.2005.01365.x

Liu, W., Wang, Y., Sun, J., Jiang, H., Xu, H., Wang, N., et al. (2019). MdMYBDL1 employed by MdHY5 increases anthocyanin accumulation via repression of MdMYB16/308 in apple. *Plant Sci.* 283, 32–40.doi: 10.1016/j.plantsci.2019.01.016

Lu, W., Chen, J., Ren, X., Yuan, J., Han, X., Mao, L., et al. (2018). One novel strawberry MADS-box transcription factor FaMADS1a acts as a negative regulator in fruit ripening. *Sci. Hortic.* 227, 124–131. doi: 10.1016/j.scienta.2017.09.042

Luo, C., Xiao, G., and Li, Q. (2015). Research advance of the transcription factors related to stress resistances in rice. *Guangxi Zhiwu/Guihaia* 35, 942–947.

Luo, Y., Xie, M., Zhang, C., Wang, W., Zhu, J., Wan, X., et al. (2018). Function analysis of rice zinc finger protein gene OsBBX22 in response to heat stress. *Genomics Appl Biol.* 37, 836–844. doi: 10.13417/j.gab.037.000836

Maier, A., Schrader, A., Kokkelink, L., Falke, C., Welter, B., Iniesto, E., et al. (2013). Light and the E3 ubiquitin ligase COP 1/SPA control the protein stability of the MYB transcription factors PAP 1 and PAP 2 involved in anthocyanin accumulation in arabidopsis. *Plant J.* 74, 638–651. doi: 10.1111/tpj.12153

Martindale, J. L., and Holbrook, N. J. (2002). Cellular response to oxidative stress: signaling for suicide and survival. *J. Cell. Physiol.* 192, 1–15. doi: 10.1002/jcp.10119

Matoušek, J., Vrba, L., Škopek, J., Orctová, L., Pešina, K., Heyerick, A., et al. (2006). Sequence analysis of a "true" chalcone synthase (chs _H1) oligofamily from hop (*Humulus lupulus L.*) and PAP1 activation of chs _H1 in heterologous systems. *J. Agric. Food Chem.* 54, 7606–7615. doi: 10.1021/jf06 1785g

Medina, E., Kim, S.-H., Yun, M., and Choi, W.-G. (2021). Recapitulation of the function and role of ROS generated in response to heat stress in plants. *Plants* 10, 371. doi: 10.3390/plants10020371

Mishra, S. K., Tripp, J., Winkelhaus, S., Tschiersch, B., Theres, K., Nover, L., et al. (2002). In the complex family of heat stress transcription factors, HsfA1 has a unique role as master regulator of thermotolerance in tomato. *Genes Dev.* 16, 1555–1567. doi: 10.1101/gad.228802

Nabavi, S. M., Šamec, D., Tomczyk, M., Milella, L., Russo, D., Habtemariam, S., et al. (2020). Flavonoid biosynthetic pathways in plants: Versatile targets for metabolic engineering. *Biotechnol. Adv.* 38, 107316. doi: 10.1016/j.biotechadv.2018.11.005

Nagar, S., Singh, V., Arora, A., Dhakar, R., and Ramakrishnan, S. (2015). Assessment of terminal heat tolerance ability of wheat genotypes based on physiological traits using multivariate analysis. *Acta physiologiae plantarum* 37, 1–9. doi: 10.1007/s11738-015-2017-2

Ni, J., Bai, S., Zhao, Y., Qian, M., Tao, R., Yin, L., et al. (2019). Ethylene response factors Pp4ERF24 and Pp12ERF96 regulate blue light-induced anthocyanin biosynthesis in 'Red Zaosu'pear fruits by interacting with MYB114. *Plant Mol. Biol.* 99, 67–78. doi: 10.1007/s11103-018-0802-1

Niu, J., Zhang, G., Zhang, W., Goltsev, V., Sun, S., Wang, J., et al. (2017). Anthocyanin concentration depends on the counterbalance between its synthesis and degradation in plum fruit at high temperature. *Sci. Rep.* 7, 1–16. doi: 10.1038/s41598-017-07896-0

Noda, N., Yoshioka, S., Kishimoto, S., Nakayama, M., Douzono, M., Tanaka, Y., et al. (2017). Generation of blue chrysanthemums by anthocyanin B-ring hydroxylation and glucosylation and its coloration mechanism. *Sci. Adv.* 3, 7. doi: 10.1126/sciadv.1602785

Nozaki, K., and Fukai, S. (2008). Effects of high temperature on floral development and flowering in spray chrysanthemum. *J. Appl. Hortic.* 10, 8–14. doi: 10.37855/jah.2008.v10i01.02

Ohama, N., Sato, H., Shinozaki, K., and Yamaguchi-Shinozaki, K. (2017). Transcriptional regulatory network of plant heat stress response. *Trends Plant Sci.* 22, 53–65. doi: 10.1016/j.tplants.2016.08.015

Onik, J. C., Hu, X., Lin, Q., and Wang, Z. (2018). Comparative transcriptomic profiling to understand pre-and post-ripening hormonal regulations and anthocyanin biosynthesis in early ripening apple fruit. *Molecules* 23, 1908. doi: 10.3390/molecules23081908

Oren-Shamir, M. (2009). Does anthocyanin degradation play a significant role in determining pigment concentration in plants? *Plant Sci.* 177, 310–316. doi: 10.1016/j.plantsci.2009.06.015

Ortiz, C., and Cardemil, L. (2001). Heat-shock responses in two leguminous plants: A comparative study. *J. Expt. Bot.* 52, 1711–1719. doi: 10.1093/jxb/52.361.1711

Petroni, K., and Tonelli, C. (2011). Recent advances on the regulation of anthocyanin synthesis in reproductive organs. *Plant Sci.* 181, 219–229. doi: 10.1016/j.plantsci.2011.05.009

Qi, F., Liu, Y., Luo, Y., Cui, Y., Lu, C., Li, H., et al. (2022). Functional analysis of the ScAG and ScAGL11 MADS-box transcription factors for anthocyanin biosynthesis and bicolour pattern formation in senecio cruentus ray florets. *Hortic. Res.* 9, uhac071. doi: 10.1093/hr/uhac071

Qi, X., Liu, C., Song, L., and Li, M. (2020). PaMADS7, a MADS-box transcription factor, regulates sweet cherry fruit ripening and softening. *Plant Sci.* 301, 110634. doi: 10.1016/j.plantsci.2020.110634

Qiu, J. (2018). Evaluation of character stability of spray cut chrysanthemum under temperature stress. Nanjing Agricultural University.

Qu, A.-L., Ding, Y.-F., Jiang, Q., and Zhu, C. (2013). Molecular mechanisms of the plant heat stress response. *Biochem. Biophys. Res. Commun.* 432, 203–207. doi: 10.1016/j.bbrc.2013.01.104

Quattrocchio, F., Verweij, W., Kroon, A., Spelt, C., Mol, J., and Koes, R. (2006). PH4 of Petunia is an R2R3 MYB protein that activates vacuolar acidification through interactions with basic-helix-loop-helix transcription factors of the anthocyanin pathway. *Plant Cell* 18, 1274–1291. doi: 10.1105/tpc.105.034041

Rai, K. K., Pandey, N., and Rai, S. P. (2020). Salicylic acid and nitric oxide signaling in plant heat stress. *Physiol. Plant.* 168, 241–255. doi: 10.1111/ppl.12958

Shi, Q., Zhou, L., Wang, Y., Li, K., Zheng, B., and Miao, K. (2015). Transcriptomic analysis of Paeonia delavayi wild population flowers to identify differentially expressed genes involved in purple-red and yellow petal pigmentation. *PLoS ONE* 10, e0135038. doi: 10.1371/journal.pone.0135038

Song, A., Zhu, X., Chen, F., Gao, H., Jiang, J., and Chen, S. (2014). A chrysanthemum heat shock protein confers tolerance to abiotic stress. *Int. J. Mol. Sci.* 15, 5063–5078. doi: 10.3390/ijms15035063

Sun, L., Fan, X., Zhang, Y., Jiang, J., Sun, H., and Liu, C. (2016). Transcriptome analysis of genes involved in anthocyanins biosynthesis and transport in berries of black and white spine grapes (Vitis davidii). *Hereditas* 153, 1–22. doi: 10.1186/s41065-016-0021-1

Tsan, M.-F., and Gao, B. (2004). Heat shock protein and innate immunity. *Cell. Mol. Immunol.* 1, 274–279.

Tunc-Ozdemir, M., Tang, C., Ishka, M. R., Brown, E., Groves, N. R., Myers, C. T., et al. (2013). A cyclic nucleotide-gated channel (CNGC16) in pollen is critical for stress tolerance in pollen reproductive development. *Plant Physiol.* 161, 1010–1020. doi: 10.1104/pp.112.206888

Ubi, B. E., Honda, C., Bessho, H., Kondo, S., Wada, M., Kobayashi, S., et al. (2006). Expression analysis of anthocyanin biosynthetic genes in apple skin: effect of UV-B and temperature. *Plant Sci.* 170, 571–578. doi: 10.1016/j.plantsci.2005.10.009

Usman, M. G., Rafii, M. Y., Ismail, M. R., Malek, M. A., and Latif, M. A. (2015). Expression of target gene Hsp70 and membrane stability determine heat tolerance in chili pepper. *J. Am. Soc. Hortic. Sci.* 140, 144–150. doi: 10.21273/JASHS.140.2.144

Usman, M. G., Rafii, M. Y., Martini, M. Y., Yusuff, O. A., Ismail, M. R., and Miah, G. (2017). Molecular analysis of Hsp70 mechanisms in plants and their function in response to stress. *Biotechnol. Genet. Eng. Rev.* 33, 26–39. doi: 10.1080/02648725.2017.1340546

Van Der Ploeg, A., and Heuvelink, E. (2015). The influence of temperature on growth and development of chrysanthemum cultivars. *J. Hortic. Sci. Biotechnol.* 81, 174–182. doi: 10.1080/14620316.2006.11512047

Verweij, W., Spelt, C. E., Bliek, M., de Vries, M., Wit, N., Faraco, M., et al. (2016). Functionally similar WRKY proteins regulate vacuolar acidification in petunia and hair development in Arabidopsis. *Plant Cell* 28, 786–803. doi: 10.1105/tpc.15.00608

Wang, L., Guo, Y., Jia, L., Chu, H., Zhou, S., Chen, K., et al. (2014). Hydrogen peroxide acts upstream of nitric oxide in the heat shock pathway in arabidopsis seedlings. *Plant Physiol.* 164, 2184–2196. doi: 10.1104/pp.113.229369

Whitley, D., Goldberg, S. P., and Jordan, W. D. (1999). Heat shock proteins: a review of the molecular chaperones. *J. Vasc. Surg.* 29, 748–751. doi: 10.1016/S0741-5214(99)70329-0

Willits, M. G., Kramer, C. M., Prata, R. T., De Luca, V., Potter, B. G., Steffens, J. C., et al. (2005). Utilization of the genetic resources of wild species to create a nontransgenic high flavonoid tomato. *J. Agric. Food Chem.* 53, 1231–1236. doi: 10.1021/jf049355i

Winkel-Shirley, B. (2002). Molecular genetics and control of anthocyanin expression. 37, 75–94. doi: 10.1016/S0065-2296(02)37044-7

Xu, W., Dubos, C., and Lepiniec, L. (2015). Transcriptional control of flavonoid biosynthesis by MYB–bHLH–WDR complexes. *Trends Plant Sci.* 20, 176–185. doi: 10.1016/j.tplants.2014.12.001

Yamagishi, M., Shimoyamada, Y., Nakatsuka, T., and Masuda, K. (2010). Two R2R3-MYB genes, homologs of petunia AN2, regulate anthocyanin biosyntheses in flower tepals, tepal spots and leaves of Asiatic hybrid lily. *Plant Cell Physiol.* 51, 463–474. doi: 10.1093/pcp/pcq011

Yang, W., Sun, Y., Chen, S., Jiang, J., Chen, F., Fang, W., et al. (2011). The effect of exogenously applied nitric oxide on photosynthesis and antioxidant activity in heat stressed chrysanthemum. *Biol. Plant.* 55, 737–740. doi: 10.1007/s10535-011-0178-4

Ye, S., Yu, S., Shu, L., Wu, J., Wu, A., and Luo, L. (2012). Expression profile analysis of 9 heat shock protein genes throughout the life cycle and under abiotic stress in rice. *Chin. Sci. Bull.* 57, 336–343. doi: 10.1007/s11434-011-4863-7

Zhang, F., Gonzalez, A., Zhao, M., Payne, C. T., and Lloyd, A. (2003). A network of redundant bHLH proteins functions in all TTG1-dependent pathways of Arabidopsis. *Development.* 130, 4859–69. doi: 10.1242/dev.00681

Zhang, H., He, H., Wang, X., Wang, X., Yang, X., Li, L., et al. (2011). Genome-wide mapping of the HY5-mediated genenetworks in Arabidopsis that involve both transcriptional and post-transcriptional regulation. *Plant J.* 65, 346–358. doi: 10.1111/j.1365-313X.2010.04426.x

Zhang, J., Liu, B., Li, J., Zhang, L., Wang, Y., Zheng, H., et al. (2015). Hsf and Hsp gene families in Populus: genome-wide identification, organization and correlated expression during development and in stress responses. *BMC Genom.* 16, 1–19. doi: 10.1186/s12864-015-1398-3

Zhang, L., Wang, L., Zeng, X., Chen, R., Yang, S., and Pan, S. (2019). Comparative transcriptome analysis reveals fruit discoloration mechanisms in postharvest strawberries in response to high ambient temperature. *Food Chemistry: X.* 2, 100025. doi: 10.1016/j.fochx.2019.100025

Zhang, Y., Butelli, E., and Martin, C. (2014). Engineering anthocyanin biosynthesis in plants. *Curr. Opin. Plant Biol.* 19, 81–90. doi: 10.1016/j.pbi.2014.05.011

Zhang, Y., Chu, G., Hu, Z., Gao, Q., Cui, B., Tian, S., et al. (2016). Genetically engineered anthocyanin pathway for high health-promoting pigment production in eggplant. *Mol. Breeding* 36, 1–14. doi: 10.1007/s11032-016-0454-2

Zhao, D., Tao, J., Han, C., and Ge, J. (2012). Flower color diversity revealed by differential expression of flavonoid biosynthetic genes and flavonoid accumulation in herbaceous peony (*Paeonia lactiflora Pall.*). *Mol. Biol. Rep.* 39, 11263–11275. doi: 10.1007/s11033-012-2036-7

Zhou, L.-J., Geng, Z., Wang, Y., Wang, Y., Liu, S., Chen, C., et al. (2021). A novel transcription factor CmMYB012 inhibits flavone and anthocyanin biosynthesis in response to high temperatures in chrysanthemum. *Horticulture Res.* 8, 248. doi: 10.1038/s41438-021-00675-z

Zhu, T., Fonseca De Lima, C. F., and De Smet, I. (2021). The heat is on: how crop growth, development, and yield respond to high temperature. *J. Exp. Bot.* 72, 7359–7373. doi: 10.1093/jxb/erab308

Zimmermann, I. M., Heim, M. A., Weisshaar, B., and Uhrig, J. F. (2004). Comprehensive identification of arabidopsis thaliana MYB transcription factors interacting with R/B-like BHLH proteins. *Plant J.* 40, 22–34. doi: 10.1111/j.1365-313X.2004.02183.x

frontiers | Frontiers in Plant Science

TYPE Original Research
PUBLISHED 23 September 2022
DOI 10.3389/fpls.2022.1009206

OPEN ACCESS

EDITED BY
Byoung Ryong Jeong,
Gyeongsang National University,
South Korea

REVIEWED BY
Rodrigo R. Amadeu,
Bayer Crop Science, United States
Zhiqiang Xia,
Chinese Academy of Tropical
Agricultural Sciences, China
Qibin Yu,
University of Florida, United States

*CORRESPONDENCE
Ezio Portis
ezio.portis@unito.it

SPECIALTY SECTION
This article was submitted to
Plant Breeding,
a section of the journal
Frontiers in Plant Science

RECEIVED 01 August 2022
ACCEPTED 02 September 2022
PUBLISHED 23 September 2022

CITATION
Martina M, Acquadro A, Gulino D,
Brusco F, Rabaglio M, Portis E and
Lanteri S (2022) First genetic maps
development and QTL mining in
Ranunculus asiaticus L.
through ddRADseq.
Front. Plant Sci. 13:1009206.
doi: 10.3389/fpls.2022.1009206

First genetic maps development and QTL mining in *Ranunculus asiaticus* L. through ddRADseq

Matteo Martina[1], Alberto Acquadro[1], Davide Gulino[1], Fabio Brusco[2], Mario Rabaglio[2], Ezio Portis[1]* and Sergio Lanteri[1]

[1]Dipartimento di Scienze Agrarie, Forestali e Alimentari (DISAFA), Plant Genetics and Breeding, University of Torino, Grugliasco, Italy, [2]Biancheri Creazioni, Camporosso, Italy

Persian Buttercup (*Ranunculus asiaticus* L.; 2x=2n=16; estimated genome size: 7.6Gb) is an ornamental and perennial crop native of Asia Minor and Mediterranean basin, marketed both as cut flower or potted plant. Currently new varieties are developed by selecting plants carrying desirable traits in segregating progenies obtained by controlled mating, which are propagated through rhizomes or micro-propagated *in vitro*. In order to escalate selection efficiency and respond to market requests, more knowledge of buttercup genetics would facilitate the identification of markers associated with loci and genes controlling key ornamental traits, opening the way for molecular assisted breeding programs. Reduced-representation sequencing (RRS) represents a powerful tool for plant genotyping, especially in case of large genomes such as the one of buttercup, and have been applied for the development of high-density genetic maps in several species. We report on the development of the first molecular-genetic maps in *R. asiaticus* based on of a two-way pseudo-testcross strategy. A double digest restriction-site associated DNA (ddRAD) approach was applied for genotyping two F_1 mapping populations, whose female parents were a genotype of a so called 'ponpon' and of a 'double flower' varieties, while the common male parental ('Cipro') was a genotype producing a simple flower. The ddRAD generated a total of ~2Gb demultiplexed reads, resulting in an average of 8,3M reads per line. The *sstacks* pipeline was applied for the construction of a mock reference genome based on sequencing data, and SNP markers segregating in only one of the parents were retained for map construction by treating the F_1 population as a backcross. The four parental maps (two of the female parents and two of the common male parent) were aligned with 106 common markers and 8 linkage groups were identified, corresponding to the haploid chromosome number of the species. An average of 586 markers were associated with each parental map, with a marker density ranging from 1 marker/cM to 4.4 markers/cM. The developed maps were used for QTL analysis for flower color, leading to the identification of major QTLs for purple pigmentation. These results contribute to dissect on

the genetics of Persian buttercup, enabling the development of new approaches for future varietal development.

KEYWORDS

ornamentals, ddRADseq, linkage maps, genetic markers, anthocyanins, QTLs

Introduction

Persian Buttercup (*Ranunculus asiaticus* L.; 2x=2n=16; estimated genome size: 7.6Gb - Goepfert, 1974) is an outcrossing ornamental and perennial crop native of Iran, Turkey and Greece. The species is marketed both as cut flowers and potted plant (De Hertogh, 1996). As reported by Berruto et al. (2019), Ranunculus counted for the 0,4% of the total turnover of cut flowers and foliage, with the highest production in Italy (132 million of stem) and 300-350 ha of cultivated surface. Due to its high level of heterozygosity and self-incompatibility, the crossing of selected genotypes originates highly segregant progenies. The development of new varieties is based on the selection within the progenies of plants carrying traits of interested, which are propagated through rhizomes or micro-propagated *in vitro* from meristematic apexes (Beruto et al., 2018). In order to escalate breeding efficiency and respond to market demand, some more knowledge of buttercup genetics is needed in order to enable the development of molecular breeding approaches.

High throughput DNA sequencing methodology (next generation sequencing; NGS) has rapidly evolved over the past 20 years (Slatko et al., 2018), and novel sequencing-associated protocols allow the access to thousands of genomic regions across the genome (Barchi et al., 2012; Víquez-Zamora et al., 2013; Scaglione et al., 2016; Vukosavljev et al., 2016; van Geest et al., 2017). The reduced-representation sequencing (RRS) represents one of most powerful tools for plant genotyping, especially in case of large genomes such as the one *R. asiaticus*. Indeed, RRS has been applied in the development of high-density genetic maps in many species (Acquadro et al., 2017; Feng et al., 2018; Jin et al., 2019; Song et al., 2020; Toppino et al., 2020; Wang et al., 2020; Valentini et al., 2021).

Here we report on the application of a double digest restriction-site associated DNA (ddRAD) approach for genotyping two F_1 mapping populations and on development of the first molecular-genetic maps in *R. asiaticus*. The strategy adopted was the two-way pseudo-testcross, previously exploited in a number of out-breeding species (Acquadro et al., 2009; Wu et al., 2010; Portis et al., 2012; Gartner et al., 2013; Torello Marinoni et al., 2018; Mariotti et al., 2020; Wang et al., 2022). The two F1 mapping populations shared a common male parental line, and four parental maps were developed (two of the female parents and two of the common male parent), then aligned on the basis of common SNPs markers. The resulting consensus map included eight linkage groups, corresponding to the haploid chromosome number of the species, and represents a background for future mapping of genes and QTLs and application of marker assisted breeding in the species. Besides, we performed QTL analysis for flower color, identifying a major locus affecting flower purple pigmentation.

Materials and methods

Mapping populations and DNA extraction

Two F_1 segregating populations were obtained by crossing the male parental genotype 'Cipro', producing white flowers with one row of petals typical of the wild-type (called 'single' flowers), with two female parental genotypes, of which one producing violet-greenish flowers with wavy margin (called 'pon pon' flowers) and one producing violet flowers with multiple rows of petals (called 'double' flowers). The progenies were respectively named PON-PON and DOUBLE (Figure 1A).

The parental genotypes were selected by Biancheri Creazioni (IM, Italy). The two F_1 progenies included 129 and 103 plants for the PON-PON and DOUBLE population respectively, and were grown in a green-house located in Camporosso (43.794, 7.632, IM – Italy) for two seasons (2020 and 2021), adopting the cultivation techniques in use for commercial production. In 2020 plants originated from seeds, while in the 2021 were vegetatively propagated through rhizomes obtained at the end of the first season. Genomic DNA was extracted from frozen leaves with the Plant DNA Kit (E.Z.N.A.®) following the manufacturer's instructions. DNA quality was assessed through the NanoDrop™ 2000 spectrophotometer, and the Qubit® 2.0 Fluorometer was used for DNA quantification.

ddRAD-seq library preparation and sequencing

The ddRAD (double digest restriction-site associated DNA) libraries were produced using a custom protocol with minor

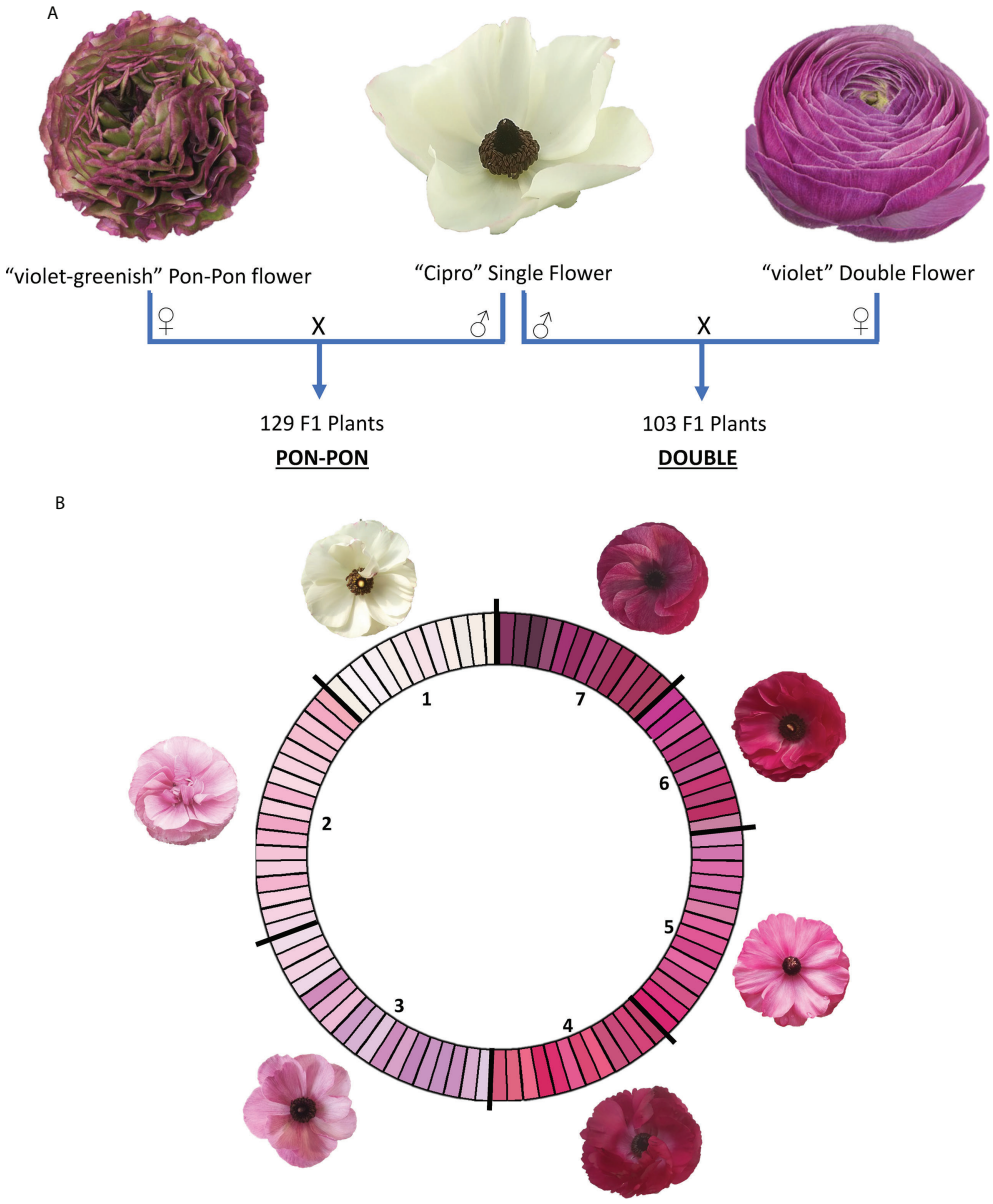

FIGURE 1
(A) Crossing scheme for the development of the two mapping populations (PON-PON and DOUBLE); **(B)** RHS-based color scale used for flower phenotyping. RHS classes were coded according to their intensity in 1-7 scale. 1: white; 2: light blue pink; 3: light violet; 4: medium purple red; 5: dark blue pink; 6: medium purple; 7: dark purple.

modifications proposed by Peterson et al. (2012). Enzyme combination was selected by *in silico* analyzing the draft genome of the related species *Anemone coronaria* L. (Martina et al., 2022), with the aim of selecting a combination predicted to produce ~30k fragments across the provided genome. After fluorometric quantification, the genomic DNA was normalized for uniforming its concentration and 375ng (10ul, ~37ng/ul) were double digested with 2.4U of both *PstI* and *EcoRI* endonucleases (New England BioLabs) in 30μL reaction, supplemented with CutSmart Buffer and incubated at 37°C for 90', followed by 20' at 65°C'. Fragmented DNA was purified with 1.5 volumes of AMPureXP beads (Agencourt) and then ligated with 200U of T4 DNA ligase (New England BioLabs) to 2.5pmol of overhang barcoded adapter for rare cut sites and to 5pmol of overhang barcoded adapter for frequent cut sites. Reactions were performed in 50μL volume at 23°C for 60' and at 20°C for 60', followed by 20' at 65°C. Samples were then pooled on multiplexing batches and bead purified as above. For each

pool, targeted fragments distribution was collected on the BluePippin instrument (Sage Science Inc.), setting the range of 380 bp – 500 bp. Gel eluted fraction was then PCR amplified with indexed primers using Phusion High-Fidelity PCR Master Mix (New England BioLabs) in a final volume of 50µL, and subjected to the following thermal protocol: [95°C, 3'] - [95°C, 30" - 60°C, 30" - 72°C, 45"] x 12 cycles - [72°C, 2']. Products were purified with 1 volume of AMPureXP beads. The resulting libraries were checked with both Qubit 2.0 Fluorometer (Invitrogen, Carlsbad, CA) and Bioanalyzer DNA assay (Agilent technologies, Santa Clara, CA). Libraries were then PE sequenced with 150 cycles on NovaSeq 6000 instrument following the manufacturer's instructions (Illumina, San Diego, CA). A low coverage sequencing and a draft assembly of the male parent ('Cipro') was obtained as reference for investigating data obtained with ddRADseq.

Sequence analysis and linkage maps development

Raw reads were demultiplexed using the *process_radtags* pipeline included in Stacks v2.53 (Catchen et al., 2013). Assembly of the short-reads of each sample into matching stacks was performed using the *ustacks* utility included in Stacks v2.53. A set of consensus loci from all the analyzed samples (catalog) was identified by the *cstacks* pipeline, and each sample was matched against the catalog using *sstack* and *tsv2bam* utilities. Sequences for each genotype were mapped to the catalog file using the Burrows-Wheeler Aligner (BWA, v0.7.17) program and the 'mem' command with the default parameters (Li and Durbin, 2009). BAM files were processed and used for SNP calling using *Samtools mpileup* (v1.6 - Danecek et al., 2021) with default parameters except for the minimum mapping quality (Q = 20). Markers were named according to the catalog sequence in which they were identified. Each name starts with an S, followed by the catalog sequence number and the position of the SNP in the sequence (i.e *S0004445_269*).

Independent framework linkage maps were constructed for each parent (male and female) from each progeny-based dataset (PON-PON and DOUBLE), using the double pseudo-testcross mapping strategy (Plomion and Durel, 1996) and JoinMap v4.0 (Van Ooijen, 2006). Four separate datasets were assembled: (i) 'Violet-greenish' - 'PP -'; (ii) Cipro I - 'C-I' -; (iii) 'Violet' - 'Db' - and (iv) Cipro II - 'C-II'. Only SNP markers in testcross configuration (expected segregation ratio of 1:1) were included in the datasets: maternal testcross markers segregating only in 'PP' or 'Db', and paternal testcross markers segregating only in 'C-I' or 'C-II'.

Genotyping data were quality filtered by removing not segregating markers, markers with >20% missing values, and skewed markers. The similarity of the loci option of JoinMap was used to identify perfectly identical markers (similarity value = 1.000), expected to map to exactly the same position. To reduce the load of calculation effort, only one representative of each group of identical loci was used for mapping. Goodness-of-fit between observed and expected segregation ratios was assessed using the χ^2 test. Markers fitting a Mendelian pattern closely associated with a χ^2 value χ^2 α = 0.1 or with only a minor deviation (χ^2 α = 0.1< χ^2 χ^2 α = 0.01) were used for map construction, provided that their inclusion did not alter the local marker order. Loci suffering from significant segregation distortion ($\chi^2 > \chi^2$ α = 0.01) were excluded.

For all maps, LGs were established based on a threshold logarithm of odds (LOD) ratio >4. To determine marker order within a linkage group (LG), the JoinMap parameters were set at Rec = 0.40, LOD = 1.0 and Jump = 5. Map distances were converted to centiMorgans (cM) using the Kosambi mapping function (Kosambi, 1943). Linkage maps were drawn using MapChart 2.2 software (Voorrips, 2002), and markers deviating in their segregation only marginally from the expected Mendelian ratio are presented with one (χ^2 α = 0.1 < χ^2 χ^2 α = 0.05) or two (χ^2 α = 0.05 < χ^2 χ^2 α = 0.01) asterisks. LG of the female and male maps were respectively named PP_01 to PP_08 and CI_01 to CI_08 for the ones present in the PON-PON dataset, and Db_01 to Db_08 and CII_01 to CII_08 for the ones present in the DOUBLE dataset (Supplemental Figure 1 and Supplemental Table 1).

Flower color assessment

The first blooming flower of market quality of each genotype was phenotyped in both seasons (2020 and 2021), as representative of the genetic potential of each individual. The main color of the internal (Main Interior Color - MiC) and external (Main Exterior Color - MeC) layer of the petals were scored following RHS classification (Figure 1B).

Statistical analyses and QTL detection

Statistical analyses were performed with R software (Team, 2016). A conventional analysis of variance was applied to estimate genotype and environment effects based on the linear model Yij = µ + gi + bj + eij, where µ, g, b and e represent the mean, the genotypic effect, the block effect and the error respectively. Correlations between traits were estimated using the Spearman coefficient, and normality, kurtosis and skewness were assessed with the Shapiro–Wilks test (α = 0.05). QTL detection was performed by considering each season independently and was based on the newly developed map using MQM mapping, as implemented in MapQTL v5 software (Van Ooijen, 2004). QTLs were initially identified using interval mapping. LOD thresholds for declaring a QTL to be significant at the 5% genome-wide probability level were

established empirically by applying 1000 permutations per trait (Doerge and Churchill, 1996). After permutation analysis, linked marker per putative QTL was treated as a co-factor in the approximate multiple QTL model. Co-factor selection and MQM analysis were repeated until no new QTL could be identified. Additive effect, as well as the percentage of the phenotypic variation (PVE) explained by each QTL, were obtained from the final multiple QTL model. Individual QTLs were prefixed by the parental line abbreviation ('PP', 'C-I', 'C-II', or 'Db'), followed by a trait abbreviation, the relevant chromosome designation, while the season was followed by a letter when there were more than one QTL for the season. Confidence interval of the QTL was calculated by considering 0.5Mb upstream and downstream the marker identified at the QTL.

Results and discussion

Sequencing and linkage map construction

The ddRAD approach generated a total of ~2Gb demultiplexed reads, and an average of 8,3M reads per genotype (detailed info about the raw data per individual can be found in Supplemental Table 1). Cleaned reads with quality scores >30 were mapped against the catalog obtained through the *stacks* pipeline (see Materials and Methods). Before filtering, ~578k polimorphisms where identified. However, after filtering at DP>15, this number was lowered to ~22k SNPs and 790 indels. Only markers heterozygous in a single parent were retained for map construction, by treating the F1 population as a backcross. For each of the parental lines, skewed markers, showing highly significant distortion from the expected 1:1 ratio, or markers with identical segregation patterns were excluded from further map construction steps (Supplemental Table 1).

Overall, 3,376 single nucleotide polymorphisms (SNPs) were identified as segregating in the PONPON population, of which 1,607 and 1,769 were used as input in JoinMap for the development of Cipro (C-I) and PonPon (PP) maps, respectively. In C-I, 732 markers were excluded by the JoinMap pipeline being co-segregating (i.e. markers showing the same segregation pattern), leading to an overall number of 875 markers used for map construction. Analogously, in PP, 796 SNPs were co-segregating, while 973 were used for map construction. A further stringent selection was applied by considering only markers grouped at LOD >4, and a set of 568 SNPs in PP, and 556 in C-I were identified as suitable for map development. The generated PP map spanned 829 cM over 8 LGs (corresponding to the haploid chromosome number of the species) ranging from 80.5 to 130.7 cM, with a marker density between 1.1 and 3 cM, and 23 gaps bigger than 5 cM. The LG7 harbored the highest number of gaps (8), while only one gap was present in LG4. The C-I map spanned 1305.8 cM across 8 LGs, ranging between 123.7 and 201.4cM and with a marker density between 1.8 and 3 cM. In this map a higher number of gaps (>5 cM) was present (60), with LG3 and LG7 including 13 and 11 gaps respectively, and LG8 harboring the lower number of gaps (3). The LGs of the two maps were aligned on the basis of 35 common markers, as shown in Figure 2.

Overall, 4,098 SNPs were identified in the DOUBLE population, of which 2,344 and 1,754 segregating in Cipro (C-II) and Double (Db) maps respectively. In C-II, 1,211 co-segregating markers were discarded and 1,113 SNPs used for

TABLE 1 Statistics of the four linkage maps.

		LG 1	LG 2	LG 3	LG 4	LG 5	LG 6	LG 7	LG 8	Average	Total
PonPon (PP)	*Size*	112.0	130.7	97.4	113.4	102.9	80.5	110.8	82.2	103.7	829.8
	N° of markers	93	83	63	82	74	58	37	78	71	568
	Marker Density	1.2	1.6	1.5	1.4	1.4	1.4	3.0	1.1	1.6	
	Gaps (> 5cM)	3	3	4	1	2	2	8	0	3	23
Cipro I (C-I)	*Size*	199.1	201.4	189.5	173.6	156.1	123.7	147.8	114.6	163.2	1305.8
	N° of markers	102	75	64	72	74	55	49	65	70	556
	Marker Density	2.0	2.7	3.0	2.4	2.1	2.2	3.0	1.8	2.4	
	Gaps (> 5cM)	5	9	13	6	4	9	11	3	8	60
Cipro II (C-II)	*Size*	226.7	160.2	116.6	132.6	151.4	149.0	127.0	118.8	147.8	1182.2
	N° of markers	152	98	113	71	49	73	50	74	85	680
	Marker Density	1.5	1.6	1.0	1.9	3.1	2.0	2.5	1.6	1.9	
	Gaps (> 5cM)	6	4	3	3	9	6	9	2	5	42
Double (Db)	*Size*	169.1	145.6	102.5	161.4	151.1	106.9	105.4	117.6	132.5	1059.7
	N° of markers	68	33	65	112	68	74	46	74	68	540
	Marker Density	2.5	4.4	1.6	1.4	2.2	1.4	2.3	1.6	2.2	
	Gaps (> 5cM)	9	12	4	4	9	2	5	6	6	51

map construction. For Db, 919 SNPs were co-segregating, leading to 835 mappable markers. A further stringent selection was applied by considering only markers grouped at LOD >4, identifying 680 loci for C-II, and 540 for Db maps development. A genetic map with an overall dimension of 829 cM was generated for Db, identifying 8 LGs ranging from 102.5 and 169.1 cM with a marker density between 1.4 and 4.4, and 51 gaps bigger than 5 cM. The highest number of gaps (12) was scored on LG2, while only two gaps were present on LG6. The 8 LGs developed for the C-II map covered 1182.2 cM, ranging between 116.6 and 226.7 cM with a marker density between 1 and 3.1 cM. Forty-two gaps were identified across LGs, with LG5 and LG7 presenting 9 gaps, and LG8 harboring only 2 gaps. Each LGs of the two maps were aligned using 27 common markers, as shown in Figure 2 and Table 1.

The 8 LGs of the two maps of the male parental genotype (C-I and C-II) were aligned by means of 44 markers. Furthermore, the four maps were aligned on the basis of 106 common markers of which 7 markers were common across PP, C-I and C-II, while one was common among the four maps. A clustering of markers was observed in some LGs, and in most cases was located in the central part of a LG. This clustering might correspond to the centromeric regions (Keim et al., 1990; Reiter et al., 1992; Tanksley et al., 1992; Vallejos et al., 1992; Ott et al., 2011), in which a reduced recombination usually takes place (Vincenten et al., 2015; Zafar et al., 2017; Acquadro et al., 2020).

An average number of 586 markers was included in each parental map, with a marker density ranging from 1 marker/cM to 4.4 markers/cM. Assuming an expected genome size of 7.6Gb (Goepfert, 1974), the average mapping length of ~1093 cM was used for estimating the physical dimension of a cM, which corresponds to a physical distance of about 7Mb. The average LG dimension ranged from 829.8 cM (PP) to 1305.8 cM (C-I).Both the male parent maps (C-I and C-II) were larger than the

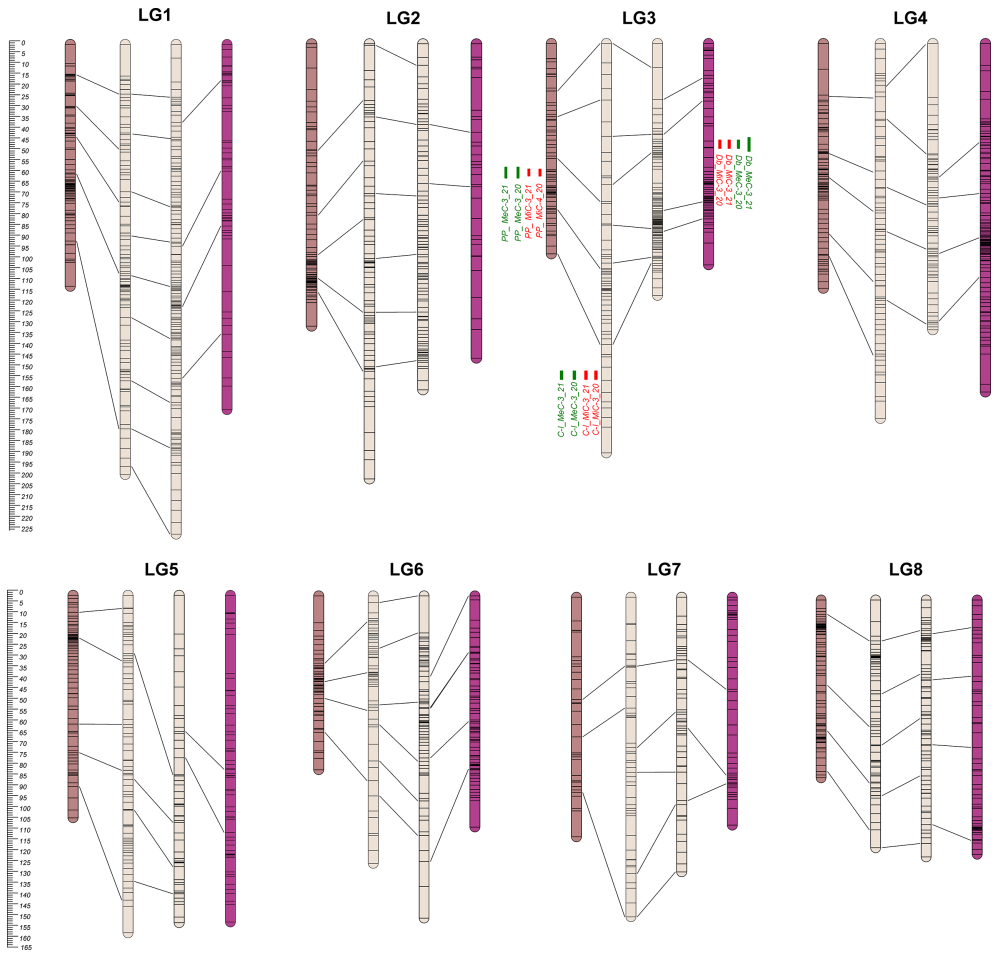

FIGURE 2
From the left to the right: PP, C-I, C-II, and Db Linkage Groups. Eight LGs (corresponding to the haploid chromosome number of the species) were identified within each parental map. C-I map was the bigger one, covering 1,305.8 cM, while the PP map was the smaller one with 829.8 cM (Table 1). QTL regions are reported as green (MeC) and red (MiC) bars on the right side of the associated LGs.

ones of the female parents (PP and Db). As previously reported (Lenormand and Dutheil, 2005), differences between paternal and maternal linkage maps could be associated with heterochiasmy (i.e., the presence of different crossover frequencies in male and female meiosis). Differential recombination rates between the sexes have been reported in several plant species, and attributed to processes such as sexually antagonistic selection acting on coding and regulatory genetic elements, female meiotic drive as well as selection during the haploid phase of the life cycle (Sardell and Kirkpatrick, 2020). The latter has been associated to the reproductive system (selfing or outcrossing) characterizing the species (Giraut et al., 2011; Mariotti et al., 2020), although even in closely related species sharing the same reproduction pattern, such as *Sinapis alba* (Nelson et al., 2013), *Brassica oleracea* (Kearsey et al., 1996) and *Brassica napus* (Kelly et al., 1997), contrasting results have been reported.

Phenotypic variation, traits correlation and QTL identification

Table 2 reports a summary of the phenotypic performance for main color of the internal (MiC) and external (MeC) layer of the petals in the parental genotypes and F1 population, together with skewness and kurtosis of the traits. The male parent 'Cipro' did not present anthocyanin content in both petal layers. Conversely, the 'Double' genotype produced violet flowers, and PonPon violet- greenish petals. While the MiC trait appears to be stable in the two seasons in the parental lines, MeC showed a certain level of variability in the PP parent. In the F1 populations transgressive segregation was observed in respect to both maternal parents, except for MeC in the DOUBLE population.

Significant inter-trait correlations were detected within and across growing seasons (Table 3), albeit detecting a certain level of variability introduced by the environment. The least correlated traits were *DB_MiC_20* and *DB_MeC_21* (+0.70), while the most highly correlated were *PP_MiC_21* and *PP_MeC_21* (+0.94).

In Season 2020, the plants originated from seeds were less vigorous in respect to plants originated from rhizomes in season 2021. The flower color was limitedly affected by the environment traits in the two seasons. However, in Season 2020 the PP population distribution appeared to be leptokurtic, while in the Season 2021 the distribution was platykurtic. Such differences did not appear in the DOUBLE population. Transgressive genotypes always deviate towards the more pigmented parent (PP and Db), with petals exceeding the parental lines in pigment accumulation. Furthermore, in some cases the petal color appeared to be not uniform and presented mottling, suggesting the involvement of regulatory elements and epigenetic mechanisms, as reported in literature (Koseki et al., 2005; Le Maitre et al., 2019; Wang et al., 2019; Zheng et al., 2021).

The genetic basis of variation in quantitative traits can traditionally be resolved by the QTL approach, which partitions the variation into distinct genomic regions defined by a linkage map (Paterson et al., 1988). One of the most important issues to determine is the stability of the trait and how stable the expression of the various loci is by repeating the phenotypic evaluation over time and/or space. QTL detection

TABLE 2 List of the traits analyzed and their code, means, standard deviations (SD), overall statistics, coefficients of variation (cv), and transgressive genotypes.

Population	**PON-PON**				**DOUBLE**			
Trait	*MiC_20*	*MiC_21*	*MeC_20*	*MeC_21*	*MiC_20*	*MiC_21*	*MeC_20*	*MeC_21*
Trait code	*PP_MiC_20*	*PP_MiC_21*	*PP_MeC_20*	*PP_MeC_21*	*Db_MiC_20*	*Db_MiC_21*	*Db_MeC_20*	*Db_MeC_21*
PP/Db mean	6	6	7	4	5	5	7	7
C mean	1	1	1	1	1	1	1	1
F1 mean	2.7	3.4	3.0	3.7	3.4	3.6	4.0	4.2
± SD	1.7	2.0	1.9	2.2	1.7	1.7	2.0	2.1
Cv	0.6	0.6	0.6	0.6	0.5	0.5	0.5	0.5
Shapiro-Wilks	0.80	0.80	0.80	0.78	0.85	0.85	0.79	0.77
Skewness	-1.13	-1.61	-1.41	-1.69	-0.18	-0.42	-0.53	-0.63
SE	0.43	0.43	0.43	0.43	0.24	0.24	0.24	0.24
Kurtosis	0.48	-0.11	0.19	-0.22	-1.20	-1.01	-1.32	-1.26
SE	0.22	0.21	0.22	0.21	0.48	0.47	0.48	0.47
Transgressive respect PP/Db	4	45	0	58	17	15	0	0
Transgressive respect C	0	0	0	0	0	0	0	0

Ponpon parent (PP) and double parent (Db) mean are reported, as well as the Cipro mean (C mean) and the average of the corresponding F1 population (F1 mean). F1 population's distribution histograms for the investigated traits can be found in in Supplemental Figure 2.

TABLE 3 Inter-trait Spearman correlations assessed in the mapping populations.

	PP_MiC_20	PP_MiC_21	PP_MeC_20	PP_MeC_21
PP_MiC_20	–			
PP_MiC_21	0.76	–		
PP_MeC_20	0.90	0.81	–	
PP_MeC_21	0.77	0.94	0.84	–
	Db_MiC_20	Db_MiC_21	Db_MeC_20	Db_MeC_21
Db_MiC_20	–			
Db_MiC_21	0.82	–		
Db_MeC_20	0.88	0.81	–	
Db_MeC_21	0.70	0.88	0.86	–

was performed considering each season independently and was based on the newly developed map using MQM mapping (see Materials and Methods). LOD score, percentage of variance explained (PVE), and confidence interval (CI) related to QTLs, are described in Table 3. QTL analyses on all traits and environments yielded a total of 12 major (PVE values >10), located on LG3 (see Figure 2 and Table 4). In both female parents (PP and Db), 8 major QTLs were located in the same scaffold (*S0004445)* for both MiC and MeC. On the other hand, QTLs were identified only in the male parental map from the PON-PON population (C-I), both for MiC and MeC. Our results highlight a very high correlation between the external (MeC) and internal (MiC) pigmentation of the flower (Table 3), suggesting that the same genomic regions affect both traits. Thus, MiC and MeC appear to be controlled by common major QTLs located on LG3, justifying a PVE ranging from 31.7 to 84%, with a LOD ranging from 11.23 to 50.6.

To the best of our knowledge, this is the first report on QTLs detection in Persian buttercup. The identified QTLsshould be further on investigated and, once validated on a large collection of breeding material, the developed molecular markers might be applied for molecular assisted breeding.

Conclusions

Genome size varies greatly across the flowering plants and has played an important role in shaping their evolution. *Ranunculus asiaticus* harbors a very large genome size of about 7Gb.Mainly as a consequence of its large genome size, the development of genomic tools in the species has been to date very limited. We have applied for the first time in Persian buttercup, a reduced -representation sequencing (RRS) approach with the goal to develop its first genetic maps. Based on the two-way pseudo test cross strategy in two F1 populations, sharing the same male parent, we constructed maps which were used for positioning the first QTLs affecting the flower anthocyanin pigmentation. Our results lay the foundations for

TABLE 4 QTL detected in the mapping population.

Map	Trait	Year	Name	Group	Pos.	Locus	LOD	CI	PVE	Add.	GW
PP	MiC	20	*PP_MiC-3_20*	LG3	60.8	S0004445_269	21.74	58.8-61.3	48.3	2.5	18
		21	*PP_MiC-3_21*	LG3	60.8	S0004445_269	38.66	58.8-61.3	67.4	3.4	23
	MeC	20	*PP_MeC-3_20*	LG3	60.8	S0004445_269	29.2	58.8-61.3	49.4	2.7	19.4
		21	*PP_MeC-3_21*	LG3	60.8	S0004445_269	46.1	58.8-61.3	71.9	3.9	25.8
C-I	MiC	20	*C-I_MiC-3_20*	LG3	155.9	S0038600_63	23.32	155.38-156.38	57.9	-2.7	18
		21	*C-I_MiC-3_21*	LG3	155.9	S0038600_63	43.45	155.38-156.38	79.3	-3.7	23.1
	MeC	20	*C-I_MeC-3_20*	LG3	155.9	S0038600_63	28.81	155.38-156.38	65.7	-3.1	19.6
		21	*C-I_MeC-3_21*	LG3	155.9	S0038600_63	50.6	155.38-156.38	84	-4.1	26
Db	MiC	20	*Db_MiC-3_20*	LG3	48.3	S0004445_68	11.23	47.565-48.796	31.7	-2.0	9.3
		21	*Db_MiC-3_21*	LG3	48.3	S0004445_68	15.62	47.565-48.796	45.1	-2.4	10.1
	MeC	20	*Db_MeC-3_20*	LG3	48.3	S0004445_68	22.37	47.565-48.796	59	-3.2	14.8
		21	*Db_MeC-3_21*	LG3	48.3	S0004445_68	21.41	47.565-48.796	58.9	-3.3	18.7

For each trait the location (LG and position), the associated marker, the LOD, confidence interval (CI), percentage of explained variation (PVE), additive effect (Add.), and the genome-wide thresholds (GW) at p = 0.05 (as determined from 1000 permutations) are indicated.

future genetic and genomic studies and provide a framework for implementing more targeted breeding programs in *R. asiaticus*.

Data availability statement

Sequencing data used in this study are openly available in the NCBI database (PRJNA876570 - https://www.ncbi.nlm.nih.gov/bioproject/PRJNA876570).

Author contributions

Conceptualization: SL, EP, AA MR, FB and MM; methodology: SL, EP, AA MR, and MM; software: AA, EP and MM; validation, MM, DG and EP; formal analysis: MM, DG and EP and AA; investigation: EP, MM, AA; resources: MR, FB, and DG; data curation: MM and EP; writing—original draft preparation: MM, AA, and EP; writing—review and editing: SL; visualization: MR, FB, and DG; supervision, EP and SL. All authors have read and agreed to the published version of the manuscript.

Funding

This research was partially funded by Biancheri Creazioni (Camporosso, Italy).

Conflict of interest

The authors declare that the research was conducted in the absence of any commercial or financial relationships that could be construed as a potential conflict of interest.

Publisher's note

All claims expressed in this article are solely those of the authors and do not necessarily represent those of their affiliated organizations, or those of the publisher, the editors and the reviewers. Any product that may be evaluated in this article, or claim that may be made by its manufacturer, is not guaranteed or endorsed by the publisher.

Supplementary material

The Supplementary Material for this article can be found online at: https://www.frontiersin.org/articles/10.3389/fpls.2022.1009206/full#supplementary-material

SUPPLEMENTARY FIGURE 1
Linkage Groups obtained after analysis, together with markers name.

SUPPLEMENTARY FIGURE 2
Distribution of the investigated traits in the two populations.

References

Acquadro, A., Barchi, L., Gramazio, P., Portis, E., Vilanova, S., Comino, C., et al. (2017). Coding SNPs analysis highlights genetic relationships and evolution pattern in eggplant complexes. *PLoS One* 12, e0180774. doi: 10.1371/journal.pone.0180774

Acquadro, A., Barchi, L., Portis, E., Nourdine, M., Carli, C., Monge, S., et al. (2020). Whole genome resequencing of four Italian sweet pepper landraces provides insights on sequence variation in genes of agronomic value. *Sci. Rep.* 10 (1), 1–16. doi: 10.1038/s41598-020-66053-2

Acquadro, A., Lanteri, S., Scaglione, D., Arens, P., Vosman, B., and Portis, E. (2009). Genetic mapping and annotation of genomic microsatellites isolated from globe artichoke. *Theor. Appl. Genet.* 118, 1573–1587. doi: 10.1007/s00122-009-1005-6

Barchi, L., Lanteri, S., Portis, E., Valè, G., Volante, A., Pulcini, L., et al. (2012). A RAD tag derived marker based eggplant linkage map and the location of QTLs determining anthocyanin pigmentation. *PloS One* 7, e43740. doi: 10.1371/journal.pone.0043740

Beruto, M., Martini, P., and Viglione, S. (2019). Ranunculus asiaticus: From research to production. *Acta Hortic.* 1237, 117–128. doi: 10.17660/ActaHortic.2019.1237.16

Beruto, M., Rabaglio, M., Viglione, S., Van Labeke, M.-C., and Dhooghe, E. (2018). *"Ranunculus," in ornamental crops handbook of plant breeding*. Ed. J. Van Huylenbroeck (Cham: Springer), 649–671. doi: 10.1007/978-3-319-90698-0_25

Catchen, J., Hohenlohe, P. A., Bassham, S., Amores, A., and Cresko, W. A. (2013). Stacks: an analysis tool set for population genomics. *Mol. Ecol.* 22, 3124–3140. doi: 10.1111/mec.12354

Danecek, P., Bonfield, J. K., Liddle, J., Marshall, J., Ohan, V., Pollard, M. O., et al. (2021). Twelve years of SAMtools and BCFtools. *Gigascience* 10, giab008. doi: 10.1093/gigascience/giab008

De Hertogh, A. A. (1996). *Holland Bulb forcer's guide. 5th ed* (The Netherlands: Alkemade Printing Lisse).

Doerge, R. W., and Churchill, G. A. (1996). Permutation tests for multiple loci affecting a quantitative character. *Genetics* 142, 285–294. doi: 10.1093/genetics/142.1.285

Feng, X., Yu, X., Fu, B., Wang, X., Liu, H., Pang, M., et al. (2018). A high-resolution genetic linkage map and QTL fine mapping for growth-related traits and sex in the Yangtze river common carp (Cyprinus carpio haematopterus). *BMC Genomics* 19, 230. doi: 10.1186/s12864-018-4613-1

Gartner, G. A. L., Mccouch, S., and Moncada, M. D. P. (2013). A genetic map of an interspecific diploid pseudo testcross population of coffee. *Euphytica* 192 (2), 305–323. doi: 10.1007/s10681-013-0926-y

Giraut, L., Falque, M., Drouaud, J., Pereira, L., Martin, O. C., and Mézard, C. (2011). Genome-wide crossover distribution in arabidopsis thaliana meiosis reveals sex-specific patterns along chromosomes. *PloS Genet.* 7, e1002354. doi: 10.1371/journal.pgen.1002354

Goepfert, D. (1974)Karyotypes and DNA content in species of ranunculus l. and related genera. In: *Botaniska notiser*. Available at: https://scholar.google.com/scholar_lookup?title=Karyotypes+and+DNA+content+in+species+of+Ranunculus+L.+and+related+genera&author=Goepfert%2C+D.&publication_year=1974 (Accessed August 1, 2022).

Jin, Y., Zhao, W., Nie, S., Liu, S.-S., El-Kassaby, Y. A., Wang, X.-R., et al. (2019). Genome-wide variant identification and high-density genetic map construction using RADseq for platycladus orientalis (Cupressaceae). *G3: Genes Genomes Genet.* 9, 3663–3672. doi: 10.1534/g3.119.400684

Kearsey, M. J., Ramsay, L. D., Jennings, D. E., Lydiate, D. J., Bohuon, E. J. R., and Marshall, a. ,. D. F. (1996). Higher recombination frequencies in female compared to male meisoses in brassica oleracea. *Theoret Appl. Genet.* 92, 363–367. doi: 10.1007/BF00223680

Keim, P., Diers, B. W., Olson, T. C., and Shoemaker, R. C. (1990). RFLP mapping in soybean: Association between marker loci and variation in quantitative traits. *Genetics* 126, 735–742. doi: 10.1093/genetics/126.3.735

Kelly, A. L., Sharpe, A. G., Nixon, J. H., Lydiate, D. J., and Evans, E. J. (1997). Indistinguishable patterns of recombination resulting from male and female meioses in brassica napus (oilseed rape). *Genome* 40, 49–56. doi: 10.1139/g97-007

Kosambi, D. D. (1943). The estimation of map distances from recombination values. *Ann. Eugenics* 12, 172–175. doi: 10.1111/j.1469-1809.1943.tb02321.x

Koseki, M., Goto, K., Masuta, C., and Kanazawa, A. (2005). The star-type color pattern in petunia hybrida 'Red star' flowers is induced by sequence-specific degradation of chalcone synthase RNA. *Plant Cell Physiol.* 46, 1879–1883. doi: 10.1093/pcp/pci192

Le Maitre, N. C., Pirie, M. D., and Bellstedt, D. U. (2019). Floral color, anthocyanin synthesis gene expression and control in cape Erica species. *Front. Plant Sci.* 10. doi: 10.3389/fpls.2019.01565

Lenormand, T., and Dutheil, J. (2005). Recombination difference between sexes: A role for haploid selection. *PloS Biol.* 3, e63. doi: 10.1371/journal.pbio.0030063

Li, H., and Durbin, R. (2009). Fast and accurate short read alignment with burrows-wheeler transform. *Bioinformatics* 25, 1754–1760. doi: 10.1093/bioinformatics/btp324

Mariotti, R., Fornasiero, A., Mousavi, S., Cultrera, N. G. M., Brizioli, F., Pandolfi, S., et al. (2020). Genetic mapping of the incompatibility locus in olive and development of a linked sequence-tagged site marker. *Front. Plant Sci.* 10. doi: 10.3389/fpls.2019.01760

Martina, M., Acquadro, A., Barchi, L., Gulino, D., Brusco, F., Rabaglio, M., et al. (2022). Genome-wide survey and development of the first microsatellite markers database (AnCorDB) in anemone coronaria l. *Int. J. Mol. Sci.* 23 (6), 3126. doi: 10.3390/ijms23063126

Nelson, D. L., Orr, H. T., and Warren, S. T. (2013). The unstable repeats - three evolving faces of neurological disease. *Neuron* 77, 825–843. doi: 10.1016/j.neuron.2013.02.022

Ott, A., Trautschold, B., and Sandhu, D. (2011). Using microsatellites to understand the physical distribution of recombination on soybean chromosomes. *PloS One* 6, e22306. doi: 10.1371/journal.pone.0022306

Paterson, A. H., Lander, E. S., Hewitt, J. D., Peterson, S., Lincoln, S. E., and Tanksley, S. D. (1988). Resolution of quantitative traits into mendelian factors by using a complete linkage map of restriction fragment length polymorphisms. *Nature* 335, 721–726. doi: 10.1038/335721a0

Peterson, B. K., Weber, J. N., Kay, E. H., Fisher, H. S., and Hoekstra, H. E. (2012). Double digest RADseq: An inexpensive method for *De novo* SNP discovery and genotyping in model and non-model species. *PLoS One* 7, e37135. doi: 10.1371/journal.pone.0037135

Plomion, C., and Durel, C. (1996). Estimation of the average effects of specific alleles detected by the pseudo-testcross QTL mapping strategy. *Genet. Selection Evol.* 28, 223. doi: 10.1186/1297-9686-28-3-223

Portis, E., Scaglione, D., Acquadro, A., Mauromicale, G., Mauro, R., Knapp, S. J., et al. (2012). Genetic mapping and identification of QTL for earliness in the globe artichoke/cultivated cardoon complex. *BMC Res. Notes* 5, 252. doi: 10.1186/1756-0500-5-252

Reiter, R. S., Williams, J. G., Feldmann, K. A., Rafalski, J. A., Tingey, S. V., and Scolnik, P. A. (1992). Global and local genome mapping in arabidopsis thaliana by using recombinant inbred lines and random amplified polymorphic DNAs. *Proc. Natl. Acad. Sci. U.S.A.* 89 (4), 1477–1481.

Sardell, J. M., and Kirkpatrick, M. (2020). Sex differences in the recombination landscape. *Am. Nat.* 195, 361–379. doi: 10.1086/704943

Scaglione, D., Reyes-Chin-Wo, S., Acquadro, A., Froenicke, L., Portis, E., Beitel, C., et al. (2016). The genome sequence of the outbreeding globe artichoke constructed *de novo* incorporating a phase-aware low-pass sequencing strategy of F1 progeny. *Sci. Rep.* 6, 19427. doi: 10.1038/srep19427

Slatko, B. E., Gardner, A. F., and Ausubel, F. M. (2018). Overview of next-generation sequencing technologies. *Curr. Protoc. Mol. Biol.* 122, e59. doi: 10.1002/cpmb.59

Song, X., Xu, Y., Gao, K., Fan, G., Zhang, F., Deng, C., et al. (2020). High-density genetic map construction and identification of loci controlling flower-type traits in chrysanthemum (Chrysanthemum × morifolium ramat.). *Horticult. Res.* 7, 108. doi: 10.1038/s41438-020-0333-1

Tanksley, S. D., Ganal, M. W., Prince, J. P., de Vicente, M. C., Bonierbale, M. W., Broun, P., et al. (1992). High density molecular linkage maps of the tomato and potato genomes. *Genetics* 132, 1141–1160. doi: 10.1093/genetics/132.4.1141

Team, R. C. (2016)R: A language and environment for statistical computing. In: *R foundation for statistical computing* (Vienna, Austria). Available at: https://cir.nii.ac.jp/crid/1574231874043578752 (Accessed August 1, 2022).

Toppino, L., Barchi, L., Mercati, F., Acciarri, N., Perrone, D., Martina, M., et al. (2020). And high-resolution genetic map of eggplant based on a RIL population, and location of QTLs related to plant anthocyanin pigmentation and seed vigour. *Genes* 11, 745. doi: 10.3390/genes11070745

Torello Marinoni, D., Valentini, N., Portis, E., Acquadro, A., Beltramo, C., and Botta, R. (2017). Construction of a high-density genetic linkage map and QTL analysis for hazelnut breeding. In *IX International Congress on Hazelnut* 1226, pp 25–30. doi: 10.17660/ActaHortic.2018.1226.3

Valentini, N., Portis, E., Botta, R., Acquadro, A., Pavese, V., Cavalet Giorsa, E., et al. (2021). Mapping the genetic regions responsible for key phenology-related traits in the European hazelnut. *Front. Plant Sci.* 12. doi: 10.3389/fpls.2021.749394

Vallejos, C. E., Sakiyama, N. S., and Chase, C. D. (1992). A molecular marker-based linkage map of phaseolus vulgaris l. *Genetics* 131, 733–740. doi: 10.1093/genetics/131.3.733

van Geest, G., Bourke, P. M., Voorrips, R. E., Marasek-Ciolakowska, A., Liao, Y., Post, A., et al. (2017). An ultra-dense integrated linkage map for hexaploid chrysanthemum enables multi-allelic QTL analysis. *Theor. Appl. Genet.* 130, 2527–2541. doi: 10.1007/s00122-017-2974-5

Van Ooijen, J. W. (2004). MapQTL® 5, software for the mapping of quantitative trait loci in experimental populations.

Van Ooijen, J. W. (2006) *JoinMap® 4, software for the calculation of genetic linkage maps in experimental populations – ScienceOpen*. Available at: https://www.scienceopen.com/document?vid=baa76c8c-fb55-4c13-a6ca-24c71002ab5a (Accessed August 1, 2022).

Vincenten, N., Kuhl, L.-M., Lam, I., Oke, A., Kerr, A. R., Hochwagen, A., et al. (2015). The kinetochore prevents centromere-proximal crossover recombination during meiosis. *Elife* 4, e10850. doi: 10.7554/eLife.10850

Víquez-Zamora, M., Vosman, B., van de Geest, H., Bovy, A., Visser, R. G., Finkers, R., et al. (2013). Tomato breeding in the genomics era: insights from a SNP array. *BMC Genomics* 14, 354. doi: 10.1186/1471-2164-14-354

Voorrips, R. E. (2002). MapChart: software for the graphical presentation of linkage maps and QTLs. *J. Hered.* 93, 77–78. doi: 10.1093/jhered/93.1.77

Vukosavljev, M., Arens, P., Voorrips, R. E., van 't Westende, W. P., Esselink, G. D., Bourke, P. M., et al. (2016). High-density SNP-based genetic maps for the parents of an outcrossed and a selfed tetraploid garden rose cross, inferred from admixed progeny using the 68k rose SNP array. *Hortic. Res.* 3, 1–8. doi: 10.1038/hortres.2016.52

Wang, Z., Lu, G., Wu, Q., Li, A., Que, Y., and Xu, L. (2022). Isolating QTL controlling sugarcane leaf blight resistance using a two-way pseudo-testcross strategy. *Crop J.* 10, 1131–1140. doi: 10.1016/j.cj.2021.11.009

Wang, Z., Song, M., Li, Y., Chen, S., and Ma, H. (2019). Differential color development and response to light deprivation of fig (Ficus carica l.) syconia peel and female flower tissues: Transcriptome elucidation. *BMC Plant Biol.* 19, 217. doi: 10.1186/s12870-019-1816-9

Wang, Z., Wei, X., Yang, J., Li, H., Ma, B., Zhang, K., et al. (2020). Heterologous expression of the apple hexose transporter md HT 2.2 altered sugar concentration with increasing cell wall invertase activity in tomato fruit. *Plant Biotechnol. J.* 18, 540–552. doi: 10.1111/pbi.13222

Wu, S., Yang, J., Huang, Y., Li, Y., Yin, T., Wullschleger, S. D., et al. (2010). An improved approach for mapping quantitative trait loci in a pseudo-testcross: Revisiting a poplar mapping study. *Bioinform. Biol. Insights* 4, BBI.S4153. doi: 10.4137/BBI.S4153

Zafar, F., Okita, A. K., Onaka, A. T., Su, J., Katahira, Y., Nakayama, J., et al. (2017). Regulation of mitotic recombination between DNA repeats in centromeres. *Nucleic Acids Res.* 45, 11222–11235. doi: 10.1093/nar/gkx763

Zheng, X., Om, K., Stanton, K. A., Thomas, D., Cheng, P. A., Eggert, A., et al. (2021). The regulatory network for petal anthocyanin pigmentation is shaped by the MYB5a/NEGAN transcription factor in mimulus. *Genetics* 217, iyaa036. doi: 10.1093/genetics/iyaa036

frontiers | Frontiers in Plant Science

TYPE Original Research
PUBLISHED 26 September 2022
DOI 10.3389/fpls.2022.1010896

OPEN ACCESS

EDITED BY
Daqiu Zhao,
Yangzhou University, China

REVIEWED BY
Qinlong Zhu,
South China Agricultural University, China
Yalong Guo,
Institute of Botany, Chinese Academy of Sciences (CAS), China

*CORRESPONDENCE
Shuangjiang Li
lishuangjiang0000@163.com
Shunzhao Sui
sszcq@swu.edu.cn

SPECIALTY SECTION
This article was submitted to Plant Breeding, a section of the journal Frontiers in Plant Science

RECEIVED 03 August 2022
ACCEPTED 29 August 2022
PUBLISHED 26 September 2022

CITATION
Zhu T, Liu B, Liu N, Xu J, Song X, Li S and Sui S (2022) Gibberellin-related genes regulate dwarfing mechanism in wintersweet. *Front. Plant Sci.* 13:1010896. doi: 10.3389/fpls.2022.1010896

Gibberellin-related genes regulate dwarfing mechanism in wintersweet

Ting Zhu[1], Bin Liu[1], Ning Liu[1], Jie Xu[1], Xingrong Song[2], Shuangjiang Li[1]* and Shunzhao Sui[1]*

[1]Key Laboratory of Horticulture Science for Southern Mountainous Regions of Ministry of Education, Chongqing Engineering Research Center for Floriculture, College of Horticulture and Landscape Architecture, Southwest University, Chongqing, China, [2]Horticulture Research Institute, Sichuan Academy of Agricultural Sciences, Chengdu, China

Chimonanthus praecox (wintersweet) is an important cut flower and pot plant with a high ornamental and economic value in China. The development of dwarf wintersweet varieties has become an important research topic for the wintersweet industry. The lack of natural dwarf germplasm has hindered research into the molecular mechanisms of developing dwarf wintersweet, limiting its cultivation. After a long-term investigation and collection of germplasm resources of *C. praecox*, we obtained the germplasm of a dwarf *C. praecox* (dw). Here, the dwarf and normal *C. praecox* (NH) were used to identify the types of hormones regulating dw formation using phenotypic identification and endogenous hormone determination. Differentially expressed genes in the dw and NH groups were screened using transcriptome analysis. The functions of key genes in the dwarf trait were verified by heterologous expression. It was found that the internode length and cell number were significantly reduced in dw than in NH, and the thickness of the xylem and pith was significantly decreased. The dwarfness of dw could be recovered by exogenous gibberellic acid (GA) application, and endogenous GA levels showed that the GA4 content of dw was substantially lower than that of NH. Transcriptome differential gene analysis showed that the elevated expression of the *CpGA2ox* gene in the GA synthesis pathway and that of *CpGAI* gene in the signal transduction pathway might be the key mechanisms leading to dwarfing. Combined with the results of weighted gene co-expression network analysis, we selected the *CpGAI* gene for analysis and functional verification. These results showed that CpGAI is a nuclear transcriptional activator. Overexpression of *CpGAI* in *Populus tomentosa* Carr. showed that *CpGAI* could lead to the dwarfing in poplar. We analyzed the dwarfing mechanism of *C. praecox*, and the results provided a reference for dwarf breeding of wintersweet.

KEYWORDS

gibberellic, DELLA, *Chimonanthus praecox*, plant height, WGCNA

Introduction

Chimonanthus praecox (wintersweet) is a traditional ornamental wood specialty plant in China. Wintersweet has a long history of flower culture with a wide variety of cultivated species and is an excellent rare garden winter flower. It is also a valuable potted and cut flower material with good market value (Lin and Chen, 2020). As potted plants can be moved and are easy to manage, they are suitable for interior decoration in public places, such as restaurants, industries, schools, and hospitals, and meet the needs of family horticulturists. Recently, wintersweet potted plants have been receiving increasing attention from the industry (Xiao, 2021). The plant height of wintersweet is generally approximately 3 m. Pruning and exogenous gibberellin inhibitors, such as chlormequat chloride, paclobutrazol, and daminozide, are used to produce dwarfs of wintersweet (Yuan and Song, 2012; Du et al., 2015). These methods have several disadvantages, namely harmful effects on growth, high labor cost, and difficulty in ensuring stability in the later period. Currently, no good solution exists for controlling the height of wintersweet plants.

Plant architecture is a result of the continuous or periodic division of the meristem. In dicotyledons, plant height is promoted mainly by the stem apical meristem (SAM), whereas the lateral meristem increases the stem diameter (Wang et al., 2018). Studies have also shown that plant height and stem diameter are positively correlated (Rezaee et al., 2009). Plant height exhibits plasticity, which depends on the coordinated regulation of environmental signals and plant hormones, and mainly regulates stem elongation by promoting cell elongation and increasing cell number (Bai et al., 2012; Oh et al., 2014). Gibberellin acid (GA), a tetracyclic diterpenoid plant hormone, is one of the most important hormones regulating plant height. Significant changes in expression of genes related to GA synthesis or signaling pathways, or mutations can lead to changes in plant height. GA biosynthesis is catalyzed by the following key enzymes, including geranylgeranyl pyrophosphate synthase (GGPS), copalyl diphosphate synthase (CPS), kaurene synthase (KS), kaurene oxidase (KO), kaurenoic acid oxidase (KAO), GA20-oxidase (GA20ox), and GA3-oxidase (GA3ox). GA deactivation is catalyzed by GA2-oxidase (GA2ox) (Hedden and Phillips, 2000). In rice, the *OsEATB* gene negatively regulates internode length by inhibiting KS transcription (Qi et al., 2011); overexpression of *OsWOX3A* results in shorter internode length by inhibiting KAO transcription (Cho et al., 2016). Both responses lead to dwarfing caused by the decreased expression of GA synthesis-related genes. A typical case of dwarfing caused by the mutation of the *sd1* gene in rice, which codes for the downstream gene *GA20ox-2* that is involved in GA synthesis, led to the "green revolution" (Ashikari et al., 2002). In GA signal transduction, DELLA protein degradation and inactivation result in internode elongation. When the N-terminal domain of the DELLA protein is mutated, DELLA protein degradation is blocked and it becomes a constitutive repressor; hence, plants show a dwarfing phenotype insensitive to GA (Dill et al., 2001; Fu and Harberd, 2003; Fu et al., 2004). In *Arabidopsis thaliana*, the NAC transcription factor *JUB1* inhibits stem elongation by increasing the transcription level of DELLA, a key factor in the GA signaling pathway (Dill et al., 2001; Shahnejat-Bushehri et al., 2016). Another representative case of the "Green Revolution" (semi-) dwarf dry wheat is that two genes encoding DELLA protein—*Rht-B1* and *Rht-D1*—are insensitive to GA signal, resulting in shorter plant height (Peng et al., 1999).

Most studies on plant height have been conducted in herbaceous model plants, such as rice, wheat, and *Arabidopsis*, while studies on the regulation mechanism of plant height in woody plants are limited. In a dwarfing study on peach, it was found that the mutation of cytosine to thymine in the sequence GID1c led to the conversion of serine (S) to phenylalanine (F). Even in the presence of GA, GID1c^{S191F} cannot interact with the growth inhibitor DELLA1, resulting in GA-insensitive dwarfs (Cheng et al., 2019). Studies on the crape myrtle, an ornamental woody plant, have shown that auxin plays a key role in cell division in the SAM and that auxin and GA4 interact to regulate the internode length (Ju et al., 2018). Most studies on wintersweet are based on characteristics, such as flower senescence and flower bud dormancy (Huang et al., 2019; Li et al., 2020), and the molecular mechanism of dwarfing has not been reported. The first dwarf material identified in this study is ideal for analyzing the dwarfing mechanism. The dwarfing mechanism of *C. praecox* was studied using cell observation, hormone determination, transcriptome analysis, and transgenic verification. This study also provides a reference for analyzing the molecular mechanism of dwarfing characteristics in woody plants.

Materials and methods

Phenotype and hormone treatment

This study used dwarf (dw) and common *C. praecox* (NH) as experimental materials. In October 2020, grafting of the two accessions was performed at the teaching base of the College of Horticulture and Landscape Architecture of Southwest University (Chongqing, China). In March 2021, the scions sprouted for follow-up experiments.

Twelve branches of each accession were randomly selected to measure branch length and internode number. Branch length was measured when the scion began to grow on March 04, 2021, and the internode number was counted when internodes became distinct on March 31, 2021. Both measurements and statistics were performed every 7 days until the summer shoot growth was completed. The internode length was obtained by dividing the branch length by the number

of internodes. Multiple comparisons and related phenotypic regression analyses were performed using SPSS 20.0.

Six branches with a length of 12 cm and three nodes were selected from dw, and the whole branch was sprayed with GA at a concentration of 150 mg/L. The treatment was administered at 9:00 a.m. on the 1st, 5th, and 10th days. Before treatment, 6 dw and 6 NH plants of the same height and node number were selected and sprayed with water as a control. These branches' height and the number of internodes were observed 14 days later.

Histological observation of the stem

The dw and NH branches with four internodes were selected for histological observation, and the stem tip, cross section, and longitudinal section of the stem segment were prepared. One branch was considered as one biological repeat and a total of three biological repeats were considered.

The tender stem tip was dissected using paraffin sections as follows. Fresh tissue from the stem tip was fixed with 50% fixative solution for more than 24 h. Dehydration boxes were placed into the dehydrator and gradient alcohol for dehydration. The wax-soaked tissues were embedded in an embedding machine. Samples were sectioned on a Leica RM2016 slicer with a thickness of 4 μm. After staining with safranin and solid green, the sections were sealed with xylene transparent and neutral gum, respectively; then, they were observed and photographed using a NIKON ECLIPSE E100 optical microscope.

The tissue of the stem segment was hard (the fourth internode from the tip down), and the cross section was obtained by hard-tissue slicing. The cells were fixed with 70% formaldehyde-acetic acid-ethanol fixative (FAA) for 48 h, dehydrated, molded, embedded successively, and then sectioned using a Leica HistoCore AUTOCUT hard tissue slicer at a thickness of 10 μm. Safranin and solid green staining, and the images were observed under a NIKON ECLIPSE E100 optical microscope and photographed using Nikon DS-U3.

The length of the stem tip was measured using the Nano Measurer software (Fudan University), and the tissue thickness and cell size of the stem sections were calculated using CaseViewer software. The number of cells in the longitudinal section of the internode was obtained by dividing the average internode length by the average cell length (Ripetti et al., 2008).

Determination of endogenous gibberellic acid content

The stem tip and the first two stem segments (excluding leaves) of *C. praecox* branches obtained in early April 2021 were used for endogenous GA content determination in three biological repeats according to the method of Pan et al. (2010). Approximately 0.5 g of fresh sample was ground to a dry powder using liquid nitrogen and placed in a glass test tube. A mixture of isopropanol-water-hydrochloric acid and 8 μL of 1 μg/mL internal standard solution was added to the glass tube and oscillated for 30 min at 4°C. Dichloromethane was then added, and the mixture was oscillated for 30 min at 4°C. The solution was centrifuged at 6,000 *g* for 5 min at 4°C, and the lower organic phase was obtained. The organic phase was dried using nitrogen and redissolved in methanol (0.1% formic acid). After centrifugation, the supernatant was passed through a 0.22-μm filter membrane and analyzed using high-performance liquid chromatography-tandem mass spectrometry (HPLC-MS/MS).

Transcriptomic and quantitative real-time PCR analysis

According to the statistical results of previous pre-experiments, we roughly divided the growth of wintersweet into three stages. The first stage occurred in mid-early March (T1 group), when wintersweet began to grow; the second stage occurred in mid-April (T2 group), when the growth rate of wintersweet was fast, and the third stage occurred in early May (T3 group), when it began to grow slowly. The stem tip and first two stem segments (excluding leaves) were selected for all three groups, and 10 branches were mixed as one biological replicate, with three biological replicates in each of the three groups.

Total RNA was extracted using the TRIzol kit (Tiangen, Beijing, China); mRNA was purified, and a cDNA library was constructed. Illumina HiSeq 4000 and PE 150 sequencing strategies were used for sequencing. Raw sequencing data were filtered to obtain clean data. The transcript was spliced using Trinity software; redundancy was removed using CD-HIT (v4.8.1), and splicing quality was evaluated using the BUSCO software. Gene expression was calculated using RSEM software, and genes with FDR < 0.05 and $|\log2\ (\text{Fold Change})| > 1$ were considered to be differentially expressed genes (DEGs).

To describe the pattern of genetic association among different samples and identify highly synergistic gene sets, we performed a weighted gene co-expression network analysis (WGCNA) using the R package "WGCNA" (Zhang and Horvath, 2005) and visualized using Cytoscape v1.7.251[1].

To verify the RNA-seq data, the expression patterns of nine related DEGs were analyzed. Specific primers designed using Primer6 were used for qRT-PCR in the Bio-Rad CFX96 system (**Supplementary Table 1**). Relative gene expression levels were calculated using the $2^{-\Delta\Delta CT}$ method (Livak and Schmittgen, 2001). Three biological replicates and three technical replicates were performed.

1 https://cytoscape.org/index.html

Gene cloning and *CpGAI* bioinformatics analysis

The first-strand cDNA was synthesized from RNA according to the manufacturer's instructions using a PrimeScript RT kit with gDNA Eraser (TaKaRa, Dalian, China). The *CpGID1, CpGAI,* and *CpGID2* genes were amplified using the Pfu DNA polymerase kit (TransGen, Beijing, China) and sequence-specific primers (*CpGID1*-F/R, *CpGID2*-F/R, and *CpGAI*-F/R, respectively) (**Supplementary Table 2**). The PCR products were cloned into the pMD19-T vector (Takara, Shiga, Japan) for sequencing.

Multiple amino acid sequences were compared using ClustalW, and the results were plotted using JalView. A phylogenetic tree was constructed using MEGA7.0 software based on the neighbor joining method, and bootstrap analysis was performed with 1,000 replications. The amino acid sequences of other plant used in this alignment and phylogenetic trees were obtained from the National Center for Biotechnology Information (NCBI).

Subcellular localization of *CpGAI*

Specific primers were designed to determine the subcellular localization of *CpGAI* (**Supplementary Table 2**). The ORF of *CpGAI* without a stop codon was cloned into the N terminus of the pCAMBIA1300 vector *GFP* (green fluorescent protein) gene using a seamless cloning kit (Yugong Biolabs, Jiangsu, China). The fusion recombinant plasmid *pCAMBIA1300-CpGAI* and empty vector *pCAMBIA1300* (positive control) were transformed into *Agrobacterium tumefaciens* and then transfected into onion epidermal cells. Simultaneously, the untransfected onion epidermis was used as the blank control. Onion cells were cultured in MS medium at 28°C in the dark for 24 h, and the nuclei of onion cells were stained with 10 μg/mL 4′, 6-diamidino-2-phenylindole (DAPI). Observations were performed using a Zeiss LSM 800 confocal excitation light microscope.

Transcriptional self-activation activity of *CpGAI*

Specific primers were designed to determine whether *CpGAI* has transcriptional self-activation activity (**Supplementary Table 2**). Similarly, *CpGAI* was cloned into the yeast expression vector pGBKT7 (Clontech, Shiga, Japan) using a seamless cloning method to construct the vector *pGBKT7-CpGAI*. According to the instructions of the yeast transformation kit (Coolaber), *pGBKT7-CpGAI*, *pGBKT7* (negative control), and *pGBKT7-TF39* (positive control) were transformed into the yeast strain Y2HGold. Exactly 10 μL of 10^0, 10^{-1}, 10^{-2}, and 10^{-3} diluents of yeast cells were selected on SD/-Trp, SD/-Trp, and X-α-gal (5-bromo-4-chloro-3-indoxyl-α-D-galactopyranoside) media. The presence of yeast plaque and whether the plaque turned blue were observed to determine whether the CpGAI protein had transcriptional activation activity. The yeast media described above were purchased from TaKaRa (BioTech, Dalian, China). All yeast cells were cultured at 29°C for 2–3 days.

CpGAI overexpression in *Populus tomentosa* Carr.

As described by Jia et al. (2010), *Agrobacterium*-mediated leaf disc transformation was performed in *P. tomentosa*. Primers for identification and expression analysis of the transgenic-positive seedlings are shown in **Supplementary Table 2**.

Results

Phenotype, exogenous gibberellic acid treatment, and endogenous gibberellic acid content determination of dwarf and NH

The statistical results of the internode length of the two accessions of *C. praecox* showed that the internode length of NH was almost three times that of dw (**Figure 1A**). The average stem tip lengths of NH and dw were 1,562 and 713 μm, respectively, in the paraffin sections (**Figures 1B,E**), indicating significant differences between the two accessions in the early stage of branch development. The transverse section of the stem (**Figures 1C,F**) showed that the difference in stem thickness of dw and NH was caused mainly by the difference in xylem thickness and pith diameter. Longitudinal hard-tissue slicing showed that the size of the dw cells was significantly smaller than that of NH cells (**Figures 1D,G**).

The initial length of dw and NH was 12 cm, and three internodes were marked. After 14 days, it was found to be 36 cm with six internodes for NH (**Figure 1H**) and 24 cm with five nodes for dw. The average branch length of dw treated with exogenous GA was 34 cm with six nodes, which was 41.7% more than the length of untreated branches, almost the same as NH. Exogenous gibberellin treatment was strongly resilient for the branch length of dw. These results suggested that the decrease in endogenous GA may cause dwarfing. Moreover, the endogenous content of GA4 in NH was determined to be significantly higher than that in dw (**Figure 1I**), which further confirmed that

10.3389/fpls.2022.1010896

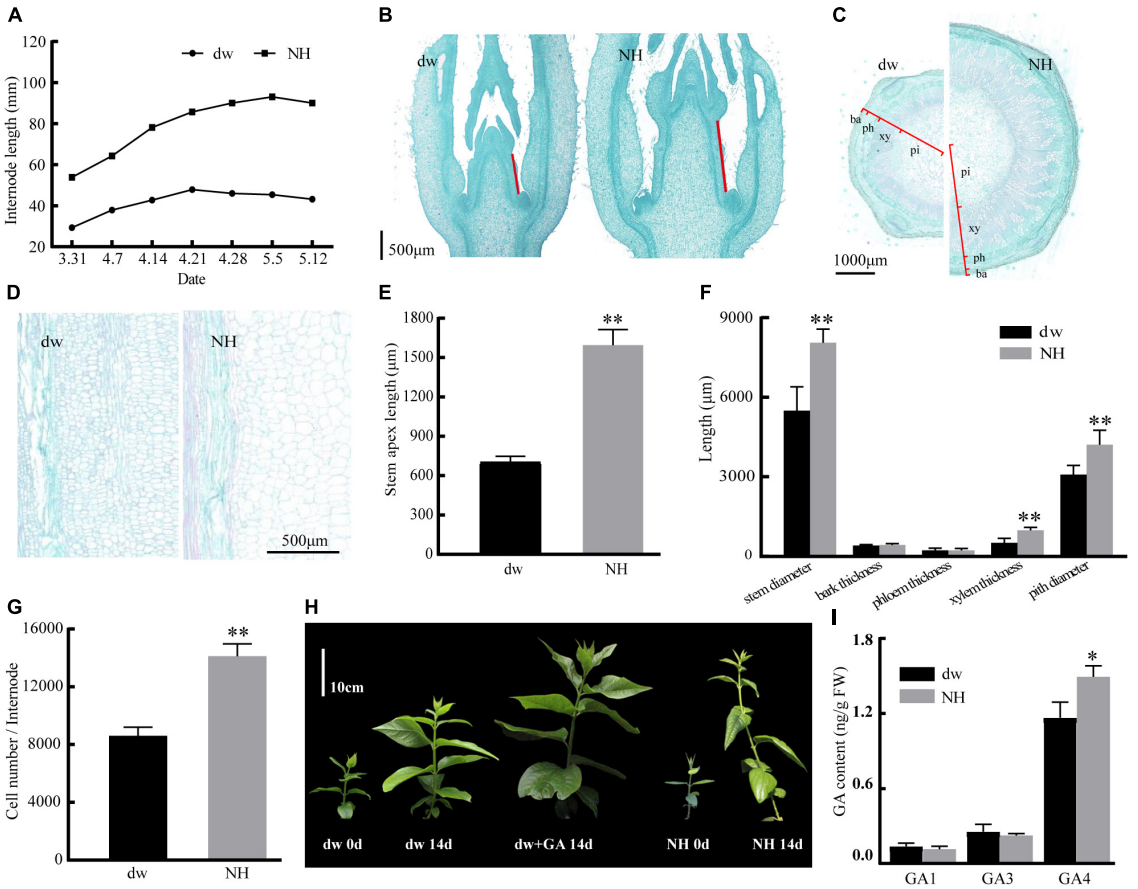

FIGURE 1
Response of internode length, slicing of dw and NH, dw to exogenous GA treatment. **(A)** Internode length in different periods. Panels **(B,E)** are the paraffin sections of the stem tip, with red lines indicating the length of the stem tip. Panels **(C,F)** are transverse sections of the stem. ba, bark; ph, phloem; xy, xylem; pi, pith. Panels **(D,G)** are the longitudinal sections of the stem. **(H)** The effect of hormone treatment on the growth of dw and NH. **(I)** Endogenous GA content. The * and ** indicate a significant difference from NH at $p < 0.05$ and $p < 0.01$, respectively, as determined by the Student *t*-test.

endogenous GA plays an important role in regulating plant height in *C. praecox*.

Transcriptome sequencing, differential genes, and functional enrichment analysis

A total of 397.53 Gb of raw reads were obtained. After quality control, 388.24 Gb clean reads were obtained. The contents of N50 and GC were 2,357 bp and 45%, respectively. Genes were annotated using functional databases (**Supplementary Figures 1A,C**, **2**). Principal component analysis showed good biological repeatability among samples (**Supplementary Figure 1B**). Nine genes were selected to test the transcriptome results' reliability and consistency. Their expression levels were assessed by qRT-PCR. The expression patterns obtained by qRT-PCR and RNA-seq analyses were similar (**Supplementary Figure 3A**). Linear regression analysis showed that the goodness of fit R^2 reached 0.92 (**Supplementary Figure 3B**), indicating the reliability of the transcriptome data.

There were differences among the T1, T2, and T3 groups (**Figure 2A**). Scatter plots of the first 20 pathways in the three groups were constructed based on the significance of enrichment. A pathway with a *P*-value less than 0.05 was defined as a significantly enriched pathway. In the T2 (**Figure 2C**) and T3 (**Figure 2D**) groups, 70 and 89 DEGs belonged to the plant hormone signal transduction pathway (red box), respectively, which was also the most significantly enriched pathway in the two groups. It suggested that plant hormone signal transduction changes greatly during T2 and T3 stages, which is probably an important pathway. Notably, all the first 20 pathways enriched in the T1 (**Figure 2B**), T2, and T3 groups include biosynthesis of secondary metabolites (green box). In addition, it was significantly enriched in the T2 ($p = 0.0406$) and T3 ($p = 0.0378$) pathways, and many terpenoids genes were found in this pathway.

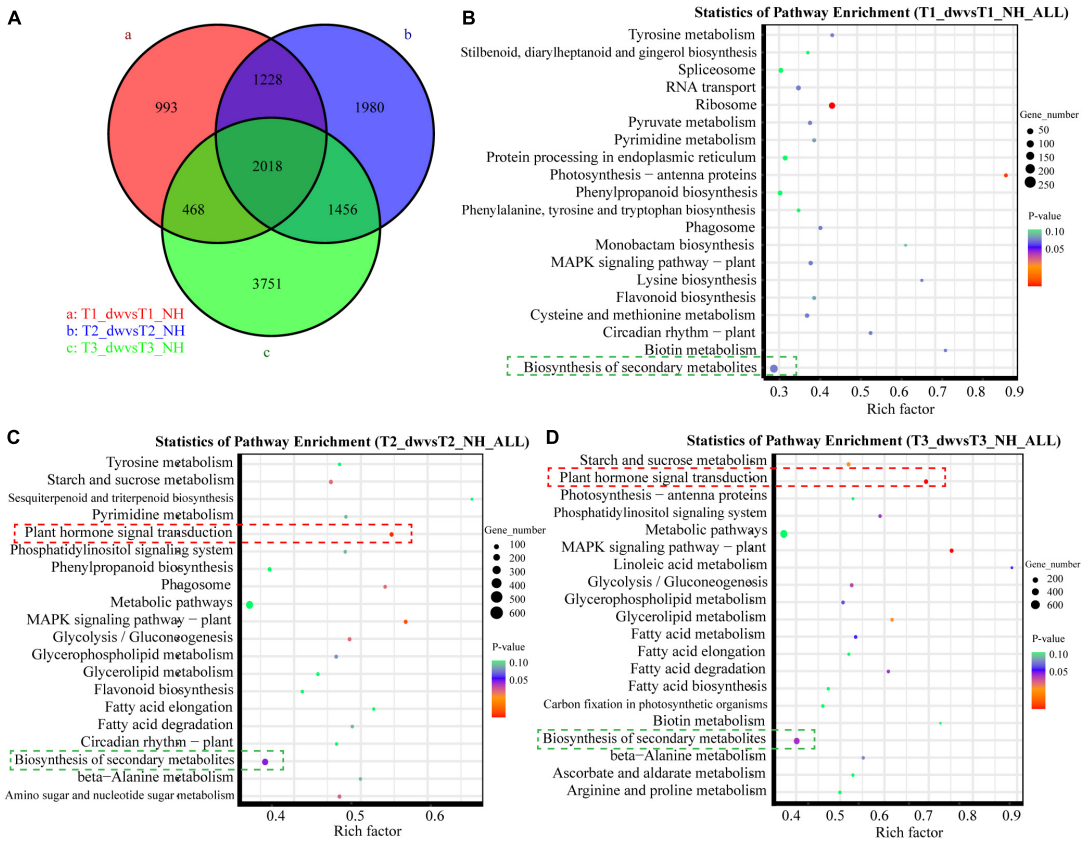

FIGURE 2
Venn diagram and KEGG function analysis of DEGs in T1, T2, and T3 groups. **(A)** Venn diagram of DEGs in three groups. Panels **(B–D)** are scatter plots of the first 20 KEGG enrichment pathways of DEGs at T1, T2, and T3 stages, respectively.

The DEGs of dw and NH at T1, T2, and T3 stages were clustered according to the change in expression to determine the up- and down-regulation of all the DEGs (a total of 11,894) in the three stages (**Figure 3A**). The results showed that profiles 19, 12, and 16 were up-regulated; 18, 9, and 15 were down-regulated, and profile 17 was up- and down-regulated. Furthermore, genes with a significant enrichment trend were analyzed using KEGG enrichment analysis (**Figure 3B**). Profiles 19, 18, 17, 16, 12, and 9 were enriched in the plant hormone signal transduction pathway (red box), and profiles 16 and 17 had differential genes enriched in the diterpenoid biosynthesis pathway (green box). These profile enrichment analyses indicate that GA synthesis and signal transduction are key pathways. Hence, future studies will be focused on these key pathways.

Differentially expressed genes involved in gibberellic acid synthesis and signaling pathways

Gibberellic acid plays an important role in regulating plant height. The above exogenous hormone treatments proved that GA played a significant role in regulating plant height in *C. praecox*. Combined with the results of the KEGG analysis of the transcriptome, we believe that the synthesis and signal transduction of GA may play a crucial role in dwarfness. Therefore, we analyzed the differential transcriptional expression of the GA pathway (at least one of the three periods was different) and drew the following heat map (**Figures 4A,B**).

Three transcripts (TRINITY_DN19832_c0_g1, TRINITY_DN24125_c2_g5, and TRINITY_DN17449_c0_g1) were found that were related to the GGPS enzyme, which catalyzes the synthesis of the diterpenoid precursor GGPP (Sun and Kamiya, 1994), and the transcriptional level of two of them in NH was significantly higher than that in dw. The expression of KO (TRINITY_DN20269_c4_g1), KAO (TRINITY_DN26616_c5_g1), and GA20ox (TRINITY_DN23673_c5_g1) transcripts was significantly higher in dw than that in NH at T3. GA2ox (TRINITY_DN23040_c1_g1) inactivates bioactive GA1 and GA4 (Hedden and Phillips, 2000), and its expression was significantly upregulated at the T1 and T3 stages. Thus, GA2ox may inactivate endogenous GA in dw. We also

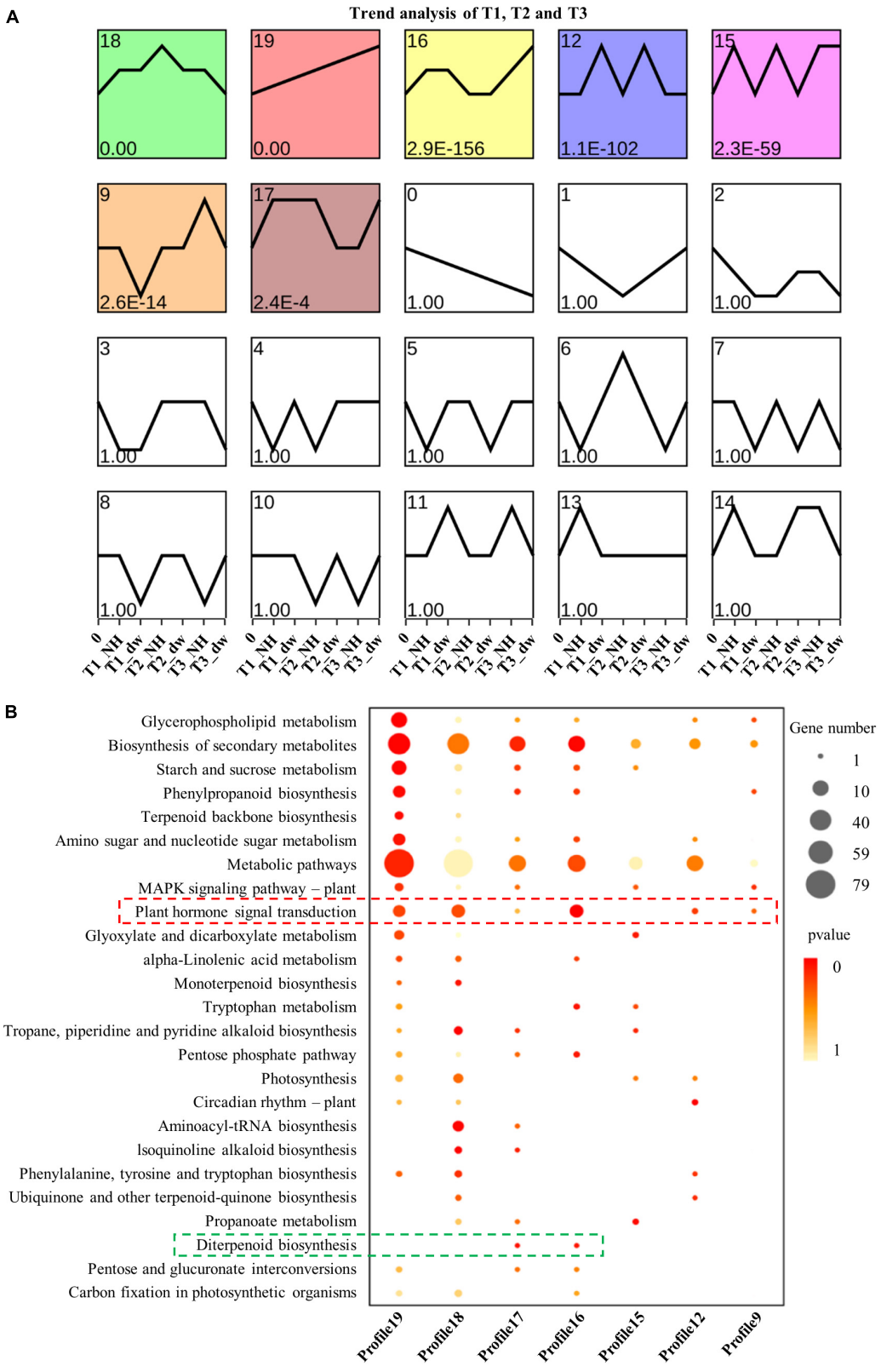

FIGURE 3
Trend analysis and KEGG enrichment analysis of significant cluster profile. **(A)** Trend cluster analysis of all DEGs at T1, T2, and T3; colored boxes represent profiles with significant differences. **(B)** KEGG enrichment and scatter plots of all genes in trend profile.

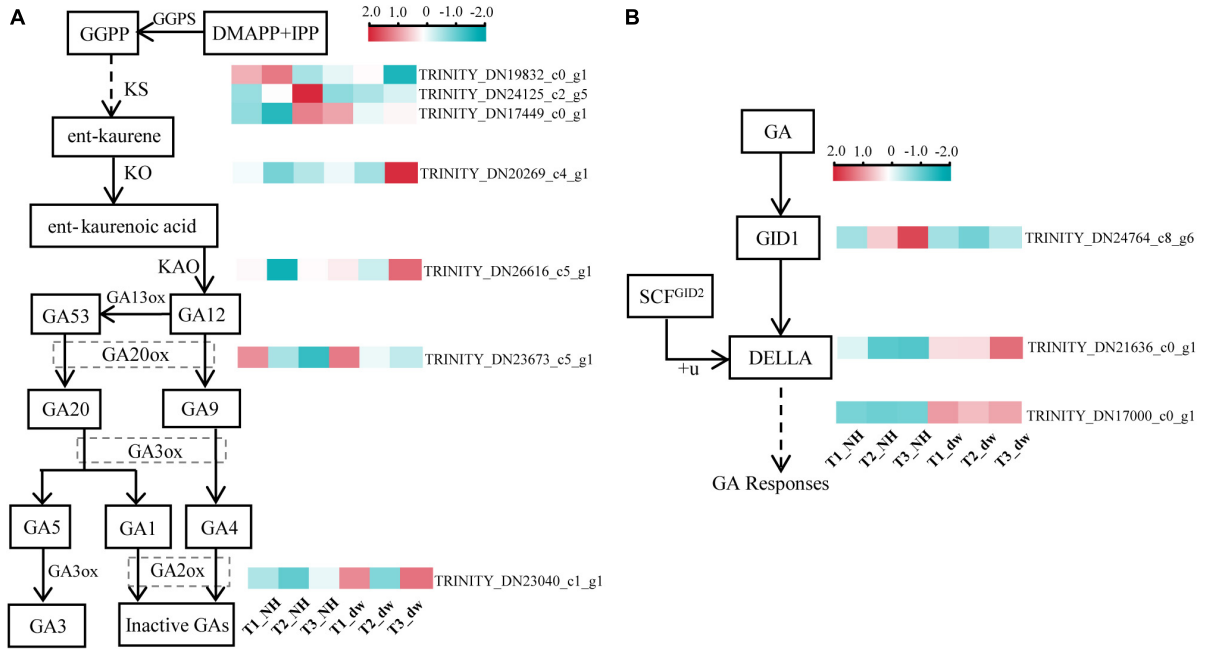

FIGURE 4
Analysis of DEGs related to GA synthesis and signal pathways. **(A)** DEGs in the GA synthesis pathway. **(B)** DEGs in GA signaling pathway. GGPS, geranylgeranyl pyrophosphate synthase; KO, ent-kaurene oxidase; KAO, ent-kaurenoic acid oxidase; GA20ox, gibberellin 20 oxidase; GA2ox, gibberellin 2-β-dioxygenase; GID1, gibberellin Insensitive Dwarf1; GAI, gibberellin-acid Insensitive; GID2, gibberellin Insensitive Dwarf2.

analyzed the transcriptional levels of three key genes in the GA signal transduction pathway (Figure 4B), including the GA receptor GID1, F-box protein GID2, and DELLA protein (Sun, 2010), in which DELLA is a negative factor for gibberellin signal transduction (Locascio et al., 2013). One GID1 transcript (TRINITY_DN24764_c8_g6) was downregulated among the DEGs in the T2 and T3 stages. The level of a typical member of the DELLA protein family, GAI1-like (TRINITY_DN21636_c0_g1), which we call *CpGAI*, was significantly higher in dw than that in NH at T2 and T3. Only one transcript of GID2 (TRINITY_DN17000_c0_g1) was upregulated in dw.

Weighted gene co-expression network analysis

To correlate plant height-related genes and phenotypic traits (pl, il, st, sd, ph, xy, and pi), we constructed a module–trait relationship using WGCNA. Among these phenotypes, ph, il, and st had the most direct relationship with plant height. Some studies have shown a strong positive correlation between stem diameter and stem height (Rezaee et al., 2009); therefore, the phenotypic characteristics of sd, ph, xy, and pi are also closely related to plant height. All genes in the 18 samples in WGCNA were divided into 26 modules (Figure 5A). According to $R^2 \geq 0.65$ and $p \leq 0.005$, four modules with the highest correlation with phenotypic characteristics were selected: turquoise, red, sienna3, and darkolivegreen. Genes related to the hormones and cell formation were common in these modules.

Module and trait correlation analysis showed that the modules most related to the phenotypes of pl, il, and st were 'turquoise' (positive correlation) and 'darkolivegreen' (negative correlation), indicating that the HUB genes of these two modules are likely to play an important role in regulating plant height (Langfelder and Horvath, 2008). The analysis of turquoise (positive correlation) module (Figure 5B, left) revealed eight HUB genes; heat maps were drawn (Figure 5C, left), and two of them were *CIGR1* homologous genes (TRINITY_DN25905_c2_g2, TRINITY_DN23034_c0_g1) of the GRAS protein family. Several genes may be involved in cell wall biosynthesis, including *GATL9* (TRINITY_DN26894_c1_g7), *CESA2* (TRINITY_DN25522_c1_g2), *CESA5* (TRINITY_DN21261_c0_g3), *XTH23* (TRINITY_DN21370_c2_g2), *CSLC12* (TRINITY_DN25596_c1_g1), and *XXT2* (TRINITY_DN23543_c5_g2).

In the dark olive green (negative correlation) module, we identified four HUB motifs (Figures 5B,C, middle) related to hormone signal transduction. The genes involved in GA signal transduction were *GID2* (TRINITY_DN17000_c0_g1), *GAI* (TRINITY_DN21636_c0_g1) (GAI was identified again), and the auxin signal transduction gene, *IAA5*

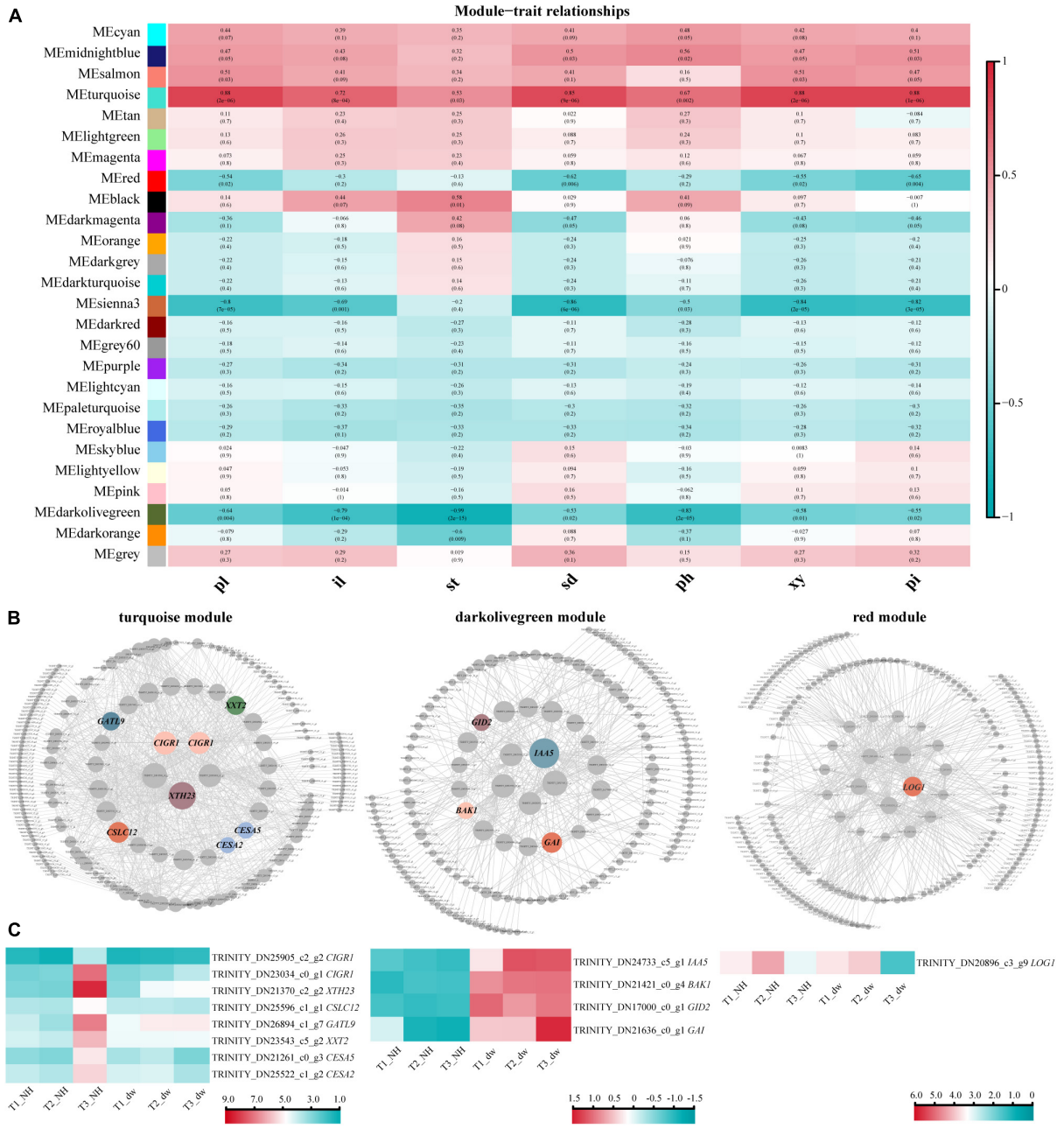

FIGURE 5
WGCNA and HUB genes of three key modules. **(A)** Association between modules and phenotypic traits. pl, plant height; il, internode length; st, length of stem tip; sd, stem diameter; ph, phloem thickness; xy, xylem thickness; pi, pith diameter. **(B)** HUB gene interaction network. CIGR1, chitin-inducible gibberellin-responsive protein 1; XTH23, probable xyloglucan endotransglucosylase/hydrolase protein 23; CSLC12, probable xyloglucan glycosyltransferase; GATL9, probable galacturonosyltransferase-like 9; XXT2, xyloglucan 6-xylosyltransferase 2; CESA2, cellulose synthase A catalytic subunit 2; CESA5, cellulose synthase A catalytic subunit 5; IAA5, auxin-responsive protein IAA5-like; BAK1, brassinosteroid insensitive 1-associated receptor kinase 1-like; LOG1, cytokinin riboside 5′-monophosphate phosphoribohydrolase LOG1. **(C)** Heat map of HUB gene expression.

(TRINITY_DN24733_c5_g1). A brassinolide signal transduction gene *BAK1* (TRINITY_DN21421_c0_g4) was also identified.

The other two modules, red and sienna3, were analyzed. In the red (negative correlation) module, a hormone-related HUB gene was identified as *LOG1* (TRINITY_DN20896_c3_g9) (Figures 5B,C, right). Although red was a negative correlation module, the expression of *LOG1* in NH was higher than that in dw at T3 stage. No significant difference was observed in the HUB genes in the sienna3 module.

Gibberellic acid signaling pathway gene cloning and *CpGAI* analysis

The level of active DELLA protein plays a key role in plant height. The above analysis showed that the expression of *CpGAI* in dw was significantly higher than that in NH, which may lead to a higher level of active DELLA protein in dw. To verify whether GID1 and GID2 interact with DELLA protein differently in the GA signal transduction pathway in the two materials, we searched for these genes in the transcriptome database and cloned them in the two materials. A typical DELLA domain was searched in the database, and a *DELLA* homologous gene, *CpGAI* (TRINITY_DN21636_c0_g1), was identified. We also searched for *CpGID1* (TRINITY_DN24764_c8_g6) and *CpGID2* (TRINITY_DN17000_c0_g1) genes. The cloning results showed no difference in the coding region sequences of the three genes in the two accessions (Gene bank accession number: *CpGAI*, OP222008; *CpGID1*, OP222009; *CpGID2*, OP222010). This indicates that the dwarfness of dw was not due to an interaction with the DELLA protein caused by a deletion or mutation of the gene sequence in the GA signal transduction pathway, but by the change at the transcriptional level.

According to the above research results, we believe that the change in *CpGAI* gene transcription level is one of the key changes that lead to the dwarfing trait in dw; therefore, *CpGAI* was evaluated further. We cloned the full-length *CpGAI* ORF of 1,740 bp in the *C. praecox* cDNA. The amino acid sequence of CpGAI was searched using NCBI pBLAST and compared with homologous proteins of other species (**Figure 6A**). The conserved domains of CpGAI and CmGAI, AfGAI, KuGAI, PsGAI, and McGRAS have high homology, suggesting that CpGAI might have the functional characteristics of the DELLA protein family. There are typical DELLA domains at the N-terminus of CpGAI, including DELLA and TVHYNP motifs (red lines), which are necessary for sensing GA signals. CpGAI also has typical GRAS domains at the C-terminus, including leucine heptad repeat I (LHR I), VHIID motif, leucine heptad repeat II (LHR II), PFYRE motif, and SAW motif (green lines) (Peng et al., 1997; Pysh et al., 1999). Phylogenetic analysis showed that CpGAI (red triangle) and GAI1-like of *Cinnamomum micranthum* had the highest homology and clustered together (**Figure 6B**).

The GAI is a transcriptional regulator (Fleck and Harberd, 2002). Therefore, we speculated that *CpGAI* might be located in the nucleus. After *A. tumefaciens*-mediated transformation and transient expression, laser confocal observation showed that the *35S:CpGAI-GFP* fusion protein was located mainly in the nucleus with a small amount in the cytoplasm, while GFP in the positive control group containing the empty vector *35S:GFP* was distributed throughout the whole cell, and only blue fluorescence was observed in the mock group, but not GFP (**Figure 7A**).

We used a yeast system to analyze the self-activating transcriptional activity of CpGAI protein to verify that *CpGAI* can activate transcription. The results showed that *pGBKT7-CpGAI*, *pGBKT7-TF39,* and *pGBKT7* strains grew normally on the YPDA medium (**Figure 7B**). A single colony was picked, shaken, and dropped on SD/-Trp and SD/-Trp (+*X*-α-gal) media. All the strains grew but did not show color on SD/-Trp medium, indicating that the above plasmids were successfully transferred into the Y2HGold strain. The negative control grew on SD/-Trp (+*X*-α-gal) medium but did not show color; the strain transfected with *pGBKT7-TF39* and *pGBKT7-CpGAI* recombinant plasmids grew, and the reaction substrate *X*-α-gal turned blue. These results suggest that CpGAI has self-activating transcriptional activity and may play a role in transcription in *C. praecox*.

Transgenic poplars overexpressing *CpGAI* became shorter

The *CpGAI* gene was overexpressed in poplar under the control of the cauliflower mosaic virus 35S promoter to assess the biological function of *CpGAI*. The transgenic lines were identified using PCR, and the expression level of *CpGAI* was determined using qRT-PCR. The results showed that the plant height of the three overexpressing lines (L2, L3, and L5) was lesser than that of the WT (**Figure 8A**), and the internode length was significantly shorter (**Figure 8B**). qRT-PCR results showed no expression of *CpGAI* in the WT lines, but it was highly expressed in the three transgenic lines (**Figure 8C**). Therefore, it is speculated that the increased expression of *CpGAI* may cause dwarfism in dw.

Discussion

The lack of endogenous gibberellic acid may be one of the reasons for the dwarfing of dwarf

The height of ornamental plants is very important for enriching horticultural materials. In this study, identifying a dwarf accession of *C. praecox* provided the experimental material for analyzing the mechanism of dwarfing in *C. praecox*. Phenotypic analysis of the dw and NH accessions revealed that decreased internode number and internode length resulted in dwarfing in dw. There was a significant difference in stem tip length between the two accessions in the paraffin sections, which may indicate that internode shortening of dw occurred at the early stage. The transverse section of the stem showed that the thickness of the xylem and pith of dw was significantly smaller than that of NH, which led to a significant difference in the stem diameter. Jiao et al. (2019) overexpressed the *MYB189*

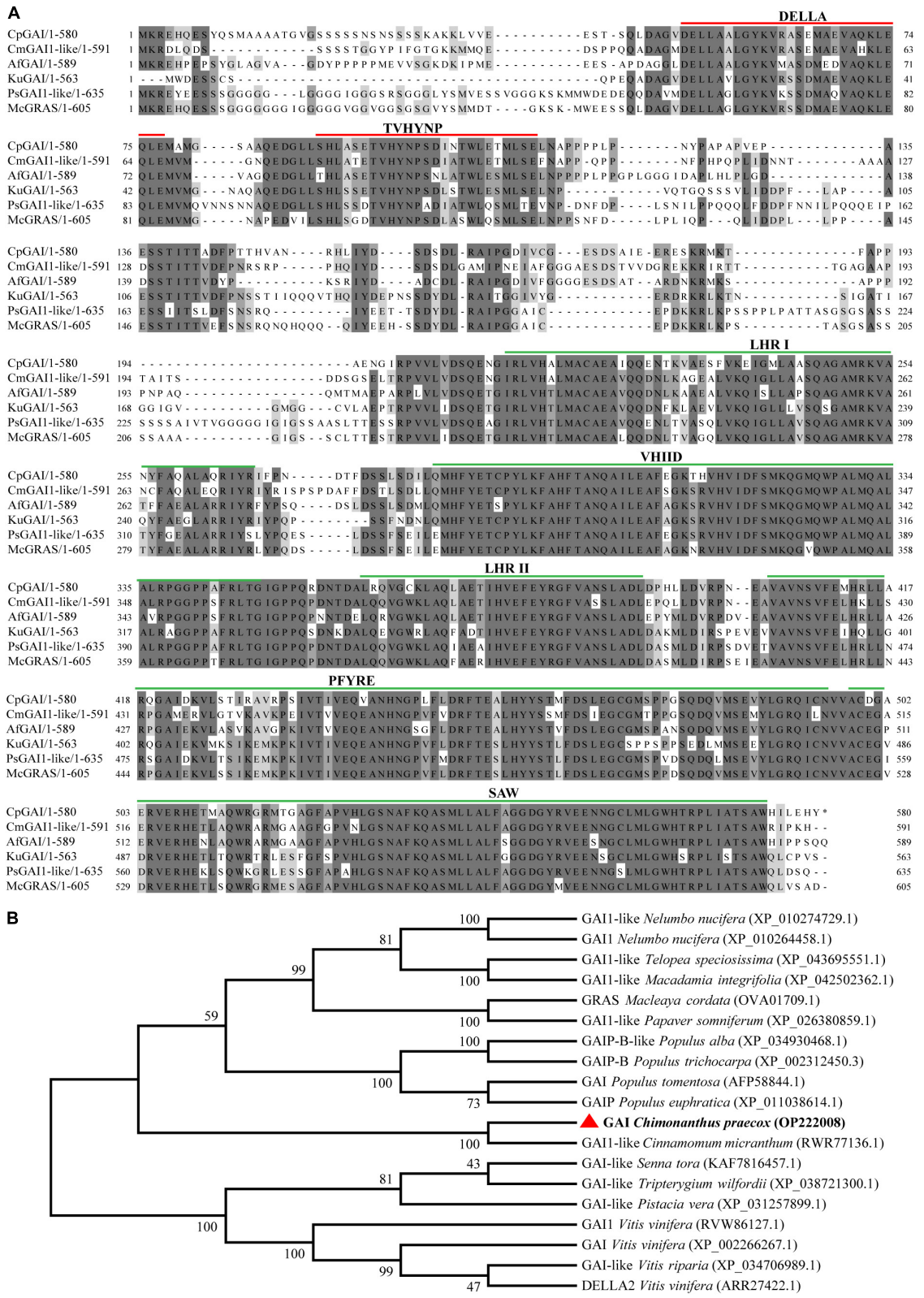

FIGURE 6
CpGAI amino acid sequence alignment and phylogenetic analysis. **(A)** Multiple sequence alignment of CpGAI protein with the proteins of *Cinnamomum micranthum*, *Aristolochia fimbriata*, *Kingdonia uniflora*, *Papaver somniferum*, and *Macleaya cordata*. The line above shows the location of the conservative area. **(B)** Phylogenetic analysis of the CpGAI protein and GAI of other species; red triangle represents CpGAI.

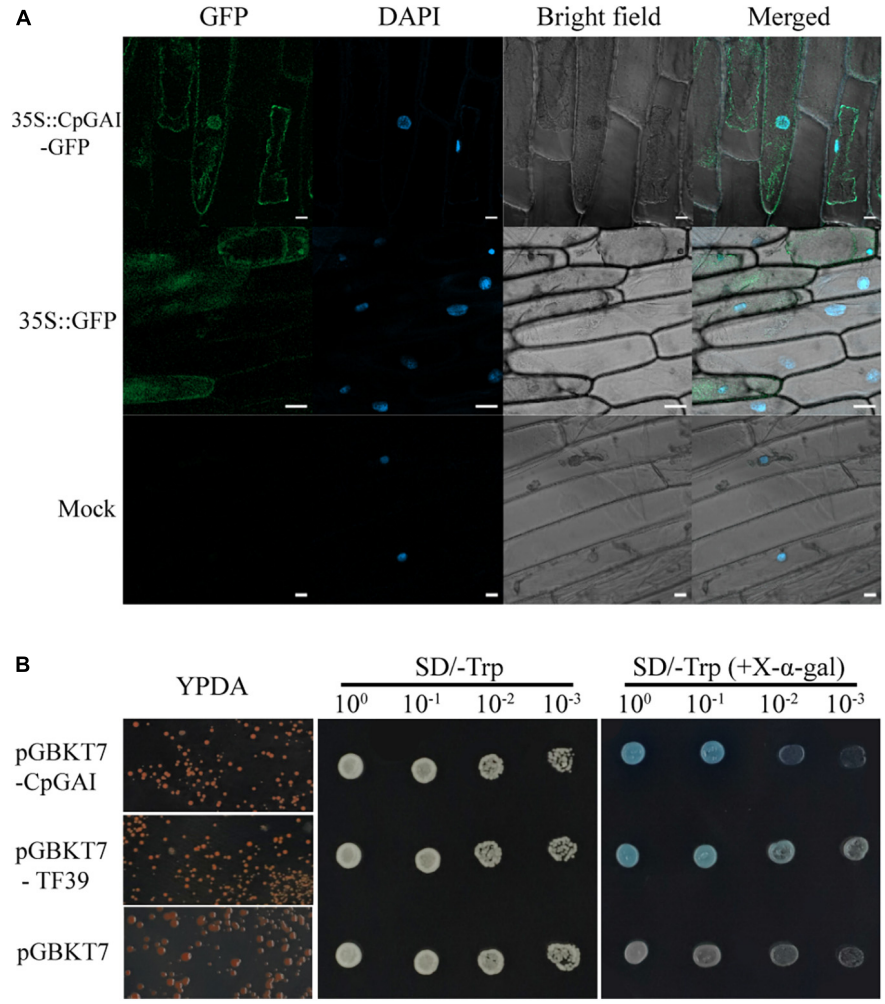

FIGURE 7
CpGAI is mainly located in the nucleus and has transcriptional self-activation activity. **(A)** Subcellular localization of *CpGAI-GFP* in onion epidermis. The short white line at the lower right of *35S:CpGAI-GFP*, *35S: GFP*, and mock represents 20, 50, and 20 μm, respectively. **(B)** Transcriptional self-activating activity of CpGAI protein in yeast cells. SD/-Trp, medium without tryptophan; SD/- trp (+*X*-α-gal), medium without tryptophan containing 5-bromo-4-chloro-3-indoxyl-α-D-galactopyranoside. pGBKT7-TF39 is the positive control, and pGBKT7 is the negative control.

gene in poplar and found that the xylem thickness of the transgenic lines was significantly reduced compared to the WT. It was accompanied by a significant decrease in plant height, suggesting that there may be a connection between xylem thickness and plant height.

The GA is an important hormone that controls plant height, mainly by increasing the number and length of cells to promote growth (Richards et al., 2001). Longitudinal sections showed that the number and size of the cells led to a shortening of the dw internodes, which suggests that the dwarfing of dw may be related to the GA pathway. The height of dw can be restored by exogenous GA treatment. Active GA1 and GA4 have been confirmed to play important roles in dwarfing in many plants (MacMillan, 2001). Endogenous GA content analysis showed that GA4 was significantly higher in NH than in dw, which further supports the hypothesis that GA causes dw dwarfing.

Key differentially expressed genes of gibberellic acid synthesis and signal transduction pathways

The results of KEGG analysis of the transcriptome showed that GA was indeed an important hormone involved in dwarfing in dw, and the transcript expression levels of GA synthesis and signal transduction-related genes in the two materials were analyzed. GA is a diterpene compound that synthesizes the diterpenoid precursor GGPP (Sun and Kamiya, 1994). Tata et al. (2016) transferred the sunflower gene

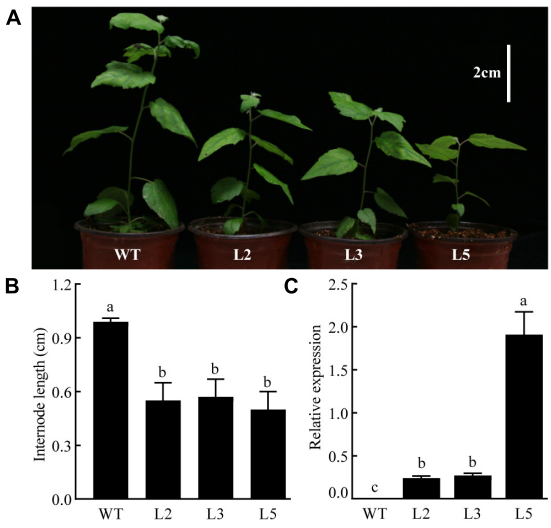

FIGURE 8
Overexpressed CpGAI lines show reduced plant height (white vertical line in the upper right corner indicates 2 cm). **(A)** Phenotypes of transgenic lines L2, L3, and L5. **(B)** Internode length of transgenic lines and WT. **(C)** Relative expression of *CpGAI* in transgenic lines and WT. Different lowercase letters **(a–c)** above bars indicate significant differences ($p < 0.05$).

HaGGPS into tobacco and found that transgenic tobacco with heterologous expression of *HaGGPS* was taller and had a higher endogenous GA content than the WT plants, indicating that GGPS can increase the content of GA in plants. Our results showed that the expression level of the two *CpGGPS* genes in NH was significantly higher than that in dw, which indicates that NH may synthesize more endogenous GA. The expression of the GA synthesis pathway genes *CpKO, CpKAO,* and *CpGA20ox* in dw was significantly higher than that in NH, which is contrary to our inference; however, the expression of *GA2ox*, which catalyzes the conversion of active GA1 and GA4 into inactive GA (Hedden and Phillips, 2000), in dw was significantly higher than that in NH. Moreover, endogenous GA4 content was substantially lower in dw, which indicates that the content of active GA4 may be decreased because of the high expression of *CpGA2ox*, resulting in dwarfing. In a study on peas, the increase in *GA2ox* expression inhibited the accumulation of active GA (Weller et al., 2009), which is consistent with our presumption of the decrease in endogenous GA4 in dw.

In the signal transduction stage, GID1, DELLA, and GID2 proteins are the three key regulatory factors in GA signal transduction (Sun, 2010). GID1 is the sensory receptor of GA. In *A. thaliana*, the three types of GID1 (a-, b-, and c-) have a higher binding ability to GA4 than the other GAs (Nakajima et al., 2006). The active GA4 content was higher in NH than in dw, which may be the reason for the increased expression of *CpGID1* in NH. The increased expression of *CpGAI* in dw may lead to the accumulation of active DELLA proteins and inhibition of growth in dw.

HUB genes related to dwarf dwarfing are involved in hormone and cell wall synthesis

Plant height regulation is complex, and we used WGCNA to identify genes closely related to plant height in the entire network. The HUB genes were related mainly to hormones and cell wall formation. The HUB genes related to GA signal transduction pathway included *CpGAI* and *CpGID2*. Two *CIGR1* homologous genes were highly expressed in the NH, similar to plant height studies in rice. The expression of CIGR in all tissues of tall rice plants was higher than that in short rice plants, especially in the young leaf sheaths that contain elongating tissue (Kovi et al., 2011). *IAA5*, an important gene in the auxin signal transduction pathway, was highly expressed in dw. AUX/IAA is an important repressor in the IAA signal transduction pathway, and its related genes regulate plant height. Transgenic rice plants overexpressing *OsIAA1* showed a reduction in plant height (Song et al., 2009). The HUB gene *CpBAK1,* related to brassinolide signal transduction, was highly expressed in dw. *AtBAK1* gene was heterogeneously expressed in rice plants, and the transgenic rice plants showed a semi-dwarfing phenotype during the growth and development stages (Wang et al., 2007). Subsequently, Li et al. (2009) overexpressed a truncated intracellular domain of *OsBAK1* in rice, which led to a dwarfing phenotype, and showed that BAK1 caused dwarfing by affecting plant brassinosteroid signal transduction. The cytokinin-related gene *CpLOG1* was identified as a HUB gene. The *LONELYGUY* (*LOG*) gene has been shown to be necessary to maintain the activity of meristems in rice. It is a cytokinin-activating enzyme that plays a role in the final step of the synthesis of active cytokinins, and its loss of function leads to early termination of the shoot meristem (Kurakawa et al., 2007). Previous phenotype results showed that the number of stem segments in dw was less than that in NH, suggesting that the low expression of *CpLOG1* in dw might lead to the early completion of SAM differentiation. Plant hormones interact with one or more other hormones to function (Santner et al., 2009). Therefore, among the identified HUB genes, it is likely that plant height is regulated by the interaction between hormones, and the mechanism of mutual regulation between hormones needs to be further studied.

The identified HUB genes included *CpXTH23, CpCSLC12, CpGATL9* (*GAUT-Like 9*), *CpXXT2,* and *CpCESA2/5*. These genes and their homologous genes are involved in cell wall formation in other plants and influence stem diameter and elongation (Turner and Somerville, 1997; Burn et al., 2002; Cocuron et al., 2007; Kong et al., 2011; Guo et al., 2020;

Sowinski et al., 2022). In rice, GA can upregulate the expression of the *OsXTH8* gene, while other hormones have little effect on *OsXTH8* (Jan et al., 2004). The expression of *XTH23* in *A. thaliana* was significantly upregulated by GA treatment (Yokoyama and Nishitani, 2001). The transcriptional level of the *GAUT* gene may be regulated by hormones other than GA (Fan et al., 2021). In crape myrtle, the number of pith cells and xylem cells was significantly higher in exogenous GA4 treated plants than that in the control (Ju et al., 2018). These results demonstrate that GA can regulate cell growth by inducing the expression of genes related to cell wall synthesis.

Up-regulation of *CpGAI* may lead to dwarfing of dwarf

Mutation in the genes related to GA signal transduction pathway leads to a change in plant height. In peach dwarfing, the GID1 mutation inhibits the interaction with DELLA protein, resulting in DELLA protein accumulation (Cheng et al., 2019). It has also been shown that DELLA protein accumulation can be induced when the DELLA or VHYNP motifs are mutated (Willige et al., 2007). We cloned *CpGAI, CpGID1,* and *CpGID2* to determine whether dwarfing was caused by gene mutations in the GA signal transduction pathway. We found that these three sequences were identical in the two accessions, respectively, which ruled out the dwarfing of dw due to a gene mutation. It was probably due to the significant upregulation of *CpGAI*. It has been confirmed that high-level transcription of the DELLA gene can inhibit stem elongation (Dill et al., 2001; Shahnejat-Bushehri et al., 2016).

Our domain analysis of CpGAI showed that its N-terminal contains a typical DELLA domain, and the C-terminal has a regular GRAS domain. Subcellular localization indicated that CpGAI was located mainly in the nucleus, with a small amount in the cytoplasm. In *A. thaliana*, sugarcane, and other plants, GAI is located in the nucleus (Dill et al., 2001; Chai et al., 2022). The presence of small amount of GFP signals in the cytoplasm might indicate the localization of free GFP that has been cleaved from the fusion protein (GAI-GFP) in the transfected cells (Quattrocchio et al., 2013). Transcriptional activation experiments further demonstrated that *CpGAI* is a typical transcription factor. DELLA represses plant growth and inhibits GA signaling in two ways (Ariizumi et al., 2008): first, the formation of the GA-GID1-DELLA protein complex enhances the interaction between DELLA and $SCF^{SLY1/GID2}$, resulting in the ubiquitination of DELLA proteins by SLY1/GID2 and degradation by the 26S proteasome (Gomi et al., 2004); second, GA binds to GID1 and directly interacts with the DELLA domain to block the inhibitory activity of DELLA and inactivate the DELLA protein, which is independent of the ubiquitin degradation of DELLA protein by GID2 (Ariizumi et al., 2008). In our results, endogenous GA4 content and the expression of

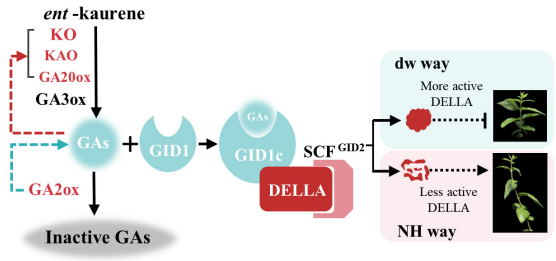

FIGURE 9
Model of plant height regulation in *C. praecox* (dw and NH). In the synthesis pathway, the red character indicates the up-regulated gene in dw. The red arrow indicates that decreased GA content promotes the up-regulation of synthetic gene expression, and the green arrow indicates that GA2ox reduces the active GA. In the signal transduction pathway, short vertical lines represent more active DELLA proteins that inhibit the elongation of *C. praecox* branches, while dotted arrows represent less active DELLA proteins that allow normal *C. praecox* growth.

CpGID1 were high in NH, which may enable the GA-GID1 complex to interact with more DELLA domains of CpGAI, thereby inhibiting DELLA activity. At the same time, the high expression of *CpGAI* in dw may lead to the accumulation of active DELLA proteins and inhibit the growth of dw. Therefore, there may be two inhibitory pathways for the DELLA protein in *C. praecox*. We verified the overexpression of *CpGAI* in *P. tomentosa*, a woody plant. The results showed that the overexpressed population's plant height and internode length decreased significantly, which confirmed the dwarfing function of *CpGAI*. In a recent study on *A. thaliana*, HB40 directly upregulated the expression of *GA2oxs* to reduce bioactive GA, whereas lower levels of active GA led to an increase in DELLA protein levels and inhibited various growth and development processes, including plant height (Dong et al., 2022), which is similar to our results.

Finally, we propose a regulatory mechanism model for dw dwarfing (**Figure 9**). In the normal plant *C. praecox* (NH), the GA synthesis pathway gene is normally expressed; active GA1, GA3, and GA4 are synthesized, and signal transduction is completed. Finally, DELLA protein is degraded or inactivated by ubiquitin, and wintersweet grows normally. In dw, the KO, KAO, and GA20ox genes that synthesize GA are highly expressed, but GA2ox, which inactivates GA, is also highly expressed and significantly reduces the active GA4 content. The decrease in GA4 results in the increase in the transcription of genes in the synthesis and metabolic pathways and induces dwarfing of dw to some extent. After entering the signal transduction stage, the elevated expression of *CpGAI* in dw leads to increased levels of active DELLA protein. A small amount of GA-GID1 complex is not enough to bind to the functional DELLA protein to inactivate it or be subsequently ubiquitinated, and the active DELLA protein further leads to dw dwarfing.

Data availability statement

Accession to RNA-seq data: all RNA-sequencing data were deposited in National Center for Biotechnology Information (NCBI) under BioProject accession number: PRJNA869201 (https://www.ncbi.nlm.nih.gov/sra/PRJNA869201). Gene bank accession numbers: CpGAI: OP222008; CpGID1: OP222009; and CpGID2: OP222010.

Author contributions

SS and SL collected the accessions. TZ and SS designed the research. TZ analyzed the sequencing data and wrote the manuscript. NL performed qPCR. BL, JX, and XS performed graphic drawing. BL and SL edited the manuscript. All authors contributed to the article and approved the submitted version.

Funding

This work was supported by the National Natural Science Foundation of China (31971711) and the Graduate Scientific Innovation Program of Chongqing, China (CYB20101).

Conflict of interest

The authors declare that the research was conducted in the absence of any commercial or financial relationships that could be construed as a potential conflict of interest.

Publisher's note

All claims expressed in this article are solely those of the authors and do not necessarily represent those of their affiliated organizations, or those of the publisher, the editors and the reviewers. Any product that may be evaluated in this article, or claim that may be made by its manufacturer, is not guaranteed or endorsed by the publisher.

Supplementary material

The Supplementary Material for this article can be found online at: https://www.frontiersin.org/articles/10.3389/fpls.2022.1010896/full#supplementary-material

References

Ariizumi, T., Murase, K., Sun, T. P., and Steber, C. M. (2008). Proteolysis-Independent Downregulation of DELLA Repression in *Arabidopsis* by the Gibberellin Receptor GIBBERELLIN INSENSITIVE DWARF1. *Plant Cell* 20, 2447–2459. doi: 10.1105/tpc.108.058487

Ashikari, M., Sasaki, A., Ueguchi-Tanaka, M., Itoh, H., Nishimura, A., Datta, S., et al. (2002). Loss-of-function of a rice gibberellin biosynthetic gene, GA20 oxidase (GA20ox-2), led to the rice 'green revolution'. *Breed. Sci.* 52, 143–150. doi: 10.1270/jsbbs.52.143

Bai, M. Y., Fan, M., Oh, E., and Wang, Z. Y. (2012). A Triple Helix-Loop-Helix/Basic Helix-Loop-Helix Cascade Controls Cell Elongation Downstream of Multiple Hormonal and Environmental Signaling Pathways in *Arabidopsis*. *Plant Cell* 24, 4917–4929. doi: 10.1105/tpc.112.105163

Burn, J. E., Hocart, C. H., Birch, R. J., Cork, A. C., and Williamson, R. E. (2002). Functional analysis of the cellulose synthase genes CesA1, CesA2, and CesA3 in *Arabidopsis*. *Plant Physiol.* 129, 797–807. doi: 10.1104/pp.010931

Chai, Z., Fang, J. L., Yao, W., Zhao, Y., Cheng, G. Y., Akbar, S., et al. (2022). ScGAIL, a sugarcane N-terminal truncated DELLA-like protein, participates in gibberellin signaling in *Arabidopsis*. *J. Exp. Bot.* 73, 3462–3476. doi: 10.1093/jxb/erac056

Cheng, J., Zhang, M. M., Tan, B., Jiang, Y. J., Zheng, X. B., Ye, X., et al. (2019). A single nucleotide mutation in GID1c disrupts its interaction with DELLA1 and causes a GA-insensitive dwarf phenotype in peach. *Plant Biotechnol. J.* 17, 1723–1735. doi: 10.1111/pbi.13094

Cho, S. H., Kang, K., Lee, S. H., Lee, I. J., and Paek, N. C. (2016). OsWOX3A is involved in negative feedback regulation of the gibberellic acid biosynthetic pathway in rice (*Oryza sativa*). *J. Exp. Bot.* 67, 1677–1687. doi: 10.1093/jxb/erv559

Cocuron, J. C., Lerouxel, O., Drakakaki, G., Alonso, A. P., Liepman, A. H., Keegstra, K., et al. (2007). A gene from the cellulose synthase-like C family encodes a beta-1,4 glucan synthase. *Proc. Natl. Acad. Sci. U. S. A.* 104, 8550–8555. doi: 10.1073/pnas.0703133104

Dill, A., Jung, H. S., and Sun, T. P. (2001). The DELLA motif is essential for gibberellin-induced degradation of RGA. *Proc. Natl. Acad. Sci. U. S. A.* 98, 14162–14167. doi: 10.1073/pnas.251534098

Dong, S. C., Tarkowska, D., Sedaghatmehr, M., Welsch, M., Gupta, S., Mueller-Roeber, B., et al. (2022). The HB40-JUB1 transcriptional regulatory network controls gibberellin homeostasis in *Arabidopsis*. *Mol. Plant* 15, 322–339. doi: 10.1016/j.molp.2021.10.007

Du, Y. Q., Tian, X. L., Gan, J. Z., Gu, H. F., Xu, M. L., and Shen, P. H. (2015). Dwarfing effects of chlormequat, paclobutrazol and daminozide applications on *Chimonanthus praecox*. *J. Beijing For. Univ.* 37, 44–47. doi: 10.13332/j.1000-1522.20150459

Fan, S., Liu, A., Zou, X., Zhang, Z., Ge, Q., Gong, W., et al. (2021). Evolution of pectin synthesis relevant galacturonosyltransferase gene family and its expression during cotton fiber development. *J. Cotton Res.* 4:22. doi: 10.1186/s42397-021-00099-z

Fleck, B., and Harberd, N. P. (2002). Evidence that the *Arabidopsis* nuclear gibberellin signalling protein GAI is not destabilised by gibberellin. *Plant J.* 32, 935–947. doi: 10.1046/j.1365-313x.2002.01478.x

Fu, X. D., and Harberd, N. P. (2003). Auxin promotes *Arabidopsis* root growth by modulating gibberellin response. *Nature* 421, 740–743. doi: 10.1038/nature01387

Fu, X. D., Richards, D. E., Fleck, B., Xie, D. X., Burton, N., and Harberd, N. P. (2004). The *Arabidopsis mutant* sleepy1(gar2-1) protein promotes plant growth by increasing the affinity of the SCFSLY1 E3 ubiquitin ligase for DELLA protein substrates. *Plant Cell* 16, 1406–1418. doi: 10.1105/tpc.021386

Gomi, K., Sasaki, A., Itoh, H., Ueguchi-Tanaka, M., Ashikari, M., Kitano, H., et al. (2004). GID2, an F-box subunit of the SCF E3 complex, specifically interacts with phosphorylated SLR1 protein and regulates the gibberellin-dependent degradation of SLR1 in rice. *Plant J.* 37, 626–634. doi: 10.1111/j.1365-313X.2003.01990.x

Guo, P., Chang, H. L., Li, Q., Wang, L. N., Ren, Z. H., Ren, H. Z., et al. (2020). Transcriptome profiling reveals genes involved in spine development during CsTTG1-regulated pathway in cucumber (*Cucumis sativus* L.). *Plant Sci.* 291:110354. doi: 10.1016/j.plantsci.2019.110354

Hedden, P., and Phillips, A. L. (2000). Gibberellin metabolism: New insights revealed by the genes. *Trends Plant Sci.* 5, 523–530. doi: 10.1016/S1360-1385(00)01790-8

Huang, R. W., Liu, D. F., Huang, M., Ma, J., Li, Z. N., Li, M. Y., et al. (2019). CpWRKY71, a WRKY Transcription Factor Gene of Wintersweet (*Chimonanthus praecox*), Promotes Flowering and Leaf Senescence in *Arabidopsis*. *Int. J. Mol. Sci.* 20:5325. doi: 10.3390/ijms20215325

Jan, A., Yang, G. X., Nakamura, H., Ichikawa, H., Kitano, H., Matsuoka, M., et al. (2004). Characterization of a xyloglucan endotransglucosylase gene that is up-regulated by gibberellin in rice. *Plant Physiol.* 136, 3670–3681. doi: 10.1104/pp.104.052274

Jia, Z. C., Sun, Y. M., Yuan, L., Tian, Q. Y., and Luo, K. M. (2010). The chitinase gene (Bbchit1) from *Beauveria bassiana* enhances resistance to *Cytospora chrysosperma* in *Populus tomentosa* Carr. *Biotechnol. Lett.* 32, 1325–1332. doi: 10.1007/s10529-010-0297-6

Jiao, B., Zhao, X., Lu, W. X., Guo, L., and Luo, K. M. (2019). The R2R3 MYB transcription factor MYB189 negatively regulates secondary cell wall biosynthesis in Populus. *Tree Physiol.* 39, 1187–1200. doi: 10.1093/treephys/tpz040

Ju, Y. Q., Feng, L., Wu, J. Y., Ye, Y. J., Zheng, T. C., Cai, M., et al. (2018). Transcriptome analysis of the genes regulating phytohormone and cellular patterning in Lagerstroemia plant architecture. *Sci. Rep.* 8:15162. doi: 10.1038/s41598-018-33506-8

Kong, Y. Z., Zhou, G. K., Yin, Y. B., Xu, Y., Pattathil, S., and Hahn, M. G. (2011). Molecular Analysis of a Family of *Arabidopsis* Genes Related to Galacturonosyltransferases. *Plant Physiol.* 155, 1791–1805. doi: 10.1104/pp.110.163220

Kovi, M., Zhang, Y. S., Yu, S. B., Yang, G. Y., Yan, W. H., and Xing, Y. Z. (2011). Candidacy of a chitin-inducible gibberellin-responsive gene for a major locus affecting plant height in rice that is closely linked to Green Revolution gene sd1. *Theor. Appl. Genet.* 123, 705–714. doi: 10.1007/s00122-011-1620-x

Kurakawa, T., Ueda, N., Maekawa, M., Kobayashi, K., Kojima, M., Nagato, Y., et al. (2007). Direct control of shoot meristem activity by a cytokinin-activating enzyme. *Nature* 445, 652–655. doi: 10.1038/nature05504

Langfelder, P., and Horvath, S. (2008). WGCNA: An R package for weighted correlation network analysis. *BMC Bioinform.* 9:559. doi: 10.1186/1471-2105-9-559

Li, D., Wang, L., Wang, M., Xu, Y. Y., Luo, W., Liu, Y. J., et al. (2009). Engineering OsBAK1 gene as a molecular tool to improve rice architecture for high yield. *Plant Biotechnol. J.* 7, 791–806. doi: 10.1111/j.1467-7652.2009.00444.x

Li, Z. N., Liu, N., Zhang, W., Wu, C. Y., Jiang, Y. J., Ma, J., et al. (2020). Integrated transcriptome and proteome analysis provides insight into chilling-induced dormancy breaking in *Chimonanthus praecox*. *Hortic. Res.* 7:198. doi: 10.1038/s41438-020-00421-x

Lin, S. Q., and Chen, D. R. (2020). Landscape Application and Industry Progress of Wintersweet. *Chin. Landscape Arch.* 36, 104–108. doi: 10.19775/j.cla.2020.S1.0104

Livak, K. J., and Schmittgen, T. D. (2001). Analysis of relative gene expression data using real-time quantitative PCR and the 2(T)(-Delta Delta C) method. *Methods* 25, 402–408. doi: 10.1006/meth.2001.1262

Locascio, A., Blazquez, M. A., and Alabadi, D. (2013). Genomic Analysis of DELLA Protein Activity. *Plant Cell Physiol.* 54, 1229–1237. doi: 10.1093/pcp/pct082

MacMillan, J. (2001). Occurrence of gibberellins in vascular plants, fungi, and bacteria. *J. Plant Growth Regul.* 20, 387–442. doi: 10.1007/s003440010038

Nakajima, M., Shimada, A., Takashi, Y., Kim, Y. C., Park, S. H., Ueguchi-Tanaka, M., et al. (2006). Identification and characterization of *Arabidopsis* gibberellin receptors. *Plant J.* 46, 880–889. doi: 10.1111/j.1365-313X.2006.02748.x

Oh, E., Zhu, J. Y., Bai, M. Y., Arenhart, R. A., Sun, Y., and Wang, Z. Y. (2014). Cell elongation is regulated through a central circuit of interacting transcription factors in the *Arabidopsis* hypocotyl. *Elife* 3:e03031. doi: 10.7554/eLife.03031

Pan, X. Q., Welti, R., and Wang, X. M. (2010). Quantitative analysis of major plant hormones in crude plant extracts by high-performance liquid chromatography-mass spectrometry. *Nat. Protoc.* 5, 986–992. doi: 10.1038/nprot.2010.37

Peng, J. R., Carol, P., Richards, D. E., King, K. E., Cowling, R. J., Murphy, G. P., et al. (1997). The *Arabidopsis* GAI gene defines a signaling pathway that negatively regulates gibberellin responses. *Genes Dev.* 11, 3194–3205. doi: 10.1101/gad.11.23.3194

Peng, J. R., Richards, D. E., Hartley, N. M., Murphy, G. P., Devos, K. M., Flintham, J. E., et al. (1999). 'Green revolution' genes encode mutant gibberellin response modulators. *Nature* 400, 256–261. doi: 10.1038/22307

Pysh, L. D., Wysocka-Diller, J. W., Camilleri, C., Bouchez, D., and Benfey, P. N. (1999). The GRAS gene family in *Arabidopsis*: Sequence characterization and basic expression analysis of the SCARECROW-LIKE genes. *Plant J.* 18, 111–119. doi: 10.1046/j.1365-313X.1999.00431.x

Qi, W. W., Sun, F., Wang, Q. J., Chen, M. L., Huang, Y. Q., Feng, Y. Q., et al. (2011). Rice Ethylene-Response AP2/ERF Factor OsEATB Restricts Internode Elongation by Down-Regulating a Gibberellin Biosynthetic Gene. *Plant Physiol.* 157, 216–228. doi: 10.1104/pp.111.179945

Quattrocchio, F. M., Spelt, C., and Koes, R. (2013). Transgenes and protein localization: Myths and legends. *Trends Plant Sci.* 18, 473–476. doi: 10.1016/j.tplants.2013.07.003

Rezaee, R., Vahdati, K., and Valizadeh, M. (2009). Variability of seedling vigour in *Persian walnut* as influenced by the vigour and bearing habit of the mother tree. *J. Hortic. Sci. Biotechnol.* 84, 228–232. doi: 10.1080/14620316.2009.11512509

Richards, D. E., King, K. E., Ait-ali, T., and Harberd, N. P. (2001). How gibberellin regulates plant growth and development: A molecular genetic analysis of gibberellin signaling. *Annu. Rev. Plant Physiol. Plant Mol. Biol.* 52, 67–88. doi: 10.1146/annurev.arplant.52.1.67

Ripetti, V., Escoute, J., Verdeil, J. L., and Costes, E. (2008). Shaping the shoot: The relative contribution of cell number and cell shape to variations in internode length between parent and hybrid apple trees. *J. Exp. Bot.* 59, 1399–1407. doi: 10.1093/jxb/ern049

Santner, A., Calderon-Villalobos, L. I. A., and Estelle, M. (2009). Plant hormones are versatile chemical regulators of plant growth. *Nat. Chem. Biol.* 5, 301–307. doi: 10.1038/nchembio.165

Shahnejat-Bushehri, S., Tarkowska, D., Sakuraba, Y., and Balazadeh, S. (2016). *Arabidopsis* NAC transcription factor JUB1 regulates GA/BR metabolism and signalling. *Nat. Plants* 2:16013. doi: 10.1038/NPLANTS.2016.13

Song, Y. L., You, J., and Xiong, L. Z. (2009). Characterization of OsIAA1 gene, a member of rice Aux/IAA family involved in auxin and brassinosteroid hormone responses and plant morphogenesis. *Plant Mol. Biol.* 70, 297–309. doi: 10.1007/s11103-009-9474-1

Sowinski, E. E., Westman, B. M., Redmond, C. R., Kong, Y. Z., Olek, A. T., Olek, J., et al. (2022). Lack of xyloglucan in the cell walls of the *Arabidopsis* xxt1/xxt2 mutant results in specific increases in homogalacturonan and glucomannan. *Plant J.* 110, 212–227. doi: 10.1111/tpj.15666

Sun, T. P. (2010). Gibberellin-GID1-DELLA: A Pivotal Regulatory Module for Plant Growth and Development. *Plant Physiol.* 154, 567–570. doi: 10.1104/pp.110.161554

Sun, T. P., and Kamiya, Y. (1994). The *Arabidopsis* Ga1 Locus Encodes the Cyclase Ent-Kaurene Synthetase-a of Gibberellin Biosynthesis. *Plant Cell* 6, 1509–1518. doi: 10.1105/tpc.6.10.1509

Tata, S. K., Jung, J., Kim, Y. H., Choi, J. Y., Jung, J. Y., Lee, I. J., et al. (2016). Heterologous expression of chloroplast-localized geranylgeranyl pyrophosphate synthase confers fast plant growth, early flowering and increased seed yield. *Plant Biotechnol. J.* 14, 29–39. doi: 10.1111/pbi.12333

Turner, S. R., and Somerville, C. R. (1997). Collapsed xylem phenotype of *Arabidopsis* identifies mutants deficient in cellulose deposition in the secondary cell wall. *Plant Cell* 9, 689–701. doi: 10.1105/tpc.9.5.689

Wang, B., Smith, S. M., and Li, J. Y. (2018). Genetic Regulation of Shoot Architecture. *Annu. Rev. Plant Biol.* 69, 437–468. doi: 10.1146/annurev-arplant-042817-040422

Wang, L., Xu, Y. Y., Li, J., Powell, R. A., Xu, Z. H., and Chong, K. (2007). Transgenic rice plants ectopically expressing AtBAK1 are semi-dwarfed and hypersensitive to 24-epibrassinolide. *J. Plant Physiol.* 164, 655–664. doi: 10.1016/j.jplph.2006.08.006

Weller, J. L., Hecht, V., Schoor, J. K. V., Davidson, S. E., and Ross, J. J. (2009). Light Regulation of Gibberellin Biosynthesis in Pea Is Mediated through the COP1/HY5 Pathway. *Plant Cell* 21, 800–813. doi: 10.1105/tpc.108.063628

Willige, B. C., Ghosh, S., Nill, C., Zourelidou, M., Dohmann, E. M. N., Maier, A., et al. (2007). The DELLA domain of GA INSENSITIVE mediates the interaction with the GA INSENSITIVE DWARF1A gibberellin receptor of *Arabidopsis*. *Plant Cell* 19, 1209–1220. doi: 10.1105/tpc.107.051441

Xiao, K. (2021). *Planning and Design of Wintersweet Industrial Park–Taking the Planning and Design of World Wintersweet Industrial Park in Yanling as an Example*. Ph.D. thesis, Beijing Forestry University, Beijing.

Yokoyama, R., and Nishitani, K. (2001). A comprehensive expression analysis of all members of a gene family encoding cell-wall enzymes allowed us to

predict cis-regulatory regions involved in cell-wall construction in specific organs of *Arabidopsis*. *Plant Cell Physiol.* 42, 1025–1033. doi: 10.1093/pcp/pce154

Yuan, P. Y., and Song, X. R. (2012). Effect of Paclobutrazol on Brachysm and Stress Resistance of Potted *Chimonanthus praecox*. *Southwest China J. Agric. Sci.* 25, 1253–1256. doi: 10.16213/j.cnki.scjas.2012.04.065

Zhang, B., and Horvath, S. (2005). A general framework for weighted gene co-expression network analysis. *Statist. Appl. Genet. Mol. Biol.* 4:Article17. doi: 10.2202/1544-6115.1128

frontiers | Frontiers in Plant Science

TYPE Original Research
PUBLISHED 06 October 2022
DOI 10.3389/fpls.2022.999433

OPEN ACCESS

EDITED BY
Shunli Wang,
Chinese Academy of Agricultural Sciences (CAAS), China

REVIEWED BY
Pandiyan Muthuramalingam,
Gyeongsang National University, South Korea
Shanker Lal Kothari,
Amity University Rajasthan, India

*CORRESPONDENCE
Xiaomei Sun
sxm7280@syau.edu.cn

†These authors have contributed equally to this work

SPECIALTY SECTION
This article was submitted to Plant Breeding, a section of the journal Frontiers in Plant Science

RECEIVED 21 July 2022
ACCEPTED 20 September 2022
PUBLISHED 06 October 2022

CITATION
Guan S, Kang X, Ge J, Fei R, Duan S and Sun X (2022) An efficient *Agrobacterium*-mediated transient transformation system and its application in gene function elucidation in *Paeonia lactiflora* Pall. *Front. Plant Sci.* 13:999433. doi: 10.3389/fpls.2022.999433

An efficient *Agrobacterium*-mediated transient transformation system and its application in gene function elucidation in *Paeonia lactiflora* Pall.

Shixin Guan[1,2†], Xuening Kang[1,2†], Jiayuan Ge[1,2], Riwen Fei[3], Siyang Duan[1,2] and Xiaomei Sun[1,2*]

[1]College of Forestry, Shenyang Agricultural University, Shenyang, China, [2]Key Laboratory of Forest Tree Genetics, Breeding and Cultivation of Liaoning Province, Shenyang Agricultural University, Shenyang, China, [3]College of Horticulture, Shenyang Agricultural University, Shenyang, China

Paeonia lactiflora Pall. is known as the king of herbaceous flowers with high ornamental and precious medicinal value. However, the lack of a stable genetic transformation system has greatly affected the research of gene function in *P. lactiflora*. The *Agrobacterium*-mediated transient gene expression is a powerful tool for the characterization of gene function in plants. In this study, the seedlings of *P. lactiflora* were used as the transformation receptor materials, and the efficient transient transformation system with a GUS reporter gene was successfully established by *Agrobacterium* harboring pCAMBIA1301. To optimize the system, we investigated the effects of germination time, *Agrobacterium* cell density, infection time, acetosyringone (AS) concentration, co-culture time, negative pressure intensity, Tween-20 concentration and different receptor materials on the transient transformation efficiency of *P. lactiflora*. The results showed that the highest transient transformation efficiency (93.3%) could be obtained when seedlings in 2-3 cm bud length were subjected to 12 h infection of resuspension solution comprising 1.2 OD_{600} *Agrobacterium*, 200 μM AS and 0.01% Tween-20 under 10 of negative pressure intensity followed by 3 days of co-culture in darkness condition. This method is more suitable for the study of gene function in *P. lactiflora*. Subsequently, stress resistance genes *PlGPAT*, *PlDHN2* and *PlHD-Zip* were used to verify the effectiveness of this transformation system. These results can provide critical information for identification of key genes in non-model plants, such as *P. lactiflora*, and promote the development of molecular biology research for *P. lactiflora*.

KEYWORDS

***Paeonia lactiflora* pall., efficient transient transformation, *Agrobacterium*-mediated, stress resistance genes, physiological indexes**

Introduction

Herbaceous peony (*Paeonia lactiflora* Pall.) belongs to the Paeoniaceae family and is known as the 'flower phase'. It is a famous traditional flower and has been cultivated for more than three thousand years in China (Li, 1999). *P. lactiflora* is widely introduced because it has medicinal and excellent ornamental value as an economic plant. *P. lactiflora* has strong cold resistance and can survive winter in the open field in the northern region. It is an important garden flower and is very popular. In recent years, with the increasing area of cultivation, the environmental challenges faced by *P. lactiflora* have become more complex. Therefore, it is important to study the functions of stress resistance-related genes in *P. lactiflora*. At present, the commonly used gene function research is to stably inherit the target gene in this plant to obtain transgenic plants. But for *P. lactiflora*, a stable genetic transformation system has not been established so far, and there are still problems in the study of tissue culture of *Paeonia* plants such as contamination, browning (Zhang et al., 2021), vitrification of explants, difficulties in redifferentiation of callus, inducing robust clumps of seedlings, and rooting sterile seedlings of *P. lactiflora* (Zhou and Huang, 2018). Presently, domestic and foreign studies on gene function of *P. lactiflora* mostly use model plants, such as tobacco and *Arabidopsis thaliana*. Thus, it is necessary to establish an *Agrobacterium*-mediated high efficiency transient transformation system suitable for studying the function of the anti-stress gene of *P. lactiflora*.

Agrobacterium-mediated transient transformation of plants is a technology that can achieve transient high-level expression of target genes in a short time (Tyurin et al., 2020), which is widely used for the gene functional verification (Vaghchhipawala et al., 2011). Compared with stable transformation, it does not rely on chromosomal integration of heterologous DNA (Zheng et al., 2012), is simpler, faster and lower cost, and the process allows the processing of large numbers of plants as well as multiple gene transient expression on a single leaf analysis (Tsubasa, 2018), making this technology a powerful tool for studying the function of plant genes without genetic transformation system (Liao et al., 2017). Currently, this technology has been successfully applied to many plants, such as *A. thaliana* (Guo et al., 2016), *Betula platyphylla* (Zheng et al., 2012), *Salix babylonica* (Ji et al., 2014), *Populus euphratica* (Takata and Eriksson, 2012), *Gossypium hirsutum* (Li et al., 2018a), *Rosa chinensis* (Lu et al., 2017), and *Anemone vitifolia* (Wang, 2014). Xie et al. (2019) first applied a Tobacco Rattle Virus (TRV)-induced gene silencing technique to the peony 'Fengdan'. After silencing the peony endogenous gene *PoPDS*, it was found that the uppermost new leaves showed a typical photobleaching phenotype. In addition, by observing the fluorescence of green fluorescent protein (GFP) in the leaves and roots of peony inoculated with TRV-GFP, it was found that TRV can silence genes in various tissues. Bian et al. (2020) used the virus-induced gene silencing (VIGS) technique to silence the *PlDELLA* gene in *P.lactiflora* and found that *PlDELLA* has a negative effect on dormancy release and plant growth. The above findings suggest that transient transformation system can be applied in the study of gene function in *Paeonia*, but mostly by means of VIGS technique (Shu et al., 2018; Wu et al., 2020). However, the overexpression of some key genes *via Agrobacterium*-mediated transient transformation system has rarely been reported in *Paeonia*.

The cold resistance of plants is closely related to the level of phosphatidylglycerol in chloroplast membrane lipids. Glycerol-3-phosphate acyltransferase (GPAT) is the first acylesterase for synthesis of phosphatidylglycerol in biofilm (Shockey et al., 2016). Recent studies revealed that the gene has a potential role in tolerance to abiotic stress in many species, such as *Ammopiptanthus mongolicus* (Xue et al., 2019), *Oryza sativa* (Imran et al., 2021) and *Forsythia viridissima* (Li et al., 2020). Li et al. (2018b) analyzed the expression level of *PlGPAT* gene under low temperature stress and found that it plays an important role in regulating the cold resistance of *P. lactiflora*. Many studies have shown that the *DHN* gene is involved in a cytoprotective mechanism that maintains the stability of cell membranes under stress conditions (Klimešová et al., 2020), and abiotic stress and hormone induce the expression of this gene (Yamasaki et al., 2013). The gene's ability to improve plant tolerance to high temperature has been confirmed in a variety of plants, such as *Capsicum annuum* (Liu, 2021), *Melilotoides ruthenica* (Shen et al., 2016) and *A. mongolicus* (Shi, 2012). Chen et al. (2017) found that the expression of *PlDHN2* gene was up-regulated after high temperature treatment, which was involved in the regulation mechanism of peony's tolerance to high temperature stress in *P. lactiflora*. Moreover, Homeodomain Leucine Zipper (HD-Zip) protein is a transcription factor specific to higher plants. A large number of research data show that HD-Zip protein plays a very important role in plant growth regulation and resistance to stress (Sessa et al., 1998). Therefore, various genes of the HD-ZIP family have been isolated and cloned from numerous plants, and their functions have been studied. Examples include *Dendrobium catenatum* (Huang et al., 2021), *Zea mays* (Wang et al., 2021) and *Arachis hypogaea* (Banavath et al., 2018). The drought tolerance function of the *P. lactiflora PlHD-Zip* gene has been confirmed by overexpression in *A. thaliana* (Wang et al., 2010).

A large number of previous studies have shown that the transient transformation efficiency of plants is influenced by the growth state of the transformed recipient material (Chen et al., 2021), *Agrobacterium* density (Li et al., 2018a), infection time (Xia et al., 2020a), acetosyringone concentration (Liu et al., 2020), co-

culture time (An et al., 2020) and some other factors. In this study, we screened each factor mentioned above and established a high-efficiency transient transformation system of *P. lactiflora* mediated by *Agrobacterium*. This system was used to transiently overexpress the stress resistance genes *PlGPAT*, *PlDHN2* and *PlHD-Zip* in *P. lactiflora*, and detect their effects on low temperature, high temperature and drought stress. Gene expression levels and physiological indicators verified the feasibility of the transient transformation system. The transient transformation protocol we developed is fast and efficient for the functional study of the stress resistance gene of *P. lactiflora*.

Materials and methods

Seed collection and seedling preparation of *P. lactiflora*

The aseptic tissue cultureseedlings cultivated from the herbaceous peony hybrid seeds ('Fen Yunu' × 'Fen Yulou') were collected from the Peony Germplasm Resource Garden of Shenyang Agricultural University. The pCAMBIA1301-GUS vector was gifted by Professor Yucheng Wang (Shenyang Agricultural University). The *Agrobacterium tumefaciens* EHA105 strain was purchased from Angyu Biotechnology Co., Ltd. (Angyu Biotechnology Co., Ltd., Shanghai, China). The trial flow is summarized in Figure 1.

Paeonia lactiflora hybrid seeds were soaked in warm water for 48 h, and the seed coats were removed. The seeds were disinfected with 75% alcohol for 30s, rinsed twice with sterile water, disinfected with 0.1% $HgCl_2$ solution for 5-6 min, and sterile-water rinsed 3-4 times for 1 min per time. Sterile water was then removed with sterile filter paper. The embryos were taken out and inoculated in the starting medium (MS + 0.5 mg·L^{-1} GA_3 + 1.0 mg·L^{-1} 6-BA + 30 g·L^{-1} sucrose + 6.5 g·L^{-1} agar, pH = 5.6), and placed under the conditions of light time of 16 h·d^{-1}, light intensity of 2000-3000 lx, and temperature of 24-26°C. The sterile tissue culture seedlings at 30, 45 and 60 d after germination were taken for *Agrobacterium*-mediated transient transformation (Figure 2).

The seeds were washed with washing powder for 20 min, and then flushed with water repeatedly until there is no foam. The seeds were soaked in water for 3 h, and the full seeds were retained. The seeds were disinfected with 0.5% $KMnO_4$ for 40 min, and then washed with water to remove all drug residues. The seeds were soaked in 45°C warm water for 24 h until the water became turbid. The new 45°C warm water was used to continue soaking for 24 h. Next, the seeds were washed, and the floating seeds were thrown away. The seeds were stored in sand at 15-20°C, and observed every 5 days. When the root length of the seeds was 3-4 cm (Figure 3A), they were placed in the 4°C incubator for germination. After two months, the seeds were removed from the incubator and placed in a 15-20°C environment. Approximately 3-7 days later, seedlings with 2-3 cm buds (Figure 3B) were taken out to compare the effects of different receptor materials on *P. lactiflora* transient transformation efficiency.

Construction of recombinant plasmids

The EASYspin Plus polysaccharide and polyphenol complex plant RNA rapid extraction kit (Aidlab, Beijing, China) was used to extract the total RNA of *P. lactiflora* seeds, and the RNA was reversely transcribed into cDNA using the PrimeScript™ II 1st Strand cDNA synthesis kit (Takara, Beijing, China). This cDNA was used as a template, PlGPAT-F/R, PlDHN2-F/R and PlHD-Zip-F/R are upstream and downstream primers for PCR amplification. The plant expression vector pCAMBIA1301 and the target gene with added restriction sites and protected bases were doubly digested with NcoI and BglII enzymes, and the empty expression vector and target gene fragment were recovered using a gel recovery kit (Aidlab, Beijing, China). The coding sequence (CDS) of the target gene was fused in-frame with the GUS coding region in the plant expression vector pCAMBIA1301 to construct the recombinant plasmid *pCAMBIA1301:PlGPAT/PlDHN2/PlHD-Zip* (Supplementary Figure 1). The empty vectors were used as control. All primers used in PCR are shown in Supplementary Table 1.

Agrobacterium-mediated transient transformation

The constructs and pCAMBIA1301 empty vector were transformed into *Agrobacterium* EHA105 by freeze-thaw method. The bacterial solution was coated on LB solid medium containing 50 mg·L^{-1} Kan and 50 mg·L^{-1} Rif and cultivated for 2-3 d at 28°C in inverted position. The single colony was inoculated to 1.5 mL of LB liquid medium containing 50 mg·L^{-1} Kan and 50 mg·L^{-1} Rif and incubated for 24 h at 28°C and 200 rpm. The 1 mL of turbid bacterial culture was taken into 100 mL of LB liquid medium containing 50 mg·L^{-1} Kan and 50 mg·L^{-1} Rif for secondary activation. The OD_{600} values of bacterial solution were incubated to 0.8, 1.0, 1.2 and 1.4, and the culture was centrifuged at 5000 rpm for 10 min. The bacterial pellets were collected and then transferred into transformation solution (MS + 1 mmol·L^{-1} MES + 2 mmol·L^{-1} $MgCl_2$ + 100, 150, 200, 250 μmol·L^{-1} AS + 30 g·L^{-1} sucrose + 0, 0.005%, 0.01%, 0.015%, 0.02% Tween-20, pH=5.6) for resuspension. The *P. lactiflora* seedlings were placed in a syringe containing *Agrobacterium* resuspension solution. The injection port was sealed and syringe was drawn 0, 5, 10 and 15 times with 3-5 cm each time for negative pressure treatment. Afterwards, they were poured into a wide-mouth conical flask containing *Agrobacterium* resuspension solution. The *P. lactiflora* seedlings were infected at 28°C and 200 rpm for 8, 12, 24 and

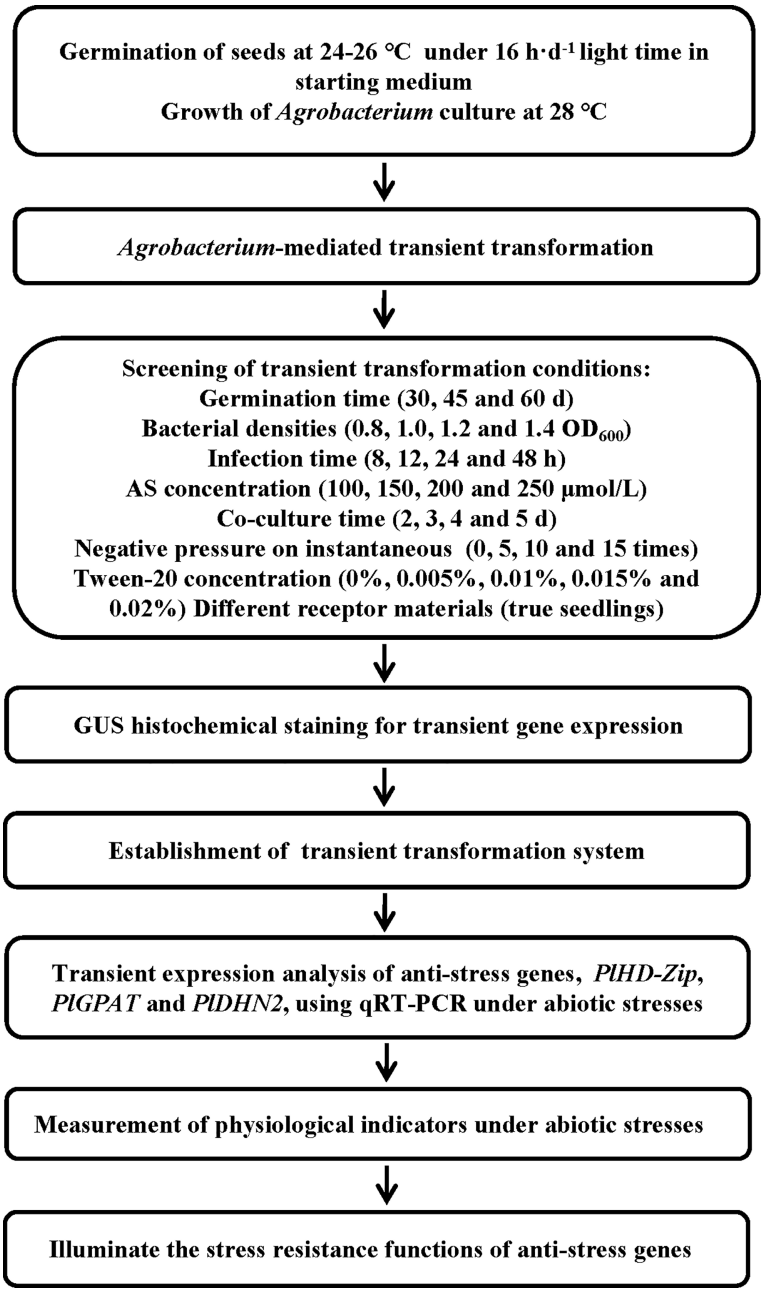

FIGURE 1
Flow chart of *Agrobacterium*-mediated transient transformation system for the development of transgenic *P. lactiflora* plants.

48 h. After that, they were rinsed twice with MS medium. Then *P. lactiflora* tissue culture seedlings were blotted on sterile filter paper and co-cultivated in medium (MS + 0.5 mg·L^{-1} GA_3 + 1.0 mg·L^{-1} 6-BA + 200 μmol·L^{-1} AS + 30 g·L^{-1} sucrose + 6.5 g·L^{-1} agar, pH=5.6) for 2, 3, 4 and 5 d under dark condition. For true seedlings, they were planted in sterilized sand, and the flower pot mouth was covered with perforated preservative film. Under dark conditions, the culture was carried out for 3 d.

Screening of transient transformation conditions of *P. lactiflora*

When *Agrobacterium* was used to infect *P. lactiflora* seedlings, the transient transformation conditions were screened, including germination time (30, 45 and 60 d), bacterial densities (0.8, 1.0, 1.2 and 1.4 OD_{600}), infection time (8, 12, 24 and 48 h), AS concentrations (100, 150, 200 and 250

FIGURE 2
Growth States of *P. lactiflora* embryos during tissue culture. **(A–C)** Embryos at 30 **(A)**, 45 **(B)** and 60 **(C)** d after germination, respectively.

μmol/L), co-culture time (2, 3, 4 and 5 d) and negative pressure intensities (0, 5, 10 and 15 times), Tween-20 concentrations (0%, 0.005%, 0.01%, 0.015% and 0.02%) and different receptor materials (true seedlings). In the process of experiment design, taking one factor as single variable and other factors as standard, the effects of different influencing factors on the transient transformation efficiency of *P. lactiflora* seedlings were observed.

GUS histochemical staining for transient gene expression

GUS staining was performed on the co-cultured *P. lactiflora* seedlings with the GUS staining kit (Real-Times, Beijing, China) for 30 plants per treatment. The seedlings were put into the GUS staining solution and placed at 37°C for 24 h in the dark. Afterwards, the seedlings were decolorized with 75% alcohol, and then transferred into 95% alcohol. The 95% alcohol was replaced 2-3 times during the period until the chlorophyll was completely destained. The blue-stained plants were considered to be positive transient transgenic plants. Transformation efficiency was calculated *via* the equation: transformation efficiency (%) = (number of seedlings stained/total number of seedlings) × 100. Three biological replicates were set for each group of experiments.

Transient expression analysis of anti-stress genes of *P. lactiflora*

The transient transgenic plants were placed in a constant temperature incubator and maintained at -4 or 40°C for low or

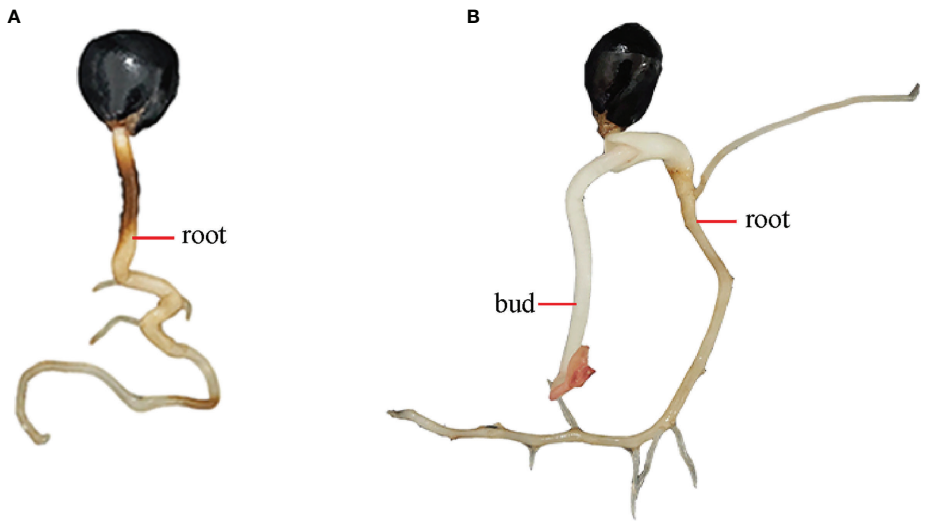

FIGURE 3
Germination states of *P. lactiflora* seed hypocotyls and epicotyls during culture. **(A)** Hypocotyl germination with the root length of 3-4 cm. **(B)** Epicotyl germination with the bud length of 2-3 cm.

high temperature stress, respectively. The transient transgenic plants were inoculated into an initial medium containing 150 mmol·L^{-1} mannitol for drought stress. Samples were collected at 0 and 2 h after each stress treatment. The obtained samples were flash-frozen using liquid nitrogen, followed by storage at -80°C until subsequent use.

The true seedlings of transient transgenic *P. lactiflora* treated for 0 and 2 h under different abiotic stresses were collected, and the total RNA was extracted from the transient transgenic *P. lactiflora* seedlings using EASYspin Plus polysaccharide and polyphenol complex plant RNA rapid extraction kit (Aidlab, Beijing, China). RT Master Mix kit (Perfect Real Time) (Takara, Beijing, China) was used to reverse-transcribe total RNA into cDNA. The StepOnePlus™ fluorescence quantifier (Takara, Beijing, China) was used in quantitative real-time PCR (qRT-PCR) analysis. The *PlActin* (GenBank accession no. JN105299) was selected as the internal reference gene (Ge et al., 2014). The reaction system contained 10 μL of 2x TB Green Premix Ex Taq™ (Tli RNaseH Plus) (Takara, Beijing, China), 0.4 μL of 50x ROX Reference Dye, 5.6 μL of ddH_2O, 1 μL of each primer (10 μM), and 2 μL of cDNA in a final volume of 20 μL. A two-step amplification standard procedure was adopted. The amplification parameters ;were as follows: predeformation at 95°C for 30 s; 40 cycles at 95°C for 5 s and 60°C for 30 s. The dissolution curve program was carried out after 40 cycles under 60-95°C at the increment of 0.5°C/5 s. The gene relative expression levels were calculated according to the $2^{-\Delta\Delta Ct}$ method (Schmittgen and Livak, 2008). Each sample included three biological replicates. All primers for qRT-PCR are shown in Supplementary Table 2.

Determination of physiological indicators of transient transgenic plants

The true seedlings of *P. lactiflora* treated with abiotic stress were collected for the determination of physiological indexes. Superoxide dismutase (SOD) and peroxidase (POD) activity assays were determined according to the method of Dhindsa et al. (1981). The activity of catalase (CAT) and the content of proline were determined following the previously described method (Li, 2000). The content of malondialdehyde (MDA) was determined according to the method of Wang et al. (2010). The measurement of soluble sugar content referred to the published method (Tang, 1999). All experiments were performed in three biological replicates and each replicate contained at least 10 transient transgenic true seedlings.

Statistical analysis

The data were analyzed with SPSS software (Version 22.0, SPSS Inc, USA). The experiments were performed in three biological replicates and subjected to one-way analysis of variance (ANOVA) followed by Duncan's multiple range test (DMRT) at $P < 0.05$ significance level.

Results

Effect of germination time on transient transformation efficiency of *P. lactiflora*

In order to study the effect of germination time on the transient transformation efficiency of *P. lactiflora*, tissue culture seedlings of *P. lactiflora* at 30, 45 and 60 d after germination were selected and transformed with *Agrobacterium* EHA105 containing *GUS* gene (Supplementary Figure 2). The cotyledons of tissue culture seedlings at 30 and 45 d after germination had blue spots, and the GUS positive tissue culture seedlings at 30 d after germination had the highest transformation rate of 33.3%. However, only one true leaf of 60-day-old tissue culture seedlings had a small area of micro-blue on the edge, indicating that GUS expression efficiency decreased with increasing number of days after germination. Therefore, in the later experiment, 30-day-old *P. lactiflora* tissue culture seedlings were selected as transformation receptor materials.

Effect of bacterial concentration on transient transformation efficiency of *P. lactiflora*

Four concentrations of *Agrobacterium* were set in this experiment, and the OD_{600} values were 0.8, 1.0, 1.2 and 1.4, respectively (Supplementary Figure 3). When the OD_{600} value increased from 0.8 to 1.2, the instantaneous transformation efficiency increased gradually. When the OD_{600} value was 1.2, the instantaneous transformation efficiency was the highest with the transformation rate of 33.3%. When the OD_{600} value increased to 1.4, the number of dead *Agrobacterium* cells increased, and the instantaneous transformation rate decreased to 30%. Therefore, in this experiment, the optimal bacterial concentration for *P. lactiflora* transient transformation system was 1.2.

Effect of infection time on transient transformation efficiency of *P. lactiflora*

In the study of the effect of infection time on the instantaneous transformation efficiency of *P. lactiflora*, we found that the instantaneous transformation efficiency of *P. lactiflora* was 26.7% with 8 h of infection period. With the increase of infection time, the instantaneous transformation

efficiency increased. The highest instantaneous transformation efficiency was obtained with 24 h of infection period, and the transformation rate reached 40%. When the tissue culture seedlings were infected for 48 h, the instantaneous transformation efficiency was the lowest (Supplementary Figure 4). The tissue culture seedlings of *P. lactiflora* appeared softening and wilting, and the state of tissue culture seedlings was still unable to recover after co-culture, which was unable to be used for subsequent research.

Effect of AS concentration on transient transformation efficiency of *P. lactiflora*

Appropriate addition of AS can improve the transformation ability of *Agrobacterium* (Zou, 2011). In this study, four concentrations of AS were set as 100 μmol·L $^{-1}$, 150 μmol·L $^{-1}$, 200 μmol·L $^{-1}$ and 250 μmol·L^{-1}. Adding appropriate amount of AS in the transformation solution could improve the instantaneous transformation efficiency of *P. lactiflora*. With the increase of AS concentration, the instantaneous transformation rate of *P. lactiflora* increased. Adding 200 μmol·L^{-1} AS to the transformation solution, the number of successfully dyed tissue culture seedlings was the largest, and the transformation rate reached 40%. When the AS concentration increased to 250 μmol·L^{-1}, the instantaneous transformation rate decreased to 36% (Supplementary Figure 5). Therefore, the optimal AS concentration in the transient transformation system of *P. lactiflora* was 200 μmol·L^{-1}.

Effect of co-culture time on transient transformation efficiency of *P. lactiflora*

Four gradients of co-culture time were set in this experiment. When the co-culture time was 2 d, the instantaneous transformation efficiency was the lowest, and the transformation rate was 17.6%. When the co-culture time increased to 3 d, the instantaneous transformation rate reached the highest value of 40% (Supplementary Figure 6). Due to the absence of antibiotics in the co-culture medium, the overgrowth of *Agrobacterium* led to browning and softening of tissue culture seedlings with the increase of co-culture time, which was consistent with the low transformation efficiency observed.

Effect of negative pressure on instantaneous transformation efficiency of *P. lactiflora*

External application of appropriate negative pressure treatment can form small wounds on the surface of plant tissue, which is helpful for the infiltration of *Agrobacterium* (Mo et al., 2019). Four different negative pressure intensities (0, 5, 10, 15) were set in this experiment. When the negative pressure treatment was not carried out, the instantaneous transformation rate of *P. lactiflora* was 40%. When the negative pressure intensity was 5, the instantaneous transformation efficiency was 50%. When the negative pressure intensity increased to 10, the instantaneous transformation efficiency of *P. lactiflora* was the highest, reaching 63.3%. This was 1.58 times higher than that of no negative pressure treatment (Supplementary Figure 7). When the negative pressure intensity was 15, the tissue culture seedlings were obviously injured, and softening and wilting occurred. It was unable to carry out subsequent experiments. Therefore, the optimum negative pressure strength for *P. lactiflora* transient transformation system was 10.

Effect of Tween-20 concentration on the instantaneous transformation efficiency of *P. lactiflora*

Tween-20 is a commonly used surfactant, and an appropriate amount of Tween-20 can help *Agrobacterium* infiltrate into the intercellular space of plant cells, thereby improving the transient transformation efficiency (Zhong et al., 2016). In this study, five gradient concentrations of Tween-20 were set in the process of transient transformation for tissue culture seedlings. There was no difference in the instantaneous transformation efficiency between 0.005% and 0% Tween-20. When the concentration of Tween-20 increased to 0.01%, the instantaneous transformation efficiency increased significantly, and the transformation rate reached 73.3%. This was 1.08 times higher than that of no Tween-20. However, when the concentration of Tween-20 increased to 0.02%, the instantaneous transformation efficiency decreased to 57% (Supplementary Figure 8). The results showed that 0.01% Tween-20 was the optimal concentration for transient transformation.

Effect of different receptor materials on transient transformation efficiency of *P. lactiflora*

In this study, the true seedlings with buds of 2-3 cm were used as the receptor materials for transient transformation of *P. lactiflora*. It was found that when the seedlings were transformed under the optimal transient transformation conditions selected in the previous study, the seedlings showed softening and wilting after 24 h of *Agrobacterium* suspension infection, indicating that the *P. lactiflora* seedlings were invaded by *Agrobacterium*. This was not conducive to the later experiment. Therefore, the infection time of 8 h, 12 h and 24 h were set in this

experiment. The instantaneous transformation rate was 63.3% when the seedlings were infected in the *Agrobacterium* suspension for 8 h. Then, the instantaneous transformation rate increased first and then decreased with the increase of infection time. The instantaneous transformation rate was the highest at 12 h, reaching 93.3%. This experiment suggested that the optimal infection time was 12 h when the *P. lactiflora* seedling was used as transformation receptor material (Supplementary Figure 9).

Identification of transient transgenic *P. lactiflora*

The constructs *pCAMBIA1301:PlGPAT/PlDHN2/PlHD-Zip* were transformed into *Agrobacterium* EHA105 by freeze-thaw method, respectively. The single colonies were selected for oscillation culture. The shaken *Agrobacterium* solution was subjected to bacterial solution PCR. The products of 1347, 399 and 972 bp were amplified from the three *Agrobacterium* solutions with different recombinant vectors, respectively. The products were all in line with the expected size, indicating functional recombinant vectors *pCAMBIA1301:PlGPAT/PlDHN2/PlHD-Zip* and successful *Agrobacterium* transformations (Figure 4).

Subsequently, the recombinant over-expression vector containing stress-resistant gene of *P. lactiflora* was transiently transformed into *P. lactiflora* true seedlings by *Agrobacterium*-mediated method, and the pCAMBIA1301 empty vector containing *GUS* reporter gene was transiently transformed into *P. lactiflora* seedlings as the blank control group. The transient transgenic *P. lactiflora* true seedlings were immersed in GUS staining solution (Figure 5). The transient transformation of *PlGPAT*, *PlDHN2* and *PlHD-Zip* genes in *P. lactiflora* seedlings elicited blue spots visible to naked eyes, indicating that the transient transformation system of *P. lactiflora* was successfully used to transiently transform the three stress-resistant genes into *P. lactiflora* seedlings.

Transient overexpression of stress-resistance gene in *P. lactiflora*

In order to verify the feasibility of the established transient transformation system, the overexpression vectors of *PlGPAT*, *PlDHN2* and *PlHD-Zip* were constructed in this study. The established transient transformation system was used to transiently transformed these constructs into *P. lactiflora* true seedlings, and the expression changes of three stress-resistant genes under abiotic stress were detected by qRT-PCR method (Figure 6). The results showed that there was no significant difference in the expression levels of stress-resistant genes between the control and transient transgenic seedlings under normal growth condition. After abiotic stress treatment, the expression levels of stress-resistant genes in the control and transient transgenic seedlings were significantly increased, and the expression levels of stress-resistant genes in the transient transgenic seedlings were significantly higher than those in the control seedlings. This indicated that *PlGPAT*, *PlDHN2* and *PlHD-Zip* were successfully transiently overexpressed in *P. lactiflora* seedlings and are responsible for stress resistance functions.

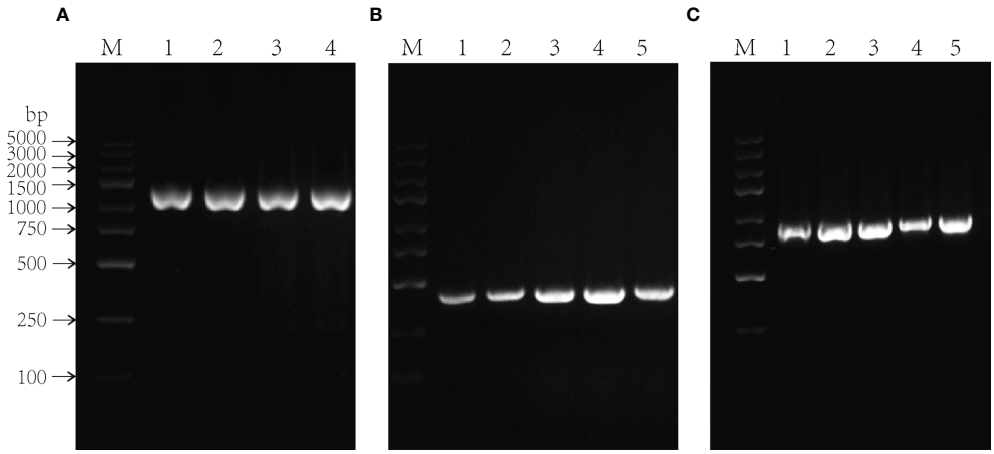

FIGURE 4
Molecular analysis of *Agrobacterium tumefaciens* containing recombinant expression vector. **(A-C)** PCR analysis of *Agrobacterium tumefaciens* using *PlGPAT* **(A)**, *PlDHN2* **(B)** and *PlHD-Zip* **(C)** gene-specific primers, respectively. PCR products in 1347, 399 and 972 bp were observed in each *Agrobacterium tumefaciens* using *PlGPAT*, *PlDHN2* and *PlHD-Zip* gene-specific primers, respectively. M, DL2000 marker; 1-5, different *Agrobacterium tumefaciens*.

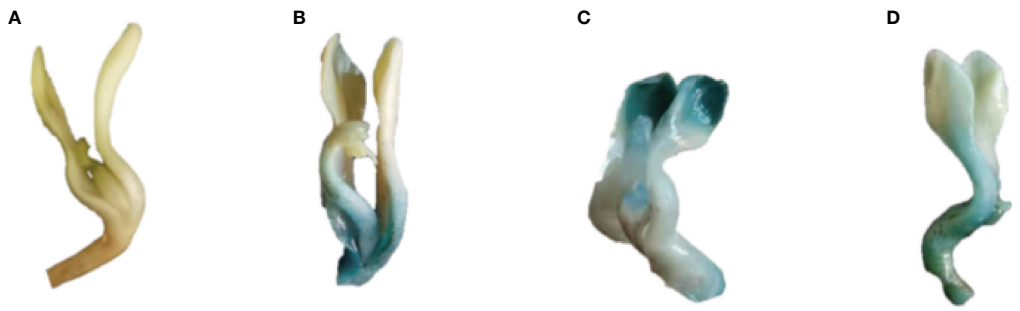

FIGURE 5
GUS staining of transient transgenic *P. lactiflora* seedlings. **(A)** Seedlings as control exhibit no GUS expression. **(B-D)** Seedlings with transient expression of *PlGPAT* **(B)**, *PlDHN2* **(C)** and *PlHD-Zip* **(D)** gene exhibit GUS expression, respectively.

Changes in physiological indexes of transient over-expression *P. lactiflora*

To further verify the function of stress resistance genes *PlGPAT*, *PlDHN2* and *PlHD-Zip*, the activities of three major antioxidant enzymes and the contents of MDA, soluble sugar and proline in transient transgenic true seedlings were measured. The results of antioxidant enzyme activities showed that there was no significant difference in SOD, POD and CAT activities between the control and transient transgenic *PlGPAT P. lactiflora* tissue culture seedlings under normal growth condition. After low temperature stress treatment, the activities of SOD, POD and CAT in *P. lactiflora* seedlings were significantly increased, and the activities of SOD, POD and CAT in transient transgenic seedlings were significantly higher than those in control seedlings. Under high temperature or drought stress, the same results were also obtained for the analysis of antioxidant enzyme activities in the seedlings of transiently transformed *PlDHN2* and *PlHD-Zip* (Figure 7). The analysis of cell membrane permeability physiological indexes showed that under normal growth conditions, there was no significant difference in MDA content between the control and transient transgenic seedlings of *P. lactiflora*. After abiotic stress, the MDA contents of the control and transient transgenic seedlings containing *PlGPAT*/*PlDHN2*/*PlHD-Zip* gene increased, and the content of transient transgenic seedling was significantly lower than that of the control seedling (Figure 8A). The content analysis of organic osmolytes showed that the soluble sugar and proline contents of the control and transient transgenic peony seedlings were significantly increased compared with the normal growth condition after abiotic stress treatment, and the soluble sugar and proline contents of the transient transgenic seedlings were significantly higher than those of the control seedlings (Figures 8B, C). The above research results demonstrated that the transient transformation system of *P. lactiflora* was successfully used to transfer the stress-resistant gene of *P. lactiflora* into the seedlings of *P. lactiflora* and exert its stress-resistant function, indicating that the transient transformation system of *P. lactiflora* established in this study could be used to study the function of the stress-resistant gene in *P. lactiflora*.

Discussion

The *Agrobacterium*-mediated transient transformation of plants is mainly involved in injection and infiltration method. In the study, these two methods were applied. With injection method, due to the thickness of leaves and tightness of cell

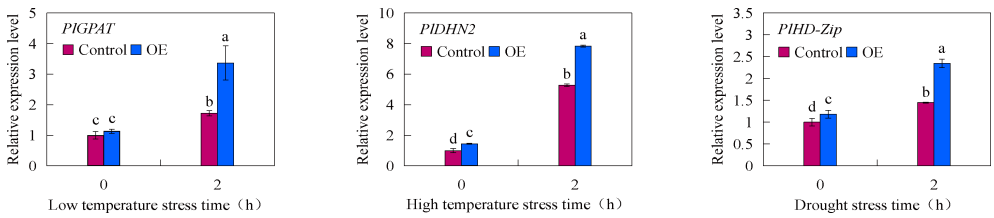

FIGURE 6
Transient expression analysis of *P. lactiflora* stress resistance genes under abiotic stresses. Error bars indicate standard deviation of three replicates. Different letters mean significantly different by Duncan's multiple range test at $P < 0.05$.

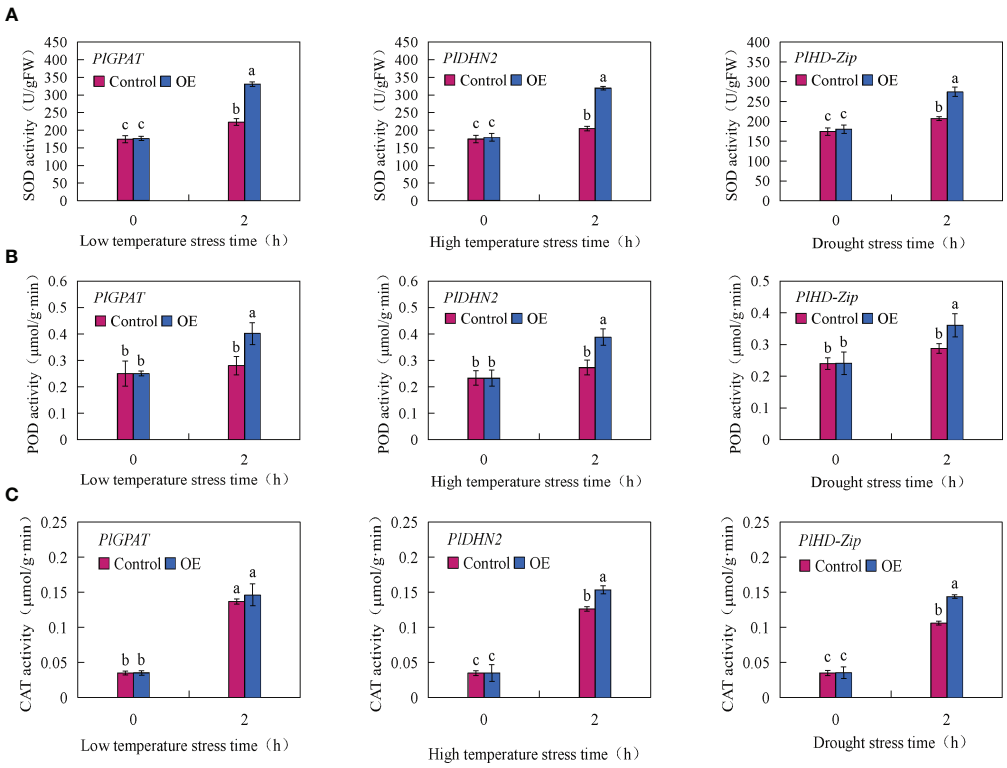

FIGURE 7
Analysis of antioxidant enzyme activity in *P. lactiflora* seedlings with transient overexpression of stress resistance genes. **(A)** SOD activity. **(B)** POD activity. **(C)** CAT activity. Error bars indicate standard deviation of three replicates. Different letters mean significantly different by Duncan's multiple range test at $P < 0.05$.

tissues of *P. lactiflora* tissue culture seedlings, the bacterial solution could not be diffused after the injection of *Agrobacterium* suspension. This resulted in a lower instantaneous transformation efficiency. In contrast, with the infiltration method, the instantaneous transformation was completed after only a few hours of submerging of whole *P. lactiflora* seedlings in *Agrobacterium* tumefaciens resuspension solution. This result suggests that *Agrobacterium* infiltration method is more suitable for transient transformation of *P. lactiflora*.

Agrobacterium-mediated transient transformation is a complex process. In order to obtain high transformation rate with high expression of target genes in the tissue culture seedlings of *P. lactiflora*, we screened the optimal transformation conditions. Firstly, the growth status of transformation receptor materials has a dramatic impact on the infection of *Agrobacterium*. After a long time of germination, seedlings had thicker cotyledons and tighter cell tissues, which could hinder the infection of *Agrobacterium*. Seedlings at 30 days after germination had tender cotyledons, which was beneficial for the infection of *Agrobacterium* and had the highest transient transformation efficiency. Wu (2015) found that fresh and tender leaves were more conducive to the improvement of transient expression efficiency than old leaves in mulberry. Takata and Eriksson. (2012) also considered that the transformation rate of young leaves was higher than that of old leaves in the establishment of transient transformation system of hybrid poplar.

Previous studies have shown that the *Agrobacterium* density and infection time directly determine the instantaneous transformation efficiency of plants (Mi et al., 2009). It is necessary to ensure that sufficient *Agrobacterium* infiltrates into plant cells without damaging the plant. In this study, we screened the concentration of bacterial solution and infection time. When the tissue culture seedlings of *P. lactiflora* were immersed in the *Agrobacterium* suspension with OD_{600} value of 1.2 for 24 h, the final number of GUS positive plants was the highest, with less toxicity in the tissue culture seedlings of *P. lactiflora*. In all previous works establishing transient transformation systems for *Malus sieversii* (Li et al., 2018c), *Pinus tabulaeformis* (Liu et al., 2020) and *Iris foetidissima* (An et al., 2020) all screened the bacterial solution concentration and infestation time were screened. The results suggested that too low a bacterial solution concentration or too short an infestation

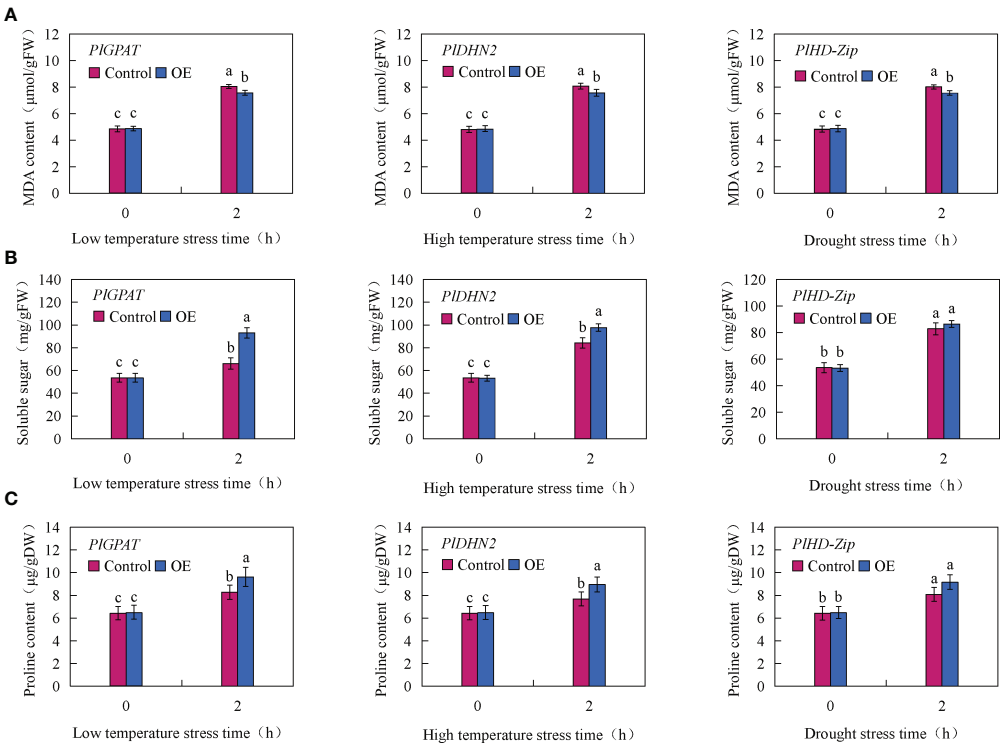

FIGURE 8
Analysis of Physiological index in *P. lactiflora* seedlings with transient overexpression of stress resistance genes. **(A)** MDA content. **(B)** soluble sugar content. **(C)** Proline content. Error bars indicate standard deviation of three replicates. Different letters mean significantly different by Duncan's multiple range test at $P < 0.05$.

time would make the infestation ineffective and lead to plant damage. In addition, it has been reported that many proteins encoded by *Vir* gene play a crucial role in *Agrobacterium*-mediated transformation, and the activity of *Vir* gene carried by Ti plasmid plays a critical role for the infection ability of *Agrobacterium* (Gelvin, 2003). *Vir* gene expression is induced by phenolic compounds, and appropriate accumulation of them can promote the integration of target genes to improve the transient transformation efficiency (Zou, 2011). AS is one of the most commonly used active phenolic compounds, which is a natural signal molecule produced by damaged plant cells. It can expand the host range of some rhizobium strains (Zheng et al., 2012). Faizal and Geelen. (2012) found that the addition of 100 μmol·L^{-1} AS in *Agrobacterium* suspension could make the transient transformation efficiency of *Maesa lanceolata* reach the highest level. This concentration was also suitable for the transient transformation of the whole bamboo (Chen et al., 2021) and *I. foetidissima* leaves (An et al., 2020). Li et al. (2018a) used three different AS concentrations in the transient transformation assay of upland cotton seedlings, and found that GUS staining and activity were the highest when the AS concentration is at 165 μmol·L^{-1}. It can be seen that the optimal AS concentrations for different plants are not the same. In this study, we found that the addition of AS with a concentration of 200 μmol·L^{-1} in the *Agrobacterium* suspension could achieve the highest transient transformation efficiency for *P. lactiflora*. This is consistent with the optimal AS concentration in the transient transformation system for *Salsola laricifolia* (Xia et al., 2020a).

It takes a certain time for *Agrobacterium* to transfer the target gene into plant cells. The transformation of plants by *Agrobacterium* will not complete if co-culture time is too short. On the other hand, it will cause excessive reproduction of *Agrobacterium* and irreversible damage to plants if co-culture time is too long, which reduces the instantaneous transformation rate. An et al. (2020) found that the best transient co-culture time of *I. foetidissima* leaves was 4 days. Both Faizal and Geelen (2012) and Li et al. (2018a) considered that the 5 days after infection of *M. lanceolata* and *G. hirsutum* was the best co-culture time for gene function research. In this experiment, since no antibiotic was added to the co-culture medium, the excessive growth of *Agrobacterium* led to browning and death of tissue culture seedlings of *P. lactiflora* with the extension of co-culture time. This was consistent with the results obtained by previous researchers (Zhuo et al., 2019). Therefore, we believed that 3 days was the optimal co-culture time for the transient transformation in *P. lactiflora*.

A previous study reported that external treatments, such as negative pressure, cotyledon puncture, and surfactant application, could significantly improve plant transient transformation efficiency (Xia et al., 2020b). In this study, sterile needles were used to scratch the cotyledon surface of *P. lactiflora* tissue culture seedlings for cotyledon puncture treatment. It was found that the transformed *P. lactiflora* tissue culture seedlings blackened due to the large scratch area, which could not meet the requirements of subsequent experiments. The negative pressure treatment was carried out on the tissue culture seedlings of *P. lactiflora*. The results showed that the treatment with intensity of 10 could significantly improve the instantaneous transformation efficiency of *P. lactiflora*. This is because the negative pressure treatment could form a slight wound on the surface of the tissue culture seedlings of *P. lactiflora*, which promoted the infection of *Agrobacterium* without harming plants. In the transient transformation assays of *Diospyros kaki* Thunb. (Mo et al., 2019), *Medicago sativa* (Wu et al., 2021) and *Caladium bicolosr* (Li, 2018), it was also found that the transient expression rate of the reporter gene was significantly increased after negative pressure treatment. Surfactants significantly decrease the surface tension by adsorption between the gas-liquid or liquid-liquid interface, This increases the permeability of plant cells and promote the transformation of *Agrobacterium*. Triton X-100, Tween-20 and Silwet L-77 are commonly used surfactants in the transient transformation process. Liu et al. (2019) found that Silwet L-77, Tween-20 and Triton X-100 all improved the transient transformation efficiency of *Caragana intermedia* to some extent. Among them, a small amount of Tween-20 can significantly improve the permeability of plant cells (Zhong et al., 2016). It helps more *Agrobacterium* enter the plant cell gap and hence improves the efficiency of transient transformation (Kalpana et al., 2016). In our study, we found that adding 0.01% Tween-20 in the *Agrobacterium* suspension could make the instantaneous transformation rate of peony reach the highest level. Mi et al. (2009) found that both 0.01% Triton X-100 and 0.01% Tween-20 could improve the transient expression efficiency of *A. thaliana*, and 0.01% Tween-20 had a better effect. Similar conclusions have been reached in the transient transformation systems of many herbaceous plants, such as *B. platyphylla*, *P. euphratica*, *Tamarindus indica*, *Duboisia myoporoides* and *S. babylonica* (Ji et al., 2014).

The culture process of *P. lactiflora* tissue culture seedlings is relatively complex, and the explants are prone to contamination. However, the culture of *P. lactiflora* true seedlings is relatively simple, and the contamination rate is low. The seeds used for the cultivation of *P. lactiflora* true seedlings can be stored in a large amount in sand, ensuring the sufficient transformation materials. In this experiment, the effects of different receptor materials on the transient transformation efficiency of *P. lactiflora* were studied on the basis of the optimal transient transformation conditions obtained by screening the tissue culture seedlings of *P. lactiflora*. The results showed that the optimal infection time was 12 h, and the transient transformation rate could reach 93.3%. Compared with tissue culture seedlings as transformation receptor materials, the instantaneous transformation operation of true seedlings was more convenient. It does not need to be carried out on ultra-clean bench, and the instantaneous transformation rate is higher. The result suggested that the transient transformation system with *P. lactiflora* true seedling as receptor material was more suitable for *P. lactiflora*.

The transient expression of plants has been widely used in gene function verification. For plants with no mature genetic transformation system such as *P. lactiflora*, it is very difficult to study the gene function associated with obvious phenotype. Therefore, it is necessary to establish transient transformation system for gene function exploration (Li et al., 2020). Currently, transient transformation systems have been widely used to study gene functions in plants. Zang et al. (2015) overexpressed the *ThZFP1* gene in *Tamarix hispida* through an *Agrobacterium*-mediated transient transformation system and verified its positive regulation in proline accumulation, as well as SOD and POD activities under salt and osmotic stress conditions. Using a transient transformation system (Liu et al., 2019), it was also found that transient expression of the *CiDREB1C* gene enhanced tolerance to drought and salt stress and reduced sensitivity to ABA in *C. intermedia* using a transient transformation system (Liu et al., 2019). Liao et al. (2021) conducted transient overexpression and gene silencing of *SgCPR1* and *SgCPR2*, and found that *SgCPR1* and *SgCPR2* played a particularly important role in the biosynthesis of mogroside in *Siraitia grosvenorii*. The system can not only overexpress endogenous genes of plants, but also transiently transform exogenous genes of other plants. For this reason, the gene function can be studied more widely. Moreover, the *Agrobacterium*-mediated transient transformation system can also be applied to promoter, transcription factor, protein subcellular localization and interaction analysis (Takata and Eriksson, 2012; Liu et al., 2020). Therefore, the establishment of *Agrobacterium*-mediated transient transformation system of *P. lactiflora* is of great research significance.

In this study, the transient overexpression of *P. lactiflora* resistance genes *PlGPAT*, *PlDHN2* and *PlHD-Zip* were carried out using the established transient transformation system in *P. lactiflora*. qRT-PCR analysis showed that the expression levels of stress-resistant genes in transgenic plants increased after abiotic stress treatment, which was significantly higher than those in control plants after abiotic stress treatment. The results of physiological index measurements showed that the proline and soluble sugar content as well as SOD, POD and CAT activity in the transiently overexpressed *P. lactiflora* resistance gene plants were significantly higher than those in control plants after abiotic stress treatment, and the MDA level was lower than that in control plants. It can be concluded that the stress

resistance genes *PlGPAT*, *PlDHN2* and *PlHD-Zip* can be successfully transferred into the *P. lactiflora* seedlings using transient transformation system, and have stress resistance functions under abiotic stresses.

Conclusion

The present study established an efficient *Agrobacterium*-mediated transient transformation system for *P. lactiflora*. The established transient transformation system was used to achieve transient overexpression of *P. lactiflora* resistance genes in a relatively short period of time, and the stress resistance indicators of transgenic plants were detected. The results showed that all three resistance genes served to enhance the resistance of *P. lactiflora* to abiotic stress treatment. The transient transformation system we developed can be successfully applied for gene transient overexpression and function analysis in *P. lactiflora*. Consequently, the transient transformation system will promote functional analyses of *P. lactiflora* stress-responsive genes.

Data availability statement

The datasets presented in this study can be found in online repositories. The names of the repository/repositories and accession number(s) can be found below: https://www.ncbi.nlm.nih.gov/genbank/, JN105299.1, https://www.ncbi.nlm.nih.gov/genbank/, KJ914575.1, https://www.ncbi.nlm.nih.gov/genbank/, KY272747.1, https://www.ncbi.nlm.nih.gov/genbank/, MN832790.1.

Author contributions

XS, XK and JG designed the project. XK and JG completed the tissue culture and seedling culture of *P. lactiflora*. XK, RF and SD completed the screening experiment of transient transformation conditions of *P. lactiflora* mediated by *Agrobacterium*. JG and SG participated in GUS staining and decolorization test. XK and RF completed the cloning of stress related genes and construction of recombinant expression vector of *P. lactiflora*. This article was written by SG, XK and JG. All authors contributed to the article and approved the submitted version.

Funding

This work was supported by the National Natural Science Foundation of China (32071814 and 31470696).

Conflict of interest

The authors declare that the research was conducted in the absence of any commercial or financial relationships that could be construed as a potential conflict of interest.

Publisher's note

All claims expressed in this article are solely those of the authors and do not necessarily represent those of their affiliated organizations, or those of the publisher, the editors and the reviewers. Any product that may be evaluated in this article, or claim that may be made by its manufacturer, is not guaranteed or endorsed by the publisher.

Supplementary material

The Supplementary Material for this article can be found online at: https://www.frontiersin.org/articles/10.3389/fpls.2022.999433/full#supplementary-material

References

An, W. J., Zhang, Y. X., and Yuan, H. Y. (2020). A system establishment of transient expression on iris foetidissima l. *Mol. Plant Breed.* 18, 6359–6363. doi: 10.13271/j.mpb.018.006359

Banavath, J. N., Thammineni, C., Varakumar, P., Konduru, S., Guduru, K. K., Akila, C. S., et al. (2018). Stress inducible overexpression of *AtHDG11* leads to improved drought and salt stress tolerance in peanut (*Arachis hypogaea* l.). *Front. Chem.* 236. doi: 10.3389/fchem.2018.00034

Bian, T. T., Ma, Y., Guo, J., Wu, Y., Shi, D. M., and Guo, X. F. (2020). Herbaceous peony (*Paeonia lactiflora* pall.) PlDELLA gene negatively regulates dormancy release and plant growth. *Plant Sci.* 297, 110539. doi: 10.1016/j.plantsci.2020.110539

Chen, K., Hu, K., Xi, F., Wang, H., Kohnen, M. V., Gao, P. F., et al. (2021). High-efficient and transient transformation of moso bamboo (Phyllostachys edulis) and ma bamboo (Dendrocalamus latiflorus Munro). *J. Plant Biol.* 4, 182–194. doi: 10.1007/s12374-020-09294-y

Chen, Y., Ma, Y., Guo, J., Li, J. J., Han, L. L., and Guo, X. F. (2017). Cloning and expression analysis of peoniflorin gene *PlDHN2* in peony (*Paeonia lactiflora*). *J. Plant Physiol.* 53, 1297–1305.

Dhindsa, R. S., Pamela, P. D., and Thorpe, T. A. (1981). Leaf senescence: Correlated with increased levels of membrane permeability and lipid peroxidation, and decreased levels of superoxide dismutase and catalase. *J. Exp. Bot.* 32, 93–101. doi: 10.1093/jxb/32.1.93

Faizal, A., and Geelen, D. (2012). Agroinfiltration of intact leaves as a method for the transient and stable transformation of saponin producing maesa lanceolata. *Plant Cell Rep.* 31, 1517–1526. doi: 10.1007/s00299-012-1266-4

Gelvin, S. B. (2003). *Agrobacterium*-mediated plant transformation:the biology behind the "Gene-jockeying" tool. *Microbiol. Mol. Biol. Rev.* 67, 16–37. doi: 10.1128/MMBR.67.1.16-37.2003

Ge, J., Zhao, D., Han, C., Wang, J., Hao, Z., and Tao, J. (2014). Cloning and expression of floral organ development-related genes in herbaceous peony (*Paeonia lactiflora* pall.). *Mol. Biol. Rep.* 41 (10), 6493–6503. doi: 10.1007/s11033-014-3532-8

Guo, Y., Wang, Y. C., and Wang, Z. B. (2016). Optimizing transient genetic transformation method on arabidopsis plants mediated by *agrobacterium tumefaciens*. *J. Northeast Forestryuniversity* 44, 41–44.

Huang, H., Wang, H., Tong, Y., and Wang, Y. H. (2021). Identification and characterization of *HD-zip* genes reveals their roles in stresses responses and facultative crassulacean acid metabolism in *dendrobium catenatum*. *Sci. Hortic-Amsterdam* 285, 110058. doi: 10.1016/j.scienta.2021.110058

Imran, S., Shao, G. N., Sheng, Z. H., Hu, P. S., and Tang, S. Q. (2021). Identification and analysis of the structure, expression and nucleotide polymorphism of the *GPAT* gene family in rice. *Plant Gene* 26, 100290. doi: 10.1016/j.plgene.2021.100290

Ji, X. Y., Zheng, L., Liu, Y. J., Nie, X. G., Liu, S. G., and Wang, Y. C. (2014). A transient transformation system for the functional characterization of genes involved in stress response. *Plant Mol. Biol. Rep.* 32, 732–739. doi: 10.1007/s11105-013-0683-z

Kalpana, N., Manoj, K. A., Lourdes, B., Elizabeth, S. A., and Miguel, L. (2016). Protoplast isolation, transient transformation of leaf mesophyll protoplasts and improved *agrobacterium*-mediated leaf disc infiltration of phaseolus vulgaris: tools for rapid gene expression analysis. *BMC Biotechnol.* 16, 53–67. doi: 10.1186/s12896-016-0283-8

Klimešová, J., Holková, L., and Středa, T. (2020). Drought stress response in maize: molecular, morphological and physiological analysis of tolerant and sensitive genotypes. *Maydica* 65, 1–9.

Li, H. S. (2000). *Principles and techniques of plant physiology and biochemistry experiments*. Beijing: Higher Education Press.

Li, J. Y. (1999). *Chinese Tree peony and herbaceous peony*. Beijing: Forestry publishing house

Li, X. (2018). *Optimization of the genetic transformation system of Caladium bicolor 'Hongtao K' and the introduction of AtPAP1 gene and maize Lc gene [master's thesis]*. [Congqing]: Xinan Agricultural University.

Liao, J. J., Niu, C. C., Xie, Q. J., Xing, Q. J., and Qi, H. Y. (2017). The recent advances of transient expression system in horticultural plants. *Acta Hortic. Sin.* 44, 1796–1810. doi: 10.16420/j.issn.0513-353x.2017-0398

Liao, J. J., Xie, L., Shi, H. W., Cui, S. R., Lan, F. S., Luo, Z. L., et al. (2021). Development of an efficient transient expression system for siraitia grosvenorii fruit and functional characterization of two NADPH-cytochrome P450 reductases. *Phytochemistry* 189, 112824–112833. doi: 10.1016/j.phytochem.2021.112824

Li, L., Gu, H., Yue, Y. Z., Yang, X. L., and Wang, L. G. (2020). Advances in transient transformation systems of woody plants. *Mol. Plant Breed.* 18, 7784–7794. doi: 10.13271/j.mpb.018.007784

Li, H. P., Li, K., Guo, Y. T., Guo, J. G., Miao, K. T., Botella, J. R., et al. (2018a). A transient transformation system for gene characterization in upland cotton (Gossypium hirsutum). *Plant Methods* 14, 50–61. doi: 10.1186/s13007-018-0319-2

Li, X. T., Liu, P., Yang, P. P., Fan, C. Z., and Sun, X. M. (2018b). Characterization of the glycerol-3-phosphate acyltransferase gene and its real-time expression under cold stress in *Paeonia lactiflora* pall. *PloS One* 13 (8), e0202168. doi: 10.1371/journal.pone.0202168

Liu, S. Y. (2021). *Study on the mechanism of dehydratin CaDHN4 gene regulating pepper stress resistance* (Xi'an (Shaanxi: Northwest A & F University).

Liu, S. W., Ma, J. J., Liu, H. M., Guo, Y. T., Li, W., and Niu, S. H. (2020). An efficient system for *agrobacterium*-mediated transient transformation in pinus tabuliformis. *Plant Methods* 16, 52–61. doi: 10.1016/S0168-9452(96)04541-4

Liu, K., Yang, Q., Yang, T. R., Wu, Y., Wang, G. X., Yang, F. Y., et al. (2019). Development of *agrobacterium*-mediated transient expression system in caragana intermedia and characterization of CiDREB1C in stress response. *BMC Plant Biol.* 19, 237–250. doi: 10.1186/s12870-019-1800-4.33

Li, X. Y., Zhang, K. C., Zhang, D. Y., Li, J., and Wang, Y. C. (2018c). Establishment and preliminary validation of transient genetic transformation method of malus sieversii. *Mol. Plant Breed.* 16, 7315–7321. doi: 10.13271/j.mpb.016.007315

Lu, J., Bai, M. J., Ren, H. R., Liu, J. Y., and Wang, C. Q. (2017). An efficient transient expression system for gene function analysis in rose. *Plant Methods* 13, 116–128. doi: 10.1186/s13007-017-0268-1

Mi, J. K., Kon, B., and Chung-Mo, P. (2009). Optimization of conditions for transient *agrobacterium*-mediated gene expression assays in arabidopsis. *Plant Cell Rep.* 28, 59–67. doi: 10.1007/s00299-009-0717-z

Mo, R. L., Yang, S. C., Zhang, Q. L., Xu, L. Q., and Luo, Z. R. (2019). Vacuum infiltration enhances the *agrobacterium*-mediated transient transformation for gene functional analysis in persimmon (Diospyros kaki thunb.). *Sci. Hortic-Amsterdam* 251, 174–180. doi: 10.1016/j.scienta.2019.03.002

Schmittgen, T. D., and Livak, K. J. (2008). Analyzing real-time PCR data by the comparative CT method. *Nat. Protoc.* 3 (6), 1101–1108. doi: 10.1038/nprot.2008.73

Sessa, G., Steindler, C., Morelli, G., and Ruberti, I. (1998). The arabidopsis athb-8, -9 and -14 genes are members of a small gene family coding for highly related HD-ZIP proteins. *Plant Mol. Biol.* 38, 609–622. doi: 10.1023/A:1006016319613

Shen, Y. F., Ma, C., Wu, X. P., Zhang, Y. M., and Wang, H. Q. (2016). The heterologous expression of sk2 dehydrin gene *mrdhn3* in medicago ruthenica increased the resistance of e.coli to salt and high temperature stress. *J. Grassl. Sci.* 25, 118–127. doi: 10.11686/cyxb2015510

Shi, J. (2012). *Cloning of KS type dehydrin gene family of ammopiptanthus mongolicus and expression and function analysis of abiotic stress related genes* (Beijing: Beijing Forestry University).

Shockey, J., Regmi, A., Cotton, K., Adhikari, N., Browse, J., and Bates, P. D. (2016). Identification of arabidopsis *GPAT9* (At5g60620) as an essential gene involved in triacylglycerol biosynthesis. *Plant Physiol.* 170, 163–179. doi: 10.1104/pp.15.01563

Shu, Q. Y., Zhu, J., Men, S. Q., Hao, Q., Wang, Q. Y., Liu, Z. A., et al. (2018). The VIGS technology system was established based on the flavonoid glycosyltransferase gene of peony. *Hortic. J.* 45, 168–176. doi: 10.16420/j.issn.0513-353x.2017-0522

Takata, N., and Eriksson, M. E. (2012). A simple and efficient transient transformation for hybrid aspen (Populus tremula × p. tremuloides). *Plant Methods* 8, 30–40. doi: 10.1186/1746-4811-8-30

Tang, Z. C. (1999). *A Guide to Modern Plant Physiology Experiments*. Shanghai: Science Press.

Tsubasa, S. (2018). Analysis of the intracellular localization of transiently expressed and fluorescently labeled copper-containing amine oxidases, diamine oxidase and n-methylputrescine oxidase in tobacco, using an *Agrobacterium* infiltration protocol. *Methods Mol. Biol.* 1694, 215–223. doi: 10.1007/978-1-4939-7398-9_20

Tyurin, A. A., Suhorukova, A. V., Kabardaeva, K. V., and Goldenkova-Pavlova, I. V. (2020). Transient gene expression is an effective experimental tool for the research into the fine mechanisms of plant gene function: advantages, limitations, and solutions. *Plants* 9, 1187–1206. doi: 10.3390/plants9091187

Vaghchhipawala, Z., Rojas, C. M., Senthil-kumar, M., and Mysore, K. S. (2011). Agroinoculation and agroinfiltration:Simple tools for complex gene function analyses. *Methods Mol. Biol.* 678, 65–76. doi: 10.1007/978-1-60761-682-5_6

Wang, L. (2014). *Establishment and application of transient expression system in cotton cotyledon* (Xi'an (Shaanxi: Shaanxi Normal University).

Wang, F., Fang, P., Yan, H. P., Ji, X. Z., and Peng, Y. L. (2021)Heterologous overexpression of ZmHDZIV13 enhanced drought and salt tolerance in arabidopsis and tobacco (Accessed July 15, 2021).

Wang, Y. C., Gao, C. Q., Liang, Y. N., Wang, C., Yang, C. P., and Liu, G. F. (2010). A novel bZIP gene from tamarix hispida mediates physiological responses to salt stress in tobacco plants. *J. Plant Physiol.* 167, 222–230. doi: 10.1016/j.jplph.2009.09.008

Wu, S. L. (2015). *Construction of transients system and function analysis of* FT *gene in mulberry (*Morus alba *L.) [master's thesis]*. [Xi'an (Shaanxi)]: Northwest A&F University.

Wu, Y. J., Leng, Y. R., Jing, S. L., Zheng, C. P., Lang, C. J., and Yang, L. P. (2021). Using vacuum infection method to transiently expression of *GUS* Gene in *Medicago sativa* L. by vacuum infiltration. *Mol. Plant Breed.* 20, 859–864.

Wu, Y., Liu, M., Chen, M., Jiang, Y., and Sun, J. (2020). The application of VIGS technology in ornamental plants. *Mol. Plant Breed.* 18, 944–951. doi: 10.13271/j.mpb.018.000944

Xia, P. G., Hu, W. Y., Liang, T. Y., Yang, D. F., and Liang, Z. S. (2020b). An attempt to establish an *agrobacterium*-mediated transient expression system in medicinal plants. *Protoplasma.* 257, 1497–1505. doi: 10.1007/s00709-020-01524-x

Xia, C. L., Li, Y. N., and Wen, Z. B. (2020a). The establishment and preliminary verification of transient transformation system of salsola laricifolia. *Arid Zone Res.* 37, 1317–1326. doi: 10.13866/j.azr.2020.05.25

Xie, L. H., Zhang, Q. Y., Sun, D. Y., Yang, W. Z., Hu, J. Y., Niu, L. X., et al. (2019). Virus-induced gene silencing in the perennial woody paeonia ostii. *PeerJ.* 7, e7001. doi: 10.7717/peerj.7001

Xue, M., Guo, T., Ren, M. Y., Wang, Z. L., Tang, K. G., Zhang, W. J., et al. (2019). Constitutive expression of chloroplast glycerol-3-phosphate acyltransferase from ammopiptanthus mongolicus enhances unsaturation of chloroplast lipids and tolerance to chilling, freezing and oxidative stress in transgenic *Arabidopsis*. *Plant Physiol.Bioch.* 143, 375–387. doi: 10.1016/j.plaphy.2019.07.019

Yamasaki, Y., Koehler, G., Blacklock, B. J., and Randall, S. K. (2013). Dehydrin expression in soybean. *Plant Physiol. Bioch.* 70, 213–220. doi: 10.1016/j.plaphy.2013.05.013

Zang, D. D., Wang, C., Ji, X. Y., and Wang, Y. C. (2015). Tamarix hispida zinc finger protein ThZFP1 participates in salt and osmotic stress tolerance by increasing proline content and SOD and POD activities. *Plant Sci.* 235, 111–121. doi: 10.1016/j.plantsci.2015.02.016

Zhang, R. L., Wang, X. B., Shao, L. M., Li, D. Q., Xia, Y. P., and Zhang, J. P. (2021). Tissue culture and genetic transformation system construction of *Paeonia lactiflora* and *Paeonia suffruticosa*. *Plant Physiol. J.* 57, 235–247.

Zheng, L., Liu, G. F., Meng, X. N., Li, Y. B., and Wang, Y. C. (2012). A versatile *Agrobacterium*-mediated transient gene expression system for herbaceous plants and trees. *Bioch. Gene.* 50, 761–769. doi: 10.1007/s10528-012-9518-0

Zhong, L. H., Zhang, Y. P., Liu, H. C., Sun, G. W., Chen, R. Y., and Song, S. W. (2016). *Agrobacterium*-mediated transient expression via root absorption in flowering Chinese cabbage. *SpringerPlus* 5, 18–25. doi: 10.1186/s40064-016-3518-1

Zhou, S. S., and Huang, Y. F. (2018). Advances in tissue culture of *Paeonia lactiflora*. *Plant Doc.* 31, 37–40.

Zhuo, L., Zhang, D. Y., Li, X. S., Yang, H. L., and Guan, K. Y. (2019). Establishment of transient genetic transformation method for syntrichia caninervis mitt. *Mol. Plant Breed.* 17, 7. doi: 10.13271/j.mpb.017.001913

Zou, Z. (2011). Advances on factors influencing induction of *Agrobacterium* tumefaciens *Virulence* Genes. *China Biotech.* 31, 126–132.

frontiers | Frontiers in Plant Science

TYPE Original Research
PUBLISHED 18 October 2022
DOI 10.3389/fpls.2022.981086

OPEN ACCESS

EDITED BY
Daqiu Zhao,
Yangzhou University, China

REVIEWED BY
Jietang Zhao,
South China Agricultural University, China
Xiang Gao,
Northeast Normal University, China

*CORRESPONDENCE
Jianxin Fu
fujx@zafu.edu.cn
Chao Zhang
zhangc@zafu.edu.cn

†These authors have contributed equally to this work and share first authorship

SPECIALTY SECTION
This article was submitted to Plant Breeding, a section of the journal Frontiers in Plant Science

RECEIVED 29 June 2022
ACCEPTED 30 September 2022
PUBLISHED 18 October 2022

CITATION
Qian J, Jiang L, Qing H, Chen J, Wan Z, Xu M, Fu J and Zhang C (2022) ZeMYB9 regulates cyanidin synthesis by activating the expression of flavonoid 3′-hydroxylase gene in *Zinnia elegans*. *Front. Plant Sci.* 13:981086. doi: 10.3389/fpls.2022.981086

ZeMYB9 regulates cyanidin synthesis by activating the expression of flavonoid 3′-hydroxylase gene in *Zinnia elegans*

Jieyu Qian[1,2,3†], Lingli Jiang[1,2,3†], Hongsheng Qing[1,2,3], Jiahong Chen[1,2,3], Ziyun Wan[1,2,3], Menghan Xu[1,2,3], Jianxin Fu[1,2,3*] and Chao Zhang[1,2,3*]

[1]Zhejiang Provincial Key Laboratory of Germplasm Innovation and Utilization for Garden Plants, Zhejiang Agriculture & Forestry University, Hangzhou, China, [2]Key Laboratory of National Forestry and Grassland Administration on Germplasm Innovation and Utilization for Southern Garden Plants, Zhejiang Agriculture & Forestry University, Hangzhou, China, [3]School of Landscape Architecture, Zhejiang Agriculture & Forestry University, Hangzhou, China

Petal color in *Zinnia elegans* is characterized mainly by anthocyanin accumulation. The difference in the content of anthocyanins, especially cyanidins, affects petal coloration in *Z. elegans*, but the underlying regulatory mechanism remains elusive. Here, we report one R2R3-MYB transcription factor from subgroup 6, ZeMYB9, acting as a positive regulator of anthocyanin accumulation in *Z. elegans*. Up-regulated expression of *ZeMYB9* and flavonoid 3′-hydroxylase gene (*ZeF3′H*) was detected in the cultivar with higher cyanidin content. ZeMYB9 could specifically activate the promoter of *ZeF3′H*, and over-expression of *ZeMYB9* induces much greater anthocyanin accumulation and higher expression level of anthocyanin biosynthetic genes in both petunia and tobacco. And then, ZeMYB9 was demonstrated to interact with ZeGL3, a bHLH transcription factor belonging to IIIf subgroup. Promoter activity of *ZeF3′H* was significantly promoted by co-expressing *ZeMYB9* and *ZeGL3* compared with expressing *ZeMYB9* alone. Moreover, transient co-expression of *ZeMYB9* and *ZeGL3* induced anthocyanin accumulation in tobacco leaves. Our results suggest that ZeMYB9 could enhance cyanidin synthesis and regulate petal color in *Z. elegans* though activating the expression of *ZeF3′H*, by itself or interacting with ZeGL3.

KEYWORDS

***Zinnia elegans*, anthocyanin, flavonoid 3′-hydroxylase, MYB, bHLH**

Introduction

Flower color, one of the most important ornamental traits for floricultural crops, is mainly due to the accumulation of three kinds of pigments: flavonoids, carotenoids and betalains (Tanaka et al., 2008). Anthocyanins, belonging to a colored class of flavonoids, make flowers with a diverse range of hues from orange, red, to blue and violet (Tanaka et al., 2008). Anthocyanin synthesis is relatively conserved in higher plants, mainly based on a series of catalytic enzymes including chalcone synthase (CHS), chalcone isomerase (CHI), flavanone 3-hydroxylase (F3H), flavonoid 3′-hydroxylase (F3′H), dihydroflavonol 4-reductase (DFR), anthocyanidin synthase (ANS), anthocyanin glucosyltransferase (GT), anthocyanin acyltransferase (AT) and methyltransferase (MT) (Tanaka et al., 2010).

The number of hydroxyl groups on the B-ring of anthocyanin is one of the essential factors affecting the color of anthocyanin pigments. Blue/violet flowers are inclined to accumulate trihydroxylated delphinidin-based anthocyanins, red/magenta flowers tend to contain cyanidin-based anthocyanins (with two hydroxyl groups on the B-ring), while orange/brick red flowers predominantly contain pelargonidin-based anthocyanins with only one hydroxyl group on the B-ring (Tanaka and Brugliera, 2013).

Two cytochromes P450, F3′H and F3′5′H play a crucial role in the determination of flower color and anthocyanin profile by introducing hydroxyl groups to the B-ring (Tanaka, 2006). Flowers could accumulate blue-flower-specific anthocyanidins, such as delphinidin, petunidin and malvidin, which is due to the presence of F3′5′H activity (Shimada et al., 2014). However, many ornamental plants, such as rose (*Rosa hybrida*), chrysanthemum (*Chrysanthemum morifolium*), carnation (*Dianthus caryophyllus*), naturally lack F3′5′H activity, so they cannot synthesize delphinidin-based anthocyanins, which leads to the deficiency of violet/blue flower colors in these plant species (Holton et al., 1993). The introduction of heterologous *F3′5′H* gene into these plants, results in novel purple/violet flowers owing to the formation and accumulation of delphinidin-based anthocyanins (Fukui et al., 2003; Katsumoto et al., 2007; Noda et al., 2017). Another cytochrome P450 F3′H can catalyze the hydroxylation at the 3′-position of the B-ring and convert dihydrokaempferol (DHK) into dihydroquercitin (DHQ), resulting in a metabolic flux shift toward cyanidin biosynthesis and the production of cyanidin-based anthocyanins (Tanaka and Brugliera, 2013). Therefore, spontaneous mutations of *F3′H* gene in the morning glory species (*Ipomoea nil*, *I. purpurea* and *I. tricolor*) lead to the change of flower color and redirection of the anthocyanin biosynthesis pathway from cyanidin into pelargonidin (Hoshino et al., 2003). In addition, the expression level of *F3′H* gene was closely associated with the anthocyanin composition and content in the fruits of different *Fragaria* species. *F.* × *ananassa* fruits with lower expression of *F3′H* showed a prevalence of pelargonidin, while *F. vesca* with up-regulated expression of *F3′H* had a higher content of cyanidin (Thill et al., 2013).

In addition to catalytic enzyme genes, anthocyanin biosynthesis is also controlled by three types of transcription factors: MYB, bHLH (basic helix-loop-helix) and WD repeat (WDR) (Albert et al., 2014; Xu et al., 2015; Zhou et al., 2019). In plants, MYB transcription factors could be divided into four main types, and the number of R2R3 type MYBs is the largest (Yanhui et al., 2006). Many plant R2R3-MYBs are reported as the key factors in regulating anthocyanin biosynthesis (LaFountain and Yuan, 2021; Yan et al., 2021), of which subgroup 6 (SG6) R2R3-MYBs act as activators of anthocyanin biosynthesis (Quattrocchio et al., 1999; Jian et al., 2019; Fang et al., 2021). Overexpression of *AtMYB75*/*PAP1*, *AtMYB90*/*PAP2*, *AtMYB113* or *AtMYB114* of SG6 promotes anthocyanin accumulation in *Arabidopsis* (Teng et al., 2005; Gonzalez et al., 2008). SG6 R2R3-MYB alone or MYB-bHLH-WDR (MBW) complex enhance anthocyanin accumulation *via* binding to a specific *cis*-acting element (C/TAACG/TG) to activate the expression of structural genes involved in anthocyanin synthesis (Gonzalez et al., 2008). In *Chrysanthemum morifolium*, *CmMYB6* directly activates the expression of *CmDFR*, which could be enhanced when CmMYB6 interacts with a IIIf bHLH protein CmbHLH2 to form a transcriptional complex (Xiang et al., 2015; Xu et al., 2015). Similarly, AcMYBF110 alone or in interaction with AcbHLH1, AcbHLH4, or AcbHLH could regulate the expression of *AcCHS, AcF3′H, AcANS, AcUFGT3a, AcUFGT6b, and AcGST1* in kiwifruit (*Actinidia chinensis*) (Liu et al., 2021).

Zinnia elegans, a popular ornamental plant, is rich in flower color and anthocyanins are the main pigments in the petals of this species (Qian et al., 2021). Four main anthocyanins, including cyanidin 3-O-(6′′-acetyl) glucoside-5-O-glucoside (Cy3AG5G), cyanidin 3-O-(6′′-acetyl)glucoside (Cy3AG), pelargonidin 3-O-(6′′-acetyl)glucoside-5-O-glucoside (Pg3AG5G) and pelargonidin 3-O-(6′′-acetyl) glucoside (Pg3AG), have been identified in previous studies (Qian et al., 2019; Qian et al., 2021). Anthocyanin profile is quite different in different color cultivars of *Z. elegans*. Pink and coral cultivars show a prevalence of pelargonidins, whereas cyanidins account for more than half of the total anthocyanins in purple and red cultivars (Qian et al., 2021). In addition, the expression levels of *ZeF3′H* gene are greatly higher in purple and red cultivars than those in pink and coral cultivars (Qian et al., 2021), suggesting a close link between *ZeF3′H* expression and cyanidin accumulation in *Z. elegans*. Among three identified SG6 R2R3-MYBs based on the petal transcriptome data, the expression level of *ZeMYB9* was significantly correlated with that of *ZeF3′H* during petal development in red cultivar of

Z. elegans (Qian et al., 2022). At present, how ZeMYB9 functions between different color cultivars of *Z. elegans* is not clear. What's more, the underlying regulatory mechanism by which ZeMYB9 activates the expression of *ZeF3'H* and enhances cyanidin biosynthesis remains unknown, and should be further addressed.

In this study, anthocyanin content and the expression pattern of *ZeMYB9* and *ZeF3'H* were analyzed between pink (lower cyanidin accumulation) and purple (higher cyanidin accumulation) cultivars. Next, yeast one-hybrid and dual luciferase assays were utilized to investigate the interaction between ZeMYB9 and the promoter of the target gene *ZeF3'H*. Using transient assays in petunia flower and stable transformation in tobacco, ZeMYB9 was demonstrated to be a positive regulator of anthocyanin biosynthesis. Furthermore, the interaction between ZeMYB9 and a IIIf bHLH protein ZeGL3, identified by yeast two-hybrid, bimolecular fluorescence complementation and luciferase complementary assays, greatly enhanced the expression of *ZeF3'H* than ZeMYB9 alone did, and also resulted in abundant anthocyanin accumulation in tobacco leaves. Our results revealed that ZeMYB9 was responsible for the difference in anthocyanin profile and petal color of different color cultivars in *Z. elegans*, which will provide insights into the regulatory mechanism of anthocyanin biosynthesis and petal color development in *Z. elegans*.

Results

Anthocyanin and petal color analyses

Similar to our previous study (Qian et al., 2021), four anthocyanins were detected in 'Dreamland Pink' (DP) with pink petal color and 'Dreamland Rose' (DRO) with purple petal color (Figure 1A), including cyanidin 3-O-(6′′-acetyl) glucoside-5-O-glucoside (Cy3AG5G), cyanidin 3-O-(6′′-acetyl) glucoside (Cy3AG), pelargonidin 3-O-(6′′-acetyl)glucoside-5-O-glucoside (Pg3AG5G) and pelargonidin 3-O-(6′′-acetyl) glucoside (Pg3AG) (Figure 1B). There was no difference in the content of pelargonidins between these two cultivars, but the content of cyanidins in DRO was significantly higher than that of DP (0.37 mg/g FW and 0.04 mg/g FW, respectively), which resulted in markedly higher total anthocyanin content (TA) in DRO (Figure 1C). Cyanidins in DRO accounted for 79.3% of TA, which was more than twice as much as that in DP

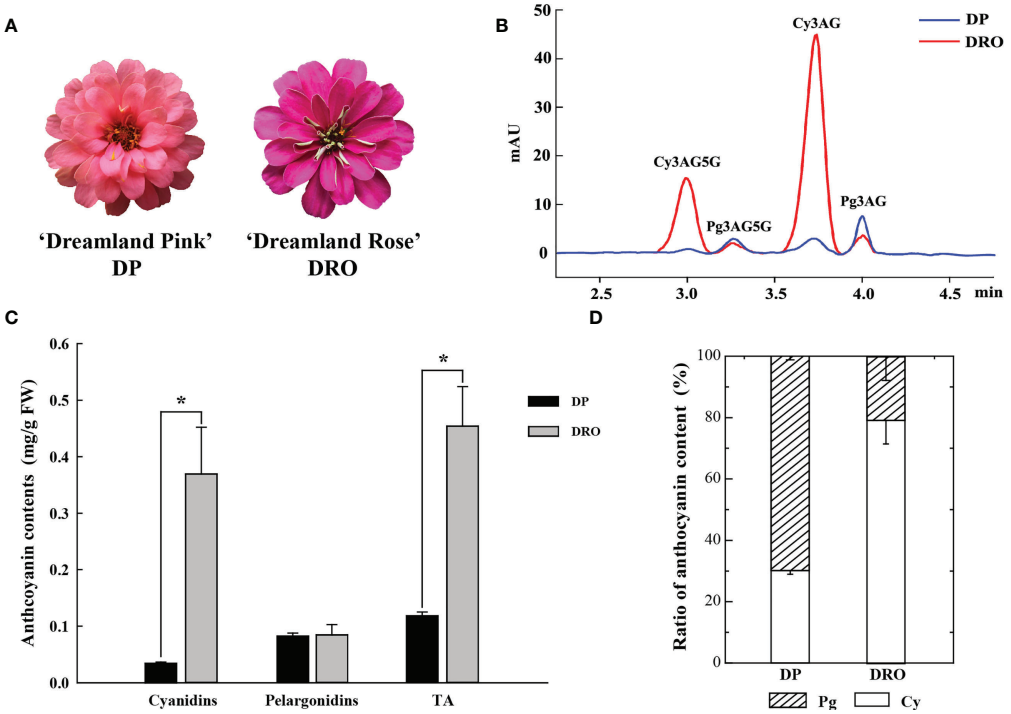

FIGURE 1
The content of anthocyanin components in two cultivars. **(A)** Inflorescences of *Zinnia elegans* 'Dreamland Pink' (DP) and 'Dreamland Rose' (DRO) at the full opening stage (S4). **(B)** UPLC chromatogram of DP and DRO at 530nm. **(C)** The comparison of the content of cyanidins, pelargonidins and total anthocyanin (TA) between DP and DRO. **(D)** Proportion analysis of the anthocyanin component contents in DP and DRO. Error bars indicated standard error (SE) of three replicates. T-test was used for statistical analyses between two cultivars (*$P < 0.05$).

10.3389/fpls.2022.981086

(Figure 1D). In addition, there was no significant difference in total flavonoids contents between these two cultivars (Figure S1A). Based on petal color analysis, DRO exhibited higher a^* and C^* values, and lower L^*, b^* and $h°$ values, compared with DP (Figure S1B). These results suggested that cyanidin content should be responsible for the color difference between these two cultivars.

Expression analysis of *ZeF3'H* and *ZeMYB9* and sequence analysis of ZeMYB9

ZeF3'H, a homologous gene of *F3'H* essential for cyanidin biosynthesis, showed significantly higher expression level in DRO than that in DP at the corresponding stage (Figure 2A). A R2R3-

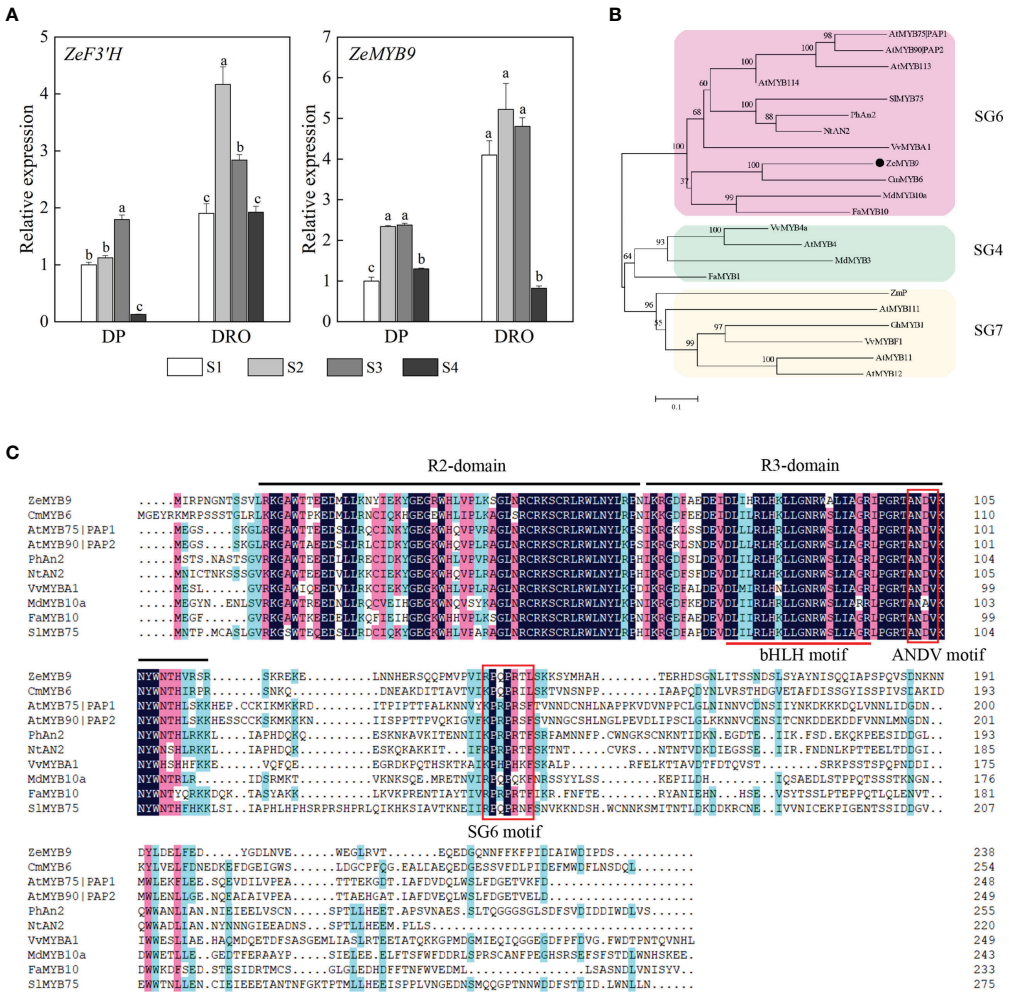

FIGURE 2
Expression analysis of *ZeF3'H* and *ZeMYB9* and sequence analysis of ZeMYB9. **(A)** Relative expression levels of *ZeF3'H* and *ZeMYB9* in the petals of DP and DRO at different developmental stages. *ZeACT* gene was used as an internal control for normalization, and three biological replicates were performed. Error bars indicated standard error (SE). And different lowercases indicate significant differences ($P < 0.05$). **(B)** Phylogenetic tree of different R2R3-MYB proteins participating in anthocyanin biosynthesis in other plants. **(C)** Multiple alignment of the amino acid sequences of SG6 R2R3-MYB proteins from different plants. The black line at the top indicated the conserved R2-domain and R3-domain. The red underline indicated a motif ([D/E]Lx_2[R/K]$x_3Lx_6Lx_3$R) interacting with a bHLH transcription factor. The red box indicated the conserved ANDV motif and SG6 motif. The GenBank accession numbers of MYB proteins from other species were as follows: the SG6 MYBs as *Arabidopsis thaliana* AtMYB75|PAP1 (AT1G56650.1), *A. thaliana* AtMYB90|PAP2 (AT1G66390.1), *A. thaliana* AtMYB113 (AT1G66370.1), *A. thaliana* AtMYB114 (AT1G66380.1), *Solanum lycopersicum* SlMYB75 (NP_001265992.1), *Petunia hybrida* PhAn2 (AAF66727.1), *Nicotiana tabacum* NtAN2 (ACO52470.1), *Vitis vinifera* VvMYBA1 (BAD18977.1), *Chrysanthemum morifolium* CmMYB6 (KR002097.1), *Malus domestica* MdMYB10a (ABB84753.1), *Fragaria ananassa* FaMYB10 (ABX79947.1); the SG4 MYBs as *V. vinifera* VvMYB4a (NP_001268129.1), *A. thaliana* AtMYB4 (AT4G38620.1), *M. domestica* MdMYB3 (AEX08668.1), *F. ananassa* FaMYB1 (AAK84064.1); the SG7 MYBs as *Zea mays* ZmP (P27898), *A. thaliana* AtMYB11 (AT3G62610.1), *A. thaliana* AtMYB12 (AT2G47460.1), *A. thaliana* AtMYB111 (AT5G49330.1), *Gerbera hybrid* GhMYB1 (CAD87007), *V. vinifera* VvMYBF1 (ACT88298).

10.3389/fpls.2022.981086

MYB protein ZeMYB9 was considered as the potential regulatory factor of *ZeF3'H* (Qian et al., 2022), and the expression level of *ZeMYB9* was also greatly higher in DRO (Figure 2A), which was highly correlated with the expression level of *ZeF3'H*. Phylogenetic analysis showed that ZeMYB9 was grouped into SG6 and closely related to CmMYB6 (GenBank Accession Number KR002097.1) from *Chrysanthemum morifolium* (Figure 2B). Multiple sequence alignment of ZeMYB9 and other SG6 MYB proteins (Figure 2C) revealed that the conserved R2 and R3 domains were at the N-termina, and a conserved bHLH motif interacting with a bHLH transcription factor and suitable identifier ANDV were all present in the R3 domain. In addition, ZeMYB9 also had SG6 motif, which was identified to positively regulate anthocyanin synthesis (Rodrigues et al., 2021).

ZeMYB9 could directly bind to and activate the promoter of *ZeF3'H*

A 1703 bp sequence ($ZeF3'H_{pro}$) upstream of the initiation codon of *ZeF3'H* was isolated, which contained four MYB elements. To identify whether ZeMYB9 can directly bind to the promoter of *ZeF3'H*, yeast one-hybrid and dual luciferase assay were carried out. Co-transformed yeasts of pGADT7-ZeMYB9 and pAbAi-ZeF3'H-Pro could survive and grow normally on the selective medium of SD/-Leu/100 ng mL^{-1} AbA, but the negative control did not survive (Figure 3A), revealing that ZeMYB9 can interact with *ZeF3'H* promoter in the yeast system. In addition, a dual luciferase assay was employed to further verify the regulation of ZeMYB9 on the

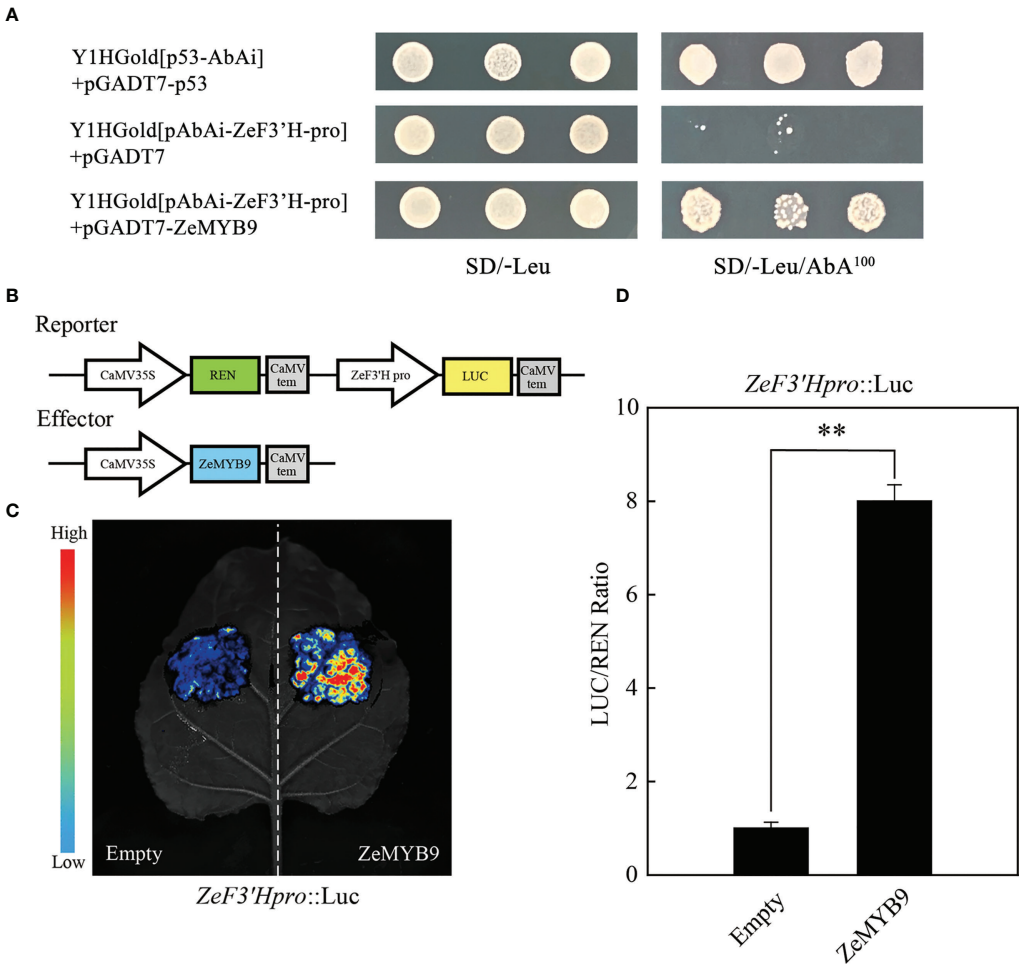

FIGURE 3
ZeMYB9 could directly bind to the promoter of *ZeF3'H*. **(A)** Yeast one-hybrid assay showing the binding of ZeMYB9 to the promoter of *ZeF3'H*. **(B)** Construction diagrams of reporter and effector vectors for dual-luciferase assays. **(C)** Graph showing the luminescence intensity of luciferase in *N. benthamiana* leaves. **(D)** Transient dual-luciferase detections of *ZeF3'H* in *N. benthamiana* leaves. Data were showed as the mean ± SE from three biological replicates. T-test was used for statistical analyses compared with corresponding control (**$P < 0.01$).

10.3389/fpls.2022.981086

ZeF3'H promoter. The reporter plasmid contained *LUC* and *REN* expressed under the control of *ZeF3'H*promoter and 35S promoter, respectively, while the effector vector carried *ZeMYB9* under the control of 35S promoter (Figure 3B). *ZeF3'H*$_{pro}$::LUC were transiently co-transformed with 35S::ZeMYB9 or 35S:: empty into *N. benthamiana* leaves. Signal of LUC was significantly increased when *ZeF3'H*$_{pro}$::LUC reporter was co-transformed with 35S::ZeMYB9 effector compared with 35S:: empty effector (Figure 3C). And the LUC/REN ratio with 35S:: ZeMYB9 effector was eight times higher than the control (Figure 3D). The results demonstrated that ZeMYB9 could bind to promoter and positively regulate the expression of *ZeF3'H*.

Heterologous expression of *ZeMYB9* strongly promoted anthocyanin accumulation in petunia and tobacco flowers

Transient transformation of petunia flowers and stable transformation of tobacco over-expressing *ZeMYB9* were used to characterize the function of *ZeMYB9*. Comparing with wild type, the petal limbs of transient petunia showed pink patches and obvious anthocyanin accumulation (Figure 4A). The content of anthocyanin in petunia petal limbs transiently expressing *ZeMYB9*, was about eight times higher than that in wild type (Figure 4B). As expected, in the transient expression

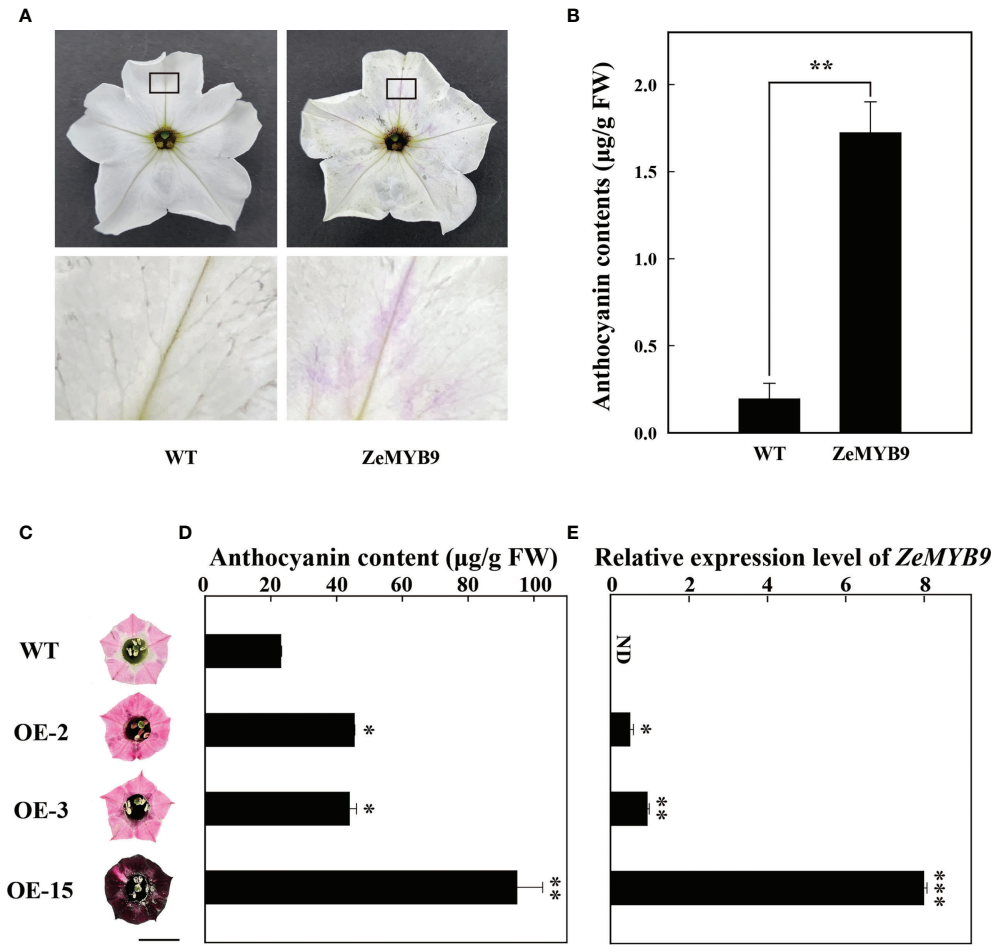

FIGURE 4
Overexpression of *ZeMYB9* in petunia and tobacco. **(A)** Phenotype of the entire (above) and the partial view (below) of petal limbs in wild type and *ZeMYB9*-overexpression flowers. **(B)** Total anthocyanin content in petal limbs of wild type and transiently transformed petunia. **(C)** Petal limb phenotype of wild-type and transgenic tobacco plants (OE-2, OE-3 and OE-15). The black line on the diagram showed a scale of 1cm. **(D)** Total anthocyanin contents in wild type and transgenic tobacco petal limbs. **(E)** Transcription levels of *ZeMYB9* in wild type and transgenic tobacco petal limbs. Data were showed as the mean ± SE from three biological replicates. T-test was used for statistical analyses compared with corresponding control (*P < 0.05, **P < 0.01, ***P < 0.001).

10.3389/fpls.2022.981086

petunia, the expression of nearly all of structural genes involved in anthocyanin synthesis was markedly upregulated (Figure S2).

ZeMYB9 driven by 35S promoter was transformed into tobacco leaf discs by an *Agrobacterium*-mediated transformation. Several transgenic plants were transplanted to a climate chamber and used for subsequent phenotypic observation. Leaves of three transgenic lines (OE-2, OE-3, and OE-15) turned into dark red (Figure S3A), while obvious pigment accumulation showed in different floral tissues of the flowers of three transgenic plants, including petal limb (Figure 5A), tube, filament and anther (Figure S3B), compared with the wild type. Surprisingly, petal limb color of OE15 showed dark wine red (Figure 4C). Determination of anthocyanins from petal limb showed that the anthocyanin content in OE-2 and OE-3 was 2-fold higher than wild type, while that in OE-15 was 4-fold higher (Figure 4D), accompanied with the highest expression level of *ZeMYB9* (Figure 4E). Expression analysis showed that compared with the wild type, all the detected anthocyanin structural genes and *NtAN1a* were significant upregulated in petal limbs of OE-3 and OE-15, while only *NtCHS*, *NtF3H* and *NtF3'H* were significantly upregulated in OE2 (Figure S4). *NtAN1b* showed higher expression level only in OE-15 (Figure S4).

ZeMYB9 could interact with ZeGL3 to activate the expression of *ZeF3'H*

bHLH proteins from IIIf subgroup are involved in the regulation of anthocyanin synthesis (Davies et al., 2012). A

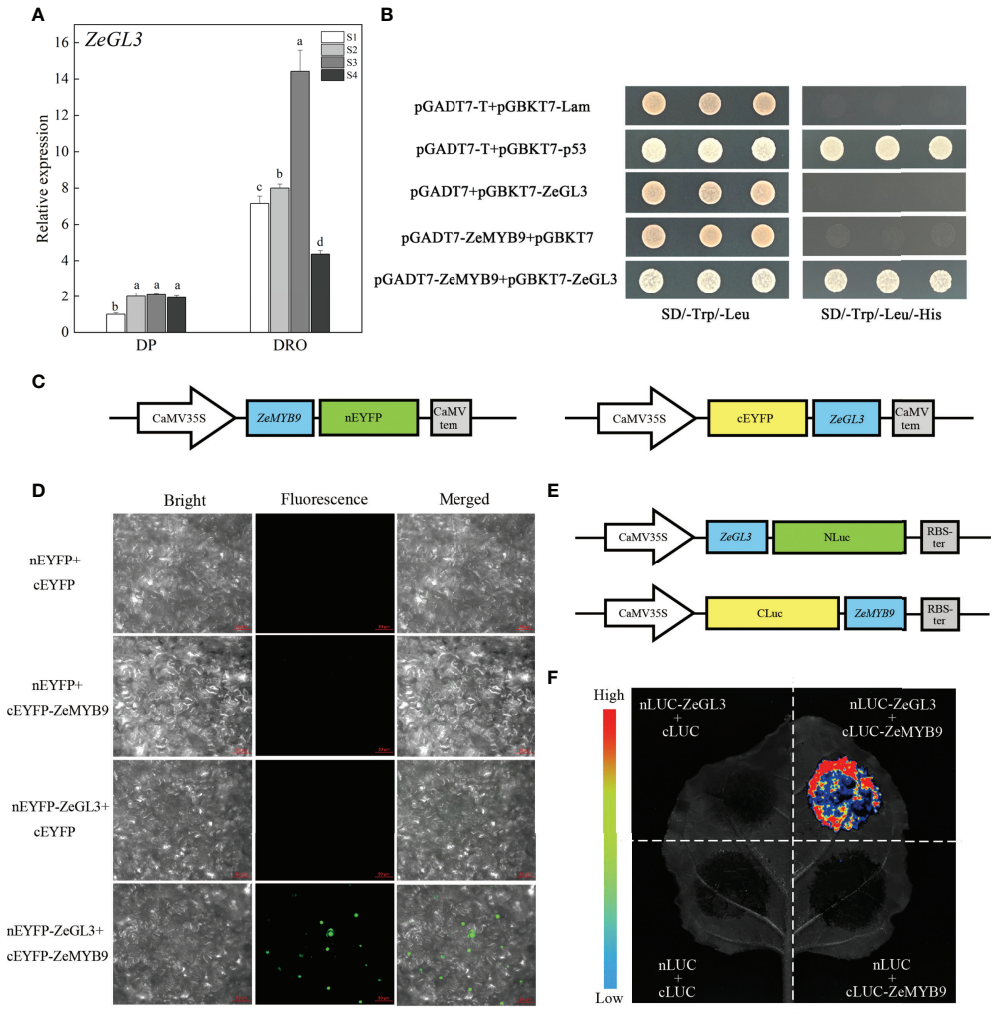

FIGURE 5
Expression analysis of ZeGL3 and interaction analysis of ZeMYB9 and ZeGL3. **(A)** Relative expression levels of ZeGL3 in the petals of DP and DRO at different developmental stages. ZeACT gene was used as an internal control for normalization, and three biological replicates were performed. Error bars indicate standard error (SE), and different lowercases indicate significant differences ($P < 0.05$). **(B)** Yeast two-hybrid assay for interaction relationship analysis between ZeMYB9 and ZeGL3. **(C)** Reporter plasmids construction diagrams for Bimolecular fluorescence complementation (BiFC) assays. **(D)** BiFC analysis between ZeMYB9 and ZeGL3 in N. benthamiana leaves. **(E)** Reporter plasmids construction diagrams for luciferase complementary assay (LCA). **(F)** ZeMYB9 could interact with ZeGL3 in LCA.

bHLH transcription factor belonging to IIIf subgroup was identified in *Z. elegans*, which was named ZeGL3 based on phylogenetic analysis that it was clustered into the clade of GL3 rather than clade of TT8 (Figure S5A). MYB-interaction region (MIR) and bHLH domain were present in ZeGL3 (Figure S5B). Similar to *ZeF3'H* and *ZeMYB9*, the expression level of *ZeGL3* was also greatly higher in DRO than that in DP (Figure 5A).

Yeast two-hybrid analysis showed that ZeGL3 and ZeMYB9 could physically interact, since yeast cells co-transformed with the positive control (pGBKT7-53+pGADT7-T) or pGADT7-ZeMYB9 with pGBKT7-ZeGL3, could grow on SD selection medium without Leu, Trp and His (Figure 5B). For BiFC assay, ZeGL3 and ZeMYB9 were individually fused with N-terminal and C-terminal fragment of enhanced yellow fluorescent protein (nEYFP and cEYFP) (Figure 5C). Then, different combinations were cotransformed into the same *N. benthamiana* leaf. No fluorescence was detected in negative control combinations, while strong fluorescence was observed in nucleus when coexpressing ZeMYB9-cEYFP and ZeGL3-nEYFP (Figure 5D). We also confirmed this result through luciferase complementary assay (LCA). ZeGL3 and ZeMYB9 were fused with NLuc and CLuc, respectively (Figure 5E). No LUC signal was detected in negative controls, while high LUC activity was present in the combination of ZeMYB9-CLuc and ZeGL3-NLuc (Figure 5F), which was consistent with the result of BiFC assay and indicated that ZeMYB9 could physically interact with ZeGL3.

Luciferase assay showed that the relative activitiy of the *ZeF3'H* promoter was enhanced with the combination of ZeGL3 and ZeMYB9, compared to ZeMYB9 alone (Figure 6). These results revealed that ZeMYB9 could form a transcriptional complex with ZeGL3 to activate the expression of *ZeF3'H*.

Co-expression of ZeMYB9 and ZeGL3 triggers the accumulation of anthocyanins in tobacco leave

To further characterize the function of *ZeMYB9* and *ZeGL3* in anthocyanin synthesis, transient transformation in tobacco leaves was carried out. The tobacco leaves turned into red in the injection area after five days which co-expressed *ZeMYB9* and *ZeGL3*, while no red pigmentation was detected infiltrating with eYFP (empty vector), *ZeMYB9* alone or *ZeGL3* alone (Figure 7A). Co-expression of *ZeMYB9* and *ZeGL3* possessed the ability to produce a dramatic accumulation of anthocyanin, but *ZeMYB9* or *ZeGL3* alone could not promote anthocyanin biosynthesis in tobacco leaves (Figure 7B). In co-expression of *ZeMYB9* and *ZeGL3*, all structural genes and two *bHLH* genes were significantly upregulated compared to the control (Figure 7D).

Discussion

The difference in the composition and content of anthocyanin provides many ornamental plants in a wide variety of colors. In flowers with pink, red or purple petal color, higher anthocyanin content is always accompanied with

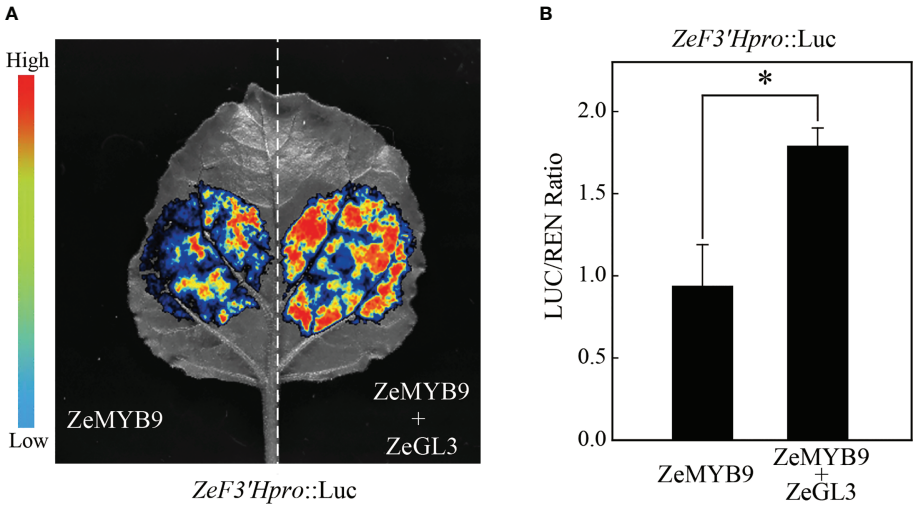

FIGURE 6
ZeMYB9 can form complexes with ZeGL3 to activate the expression of *ZeF3'H*. **(A)** Dual-luciferase assay in *N. benthamiana* leaves. **(B)** Ratio of LUC to REN activity. The data were the mean ± SE from three biological replicates. T-test was used for statistical analyses compared with corresponding control (*$P < 0.05$).

10.3389/fpls.2022.981086

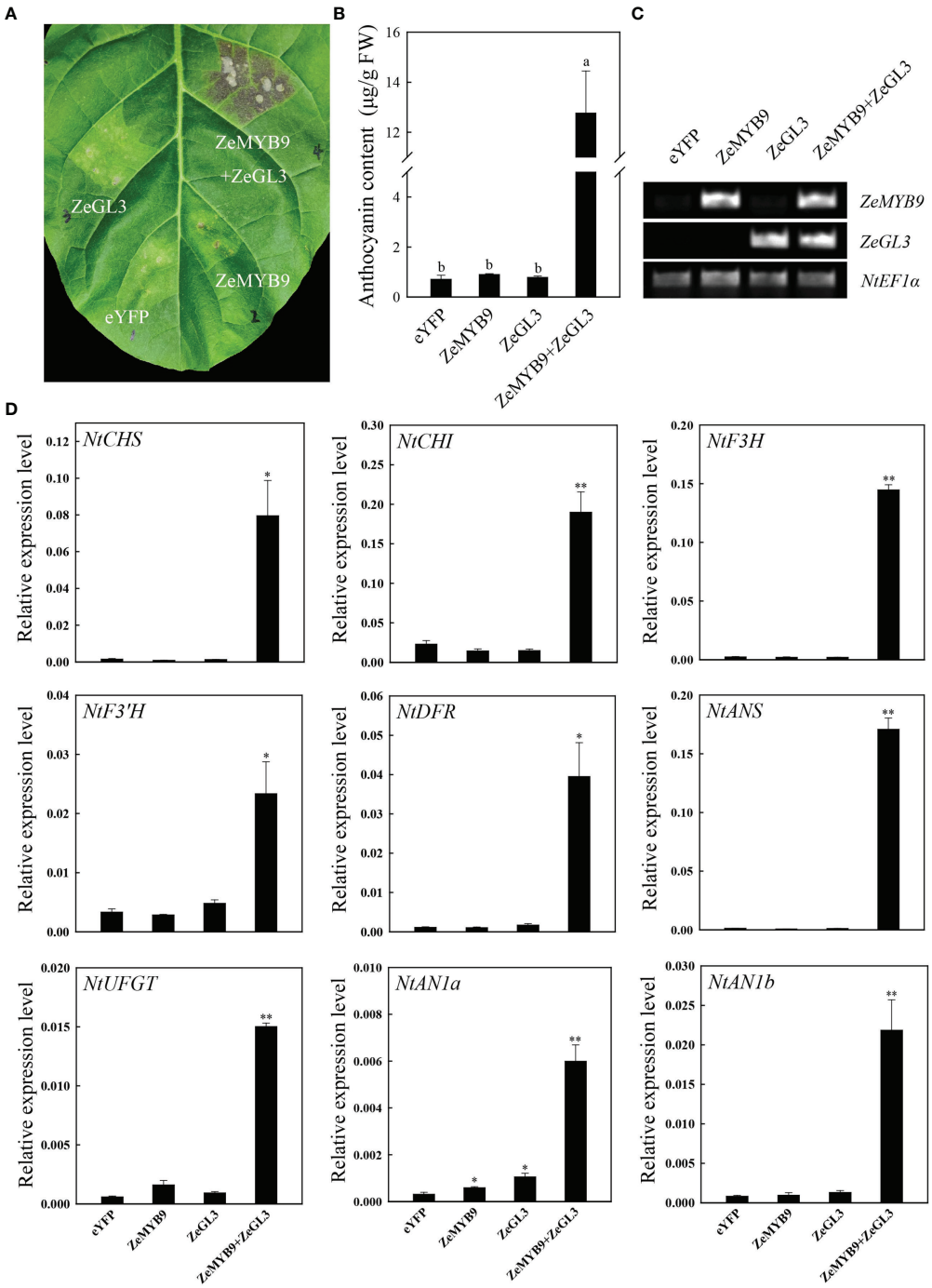

FIGURE 7
Co-expression of ZeMYB9 and ZeGL3 induces anthocyanin accumulation in tobacco leaves. **(A)** The tobacco leaves were photographed by camera and the location of gene injection was indicated on the graph. **(B)** Analysis of total anthocyanin content. Error bars indicate standard error (SE). And different lowercases indicate significant differences ($P < 0.05$). **(C)** Transcription levels of *ZeMYB9* and *ZeGL3* in the control and transient transformation of tobacco. *NtEF1α* was used as the reference gene. **(D)** Relative expression levels of the anthocyanin biosynthesis related structural genes and *bHLHs* (*AN1a* and *AN1b*). *NtEF1α* gene was used as an internal control for normalization, and three biological replicates were performed for qRT-PCR analysis. T-test was used for statistical analyses compared with corresponding control (*$P < 0.05$, **$P < 0.01$).

higher values of color parameters a^* and C^* and low value of color parameter L^* (Zhang et al., 2014; Deng et al., 2019). Similarly, compared to DP cultviar, DRO higher anthocyanin accumulation exhibited higher a^* and C^* values, and lower L^* value (Figure S1B). The synthesis of anthocyanin in petals is affected by the regulation of anthocyanin structural genes (Tanaka and Ohmiya, 2008). F3'H, a cytochrome P450 protein, belongs to CYP75B (Tanaka and Brugliera, 2013). *F3'H* gene could redirect the anthocyanin synthesis into cyanidin pathway and yield intense red color (Hoshino et al., 2003). The pink variety 'Albert heijn' of *Tulipa fosteriana* accumulated more cyanidins than the orange variety 'SN09', due to higher *F3'H* transcription leve (Yuan et al., 2014). When the expression levels of *F3'Hs* were downregulated, nearly only pelargonidin derivatives was accumulated in the pink flower varieties of *S. cruentus* (Jin et al., 2016). The pink and red flowers of *C. cyanus* had no cyanidins due to the open reading frame of *F3'H* were truncated and loss of a haem binding site (Deng et al., 2019). Similarly, we found the expression level of *ZeF3'H* in DRO was significantly higher than in DP (Figure 2A), accompanying with more accumulation of cyanidins in DRO (Figure 1).

Anthocyanin synthesis is controlled not only by structural genes, but also by regulatory genes. Currently, anthocyanin accumulation in many plants is regulated by R2R3-MYB transcription factors (Xu et al., 2015). R2R3-MYBs from *A. thaliana* could be divided into several subfamilies according to the conserved motifs, of which SG6 R2R3-MYBs act as activators of anthocyanin biosynthesis (Quattrocchio et al., 1999; Jian et al., 2019; Fang et al., 2021). ZeMYB9, a typical SG6 R2R3-MYB with conserved SG6 motif (Figure 2C) was proven to be a positive regulator of anthocyanin synthesis, because overexpression of this gene could greatly promote anthocyanin accumulation in petunia and tobacco flowers (Figure 4). SG6 R2R3-MYBs, such as MYB6 from *Populus tomentosa* and RH1 from *Medicago truncatula*, could directly bind to the MYB element on the promoter of the structural gene on the anthocyanin synthesis pathway to promote anthocyanin accumulation (Wang et al., 2019a; Wang et al., 2021). Similar to the expression pattern of *MaMybA* in grape hyacinth (*Muscari armeniacum*) (Chen et al., 2019), the expression of *ZeMYB9* increased first and then decreased with the development of flowers. What's more, *ZeMYB9* showed a significant positive correlation with *ZeF3'H* expression level and specifically activated the promoter of *ZeF3'H* based on yeast one-hybrid and dual luciferase assays (Figure 3). It was suggested that ZeMYB9 can alter anthocyanin profile by regulating the expression of *ZeF3'H* in *Z. elegans*.

Numerous studies have identified that a conserved motif [D/E]Lx$_2$[R/K]x$_3$Lx$_6$Lx$_3$R in the R3 domain of R2R3-MYB could interact with bHLH of IIIf subgroup to form MYB-bHLH complex in all anthocyanin-accumulating plants (Feller et al., 2011). In *A. thaliana*, IIIf bHLH transcription factors are mainly divided into TT8 and GL3 clades. AtTT8 can interact with MYB and WD40 to regulate the synthesis of anthocyanin and proanthocyanidins (Baudry et al., 2004; Gonzalez et al., 2008). AtGL3 and AtEGL3 can also coordinate with MYB transcription factors to regulate the synthesis of anthocyanin but not proanthocyanidins (Payne et al., 2000; Morohashi et al., 2007). *PbbHLH2* from *Pyrus bretschneideri*, interacts with MYB through the N-terminal MIR domain to promote anthocyanin synthesis (Li et al., 2021). Evolutionary analysis showed that ZeGL3 belonged to the GL3 clade and there was a MIR domain region present in its N-terminal (Figure S5), suggesting that this protein may possess positive regulation on anthocyanin synthesis. In our study, yeast two-hybrid, LCA and BiFC assays illustrated the interaction between ZeMYB9 and ZeGL3 proteins (Figure 5). AcMYB123 and AcbHLH42 in *Actinidia chinensis* cv. Hongyang could interact to induce anthocyanin accumulation in tobacco leaves and activate the expression of *AcF3GT1* and *AcANS* promoter (Wang et al., 2019b). Similar positive function of MYB-bHLH complex on the expression of anthocyanin structural genes was well conserved in many plants, such as *Anthurium andraeanum* (Li et al., 2019a), *P. qiui* (Liu et al., 2022), *Medicago truncatula* (Li et al., 2016), etc. In our study, the interaction of ZeMYB9 and ZeGL3 proteins could enhance the activation of *ZeF3'H* expression (Figure 6) and trigger anthocyanin accumulation in tobacco leaves (Figure 7).

On the basis of the above results, we propose a regulatory network of anthocyanin biosynthesis in *Z. elegans*, which was controlled by *ZeMYB9* (Figure 8). ZeMYB9 could directly or in the form of ZeMYB9-ZeGL3 complex bind to the promoter of *ZeF3'H*. Higher expression of *ZeMYB9* increased the expression of *ZeF3'H*, thereby anthocyanin synthesis was more directed to the DHQ pathway and eventually to the synthesis of cyanidins in DRO. Meanwhile, the expression of *ZeMYB9* in DP was relatively lower, resulting in downregulated expression of *ZeF3'H*, so the synthesis of anthocyanin mainly led to the accumulation of pelargonidins. These results would significantly expand the current understanding of transcriptional regulation of flower color in *Z. elegans*, and also provide theoretical basis for flower color breeding in Compositae flowers.

Conclusion

Cyanidins were the main pigments that affected the color of DP and DRO petals. We found a positive MYB regulator of the S6 subfamily, ZeMYB9, which was positively correlated with *ZeF3'H* expression and higher expression of *ZeMYB9* and *ZeF3'H* was detected in the DRO cultivar with higher cyanidin content. ZeMYB9 could significantly activate the expression of *ZeF3'H* promoter and promoted anthocyanin accumulation in petunia and tobacco corolla. ZeMYB9 was also

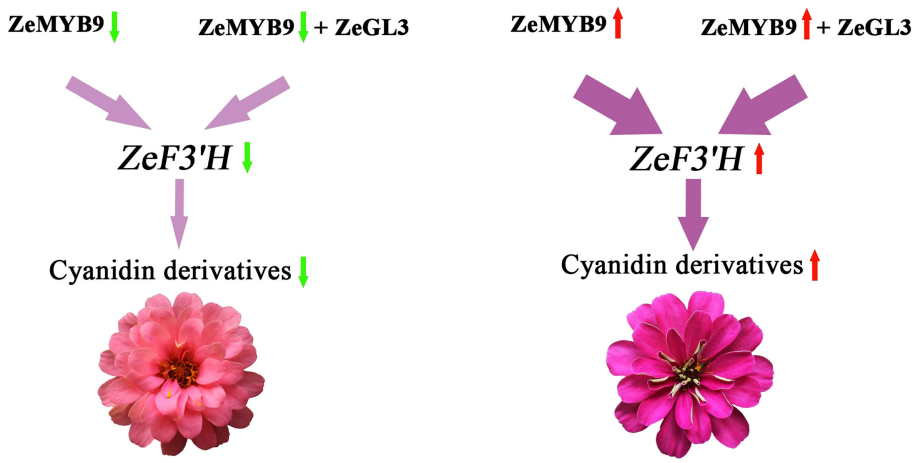

FIGURE 8
Diagram of regulatory pattern of *ZeMYB9* in *Z. elagans*.

shown to interact with a IIIf subfamily of bhLH transcription factor ZeGL3 to promote *ZeF3'H* promoter expression and induce anthocyanin synthesis in tobacco leaves. This study revealed the regulation mechanism of color difference of different *Z. elagans* cultivars, which provides useful resources for future studies on the molecular breeding of flowers color in Compositae flowers.

Materials and methods

Plant materials and growth conditions

Z. elegans 'Dreamland Pink' (DP) with pink petal color and 'Dreamland Rose' (DRO) with purple petal color, were chosen as materials (Figure 1A). These plant materials were grown in climatic chamber with a relative humidity of 60% and long-day conditions (16 h/8 h light/dark, 25°C/18°C). Flower opening process of *Z. elegans* could be divided into four developmental stages (Qian et al., 2021): S1 was defined as when the ray florets were acicular and had barely outgrown the bract; S2 was defined as when the ray florets clearly outgrew and began to colored, the bract and the angle between the ray florets and the stem was equal to or less than 45°; S3 was defined as when petals of the ray florets were slightly flattened and completed coloring, the angle between the ray florets and the stem was about 90°; S4 was defined as when petals of the ray florets were flattened. The ray florets at the four developmental stages of DP and DRO were separated, immediately frozen in liquid nitrogen and stored at -80°C until use. Tobacco (*Nicotiana tabacum* 'NC89' or *N. benthamiana*) and *Petunia hybrida* 'Mitchell' used for subsequent experiments were also cultivated in long-day climatic chamber (16 h/8 h light/dark, 25°C/18°C).

Color parameters and total flavonoids measurement

Color parameters of the middle part of ray florets in DP and DRO at S4 were determined by the color reader CR-10 (Konica Minolta Optics, Inc., Sakai, Japan). Lightness (L^*) and two chromatic components a^* and b^* were analyzed using the International Commission on Illumination (CIE) $L^*a^*b^*$system (Gonnet, 1993). Chroma (C^*) and hue angle ($h°$) were calculated by L^*, a^* and b^* values: $C^*=(a^{*2}+b^{*2})^{1/2}$, $h°$=arctan (b^*/a^*) (McGuire, 1992).

The total flavonoids contents in the ray florets of DP and DRO at S4 were quantified as described by Sakata (Sakata et al., 1995) and the content was calculated by a standard curve drawn with rutin as the standard substance: Total flavonoids=0.0078*A_{405} (R^2 = 0.993).

Extraction and component analysis of anthocyanins

0.2 g fresh ray florets of DP and DRO at S4 were weighed and ground into powder using liquid nitrogen. Then, they were incubated in 2 mL extracting solution containing 2% formic acid and 70% methyl alcohol overnight at 4°C (Qian et al., 2021). The combined supernatants were filtered through 0.22 μm micropore filter for further analysis by UPLC. The UPLC (Waters Acquity H-Class) was equipped with chromatographic column using Acquity UPLC® HSS T3 (Waters, 1.8 μm, 2.1×100 mm) and the column temperature was 30°C. The analytical column was eluted with mobile phase A (formic acid: water, 1:99, v/v) and mobile phase B (acetonitrile) at a rate of 0.4 mL min^{-1}. The gradient elution condition was: 0-15 min, 95%-5% A,

5%-95% B; 15-16 min, 5% A, 95% B; 16.0-16.1 min, 5%-95% A, 95%-5% B; 16.1-19.0 min, 95% A, 5% B. The UV detection wavelength was set at 530 nm. Quantitative analysis of each component was conducted by external standard method using cyanidin-3-*O*-rutinoside as a standard.

Gene sequence and phylogenetic analysis

Gene sequences of *ZeMYB9* and *ZeGL3* were identified from petal transcriptome of *Z. elegans*. The amino acid sequences of *ZeMYB9* and *ZeGL3* were subjected to multiple sequence alignment by DANMAN and phylogenetic tree analysis by MEGA 6 (Tamura et al., 2011) with the neighbor-joining method (1000 bootstrap replicates). The anthocyanidin-related MYB and bHLH proteins in *Arabidopsis thaliana* and other species were obtained from the TAIR (https://www.arabidopsis.org/) and NCBI (https://www.ncbi.nlm.nih.gov/) databases.

RNA extraction and cDNA synthesis

Total RNA was extracted using the FastPure Plant Total RNA Isolation Kit (Vazyme, Nanjing, China). The cDNA was synthesized from the PrimeScript™ RT Master Mix (Takara, Dalian, China).

qRT-PCR analysis

The expression of *ZeMYB9*, *ZeF3'H* and *ZeGL3* at four developmental stages in two cultivars was analyzed. The RT-PCR reactions were performed using AceQ Universal SYBR qPCR Master Mix (Vazyme, China) on LightCycler® 480 II (Roche Diagnostics, Germany). Reactions were run with three biological replicates and the amplification program consisted of one cycle of 95°C for 5 min followed by 40 cycles of 95°C for 10 s and 60°C for 30 s with melt curve program. The *ZeACT* gene was used to normalize the samples. Relative expression of the target genes was calculated by $2^{-\Delta\Delta Ct}$ (Livak and Schmittgen, 2001). qRT-PCR data were presented here as the mean ± SE of three biological replicates. All primer sequences were available in Table S1.

ZeF3'H promoter isolation and analysis

ZeF3'H gene was predicted as the key anthocyanin biosynthetic gene determining the synthesis of cyanidins in *Z. elegans* (Qian et al., 2021). The promoter of *ZeF3'H* was isolated with genomic walking FPNI-PCR (Wang et al., 2011) from genomic DNA of young leaves extracted with CTAB method (Murray and Thompson, 1980). Primers used in FPNI-PCR were showed in Table S2. And the *cis*-elements of *ZeF3'H* promoter sequence were predicted by PlantCARE (http://bioinformatics.psb.ugent.be/webtools/plantcare/html/).

Yeast one-hybrid assay

The promoter sequence of *ZeF3'H* (ZeF3'H-Pro) was amplified with primers in Table S2 and inserted into the pAbAi vector, and the CDS of *ZeMYB9* was cloned into the pGADT7 vector with the primers listed in Table S3. pAbAi-ZeF3'H-Pro was transformed into Y1H Gold according to the protocol of Yeastmaker™ Yeast Transformation System 2 User Manual, and the lowest inhibitory concentration of aureobasidin A (AbA) for the bait strain was tested on SD/-Ura media. The prey and was transformed into yeast cells containing recombinant pAbAi vector and then incubated on SD/-Leu medium at 30°C for 3 days. The interactions between pGADT7-ZeMYB9 and pAbAi-ZeF3'H-Pro were detected on SD/-Leu medium with 100 ng mL^{-1} AbA at 30°C for 4 days.

Dual luciferase assay

The full-length fragment of the *ZeF3'H* promoter was cloned into pGreenII 0800-LUC vector and the CDS of *ZeMYB9* and *ZeGL3* were inserted into pCNHP-eYFP vector, respectively. The recombinant plasmids and empty vector were transformed into *Agrobacterium* strain GV3101 or GV3101 (pSoup). The *Agrobacterium* strain bacteria that carried transcription factor or the promoter were resuspended in infiltration medium (10 mM $MgCl_2$ and 200 μM acetosyringone) and mixed when OD_{600} reached to 0.8. Then the mixtures were injected into tobacco leaves without needle. After three days, the transformed tobacco leaves were sprayed with D-luciferin sodium salt (Coolaber, Beijing, China) and then observed using Fuison-FX7 multi-imaging apparatus (Vilber, France). Enzyme activities of Firefly luciferase (LUC) and Renilla luciferase (REN) were tested using Dual Luciferase Reporter Assay Kit (Vazyme, China).

Transient transformation of petunia flowers

In order to verify the function of *ZeMYB9* in the regulation of anthocyanin biosynthesis, transient overexpression of *ZeMYB9* in petunia flowers were infiltrated by vacuum

infiltration method. Day 1 petunia flowers were respectively submerged in infiltration containing *Agrobacterium* (OD_{600} = 1.0) harboring pCNHP-eYFP-*ZeMYB9* or empty vector and subjected to vacuum condition of -13 psi. After releasing the vacuum, the petals were cultured in 2 mL tubes containing 3% sucrose for five days. And then, the petal limbs were observed and sampled for anthocyanin measurement and gene expression analysis. The expression level of *ZeMYB9* and anthocyanin related genes in petunia petals were analyzed by using qRT-PCR. The qRT-PCR primers for petunia anthocyanin-related structural genes and *PhEF1α* were obtained from the previous study (Zhang et al., 2021).

Stable tobacco transformation

The CDS of *ZeMYB9* was inserted into pCNH-Flag vector, and the recombinant plasmid was transformed into *Agrobacterium* strain GV3101 for transformation. Then the *Agrobacterium* carrying pCNH-Flag-*ZeMYB9* plasmid inflected *N. tabacum* 'NC89' leaf disks according to the protocol described by Li's methods (Li et al., 2019b). The transformed tobacco plants were screened using 10 mg L^{-1} hygromycin antibiotic. The petal limbs of transgenic plants and wild-type tobacco were used for analyzing anthocyanin contents and gene expression levels. The expression level of *ZeMYB9* and anthocyanin related genes in tobacco petal limbs was analyzed by qRT-PCR. The qRT-PCR primers for tobacco anthocyanin-related structural genes and *NtEF1α* were obtained from the previous study (Li et al., 2019b).

Yeast two-hybrid assay

The full-length coding sequences of *ZeMYB9* and *ZeGL3* were respectively introduced into pGADT7 and pGBKT7 vectors. Various combinations of BD and AD vectors were cotransformed into the yeast strain Y2H Gold and grown on SD/-Leu-Trp medium at 30°C for 3-4 days. The clones were subsequently grown on SD/-His-Leu-Trp medium at 30°C for 4 days to test the interaction between ZeMYB9 and ZeGL3.

BiFC assay and LCA

Bimolecular fluorescence complementation (BiFC) and luciferase complementary assay (LCA) were used to analyze the interaction between ZeMYB9 and ZeGL3 proteins. Full-length sequences of ZeMYB9 and ZebHLH1 were cloned into the vector pCNHP-cEYFP and pCNHP-nEYFP, respectively. The recombinant plasmids were respectively transformed into *Agrobacterium* strain GV3101 and then different combinations of *Agrobacterium* strains were co-transformed into four-week tobacco leaves with needleless syringes which resuspended in infiltration medium (10 mM $MgCl_2$ and 200 μM acetosyringone) to each OD_{600} of 0.8. After 48 h of the injection, EYFP fluorescence was detected using Fluorescence microscope of Axio Imager A2 (ZEISS, Germany).

Full-length sequences of *ZeMYB9* and *ZeGL3* were inserted into the pCAMBIAI1300-Cluc and pCAMBIAI1300-Nluc plasmids, respectively. All combinations of *Agrobacterium* strains cell containing recombinant plasmids were infiltrated into tobacco leaves. The infiltrated tobacco leaves were sprayed with D-luciferin sodium salt (Coolaber, Beijing, China) and detected after three days using Fuison-FX7 multi-imaging apparatus (Vilber, France).

Transient transformation of tobacco

Transient co-expression of *ZeMYB9* and *ZeGL3* in *N. tabacum* 'NC89' leaves was conducted based on a modified method (Sparkes et al., 2006). *Agrobacterium* containing pCNHP-eYFP-*ZeMYB9*, pCNHP-eYFP-*ZeGL3* or the mixture were infiltrated into tobacco leaves and the plants were cultured in phytotron under normal condition for five days. Transcription of *ZeMYB9* or *ZeGL3* was analyzed by RT-PCR, while anthocyanin biosynthesis-related structural genes and *bHLHs* (*AN1a* and *AN1b*) were analyzed by qRT-PCR. The *NtEF1α* gene was used to normalize the target genes.

Total anthocyanin determination

Anthocyanin contents were measured using the procedure of previous study (Stevenson and Harrington, 2009). The injected tobacco leaves or petunia flowers were ground to a powder in liquid nitrogen and then extracted in 2 mL of acidified methanol (1% HCl) overnight at 4°C and in the dark. Chloroform was added to remove chlorophyll that tobacco leaves to prevent interference with absorbance, and anthocyanin were measured at 530 and 657 nm. Relative anthocyanin content was calculated on a formula: $(A_{530} - 0.25 * A_{657})$/mg FW.

Statistical analysis

One-way analysis of variance (ANOVA) or T-test was considered appropriate to determine significant differences between pairwise comparisons in the analyses of color parameters, pigment contents or gene expression level with SPSS software version 20.0 (SPSS Inc., Chicago, IL, USA). Photographs were created using SigmaPlot software version 14.0 (Systat Software, San Jose, CA, USA), Adobe Photoshop

CC 2019 and Adobe Illustrator CC 2019 (Adobe Systems, Inc., San Jose, CA, USA).

Data availability statement

The sequence data presented in the study are deposited in the NCBI GenBank database, accession numbers MT815440, ON959236 and ON959237 for *ZeF3'H*, *ZeMYB9* and *ZeGL3*, respectively.

Author contributions

CZ and JF designed and supervised this study. JQ and LJ performed the experiments and analyzed the data. HQ, JC, ZW and MX assisted with doing the experiments. JQ, LJ and CZ wrote the article. All authors contributed to the article and approved the submitted version.

Funding

This research was supported by National College Students Innovation and Entrepreneurship Training Program (No. 202010341022), College Students Research Training Program of Zhejiang Agriculture and Forestry University (No. 2021KX0069 and S202210341185), and the Open Fund of Zhejiang Provincial Key Laboratory of Germplasm Innovation and Utilization for Garden Plants (K202105).

Acknowledgments

We are grateful to Dr. Xing-Qi Huang for the gift of plasmids pCNHP-eYFP, pCNHP-cEYFP, pCNHP-nEYFP and pCNH-Flag.

Conflict of interest

The authors declare that the research was conducted in the absence of any commercial or financial relationships that could be construed as a potential conflict of interest.

Publisher's note

Supplementary material

The Supplementary Material for this article can be found online at: https://www.frontiersin.org/articles/10.3389/fpls.2022.981086/full#supplementary-material

SUPPLEMENTARY FIGURE 1
Color parameters and total flavonoid content analysis of DP and DRO. **(A)** Total flavonoid content in DP and DRO. **(B)** The flower color parameter values of DP and DRO. *L**, lightness; *a**, redness; *b**, yellowness; *C**, chroma; *h°*, hue angle. Three biological replicates were performed for content analysis. T-test was used for statistical analyses compared with corresponding control (**P* < 0.05, ***P* < 0.01).

SUPPLEMENTARY FIGURE 2
Relative expression levels of *ZeMYB9* and structural genes in the anthocyanin biosynthesis pathway in the petal limbs of wild type and transgenic petunia. *PhEF1α* gene was used as an internal control for normalization, and three biological replicates were performed. Error bars indicated standard error (SE). T-test was used for statistical analyses compared with wild type (**P* < 0.05, ***P* < 0.01).

SUPPLEMENTARY FIGURE 3
Phenotypic observation of wild type and three transgenic lines (OE-2, OE-3 and OE-15). **(A)** Phenotypic observations of the entire plants. **(B)** Phenotypic observations of tubes, calyxs, anthers, filaments, and ovaries. The black line on the diagram showed a scale of 1cm.

SUPPLEMENTARY FIGURE 4
Relative expression levels of *ZeMYB9* and structural genes in the anthocyanin biosynthesis pathway in the petal limbs of wild type and transgenic tobacco. *NtEF1α* gene was used as an internal control for normalization, and three biological replicates were performed. Error bars indicated standard error (SE). T-test was used for statistical analyses compared with corresponding control (*P < 0.05, **P < 0.01, ***P < 0.001).

SUPPLEMENTARY FIGURE 5
Analysis of ZeGL3 from IIIf subgroup in *Zinnia elegans*. **(A)** Phylogenetic tree of different GL3 and TT8 proteins participating in anthocyanin biosynthesis in other plants. **(B)** Multiple alignment of the amino acid sequences of bHLH IIIf subgroup proteins from different plants. The black line at the top indicated the conserved MYB-interaction region (MIR) at the N-terminal. The alternating red and black lines indicated a bHLH domain at the C-terminal. The GenBank accession numbers of these bHLH proteins were as follows: the GL3 clade as Arabidopsis thaliana AtMYB75|PAP1 (AT1G56650.1), *Malus domestica* MdbHLH33 (ABB84474.1), *Fragaria ananass* FabHLH33 (AFL02465.1), *Vitis vinifera* VvMYCA1 (ABM92333.3), *Arabidopsis thaliana* AtGL3 (NP_001333705.1), *Antirrhinum majus* AmDEL (AAA33663.1); the TT8 clade as *Chrysanthemum morifolium* CmbHLH2 (ALR72603.1), *A. thaliana* AtTT8 (CAC14865.1), *Nicotiana tabacum* NtAn1a (AEE99257.1).

SUPPLEMENTARY TABLE 1
Primer sequences for qRT-PCR.

SUPPLEMENTARY TABLE 2
Primer sequences for promoter cloning.

SUPPLEMENTARY TABLE 3
Primer sequences for vector construction.

References

Albert, N. W., Davies, K. M., Lewis, D. H., Zhang, H., Montefiori, M., Brendolise, C., et al. (2014). A conserved network of transcriptional activators and repressors regulates anthocyanin pigmentation in eudicots. *Plant Cell* 26, 962–980. doi: 10.1105/tpc.113.122069

Baudry, A., Heim, M. A., Dubreucq, B., Caboche, M., Weisshaar, B., and Lepiniec, L. (2004). TT2, TT8, and TTG1 synergistically specify the expression of *BANYULS* and proanthocyanidin biosynthesis in *Arabidopsis thaliana*. *Plant J.* 39, 366–380. doi: 10.1111/j.1365-313X.2004.02138.x

Chen, K., Du, L., Liu, H., and Liu, Y. (2019). A novel R2R3-MYB from grape hyacinth, MaMybA, which is different from MaAN2, confers intense and magenta anthocyanin pigmentation in tobacco. *BMC Plant Biol.* 19, 390. doi: 10.1186/s12870-019-1999-0

Davies, K. M., Albert, N. W., and Schwinn, K. E. (2012). From landing lights to mimicry: the molecular regulation of flower colouration and mechanisms for pigmentation patterning. *Funct. Plant Biol.* 39, 619–638. doi: 10.1071/FP12195

Deng, C., Li, S., Feng, C., Hong, Y., Huang, H., Wang, J., et al. (2019). Metabolite and gene expression analysis reveal the molecular mechanism for petal colour variation in six *Centaurea cyanus* cultivars. *Plant Physiol. Biochem.* 142, 22–33. doi: 10.1016/j.plaphy.2019.06.018

Fang, Z.-Z., Lin-Wang, K., Zhou, D.-R., Lin, Y.-J., Jiang, C.-C., Pan, S.-L., et al. (2021). Activation of *PsMYB10.2* pranscription causes anthocyanin accumulation in flesh of the red-fleshed mutant of 'Sanyueli' (*Prunus salicina* lindl.). *Front. Plant Sci.* 12. doi: 10.3389/fpls.2021.680469

Feller, A., Machemer, K., Braun, E. L., and Grotewold, E. (2011). Evolutionary and comparative analysis of MYB and bHLH plant transcription factors. *Plant J.* 66, 94–116. doi: 10.1111/j.1365-313X.2010.04459.x

Fukui, Y., Tanaka, Y., Kusumi, T., Iwashita, T., and Nomoto, K. (2003). A rationale for the shift in colour towards blue in transgenic carnation flowers expressing the flavonoid 3',5'-hydroxylase gene. *Phytochem* 63, 15–23. doi: 10.1016/S0031-9422(02)00684-2

Gonnet, J. F. (1993). CIELab measurement, a precise communication in flower colour: An example with carnation (*Dianthus caryophyllus*) cultivars. *J. Hortic. Sci.* 68, 499–510. doi: 10.1080/00221589.1993.11516378

Gonzalez, A., Zhao, M., Leavitt, J. M., and Lloyd, A. M. (2008). Regulation of the anthocyanin biosynthetic pathway by the TTG1/bHLH/Myb transcriptional complex in *Arabidopsis* seedlings. *Plant J.* 53, 814–827. doi: 10.1111/j.1365-313X.2007.03373.x

Holton, T. A., Brugliera, F., Lester, D. R., Tanaka, Y., Hyland, C. D., Menting, J. G., et al. (1993). Cloning and expression of cytochrome P450 genes controlling flower colour. *Nature* 366, 276–279. doi: 10.1038/366276a0

Hoshino, A., Morita, Y., Choi, J.-D., Saito, N., Toki, K., Tanaka, Y., et al. (2003). Spontaneous mutations of the flavonoid 3'-hydroxylase gene conferring reddish flowers in the three morning glory species. *Plant Cell Physiol.* 44, 990–1001. doi: 10.1093/pcp/pcg143

Jian, W., Cao, H., Yuan, S., Liu, Y., Lu, J., Lu, W., et al. (2019). SlMYB75, an MYB-type transcription factor, promotes anthocyanin accumulation and enhances volatile aroma production in tomato fruits. *Hortic. Res.* 6, 22. doi: 10.1038/s41438-018-0098-y

Jin, X., Huang, H., Wang, L., Sun, Y., and Dai, S. (2016). Transcriptomics and metabolite analysis reveals the molecular mechanism of anthocyanin biosynthesis branch pathway in different *Senecio cruentus* cultivars. *Front. Plant Sci.* 7. doi: 10.3389/fpls.2016.01307

Katsumoto, Y., Fukuchi-Mizutani, M., Fukui, Y., Brugliera, F., Holton, T. A., Karan, M., et al. (2007). Engineering of the rose flavonoid biosynthetic pathway successfully generated blue-hued flowers accumulating delphinidin. *Plant Cell Physiol.* 48, 1589–1600. doi: 10.1093/pcp/pcm131

LaFountain, A. M., and Yuan, Y. W. (2021). Repressors of anthocyanin biosynthesis. *New Phytol.* 231, 933–949. doi: 10.1111/nph.17397

Li, P., Chen, B., Zhang, G., Chen, L., Dong, Q., Wen, J., et al. (2016). Regulation of anthocyanin and proanthocyanidin biosynthesis by *Medicago truncatula* bHLH transcription factor MtTT8. *New Phytol.* 210, 905–921. doi: 10.1111/nph.13816

Li, Z., Chen, W., Zhang, C., Du, C., Shao, G., Cui, Y., et al. (2019b). *RcMYBPA2* of *Rosa chinensis* functions in proanthocyanidin biosynthesis and enhances abiotic stress tolerance in transgenic tobacco. *Plant Cell Tiss. Org. Cult.* 137, 441–454. doi: 10.1007/s11240-019-01580-z

Li, C., Qiu, J., Huang, S., Yin, J., and Yang, G. (2019a). AaMYB3 interacts with AabHLH1 to regulate proanthocyanidin accumulation in *Anthurium andraeanum* (Hort.)–another strategy to modulate pigmentation. *Hortic. Res.* 6, 14. doi: 10.1038/s41438-018-0102-6

Liu, X., Duan, J., Huo, D., Li, Q., Wang, Q., Zhang, Y., et al. (2022). The *Paeonia qiui* R2R3-MYB transcription factor PqMYB113 positively regulates anthocyanin accumulation in *Arabidopsis thaliana* and tobacco. *Front. Plant Sci.* 12. doi: 10.3389/fpls.2021.810990

Liu, Y., Ma, K., Qi, Y., Lv, G., Ren, X., Liu, Z., et al. (2021). Transcriptional regulation of anthocyanin synthesis by MYB-bHLH-WDR complexes in kiwifruit (*Actinidia chinensis*). *J. Agric. Food Chem.* 69, 3677–3691. doi: 10.1021/acs.jafc.0c07037

Livak, K. J., and Schmittgen, T. D. (2001). Analysis of relative gene expression data using real-time quantitative PCR and the $2^{-\Delta\Delta CT}$ method. *Methods* 25, 402–408. doi: 10.1006/meth.2001.1262

Li, X., Xiang, F., Han, W., Qie, B., Zhai, R., Yang, C., et al. (2021). The MIR-domain of PbbHLH2 is involved in regulation of the anthocyanin biosynthetic pathway in "Red zaosu" (*Pyrus bretschneideri* rehd.) pear fruit. *Int. J. Mol. Sci.* 22, 3026. doi: 10.3390/ijms22063026

McGuire, R. G. (1992). Reporting of objective color measurements. *HortScience* 27, 1254–1255. doi: 10.1016/0304-4238(93)90147-I

Morohashi, K., Zhao, M., Yang, M., Read, B., Lloyd, A., Lamb, R., et al. (2007). Participation of the *Arabidopsis* bHLH factor GL3 in trichome initiation regulatory events. *Plant Physiol.* 145, 736–746. doi: 10.1104/pp.107.104521

Murray, M. G., and Thompson, W. F. (1980). Rapid isolation of high molecular weight plant DNA. *Nucleic Acids Res.* 8, 4321–4326. doi: 10.1093/nar/8.19.4321

Noda, N., Yoshioka, S., Kishimoto, S., Nakayama, M., Douzono, M., Tanaka, Y., et al. (2017). Generation of blue chrysanthemums by anthocyanin b-ring hydroxylation and glucosylation and its coloration mechanism. *Sci. Adv.* 3, e1602785. doi: 10.1126/sciadv.1602785

Payne, C. T., Zhang, F., and Lloyd, A. M. (2000). *GL3* encodes a bHLH protein that regulates trichome development in arabidopsis through interaction with GL1 and TTG1. *Genetics* 156, 1349–1362. doi: 10.1093/genetics/156.3.1349

Qian, J., Jiang, L., Zheng, G., Chen, J., Lai, W., Xu, M., et al. (2022). Identification and expression analysis of MYB transcription factors regulating the anthocyanin biosynthesis in *Zinnia elegans* and function research of *ZeMYB9*. *Acta Hortic. Sin.* 49, 1505–1518. doi: 10.16420/j.issn.0513-353x.2021-0474

Qian, J., Lai, W., Jiang, L., Zhan, H., Zhai, M., Fu, J., et al. (2021). Association between differential gene expression and anthocyanin biosynthesis underlying the diverse array of petal colors in *Zinnia elegans*. *Sci. Hortic.* 277, 109809. doi: 10.1016/j.scienta.2020.109809

Qian, J., Zhan, H., Zhai, M., Lai, W., Pang, T., Fu, J., et al. (2019). "Composition and content analysis of anthocyanidins in the petals of zinnia elegans In," in *Advances in ornamental horticulture of chin*. Ed. Q. Zhang (, Beijing: China Forestry Publishing House), 479–483.

Quattrocchio, F., Wing, J., van der Woude, K., Souer, E., de Vetten, N., Mol, J., et al. (1999). Molecular analysis of the *anthocyanin2* gene of petunia and its role in the evolution of flower color. *Plant Cell* 11, 1433–1444. doi: 10.1105/tpc.11.8.1433

Rodrigues, J. A., Espley, R. V., and Allan, A. C. (2021). Genomic analysis uncovers functional variation in the c-terminus of anthocyanin-activating MYB transcription factors. *Hortic. Res.* 8, 77. doi: 10.1038/s41438-021-00514-1

Sakata, Y., Aoki, N., Tsunematsu, S., Nishikouri, H., and Johjima, T. (1995). Petal coloration and pigmentation of tree peony bred and selected in daikon island (shimane prefecture). *J. Jpn. Soc Hortic. Sci.* 64, 351–357. doi: 10.2503/jjshs.64.351/

Shimada, Y., Ohbayashi, M., Nakano-Shimada, R., Okinaka, Y., Kiyokawa, S., and Kikuchi, Y. (2014). Genetic engineering of the anthocyanin biosynthetic pathway with flavonoid-3',5'-hydroxylase: specific switching of the pathway in petunia. *Plant Cell Rep.* 20, 456–462. doi: 10.1007/s002990100319

Sparkes, I. A., Runions, J., Kearns, A., and Hawes, C. (2006). Rapid, transient expression of fluorescent fusion proteins in tobacco plants and generation of stably transformed plants. *Nat. Protoc.* 1, 2019–2025. doi: 10.1038/nprot.2006.286

Stevenson, C. C., and Harrington, G. N. (2009). The impact of supplemental carbon sources on *Arabidopsis thaliana* growth, chlorophyll content and anthocyanin accumulation. *Plant Growth Regul.* 59, 255–271. doi: 10.1007/s10725-009-9412-x

Tamura, K., Peterson, D., Peterson, N., Stecher, G., Nei, M., and Kumar, S. (2011). MEGA5: molecular evolutionary genetics analysis using maximum likelihood, evolutionary distance, and maximum parsimony methods. *Mol. Biol. Evol.* 28, 2731–2739. doi: 10.1093/molbev/msr121

Tanaka, Y. (2006). Flower colour and cytochromes P450. *Phytochem. Rev.* 5, 283–291. doi: 10.1007/s11101-006-9003-7

Tanaka, Y., and Brugliera, F. (2013). Flower colour and cytochromes P450. *Philos. Trans. R. Soc Lond B. Biol. Sci.* 368, 20120432. doi: 10.1098/rstb.2012.0432

Tanaka, Y., Brugliera, F., Kalc, G., Senior, M., Dyson, B., Nakamura, N., et al. (2010). Flower color modification by engineering of the flavonoid biosynthetic pathway: practical perspectives. *Biosci. Biotechnol. Biochem.* 74, 1760–1769. doi: 10.1271/bbb.100358

Tanaka, Y., and Ohmiya, A. (2008). Seeing is believing: engineering anthocyanin and carotenoid biosynthetic pathways. *Curr. Opin. Biotechnol.* 19, 190–197. doi: 10.1016/j.copbio.2008.02.015

Tanaka, Y., Sasaki, N., and Ohmiya, A. (2008). Biosynthesis of plant pigments: anthocyanins, betalains and carotenoids. *Plant J.* 54, 733–749. doi: 10.1111/j.1365-313X.2008.03447.x

Teng, S., Keurentjes, J., Bentsink, L., Koornneef, M., and Smeekens, S. (2005). Sucrose-specific induction of anthocyanin biosynthesis in arabidopsis requires the MYB75/PAP1 gene. *Plant Physiol.* 139, 1840–1852. doi: 10.1104/pp.105.066688

Thill, J., Miosic, S., Gotame, T. P., Mikulic-Petkovsek, M., Gosch, C., Veberic, R., et al. (2013). Differential expression of flavonoid 3'-hydroxylase during fruit development establishes the different b-ring hydroxylation patterns of flavonoids in *Fragaria* × *ananassa* and *Fragaria vesca*. *Plant Physiol. Biochem.* 72, 72–78. doi: 10.1016/j.plaphy.2013.03.019

Wang, C., Ji, W., Liu, Y., Zhou, P., Meng, Y., Zhang, P., et al. (2021). The antagonistic MYB paralogs *RH1* and *RH2* govern anthocyanin leaf markings in *Medicago truncatula*. *New Phytol.* 229, 3330–3344. doi: 10.1111/nph.17097

Wang, L., Lu, W., Ran, L., Dou, L., Yao, S., Hu, J., et al. (2019a). R2R3-MYB transcription factor MYB6 promotes anthocyanin and proanthocyanidin biosynthesis but inhibits secondary cell wall formation in *Populus tomentosa*. *Plant J.* 99, 733–751. doi: 10.1111/tpj.14364

Wang, L., Tang, W., Hu, Y., Zhang, Y., Sun, J., Guo, X., et al. (2019b). A MYB/bHLH complex regulates tissue-specific anthocyanin biosynthesis in the inner pericarp of red-centered kiwifruit *Actinidia chinensis* cv. hongyang. *Plant J.* 99, 359–378. doi: 10.1111/tpj.14330

Wang, Z., Ye, S., Li, J., Zheng, B., Bao, M., and Ning, G. (2011). Fusion primer and nested integrated PCR (*FPNI-PCR*): a new high-efficiency strategy for rapid chromosome walking or flanking sequence cloning. *BMC Biotechnol.* 11, 109–120. doi: 10.1186/1472-6750-11-109

Xiang, L. L., Liu, X. F., Li, X., Yin, X. R., Grierson, D., Li, F., et al. (2015). A novel *bHLH* transcription factor involved in regulating anthocyanin biosynthesis in *Chrysanthemums* (*Chrysanthemum morifolium* ramat.). *PloS One* 10, e0143892. doi: 10.1371/journal.pone.0143892

Xu, W., Dubos, C., and Lepiniec, L. (2015). Transcriptional control of flavonoid biosynthesis by MYB-bHLH-WDR complexes. *Trends Plant Sci.* 20, 176–185. doi: 10.1016/j.tplants.2014.12.001

Yanhui, C., Xiaoyuan, Y., Kun, H., Meihua, L., Jigang, L., Zhaofeng, G., et al. (2006). The MYB transcription factor superfamily of *Arabidopsis*: expression analysis and phylogenetic comparison with the rice MYB family. *Plant Mol. Biol.* 60, 107–124. doi: 10.1007/s11103-005-2910-y

Yan, H., Pei, X., Zhang, H., Li, X., Zhang, X., Zhao, M., et al. (2021). MYB-mediated regulation of anthocyanin biosynthesis. *Int. J. Mol. Sci.* 22, 3103. doi: 10.3390/ijms22063103

Yuan, Y., Ma, X., Tang, D., and Shi, Y. (2014). Comparison of anthocyanin components, expression of anthocyanin biosynthetic structural genes, and *TfF3'H1* sequences between *Tulipa fosteriana* 'Albert heijn' and its reddish sport. *Sci. Hortic.* 175, 16–26. doi: 10.1016/j.scienta.2014.05.032

Zhang, C., Wang, W., Wang, Y., Gao, S., Du, D., Fu, J., et al. (2014). Anthocyanin biosynthesis and accumulation in developing flowers of tree peony (*Paeonia suffruticosa*) 'Luoyang hong'. *Postharvest Biol. Technol.* 97, 11–22. doi: 10.1016/j.postharvbio.2014.05.019

Zhang, B., Xu, X., Huang, R., Yang, S., Li, M., and Guo, Y. (2021). CRISPR/Cas9-mediated targeted mutation reveals a role for *AN4* rather than *DPL* in regulating venation formation in the corolla tube of *Petunia hybrida*. *Hortic. Res.* 8, 116. doi: 10.1038/s41438-021-00555-6

Zhou, H., Lin-Wang, K., Wang, F., Espley, R. V., Ren, F., Zhao, J., et al. (2019). Activator-type R2R3-MYB genes induce a repressor-type R2R3-MYB gene to balance anthocyanin and proanthocyanidin accumulation. *New Phytol.* 221, 1919–1934. doi: 10.1111/nph.15486

frontiers | Frontiers in Plant Science

TYPE Original Research
PUBLISHED 20 October 2022
DOI 10.3389/fpls.2022.1004732

OPEN ACCESS

EDITED BY
Daqiu Zhao,
Yangzhou University, China

REVIEWED BY
Michael Tellier,
University of Oxford, United Kingdom
Sharmistha M,
Indian Institute of Technology Gandhinagar, India
Corentin Claeys Bouuaert,
Université catholique de Louvain, Belgium

*CORRESPONDENCE
Mingbing Zhou
zhoumingbing@zafu.edu.cn

SPECIALTY SECTION
This article was submitted to Plant Breeding, a section of the journal Frontiers in Plant Science

RECEIVED 27 July 2022
ACCEPTED 07 October 2022
PUBLISHED 20 October 2022

CITATION
Zhou X, Xie J, Xu C, Cao X, Zou L-H and Zhou M (2022) Artificial optimization of bamboo *Ppmar2* transposase and host factors effects on *Ppmar2* transposition in yeast. *Front. Plant Sci.* 13:1004732. doi: 10.3389/fpls.2022.1004732

Artificial optimization of bamboo *Ppmar2* transposase and host factors effects on *Ppmar2* transposition in yeast

Xiaohong Zhou, Jiamin Xie, Chao Xu, Xiuling Cao, Long-Hai Zou and Mingbing Zhou*

State Key Laboratory of Subtropical Silviculture, Institute of Bamboo Research, Zhejiang A&F University, Hangzhou, China

Mariner-like elements (*MLEs*) are promising tools for gene cloning, gene expression, and gene tagging. We have characterized two *MLE* transposons from moso bamboo, *Ppmar1* and *Ppmar2*. *Ppmar2*, is smaller in size and has higher natural activities, thus making it a more potential genomic tool compared to *Ppmar1*. Using a two-component system consisting of a transposase expression cassette and a non-autonomous transposon cotransformed in yeast, we investigated the transposition activity of *Ppmar2* and created hyperactive transposases. Five out of 19 amino acid mutations in *Ppmar2* outperformed the wild-type in terms of catalytic activities, especially with the S347R mutant having 6.7-fold higher transposition activity. Moreover, 36 yeast mutants with single-gene deletion were chosen to screen the effects of the host factors on *Ppmar2NA* transposition. Compared to the control strain (*his3Δ*), the mobility of *Ppmar2* was greatly increased in 9 mutants and dramatically decreased in 7 mutants. The transposition ability in the *efm1Δ* mutant was 15-fold higher than in the control, while it was lowered to 1/66 in the *rtt10Δ* mutant. Transcriptomic analysis exhibited that *EFM1* defection led to the significantly impaired *DDR2*, *HSP70* expression and dramatically boosted *JEN1* expression, whereas *RTT10* defection resulted in significantly suppressed expression of *UTP20*, *RPA190* and *RRP5*. Protein methylation, chromatin and RNA transcription may affect the *Ppmar2NA* transposition efficiency in yeast. Overall, the findings provided evidence for transposition regulation and offered an alternative genomic tool for moso bamboo and other plants.

KEYWORDS

***mariner-like element (MLE)*, artificial optimization, transposase, host factor, bamboo, yeast**

Introduction

Transposons are found in a wide variety of species and migrate across the genome. There are two types of transposons: DNA transposons and RNA transposons. *Mariner-like elements* (*MLEs*) belong to the DNA transposon family. *Mariner* transposon was first characterized in the *Drosophila mauritania* mutant with white eyes, and later homologous elements were discovered in abundance in plant and animal genomes (Hartl et al., 1997). *MLEs* are typically comprised of an Open Reading Frame (ORF) that encodes the transposase (Tpase), which locates between two paired Terminal Inverted Repeats (TIRs) and Target Site Duplications (TSDs) (Plasterk et al., 1999). Transposase has three well-defined domains. The N-terminal domain contains helix-turn-helix (HTH) motifs that recognize and bind the TIRs. The C-terminus contains a catalytic domain with a DDE/D triad (Yuan and Wessler, 2011). The two aspartic acid residues (D) and a glutamic acid (E) or another aspartic acid (D) are commonly located 34 or 39 amino acids apart in animal and plant transposases (DD34E/D, DD39D, respectively) (Hartl et al., 1997; Feschotte and Wessler, 2002). The Linker region, harboring a conserved WVPHEL motif, connects the HTH motif and catalytic domain (Liu and Chalmers, 2014).

The conservation of the transposase sequence has a significant impact on transposition efficiency. The three most well-studied *MLE*s to date are *Sleeping Beauty* (*SB*) from fish (Ivics et al., 1997), *Mos1* from *Drosophila mauritiana* (Bryan et al., 1990), as well as *Himar1* from *Haematobia irritans* (Robertson and Lampe, 1995). In *SB*, a single amino acid mutation yielded around 2-3-fold transposition efficiency, and 9 amino acid mutations (K14R, K33A, R115H, RKEN214-217DAVQ, M243H, T314N) by DNA shuffling resulted in a hyperactive mutant SB100X with a 100-fold increase in transposition activity (Mátés et al., 2009). Germon et al. (2009) used systematic single amino acid substitutions to create two hyperactive *Mos1* mutants (FETY and FET) that were 60- and 800-fold more active than the wild-type *Mos1* version. The Linker region is also important for transposition efficiency. Almost all single mutations of the WVPHEL motif in *Himar1* and *Hsmar1* transposase led to highly active transposase variants, but which easily produce non-productive DNA double-strand breaks that can induce DNA damage and mutations (Butler et al., 2006; Lampe, 2010; Liu and Chalmers, 2014).

Besides the sequences of transposases, DNA methylation, chromatin status, over-production inhibition (OPI) and host proteins may influence the transposition frequency. It was shown that the methylated *SB* was at least 100-fold more active than the unmethylated version. CpG methylation of the *SB* region and heterochromatin formation facilitated the transposition reaction (Yusa et al., 2004). The MLE transposase activity was also inhibited by OPI (Lohe and Hartl, 1996). Overproduction of wild-type transposase enhanced the attachment of the transposase dimer and competition for free transposon ends, ultimately lowering the transposase activity. OPI started to occur when the number of transposase dimers was superior to the number of available TIRs (Claeys et al., 2013). High Mobility Group B1 (HMGB1) was a host-encoded cofactor of *SB* transposition and was involved in the formation of transposase-transposon complexes. Transposition of *SB* was severely suppressed in the HMGB1-deficient mouse cells (Zayed et al., 2003). In yeast (*Saccharomyces cerevisiae*), more than 200 host factors have been found to be associated with *Ty1* and *Ty3* retrotransposon (Irwin et al., 2005; Curcio et al., 2015). These factors were hypothesized of being involved in chromatin and transcript elongation, translation and cytoplasmic RNA processing, vesicular trafficking, nuclear transport, and DNA maintenance.

Two full-length *MLEs* named *Ppmar1* and *Ppmar2* were previously identified from the genome of moso bamboo (*Phyllostachys edulis*) (Zhou et al., 2015). *Ppmar1* and *Ppmar2* were shown to be transposable in *Arabidopsis thaliana* and yeast (Zhou et al., 2016; Zhou et al., 2017; Ramakrishnan et al., 2019a; Ramakrishnan et al., 2019b). Site-directed mutation boosted the activity of the *Ppmar1* mutant (*S171A*) by more than 10-fold (Zhou et al., 2017). *Ppmar2* is smaller in size (Zhou et al., 2016) and has a higher natural activity (Zhou et al., 2017), thus making it a more potential genomic tool compared to *Ppmar1*. Moso bamboo has a very lengthy vegetative growth cycle (~60 years), and hence rarely reproduces sexually, but reproduces *via* rhizomes during the vegetative period (Janzen, 1976; Watanabe et al., 1982). Breeding of moso bamboo *via* hybridization is extremely difficult due to its occasional sexual reproduction. So, a bamboo mutant library *via* an efficient transformation system will be a preference for future breeding. Currently, the most used genomic tools are T-DNA insertion and gene targeting (e.g., CRISPR/Cas). Insertional mutagenesis based on active transposons may be a promising tool to manipulate the genome of moso bamboo.

In the present study, we focused on the *Ppmar2* transposon to develop hyperactive *Ppmar2* mutants by rational mutagenesis. The host factors in yeast which regulated *Ppmar2* transposition were also screened. The hyperactive *Ppmar2* transposon system reported in this study with its outstanding features including its compact size and non-linked insertion sites could provide an alternative genomic tool for moso bamboo and other plants.

Methods

Construction of the *Ppmar2* transposition system in yeast

The *Ppmar2* transposition system was constructed using the transposon donor vector, pWL89A, and the transposase

expression vector, pAG415gal-ccdB, as described by Ramakrishnan et al. (2019a; 2019b). *Ppmar2* non-autonomous transposon (*Ppmar2NA*) was cloned by amplifying its 5' and 3' TIRs as well as the adjacent sequence, followed by an overlap PCR. *Ppmar2NA* was inserted into the *Xho I* site at the 5' untranslated region (UTR) of the *Ade2* gene in the vector pWL89A possessing two selectable markers, *Ura3* and *Ade2*. The transposon donor vector was named pWL89A-Ppmar2NA. The *Ppmar2* transposase sequences were amplified by adding *Not I* and *EcoR V* sites at both ends to fit the pAG415gal-ccdB vector. Both restriction enzymes cut the pAG415gal-ccdB vector. The transposase fragment and the backbone of pAG415gal-ccdB were then ligated by T4 DNA ligase to obtain the recombined vectors pAG415gal-transposase with *Leu2* selectable marker. The transposase was promoted to be expressed under the *gal* promoter.

Yeast transposition assay

The two prepared plasmids (pWL89a-Ppmar2NA and pAG415gal-transposase) were co-transformed into *S. cerevisiae* strain DG2523. Transformed yeast strains were grown on medium lacking Leucine and uracil (SD-his-ura) but with 2% galactose at 30°C in the dark for 3 days, followed by the suspension of single colonies in 150 μl water and plating onto medium lacking adenine, Leucine, and uracil (SD-ade-his-ura) with 2% galactose as the carbon sources. The plates were incubated at 30°C in the dark for about 3 days to allow the growth of ADE2 revertant colonies.

Transposition footprints analysis

The fragments covered *Ppmar2NA* excision spots on pWL89a were amplified using primers of yeast T-5 (5'-CAC CCC AGG CTT TAC ACT TTA TG-3') and T-3 (5'-GTT GCT TAT TTG TTT GGC AGG AG-3'). PCR products were cloned into the pUC18-T vector for sequencing.

Insertion sites and insertion bias analysis

Genomic DNA was extracted from the single ADE2 revertant colonies and then was sheared into 500-bp fragments using Covaris E220 ultrasonicator (Covaris, UK). The libraries were normalized, pooled, and sequenced *via* Illumina high-throughput sequencing platform NovaSeq 6000 (2×250 bp paired-end run). Low-quality sequences were filtered by Sickle (v1.33) with Q30 and 125bp minimal length (Joshi and Fass, 2011). Filtered reads were aligned to the *Ppmar2NA* sequence through the local blast. Subsequently, the reads containing the *Ppmar2NA* sequence and adjacent sequence were aligned to the *S. cerevisiae* reference genome (https://yeastgenome.org/) to identify the insertion sites. The 20bp upstream and downstream of the insertion sites were aligned to verify the nucleotide distribution characteristics of the *Ppmar2NA* insertion sites.

Site-directed mutagenesis of *Ppmar2* transposase

To identify *Ppmar2* non-conserved transposase sites, we downloaded 22 *MLE* transposase sequences from GenBank and aligned them with the *Ppmar2* transposase using MEGA11.0.10 (Tamura et al., 2021). Mutagenesis was performed with the QuikChange Lightning Site-Directed Mutagenesis Kit using the primers listed in Supplementary Table S1. The selected sites of the *Ppmar2* transposase were mutated into corresponding amino acids (Supplementary Table S2). The mutated *Ppmar2* transposases then replaced the template on pAG415gal-transposase to examine the transposition activities. All plasmids were sequenced to confirm the presence of the targeted mutation. Homologous hyperactive mutation sites in the *Mos1* and *Himar1* transposase were mutated into the corresponding amino acid in the *Ppmar2* transposase.

Transposition frequency of *Ppmar2* mutants

The transposition frequencies of *Ppmar2* mutants were evaluated by ADE2 revertant frequencies. Each galactose-induced colony was suspended in 50 μl of water and plated on media without adenine. The cell suspension was equally diluted to 1×10^{-5} volume and was plated on SD media lacking adenine, Leucine and uracil (SD-ade-his-ura) to obtain the total number of galactose-induced colonies. The assay of each mutant was performed with six biological replicates.

Transposition frequency analysis of *Ppmar2* in yeast mutants

To examine the host factors' effects on *Ppmar2* transposition in yeast, 36 mutants with single-gene deletions were selected (Table S3) which were kindly provided by Charles Boone (Toronto University, Toronto, in Canada), and *His3Δ* was used as the control strain. These genes are involved in methylation, DNA replication, transcription, translation, as well as the regulation of retrotransposon (*Ty1* and *Ty3*) (Irwin et al., 2005; Curcio et al., 2015).

Gene expression *via* RNA-seq

The *efm1Δ*, *rtt10Δ* mutants and the wild type yeast *His3Δ* were cotransformed with pWL89a-Ppmar2NA and pAG415gal-transposase plasmids with three colonies for each genotype. The mRNA of the single ADE2 revertant colonies was extracted, when strains grew in YPD liquid medium with the OD600 of 0.5, and was synthesized into cDNA strands with dNTPs and DNA polymerase I. The final cDNA library was obtained through the AMPure XP system and was sequenced on an Illumina Hiseq 2000 platform (Tianjin Nuohe Zhiyuan Bioinformatics Co., Ltd.) to generate 125 bp/150 bp paired-end reads. The adapter, ploy-N and low-quality reads from raw data were removed using Illumina PIPELINE software. Index of the yeast genome has been built using STAR (v2.5.1b) and paired-end clean reads were aligned to the yeast reference genome (https://yeastgenome.org/) with TopHat v2.0.12. The reads mapped to each gene were counted by HTSeq v0.6.0 and were normalized to fragments per kilobase of exon per million fragments mapped (FPKM) (Trapnell et al., 2010). The method of Benjamini and Hochberg was used to adjust the *P*-value to control the error detection rate (Haynes, 2013). In this experiment, the correction of $p < 0.05$, with | log2foldchange | > 1 was used for screening differentially expressed genes (DEGs).

Quantitative real-time PCR analysis

Eight DEGs were selected for qRT-PCR analysis. One μg total RNA of each sample was reverse-transcribed using PrimeScript™ RT reagent Kit with gDNA Eraser. The qRT-PCR was performed using the SYBR® Premix Ex Taq™ II (Tli RNaseH Plus) on the iQ™5 Multi-channel Real-time PCR Detection System (Bio-Rad). The relative abundance of each gene expression was calculated from the 2-ΔΔCt values between the target gene and *ALG9 (Protein amino acid glycosylase 9)* (Teste et al., 2009). The results were analyzed by Bio-Rad CFX Manager 3.1 software. Each reaction was performed at least three times.

Results

Verification of the *Ppmar2* transposition potential in yeast

To determine whether *Ppmar2* can transpose in the yeast genome, we performed transposition assays in yeast utilizing the methods described previously (Ramakrishnan et al., 2019a; Ramakrishnan et al., 2019b). The assays used two constructs, one transposase expression vector and one transposon donor vector. In the transposase expression plasmid, the *Ppmar2* transposase coding sequence was fused to the inducible *GAL1* promoter, and *Leu2* served as the selectable marker. In the transposon donor plasmid, the non-autonomous *Ppmar2NA* element was inserted in the 5'UTR of the *ADE2* reporter gene, and *Ura3* served as the selectable marker. Transformants containing both plasmids were selected on a medium with 2% galactose but lacking Leucine and uracil. Colonies of the double transformants were picked and regrown on agar plates without adenine for the selection of *ADE2* revertants, which represented the excision of the *Ppmar2NA*. Notably, *ADE2* revertant colonies were obtained in the presence of the *Ppmar2* transposase, but none when the control plasmid, pAG415-ccdB, was used.

Plasmid DNA was prepared from the independent *ADE2* revertants, and the excision products of *Ppmar2NA* in the *ADE2* 5'UTR region were PCR amplified using primers of yeast T-5 and T-3. Sequencing results revealed diverse footprints of excision were generated by *Ppmar2NA* in the donor plasmid. Between two *Ppmar2NA* TIRs, one to four bases were retained (Figure 1).

Reinsertion preferences of the excised *Ppmar2NA*

To follow the fate of the excised *Ppmar2NA* and localize the reinsertion sites in the yeast genome, genomic DNA was extracted from the independent *ADE2* revertants, and sequenced (with 30 times coverage). Following alignment, we identified 7 genetic integration events on 6 yeast chromosomes. All insertions occurred within ~500 bp of the coding regions, with one insertion occurring within the gene (Table 1). As expected, *Ppmar2NA* in all detected events was inserted into a TA dinucleotide where the AT content of 50 bp sequences nearby the insertion sites was more than 60% (Figure 2). To further validate the *Ppmar2NA* insertion bias, we analysed the 20 bp sequences flanking the TA on both sides. Alignment of the 7 integration sites revealed that the excised *Ppmar2NA* was preferentially inserted into AT-rich regions (Figure 2 and Table 1).

Targeted mutagenesis of the *Ppmar2* transposase to enhance *Ppmar2NA* transposition in yeast

To improve the transposition activity of *Ppmar2*, the transposase was modified following the strategy as described (Zhou et al., 2017). We selected 22 *MLE* transposase sequences from animals and plants, including *Mos1* from *D. mauritiana* (Bryan et al., 1990), *Himar1* from *H. irritans* (Robertson and Lampe, 1995), *Ppmar1* from Moso bamboo, and three *MLE*

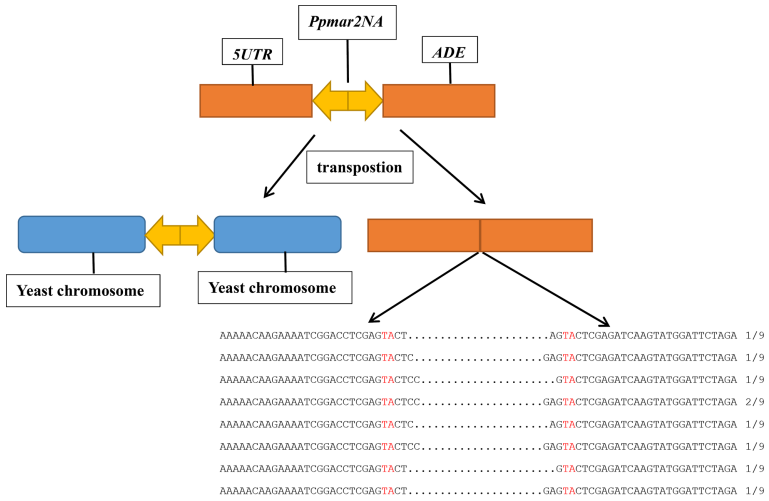

FIGURE 1
Sequence alignment of *Ppmar2NA* at excision spots on pWL89a. Sequences of *Ppmar2NA* at excision spots were amplified using primers yeast T-5 and T-3. The TA-target sites of TSDs are marked in red, and the interval between the red TA represents the footprints after cleavages.

transposases from rice (Yang et al., 2006; Yang et al., 2009) (Figure 3). Other sequences were filtered in the NCBI database by blast using the *Ppmar2* transposase sequence as a query, which showed high homology with the *Ppmar2* transposase. We examined amino acid residues that were partially conserved in *MLEs* but not in the *Ppmar2* transposase after alignment. Thirteen such sites scattered across the three conserved domains of the *Ppmar1* transposase (the DNA binding domain, the Linker domain, and the catalytic domain) were identified (Figure 3). Moreover, we selected six homology sites in the *Ppmar2* transposase that corresponded to the hyperactive mutation sites in the *Mos1* and *Himar1* transposase (D129A, D129R, G132A, A168R, L174K and K289A) (Figure 3) (Butler et al., 2006; Germon et al., 2009). The 18 candidate sites, including four in the HTH binding domain, three in the Linker region, and eleven in the catalytic domain, were systematically modified one by one, and the transposase variants were evaluated in the yeast excision assay (Table S2).

Among the 19 transposase mutations (two mutations at the 129th amino acid), 5 of them (L235F, K243R, S347R, S292I, and L174K) dramatically enhanced the *Ppmar2* excision activity by more than 2-fold (Figure 4). Four amino acid substitutions, including L266P, L309P, D333P, and A168R, suppressed the transposition. The remaining 10 amino acid substitutions had no significant effects (Figure 4). The S347R mutant exhibited the highest transposition activity, which was 6.7-fold that of the wild type (Figure 4).

Host factors' effects on *Ppmar2* transposition in yeast

To investigate the effects of host factors on transposition efficiency, 36 yeast mutants with single-gene deletions were screened (Table S2). Of the 36 genes, 8 genes were involved in methylation, 7 genes in DNA replication, transcription, and translation, and 21 genes were host factors of retrotransposons

TABLE 1 Details of *Ppmar2NA* reinsertion sites.

No. of chromosome	Insert site	AT content of 50 bp sequences around the insertion sites	Distance from the nearest gene
I	138841	68%	495 bp upstream from *ERP2* gene
IV	26011	79%	33 bp downstream from *LRG1* gene
IV	524715	62%	20 bp upstream from *EHD3*
IX	33347	65%	380 bp downstream from *YIL165C* gene
X	585548	66%	110 bp upstream from *YJR085C* gene
XIII	302740	63%	254 bp upstream from *ERG5* gene
XVI	541299	61%	Coding region of *CHL1* gene

FIGURE 2
Reinsertion preference analysis of excised *Ppmar2NA*. The pictogram shows the relative nucleotide frequencies of the 7 detected insertion events in the yeast genome. On either side of the reinserted *Ppmar2NA* elements, 20 bases flank the conserved TA insertion spot. The nucleotide A is shown in green, C in red, G in blue, and T in yellow. The lightning symbol indicates the *Ppmar2NA* reinsertion site.

(*Ty1* and *Ty3*) (Irwin et al., 2005; Curcio et al., 2015). The 36 yeast mutants were double transformed with pWL89a-Ppmar2NA and pAG415gal-transposase. The positive colony assay in each yeast mutant revealed that the transposition frequency was significantly higher in 9 yeast mutants (*tmt1Δ*, *efm1Δ*, *efm5Δ*, *mgt1Δ*, *pdr3Δ*, *rtt102Δ*, *chd1Δ*, *exg2Δ*, and *cur1Δ*) than in the control strain (*His3Δ*), but significantly lower in 7 yeast mutants (*set2Δ*, *rtt106Δ*, *rtt10Δ*, *mlh2Δ*, *vac7Δ*, *mrpl10Δ*, and *itr2Δ*), with no obvious differences in the other 20 yeast mutants (Figure 5). *Ppmar2NA* showed the most active transposition in the *efm1Δ* mutant, which was 15-fold higher than in *His3Δ*. *Ppmar2NA* had the lowest transposition frequency in the *rtt10Δ* mutant, which was only 1/66 that in the *His3Δ* strain.

DEGs in the mutants with dramatically distinct transposition ability *Ppmar2NA*

To explore the host factors' effects and investigate the DEGs involved in the transposition regulation, we performed the transcriptome analyses for the strains with distinct

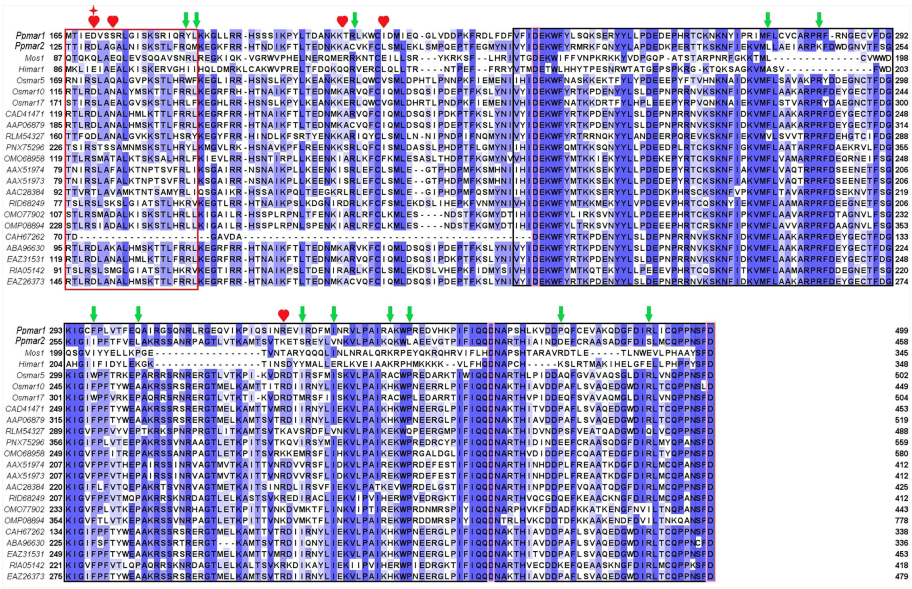

FIGURE 3
Homology alignment of 22 *MLE* transposases. The red box is the HTH domain, the black box is the DDD domain, and the Linker area is in the middle. Three aspartic acid residues (D) in the DDD domain were highlighted with pink boxes. *Mos1* from *D. mauritiana* (Bryan et al., 1990), *Himar1* from *H. irritans* (Robertson and Lampe, 1995), *Ppmar1* from moso bamboo and three *MLE* transposases (*Osmar5, Osmar10, Osmar17*) from rice (Yang et al., 2009). Other entries are named according to the first letter of the genus name and the species name, followed by the GenBank accession number. The 12 non-conserved sites (marked by green arrows) of the *Ppmar2* transposase were mutated into corresponding conserved amino acids. The 6 homologous hyperactive mutation sites in the *Mos1* and *Himar1* transposase were mutated into the corresponding amino acid in the *Ppmar2* transposase (marked by a red heart shape). The amino acid at the 129th position was mutated into two different amino acids (marked by a red star).

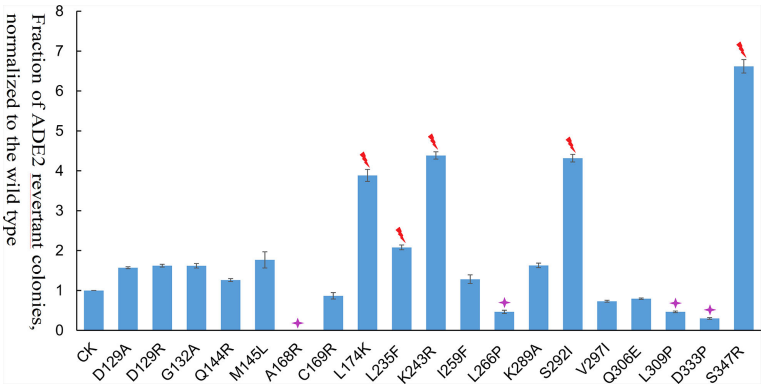

FIGURE 4
Transposition frequencies catalyzed by *Ppmar2* transposase mutants (CK is the wild type *Ppmar2* transposase). The mean excision frequency of the 19 *Ppmar2* mutants was normalized by that of the wild type. Y-axis represents the fraction of ADE2 revertant colonies, normalized to the wild type. Each excision assay was conducted with six biological replicates. The transposase mutations were marked by red heart shapes which dramatically enhanced *Ppmar2* transposase catalytic activity by more than 2-fold. The transposase mutations were marked by pink star shapes which dramatically reduced *Ppmar2* transposase catalytic activity to less than 1/2-fold.

transposition competence *Ppmar2NA* (*efm1Δ* vs. *His3Δ* and *rtt10Δ* vs. *His3Δ*). Sixty-seven DEGs were validated with a *P*-value lower than 0.0001 (Figure 6) and enriched *via* GO and KEGG. These DEGs were related to ribosome biogenesis, RNA modification and DNA modifications which might be involved in the regulation the *Ppmar2* transposition (Figures 1S, 2S). In the mutant *efm1Δ* with highly active *Ppmar2NA*, three genes linked with DNA repair and RNA transcription (*DNA Damage Responsive 2* (*DDR2*), *Heat Shock Protein 70* (*HSP70*) and *Monocarboxylate/proton symporter of the plasma membrane* (*JEN1*)), might be likely related to regulation of the *Ppmar2NA* transposition. *DDR2* and *HSP70* were highly expressed in the *efm1Δ* strain, while the expression of *JEN1* was repressed. In the *rtt10Δ* null mutant, three genes (*U3 snoRNA-associated protein 20* (*UTP20*), *DNA-directed RNA polymerase I subunit* (*RPA190*), *U3 small nucleolar RNA-associated protein* (*RRP5*)), involved in ribosome assembly and RNA polymerase synthesis, were markedly downregulated.

qRT-PCR was performed to validate the RNA-seq data by checking the expression levels of *Elongation Factor Methyltransferase (EFM1)*, Regulator of Ty1 Transposition (*RTT10*), *DDR2, HSP70, JEN1, UTP20, RPA190* and *RRP5*. No expression of *EFM1* was detected in *efm1Δ*, and a low-level expression of *RTT10* in *rtt10Δ*, as predicted. The other gene expression patterns displayed *via* qRT-PCR were completely consistent with the RNA-seq data-derived gene expression pattern (Supplementary Figure 3).

Discussion

Yeast has been widely used as a heterologous host to evaluate the transposition activity of plant DNA transposons, such as *Osmar5* and *Stowaways MITE* in rice (Yang et al., 2006; Yang et al., 2009), and *Ac/Ds* in maize (Lazarow et al., 2012). We have identified two *MLE* transposons in moso bamboo, *Ppmar1* and

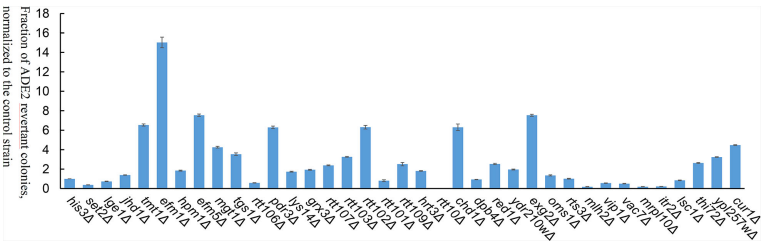

FIGURE 5
Transposition efficiency of *Ppmar2NA* in 36 yeast single-gene mutants. The mean excision frequency of *Ppmar2NA* in the 36 yeast mutants was normalized to that of the control strain (*His3Δ*). Y-axis represents the fraction of ADE2 revertant colonies, normalized to the control strain. Each excision assay was conducted with six biological replicates.

10.3389/fpls.2022.1004732

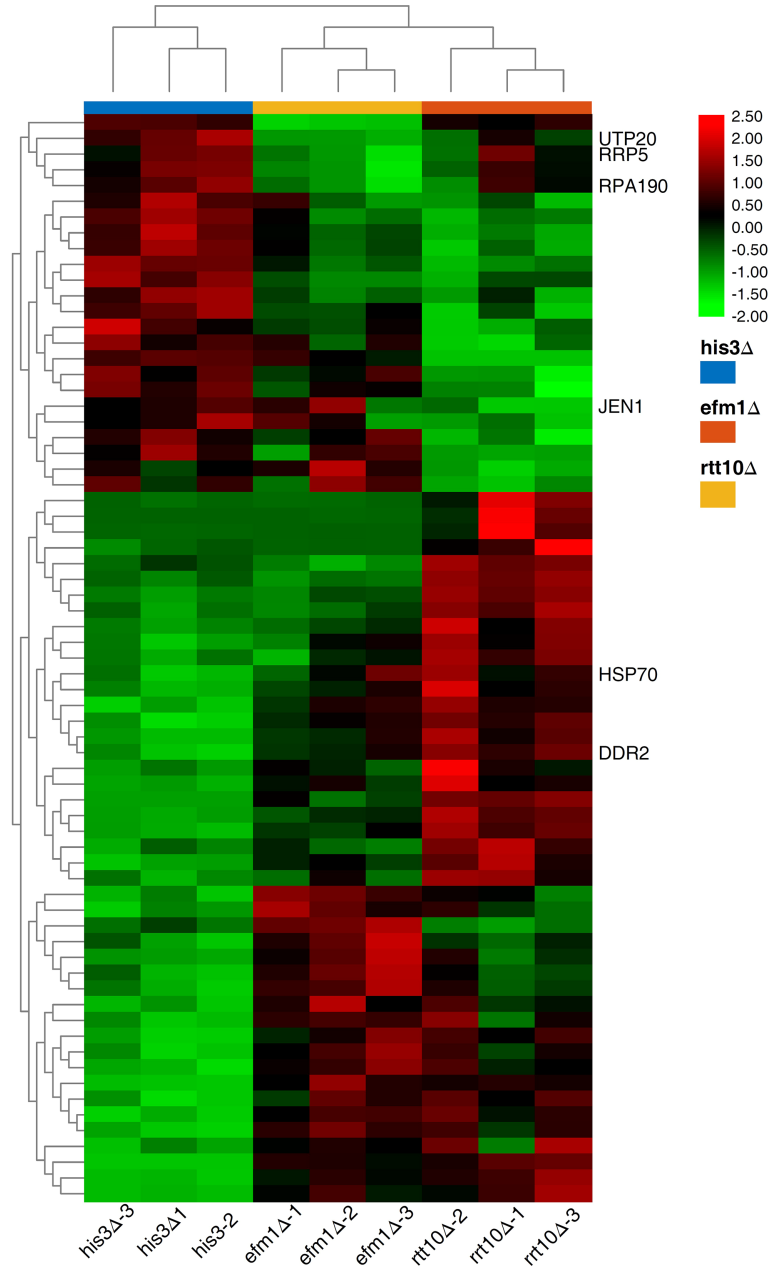

FIGURE 6
Heat map of DEGs expression in *HisΔ3, efm1Δ, rtt10Δ* strains. The expression patterns of *DDR2, HSP70, JEN1, UTP20, RPA190* and *RRP5* genes were marked. The color scale indicates the relative expression level.

Ppmar2, which both could jump in *Arabidopsis thaliana* and yeast genome (Zhou et al., 2016; Zhou et al., 2017; Ramakrishnan et al., 2019a; Ramakrishnan et al., 2019b). *Ppmar2* has a relatively smaller size and naturally higher activity than *Ppmar1*, thus making it a more potential genomic tool. To improve the transposition efficiency and develop an alternative gene-tagging tool, we create a hyperactive *Ppmar2 via* mutagenesis and screen the host factors influencing transposition of *Ppmar2* in yeast.

Ppmar2NA's transposition footprints and insertion preferences resembled the other *MLEs*

Using a two-component system consisting of a transposase expression cassette and a non-autonomous transposon cotransformed in yeast, we examined the transposition activity of *Ppmar2NA*. The footprints of *Ppmar2NA* after excision

revealed that *Ppmar2NA* was preferentially cut between the two TIRs, leaving 1-4 staggered nucleotides (Figure 1). Similarly, the *Osmar5* transposase generated a staggered cut with one to four nucleotides at both ends of the transposon element (Yang et al., 2006), whereas the animal transposases *Mos1*, *Sleeping Beauty*, and *Frog Prince* were cleaved but left no more than three nucleotides (Luo et al., 1998; Dawson and Finnegan, 2003; Miskey et al., 2003). On the other hand, *Ppmar2NA* tended to insert into the TA-rich regions and generated AT TSDs (Figure 2). In short, as a member of the *MLEs* family transposons, *Ppmar2NA* shared a similar cleavage footprint and insertion preference.

Some amino acids in key sites are important for the catalytic activity of *Ppmar2* transposase

Eighteen non-conversed amino acids in *Ppmar2* transposase, including 4 in the HTH binding domain, 3 in the linker junction region, and 11 in the DDD catalytic domain, were selected for mutagenesis to improve the transposition activity (Figure 3). Another 6 homology sites in *Ppmar2* corresponding to hyperactive mutation sites in *Mos1* and *Himar1* were also chosen (D129A, D129R, G132A, A168R, L174K and K289A) (Butler et al., 2006; Germon et al., 2009). The catalytic activities in five of the six mutants were improved, which was consistent with the mutation effect in *Mos1* and *Himar1* except for A168R (Figure 4) (Butler et al., 2006; Germon et al., 2009). Strangely, the five hyperactive mutation sites are not conserved in the sequences of *Ppmar2* transposase (Figure 4).

The linker region connects the HTH motif and catalytic domain, which are not conserved as WVPHEL motif in *Ppmar2* transposase. Three mutations (A168R, C169R, and L174K) located in the Linker region of the *Ppmar2* transposase, which regulated the spatial structure of the transposase, exhibited divergent transposition actives (Butler et al., 2006; Liu and Chalmers, 2014). The catalytic activity of the C169R mutation did not change significantly, but the A168R mutant totally lost the catalytic activity. The L174K transposase mutant, on the other hand, showed considerably higher catalytic activity than the wild type (Figure 4). The catalytic domain featured by a conserved DDE/D motif played a vital role in transposition activity (Yang et al., 2006). It has been reported that substitution of the DDD to the DDE in the *Tc1* family abolished the transposase activity (Lohe et al., 1997). The transposition efficiency of *Ppmar2* transposase varied among the targeted mutation sites (L235F, K243R, I259F, L266P, K289A, S292I, V297I, Q306E, L309P, D333P, and S347R). The L235F, K243R, S347R and S292I mutation greatly boosted the transposition. Especially, the S347R mutation resulted in a 6.7-fold higher transposition frequency (Figure 4). The hyperactive *Ppmar2* system would be used in plant genomic engineering as an alternative transposon-based technique.

It should be noted that the high catalytic activity of transposase mutations may not directly lead to high-frequency transposition due to OPI. Construction of transposase mutations which are usually less sensitive to OPI, e.g. low TIR binding affinity, and low stability of the transposase dimers will contribute to the high transposition frequency (Liu and Chalmers, 2014; Tellier and Chalmers, 2020). In the following, mutations that change in *Ppmar2* transposition kinetics that shift the OPI equilibrium will be considered.

Host factors, including *EFM1* and *RTT10* genes, significantly affected the transposition frequency of *Ppmar2NA* in yeast

The yeast single-gene deletion mutant library was effectively used to investigate the impact of host factors on the activity of retrotransposons *Ty1* and *Ty3*. More than 200 host factors, including those involved in chromatin and transcript elongation, translation and cytoplasmic RNA processing, vesicular trafficking, nuclear transport, and DNA maintenance, regulated the transposon activity of yeast *Ty1* (Curcio et al., 2015) and *Ty3* (Irwin et al., 2005). The 36 related yeast mutants with single gene deletions were selected in this study. The transposition efficiencies of *Ppmar2NA* in 9 yeast mutants (*tmt1Δ, efm1Δ, efm5Δ, mgt1Δ, chd1Δ, pdr3Δ, cur1Δ, exg2Δ*, and *rtt102Δ*) were 2-fold more active than that in the control yeast. Notably, in the *efm1Δ* mutant, the transposition efficiency increased by 15-fold. Among the 9 genes, four are related to protein methylation, one to DNA methylation, one to chromatin organization, and the remaining 4 were host factors of retrotransposon. In another 5 yeast mutants (*set2Δ, rtt10Δ, mlh2Δ, mrpl10Δ*, and *itr2Δ*), the transposition efficiency of *Ppmar2NA* was at least 1/2 less active than in the control strain *His3Δ*, especially in *rtt10Δ* mutant, where the transposition efficiency decreased by more than 65-fold. One of the 5 genes was associated with histone methylation, whereas the other 4 genes were host factors of retrotransposon. These findings indicated that DNA transposon and RNA transposon may share common host factors (Irwin et al., 2005; Curcio et al., 2015).

In yeast, *Elongation Factor Methyltransferase (EFM1)*, which encoded lysine methyltransferase SET8, may characteristically methylate H4K20 (Zhang and Bruice, 2008) and function in

protein modification, chromosome-protein binding regulation, and gene transcription and translation. Studies have shown that *EFM1* methylates H4K20 into three proteins H4K20me1, H4K20me2 and H4K20me3 (Yang and Mizzen, 2009). H4K20me1 could further promote chromatin condensation with the help of Condensin II (Weirich et al., 2015). Also, H4K20me1 and H4K20me2 inhibited gene transcription and chromosomal shrinkage by binding to the Lethal (3) Malignant Brain Tumor-Like Protein 1 (L3MBTL1) (Li et al., 2007). H4K20me3 was generally regarded as a marker of transcriptional inhibition in heterochromatin (Schotta et al., 2004). H4K20 was not methylated when the *EFM1* gene was knocked out, which might be related to the high transposition frequency of the *Ppmar2* in the *efm1Δ* mutant yeast.

The DEGs identified with the comparison of *efm1Δ* and *His3Δ* revealed that the *efm1Δ* cell conditions were changed significantly. The *DDR2* gene encoded a stress protein involved in DNA repair (Kobayashi et al., 1996). The expression of this gene was dramatically elevated in the *efm1Δ* mutant, suggesting that it may efficiently repair the damaged DNA. The HSP70, which encoded heat shock factor (Abrams et al., 2014), was also obviously upregulated in the *efm1Δ* mutant. Jardim et al. (2015) found evidence that *mos1* may be co-activated with *HSP70* genes. *JEN1* mediated high-affinity uptake of carbon sources lactate, pyruvate, acetate, and micronutrient selenite, *JEN1* expression and localization are tightly regulated, with transcription repression, mRNA degradation, and protein endocytosis and degradation all occurring in the presence of glucose (Haurie et al., 2001).

The *RTT10* gene, which encoded a member of the WD40 protein family, was a retrotransposition-related gene. *Ty1* was more active in the *rtt10Δ* mutant than in the *His3Δ* strain, and the *RTT10* gene might prevent *Ty1* RNA from being reversely transcribed into cDNA (Scholes et al., 2001). Moreover, *RTT10* contributed to the synthesis of transcription factor *TFIID*, regulating the ribosome small subunit rRNA synthesis (Dragon et al., 2002). Three DEGs (*UTP20*, *RPA190* and *RRP5*) in the *rtt10Δ* mutant might be related to the lowered transposition activity. The UTP20 protein was a component of the small-subunit (SSU) processome, which modulated the 18S rRNA synthesis (Gallagher et al., 2004). The expression level of this gene in the *rtt10Δ* mutant was significantly lowered. RRP5 was another component of the SSU processome and 90S preribosome related to the synthesis of 18S and 5.8S rRNAs (Venema and Tollervey, 1996). The expression level was much lower in the *rtt10Δ* mutant than in *His3Δ*. *RPA190*, encoding RNA polymerase A (Mémet et al., 1988), was also downregulated in the *rtt10Δ* mutant. The discovery of host factors associated with *Ppmar2* mobility lays an important foundation for understanding the mechanism of *Ppmar2* transposition in the heterologous host.

In the present study, we created hyperactive *Ppmar2* transposons *via* site-direct mutagenesis and screened the heterologous host factors that influenced the transposition activity. *Ppmar2* was proved to efficient to able to excision and reinserted into the TA-rich region, which was the same as the other *MLEs* in plants. *EFM1* and *RTT10* related to protein methylation, chromatin and RNA transcription greatly impact the heterologous transposition efficiency of *Ppmar2* in yeast. The *Ppmar2* transposon system is a promising tool for insertion mutagenesis in moso bamboo and might be used as an alternative to the existing transposon tagging systems in the other plants.

Data availability statement

The datasets presented in this study can be found in online repositories. The names of the repository/repositories and accession number(s) can be found in the article/Supplementary Material.

Author contributions

MZ designed the experiments; XZ and JX performed the research; CX, XC and L-HZ participated in the research; MZ and XZ wrote the manuscript. All authors have read and approved the manuscript.

Funding

This work was funded by grants from the Zhejiang Provincial Natural Science Foundation of China (No. LZ19C160001 and LQ21C160003), the National Natural Science Foundation of China (No. 31870656, 31470615 and 32001326), the Talent Research Foundation of Zhejiang A&F University (No. 2019FR055) and Independent research project of state key laboratory of subtropical silviculture (ZY20200301).

Acknowledgments

We would like to extend our sincere gratitude and appreciation to all reviewers for their valuable comments.

Conflict of interest

The authors declare that the research was conducted in the absence of any commercial or financial relationships that could be construed as a potential conflict of interest.

Publisher's note

All claims expressed in this article are solely those of the authors and do not necessarily represent those of their affiliated

organizations, or those of the publisher, the editors and the reviewers. Any product that may be evaluated in this article, or claim that may be made by its manufacturer, is not guaranteed or endorsed by the publisher.

Supplementary material

The Supplementary Material for this article can be found online at: https://www.frontiersin.org/articles/10.3389/fpls.2022.1004732/full#supplementary-material

References

Abrams, J. L., Verghese, J., Gibney, P. A., and Morano, K. A. (2014). Hierarchical functional specificity of cytosolic heat shock protein 70 (Hsp70) nucleotide exchange factors in yeast. *J. Biol. Chem.* 289 (19), 13155–13167. doi: 10.1074/jbc.M113.530014

Bryan, G., Garza, D., and Hartl, D. (1990). Insertion and excision of the transposable element mariner in *Drosophila*. *Genetics* 125 (1), 103–114. doi: 10.1093/genetics/125.1.103

Butler, M. G., Chakraborty, S. A., and Lampe, D. J. (2006). The n-terminus of Himar1 mariner transposase mediates multiple activities during transposition. *Genetica* 127 (1-3), 351–366. doi: 10.1007/s10709-006-6250-x

Claeys, B., Lipkow, K., Andrews, S. S., Liu, D., and Chalmers, R. (2013). The autoregulation of a eukaryotic DNA transposon. *Elife* 2, e00668. doi: 10.7554/eLife.00668

Curcio, M. J., Lutz, S., and Lesage, P. (2015). The Ty1 LTR-retrotransposon of budding yeast, *Saccharomyces cerevisiae*. *Microbiol. Spectr.* 3 (2), MDNA3–0053-2014. doi: 10.1128/microbiolspec.MDNA3-0053-2014

Dawson, A., and Finnegan, D. J. (2003). Excision of the *Drosophila* mariner transposon Mos1: Comparison with bacterial transposition and V(D)J recombination. *Mol. Cell* 11 (1), 225–235. doi: 10.1016/S1097-2765(02)00798-0

Dragon, F., Gallagher, J., Compagnone-Post, P. A., Mitchell, B. M., Porwancher, K. A., Wehner, K. A., et al. (2002). A large nucleolar U3 ribonucleoprotein required for 18S ribosomal RNA biogenesis. *Nature* 417 (6892), 967–970. doi: 10.1038/nature00769

Feschotte, C., and Wessler, S. R. (2002). *Mariner*-like transposases are widespread and diverse in flowering plants. *Proc. Natl. Acad. Sci. U.S.A.* 99 (1), 280–285. doi: 10.1073/pnas.022626699

Gallagher, J. E., Dunbar, D. A., Granneman, S., Mitchell, B. M., Osheim, Y., Beyer, A. L., et al. (2004). RNA Polymerase I transcription and pre-rRNA processing are linked by specific SSU processome components. *Genes Dev.* 18 (20), 2506–2517. doi: 10.1101/gad.1226604

Germon, S., Bouchet, N., Casteret, S., Carpentier, G., Adet, J., Bigot, Y., et al. (2009). *Mariner Mos1* transposase optimization by rational mutagenesis. *Genetica* 137 (3), 265–276. doi: 10.1007/s10709-009-9375-x

Hartl, D., Lohe, L., and Lozovskaya, E. R. (1997). Modern thoughts of an ancyent *marinere*: Function, evolution, regulation. *Annu. Rev. Genet.* 31: 337–358. doi: 10.1146/annurev.genet.31.1.337

Haurie, V., Perrot, M., Mini, T., Jeno, P., Sagliocco, F., and Boucherie, H. (2001). The transcriptional activator Cat8p provides a major contribution to the reprogramming of carbon metabolism during the diauxic shift in *Saccharomyces cerevisiae*. *J. Biol. Chem.* 276 (1), 76–85. doi: 10.1074/jbc.M008752200

Haynes, W. (2013). "Benjamini–hochberg method," in *Encyclopedia of systems biology*. Eds. W. Dubitzky, O. Wolkenhauer, K.-H. Cho and H. Yokota (New York, NY: Springer New York), 78–78.

Irwin, B., Aye, M., Baldi, P., Beliakova-Bethell, N., Cheng, H., Dou, Y., et al. (2005). Retroviruses and yeast retrotransposons use overlapping sets of host genes. *Genome Res.* 15 (5), 641–654. doi: 10.1101/gr.3739005

Ivics, Z., Hackett, P. B., Plasterk, R. H., and Izsvák, Z. (1997). Molecular reconstruction of *Sleeping beauty*, a *Tc1*-like transposon from fish, and its transposition in human cells. *Cell* 91 (4), 501–510. doi: 10.1016/S0092-8674(00)80436-5

Janzen, D. H. (1976). Why bamboos wait so long to flower. *Annu. Rev. Ecol. syst.* 7 (1), 347–391. doi: 10.1146/annurev.es.07.110176.002023

Jardim, S. S., Schuch, A. P., Pereira, C. M., and Loreto, E. L. (2015). Effects of heat and UV radiation on the mobilization of transposon *mariner-Mos1*. *Cell Stress Chaperones* 20 (5), 843–851. doi: 10.1007/s12192-015-0611-2

Joshi, N., and Fass, J. (2011). *"Sickle: A sliding-window, adaptive, quality-based trimming tool for FastQ files (Version 1.33)[Software]"*. Available at:https://github.com/najoshi/sickle.

Kobayashi, N., Mcclanahan, T. K., Simon, J. R., Treger, J. M., and Mcentee, K. (1996). Structure and functional analysis of the multistress response gene *DDR2* from *Saccharomyces cerevisiae*. *Biochem. Biophys. Res. Commun.* 229 (2), 540–547. doi: 10.1006/bbrc.1996.1840

Lampe, D. J. (2010). Bacterial genetic methods to explore the biology of *mariner* transposons. *Genetica* 138 (5), 499–508. doi: 10.1007/s10709-009-9401-z

Lazarow, K., Du, M. L., Weimer, R., and Kunze, R. (2012). A hyperactive transposase of the maize transposable element *activator* (*Ac*). *Genetics* 191 (3), 747–756. doi: 10.1534/genetics.112.139642

Li, H., Fischle, W., Wang, W., Duncan, E. M., Liang, L., Murakami-Ishibe, S., et al. (2007). Structural basis for lower lysine methylation state-specific readout by MBT repeats of L3MBTL1 and an engineered PHD finger. *Mol. Cell* 28 (4), 677–691. doi: 10.1016/j.molcel.2007.10.023

Liu, D., and Chalmers, R. (2014). Hyperactive mariner transposons are created by mutations that disrupt allosterism and increase the rate of transposon end synapsis. *Nucleic Acids Res.* 42 (4), 2637–2645. doi: 10.1093/nar/gkt1218

Lohe, A. R., De Aguiar, D., and Hartl, D. L. (1997). Mutations in the *mariner* transposase: the D,D(35)E consensus sequence is nonfunctional. *Proc. Natl. Acad. Sci.* 94 (4), 1293–1297. doi: 10.1073/pnas.94.4.1293

Lohe, A. R., and Hartl, D. L. (1996). Autoregulation of *mariner* transposase activity by overproduction and dominant-negative complementation. *Mol. Biol. Evol.* 13 (4), 549–555. doi: 10.1093/oxfordjournals.molbev.a025615

Luo, G., Ivics, Z., Izsvák, Z., and Bradley, A. (1998). Chromosomal transposition of a Tc1/mariner-like element in mouse embryonic stem cells. *Proc. Natl. Acad. Sci. United States America* 95, 10769–10773. doi: 10.1073/pnas.95.18.10769

Mátés, L., Chuah, M. K., Belay, E., Jerchow, B., Manoj, N., Acosta-Sanchez, A., et al. (2009). Molecular evolution of a novel hyperactive *Sleeping beauty* transposase enables robust stable gene transfer in vertebrates. *Nat. Genet.* 41 (6), 753–761. doi: 10.1038/ng.343

Mémet, S., Gouy, M., Marck, C., Sentenac, A., and Buhler, J. M. (1988). *RPA190*, the gene coding for the largest subunit of yeast RNA polymerase a. *J. Biol. Chem.* 263 (6), 2830–2839. doi: 10.1016/s0021-9258(18)69144-6

Miskey, C., Izsvak, Z., Plasterk, R. H., and Ivics, Z. (2003). The *Frog prince*: a reconstructed transposon from *Rana pipiens* with high transpositional activity in vertebrate cells. *Nucleic Acids Res.* 31 (23), 6873–6881. doi: 10.1093/nar/gkg910

Plasterk, R. H., Izsvák, Z., and Ivics, Z. (1999). Resident aliens: the Tc1/*mariner* superfamily of transposable elements. *Trends Genet.* 15 (8), 326–332. doi: 10.1016/s0168-9525(99)01777-1

Ramakrishnan, M., Zhou, M., Pan, C., Hanninen, H., Yrjala, K., Vinod, K. K., et al. (2019a). Affinities of terminal inverted repeats to DNA binding domain of transposase affect the transposition activity of bamboo *Ppmar2* mariner-like element. *Int. J. Mol. Sci.* 20 (15), 3692. doi: 10.3390/ijms20153692

Ramakrishnan, M., Zhou, M. B., Pan, C. F., Hanninen, H., Tang, D. Q., and Vinod, K. K. (2019b). Nuclear export signal (NES) of transposases affects the transposition activity of mariner-like elements *Ppmar1* and *Ppmar2* of moso bamboo. *Mob DNA* 10, 35. doi: 10.1186/s13100-019-0179-y

Robertson, H. M., and Lampe, D. J. (1995). Recent horizontal transfer of a *mariner* transposable element among and between diptera and neuroptera. *Mol. Biol. Evol.* 12 (5), 850–862. doi: 10.1093/oxfordjournals.molbev.a040262

Scholes, D. T., Banerjee, M., Bowen, B., and Curcio, M. J. (2001). Multiple regulators of Ty1 transposition in *Saccharomyces cerevisiae* have conserved roles in genome maintenance. *Genetics* 159 (4), 1449–1465. doi: 10.1093/genetics/159.4.1449

Schotta, G., Lachner, M., Sarma, K., Ebert, A., Sengupta, R., Reuter, G., et al. (2004). A silencing pathway to induce H3-K9 and H4-K20 trimethylation at constitutive heterochromatin. *Genes Dev.* 18 (11), 1251–1262. doi: 10.1101/gad.300704

Tamura, K., Stecher, G., and Kumar, S. (2021). MEGA11: Molecular evolutionary genetics analysis version 11. *Mol. Biol. Evol.* 38 (7), 3022–3027. doi: 10.1093/molbev/msab120

Tellier, M., and Chalmers, R. (2020). Compensating for over-production inhibition of the Hsmar1 transposon in escherichia coli using a series of constitutive promoters. *Mobile DNA* 11, 5. doi: 10.1186/s13100-020-0200-5

Teste, M. A., Duquenne, M., Francois, J. M., and Parrou, J. L. (2009). Validation of reference genes for quantitative expression analysis by real-time RT-PCR in *Saccharomyces cerevisiae*. *BMC Mol. Biol.* 10, 99. doi: 10.1186/1471-2199-10-99

Trapnell, C., Williams, B. A., Pertea, G., Mortazavi, A., Kwan, G., van Baren, M. J., et al. (2010). Transcript assembly and quantification by RNA-seq reveals unannotated transcripts and isoform switching during cell differentiation. *Nat. Biotechnol.* 28 (5), 511–515. doi: 10.1038/nbt.1621

Venema, J., and Tollervey, D. (1996). *RRP5* is required for formation of both 18S and 5.8S rRNA in yeast. *EMBO J.* 15 (20), 5701–5714. doi: 10.1002/j.1460-2075.1996.tb00954.x

Watanabe, M., Ueda, K., Manabe, I., and Akai, T. (1982). Flowering, seeding, germination, and flowering periodicity of *Phyllostachys pubescens*. *J. Japanese Forestry Soc.* 64 (3), 107–111. doi: 10.11519/jjfs1953.64.3_107

Weirich, S., Kusevic, D., Kudithipudi, S., and Jeltsch, A. (2015). Investigation of the methylation of numb by the SET8 protein lysine methyltransferase. *Sci. Rep.* 5, 13813. doi: 10.1038/srep13813

Yang, H., and Mizzen, C. A. (2009). The multiple facets of histone H4-lysine 20 methylation. *Biochem. Cell Biol.* 87 (1), 151–161. doi: 10.1139/O08-131

Yang, G., Nagel, D. H., Feschotte, C., Hancock, C. N., and Wessler, S. R. (2009). Tuned for transposition: molecular determinants underlying the hyperactivity of a *Stowaway* MITE. *science* 325 (5946), 1391–1394. doi: 10.1126/science.1175688

Yang, G., Weil, C. F., and Wessler, S. R. (2006). A rice *Tc1/mariner*-like element transposes in yeast. *Plant Cell* 18 (10), 2469–2478. doi: 10.1105/tpc.106.045906

Yuan, Y. W., and Wessler, S. R. (2011). The catalytic domain of all eukaryotic cut-and-paste transposase superfamilies. *Proc. Natl. Acad. Sci. U.S.A.* 108 (19), 7884–7889. doi: 10.1073/pnas.1104208108

Yusa, K., Takeda, J., and Horie, K. (2004). Enhancement of *Sleeping beauty* transposition by CpG methylation: possible role of heterochromatin formation. *Mol. Cell Biol.* 24 (9), 4004–4018. doi: 10.1128/MCB.24.9.4004-4018.2004

Zayed, H., Izsvak, Z., Khare, D., Heinemann, U., and Ivics, Z. (2003). The DNA-bending protein HMGB1 is a cellular cofactor of *Sleeping beauty* transposition. *Nucleic Acids Res.* 31 (9), 2313–2322. doi: 10.1093/nar/gkg341

Zhang, X., and Bruice, T. C. (2008). Product specificity and mechanism of protein lysine methyltransferases: Insights from the histone lysine methyltransferase SET8. *Biochemistry* 47 (25), 6671–6677. doi: 10.1021/bi800244s

Zhou, M. B., Zhong, H., Hu, J. L., and Tang, D. Q. (2015). *Ppmar1* and *Ppmar2*: the first two complete and intact full-length *mariner*-like elements isolated in *Phyllostachys edulis*. *Acta Botanica Gallica* 162 (2), 127–137. doi: 10.1080/12538078.2014.999117

Zhou, M., Hu, H., Liu, Z., and Tang, D. (2016). Two active bamboo *mariner*-like transposable elements (*Ppmar1* and *Ppmar2*) identified as the transposon-based genetic tools for mutagenesis. *Mol. Breed.* 36 (12), 163. doi: 10.1007/s11032-016-0588-2

Zhou, M. B., Hu, H., Miskey, C., Lazarow, K., Ivics, Z., Kunze, R., et al. (2017). Transposition of the bamboo *Mariner*-like element *Ppmar1* in yeast. *Mol. Phylogenet Evol.* 109, 367–374. doi: 10.1016/j.ympev.2017.02.005

frontiers | Frontiers in Plant Science

TYPE Original Research
PUBLISHED 03 November 2022
DOI 10.3389/fpls.2022.943225

OPEN ACCESS

EDITED BY
Daqiu Zhao,
Yangzhou University, China

REVIEWED BY
John M. Braverman,
Saint Joseph's University, United States
Shuyan Lin,
Nanjing Forestry University, China

*CORRESPONDENCE
Zhaoxia Dai
Daizhaoxia1999@163.com

SPECIALTY SECTION
This article was submitted to Plant Breeding, a section of the journal Frontiers in Plant Science

RECEIVED 13 May 2022
ACCEPTED 06 October 2022
PUBLISHED 03 November 2022

CITATION
Liu Y, Wu M, Xu X, Zhu X, Dai Z and Gou G (2022) Genetic diversity and phylogeography of the endemic species *Chimonobambusa utilis* growing in southwest China: Chloroplast DNA sequence and microsatellite marker analyses. *Front. Plant Sci.* 13:943225. doi: 10.3389/fpls.2022.943225

Genetic diversity and phylogeography of the endemic species *Chimonobambusa utilis* growing in southwest China: Chloroplast DNA sequence and microsatellite marker analyses

Yanjiang Liu[1,2], Mingli Wu[1,2], Xue Xu[1,2], Xiao Zhu[1,2], Zhaoxia Dai[2,3]* and Guangqian Gou[1,2]

[1]Key laboratory of Plant Resource Conservation and Germplasm Innovation in Mountainous Region (Ministry of Education), College of Life Sciences/Institute of Agro-Bioengineering, Guizhou University, Guiyang, China, [2]Bamboo Research Institute, Guizhou University, Guiyang, China, [3]College of Forestry, Guizhou University, Guiyang, China

Chimonobambusa utilis (Keng) Keng F is an endemic species distributed only in the Daluoshan Mountains, southwest China. *Ch. utilis* is popular due to its unique flavor and deliciousness and plays an important role in the industrial revolution in many counties in China. A total of 20 natural populations were sampled from the entire distribution range of *Ch. utilis*. In the present study, we used five EST-SSR molecular markers, three chloroplast DNA (*trn*H-*psb*A, *atp*F-*atp*H, and *psb*K-*psb*I), and one ITS molecular marker to elucidate the genetic diversity and phylogeography analyses of these *Ch. utilis* populations. The results exhibited that *Ch. utilis* populations showed lower genetic diversity than other angiosperms (H_T = 0.752, H_S = 0.364, and F_{ST} = 0.05021 for EST-SSR; H_T = 0.956, *Hs* = 0.507, and F_{ST} = 0.70121 for cpDNA; H_T = 0.868, *Hs* = 0.495, and F_{ST} = 0.70121 for nrDNA). A total of 40 alleles were detected for five polymorphic loci. We detected 20 polymorphic sites and 11 haplotypes within 1,398 bp of cpDNA and 59 polymorphic sites and 32 haplotypes within the 589 bp of the ITS sequence. Based on the haplotype distribution, we infer that there were at least two glacial refuges of *Ch. utilis* populations during the Quaternary Ice Age. The genetic and geographic distance were correlated ($p < 0.05$), indicating that narrow distribution might be the primary cause of the low genetic differentiation of *Ch. utilis* populations. Based on the genetic diversity of *Ch. utilis* populations, we recommend implementing effective genetic resource management and sustainable utilization.

KEYWORDS

***chimonobambusa utilis*, genetic diversity, endemic plant, historical dynamics, haplotype**

Introduction

Chimonobambusa utilis, a member of the Poaceae family *Chimonobambusa*, is an endemic species of southwest China and is widely distributed in the Daloushan Mountain area within an altitude range of 1,000 to 2,300 m. It has strong soil adaptability with pH 4.0–8.0, such as black forest soil, nursery loam, and even karst environment (Lou, 2021). The bamboo shoots of *Ch. utilis* can be eaten fresh or processed into dried shoots, flavor snacks, or canned foods. They have become a favorite food in people's daily lives and are also used in medicine, healthcare, feeding, and other functions (Liu et al., 2013; Li et al., 2015; Liu et al., 2018). In addition, because of its strong leaves, moderate number of leaves, and colorful shoots, the transition period from bamboo shoots to bamboo can be as long as half a year, and a bamboo forest is quiet and pleasant, thus having high ornamental value (Lou et al., 2021). Growing bamboo for its economic value has become popular in southwest China, where it plays an essential role in establishing urban ecological landscapes and the growth of the tourist industry. At present, the main research direction is to study the germplasm resources, growth dynamics, cultivation, and nutritional components of *Ch. utilis* (Tang et al., 2019; Ren et al., 2021; Zhu et al., 2021), but there are few reports on the population of *Ch. utilis* at the molecular level. Due to the distinctive features of bamboo, the flowering cycle is long and complicated, and environmental changes frequently make it challenging to identify the reproductive and nutritional traits that can be observed morphologically. As a consequence, systematic study findings based on the approach of categorization that simply considers morphological identification are often questioned and may not be reliable (Das et al., 2007). With the advancement of molecular biology and development of sequencing technology, researchers are constantly studying the genetic diversity, species formation, and genetic differentiation of plants (Li et al., 2019; Chen et al., 2021; Djedid et al., 2022). Therefore, we can rely on plant DNA molecular technology to distinguish different germplasm and study the population genetic differentiation, genetic structure, and pedigree geography of bamboo species.

The topography of mountainous areas in southwest China is characterized by a mountainous landscape and geomorphic features (Xie et al., 2017; Du et al., 2019). This region is considered as one of the richest and most diverse biodiversity hotspots. (Kang et al., 2014; Tian and Wariss, 2021). Historical orogeny and climate change will lead to the habitat fragmentation of species, which will split a habitat into multiple plate populations, which may lead to high gene flow and gene drift between or within populations, and eventually, alien differentiation will occur and form new species. Genetic diversity plays an important role in protecting genetic diversity, which is the basis of ecosystem diversity and species diversity and the premise of adaptation, development, and evolution of species in the process of evolution (Shen et al., 2022). The spatial distribution pattern of species determines the genetic diversity of species, historical evolution, geological climate change, and other factors (Ren et al., 2017; Zhao et al., 2021), and its size determines the ability of a population or species to open up a new environment and adapt to environmental changes. It can further analyze its evolutionary potential and provide important data support for future development (Yu et al., 2020).

Therefore, the genetic background of *Ch. utilis* was studied using molecular markers. The level of genetic diversity and genetic structure of the natural population in *Ch. utilis* was revealed, the population dynamics and distribution pattern were discussed, and the excellent provenance population was selected, providing a theoretical basis for auxiliary breeding, construction of DNA fingerprinting approaches, and exploitation and utilization of seed resources. This study aims to provide strategic help for the rational planting, cultivation, and management of *Ch. utilis* and to provide a reference for studies addressing the effects of complex geographical environments and climate fluctuations on the genetic differentiation and distribution pattern of species in southwest China.

Here, after a comprehensive investigation and extensive sampling of the natural population of *Ch. utilis*, molecular markers with different genetic backgrounds and evolution rates were combined for the first time using five EST-SSR markers and three cpDNA regions (*trn*A-*trn*H, *atp*F-*atp*H, and *psb*K-*psb*I) and one ITS sequence to make the results more comprehensive and reliable. We expect to find the causes of the genetic variation by studying the genetic diversity and phylogenetic geography of *Ch. utilis*, and based on the level of genetic diversity and genetic differentiation of *Ch. utilis*. Finally, based on the discussion of various conclusions, put forward the management strategy of scientific and feasible protection measures, and provide a certain scientific theoretical basis for the protection, development, and utilization of the *Ch. utilis* germplasm resources.

Materials and methods

Plant sampling

We have collected more than 400 natural individuals of *Ch. utilis* from 20 populations, which presents its entire geographical distribution. Twenty to twenty-five individuals were collected from each population, and each individual was 45 m apart (Chen, 2018). Fresh, tender leaves without obvious diseases and insect pests were collected by GPS software and dried with silica gel for total DNA extraction (Figure 1, Table 1). Among them, 14 representative populations and 140 individuals were used for EST-SSR molecular marker selection (Supplementary Table 1). All specimens were stored in the Natural Museum of Guizhou University (accession number: GACP), Guizhou University, China.

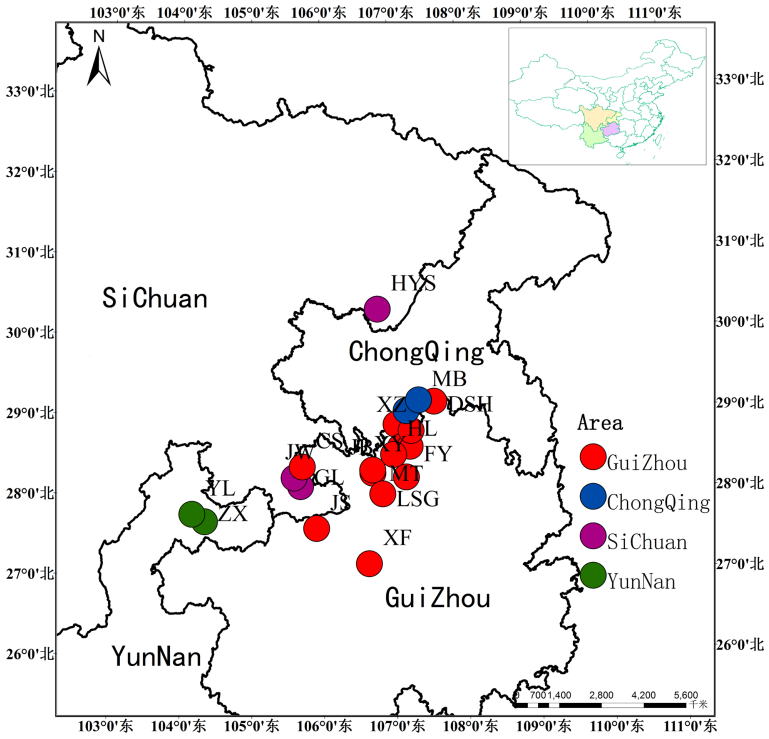

FIGURE 1
Sampling distribution of *Ch. utilis* in southwest China.

TABLE 1 Sampling information of *Ch. utilis*.

ID	Location	Individuals (*n*)	Latitude (N)	Longitude (E)	Altitude (m)
KKS	Kuankuoshui, GuiZhou	20	107.17	28.20	1,433
JB	Jiuba, GuiZhou	20	106.70	28.86	1,354
QB	Qingba, GuiZhou	20	107.04	28.26	1,781
XF	Fengcisi, GuiZhou	20	106.63	28.30	1,431
JS	Taiping, GuiZhou	20	105.90	27.13	1,324.43
MT	Miaotang, GuiZhou	20	107.09	29.14	1,577
XY	Xianyuan, GuiZhou	20	106.70	28.78	1,633.75
LSG	Loushanguan, GuiZhou	20	106.83	28.58	1,724.86
DSH	Dashahe, GuiZhou	20	107.58	28.57	1,351.06
FY	Fuyan, GuiZhou	20	107.23	28.00	1,544.97
XZ	XinZhou, GuiZhou	20	107.25	28.78	1,394.94
HL	Cuanglian, GuiZhou	20	106.99	28.49	1,715.13
GFD	Gufodong, ChongQing	20	107.18	29.03	2,074.47
HYS	Huayingshan, SiChuan	20	106.79	30.30	1,972.11
MB	Miaoba, ChongQing	21	107.36	29.16	1,348.62
GL	Gulin, SiChuan	20	105.68	28.10	1,533.77
JW	Xuyong, SiChuan	20	105.59	28.21	1,320.04
ZX	Zhenxiong, YunNan	25	104.33	27.66	1,799.96
YL	Yiliang, YunNan	22	104.16	27.75	1,832.11
CS	Liangkouhe, GuiZhou	22	105.71	28.35	1,260.49

DNA extraction and procedures

DNA was extracted from dried leaves using the Plant Genomic DNA Kit (Tiangen Biotech, Beijing, China). DNA quality was tested using 1.5% agarose gel electrophoresis. The amount of DNA was estimated by spectrophotometry (Meipuda, Shanghai, China). Then, dilution was performed by standardizing all samples to 20 ng DNA/μl and storing it at −80°C.

Microsatellite markers were selected from previously optimized markers in our laboratory and the published literature for screening (Li, 2008; Zhu et al., 2021). Internal transcribed spacer (ITS) sequences and cpDNA fragments (*trn*H-*psb*A, *atp*F-*atp*H, and *psb*K-*psb*I) were amplified (Cai et al., 2012; Supplementary Table 2).

The PCR amplification of cpDNA and ITS regions were performed in 17-μl reaction volumes containing 7 μl of 2× Taq PCR Master Mix (Tiangen Biotech, Beijing, China), 0.5 μl of each primer, 1 μl of template DNA, and 8 μl of double-distilled water. The reactions were conducted with the following conditions: initial 2-min denaturation at 95°C followed by 30 cycles of 1-min denaturation at 95°C, 55°C for 10 s with a ramp of 0.3°C/s to 65°C, and 65°C for 1 min, with a final extension at 65°C for 10 min. Agarose gel electrophoresis detection of all PCR products showed clear bands without the occurrence of the indistinct band; obvious primer dimmer and tailing phenomena were directly purified and sequenced. The purified PCR products were sequenced in an ABI 3730 (Thermo Fisher Scientific). The results of chloroplast DNA sequences and nuclear fragments were checked using Chromas 2.6, then manually aligned employing CLUSTAL W in MEGA 6 and adjusted (Tamura et al., 2013). All sequence results were deposited in the GenBank database under accession numbers (ON211020–ON211030 for cpDNA and ON206010–ON206041 for ITS).

Twenty pairs of EST-SSR primers were selected, from which five pairs of EST-SSR primers were successfully amplified with high polymorphism and homology (Supplementary Table 3). The volume of the PCR mix was 25 μl: 12.5 μl 2× Taq PCR Master Mix, the upstream and downstream primers (1 μl each), 1 μl of DNA template, and 9.5 μl of ddH_2O. The reaction parameters of PCR amplifications were as follows: pre-denaturation at 94°C for 3 min, denaturation at 94°C for 30 s, annealing at 55–60.2°C for 30 s, extension at 72°C for 1 min, a total of 30 cycles, and extension at 72°C for 5 min. The selected primer pairs were labeled with a fluorescent dye (FAM) at the 5′ end, and PCR products were analyzed using an ABI3730.

cpDNA and ITS sequences

Sequences from three cpDNA fragments and ITS sequences were concatenated into a sequence by the software PhyloSuite v1.1.15 (Zhang et al., 2019). The DnaSP version 5.0 (Librado and Rozas, 2009) was used to identify different haplotypes (n), haplotype diversity (*Hd*), nucleotide diversity (*Pi*), and the number of polymorphic sites (π). Population differentiation indices (*Gst* and *Nst*) were calculated using the program PERMUT with 1,000 permutations (Pons and Petit, 1996). The genealogical relationships among all the haplotypes were performed using a median-joining method in Network v.5 (Bandelt et al., 1999; http://www.fluxus-engineering.com/sharenet.htm). The geographical distribution of populations and haplotypes was mapped in ArcGIS v.10.2.

Average genetic diversity within populations (*HS*), total genetic diversity (*HT*), and the genetic variation, differentiation, and pairwise fixation indices (F_{ST}) within and among populations were statistically tested through analyses of molecular variance (AMOVAs) in ARELQUIN v3.1.16 (https://www.fousoft.com/arlequin.html). To better understand the population growth and expansion of cpDNA and nrDNA fragments of *Ch. utilis*, both neutrality tests and mismatch analysis were implemented in DnaSP v.5.

EST-SSR analysis

Peak analysis was performed with Gene Mapper 4.1 software, the signal value of the peak was above 200 bp, and the peak shapes are similar at the same site. For each microsatellite locus, the expected heterozygosity (*He*), observed heterozygosity (*Ho*), effective numbers of alleles (*Ne*), the mean number of alleles (*Na*), percentage of polymorphic loci (PPB), and Wright's *F* statistics parameters (F_{IS}, F_{IT}, and F_{ST}) were analyzed using GenAIEx6.5 (Peakall and Smouse, 2012). The polymorphism information content (PIC) is one of the important indexes to measure the polymorphism of SSR locus using CERVUS 3.0 (Kalinowski et al., 2007). The cluster analysis was carried out to characterize population structure in STRUCTURE version 2.3 (Pritchard et al., 2009). The parameter settings of about 20 independent simulations were run for a *K*-value of 2–15 with 10,000 length of burnin period and a number of MCMC reps after burnin of 100,000. Structure harvester was then utilized to estimate the most likely number (*K*) (Earl, 2012; http://taylor0.biology.ucla.edu/structureHarvester/) of genetic clusters based on both log-likelihood L (*K*) and Delta *K* (Δ*K*) (Evanno et al., 2005) methods. Principal coordinate analysis (PCoA) and Mantel tests were carried out using GenAIEx6.5 based on Nei's genetic distance for EST-SSR data. An AMOVA among and within populations was carried out using the program Arlequin version 3.5 to ensure the accuracy of the estimation of variance components (Excoffier and Lischer 2010).

PopGene32 software (Yeh et al., 1997) was used to calculate Nei's genetic distance of 14 populations of *Ch. utilis*. The software was then used to detect correlations between genetic distance and geographical distance, genetic distance, and

population altitude. Bottleneck 1.2.02 (Cornuet and Luikart, 1996) was used to test for recent bottleneck events in the species. The demographic history of populations was explored under the stepwise mutation model (SMM) and two-phase model (TPM) and by a heterozygosity excess test. Computation was performed using two methods (Sign and Wilcoxon tests) appropriate for a population number < 20.

Results

cpDNA and ITS sequences analysis

We identified the cpDNA consensus sequences from 410 individuals in 20 populations with a total of 1,398 bp in length containing 20 polymorphic sites (Supplementary Table 4), and the total GC content was 34.68%. We found 11 chloroplast haplotypes (H1–H11); among them, H1 was the most common, occurring in 296 individuals with a wide distribution in 16 populations, suggesting that it is the most ancient haplotype. Haplotypes H4–H11 were unique haplotypes. Haplotype H4 was unique to the GL population; haplotype H5 was unique to the ZX population. Haplotypes H6 and H7 appeared in the KKS population (Figure 2A). The total nucleotide diversity (*Pi*) of all populations was 0.00038, with most populations having a null value, and the average was 0.00013. Total haplotype diversity (*Hd*) was 0.4641, and the average was 0.4343 (Table 2). It is noteworthy that the DSH population had the highest cpDNA nucleotide and haplotype diversity in *Ch. utilis* (0.000760 and 0.511, respectively).

For ITS data, the total length was 589 bp, including 59 polymorphic sites, and the content of GC was 70.29%. A total of 32 haplotypes (H1–H32) were identified based on nrDNA fragments. Among them, haplotype H3 contains 105 individuals with the highest frequency and the widest range of distribution, and we speculate that this is an ancient haplotype. At the species level, using ITS data, the *Pi* value was 6.13×10^{-3}, with an average value was 1.8325×10^{-3}. The *Hd* value was 0.841, with an average value of 0.4343 (Table 3; Figure 2B).

The AMOVA based on the cpDNA and ITS sequences data further revealed the genetic structure from populations of *Ch. utilis*. It is apparent that a higher genetic variation was observed between populations (84.14%, $p < 0.001$) than within populations (15.86%, $p < 0.001$) at the cpDNA level. The F_{ST} value was 0.84135, which also indicates a significant level. The ITS sequence shows the same result, similar to those of cpDNA, the variation came from among populations, and the F_{ST} value was 0.84135 (Table 4).

Genetic structure analysis of *Ch. utilis* (based on cpDNA and ITS sequences) was done using Permut v.2.0 (Table 5). It is apparent from this table that the total genetic (H_T) and the average within-population diversity (H_S) were 0.956 and 0.507, respectively, based on combined cpDNA sequences. The population genetic differentiation coefficients (G_{ST}= 0.470, N_{ST} = 0.976, $N_{ST} > G_{ST}$, $p < 0.05$) showed a significant pedigree geographical structure among populations of *Ch. utilis*. The ITS sequence shows that total genetic (H_T) and the average within-population diversity (H_S) were 0.868 and 0.495, respectively. The population genetic differentiation coefficients are similar to the cpDNA data (G_{ST} = 0.430, N_{ST} = 0.543, $N_{ST} > G_{ST}$, $p < 0.05$). The gene flow based on the two molecular markers was 0.11 and 0.56, respectively.

For combined cpDNA, the H1 haplotype has the widest distribution and the highest frequency, followed by haplotype H3. According to the NETWORK analysis, these two widespread haplotypes are located at the central position of the network diagram and are likely the ancestral haplotypes. The

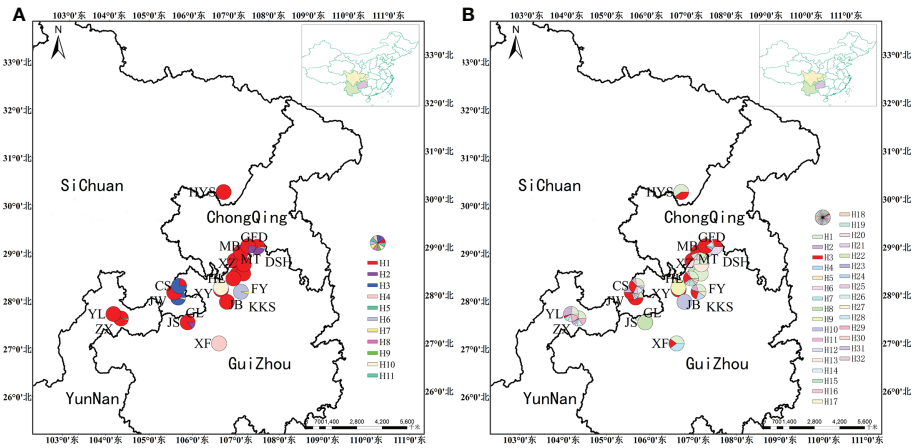

FIGURE 2
Geographic distribution of haplotype based on cpDNA **(A)** and nrDNA **(B)** sequences.

TABLE 2 Distribution and genetic diversity parameters of cpDNA haplotypes in *Ch. utilis*.

No.	Population	cpDNA					No.	Population	cpDNA				
		N	*Nh*	π (×10^{-3})	H_d	Haplotypes (*N*)			*N*	*Nh*	π (×10^{-3})	H_d	Haplotypes (*N*)
1	KKS	20	2	0.070	0.100	**H6 (19)**, **H7 (1)**	11	XZ	20	1	0	0	H1 (20)
2	JB	20	2	0.070	0.100	H1 (19), **H8 (1)**	12	HL	20	1	0	0	H1 (20)
3	QB	20	1	0	0	H1 (20)	13	GFD	20	1	0	0	H1 (20)
4	XF	20	1	0	0	**H9 (20)**	14	HYS	20	1	0	0	H1 (20)
5	JS	20	2	0. 390	0.268	H1 (17), H2 (3)	15	MB	21	2	0. 550	0.381	H1 (16), H2 (5)
6	MT	20	1	0	0	H1 (20)	16	GL	20	2	0.430	0.100	H3 (19), **H4 (1)**
7	XY	20	1	0	0	**H10 (20)**	17	JW	20	1	0	0	H1 (20)
8	LSG	20	1	0	0	H1 (20)	18	ZX	25	2	0.064	0.080	H1 (24), **H5 (1)**
9	DSH	20	3	0. 760	0.511	H1 (13), H2 (6), **H11 (1)**	19	YL	22	1	0	0	H1 (22)
10	FY	20	1	0	0	H1 (20)	20	CS	22	2	0.260	0.368	H1 (5), H3 (17)

Bold represents the unique haplotype, N represents the number of individuals, Nh represents the number of haplotypes, π represents the nucleotide diversity, and H_d represents the haplotype diversity.

remaining eight haplotypes with low frequency were located at external positions relative to the two main haplotypes; these may be young haplotypes derived from recent differentiation. The ITS sequence haplotype network diagram results supported the congruent cpDNA haplotypes, which showed that the haplotypes H3 and H1 were distributed in the central position and that the remaining haplotypes were distributed in the outside nodes of the network diagram (Figure 3).

To further understand the phylogenetic analysis of *Ch. utilis*, maximum likelihood analysis was performed for the 11 cpDNA haplotypes and 32 ITS haplotypes with *Chimonobambusa hejiangensis* as an outgroup, with 1,000 bootstrap replications (Figure 4). All haplotypes were divided into two clades with low statistical support, possibly due to the short time of intraspecific variations. These results are consistent with the haplotype network diagrams based on cpDNA and ITS sequences.

TABLE 3 Distribution and genetic diversity parameters of nrDNA haplotypes in *Ch. utilis*.

No.	Population	nrDNA				
		N	*Nh*	π (×10^{-3})	H_d	Haplotypes (*N*)
1	KKS	20	5	2.350	0.795	H1 (6), H2 (3), H3 (5), H4 (4), H5 (2)
2	JB	20	3	0.820	0.405	H1 (4), H2 (1), H3 (15)
3	QB	20	3	1.150	0.595	H1 (2), H3 (10), H6 (8)
4	XF	20	3	0.560	0.328	H1 (8), H3 (4), H7 (8)
5	JS	20	1	0	0	H8 (20)
6	MT	20	1	0	0	H8 (20)
7	XY	20	1	0	0	**H9 (20)**
8	LSG	20	1	0	0	**H10 (20)**
9	DSH	20	3	1.500	0.695	H3 (6), **H11 (6)**, **H12 (8)**
10	FY	20	1	0	0	H1 (20)
11	XZ	20	1	0	0	**H13 (20)**
12	HL	20	9	4.030	0.853	H1 (6), H2 (1), H3 (5), H4 (1), **H14 (1)**, **H15 (3)**, **H16 (1)**, **H17** (1), **H18** (1)
13	GFD	20	5	15.670	0.668	H3 (11), **H19(2)**, **H20 (1)**, **H21 (2)**, **H22 (4)**
14	HYS	20	2	0.860	0.505	H1 (12), H3 (8)
15	MB	21	4	1.410	0.348	H1 (2), H3 (17), **H23 (1)**, **H24 (1)**
16	GL	20	2	0.890	0.526	H1 (10), H3 (10)
17	JW	20	7	1.720	0.726	H1 (4), H2 (6), H3 (6), H4 (1), H7 (1), H25 (1), H26 (1)
18	ZX	25	7	1.730	0.757	H1 (8), H2 (7), H7 (1), H25 (1), **H27 (1)**, H28 (3), H29 (4)
19	YL	22	7	1.800	0.771	H1 (5), H2 (7), H3 (1), H7 (2), H28 (2), H29 (4), **H30 (1)**
20	CS	22	7	2.160	0.714	H1 (6), H2 (2), H3(7), H25 (2), H26 (3), **H31 (1)**, **H32 (1)**

Bold black represents the unique haplotype, N represents the number of individuals, Nh represents the number of haplotypes, π represents the nucleotide diversity, Hd represents the Haplotype diversity.

TABLE 4 AMOVA analysis based on the cpDNA and nrDNA for *Ch. utilis* populations.

Source of variation	cpDNA					nrDNA				
	d.f.	Sum of squares	Variance components	Percentage of variation	Fixation Index	d.f.	Sum of squares	Variance components	Percentage of variation	Fixation Index
Among populations	19	188.078	0.47856	84.14	0.84135	19	611.693	1.53875	70.12	0.70121
Within populations	390	35.193	0.09024	15.86		390	255.709	0.65566	29.88	
Total	409	223.271	0.56879			409	867.402	2.19442		

To gain insight into the population and dynamic history of *Ch. utilis*, the mismatch analysis and neutrality test results supported expansions by cpDNA and ITS data. Based on cpDNA combined sequences, the mismatch analysis was unimodal, and the expected value was consistent with the observed value, indicating that this species had recently undergone population expansion. The Neutrality Test showed both significant negative Tajima's D value (Tajima's D = −1.60601, $0.10 < p < 0.05$) and Fu and Li's F* (Fu and Lis F* = −4.24699, $p < 0.02$), implying that the populations had experienced directional selection or population expansion. The ITS sequence displayed a significant negative Tajima's D value (Tajima' s D = −1.76916, $p < 0.05$) and non-significant negative Fu and Li's F* value (Fu and Li's F* = −1.80003, $p > 0.01$), whereas the mismatch distribution analysis was bimodal with ITS data (Figure 5).

EST-SSR data analysis

To assess the diversity of *Ch. utilis* populations, five primers were polymorphic. The observed allele number (*Na*) per locus ranged from 3.143 (EST-SSR5) to 4.741 (EST-SSR1), with a mean of 3.848. The effective allele number (*Ne*) per locus ranged from 2.544 (EST-SSR3) to 3.767 (EST-SSR1), with an average value of 3.111. Shannon's Information Index (*I*) had an average of 0.170 and ranged from 0.991 (EST-SSR3) to 1.373 (EST-SSR1). The observed heterozygosity (*Ho*) and expected heterozygosity (*He*) varied from 0.993 (EST-SSR5) to 1.000 (EST-SSR1–4), and from 0.596 (EST-SSR3) to 0.886 (EST-SSR2), with an average of 0.999 and 0.653, respectively. The value of the polymorphism information content (*PIC*) ranged from 0.592 (EST-SSR3) to 0.886 (EST-SSR2) with a mean of 0.732, showing highly polymorphic loci for five primers. In summary, the highest level of genetic diversity was detected in the locus EST-SSR1, while the lowest level of genetic diversity was detected in the locus EST-SSR3 (Supplementary Table 5).

Table 6 provides the *Ch. utilis* genetic diversity at the population levels. The *Na* and *Ne* per population ranged from 3.000 (CS) to 4.800 (XZ) and from 2.448 (HYS) to 3.714 (QB), with mean values of 3.843 and 3.111, respectively. The *PIC* value shows the genetic diversity of populations; its value ranged from 0.948 (HYS) to 1.346 (YL), with an average of 1.170. The *Ho* value was 1.000 in all populations apart from the QB population (*Ho* = 0.980), with an average of 0.999. The *He* reflected the richness and evenness of the population and varied from 0.584 (HYS) to 0.712 (YL), with an average of 0.653. The genetic diversity of the XZ, QB, YL, and GL populations investigated in the present study was high; however, the genetic diversity of the HYS and CS populations was low. At the population level, the polymorphic loci (PPL) percentage was 100% in all populations (Table 6).

AMOVA based on EST-SSR data among 14 populations of *Ch. utilis* showed that a higher genetic variation was observed within populations (94.98%) than among populations (5.02%), which indicated that the genetic variation mainly occurred within populations. Moreover, the Fixation Index (F_{ST}) was 0.05021 at the population level (Supplementary Table 6). The Bayesian cluster analysis of EST-SSR showed that $K = 3$ was the optimum number of subpopulations, revealing that at least three distinct groups existed among 14 populations. The highest peak (Delta K = 13.7167) was at the value $K = 3$. Overall, there were different degrees of introgression among 140 individuals from different populations (Figure 6).

AUPGMA dendrogram was constructed based on Nei's genetic distances. PCoA results showed that all individuals were divided into three groups, which are identical to those determined by the UPGMA analysis. The first, second, and third components accounted for 16.01%, 26.67%, and 35.22% of the genetic similarity among all individuals, respectively (Figure 7).

TABLE 5 The genetic parameters and gene flow of cpDNA and nrDNA.

	Ht	*Hs*	G_{ST}	N_{ST}	N_{ST}:G_{ST}	Nm
cpDNA	0.956	0.507	0.470	0.976	$N_{ST} > G_{ST}$	0.11
nrDNA	0.868	0.495	0.430	0.543	$N_{ST} > G_{ST}$	0.56

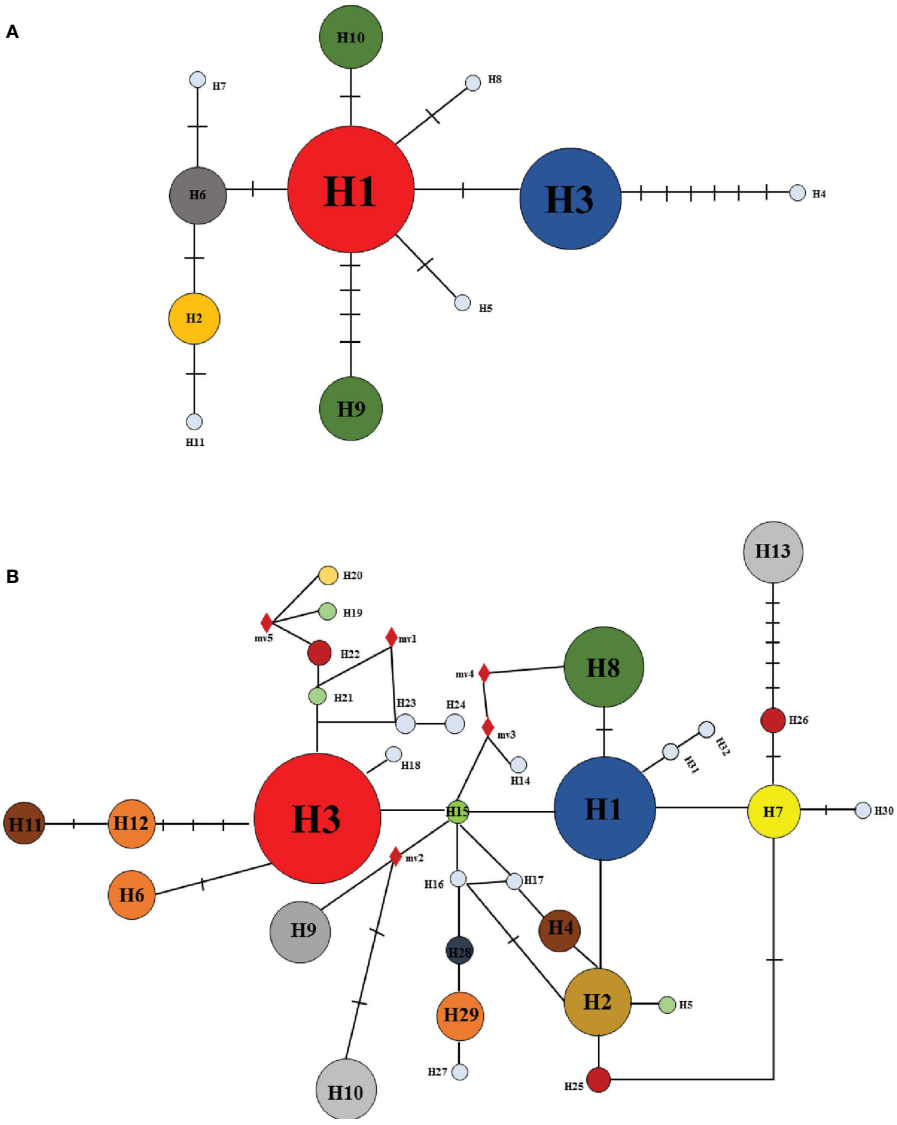

FIGURE 3
Haplotype relationships based on cpDNA **(A)** and nrDNA **(B)** by the median-joining network.

Combined with geographical distribution, all populations were divided into three sites (Figure 8): the southern region (Group A), the northern region (Group B), and the northwestern region (Group B).

Furthermore, the Mantel test revealed a significant positive correlation between genetic distance and geographic distance in *Ch. utilis* (R^2 = 0.0273, p = 0.000; Figure 9A). However, the Mantel test of genetic distance and altitude showed no significant positive correlation. These results provided further evidence that geographic isolation was the primary factor leading to the genetic differentiation of *Ch. utilis* (R^2 = 0.0006, p = 0.177; Figure 9B). Bottleneck analysis indicated that except for populations KKS and CS, the bottleneck effect was not detected in other populations based on Sign tests ($p < 0.05$) under the IAM, TPM, and SMM models. Also, the significant probabilities of Wilcoxon ($p > 0.05$) showed that some populations, such as KKS, QB, JS, XZ, HYS, and CS, experienced a recent bottleneck event (Supplementary Table 7).

Discussion

Genetic variations and differentiation

Biodiversity is the basis of human survival and is characterized by a complex ecological mixture of all biological

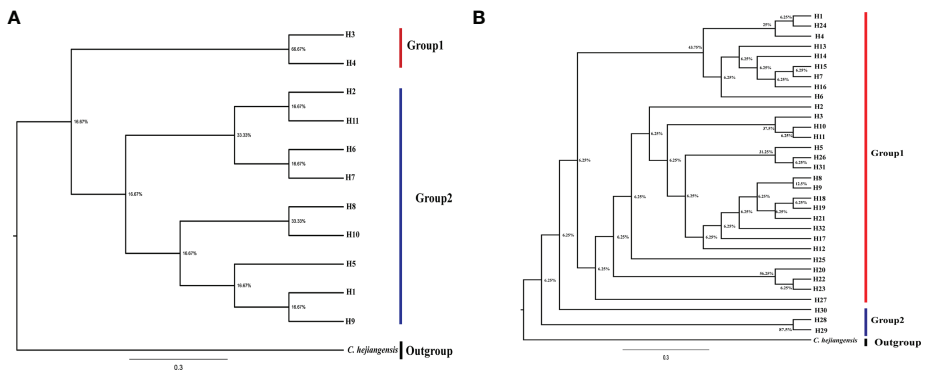

FIGURE 4
Phylogenetic Tree of *Ch. utilis* based on cpDNA **(A)** and nrDNA **(B)** haplotypes by IQ- tree.

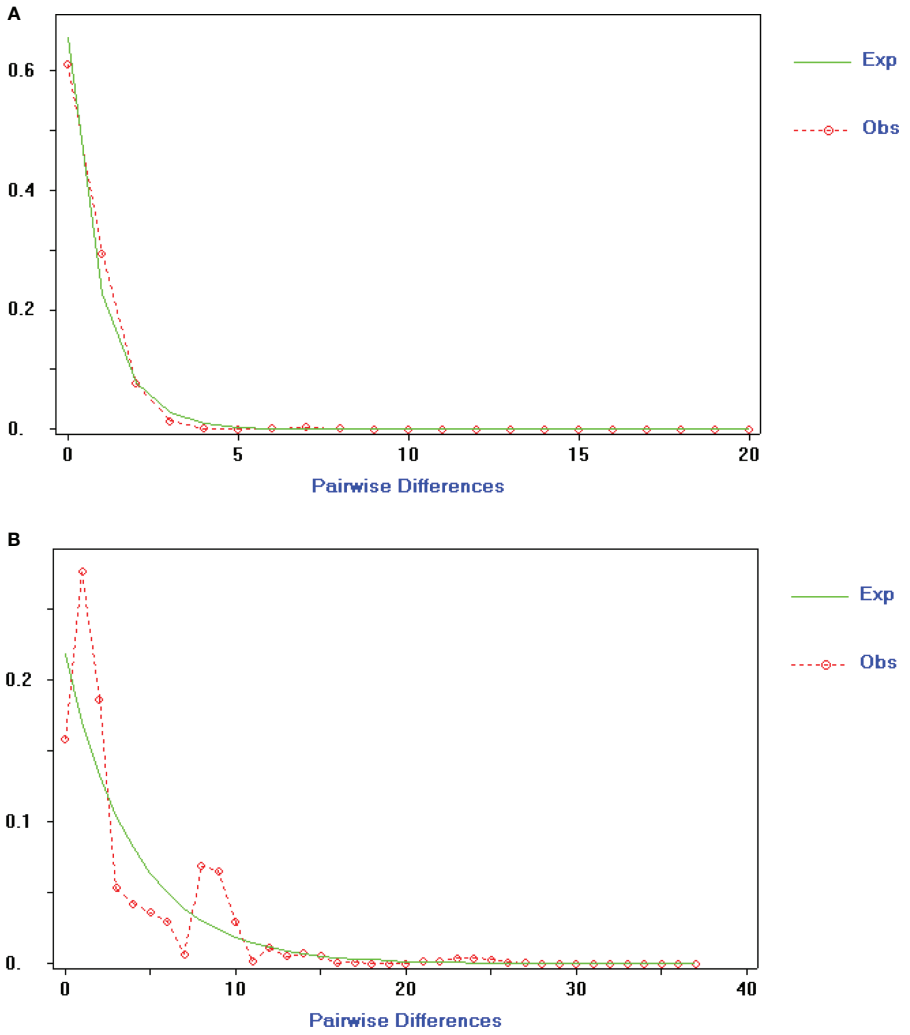

FIGURE 5
Mismatch-distribution analysis of cpDNA **(A)** and nrDNA **(B)** haplotypes for *Ch. utilis*.

TABLE 6 Polymorphism analysis of 14 *Ch. utilis* populations based on EST-SSR.

Population	*Na*	*Ne*	*I*	*Ho*	*He*	PPL (%)
KKS	3.200	2.824	1.046	1.000	0.620	100.00
QB	4.600	3.714	1.289	0.980	0.675	100.00
XF	4.200	3.256	1.225	1.000	0.665	100.00
JS	4.000	3.319	1.261	1.000	0.691	100.00
MT	3.400	2.816	1.111	1.000	0.643	100.00
XY	4.200	3.487	1.242	1.000	0.669	100.00
DSH	3.800	3.210	1.190	1.000	0.664	100.00
XZ	4.800	3.388	1.340	1.000	0.699	100.00
GFD	3.400	2.575	1.010	1.000	0.600	100.00
HYS	3.000	2.448	0.948	1.000	0.584	100.00
GL	4.000	3.302	1.221	1.000	0.669	100.00
JW	3.800	3.028	1.165	1.000	0.653	100.00
YL	4.400	3.633	1.346	1.000	0.712	100.00
CS	3.000	2.558	0.987	1.000	0.602	100.00
Mean	3.843	3.111	1.170	0.999	0.653	100.00

species and their living environment. Biodiversity is mainly divided into three levels: species diversity, genetic diversity, and ecosystem diversity. Genetic diversity generally refers to the sum of genetic variation of all individuals in different populations within a species, which has become a key metric in conservation biology research. Studying the origin and evolution of species provides a basis for the rational utilization of species and the formulation of conservation measures. *Ch. utilis* is mainly distributed in the Daluoshan Mountains and is characterized by a narrow distribution. *Camellia huana*, also distributed in the limestone-hilly areas of southern Guizhou and northern Guangxi, is an endangered species. A total of 99 alleles were detected in 12 populations of *C. huana* using 12 pairs of SSR molecular markers, indicating a low level of genetic diversity (Li et al., 2020). The present study detected higher genetic variations than endangered species, such as *Ipomoea cavalcantei* and *Pityopsis ruthii* (Hatmaker et al., 2018; Lanes et al., 2018). However, using cpDNA and ITS markers, the degree of genetic diversity of *Ch. utilis* is low relative to other angiosperms. Generally, the species with wide geographical distribution and large populations have a higher level of genetic diversity and a relatively rich gene pool, so they have a strong ability to adapt to different environments. For *Oxytenanthera abyssinica*, which mainly grows in the African continent (altitude range is 540 m to 1,750 m), the range of nucleotide polymorphism (π) ranged from 0.5×10^{-3} to 6.3×10^{-3} based on cpDNA fragment analysis (Oumer et al., 2021), which is higher than that of *Ch. utilis* in this study. In addition, there is little gene flow and high genetic differentiation among long-distance populations of *O. abyssinica*, which is similar to the results of this study. We speculate that this is mainly a result of geographical obstacles.

In this study, there are great differences in genetic diversity among different populations of *Ch. utilis*. Combined with the geographical distribution map, populations MB and DSH in the north and populations JS, GL, and CS in the southwest of the Daluoshan Mountains have high haplotype polymorphism and nucleotide polymorphism. Genetic diversity is an important indicator to measure the degree of variation in a population. The higher the degree of the population, the higher the genetic diversity and richer genetic resources, which helps to improve the adaptability of the species to climate change and historical events and provides a theoretical basis for screening for good populations.

Relationships and structure in the *Ch. utilis* populations

Bambusoideae is the only herbaceous plant with lignification under Poaceae. Bamboo has strong adaptability to the environment and easily forms varieties because of different habitats, genetic drift, human transplanting, and other factors. In addition, China has a vast territory and complex topographic and climatic changes. Incomplete statistics show that there are more than 100 varieties or forms of bamboo in China (Qiu et al., 2001). This complicates the traditional classification methods, which are mainly based on the morphological characteristics of flowers and fruits. Therefore, the study on the genetic diversity of bamboos can provide a molecular basis for controversial morphological classification results.

Barkley et al. (2005) used EST-SSR molecular markers to detect the genetic variation among 92 individuals of 44 bamboo species in 11 genera, and the UPGMA clustering method was used to classify these bamboo species into two categories, which was consistent with the morphological classification according to the different sympodial and monopodial. Mukherjee et al. (2010) used four pairs of EST-SSR primers to carry out UPGMA and SAHN cluster analysis of 20 bamboo species growing in India. It was found that the systematic location of a few bamboo species was not consistent with the morphological classification results, forming other evolutionary branches, requiring further detailed taxonomic study.

In this study, based on the structural analysis results, 14 populations of *Ch. utilis* could be divided into three groups according to the most suitable K value. According to their geographical distribution, all populations could be divided into southern, northern, and western regions along the Daluoshan Mountains. The results of the NJ tree and PCoA analysis based on Nei's genetic distance supported the division of *Ch. utilis* into three groups. Southwest China has a varied terrain, as well as a great diversity of climates; therefore, the general division of *Ch. utilis* populations into three groups may be affected by its own environmental tolerance, diffusion capacity, geological events, and climate fluctuations.

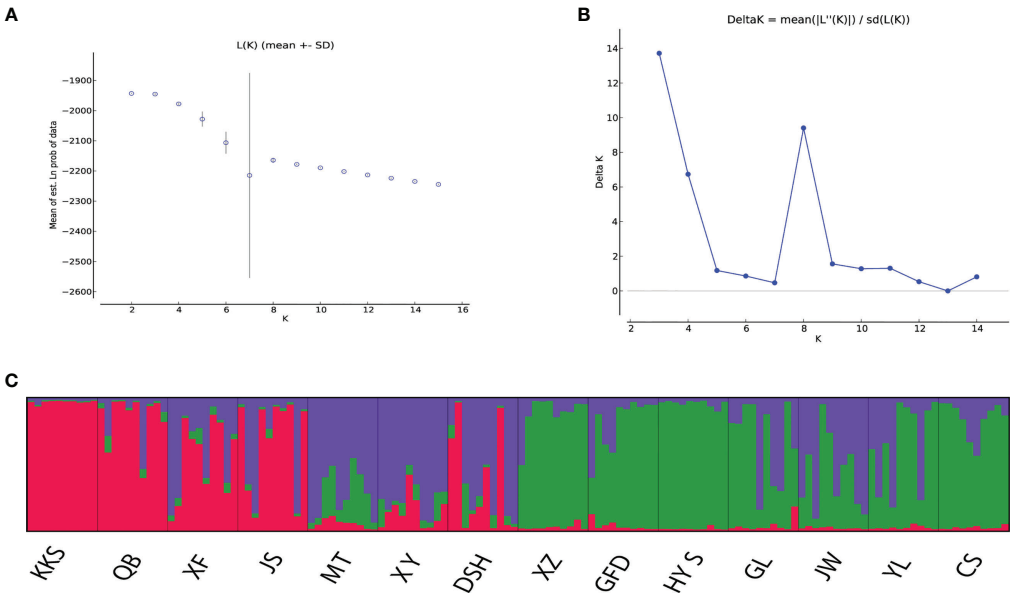

FIGURE 6
Results of STRUCTURE cluster of 140 individuals of *Ch. utilis*. **(A)** Mean log-likelihood (Ln(K)±S.D.). **(B)** Values of logarithm likelihood based on analysis by structure program. **(C)** Each of color bars represents a kind of genotypic group.

CpDNA data showed that the G_{ST} of the *Ch. utilis* population in *Ch. utilis* was lower than the average G_{ST}(G_{ST} = 0.470) of the other 124 angiosperms (by 0.637). However, compared with the above cpDNA data, the results based on nrDNA analysis showed that the G_{ST} of *Ch. utilis* was higher than the average G_{ST} (G_{ST} = 0.430) of 77 angiosperms by 0.184 (Petit et al., 2005). Liu et al. (2012) analyzed the genetic structure of 21 natural populations of *Camellia taliensis* using cpDNA gene fragments and ITS sequences. These authors found that, based on cpDNA data, the degree of genetic differentiation among *Camellia taliensis* populations (G_{ST} = 0.988, N_{ST} = 0.989) was higher than that of the *Ch. utilis* population (G_{ST} = 0.470, N_{ST} = 0.976). This may be because the effective population size of the organelle DNA of *C. taliensis* is smaller than that of nuclear DNA, resulting in strong genetic drift and a higher level of population differentiation. However, the degree of genetic differentiation among populations of *Ch. utilis* was higher than that of some conifers (Hamrick and Godt 1996; Petit et al., 2005).

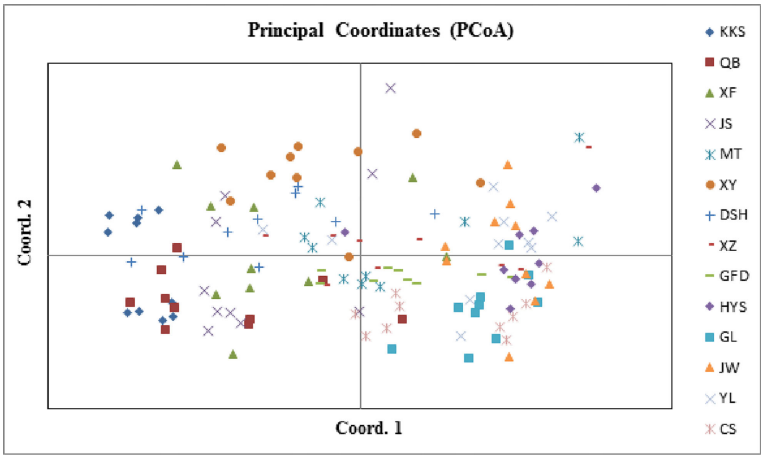

FIGURE 7
Principal coordinates analysis of *Ch. utilis* individuals.

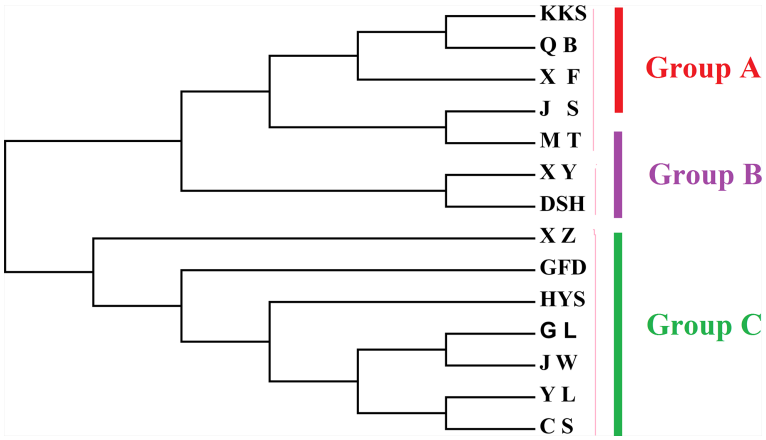

FIGURE 8
NJ tree of *Ch. utilis* populations based on Nei's genetic distance.

In this study, data analysis based on cpDNA and nrDNA showed that chloroplast haplotype H1 and ribosomal haplotype H3 are at the center of the haplotype network diagram, respectively, with a large proportion and the most widespread distribution. Therefore, we speculate that haplotypes H1 and H3 are ancient haplotypes of the *Ch. utilis* population. In addition, the haplotype phylogenetic tree based on cpDNA data divides all groups into two groups. According to the geographical distribution characteristics, the southwest side of the Daloushan Mountains is blocked by the Yunnan-Guizhou Plateau, and there are Wuling Mountains in the northeast. Therefore, populations DSH, GL, ZX, and XF in these two locations of the Daluoshan Mountains contain stable and unique haplotypes H11, H4, H5, and H9, respectively. Its haplotype diversity and nucleotide diversity are also high, and it is geographically far away from the Daluoshan Mountains. Rich haplotypes and genetic diversity allow post-glacial species to re-expand from glacial sanctuaries. Therefore, based on further analysis of nrDNA data, this study speculated that there were at least two *Ch. utilis* population refuges during the glacial period.

Management and protection strategy

Maintaining population genetic diversity and intraspecific genetic variation is not only a source of biological evolution but also a prerequisite for the sustainable development of this species and an important part of biodiversity conservation (Rao, 2004).

Based on the distribution characteristics of the *Ch. utilis* populations and the significant genetic differentiation among populations, it is necessary to protect the existing populations through *in situ* and *ex situ* conservation efforts. This study showed that the genetic diversity of *Ch. utilis* populations was highest in the north and southwest Daloushan Mountains. In the EST-SSR analysis, XZ, QB, YL, GL, and other populations in these two regions had a high level of genetic diversity. The cpDNA and ITS sequence analyses detected many haplotypes and endemic haplotypes in these two regions, and they have high haplotype polymorphism and nucleotide polymorphism. Therefore, to effectively protect the genetic germplasm resources of *Ch. utilis* in these two areas, especially the populations that have recently experienced bottleneck effects (such as HYS and CS populations), we should implement conservation *in situ* strategies to maintain the existing population size, avoid the loss of haplotypes caused by environmental changes, and improve the adaptability of the population. At the same time, special haplotype populations are transplanted to places with similar environments, and conservation *ex situ* strategies are implemented. For example, the construction of seed resources or nature reserves, such as the established Dashahe Nature Reserve and Kuanshui Nature Reserve, improves the survival rate of cultivation and improves management.

Conclusion

In this study, 20 populations of *Ch. utilis* were collected, including 13 populations in Guizhou Province, two populations in Chongqing, two populations in Yunnan Province, and three populations in Sichuan Province. Five pairs of EST-SSR molecular markers were used to analyze the genetic diversity, genetic structure, and bottleneck effect of 14 populations. Three cpDNA fragments (*trn*H-*psb*A, *atp*F-*atp*H, and *psb*K-*psb*I) with uniparental inheritance and one ITS sequence with biparental inheritance were used to study the genetic diversity, genetic structure, and dynamic population history of 410 individuals

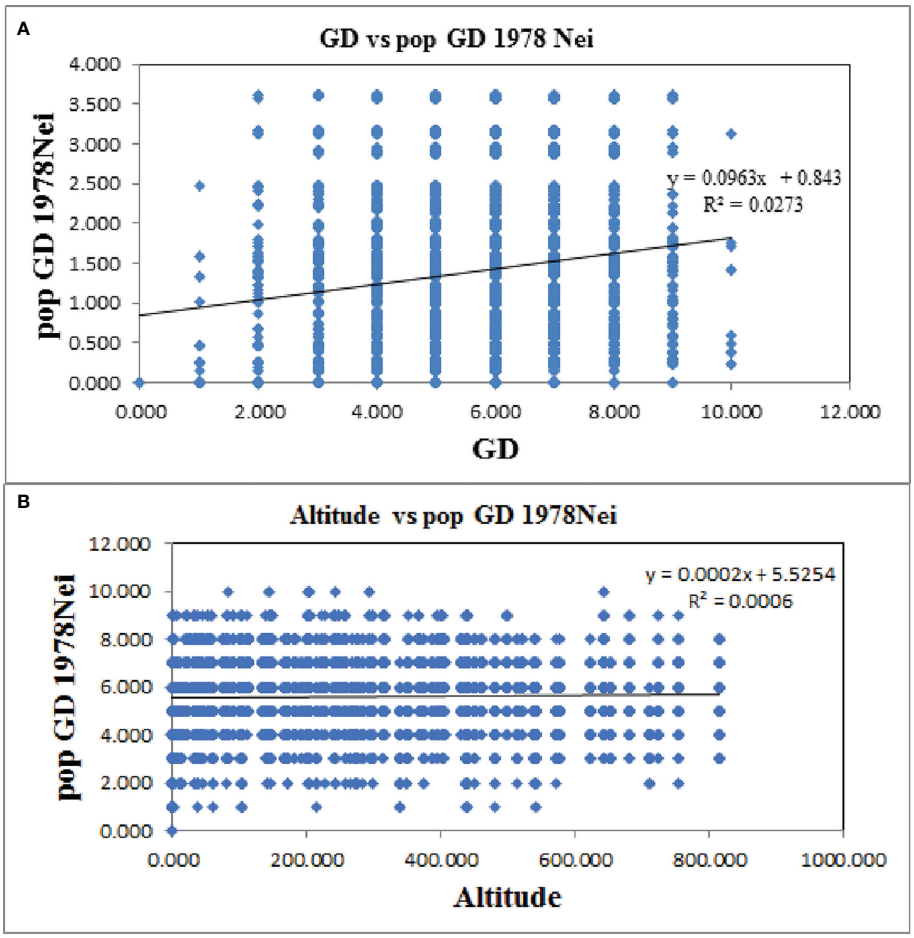

FIGURE 9
Mantel test between genetic distance **(A)** and geographic distance **(B)** of *Ch. utilis* based on EST-SSR marker.

from 20 populations of *Ch. utilis*. We detected a very significant positive correlation between genetic distance and geographical distance among populations, indicating that the genetic variation among populations of *Ch. utilis* is mainly affected by geographical barriers. In addition, the neutral test results of the two markers were significantly negative, indicating that the population of *Ch. utilis* underwent a recent rapid expansion event. Based on the present population distribution, genetic diversity, and geographical pedigree structure of *Ch. utilis*, a scientific and feasible strategy for protection and utilization was put forward. This study aimed to provide a theoretical basis for an in-depth understanding of the population genetic structure, germplasm sampling, geological events, and climate change on the genetic differentiation and geographical distribution pattern formation mechanism of *Ch. utilis*.

Data availability statement

The datasets presented in this study can be found in online repositories. The names of the repository/repositories and accession number(s) can be found in the article/Supplementary Material.

Author contributions

YL performed the experiments, analyzed the data, and approved the final draft. MW contributed to the investigation. XX and ZX prepared figures and/or tables. ZD and GG conceived and designed the experiments. All authors agree to be accountable for the final manuscript. All authors contributed to the article and approved the submitted version.

Funding

This work was supported by the Breeding of Improved Bamboo Varieties for Shoot (Te-Lin-Yan 2020-17).

Acknowledgments

We thank the Investigation of Bamboo Resources and Excavation of Economic Bamboo Species in Guizhou Province.

Conflict of interest

The authors declare that the research was conducted in the absence of any commercial or financial relationships that could be construed as a potential conflict of interest.

Publisher's note

Supplementary material

The Supplementary Material for this article can be found online at: https://www.frontiersin.org/articles/10.3389/fpls.2022.943225/full#supplementary-material

References

Bandelt, H. J., Forster, P., and Röhl, A. (1999). Median-joining networks for inferring intraspecific phylogenies. *Mol. Biol. Evolution.* 16 (1), 37–48. doi: 10.1093/oxfordjournals.molbev.a026036

Barkley, N. A., Newman, M. L., Wang, M. L., Hotchkiss, M. W., and Pederson, G. A. (2005). Assessment of the genetic diversity and phylogenetic relationships of a temperate bamboo collection by using transferred EST-SSR markers. *Genome* 48 (4), 731–737. doi: 10.1139/g05-022

Cai, Z. M., Zhang, Y. X., Zhang, L. N., Gao, L. M., and Li, D. Z. (2012). Testing four candidate barcoding markers in temperate woody bamboos (Poaceae: Bambusoideae). *J. Systematics Evol.* 50 (6), 527–539. doi: 10.1111/j.1759-6831.2012.00216.x

Chen, Y. F. (2018). *Study on sampling strategy of* chimonobambusa utilis *based on genetic diversity* (Guizhou: Guizhou University, Guiyang).

Chen, X. D., Yang, J., Guo, Y. F., Zhao, Y. M., Zhou, T., Zhang, X., et al. (2021). Spatial genetic structure and demographic history of the dominant forest oak *Quercus fabri* hance in subtropical China. *Front. Plant Sci.* 11. doi: 10.3389/fpls.2020.583284

Cornuet, J. M., and Luikart, G. (1996). Description and power analysis of two tests for detecting recent population bottlenecks from allele frequency data. *Genetics.* 144 (4), 2001–2014. doi: 10.1093/genetics/144.4.2001

Das, M., Bhattacharya, S., Basak, J., and Pal, A. (2007). Phylogenetic relationships among the bamboo species as revealed by morphological characters and polymorphism analyses. *Biol. Plant* 51, 667–672. doi: 10.1007/s10535-007-0140-7

Djedid, I. K., Terzaghi, M., Brundu, G., Cicatelli, A., Laouar, M., et al. (2022). Genetic diversity and differentiation of eleven medicago species from campania region revealed by nuclear and chloroplast microsatellites markers. *Plant Genet. Genomics* 13 (1), 97. doi: 10.3390/genes13010097

Du, H., Liu, L., Su, L., Zeng, F. P., Wang, K. L., Peng, W. X., et al. (2019). "Seasonal changes and vertical distribution of fine root biomass During vegetation restoration in a karst area, Southwest China. *Front. Plant Sci.* 9, 2001. doi: 10.3389/fpls.2018.02001

Earl, D. A. (2012). STRUCTURE HARVESTER: a website and program for visualizing STRUCTURE output and implementing the evanno method. *Conserv. Genet. Resour.* 4 (2), 359–361. doi: 10.1007/s12686-011-9548-7

Evanno, G., Regnaut, S., and Goudet, J. (2005). Detecting the number of clusters of individuals using the software structure: a simulation study. *Mol. Ecol.* 14 (8), 2611–2620. doi: 10.1111/j.1365-294X.2005.02553.x

Excoffier, L., and Lischer, H. E. (2010). Arlequin suite ver 3.5: a new series of programs to perform population genetics analyses under Linux and windows. *Mol. Ecol. Resour.* 10 (3), 564–567. doi: 10.1111/j.1755-0998.2010.02847.x

Hamrick, J. L., and Godt, M. J. W. (1996). Effects of life history traits on genetic diversity in plant species. *Philos. Trans. Biol. Sci.* 351 (1345), 1291–1298. doi: 10.1098/rstb.1996.0112

Hatmaker, E. A., Staton, M. E., Dattilo, A. J., Hadziabdic, Đ., Rinehart, T. A., Schilling, E. E., et al. (2018). Population structure and genetic diversity within the endangered species pityopsis ruthii (Asteraceae). *Front. Plant Sci.* 9, 943. doi: 10.3389/fpls.2018.00943

Kalinowski, S. T., Taper, M. L., and Marshall, T. C. (2007). Revising how the computer program CERVUS accommodates genotyping error increases success in paternity assignment. *Mol. Ecology.* 16 (5), 1099–1106. doi: 10.1111/j.1365-294X.2007.03089.x

Kang, M., Tao., J., Wang, J., Ren, C., Qi, Q. W., Xiang, Q. Y., et al. (2014). Adaptive and nonadaptive genome size evolution in karst endemic flora of China. *New Phytologist.* 202 (4), 1371–1381. doi: 10.1111/nph.12726

Lanes, É.C., Pope, N. S., Alves, R., Carvalho Filho, N. M., Giannini, T. C., Giuliettiet, A. M., et al. (2018). Landscape genomic conservation assessment of a narrow-endemic and a widespread morning glory from Amazonian savannas. *Front. Plant Sci.* 9, 532. doi: 10.3389/fpls.2018.00532

Li, T. (2008). *Research and application of EST-SSR marker in bambuseae taxonomy* (Zhejiang: Zhejiang UniversityUniversity, Hangzhou.).

Librado, P., and Rozas, J. (2009). DnaSP v5: a software for comprehensive analysis of DNA polymorphism data. *Bioinformatics.* 25 (11), 1451–1452. doi: 10.1093/bioinformatics/btp187

Li, S., Liu, S. L., Pei, S. Y., Ning, M. M., and Tang, S. Q. (2020). Genetic diversity and population structure of *Camellia huana* (Theaceae), a limestone species with narrow geographic range, based on chloroplast DNA sequence and microsatellite markers. *Plant Diversity.* 42 (5), 343–350. doi: 10.1016/j.pld.2020.06.003

Liu, Y. T., Ruan, H. X., Liu, J., Gao, M., Huang, Y., and Zhang, R. H. (2013). Antimutagenic effect of *Chimonobambusa utilis* in tongzi county of guizhou province. *J. Chin. J. Public Health Engineering.* 12, 365–367+371.

Liu, Y., Yang, S. X., Ji, P. Z., and Gao, L. Z. (2012). Phylogeography of camellia taliensis (Theaceae) inferred from chloroplast and nuclear DNA: insights into evolutionary history and conservation. *BMC Evol. Biol* 12, 92. doi: 10.1186/1471-2148-12-92

Liu, W. F., Zhang, L., Cui, X., Li, W., Zhang, W. B., and Wang, Y. H. (2018). Pyrolysis of *Chimonobambusa utilis* (Keng) keng f. and characteristics of its carbonization products. *J. Bamboo Res.* 37, 85–92. doi: 10.19560/j.cnki.issn1000-6567.2018.03.014

Li, M., Xie, D., Xie, C., Deng, Y., Zhong, Y., Yu, Y., et al. (2019). A phytogeographic divide along the 500 mm isohyet in the qinghai-Tibet plateau: Insights from the phylogeographic evidence of Chinese *Alliums* (Amaryllidaceae). *Front. Plant Sci.* 10, 149. doi: 10.3389/fpls.2019.00149

Li, G. J., Xu, Y. X., Zhang, T. H., Deng, G., Liang, Y., Luo, D. Y., et al. (2015). Preventive effect of fermented square bamboo shoots on constipation induced by montmorillonite powder. *J. Southwest China Normal University.* 40, 36–41. doi: 10.13718/j.cnki.xsxb.2015.04.008

Lou, Y. L. (2021). Investigation of workable soil characteristics and morphological diversity of *Chimonobambusa utilis*. *J. World Bamboo Rattan.* 19, 48–52.

Lou, Y. L., Chen, R. X., Zhang, G., Hu, G., Tan, L., Chen, C., et al. (2021). Afforestation effect of *Chimonobambusa utilis* at forestland of different types in bamboo forest park in central guizhou province. *World Bamboo Rattan.* 19, 61–64.

Mukherjee, A. K., Ratha, S., Dhar, S., Debata, A. K., Acharya, P. K., Mandal, S., et al. (2010). Genetic relationships among 22 taxa of bamboo revealed by ISSR and EST-based random primers. *Biochem. Genet.* 48 (11–12), 1015–1025. doi: 10.1007/s10528-010-9390-8

Oumer, O. A., Tesfaye, K., Feyissa, T., Yibeyen, D., Durai, J., Hyder, M. Z., et al. (2021). CpDNA-gene- sequence-based genetic diversity, population structure, and gene flow analysis of Ethiopian lowland bamboo (Bambusinea: *Oxytenanthera abyssinica* (A. rich.) Munro). *Int. J. Forestry Res.* 1, 1–13. doi: 10.1155/2021/9976087

Peakall, R., and Smouse, P. E. (2012). GenAlEx 6.5: genetic analysis in excel. population genetic software for teaching and research: an update. *Bioinformatics.* 28 (19), 2537–2539. doi: 10.1093/bioinformatics/bts460

Petit, R. J., Duminil, J., Fineschi, S., Hampe, A., Salvini, D., and Vendramin, G. G. (2005). Comparative organization of chloroplast, mitochondrial and nuclear diversity in plant populations. *Mol. Ecol.* 14 (3), 689–701. doi: 10.1111/j.1365-294X.2004.02410.x

Pons, O., and Petit, R. J. (1996). Measuring and testing genetic differentiation with ordered versus unordered alleles. *Genetics.* 144 (3), 1237–1245. doi: 10.1093/genetics/144.3.1237

Pritchard, J. K., Wen, X., and Falush, D. (2009). "STRUCTURE ver. 2.3," in *Http://pritch.bsd.uchicago.edu* (Chicago, IL: University of Chicago).

Qiu, E. F., Hong, W., and Zheng, Y. S. (2001). Review on diversity and utilization of bamboo in China. *J. Bamboo Res.* 2, 11–14.

Rao, N. K. (20042004). Plant genetic resources: Advancing conservation and use through biotechnology. *Afr. J. Biotechnol.* 3 (2), 136–145. doi: 10.5897/AJB2004.000-2025

Ren, C. C., Jia, Y. L., Lou, Y. L., Qiao, S. Y., Xu, W. J., and Qin, L. K. (2021). Analysis of nutritional and functional components of bamboo shoots in *Chimonobambusa utilis*, Guizhou. *Food Ferment. Indus.* 47 (10), 214–221. doi: 10.13995/j.cnki.11-1802/ts.026330

Ren, G. P., Mateo, R. G., Liu, J., Suchan, T., Alvarez, N., et al. (2017). Genetic consequences of quaternary climatic oscillations in the Himalayas: *Primula tibetica* as a case study based on restriction site-associated DNA sequencing. *New Phytol.* 213 (3), 1500–1512. doi: 10.1111/nph.14221

Shen, Y. F., Hui, X., Tu, Z. H., Zong, Y. X., Yang, L. C., Li, H. G., et al. (2022). Genetic divergence and local adaptation of liriodendron driven by heterogeneous environments. *Mol. Ecol.* 31 (3), 916–933. doi: 10.1111/mec.16271

Tang, Z. S., Li, Z. Y., Ding, Y. P., and Yu, Y. P. (2019). Tiller planting technique of *Chimonobabusa utilis* mother bamboo under magnolia officinalis forest. *Modern Agric. Sci. Technology.* 23, 133–134.

Tian, X., and Wariss, H. M. (2021). The complete chloroplast genome sequence of *Metabriggsia ovalifolia* w. t. Wang (Gesneriaceae), a national key protected plant endemic to karst areas in China. *Mitochondrial DNA B Resour.* 6, 833–834. doi: 10.1080/23802359.2021.1884021

Xie, D. F., Li, M. J., Tan, J. B., Price, M., Xiao, Q. Y., Zhou, S. D., et al. (2017). Phylogeography and genetic effects of habitat fragmentation on endemic urophysa (Ranunculaceae) in yungui plateau and adjacent regions. *PloS One* 12 (10), e0186378. doi: 10.1371/journal.pone.0186378

Yeh, F. C., Yang, R., Boyle, T. J., Ye, Z., and Xiyan, J. M. (1997). *PopGene32, Microsoft windows-based freeware for population genetic analysis, version 1.32* (University of Alberta, Edmonton, Alberta, Canada: Molecular Biology and Biotechnology Centre).

Yu, H. B., Miao, S. Y., Xie, G. W., Guo, X. Y., Chen, Z., Favre, A., et al. (2020). Contrasting floristic diversity of the hengduan mountains, the Himalayas and the qinghai-Tibet plateau sensu stricto in China. *Front. Ecol. Evol.* 8, 136. doi: 10.3389/fevo.2020.00136

Zhang, D., Gao, F., Li, W. X., Jakovlić, I., Zou, H., Zhang, J., et al. (2019). PhyloSuite: an integrated and scalable desktop platform for streamlined molecular sequence data management and evolutionary phylogenetics studies. *Mol. Ecol. Resour.* 20 (1), 348–355. doi: 10.1111/1755-0998.13096

Zhao, J. L., Paudel, B. R., Yu, X. Q., Zhang, J., and Li, Q. J. (2021). Speciation along the elevation gradient: divergence of roscoea species within the south slope of the Himalayas. *Mol. Phylogenet. Evolution.* 164, 107292. doi: 10.1016/j.ympev.2021.107292

Zhu, X., Dai, Z. X., Wang, D., Liu, Y. J., and Gou, G. Q. (2021). Study on the grading standard of annual container seedlings of phyllostachys edulis and *Chimonobambusa utilis*. *J. Mountain Agric. Biol.* 40, 48–53.

frontiers | Frontiers in Plant Science

TYPE Original Research
PUBLISHED 15 November 2022
DOI 10.3389/fpls.2022.1000160

OPEN ACCESS

EDITED BY
Shunli Wang,
Chinese Academy of Agricultural Sciences (CAAS), China

REVIEWED BY
Xiangtao Zhu,
Zhejiang Agriculture and Forestry University, China
Weibing Zhuang,
Jiangsu Province and Chinese Academy of Sciences, China

*CORRESPONDENCE
Ming Sun
sun.sm@163.com
Xiaoying Yu
475705701@qq.com
Yanlin Li
liyanlin@hunau.edu.cn

†These authors have contributed equally to this work and share first authorship

SPECIALTY SECTION
This article was submitted to Plant Breeding, a section of the journal Frontiers in Plant Science

RECEIVED 21 July 2022
ACCEPTED 01 November 2022
PUBLISHED 15 November 2022

CITATION
Zhang D, Chen Q, Zhang X, Lin L, Cai M, Cai W, Liu Y, Xiang L, Sun M, Yu X and Li Y (2022) Effects of low temperature on flowering and the expression of related genes in *Loropetalum chinense* var. *rubrum*. *Front. Plant Sci.* 13:1000160. doi: 10.3389/fpls.2022.1000160

Effects of low temperature on flowering and the expression of related genes in *Loropetalum chinense* var. *rubrum*

Damao Zhang[1,2,3†], Qianru Chen[1,2,3†], Xia Zhang[1,2,3], Ling Lin[4], Ming Cai[5], Wenqi Cai[1,2,3], Yang Liu[1,2,3], Lili Xiang[1,2,3], Ming Sun[5*], Xiaoying Yu[1,2,3*] and Yanlin Li[1,2,3,6*]

[1]Hunan Agricultural University, College of Horticulture, Changsha, Hunan, China, [2]Engineering Research Center for Horticultural Crop Germplasm Creation and New Variety Breeding, Ministry of Education, Changsha, China, [3]Hunan Mid-Subtropical Quality Plant Breeding and Utilization Engineering Technology Research Center, Changsha, China, [4]School of Economics, Hunan Agricultural University, Changsha, China, [5]Beijing Key Laboratory of Ornamental Plants Germplasm Innovation and Molecular Breeding, National Engineering Research Center for Floriculture, Beijing Laboratory of Urban and Rural Ecological Environment, Key Laboratory of Genetics and Breeding in Forest Trees and Ornamental Plants of Ministry of Education, School of Landscape Architecture, Beijing Forestry University, Beijing, China, [6]Kunpeng Institute of Modern Agriculture, Foshan, China

Introduction: *Loropetalum chinense* var. *rubrum* blooms 2-3 times a year, among which the autumn flowering period has great potential for exploitation, but the number of flowers in the autumn flowering period is much smaller than that in the spring flowering period.

Methods: Using 'Hei Zhenzhu' and 'Xiangnong Xiangyun' as experimental materials, the winter growth environment of *L. chinense* var. *rubrum* in Changsha, Hunan Province was simulated by setting a low temperature of 6-10°C in an artificial climate chamber to investigate the effect of winter low temperature on the flowering traits and related gene expression of *L. chinense* var. *rubrum*.

Results: The results showed that after 45 days of low temperature culture and a subsequent period of 25°C greenhouse culture, flower buds and flowers started to appear on days 24 and 33 of 25°C greenhouse culture for 'Hei Zhenzhu', and flower buds and flowers started to appear on days 21 and 33 of 25°C greenhouse culture for 'Xiangnong Xiangyun'. The absolute growth rate of buds showed a 'Up-Down' pattern during the 7-28 days of low temperature culture; the chlorophyll fluorescence decay rate (Rfd) of both materials showed a 'Down-Up-Down' pattern during this period. The non-photochemical quenching coefficient (NPQ) showed the same trend as Rfd, and the photochemical quenching coefficient (QP) fluctuated above and below 0.05. The expression of *AP1* and *FT* similar genes of *L. chinense* var. *rubrum* gradually increased after the beginning of low temperature culture, reaching the highest expression on day 14 and day 28, respectively, and the expression of both in the experimental group was higher than that in the control group. The expressions of *FLC*, *SVP* and *TFL1* similar genes all decreased gradually with low

temperature culture, among which the expressions of *FLC* similar genes and *TFL1* similar genes in the experimental group were extremely significantly lower than those in the control group; in the experimental group, the expressions of *GA3* similar genes were all extremely significantly higher than those in the control group, and the expressions all increased with the increase of low temperature culture time.

Discussion: We found that the high expression of gibberellin genes may play an important role in the process of low temperature promotion of *L. chinense* var. *rubrum* flowering, and in the future, it may be possible to regulate *L. chinense* var. *rubrum* flowering by simply spraying exogenous gibberellin instead of the promotion effect of low temperature.

KEYWORDS

low temperature, flowering, bud, gibberellin, FLC, FT, Ap1

1. Introduction

Loropetalum chinense var. *rubrum*, an evergreen shrub or small tree (Xia et al., 2020), which with bright leaves and as an important landscape application tree species in Hunan and even the middle and lower reaches of the Yangtze River (Runmin and Xiaoying, 2012). The flower color of *L.chinense* var. *rubrum* is absolutely gorgeous (Zhang et al., 2022)and annual flowering 2-3 times. The spring flowers is in March-April, while autumn flowers are in October-November. Although the large amount of flowers opened in spring, the flowering period of *L.chinense* coincides with other ornamental plants, which resulting in no competitive advantage in the application direction of flowering. The autumn flowering period coincides with the National Day, and its bright red flower color complements the atmosphere of the National Day celebration, which provides a new idea for the development of its flowering value. However, the number of spring flowers is much larger than that of autumn flowers in the natural environment (Bao et al., 2007). Whether this phenomenon is related to the low temperature in winter has not yet been proved. Clarifying this relationship has certain help for the excavation of the flower value of *L.chinense* var. *rubrum.*

Numerous studies have shown that photoperiod and low temperature induction are the main inducers of flowering in most plants, and that changes in these environmental conditions ultimately regulate flowering through substances in the leaves called 'florigen' (Taoka et al., 2013). Low temperature in winter is an important environmental condition for inducing and accelerating the flowering of many plants (Lina et al., 2003; Zhonghua et al., 2006). Plants start the transformation from vegetative growth to reproductive growth under the induction of low temperature, which is also called vernalization (Alexandre and Hennig, 2008). *FLC* plays an important role in floral transition by encoding a MADS-box transcription factor (Changsheng et al., 2021). It was shown that the expression of the *FLC*-like gene *VRN2* was suppressed in wheat leaves after vernalization induction, reducing the suppression of a MADS box protein-containing *VRN1* gene (with high homology to the downstream flowering regulator *AP1* in Arabidopsis) in leaves, thereby promoting flowering (Yan et al., 2004). The results showed that the transcription level of *FLC* gene was higher in cabbage without vernalization. At this time, cabbage showed late flowering traits. After 10 days of induction at 4°C, the expression level of *FLC* gene in cabbage with early flowering traits decreased significantly (Kim et al., 2007; Kitamoto et al., 2013). During vernalization, *FLC* not only suppresses the transcriptional expression of *FT* by binding to the promoter of the downstream gene *FT*, but also hinders the regulation of the floral meristem gene *AP1* by *FT* and inhibits the flower-forming transition, but also binds to the transcription factor *SVP* to form heterodimer, which jointly negatively regulates the expression of *FT* gene, thereby inhibiting flowering (Mateos et al., 2015; Luo et al., 2019; Kinmonth-Schultz et al., 2021). *FT* gene can also inhibit the expression of *FLC* gene in vegetative and reproductive growth stages, especially in seed development stages (Chen and Penfield, 2018). In 2007, it was shown that FT proteins in leaves are 'florigen' that bind to FD proteins in stem tips and promote the expression of genes in downstream floral meristems, thus promoting flowering (Taoka et al., 2011). *FT* and *TFL1* belong to the same family of PEBPs and share 98% amino acid sequence similarity, but they have opposing functions (Kobayashi et al., 1999; Karlgren et al., 2011; Sriboon et al., 2020). The balance

between *FT* and *TFL1* determines the early and late flowering of pear trees, and they are antagonistic. The flowering time is controlled by the combination of competition and *FD* to activate the transcription and expression of downstream floral meristem gene *AP1* (Abe et al., 2005; Hanano and Goto, 2011; Ito et al., 2022). AP1 gene, as an important member of the ABCDE model of floral development, which can identify and accept a large number of signal pathways. These signals can guide floral meristem development into flowers by inhibiting or promoting the expression of *AP1* (Wellmer and Riechmann, 2010; O'Maoileidigh et al., 2014).

The initiation of flower bud differentiation marks the transition of plants from vegetative growth to reproductive growth. In this process, a large number of nutrients, endogenous hormones and other contents are changed (Blázquez et al., 1998; Han et al., 2016; Rizza and Jones, 2019). The changes in gibberellin content are interspersed throughout the developmental stages of flowers and make a difference (Shihao et al., 2008; Wang et al., 2015). When exogenous gibberellin is applied, it induces flowering in long-day plants instead of low temperature, while when endogenous *GA* synthesis is blocked, flowering is delayed (Qiaoxia et al., 2019). This is the well-known gibberellin pathway that promotes flowering by inhibiting *SVP* gene expression and positively regulating *FT* and *SOC1* genes (Mateos et al., 2015). At the same time, the increase of gibberellin content in the process of flowering induction can improve the photosynthetic capacity of plant leaves (Weicai et al., 2014), then providing more energy for the flowering process and ensuring the successful completion of the flowering process (Christiaens et al., 2015).

This experiment was conducted with a new varieties of *L.chinense* and a *L.chinense* var. *rubrum*, and the experiment was carried out after the end of their autumn flowering period. The low-temperature environmental conditions in winter were simulated by low-temperature incubation at 6-10°C, and the effect of winter low temperature on the flowering of red frond was initially investigated by combining parameters such as the number of flowers, chlorophyll fluorescence parameters, and the expression of related genes.

2. Materials and methods

2.1 Materials

The experimental materials included a new variety 'Xiangnong Xiangyun' selected by Hunan Agricultural University (variety registration number: 20201102, variety registration agency: State Forestry and Grassland Administration) and 'Hei Zhenzhu'. Among them, 'Xiangnong Xiangyun' is the *L. chinense* of the *Loropetalum*, which blooms 1-2 times a year, with a large number of flowers, and the petal color is pure white or light beige; 'Hei Zhenzhu' is the *L.chinense* var. *rubrum* of the *Loropetalum*, which blooms 1-2 times a year, blooms in large numbers, and the petal color is magenta or rose. All experimental materials were the progeny of cuttings from both cultured for two years with stable genetic background. The experimental sites include the artificial climate room at Hunan Agricultural University (Room 007, 11th Teaching Building, Hunan Agricultural University) and the intelligent greenhouse in the flower base of Hunan Agricultural University.

The experiment started in November 2020 after the end of the autumn flowering period of Loropetalum Chinense.Eight pots each of 'Xiangnong Xiangyun' and 'Hei Zhenzhu' with good growth and consistent crown size were selected and numbered X.T1-X.T8 and H.T1-H.T8, respectively. After 5 days of gradient low temperature exercise (Starting from 25°C, adjust the parameters of the artificial climate chamber to reduce the ambient temperature by 3°C per day and end with 10°C), the above 16 pots of material were sequentially transferred to the artificial climate chamber for low temperature culture. The artificial climate chamber was set for a total of five cycles, 8:00-12:00, 8°C, light; 12:00-14:00, 10°C, light; 14:00-18:00, 8°C, light; 18:00-8:00 the next day, 6°C, dark. At the same time, the ambient temperature in the smart greenhouse was maintained at 25°C. After 42 days of continuous incubation in the artificial climate chamber, the plants were moved into the smart greenhouse sequentially after 3 days of gradient warming in the artificial climate chamber and incubated in the same environment as the control plants for subsequent observation (Starting from 10°C, adjust the parameters of the artificial climate chamber to increase the ambient temperature by 5°C per day and end with a warming of 25°C).During the experimental cycle, the water and fertilizer management was kept consistent for all plants, watering once every 3 days and fertilizing moderately once every 15 days.

2.2 Methods

2.2.1 Observation of buds

After the experiment started, the maximum transverse diameter and the longest longitudinal diameter of their shoots were measured sequentially every 7 days using a digital vernier caliper, and the shoots from the same part of the same plant were taken each time and repeated three times and recorded. After the low-temperature culture ended and the room-temperature culture started, the status of each plant bud was observed once every 3 days, and the number and time of present buds and flowers were recorded.

2.2.2 Determination of chlorophyll fluorescence parameters

Chlorophyll fluorescence parameters were measured randomly every 3 days after the start of the experiment using a hand-held chlorophyll fluorometer on leaves from the same

location of the same plant. For the measurement, the leaves to be measured are first held in a dark adaptation using a leaf clamp for 30 minutes. After dark adaptation, chlorophyll fluorescence parameters were measured sequentially using the 'OJIP' and 'NPQ3' programs in the instrument, and each measurement was repeated three times.

2.2.3 Detection of gene expression

During the experiment, 7-8 pieces of apical leaves from different plants of the same species were taken every 7 days in lyophilization tubes, snap-frozen in liquid nitrogen and stored in an ultra-low temperature refrigerator at -80°C. Two tubes were sampled and stored each time. Refer to the StarSpin HiPure Plant RNA Mini Kit (GeneStar, Beijing) kit instructions to extract total RNA. The cDNA was synthesized by referring to the Evo M-MLV (Ekore, Hunan) reverse transcription kit instructions. And we compared the protein sequences of the related genes of *L.chinense* var. *rubrum* in NCBI (https://www.ncbi.nlm.nih.gov/Structure/bwrpsb/bwrpsb.cgi), and preliminarily identified the similar functions of the related genes and similar genes through the protein domain, and the identification results were provided in the form of supplementary figures, primers were designed using Beacon Designer 8 (Table 1).The PCR reaction system was 2X SYBR Green Pro Taq HS Premix*5μL, 0.8μL each of upstream and downstream primers (10μmol/L), 1μL of cDNA, and ddH2O to make up to 10μL.PCR amplification conditions were: step 1, 95°C for 30 seconds, step 2, 95°C for 5 seconds, 60°C for 30 seconds, 72°C for 10 minutes for 40 cycles, 65°C for 5 seconds, 95°C for 5 seconds, 3 repetitions, and the relative expression of the target gene was calculated according to the $2^{-\Delta Ct}$ method.

2.3 Statistical analysis

The experimental data were statistically analyzed using SPAS 22.0, the Duncan method was used for multiple comparisons, Origin 2019b was used for graph drawing.

3 Results

3.1 Effect of low temperature on flowering

Combined with Tables 2 and 3, 'Xiangnong Xiangyun' and 'Hei Zhenzhu', which were cultured at low temperature and then at room temperature, were able to flower, and both had the maximum number of flower buds of 33 and 22 on days 27 and 30, respectively, after being cultured at room temperature. The maximum number of flowering was 39 and 16 on day 36, respectively. The flowering process was the same for both, but 'Xiangnong Xiangyun' had more buds and flowers than 'Hei

TABLE 1 Real-time fluorescence quantitative PCR primer information for *L.chinense* var. *rubrum*.

Gene type	Gene		Primer sequence (5′-3′)
Internal reference genes	β-actin2	F	CCACAAGGCTTATTGATAGAAT
		R	CAATGGTTGAACCTGAATACT
AP1-like gene	augustus40012	F	CCAGCTTGATAATGCTCTTAA
		R	GTGCCTTCTCCTTCTCTT
FT-like genes	augustus63326	F	ATCTTAGGACCTTCTACACTC
		R	AATATCAGTCACCAACCAATG
	augustus34660	F	GTCTCTACCGATCTCTACAC
		R	CTTCTGGAATGTCAACAACA
SVP-like gene	augustus15211	F	CAGCCATCTCCATCTCTT
		R	ACACGACTCAATCCAACT
FLC-like gene	augustus27517	F	GTTTCTTCCTCAAATTCAACTTT
		R	CTACCATCCTCATTATTCTTCTTAT
TFL1-like gene	augustus62587	F	CTAGAAGAGAGGTGGTGAC
		R	CAGTGAAGAAGGTGGAGTA
GA-like genes	augustus49213	F	CACATTCTCGGCATTATCAA
		R	TCACCACCTTGTCTTCTC
	augustus58706	F	TCCTACCTCCTTAACTATACTTC
		R	CCTGTTCACTATTGCTCTATG
	augustus63711	F	GGTGAGCACTGTGGATAT
		R	CCTCGCAATAGTCCTGAT

TABLE 2 Number of flower buds and time to bud emergence under normothermic (25°C) culture after low-temperature induction.

Date	Time/day	Number of flowering bud	
		Hei Zhenzhu	Xiangnong Xiangyun
20210108	20	0	0
20210109	21	0	6
20210112	24	5	13
20210115	27	21	33
20210118	30	22	32
20210121	33	14	25
20210124	36	4	3
20210125	37	0	0

No flower buds were seen for the two experimental materials that were continuously incubated at 25°C throughout the experimental cycle.

Zhenzhu'. In contrast, the two experimental materials, which were continuously cultured at 25°C, did not show buds or flowers throughout the experimental cycle.

3.2 Effect of low temperature on bud growth rate and photosystem

From Figure 1, the absolute growth rates of 'Xiangnong Xiangyun' and 'Hei Zhenzhu' showed a 'Up-Down' pattern during the 7-28 days of low temperature culture, after which the absolute growth rates of shoots continued to increase. In combination with the Rfd curve of chlorophyll fluorescence decay rate (right 1) and the NPQ curve of non-photochemical quenching coefficient (middle) in Figure 2, the Rfd curves of 'Xiangnong Xiangyun' and 'Hei Zhenzhu' showed an overall pattern of 'Down-Up- Down'. And reached a higher level on day 21 of this period, the trend of NPQ curve was consistent with Rfd, and the value of photochemical quenching coefficient QP fluctuated regularly above and below 0.05.

3.3 Effect of low temperature on the expression of flowering-related genes

3.3.1 Effect of low temperature on *AP1* gene expression

The expression of agustus40012, a similar gene of *AP1* in *L. chinense* var. *rubrum*, was generally in an up-regulated state as the low-temperature induction time progressed. In particular, the expression reached the highest level in the leaves of 'Xiangnong Xiangyun' and 'Hei Zhenzhu' on day 14 after the beginning of low-temperature induction, the expression in the leaves of 'Xiangnong Xiangyun' is 7.74 times that of the T0 period (Figure 3A), and the expression in the leaves of 'Hei Zhenzhu' is 20.78 times that of the T0 period (Figure 3B), and the expression in the leaves of both reaches the highest state at this time. The expression at T28 was still 2.39 and 3.44 times higher than that at T0, which was still in an up-regulated expression state. Moreover, in the period from T7 to T28, the expression of this gene in the T group was significantly higher than that in the CK group. It can also be seen that in the CK group, the expression of AP1-like genes in the leaves of both

TABLE 3 Flowering number and flowering time under normothermic (25°C) culture after low-temperature induction.

Date	Time/day	Number of flowering bud	
		Hei Zhenzhu	Xiangnong Xiangyun
20210117	29	0	0
20210118	30	0	1
20210121	33	8	19
20210124	36	16	39
20210127	39	6	12
20210130	42	0	2
20210131	43	0	0

The two experimental materials incubated continuously at 25°C throughout the experimental cycle did not see flowering.

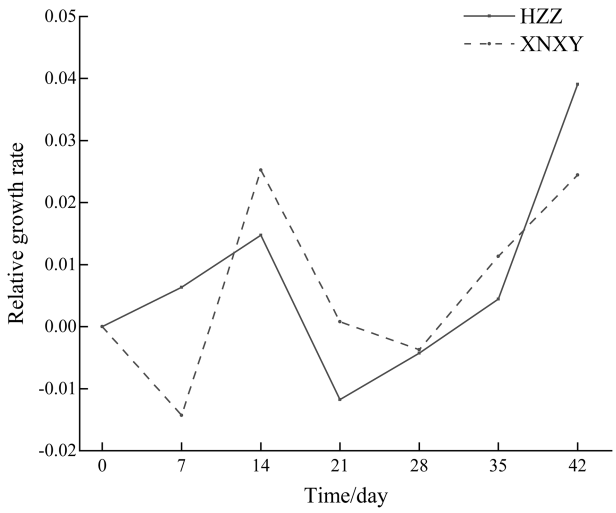

FIGURE 1
Absolute growth rate of shoots of 'Xiangnong Xiangyun' and 'Hei Zhenzhu' during low temperature culture. 'XNXY' stands for 'Xiangnong Xiangyun', 'HZZ' stands for 'Hei Zhenzhu'.

experimental subjects in the T0 period is higher than that in the T7 to T28 period.

3.3.2 Effect of low temperature on *FT* gene expression

Since the beginning of low temperature culture, *FT* similar genes in the low temperature treatment group had similar expression phenomena in 'Xiangnong Xiangyun' and 'Hei Zhenzhu'. Both genes showed up-regulated expression in general, but the expression of augustus63326 appeared to increase and then decrease during the low-temperature culture. In 'Xiangnong Xiangyun', the expression of augustus63326 was 2.63 times higher at T14 than at T0 and 2.52 times higher at T21 than at T0, and the gene had higher expression in both periods (Figure 4A1). In 'Hei Zhenzhu', augustus63326 is expressed 4.40 times more in the T14 period than in the T0 period, and augustus63326 is expressed in the T21 period is 5.28 times that in the T0 period, both of which also have higher expression (Figure 4B1). The expression of augustus63326 in both subjects decreased in the T28 period, but it was still 1.26 times and 2.56 times that of the T0 period. The expression of this gene in the T28 period was 68.79 times (Figure 4A2) and 6.50 times (Figure 4B2) higher than that in the T0 period, both reaching the highest values in 'Xiangnong Xiangyun' and 'Hei Zhenzhu'. At the same time, the expression of augustus34660 was significantly higher than that of the CK group in all periods under low temperature treatment. It can be found that except for augustus63326 of 'Xiangnong Xiangyun', the expression of FT-like genes in the low-

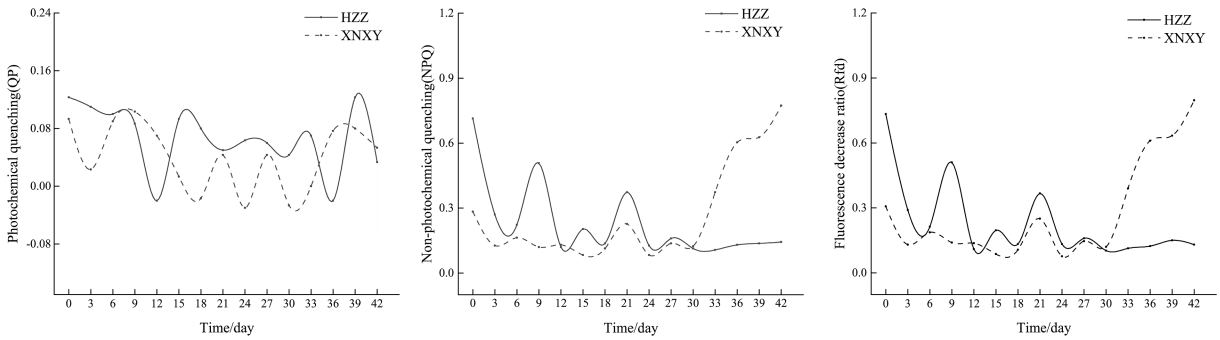

FIGURE 2
Changes in chlorophyll fluorescence parameters of 'Xiangnong Xiangyun' and 'Hei Zhenzhu' during low temperature culture. 'XNXY' stands for 'Xiangnong Xiangyun', 'HZZ' stands for 'Hei Zhenzhu'.

temperature treatment group was higher than that in the CK group in all periods.

3.3.3 Effect of low temperature on *SVP*, *FLC* and *TFL1* gene expression

After the experiment started, with the experimental time, the similar genes of *SVP* and *FLC* in the low temperature treatment group were consistently down-regulated in the leaves of 'Xiangnong Xiangyun' and 'Hei Zhenzhu'. The expression of augustus15211 reached the lowest expression at T21, 0.39 (Figure 5) and 0.42 (Figure 5) times that of T0, respectively. augustus27517 had lower expression at T28, 0.44 (Figure 5) and 2.64 (Figure 5) times that of T0, respectively, and The expression of augustus27517 was overall highly significant higher in the CK-treated group than in the low-temperature-treated group. Except for the T21 period, the expression of augustus62587, a similar gene of *TFL1*, was extremely significantly lower in both 'Xiangnong Xiangyun' and 'Hei Zhenzhu' under low temperature treatment than in the CK treatment group. In the T21 period, the expression of augustus62587 showed extreme values in both materials, at which time the highest expression of augustus62587 appeared in both materials under low temperature treatment, which were 1.27 (Figure 5) and 3.25 (Figure 5) times higher than in the T0 period, respectively. While the lowest expression of augustus62587 appeared in both materials in the CK group, which were 0.62 (Figure 5) and 2.33 (Figure 5) times higher than that in the T0 period, respectively.

3.3.4 Effect of low temperature on *GA* gene expression

Overall, the expression of the similar genes of *GA* in the low-temperature treatment group increased sharply within 7 days after the start of the low-temperature treatment. Among the three, except for augustus58706, the expression of the other two genes under low temperature treatment was very different from that in the period before low temperature treatment was started, and the extreme values were: the expression in the T7 period was 28.50 times that of the T0 period (Figure 6A1), the expression in the T14 period was 81.31 times that in the T0 period (Figure 6B1), and the expression in the T21 period was 26.81 times that in the T0 period (Figure 6A3), The expression in the T28 period is 6.13 times that in the T0 period (Figure 6B3). The expression of augustus58706 under low temperature treatment was not much different from that in the non-low temperature treatment period, and the highest expression was 2.09 times (Figure 6A2) and 1.13 times (Figure 6B2) of the T0 period, respectively. In general, the expression of the T group was significantly higher than that of the CK group in all periods. It can also be seen that the expression of all three in the CK group is at a very low level.

4 Discussion

On the one hand, some deciduous and evergreen plants escape the cold by losing their leaves and changing their leaf structure to minimize respiration and photosynthesis during winter (Oquist and Huner, 2003), and some plants, such as hostas (Hawryzki et al., 2011), escape the cold by cutting themselves above ground and keeping the lower part of the ground in a dormant state (Dogramaci et al., 2010; Yu et al., 2010). On the other hand, through long-term adaptation, most plants have evolved a trait that needs to be induced by low winter

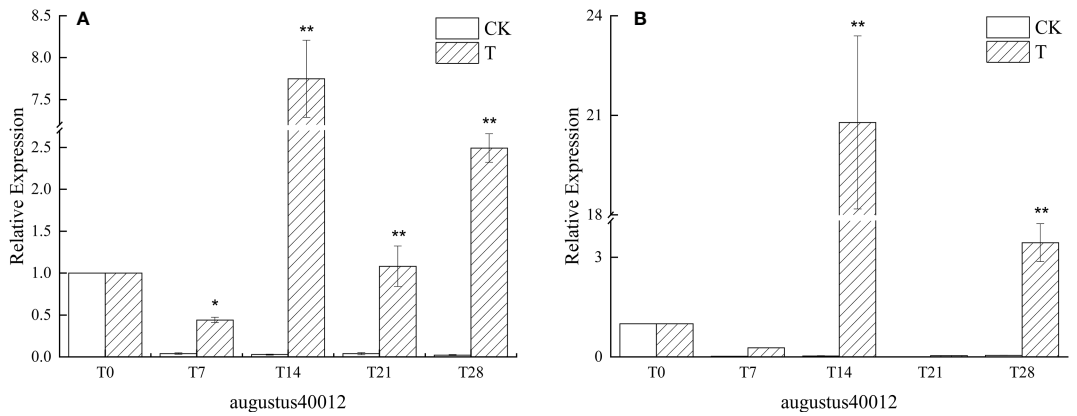

FIGURE 3
Relative expression of the similar gene augustus40012 of *AP1* in the leaves of plants with different treatments in *L. chinense* var. *rubrum*. '**(A)**' represents the relative expression of similar genes of *AP1* in leaves of 'Xiangnong Xiangyun' under different treatments. '**(B)**' represents the relative expression of similar genes of *AP1* in leaves of 'Hei Zhenzhu' under different treatments. 'T' represents the low-temperature treatment group and 'CK' represents the blank control group treated at 25°C. '*' significant difference, '**' extremely significant difference.

10.3389/fpls.2022.1000160

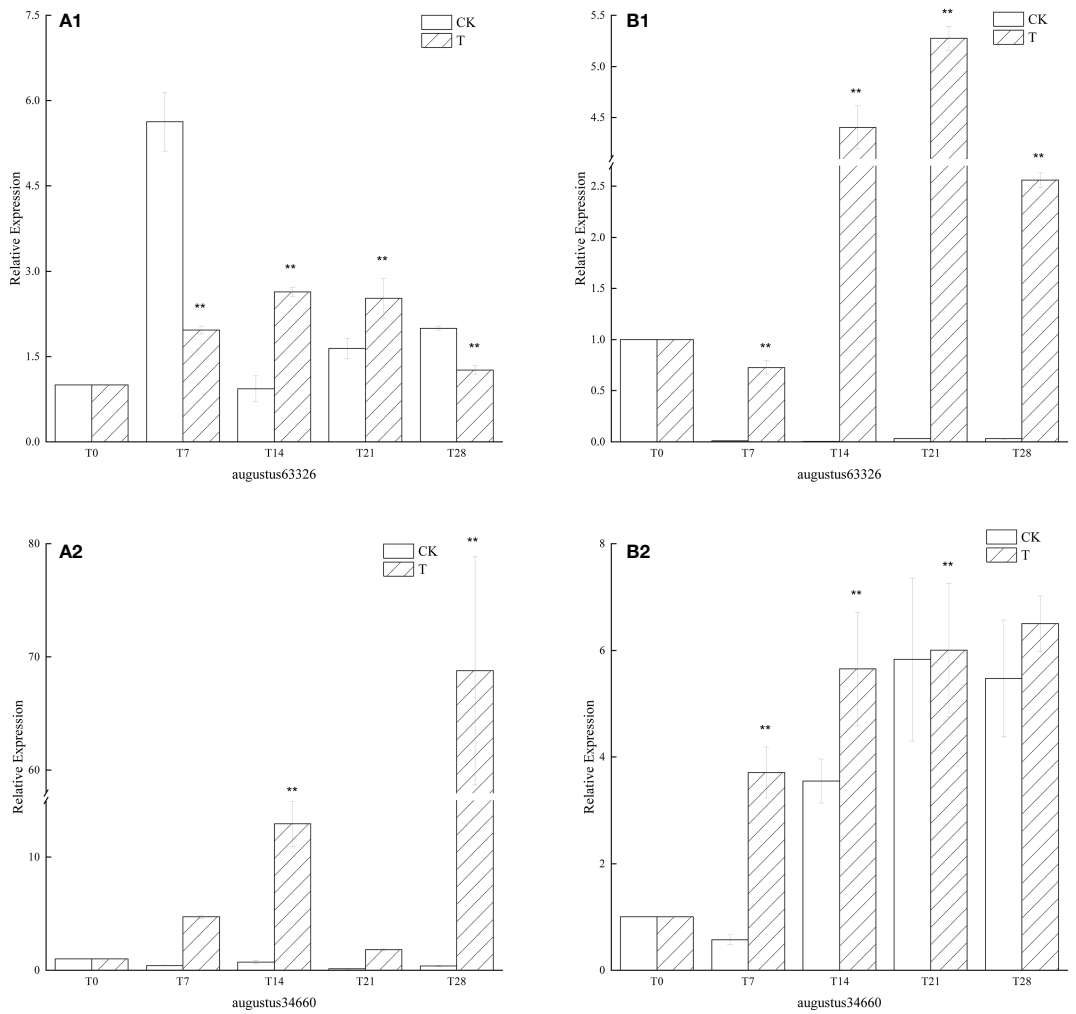

FIGURE 4
Relative expression of similar genes augustus63326 and augustus34660 of *FT* in the leaves of plants with different treatments in *L. chinense* var. *rubrum*. '**(A)**' represents the relative expression of similar genes of *FT* in leaves of 'Xiangnong Xiangyun' under different treatments. '**(B)**' represents the relative expression of similar genes of *FT* in leaves of 'Hei Zhenzhu' under different treatments. 'T' represents the low-temperature treatment group and 'CK' represents the blank control group treated at 25°C. ** extremely significant difference.

temperatures to flower and bear fruit, a phenomenon called vernalization.

In this study, it was found that after low-temperature induction, the *L. chinense* var. *rubrum* can still flower successfully even if the autumn flowering period has passed, while no flowering was seen in the same batch of *L. chinense* var. *rubrum* cultured at a constant temperature of 25°C. It shows that appropriate low-temperature induction can promote not only flowering and fruiting of some plants, but also flowering of *L. chinense* var. *rubrum*. Similarly, when Satsuma mandarins are grown continuously at 25°C, they have only nutritional growth, whereas when they are cultivated at a relatively low temperature of 15°C there is a distinction between nutritional and reproductive growth (Agusti et al., 2022). Combined with the absolute growth rate of buds in Figure 1, we found that when the low temperature started, the growth rate of buds was very low, and the plant responded to the low temperature environment by weakening its various physiological activities at low temperature (Sønstebya and Heideb, 2019), indicating that the various physiological activities of *L. chinense* var. *rubrum* itself had been weakened at this time. Subsequently, with the continuation of low temperature culture time, the growth rate of buds began to rise, at this time the *L. chinense* var. *rubrum* has adapted to the low temperature environment, and by the low temperature induced after the promotion of buds began to undergo transformation, in the low temperature buds from the

10.3389/fpls.2022.1000160

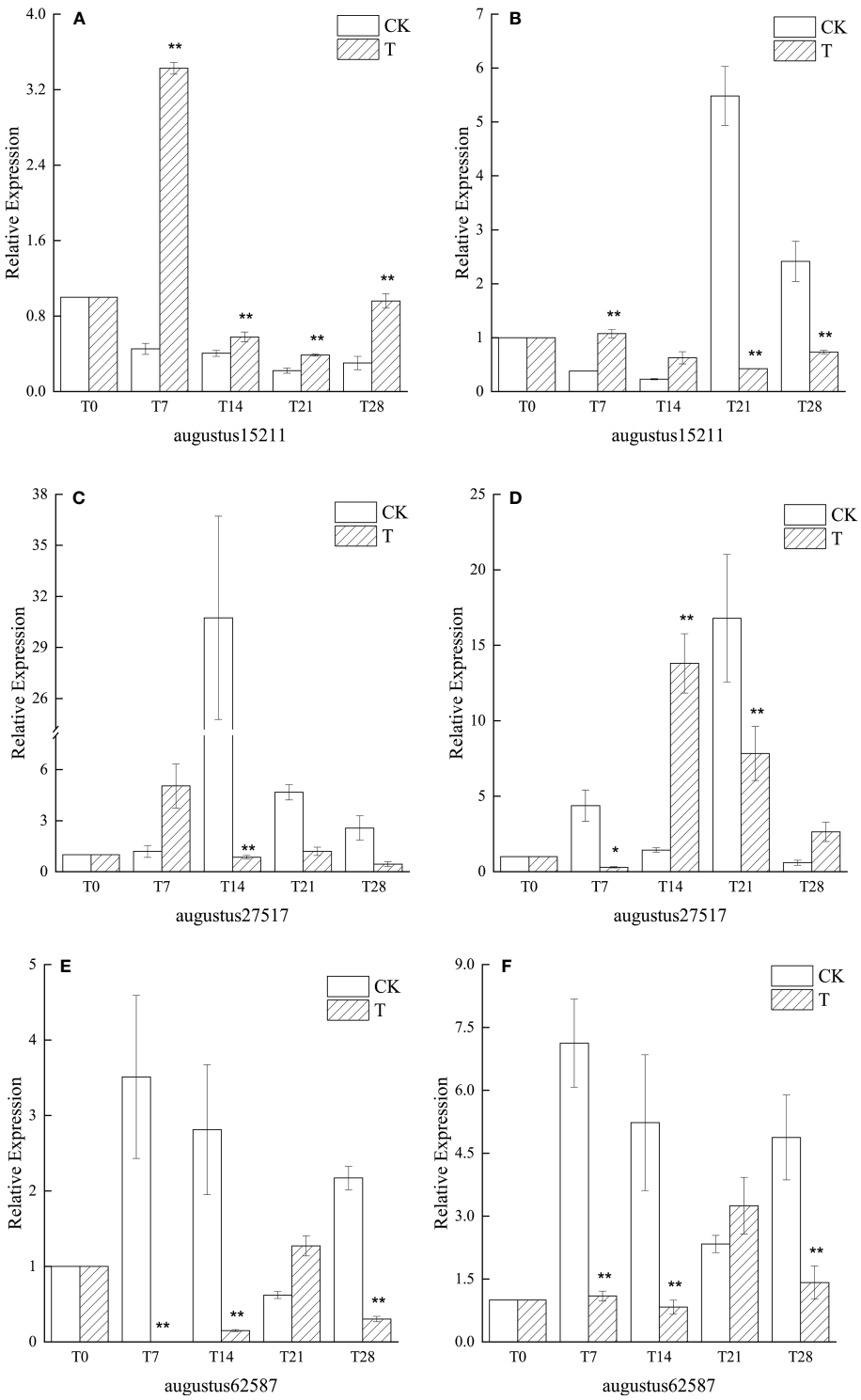

FIGURE 5
Relative expression of similar genes augustus15211, augustus27517, and augustus62587 of *SVP*, *FLC*, and *TFL1* in leaves of plants with different treatments of *L. chinense* var. *rubrum*. '**(A)**', '**(C)**' and '**(E)**' represent the relative expressions of *SVP*, *FLC* and *TFL1* similar genes in leaves of 'Xiangnong Xiangyun' under different treatments, respectively. '**(B)**', '**(D)**' and '**(F)**' represent the relative expression of similar genes of *SVP*, *FLC* and *TFL1* of 'Hei Zhenzhu' in leaves under different treatments, respectively. 'T' represents the low-temperature treatment group and 'CK' represents the blank control group treated at 25°C. '*' significant difference, '**' extremely significant difference.

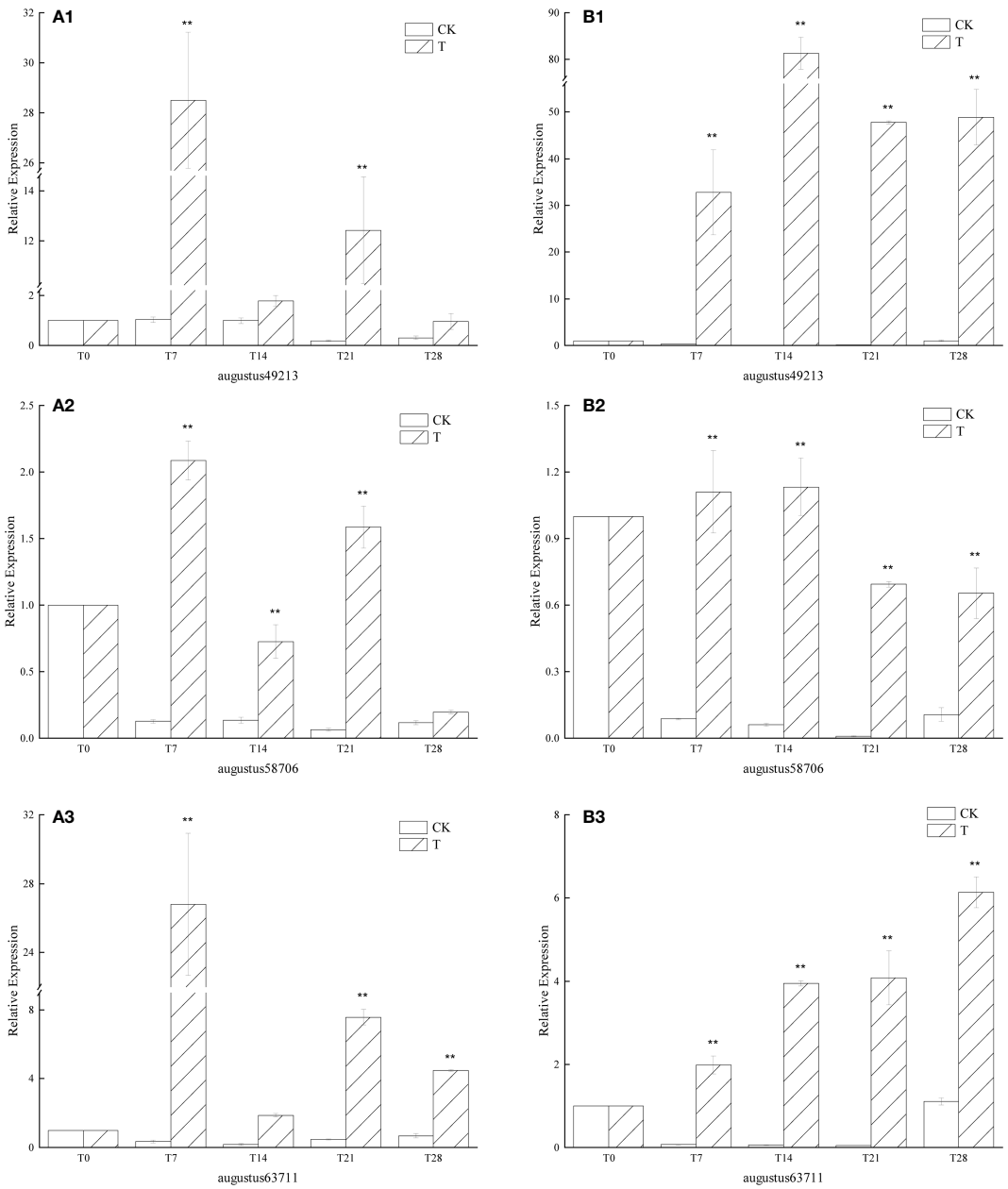

FIGURE 6
Relative expression of similar genes augustus49213, augustus58706 and augustus63711 of *GA* in the leaves of plants with different treatments of *L. chinense* var. *rubrum*. '**(A)**' represents the relative expression of *GA* similar genes in leaves of 'Xiangnong Xiangyun' under different treatments. '**(B)**' represents the relative expression of *GA* similar genes in leaves of 'Hei Zhenzhu' under different treatments. 'T' represents the low-temperature treatment group, 'CK'represents the blank control group treated at 25°C. ** extremely significant difference.

original dormant state or nutrient growth state to reproductive growth state. After that the growth rate of the buds of the *L. chinense* var. *rubrum* decreased and then increased again. During this stage, the buds may pass through a period of low temperature induction before first completing part of the process of transition to reproductive growth and then entering dormancy again. After a period of time, with the continuation of the low temperature induction, the buds are prompted to complete the subsequent stage of floral bud differentiation.

The inhibition of plant growth and physiological functions in low temperature environments is related to the reduction in the activity of photosystem II and photosystem I at low temperatures (Tang et al., 2020). The energy conversion efficiency of photosystem II can be visualized by chlorophyll

fluorescence parameters (Maxwell and Johnson, 2000), in agriculture, real-time monitoring of chlorophyll fluorescence parameters of crops enables accurate measurement of crop photosynthesis, allowing more accurate prediction of agricultural productivity and climate effects on crop yield. And the efficiency of photosystem II can usually be reflected by the value of Fv/Fm, while Rfd is a more sensitive indicator of plant vigor and photosynthetic rate than Fv/Fm (Lysenko et al., 2014; Shin et al., 2017). It can be seen that the Rfd values of the *L. chinense* var. *rubrum* in this experiment decreased sharply after the beginning of the experiment, indicating that the photosynthetic efficiency and physiological activities of the *L. chinense* var. *rubrum* at the initial stage of low temperature decreased rapidly, which is consistent with the result that the growth rate of the buds of the *L. chinense* var. *rubrum* decreased at the beginning of the experiment. From the 6th day of the experiment, the trend of Rfd was opposite to the growth rate of the shoots, and the growth rate of the shoots started to decrease when the value of Rfd increased. When plants suddenly enter reproductive growth, nutritional growth will suffer inhibition, inhibited nutritional growth will in turn inhibit reproductive growth (Gaaliche et al., 2011; Li and Zhang, 2012; Rosati et al., 2018), reproductive growth intervenes, the increase in photosystem activity of the leaves to obtain more nutrients to supply reproductive growth (Yang et al., 2012a; Yang et al., 2019). At this time, the supply of nutritional growth of buds is reduced, and the growth rate is reduced, followed by the inhibition of reproductive growth by nutritional growth, and the combined effect of the low temperature environment causes a decrease in photosynthetic efficiency and a decrease in the value of Rfd. This was repeated until the flower bud differentiation was completed in the low temperature environment. In the low temperature environment, the trend of NPQ is consistent with Rfd (Shin et al., 2021), therefore, the NPQ curve of *L. chinense* var. *rubrum* under low temperature treatment has a similar trend to the Rfd curve. The magnitude of the QP value reflects the photosynthetic efficiency of photosystem II to a certain extent (Shouren, 1999; Xin and Jirui, 2012), and the QP value of *L. chinense* var. *rubrum* under low-temperature environment remained above and below 0.05, indicating that photosystem II of redbud suffered a stronger inhibition under low-temperature conditions. Combined with Figure 2 , the phenomenon that 'Xiangnong Xiangyun' has more buds and flowers can be explained because the Rfd value of 'Xiangnong Xiangyun' showed a rapid increasing trend in the late low temperature culture, indicating that its photosystem II recovered some activity at this time. The photosynthetic efficiency of 'Xiangnong Xiangyun' was much higher than that of 'Hei Zhenzhu', which caused 'Xiangnong Xiangyun' to obtain more organic assimilated material to provide more energy for reproductive growth. Eventually, 'Xiangnong Xiangyun' had more flower buds to complete the transformation.

Among the four pathways that regulate flowering in plants, the main signal for the vernalization pathway is low temperature from the environment (Bond et al., 2011). The most important gene in the vernalization pathway is *FLC*, which encodes a MADS-box transcription factor and a flowering repressor, and the higher the expression, the stronger the repression of flowering (Yang et al., 2012b), its expression is inhibited by low temperatures during vernalization (Helliwell et al., 2006). *FLC* can inhibit flowering by interacting with *SVP* to form a dimer (Mateos et al., 2015), and by binding to the first intron region of *FT*, it strongly inhibits *FT* transcription and thus prevents bud differentiation (Li et al., 2008). *FT* is highly conserved in flowering plants and it can integrate regulatory signals from different pathways to regulate flowering (Sheng et al., 2013; Song et al., 2013), it promotes flowering when its expression is upregulated and loses its ability to promote flowering when it is downregulated (Nishikawa et al., 2007). As for *TFL1*, which belongs to the same PEPB family, its function is contrary to that of *FT* due to the alteration of a key amino acid residue in its PEPB structural domain (Klintenäs et al., 2012), and the two regulate the expression of downstream flowering genes such as *AP1* by competitively binding FD proteins (Corbesier et al., 2007; Zhu et al., 2020). As can be seen from Figure 5, the similar genes augustus27517 and augustus15211 of *FLC* and *SVP*, both of which showed a decreasing trend in expression since the beginning of low-temperature culture, while in CK both of which were maintained at high levels, indicating that the low-temperature culture environment in the experiment suppressed the expression of similar genes of *FLC* and *SVP* in *L. chinense* var. *rubrum*. The similar gene augustus62587 of *TFL1* was also at a low expression level under low temperature conditions, and was at a disadvantage when competing with *FT* to bind FD protein and therefore promoted flowering, while augustus62587 in the CK group was at a high expression level and was at an advantage in the competition and therefore inhibited flowering. Combined with Figure 4, the expression of both *FT* similar genes in the low temperature treatment group was consistently elevated, while the expression of *FT* genes in the CK group were maintained at low levels. the high level of *FT* expression again indicated that the low temperature treatment suppressed the expression of *FLC* and *SVP*, while the high level of *FT* expression was at an advantage relative to *TFL1* when competing for FD proteins, thus promoting bud differentiation and flowering.

During plant flower formation, various regulatory signals are eventually fed back to *AP1* through different pathways (Quan et al., 2019). The above *FT* integrator signal is also ultimately delivered to the *AP1* gene *via* the FD protein in order to function (Wigge et al., 2005). *AP1* is a floral meristem characteristic gene in the ABCDE model of flower development and belongs to the MADS-box family, which plays an extremely important role in the flower-forming transition (Li et al., 2021). As shown in

Figure 3 , the similar gene augustus40012 of *AP1* maintained a higher expression level in the low temperature treatment group, while the expression level of augustus40012 was at a lower expression level in the CK group, indicating that the above genes together increased the expression level of augustus40012 under low temperature through different pathways and ways, thus promoting flowering.

Flower bud differentiation is the process of transition from nutritional to reproductive growth, and the process of breaking the hormonal balance in the plant (Munne-Bosch and Lalueza, 2007; Pan et al., 2012). Among the many endogenous plant hormones, gibberellin (GA) has been shown to be closely related to flowering (Zhang et al., 2018). In the gibberellin flowering pathway, exogenous gibberellin regulates the up-regulated expression of AP1 gene to promote flowering in Arabidopsis under short sunlight with LFY protein as an intermediate (Eriksson et al., 2006). It has been shown that the internal active gibberellin content of *Brassica juncea* gradually increased to a peak during its floral bud differentiation after vernalization treatment, indicating that low temperature also promotes the expression of GA genes (Shang et al., 2017). Combined with Figure 6, in this study, the similar genes augustus49213, augustus58706 and augustus63711 of *GA* were maintained at higher expression levels during the low temperature treatment, while the gibberellin content in the CK group in all periods was always lower than that in the T0 period, indicating that low temperature promoted the expression of augustus49213, augustus58706 and augustus63711 in *L. chinense* var. *rubrum*. The up-regulation of gibberellin-related gene expression and low temperature together activated the gibberellin flowering pathway and promoted flowering in *L. chinense* var. *rubrum*.

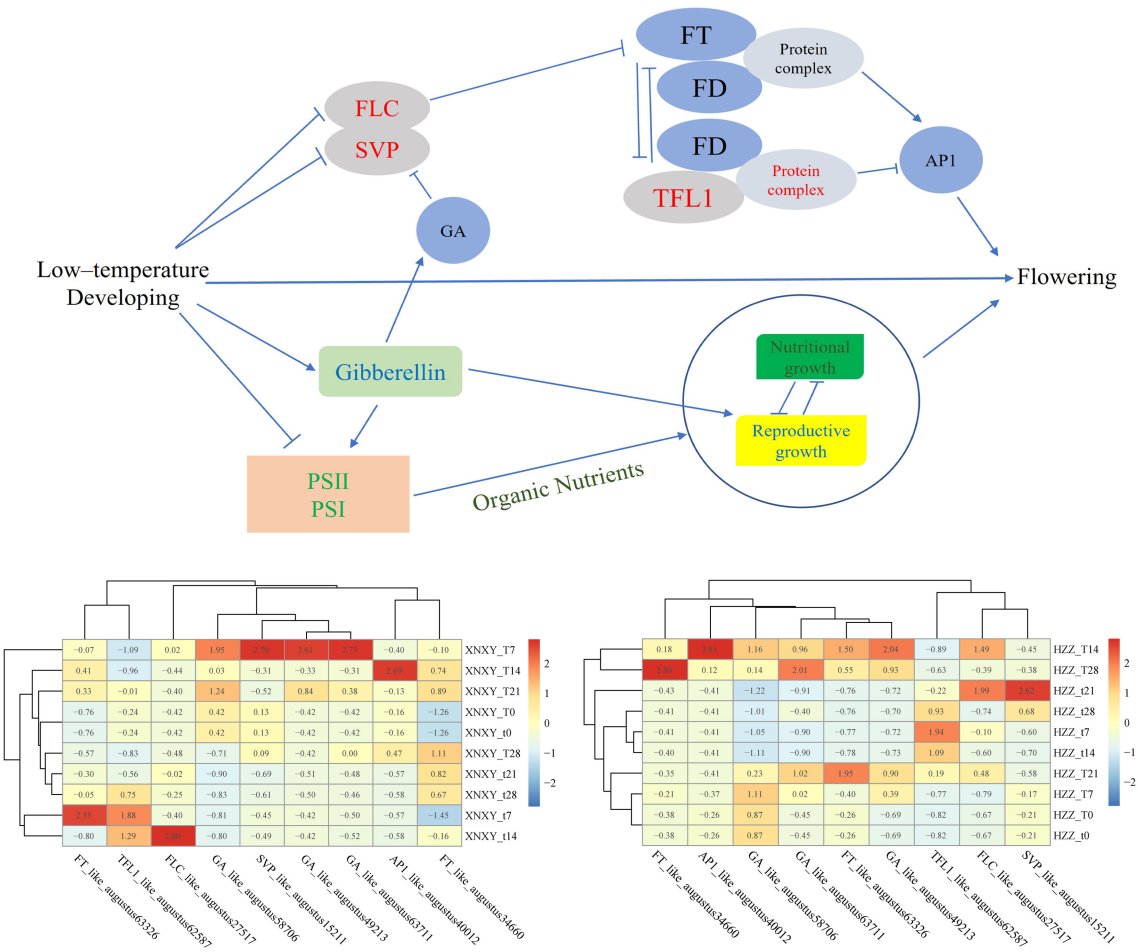

FIGURE 7
Regulation model for low temperature promotion of flowering in Eryngium. The gene expression values in the heat map are obtained from the original values after homogenization by the scale function. 'T' represents the low-temperature treatment group and 't' represents the blank control group treated at 25°C, 'XNXY' represents the 'Xiangnong Xiangyun' and 'HZZ' represents the 'Hei Zhenzhu'.

5 Conclusion

In summary, low-temperature culture is a reliable way to promote the flowering of *L. chinense* var. *rubrum* as a form of regulation, and low-temperature induction in winter is one of the reasons why the number of flowers in the spring flowering period of *L. chinense* var. *rubrum* is more than the number of flowers in the autumn flowering period. The molecular regulatory network of low temperature-promoted flowering is complex (Bond et al., 2011), the most critical of which is that the genes *FLC* and *SVP*, which are repressors of flowering formation, suffer from repression of transcript levels at low temperatures (Yan et al., 2006), and that low temperature conditions promote the expression of *GA* genes activating the gibberellin flowering pathway, which together activate the expression of the downstream flowering-promoting gene FT, which is capable of integrating multiple signals (Xu et al., 2012), and ultimately the *FT* gene positively regulates the expression of the floral meristem gene *AP1* to promote flowering transformation (Wellmer and Riechmann, 2010), based on these results we can obtain Figure 7. Through our research, we can lay the foundation for the subsequent development and use of exogenous gibberellin spraying to regulate the flowering of *L. chinense* var. *rubrum*, so that the goal of making full use of autumn flowers of *L. chinense* var. *rubrum* can be realized.

Data availability statement

The original contributions presented in the study are included in the article/Supplementary Material. Further inquiries can be directed to the corresponding authors.

Author contributions

DZ conceived and designed the experiments, performed the experiments, analyzed the data, prepared figures and/or tables, authored or reviewed drafts of the paper, and approved the final draft. QC performed the experiments, analyzed the data, authored or reviewed drafts of the paper, and approved the final draft. XZ and LL analyzed the data, authored or reviewed drafts of the paper, and approved the final draft. MC and LX conceived and designed the experiments, authored or reviewed drafts of the paper, and approved the final draft. WC analyzed the data, prepared figures and/or tables, and approved the final draft. YL performed the experiments, prepared figures and/or tables, and approved the final draft. MS, XY and YLL conceived and designed the experiments, prepared figures and/or tables, authored or reviewed drafts of the paper, and approved the final draft.

Funding

The work is funded by the Innovation training program for college students of Hunan Agricultural University (XCX2021044), National Innovation and Entrepreneurship Training Program for College Students (202112653017X), Open Project of Horticulture Discipline of Hunan Agricultural University (2021YYXK001), The Forestry Science and Technology Innovation Foundation of Hunan Province for Distinguished Young Scholarship (XLKJ202205), Innovation and Entrepreneurship Training Program of Hunan Province for College Students (201941937227), The Found of Changsha Municipal Science and Technology Bureau (KQ2202227), Hunan Provincial Natural Science Youth Foundation Project (2020JJ5264), Hunan Provincial Education Department Teaching reform Project (2021JGYB101), Hunan Agricultural University Teaching reform research project (XJJG-2020-071).

Conflict of interest

The authors declare that the research was conducted in the absence of any commercial or financial relationships that could be construed as a potential conflict of interest.

Publisher's note

Supplementary material

The Supplementary Material for this article can be found online at: https://www.frontiersin.org/articles/10.3389/fpls.2022.1000160/full#supplementary-material

References

Abe, M., Kobayashi, Y., Yamamoto, S., Daimon, Y., Yamaguchi, A., Ikeda, Y., et al. (2005). FD, a bZIP protein mediating signals from the floral pathway integrator FT at the shoot apex. *Science* 309, 1052–1056. doi: 10.1126/science.1115983

Agusti, M., Reig, C., Martinez-Fuentes, A., and Mesejo, C. (2022). Advances in citrus flowering: A review. *Front. Plant Sci.* 13, 1–17. doi: 10.3389/fpls.2022.868831

Alexandre, C. M., and Hennig, L. (2008). FLC or not FLC: the other side of vernalization. *J. Exp. Bot.* 59, 1127–1135. doi: 10.1093/jxb/ern070

Bao, Z., Chen, B., and Zhang, H. (2007). Variation in morphological traits among *Loropetalum chinense* var. *rubrum* accessions. *HORTSCIENCE* 42, 399–402. doi: 10.21273/HORTSCI.42.2.399

Blázquez, M. A., Green, R., Nilsson, O., Sussman, M. R., and Weigel, D. (1998). Gibberellins promote flowering of arabidopsis by activating the *LEAFY* promoter. *Plant Cell* 10, 791–800. doi: 10.1105/tpc.10.5.791

Bond, D. M., Dennis, E. S., and Finnegan, E. J. (2011). The low temperature response pathways for cold acclimation and vernalization are independent. *Plant Cell Environ.* 34, 1737–1748. doi: 10.1111/j.1365-3040.2011.02370.x

Changsheng, Z., Tao, W., Yuping, Z., Tian, F., Tianxiao, L., and Changen, T. (2021). Progress in flowering regulation mechanisms of *FLC*. *Chin. Bull. Bot.* 56, 651–663. doi: 10.11983/CBB21103

Chen, M., and Penfield, S. (2018). Feedback regulation of COOLAIR expression controls seed dormancy and flowering time. *Science* 360, 1014–1017. doi: 10.1126/science.aar7361

Christiaens, A., De Keyser, E., Lootens, P., Pauwels, E., Roldán-Ruiz, I., De Riek, J., et al. (2015). Cold storage to overcome dormancy affects the carbohydrate status and photosynthetic capacity ofRhododendron simsii. *Plant Biol.* 17, 97–105. doi: 10.1111/plb.12195

Corbesier, L., Vincent, C., Jang, S., Fornara, F., Fan, Q., Searle, I., et al. (2007). FT protein movement contributes to long-distance signaling in floral induction of *Arabidopsis*. *Science* 316, 1030–1033. doi: 10.1126/science.1141752

Dogramaci, M., Horvath, D. P., Chao, W. S., Foley, M. E., Christoffers, M. J., and Anderson, J. V. (2010). Low temperatures impact dormancy status, flowering competence, and transcript profiles in crown buds of leafy spurge. *Plant Mol. Biol.* 73, 207–226. doi: 10.1007/s11103-010-9621-8

Eriksson, S., Bohlenius, H., Moritz, T., and Nilsson, O. (2006). GA_4 is the active gibberellin in the regulation of *LEAFY* transcription and *Arabidopsis* floral initiation. *Plant Cell* 18, 2172–2181. doi: 10.1105/tpc.106.042317

Gaaliche, B., Lauri, P.-E., Trad, M., Costes, E., and Mars, M. (2011). Interactions between vegetative and generative growth and between crop generations in fig tree (Ficus carica l.). *Scientia Hortic.* 131, 22–28. doi: 10.1016/j.scienta.2011.09.022

Hanano, S., and Goto, K. (2011). *Arabidopsis* TERMINAL FLOWER1 is involved in the regulation of flowering time and inflorescence development through transcriptional repression. *Plant Cell* 23, 3172–3184. doi: 10.1105/tpc.111.088641

Han, Y., Chen, Z., Lv, S., Ning, K., Ji, X., Liu, X., et al. (2016). MADS-box genes and gibberellins regulate bolting in lettuce (*Lactuca sativa* l.). *Front. Plant Sci.* 7, 1–14. doi: 10.3389/fpls.2016.01889

Hawryzki, A. R., Allen, G. A., and Antos, J. A. (2011). Prolonged dormancy in the geophyte *Allium amplectens* on Vancouver island. *Botany* 89, 737–744. doi: 10.1139/b11-057

Helliwell, C. A., Wood, C. C., Robertson, M., James Peacock, W., and Dennis, E. S. (2006). The arabidopsis FLC protein interacts directly *in vivo* with *SOC1* and *FT* chromatin and is part of a high-molecular-weight protein complex. *Plant J.* 46, 183–192. doi: 10.1111/j.1365-313X.2006.02686.x

Ito, A., Saito, T., Sakamoto, D., Sugiura, T., Bai, S., and Moriguchi, T. (2022). Physiological differences between bud breaking and flowering after dormancy completion revealed by *DAM* and *FT/TFL1* expression in Japanese pear (*Pyrus pyrifolia*). *Tree Physiol.* 36, 109–120. doi: 10.1093/treephys/tpv115

Karlgren, A., Gyllenstrand, N., Kallman, T., Sundstrom, J. F., Moore, D., Lascoux, M., et al. (2011). Evolution of the PEBP gene family in plants: functional diversification in seed plant evolution. *Plant Physiol.* 156, 1967–1977. doi: 10.1104/pp.111.176206

Kim, S. Y., Park, B. S., Kwon, S. J., Kim, J., Lim, M. H., Park, Y. D., et al. (2007). Delayed flowering time in arabidopsis and brassica rapa by the overexpression of FLOWERING LOCUS c (FLC) homologs isolated from Chinese cabbage (Brassica rapa l.: ssp. pekinensis). *Plant Cell Rep.* 26, 327–336. doi: 10.1007/s00299-006-0243-1

Kinmonth-Schultz, H., Lewandowska-Sabat, A., Imaizumi, T., Ward, J. K., Rognli, O. A., and Fjellheim, S. (2021). Flowering times of wild arabidopsis accessions from across Norway correlate with expression levels of *FT*, *CO*, and *FLC* genes. *Front. Plant Sci.* 12, 740–747. doi: 10.3389/fpls.2021.747740

Kitamoto, N., Yui, S., Nishikawa, K., Takahata, Y., and Yokoi, S. (2013). A naturally occurring long insertion in the first intron in the *Brassica rapa FLC2* gene causes delayed bolting. *Euphytica* 196, 213–223. doi: 10.1007/s10681-013-1025-9

Klintenäs, M., Pin, P. A., Benlloch, R., Ingvarsson, P. K., and Nilsson, O. (2012). Analysis of conifer *FLOWERING LOCUS T/TERMINAL FLOWER1*-like genes provides evidence for dramatic biochemical evolution in the angiosperm *FT* lineage. *New Phytol.* 196, 1260–1273. doi: 10.1111/j.1469-8137.2012.04332.x

Kobayashi, Y., Kaya, H., Goto, K., Lwabuchi, M., and Araki, T. (1999). A pair of related genes with antagonistic roles in mediating flowering signals. *science* 286, 1960–1962. doi: 10.1126/science.286.5446.1960

Li, Y., An, S., Cheng, Q., Zong, Y., Chen, W., Guo, W., et al. (2021). Analysis of evolution, expression and genetic transformation of TCP transcription factors in blueberry reveal that *VcTCP18* negatively regulates the release of flower bud dormancy. *Front. Plant Sci.* 12, 1–19. doi: 10.3389/fpls.2021.697609

Li, D., Liu, C., Shen, L., Wu, Y., Chen, H., Robertson, M., et al. (2008). A repressor complex governs the integration of flowering signals in *Arabidopsis*. *Dev. Cell* 15, 110–120. doi: 10.1016/j.devcel.2008.05.002

Lina, L., Wei, L., and Qingsheng, Y. (2003). Advances on research of vernalizat ion-related gene *FLC*. *Acta Botanica Boreali-Occidentalia Sin.* 23, 2229–2234. doi: 10.3321/j.issn:1000-4025.2003.12.035

Li, Y. L., and Zhang, A. M. (2012). Analysis on the dialectical relationship between plant vegetative growth and reproductive growth. *Chin. Horticulture Abstracts* 28, 36–37. doi: 10.3969/j.issn.1672-0873.2012.02.017

Luo, X., Chen, T., Zeng, X., He, D., and He, Y. (2019). Feedback regulation of *FLC* by *FLOWERING LOCUS T (FT)* and *FD* through a *5′ FLC* promoter region in *Arabidopsis*. *Mol. Plant* 12, 285–288. doi: 10.1016/j.molp.2019.01.013

Lysenko, V. S., Varduny, T. V., Kosenko, P. O., Kosenko, Y. V., Chugueva, O. I., Semin, L. V., et al. (2014). Video registration as a method for studying kinetic parameters of chlorophyll fluorescence in ficus benjamina leaves. *Russian J. Plant Physiol.* 61, 419–425. doi: 10.1134/S102144371403008X

Mateos, J. L., Madrigal, P., Tsuda, K., Rawat, V., Richter, R., Romera-Branchat, M., et al. (2015). Combinatorial activities of SHORT VEGETATIVE PHASE and FLOWERING LOCUS c define distinct modes of flowering regulation in *Arabidopsis*. *Genome Biol.* 16, 1–23. doi: 10.1186/s13059-015-0597-1

Maxwell, K., and Johnson, G. N. (2000). Chlorophyll fluorescence–a practical guide. *J. Exp. Bot.* 51, 659–668. doi: 10.1093/jexbot/51.345.659

Munne-Bosch, S., and Lalueza, P. (2007). Age-related changes in oxidative stress markers and abscisic acid levels in a drought-tolerant shrub, *Cistus clusii* grown under Mediterranean field conditions. *Planta* 225, 1039–1049. doi: 10.1007/s00425-006-0412-z

Nishikawa, F., Endo, T., Shimada, T., Fujii, H., Shimizu, T., Omura, M., et al. (2007). Increased CiFT abundance in the stem correlates with floral induction by low temperature in Satsuma mandarin (Citrus unshiu marc.). *J. Exp. Bot.* 58, 3915–3927. doi: 10.1093/jxb/erm246

O'maoileidigh, D. S., Graciet, E., and Wellmer, F. (2014). Gene networks controlling arabidopsis thaliana flower development. *New Phytol.* 201, 16–30. doi: 10.1111/nph.12444

Oquist, G., and Huner, N. P. (2003). Photosynthesis of overwintering evergreen plants. *Annu. Rev. Plant Biol.* 54, 329–355. doi: 10.1146/annurev.arplant.54.072402.115741

Pan, H., Chuan, W., Junhui, W., Zirui, J., and Yongfang, Z. (2012). Content changes of endogenous hormones during flower bud differentiation of *Picea crassifolia*. *Acta Botanica Boreali-Occidentalia Sin.* 32, 0540–0545. doi: 10.3969/j.issn.1000-4025.2012.03.016

Qiaoxia, L., Li, Z., Yu, W., and Xiaoxia, H. (2019). The research progress of gibberellin on the regulation of flowering and floral organ development in plant. *Chin. J. Cell Biol.* 41, 746–758. doi: 10.11844/cjcb.2019.04.0026

Quan, S., Niu, J., Zhou, L., Xu, H., Ma, L., and Qin, Y. (2019). Stages identifying and transcriptome profiling of the floral transition in *Juglans regia*. *Sci. Rep.* 9, 1–14. doi: 10.1038/s41598-019-43582-z

Rizza, A., and Jones, A. M. (2019). The makings of a gradient: spatiotemporal distribution of gibberellins in plant development. *Curr. Opin. Plant Biol.* 47, 9–15. doi: 10.1016/j.pbi.2018.08.001

Rosati, A., Paoletti, A., Al Hariri, R., Morelli, A., and Famiani, F. (2018). Resource investments in reproductive growth proportionately limit investments in whole-tree vegetative growth in young olive trees with varying crop loads. *Tree Physiol.* 38, 1267–1277. doi: 10.1093/treephys/tpy011

Runmin, P., and Xiaoying, Y. (2012). Investigation and analysis of the landscape application present situation of *Loropetalum* in hunan province. *Tianjin Agric. Sci.* 18, 152–155. doi: 10.3969/j.issn.1006-6500.2012.06.039

Sønstebya, A., and Heideb, O. M. (2019). Temperature effects on growth and floral initiation in sweet cherry (*Prunus avium* l.). *Scientia Hortic.* 257, 1–8. doi: 10.1016/j.scienta.2019.108762

Shang, M., Wang, X., Zhang, J., Qi, X., Ping, A., Hou, L., et al. (2017). Genetic regulation of GA metabolism during vernalization, floral bud initiation and development in pak choi (*Brassica rapa* ssp. *chinensis* makino). *Front. Plant Sci.* 8, 1–10. doi: 10.3389/fpls.2017.01533

Sheng, A., Liu, N., Zhang, S., and Ye, X. (2013). Flowering, morphological observations and *FT* expression of *Curcuma kwangsiensis* var *nanlingensis* bud in development process. *Scientia Hortic.* 160, 383–388. doi: 10.1016/j.scienta.2013.06.006

Shihao, J., Jiliang, P., Lilin, W., and Haiman, L. (2008). Molecular mechanism of gibberellin promotion on floral development. *Plant Physiol. J.* 44, 835–843.

Shin, Y. K., Bhandari, S. R., Jo, J. S., Song, J. W., and Lee, J. G. (2017). Effect of drought stress on chlorophyll fluorescence parameters, phytochemical contents, and antioxidant activities in lettuce seedlings. *Horticulturae* 7, 1–16. doi: 10.3390/horticulturae7080238

Shin, Y. K., Bhandari, S. R., and Lee, J. G. (2021). Monitoring of salinity, temperature, and drought stress in grafted watermelon seedlings using chlorophyll fluorescence. *Front. Plant Sci.* 12, 1–17. doi: 10.3389/fpls.2021.786309

Shouren, Z. (1999). A discussion on chlorophyll fluorescence kinetics parameters and their significance. *Chin. Bull. Bot.* 16, 444–448. doi: 10.3969/j.issn.1674-3466.1999.04.021

Song, Y. H., Ito, S., and Imaizumi, T. (2013). Flowering time regulation photoperiod- and temperature-sensing in leaves. *Trends Plant Sci.* 18, 575–583. doi: 10.1016/j.tplants.2013.05.003

Sriboon, S., Li, H., Guo, C., Senkhamwong, T., Dai, C., and Liu, K. (2020). Knock-out of TERMINAL FLOWER 1 genes altered flowering time and plant architecture in brassica napus. *BMC Genet.* 21, 1–13. doi: 10.1186/s12863-020-00857-z

Tang, X., An, B., Cao, D., Xu, R., Wang, S., Zhang, Z., et al. (2020). Improving photosynthetic capacity, alleviating photosynthetic inhibition and oxidative stress under low temperature stress with exogenous hydrogen sulfide in blueberry seedlings. *Front. Plant Sci.* 11, 1–13. doi: 10.3389/fpls.2020.00108

Taoka, K., Ohki, I., Tsuji, H., Furuita, K., Hayashi, K., Yanase, T., et al. (2011). 14-3-3 proteins act as intracellular receptors for rice Hd3a florigen. *Nature* 476, 332–335. doi: 10.1038/nature10272

Taoka, K., Ohki, I., Tsuji, H., Kojima, C., and Shimamoto, K. (2013). Structure and function of florigen and the receptor complex. *Trends Plant Sci.* 18, 287–294. doi: 10.1016/j.tplants.2013.02.002

Wang, G. L., Que, F., Xu, Z. S., Wang, F., and Xiong, A. S. (2015). Exogenous gibberellin altered morphology, anatomic and transcriptional regulatory networks of hormones in carrot root and shoot. *BMC Plant Biol.* 15, 1–12. doi: 10.1186/s12870-015-0679-y

Weicai, L., Hongna, Z., Shengyou, S., Liqin, L., Bo, S., Qingzhi, L., et al. (2014). Effects of s-3307 and GA3 on fluorescence characteristics of litchi leaves during floral induction. *Chin. J. Trop. Crops* 35, 2414–2419. doi: 10.3969/j.issn.1000-2561.2014.12.017

Wellmer, F., and Riechmann, J. L. (2010). Gene networks controlling the initiation of flower development. *Trends Genet.* 26, 519–527. doi: 10.1016/j.tig.2010.09.001

Wigge, P. A., Kim, M. C., Jaeger, K. E., Busch, W., Schmid, M., Lohmann, J. U., et al. (2005). Integration of spatial and temporal information during floral induction in *Arabidopsis*. *Science* 309, 1056–1059. doi: 10.1126/science.1114358

Xia, Z., Damao, Z., Li, Z., Xiangfei, W., Xingyao, X., Dexin, G., et al. (2020). The whole genome analysis of *Loropetalum chinense* var. *Rubrum*. *Mol. Plant Breed.* 18, 7023–7029. doi: 10.13271/j.mpb.018.007023

Xin, Y., and Jirui, G. (2012). Significance and application of chlorophyll fluorescence dynamics process parameters. *J. West China Forestry Sci.* 41, 90–94. doi: 10.3969j.issn.1672-8246.2012.05.017

Xu, F., Rong, X., Huang, X., and Cheng, S. (2012). Recent advances of *Flowering locus t* gene in higher plants. *Int. J. Mol. Sci.* 13, 3773–3781. doi: 10.3390/ijms13033773

Yan, L., Fu, D., Li, C., Blechl, A., Tranquilli, G., Bonafede, M., et al. (2006). The wheat and barley vernalization gene *VRN3* is an orthologue of *FT*. *PNAS* 103, 19581–19586. doi: 10.1073/pnas.0607142103

Yang, Y., Chen, M., Tian, J., Xiao, F., Xu, S., Zuo, W., et al. (2019). Improved photosynthetic capacity during the mid- and late reproductive stages contributed to increased cotton yield across four breeding eras in xinjiang, China. *Field Crops Res.* 240, 177–184. doi: 10.1016/j.fcr.2018.11.003

Yang, H., Han, Z., Cao, Y., Fan, D., Li, H., Mo, H., et al. (2012b). A companion cell-dominant and developmentally regulated H3K4 demethylase controls flowering time in *Arabidopsis via* the repression of *FLC* expression. *PLoS Genet.* 8, 1–17. doi: 10.1371/journal.pgen.1002664

Yang, G., Tang, H., Tong, J., Nie, Y., and Zhang, X. (2012a). Effect of fertilization frequency on cotton yield and biomass accumulation. *Field Crops Res.* 125, 161–166. doi: 10.1016/j.fcr.2011.08.008

Yan, L., Loukoianov, A., Blechl, A., Tranquilli, G., Ramakrishna, W., Sanmiguel, P., et al. (2004). The wheat VRN2 gene is a flowering repressor down-regulated by vernalization. *science* 303, 1640–1643. doi: 10.1126/science.1094305

Yu, H., Luedeling, E., and Xua, J. (2010). Winter and spring warming result in delayed spring phenology on the Tibetan plateau. *PNAS* 107, 22151–22156. doi: 10.1073/pnas.1012490107

Zhang, D., Cai, W., Zhang, X., Li, W., Zhou, Y., Chen, Y., et al. (2022). Different pruning level effects on flowering period and chlorophyll fluorescence parameters of *Loropetalum chinense* var. *rubrum*. *PeerJ* 10, 1–17. doi: 10.7717/peerj.13406

Zhang, Z., Zhuo, X., Zhao, K., Zheng, T., Han, Y., Yuan, C., et al. (2018). Transcriptome profiles reveal the crucial roles of hormone and sugar in the bud dormancy of *Prunus mume*. *Sci. Rep.* 8, 5090–5104. doi: 10.1038/s41598-018-23108-9

Zhonghua, Z., Qun, Z., and Shuqing, Z. (2006). The molecular mechanism of vernalization in plants. *Chin. Bull. Bot.* 23, 60–67. doi: 10.3969j.issn.1674-3466.2006.01.009

Zhu, Y., Klasfeld, S., Jeong, C. W., Jin, R., Goto, K., Yamaguchi, N., et al. (2020). TERMINAL FLOWER 1-FD complex target genes and competition with FLOWERING LOCUS T. *Nat. Commun.* 11, 1–12. doi: 10.1038/s41467-020-18782-1

frontiers | Frontiers in Plant Science

TYPE Original Research
PUBLISHED 16 December 2022
DOI 10.3389/fpls.2022.996690

OPEN ACCESS

EDITED BY
Shunli Wang,
Chinese Academy of Agricultural Sciences (CAAS), China

REVIEWED BY
Xiaonan Yu,
Beijing Forestry University, China
Zheng Wang,
Henan Agricultural University, China

*CORRESPONDENCE
Xiaomei Sun
sxm7280@syau.edu.cn

†These authors have contributed equally to this work

SPECIALTY SECTION
This article was submitted to Plant Breeding, a section of the journal Frontiers in Plant Science

RECEIVED 18 July 2022
ACCEPTED 30 November 2022
PUBLISHED 16 December 2022

CITATION
Duan S, Xin R, Guan S, Li X, Fei R, Cheng W, Pan Q and Sun X (2022) Optimization of callus induction and proliferation of *Paeonia lactiflora* Pall. and *Agrobacterium*-mediated genetic transformation. *Front. Plant Sci.* 13:996690. doi: 10.3389/fpls.2022.996690

Optimization of callus induction and proliferation of *Paeonia lactiflora* Pall. and *Agrobacterium*-mediated genetic transformation

Siyang Duan[1,2†], Rujie Xin[1,2†], Shixin Guan[1,2], Xueting Li[3], Riwen Fei[3], Wan Cheng[1,2], Qing Pan[1,2] and Xiaomei Sun[1,2*]

[1]College of Forestry, Shenyang Agricultural University, Shenyang, China, [2]Key Laboratory of Forest Tree Genetics, Breeding and Cultivation of Liaoning Province, Shenyang Agricultural University, Shenyang, China, [3]College of Horticulture, Shenyang Agricultural University, Shenyang, China

Paeonia lactiflora Pall. is an important ornamental plant with high economic and medicinal value, which has considerable development prospects worldwide. The lack of efficient tissue culture techniques and genetic transformation systems has become a master obstacle for *P. lactiflora* research. The purpose of the present study focuses on obtaining an efficient and stable genetic transformation method using callus as the receptor and exploring an efficient protocol for callus induction and proliferation associated with *P. lactiflora*. Callus induction and proliferation were performed using MS medium with various concentrations of 2,4-Dichlorophenoxyacetic acid (2,4-D), 1-Naphthaleneacetic acid (NAA), 6-Benzylaminopurine (6-BA) and thidiazuron (TDZ). The sensitivity of callus to kanamycin and cefotaxime was determined. Several parameters such as *Agrobacterium* cell density, infection time and co-culture duration were studied to optimize transformation efficiency. *Agrobacterium* strains EHA105 and pBI121 binary vector harboring the *β-glucuronidase* (GUS) gene were used for transformation. Expression of the GUS reporter gene was detected by GUS assay, polymerase chain reaction (PCR) and Quantitative Real-time PCR (RT-qPCR). The MS medium containing 1.0 mg·L^{-1} NAA, 0.5 mg·L^{-1} 2,4-D and 0.5 mg·L^{-1} TDZ was optimal for callus induction and MS medium containing 0.5 mg·L^{-1} NAA, 1.0 mg·L^{-1} 2,4-D and 0.5 mg·L^{-1} TDZ was the best for callus proliferation. The concentrations of kanamycin and cefotaxime used for screening positive callus were 125 mg·L^{-1} and 200 mg·L^{-1}, respectively. Among various combinations analyzed, the best transformation result was obtained *via* the 25 min of infection of *Agrobacterium* at 0.6 OD_{600} and 3 d of co-culture. Overall, this study provided technical support and theoretical guidance for improving the callus induction and proliferation efficiency and the study of gene function in *P. lactiflora*.

KEYWORDS

herbaceous peony, callus, induction, proliferation, *Agrobacterium*, genetic transformation, GUS expression

Introduction

Herbaceous peony (*Paeonia lactiflora* Pall.) is a perennial herbaceous plant of the genus *Paeonia* (Zhang et al., 2022). Because of its large, colorful and diverse flowers, herbaceous peony is used as garden, potted, cut and dried flowers in many countries and regions (Zhao et al., 2017; Liu et al., 2022). In addition, it is also used as an important source of crude drugs in traditional Chinese medicine (Hu et al., 2015; Sun et al., 2021). Due to its high ornamental, medicinal and economic value, herbaceous peony is widely cultivated in the world (Xue et al., 2018; Zhao et al., 2019).

Seed and dividing are the traditional propagation methods of herbaceous peony. However, due to the special epicotyl and hypocotyl double dormancy characteristics of herbaceous peony seeds, it usually takes 3-5 years from seed germination to flowering, which makes it difficult for traditional breeding methods to meet the needs of commercial production (Shen et al., 2014). Finding efficient propagation methods of herbaceous peony has become a significant and meaningful research task. In recent years, there is an increasing and new interest to plant tissue culture (Georgiev et al., 2018). Tissue culture can increase the propagation rate, and is an important way to rapidly propagate plants, improve popular plant varieties or select new plant varieties (Osakabe et al., 2018). Although various studies have been studied on vitro culture of herbaceous peony (Jana et al., 2013; Shen et al., 2014; Zhao et al., 2017), many problems continue to be encountered on establishing faster and more efficient methods of tissue culture and its large-scale production. Numerous hurdles related to the tissue culture, such as low efficiency in direct or indirect induction of adventitious shoots, high levels of contamination, browning, poor rooting, and difficulties in transplanting and acclimatization, still need to be solved (Sivanesan et al., 2021). Therefore, it is necessary to establish an efficient and stable method of callus induction and proliferation to alleviate or even solve the above problems, and to establish a basis for the establishment of stable regeneration system of herbaceous peony.

Transgenic plants are commonly used in molecular biology to understand the function of specific genes(Chakraborty et al., 2020). The establishment of an efficient, stable and regenerating receptor system is the basis for genetic transformation. However, there are still so many obstacles on the establishment of the regeneration system associated with herbaceous peony, which not only affect the tissue culture, but also hinder the molecular biology research. Due to the difficulty in regeneration of herbaceous peony during tissue culture, there is no stable genetic transformation system and transgenic plants cannot be obtained, which greatly limits the transgenic work of herbaceous peony (Wang et al., 2021a). Therefore, at present, studies on gene function verification of *P. lactiflora* are carried out either through heterologous transformation or homologous transient expression (Ni et al., 2018; Bai et al., 2019; Lv et al., 2019). Based on this situation, finding other transgenic receptors to carry out molecular biological research of herbaceous peony has been the focus of scholars (Shen et al., 2012). Gene transformation using callus as receptor has the advantages of high efficiency and short transformation time, and has been widely used in functional analysis of related genes in apple, citrus, grape and other plants (Wu et al., 2017; Xu et al., 2017; Osakabe et al., 2018). Callus of herbaceous peony is easy to obtain, has strong proliferation ability, and can also be used as receptor material for transgene (Guo and Jeong, 2021). At the same time, with the rapid development of plant genetic transformation research, *Agrobacterium*-mediated transformation has become a convenient tool to transfer favorable traits to plants, and has already successfully applied to many plants (Chetty et al., 2013; Mayavan et al., 2013; Chen et al., 2014; Palla and Pijut, 2014; Liu et al., 2015; Singh et al., 2016; Sedaghati et al., 2018; Sun et al., 2019). However, there are few reports on *Agrobacterium*-mediated genetic transformation using herbaceous peony callus as receptor. By transferring genes into callus, the function and molecular mechanism of many important genes in *P. lactiflora* can be determined (An et al., 2018; Qi et al., 2018; Wang et al., 2018; Lu et al., 2019; Zhao et al., 2019b).

To help solve the above problems, in this study, we optimized the callus induction and proliferation protocol of *P. lactiflora* and further established an efficient *Agrobacterium*-mediated transgenic method with callus as receptor. We believe that our results provide a theoretical basis and technical support for the establishment of tissue culture regeneration system and further verification of gene function of herbaceous peony.

Materials and methods

Plant material and treatment

Herbaceous peony hybrid seeds ('Fen Yu Nu'×'Xi Shi Fen') were harvested in the germplasm resource nursery of Shenyang Agricultural University, Liaoning, China. Full and large seeds were chosen and washed under the running tap water for 10 min. After soaking in distilled water for 48 h, the seed coat was removed. Subsequently, they were transferred to a clean bench for further sterilization. The seeds were dipped in 75% (v/v) ethanol for 30 s, and rinsed 2 times with sterile distilled water. Followed by 15 min sterilization with sodium hypochlorite solution (1.5%, w/v), and the seeds were finally rinsed three times in sterile distilled water. After sterilization, the much of endosperm in each seed was removed to leave isolated embryo with a bit of endosperm, which was cultured on Murashige and Skoog (MS) medium supplemented with 0.5 $mg{\cdot}L^{-1}$ GA_3 (initiation medium) for 45 d to obtain sterile seedlings. All medium and agar used in this article were purchased from Beijing Solarbio Science & Technology Co., LTD. All plant

growth regulators (PGRs) were purchased from Shanghai Yien Chemical Technology Co., LTD.

Culture and growing conditions

The culture vessels were 100 mL Erlenmeyer flasks with 30 mL of medium. Plants were grown in a tissue culture room at 25 ± 2°C with a 16 h light/8 h dark photoperiod in 50 $\mu mol \cdot m^{-2} \cdot s^{-1}$ photosynthetic photon flux density of cool white fluorescent tubes.

Callus induction

The epicotyl stems were cut into 8-10 mm lengths, and both the leaves and cotyledons were cut into 8 mm × 8 mm squares. They were both transferred to MS medium supplemented PGRs, including 0.5 $mg \cdot L^{-1}$ 6-Benzyleaminopurine (6-BA), 1.0 $mg \cdot L^{-1}$ 1-Naphthylacetic acid (NAA) and 1.0 $mg \cdot L^{-1}$ 2,4-dichlorophenoxyacetic acid (2,4-D). Since cotyledons had the best callus induction effect and were easy to obtain, the effects of different PGRs on callus induction were studied by taking sterile cotyledons as explants. According to the results of the preliminary experiment, they were transferred to MS medium containing various concentrations of PGRs alone or in combination, including 6-BA (0.1 $mg \cdot L^{-1}$, 0.5 $mg \cdot L^{-1}$, 1.0 $mg \cdot L^{-1}$), 2,4-D (0.1 $mg \cdot L^{-1}$, 0.5 $mg \cdot L^{-1}$, 1.0 $mg \cdot L^{-1}$), NAA (0.1 $mg \cdot L^{-1}$, 0.5 $mg \cdot L^{-1}$, 1.0 $mg \cdot L^{-1}$) and Thidiazuron (TDZ) (0.5 $mg \cdot L^{-1}$, 1.0 $mg \cdot L^{-1}$, 2.0 $mg \cdot L^{-1}$) (Table 1). Each of the treatments was conducted with at least 30 explants. The callus induction rate was calculated and the callus growth state was observed after 30 d of culture.

Callus proliferation

Callus from the sterile stem, leave and cotyledon were transferred respectively to MS medium containing 1.0 $mg \cdot L^{-1}$ TDZ, 1.0 $mg \cdot L^{-1}$ NAA and 0.5 $mg \cdot L^{-1}$ 2,4-D to observe their

TABLE 1 Effect of 2.4-D ($mg \cdot L_{-1}$), NAA, TDZ and 6-BA on *P. lactiflora* callus induction.

Groups	2, 4-D ($mg \cdot L^{-1}$)	NAA ($mg \cdot L^{-1}$)	TDZ ($mg \cdot L^{-1}$)	6-BA ($mg \cdot L^{-1}$)	Induction rate (%)	Growth state
	0.1	–	–	–	41.11 ± 1.92c	emerald-green and loose-crunchy
1	0.5	–	–	–	50.00 ± 3.33b	emerald-green and tight-dense
	1.0	–	–	–	57.78 ± 5.09a	light-green and tight-dense
	–	0.1	–	–	46.67 ± 3.33b	yellow-white and loose
2	–	0.5	–	–	54.44 ± 1.92a	yellow-white and loose
	–	1.0	–	–	41.11 ± 1.92c	yellow-white and loose
	1.0	–	0.5	–	23.33 ± 5.78b	emerald-green and loose-crunchy
3	1.0	–	1.0	–	67.78 ± 1.92a	emerald-green and loose-crunchy
	1.0	–	2.0	–	26.67 ± 3.33b	emerald-green and loose-crunchy
	1.0	–	–	0.5	44.44 ± 1.92b	yellow-green and tight-dense
4	1.0	–	–	1.0	57.78 ± 1.92 a	yellow-green and tight-dense
	1.0	–	–	2.0	53.33 ± 3.33 a	yellow-green and tight-dense
	0.1	0.1	0.5	–	58.89 ± 1.82 c	emerald-green and tight-dense
	0.1	0.5	1.0	–	52.22 ± 1.92 d	emerald-green and tight-dense
	0.1	1.0	2.0	–	46.67 ± 5.78 e	green and tight-dense
	0.5	0.1	1.0	–	62.22 ± 1.92 c	emerald-green and tight-dense
5	0.5	0.5	2.0	–	78.89 ± 1.92 b	emerald-green and tight-dense
	0.5	1.0	0.5	–	86.67 ± 3.33 a	green and tight-dense
	1.0	0.1	2.0	–	76.67 ± 3.33 b	emerald-green and tight-dense
	1.0	0.5	0.5	–	86.67 ± 3.33a	emerald-green and tight-dense
	1.0	1.0	1.0	–	81.11 ± 1.92b	green and tight-dense

Statistical analysis performed within each group. The values represented mean ± SD, and different letters within a column marked significant differences ($p < 0.05$).

proliferation abilities. For the best proliferation effect, the effects of different PGRs on callus proliferation were studied by taking sterile cotyledons as explants. They were transferred to MS medium containing 2,4-D (0.1 mg·L^{-1}, 0.5 mg·L^{-1}, 1.0 mg·L^{-1}), NAA (0.1 mg·L^{-1}, 0.5 mg·L^{-1}, 1.0 mg·L^{-1}) and TDZ (0.5 mg·L^{-1}, 1.0 mg·L^{-1}, 2.0 mg·L^{-1}) alone or in combination (Table 2). There were at least 30 calluses in each treatment. The callus proliferation coefficient and browning rate were calculated after 30 d of culture.

Antibiotic sensitivity assay of *P. lactiflora* callus

The tolerance limits of cotyledone-induced callus to antibiotic kanamycin (Kan) and cefotaxime (Cef) were assessed prior to *Agrobacterium*-mediated transformation. The Kan and Cef were sterilized by filter and added to the medium when the medium temperature cooled down to about 40°C. The callus was cultured on a proliferation medium supplemented with different concentrations of Kan (0, 75, 100, 125 and 150 mg·L^{-1}) or Cef (0, 100, 200, 300 and 400 mg·L^{-1}) to determine the concentration of antibiotic needed for the effective selection of transgenic callus. The callus growth state was observed after 14 d of culture. The Kan and Cef were purchased from Beijing Solarbio Science & Technology Co., LTD.

Inhibition test of cefotaxime against *Agrobacterium*

The 20 µL of overnight *Agrobacterium tumefaciens* EHA105 culture was added to a liquid Luria Bertani (LB) medium containing different concentrations of Cef (0, 100, 200, 300 and 400 mg·L^{-1}) with three biological replicates. After 48 h of incubation, the OD_{600} value was determined by ultraviolet (UV) spectrophotometer (Qingdao Juchuang Environmental Protection Group Co. LTD, Qingdao, China).

Optimization of *Agrobacterium*-mediated transformation factors

The binary vector pBI121-GUS purchased from Shanghai Maokang Biotechnology Co., LTD. was transformed into the *Agrobacterium* strain EHA105 purchased from Shanghai Angyu Technology Co., LTD. 1000 ng pBI121-GUS vector plasmid was added to 100 µl of *Agrobacterium* EHA105 competent cells and gently mixed, then placed in ice, liquid nitrogen and water at 28°C for 5 min, and finally another ice bath for 5 min. 700 µl LB liquid medium was added to the above products and incubated for 3 h in an incubator at 28°C by shaking. After the shock culture, the bacteria were dipped and coated on solid LB medium containing 50 mg·L^{-1} Kan and incubated upside down for 2 days at 28°C. Single colonies on the above medium were selected for PCR

TABLE 2 Effects of NAA, 2, 4-D and TDZ on *P. lactiflora* callus proliferation.

Groups	NAA	2,4-D	TDZ	Proliferation coefficient	Browning rate (%)
	–	0.1	0.5	1.96 ± 0.10a	25.56 ± 3.85b
1	–	0.5	0.5	2.05 ± 0.10a	22.22 ± 3.85b
	–	1.0	0.5	1.95± 0.11a	33.33 ± 3.33a
	0.1	–	0.5	1.56 ± 0.03b	34.44 ± 6.94a
2	0.5	–	0.5	1.68 ± 0.04a	23.33 ± 3.33b
	1.0	–	0.5	1.47 ± 0.17b	40.00 ± 5.77a
	0.1	0.1	0.5	1.85 ± 0.04e	27.78 ± 1.92cd
	0.1	0.5	1.0	1.76 ± 0.04f	22.22 ± 3.85de
	0.1	1.0	2.0	1.79 ± 0.03ef	34.44 ± 1.92b
	0.5	0.1	1.0	1.56 ± 0.02g	32.22 ± 3.84bc
3	0.5	0.5	2.0	1.97 ± 0.06d	24.44 ± 1.92de
	0.5	1.0	0.5	3.21 ± 0.06a	33.33 ± 5.78bc
	1.0	0.1	2.0	1.78 ± 0.04ef	18.89 ± 3.85e
	1.0	0.5	0.5	2.80 ± 0.04b	41.11 ± 1.92a
	1.0	1.0	1.0	2.07 ± 0.03c	41.11 ± 1.92a

Plant growth regulators unit: mg·L^{-1}. Statistical analysis performed within each group. The values represented mean ± SD, and different letters within a column marked significant differences ($p < 0.05$).

validation to obtain positive strains. Then a positive transformant was picked and inoculated overnight in 2 mL fresh liquid LB medium containing 50 mg·L^{-1} rifampicin and 50 mg·L^{-1} Kan at 28 °C in 200×g. The overnight culture liquid was transferred to a 50 ml liquid LB medium at a ratio of 1:50 and then cultured until the *Agrobacterium* cell density (OD_{600}) reached 0.2-1.0, and then the culture was centrifuged at 5000×g for 10 min. The resuspension solution containing 5% sucrose and 100 μM filter-sterilized acetosyringone was used to resuspend the *Agrobacterium* as the infection solution. The healthy callus was soaked in the above prepared infection solution for infection, and the callus was gently shaken to make it fully infected. After infection, the callus was transferred to sterile filter paper until almost dry, and then transferred to the co-culture medium (MS medium containing 0.5 mg·L^{-1} NAA, 1.0 mg·L^{-1} 2,4-D and 0.5 mg·L^{-1}TDZ), dark culture was carried out at 28 °C. After three times of rinse in sterile water containing Cef of 200 mg·L^{-1} and blotting on sterile filter paper, the calluses were cultured on MS medium containing 0.5 mg·L^{-1} NAA, 1.0 mg·L^{-1} 2,4-D, 0.5 mg·L^{-1} TDZ and 200 mg·L^{-1} Cef. Again, three times of rinse in sterile water containing Cef of 200 mg L^{-1} and blotting on sterile filter paper, the calluses were transferred to a selection medium (MS medium containing 0.5 mg·L^{-1} NAA, 1.0 mg·L^{-1} 2,4-D, 0.5 mg·L^{-1} TDZ and 125 mg·L^{-1} Kan). After 49 d of culture, part of the resistant callus was taken for GUS staining and Molecular identification. To improve transformation efficiency, the key factors affecting transformation efficiency were optimized, including *Agrobacterium* cell density (0.2, 0.4, 0.6, 0.8 and 1.0 OD_{600}), infection duration (10, 15, 20, 25 and 30 min) and co-culture duration (0, 1, 2, 3 and 4 d).

GUS histochemical assay

GUS histochemical assay was conducted according to the described procedure (Jefferson, 1987). The resistant callus was divided into two parts, one part was stained with GUS solution, and wild-type callus was used as negative control. The staining results were observed and counted. The other part was used for molecular identification.

Molecular identification of transgenic callus

Genomic DNA was extracted from the transformed and non-transformed callus using an extraction kit (Aidlab, Beijing, China). The sequence of primers used for *GUS* gene (1182bp): forward primer(5'-ATACCGAAAGGTTGGGCAGG-3'), and reverse primer(5'-ATAACGGTTCAGGCACAGCA-3'). The PCR procedure were as followed: pre-denaturation at 94°C for 3 min, followed by 35 cycles at 94°C for 30 s, 56°C for 30 s, and 72°C for 1 min, and final extension at 72°C for 5 min. The amplified products were analyzed by electrophoresis in 1.2% (w/v) agarose gels. Total RNAs of callus were extracted by RNAprep pure Plant Kit (TianGen, Beijing, China). The cDNAs were synthesized by PrimeScript™ RT Master Mix kit (Perfect Real Time) (Takara, Beijing, China). The RT-qPCR primers were designed with the Primer Premier 5.0 software based on the GUS gene: forward primer (5'-AAGAGCG ATGAGCACGAGTA-3'), and reverse primer (5'-AGAAATC AAACAACCCACGA-3'). *PlACTIN* (GenBank accession no. JN105299.1) was used as an internal control (Li et al., 2020). The Actin genes were detected using primers as followed: forward primer (5'-GGTCTATTCTTGCTTCCCTC-3') and reverse primer (5'-CCCTCTGCGTCTACACTTTC-3'). The RT-qPCR was performed with StepOne™ 7500 Real-Time PCR using the TB Green ® Premix Ex Taq™ II (Tli RNaseH Plus) (Takara, Beijing, China). The reactions were accomplished according to the following method, holding stage: 95°C for 30 s; cycling stage: 40 cycles of 95°C for 5 s, 60°C for 30 s; melt curve stage: 95°C for 15 s, 60°C for 1 min, 95°C for 15 s. Each experiment was performed with three biological and technical replicates. The results were analyzed according to the $2^{-\Delta\Delta Ct}$ methods, and exhibited by GraphPad Prism 8.0.

Statistical analysis

Three biological replicates were performed for all experimental treatments in this article. We used SPSS22.0 software to perform one-way analysis of variance (ANOVA) and Duncan's method for multiple comparisons of the obtained data to determine whether the differences between the data were significant. The important data involved in the paper are calculated as follows: Induction rate = the number of inducted explants/total explants × 100%, Mortality rate = number of dead explants/total explants × 100%, Proliferation coefficient = weight of fresh proliferated callus/weight of inoculated callus, Browning rate = number of browned explants/total explants × 100%, GUS expression rate = the number of GUS-positive receptors/total number stained × 100%.

Results

Effect of different explant on inducing callus

The cotyledons are the most likely to produce callus (Figure 1A). Cotyledons became thicker after 3 d of culture, and light green callus was generated after 10 d. It had the highest induction rate (92.33%) and the lowest mortality rate (7.67%) (Figure 2). After 10 d of culture, the stem generated green callus gradually, with induction rate and mortality rate were 55.33% and 44.33%, respectively (Figures 1B and 2). However, leaves

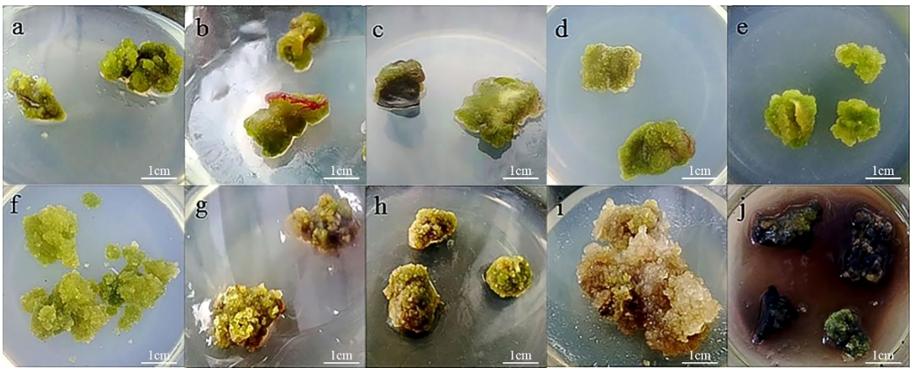

FIGURE 1
Callus induction and proliferation of *P. lactiflora*. **(A)** callus from cotyledon, **(B)** callus from stem, **(C)** callus from leave, **(D)** callus induction on MS medium containing 1.0 mg·L^{-1} 2,4-D, 0.5 mg·L^{-1} NAA and 0.5 mg·L^{-1} TDZ after culture for 30 days, **(E)** callus induction on MS medium containing 0.5 mg·L^{-1} 2,4-D, 1.0 mg·L^{-1} NAA and 0.5 mg·L^{-1} TDZ after culture for 30 days, **(F)** proliferation of callus from cotyledon, **(G)** proliferation of callus from stem, **(H)** proliferation of callus from leave, **(I)** waterlogged callus, **(J)** browned callus.

were not suitable for inducing callus. Although some leaves could generate calluses after 10 d of culture, most leaves died after 20 d with the highest mortality rate (66.33%) and the lowest induction rate (33.00%) (Figures 1C and 2). Thus, the optimal explant for callus induction is the cotyledon.

Effect of 2, 4-D, NAA, TDZ and 6-BA on callus induction

Auxin had an important influence on the induction rate of callus. After 20 d of culture on MS medium containing 2,4-D, the callus produced and grew slowly. With the increase of 2,4-D concentration, the induction rate increased gradually. The highest value was 57.78% when treated with 1.0 mg·L^{-1} 2,4-D. The calluses in Group 1 were in a better growth state and presented green and full of vitality (Table 1). While on MS medium containing NAA, the cotyledon generated callus only after 7 d of culture. After 20 d, the whole cotyledon became callus. When the concentration of NAA was 0.5 mg·L^{-1}, the callus in Group 2 induction rate reached the maximum (Table 1). However, the callus presented as unhealthy, waterlogged, yellow-white and loose. Some callus stopped growing and even died due to browning. Therefore, 2,4-D was beneficial to callus growth, while NAA could decrease the time required for callus induction.

Cytokinin is also indispensable in the process of inducing callus. Cytokinin promotes cell division and differentiation. An appropriate concentration of cytokinin and auxin will effectively improve the induction efficiency of callus. Based on the results described, 1.0 mg·L^{-1} 2,4-D was added to MS medium. At the same time, different concentrations of 6-BA or TDZ were added. After adding cytokinin, the whole cotyledon became calluses for an average culture of 15 d, and the callus growth state was

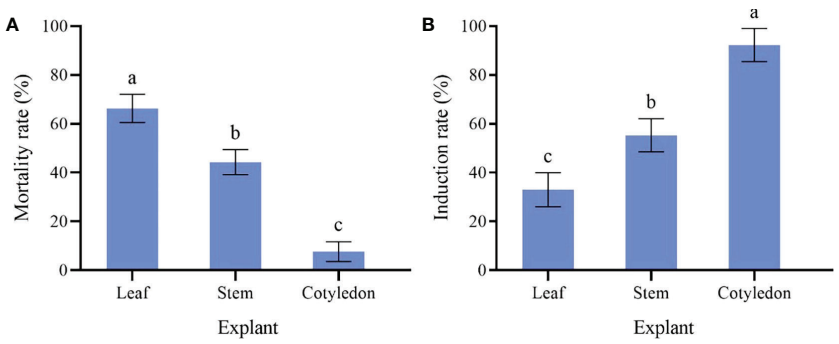

FIGURE 2
Effect of different explant of sterile seedling on *P. lactiflora* callus induction. **(A)** mortality rate of callus induced by different explants, **(B)** induction rate of callus induced by different explants, the different letters within a column marked significant differences ($p < 0.05$).

effectively improved. High or low TDZ concentration was not conducive to the callus induction. The highest rate of callus induction (67.78%) was in Group 3, which was observed from the 1.0 mg·L^{-1} TDZ (Table 1). The callus was fresh green and loose. Although there was a small amount of browning, it was effectively improved by transferring to a fresh medium. It could be seen from the fourth group that 1.0 mg·L^{-1} 6-BA had the highest induction efficiency (Table 1). The callus presented yellow-green and dense. After 40 d, the callus browning occurred and the browning degree did not decrease after transferring to a fresh medium. Thus, TDZ was more effective on callus induction than 6-BA.

The presence of 2,4-D was important to ensure callus growth state, while NAA was important for the velocity of callus induction. We found that the combination of NAA, 2,4-D and TDZ was more conducive to the callus induction. Meanwhile, the callus presented fresh green, dense and full of vitality (Table 1). On the average culture of 10 d, the whole cotyledon became callus. The highest induction rate (86.67%) was observed on MS medium supplemented with 1.0 mg·L^{-1}2,4-D, 0.5 mg·L^{-1}NAA and 0.5 mg·L^{-1} TDZ or MS medium supplemented with 0.5 mg·L^{-1} 2,4-D, 1.0 mg·L^{-1} NAA and 0.5 mg·L^{-1} TDZ. The latter was in a better growth state and presented less browning after culture (Figure 1D and Figure 1E). Therefore, the optimal medium for callus induction was MS medium containing 0.5 mg·L^{-1} 2,4-D, 1.0 mg·L^{-1} NAA and 0.5 mg·L^{-1} TDZ.

Effect of different explants on callus proliferation

The proliferation of callus from the cotyledon was fast, which presented emerald green, tight and uniform texture (Figure 1F). The highest proliferation coefficient (2.31) was observed on callus from the cotyledon and the browning rate was 13.33% (Figure 3). Callus induced from the stem had the lowest proliferation coefficient (1.12) and poor growth status. Reduced fullness and soft texture were observed during the culture (Figure 1G), with the highest browning rate (26.67%) and a serious browning degree (Figure 3). The proliferation coefficient was 1.63 of leaf callus. Its texture was compact (Figure 1H) and the proliferation rate was slower, while the browning rate was lower (10.00%). Therefore, callus from the cotyledon was the best choice for callus proliferation.

Effects of NAA, 2, 4-D and TDZ on callus proliferation

Considering that the effect of 6-BA on callus was not as good as TDZ, we did not use 6-BA in this experiment. When the concentration of TDZ was constant, 2,4-D and NAA had different effects on callus proliferation. Different concentrations of 2,4-D resulted in no significant difference in proliferation coefficient, while the browning rate increased gradually with the increase of 2,4-D concentration (Table 2, Group 1). When the concentration of TDZ was the constant, high or low concentration of NAA was not conducive to the callus proliferation. The maximum proliferation coefficient (1.68) and lowest browning rate (23.33%) were observed when 0.5 mg·L^{-1} NAA was applied (Table 2, Group 2). The callus presented yellow-green and loose with the supplement of 2,4-D, while the callus showed different degrees of green, full and loose texture due to the NAA supplement. On these two mediums, the callus will gradually brown from the inside to the outside after a culture of 30 d. Although browning will be effectively alleviated by transfer, the callus aged and even produced white aerial roots. According to this study, 2,4-D was better than NAA on improving callus proliferation coefficient, and the browning rate was lower (Table 2). As for the growth state, NAA had a better effect.

Based on the results of callus proliferation, NAA, 2,4-D and TDZ were combined to improve the callus proliferation

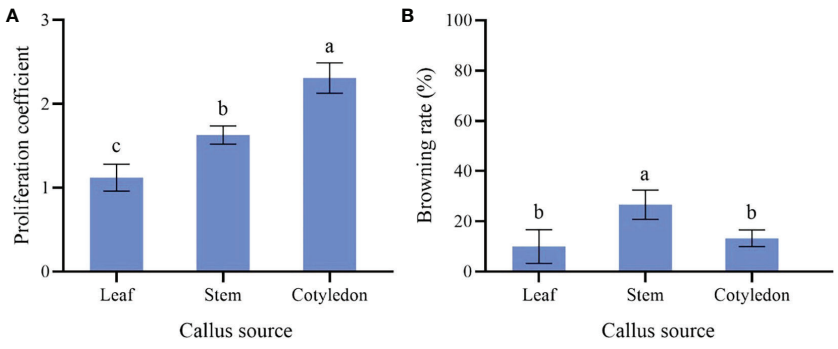

FIGURE 3
Effect of different explants on *P. lactiflora* callus proliferation. **(A)** proliferation coefficient of callus induced by different explants, **(B)** browning rate of callus induced by different explants, the different letters within a column marked significant differences ($p < 0.05$).

10.3389/fpls.2022.996690

and this brought a better effect (Table 2, Group 3). After being transferred to a proliferation medium for 20 d, the callus proliferated vigorously and presented a green, full and loose growth state. However, browning occurred at varying degrees. The callus proliferation coefficient reached the highest value (3.21) on the MS medium containing 0.5 mg·L^{-1}NAA, 1.0 mg·L^{-1}2,4-D and 0.5 mg·L^{-1} TDZ, followed by the 2.80, which was observed on the MS medium containing 1.0 mg·L^{-1} NAA, 0.5 mg·L^{-1} 2,4-D and 0.5 mg·L^{-1} TDZ. Their browning rates were 33.33% and 41.11%, respectively. Therefore, the optimal medium for callus proliferation was MS medium containing 0.5 mg·L^{-1} NAA, 1.0 mg·L^{-1} 2,4-D and 0.5 mg·L^{-1} TDZ.

Effect of different kanamycin and cefotaxime concentration on *P. lactiflora* callus growth

In this assay, the growth state of *P. lactiflora* callus was observed on a proliferation medium containing various concentrations of Kan or Cef (Figure 4). The callus was more sensitive to Kan. 75~150 mg·L^{-1} of Kan could strongly inhibit the growth of *P. lactiflora* callus. The higher concentration led to the lower proliferation rate and more serious browning of calluses, and even dead calluses (Table 3). According to the growth state, 125 mg·L^{-1} Kan was chosen to screen transformed callus of *P. lactiflora*.

Cef could inhibit the growth of *P. lactiflora* callus. The callus was less sensitive to Cef compared with Kan. Both 100, 200 and 300 mg·L^{-1} of Cef had an insignificant impact on the growth and proliferation of callus, while 400 mg·L^{-1} Cef could inhibit the callus obviously. Each callus presented browning. Combining its effect on *Agrobacterium* growth (Table 4), the optimal concentration of Cef might be 200 mg·L^{-1}.

Inhibitory effect of cefotaxime on *Agrobacterium* tumefaciens

For exploring the inhibitory effect of cefotaxime on *Agrobacterium tumefaciens*, we carried out the inhibition test of cefotaxime on *Agrobacterium*. The results showed that the OD_{600} value could not be detected when the concentration of cefotaxime was 200, 300 and 400 mg·L^{-1} (Table 4). Considering the effect of Cef on the callus growth of *P. lactiflora*, the optimal concentration of Cef was 200 mg·L^{-1}.

Transformation and obtaining of transgenic callus

In order to establish genetic transformation system and obtain transgenic callus, *Agrobacterium* strain EHA105 harboring the binary vector pBI121-GUS was used to infect callus. Various combinations of cell densities of *Agrobacterium* suspension at OD_{600} (0.2, 0.4, 0.6, 0.8 and 1.0), infection duration (10, 15, 20, 25 and 30 min) and co-culture duration (0, 1, 2, 3 and 4 d) were carried out to select the optimum transgenic system. Then, the GUS staining was used for the identification of transgenic callus after selection culture for 49 d (Figure 5).

Calluses induced by cotyledons with good and consistent growth were selected for *Agrobacterium* transformation in this experiment. *Agrobacterium* cell densities, infection and co-culture duration are key transformation factors directly affecting genetic transformation. Our results showed that the effects of different *Agrobacterium* cell densities were quite different (Figure 6). High or low cell densities were not conducive to the genetic transformation of *P. lactiflora* callus. When OD_{600} was 0.6, the callus attained the maximum GUS expression rate (53.33%). In the same way, we also found that 25 min of infection and 3 d of co-culture led to the highest GUS expression rate, with 68.33%

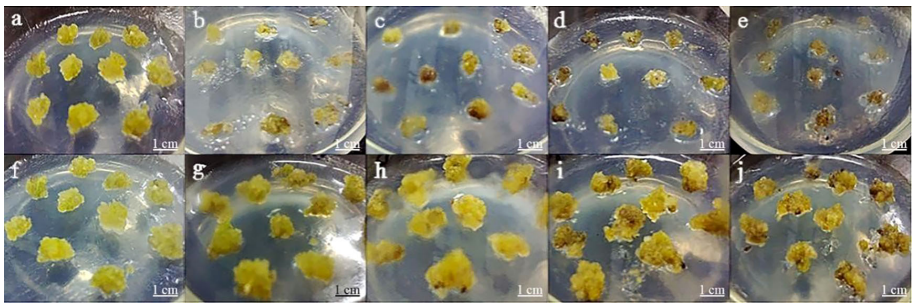

FIGURE 4
Antibiotic sensitivity assay of *P. lactiflora* callus. **(A–E)** kanamycin concentrations were 0, 75, 100, 125 and 150 mg·L^{-1}, respectively. **(F–J)** cefotaxime concentrations were 0, 100, 200, 300, and 400 mg·L^{-1}, respectively.

10.3389/fpls.2022.996690

TABLE 3 Kanamycin effects on *P. lactiflora* callus proliferation.

Concentration of kanamycin (mg·L^{-1})	0	75	100	125	150
Proliferation rate (%)	100 ± 0.01a	10.8 ± 0.58b	5.4 ± 0.79bc	0.00 ± 0.00c	0.00 ± 0.00c
Browning rate (%)	18,97 ± 2.33e	26.64 ± 1.86cd	27.68 ± 1.92bc	29.06 ± 1.32b	32.7 ± 1.47a

The values represented mean ± SD, and different letters marked significant differences ($p < 0.05$).

TABLE 4 Cefotaxime effects on *Agrobacterium* growth.

Concentration of cefotaxime (mg·L^{-1})	0	100	200	300	400
Cell density of *Agrobacterium* (OD_{600})	1.17 ± 0.01a	0.12 ± 0.01b	0.00 ± 0.00c	0.00 ± 0.00c	0.00 ± 0.00c

The values represented mean ± SD, and different letters marked significant differences ($p < 0.05$).

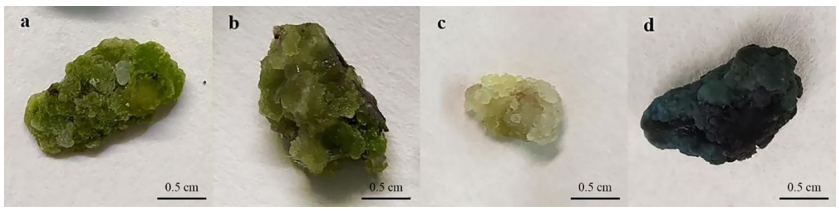

FIGURE 5
Genetic transformation of *P. lactiflora* callus by *Agrobacterium*-mediated transformation. **(A)** callus before *Agrobacterium* infection, **(B)** callus after *Agrobacterium* infection, **(C)** GUS expression in control callus, **(D)** GUS expression in transgenic callus.

and 61.67%, respectively. Therefore, OD_{600} = 0.6, 25 min for infection and co-culture for 3 d were chosen as the optimal *Agrobacterium* transformation conditions.

Molecular identification of transformants

Further molecular identification of the resistant calluses was confirmed by PCR and RT-qPCR. GUS-positive resistant calluses were selected randomly and confirmed by PCR and RT-qPCR. In PCR validation test, plasmid pBI121 was used as the positive control and non-transgenic callus DNA was used as the negative control. The presence of amplified fragments in GUS-positive resistant calluses samples and pBI121 plasmid confirmed the presence and integration of the *GUS* gene in the *P. lactiflora* genome. Non-transgenic callus genomic DNA did not show any amplified fragments (Figure 7). In order to further identify the transgenic callus at the transcriptional level, RT-

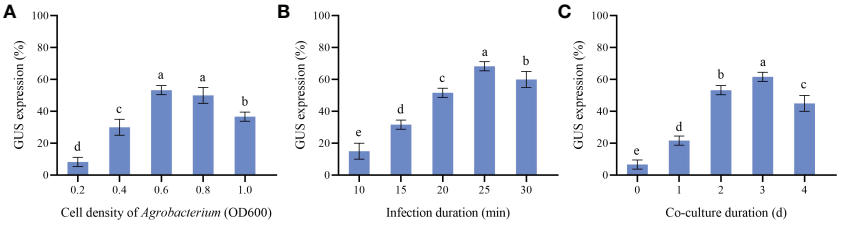

FIGURE 6
Parameters affecting transformation efficiency. **(A)** GUS expression at different *Agrobacterium* cell density, **(B)** GUS expression at different Infection duration, **(C)** GUS expression at different Co-culture duration, the different letters within a column marked significant differences ($p < 0.05$).

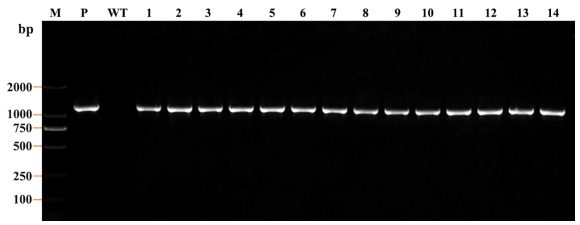

FIGURE 7
PCR analysis of the GUS-positive resistant callus of *P. lactiflora*. PCR product in 1182 bp was observed in each positive callus except wild-type with *GUS* gene-specific primer. Lane M, DL2000 DNA marker; lane P, plasmid control; lane WT, wild-type callus; lanes 1-14, different GUS-positive callus.

qPCR was used to detect the expression level of the *GUS* gene in non-transgenic callus and GUS-positive resistant calluses. The results showed that the *GUS* gene expression was not detected in the non-transgenic callus, but it was detected in GUS-positive resistant calluses (Figure 8).

Discussion

Plant callus is considered to have the potential to be used in rapid mass propagation of plants because of its advantages of easy access, strong ability of proliferation and differentiation (Wang et al., 2021b). However, callus induction and proliferation are distinct in different plant species (Xu et al., 2017). The success of callus induction is strongly related to the choice of the explant. Explant source and growth physiological state will directly affect the process of callus induction (Guo and Jeong, 2021). Seeds, cotyledons, stems, leaves, anthers, short limbs and even young fruits are usually used as explants for callus induction (Singh et al., 2015; Din et al., 2016; Bai et al., 2019). In fact, there have been many studies on callus induction in herbaceous peony, in which explants selection has been generally concerned (Shen et al., 2012). When the

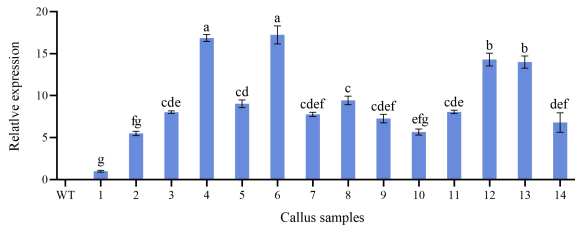

FIGURE 8
Relative expression level of *GUS* gene in non-transformed and transgenic callus. WT, non-transformed callus; 1-14, different transgenic callus, the different letters within a column marked significant differences ($p < 0.05$).

underground buds of *P. lacactiflora* were used as explants, the buds developed well and had strong ability to differentiate and proliferate *in vitro* (Tian et al., 2010). Orlikowska et al. used petioles, leaves and young stems of *Paeonia loniflorica* as explants for induction experiments. Their results showed that whether these explants could induce callus successfully depended on their culture conditions in the first 1.5 months, and the young stems were considered to have the most differentiation potential (Orlikowska et al.,1998). For wild herbaceous peony, the callus induction from vegetative organs was not only limited by season, but also complicated and ineffective in sterilization (Shen et al., 2012). In the present study, we further optimized the selection of explants based on the experience of previous studies. We induced callus using different parts of sterile seedlings obtained from cultivated seeds. The reason we did this is that seeds are easy to preserve and obtain, ensuring that explants are available regardless of time and season. In addition, the obtained sterile seedlings don't need to be sterilized, which could improve the induction efficiency. In our study, the most suitable explant for callus induction was sterile seedling cotyledon (Figure 2), and the order of proliferation ability of callus from different explants was cotyledon > leaf > stem (Figure 3). Therefore, cotyledons obtained from seed culture was most suitable for callus induction and proliferation. The reason for this result, we believe, is that cotyledon emerges at the early stage of growth and development, and the meristem cells are more active (Hu et al., 2015). Just because of this reason, we further speculated that the callus induced by cotyledon had strong growth vigor and high proliferation efficiency. Stem and leaf are at the mid-growth stage. Although their cells are totipotent, the cells of plant organs have already differentiated. So, the dedifferentiation ability of stem and leaf is relatively reduced, which may cause low efficiency in the callus induction and proliferation.

Adding plant growth regulators to the basal medium will make different effects on callus induction and proliferation (Kotb et al., 2020). Many previous studies have proved that PGRs are very important for plant callus induction and proliferation. The combination of auxin and cytokinin could improve the induction rate of callus, and the induction rate was higher when the ratio of cytokinin to auxin was between 1:1.4 and 1:5 (Shen et al., 2012). TDZ and 6-BA are both important cytokinins and play a significant role in the induction and proliferation of plant callus (Roy et al., 2012). TDZ has stronger cytokinin activity, and is superior to 6-BA in both callus and branch proliferation (Zhao et al., 2017). Similarly, our results proved that TDZ was also superior to 6-BA in callus induction of *P.lactiflora* (Table 1). In this study, on the basis of previous studies, we further optimized the components of the culture medium for callus induction from *P. lactiflora*.The results showed that two auxins, 2,4-D and NAA, affected *P. lactiflora* callus induction significantly. On 2,4-D supplemented medium, the induced callus was bright green, dense and high viable, while

the induced callus was loose, water-stained, low viable and browning occurred on NAA supplemented medium (Table 1). Therefore, we believe that 2,4-D had a better effect on callus induction than NAA, which was consistent with the previous study (Wang et al., 2010). Our results also show that when combined with TDZ in the process of proliferation, the callus proliferation coefficient was greater in a medium containing 2,4-D than that in a medium containing NAA at the same concentration. The combination of 2,4-D, NAA and TDZ were more effective in both the callus induction and proliferation process, maintaining a higher induction rate and proliferation coefficient as well as a better callus growth state. These results again indicate that 2, 4-D, NAA and TDZ play an important role in callus proliferation.In the course of our experiments, we unexpectedly discovered some preliminary methods that may reduce the browning in *P. lactiflora* tissue culture. Browning is a common phenomenon in plant tissue culture and has always been a big hurdle in the tissue culture of *P. lactiflora* (Gao et al., 2020). The explants release brown substances or phenolics into the medium in the course of plant tissue culture, which can inhibit the normal growth and differentiation of cell tissues, and even lead to death (Shen et al., 2012). Plant growth regulators have a certain effect on the browning of callus (Shen et al., 2012). In our present study, in the medium supplemented with 2,4-D, the callus was lightly browned and browning could be effectively suppressed by transferring to a new medium, while callus browning increased in the NAA-added medium. When the ratio of auxin and cytokinin varied from 1:1 to 2:1, the browning degree was lighter. Moreover, frequent transfer could slightly reduce the degree of browning but the callus gradually stopped growing after multiple transfers. Our findings may be helpful in alleviating the browning of *P. lactiflora* tissue culture, but the novel methods and mechanisms of browning prevention have yet to be obtained.

During genetic transformation, the main role of antibiotics such as Kan and Cef is to screen resistant plants or to inhibit the overgrowth of *Agrobacterium*. Previous studies have reported the optimal concentration of Kan (5-100 $mg{\cdot}L^{-1}$) and Cef (50-400 $mg{\cdot}L^{-1}$) in plants of different genera (Matsuda et al., 2005; Freiman et al., 2012; Yang et al., 2017). These studies indicated that different genotypes have different degrees of sensitivity to antibiotics, suggesting the importance of screening antibiotic concentration during transformation. In our study, we found that 125 $mg{\cdot}L^{-1}$ Kan could completely inhibit the growth of callus, and 200 $mg{\cdot}L^{-1}$ Cef was the optimal concentration to inhibit the growth of *Agrobacterium* without affecting the growth of callus. (Table 4 and Figure 4). We believe that under the action of these two antibiotics, not only positive transgenic callus can be obtained, but also the growth of *Agrobacterium* can be completely inhibited, so as to avoid the pollution caused by *Agrobacterium* attachment during molecular identification.

The *Agrobacterium*-mediated genetic transformation is the most widely used transformation method (Liu et al., 2021). However, there were few applications on *P. lactiflora*. Transformation receptor and condition are key factors affecting genetic transformation (Shen et al., 2012). Plant callus is very suitable as transformation receptor (Liu et al., 2021). It is generally believed that the pre-culture and wound of explants before transformation can improve the transformation rate of exogenous genes (Wu et al., 2014; Yan et al., 2019). Nevertheless, callus can be used as acceptor material without considering these steps (Sedaghati et al., 2018). *Agrobacterium* cell density, infection time and co-culture time have important effects on genetic transformation efficiency, and optimal parameters vary depending on the plant materials and/or acceptor types (Sedaghati et al., 2018; Yan et al., 2019). Low cell density may not provide sufficient bacteria and short periods are not conducive to establish contact between the acceptor material and *Agrobacterium*. High cell density or long co-culture time will easily cause contamination (Yan et al., 2019). Extreme cell density and infection time affect the transformation efficiency because of the *Agrobacterium* toxicosis or incomplete contact with the surface of callus (Ahmed et al., 2015). Short co-culture time may lead to incomplete T-DNA transfer process. Conversely, long co-culture time will lead to the excessive multiplication of *Agrobacterium*, which poisons the callus (Wu et al., 2015). In order to determine the optimal transformation conditions for *Agrobacterium*-mediated genetic transformation and whether the target gene can be effectively transferred into peony callus, we used GUS staining experiment to observe the transformation efficiency of the target gene. From the results, we can also see that different amounts of GUS chromogenesis were observed under various transformation conditions designed by us. *Agrobacterium* cell density at 0.6 OD_{600}, 25 min of infection and 3 d of co-culture showed high GUS staining positive rate during the screening process (Figure 6). PCR and RT-qPCR are commonly used to detect transgenic plants (Rajeevkumar et al., 2015; Wu et al., 2019; Wang et al., 2021b). As can be seen from PCR results, clear and bright amplified fragments were observed in 14 GUS-positive samples randomly selected, and the length of the fragments was consistent with the target gene (Figure 7). This indicates that our method can successfully transfer the target gene into the callus of *P. lactiflora*. RT-qPCR results also showed that GUS gene expression was detected in all GUS-positive resistant calluses compared with the non-transgenic callus, although GUS gene expression was slightly different in different GUS-positive resistant calluses (Figure 8). However, from the results, the

relative expression levels of target genes in most samples are relatively stable, which indicates that our method is feasible.

Conclusion

In conclusion, this study optimized and established an efficient method for callus induction and proliferation of *P. lactiflora*. Based on this method, cotyledons were used as explants to induce and proliferate high-quality callus, and then an efficient transgenic method using callus of *P. lactiflora* was established through *Agrobacterium* mediated genetic transformation. Our results provide theoretical basis and technical support for the establishment of a complete and stable genetic transformation system of herbaceous peony and further understanding of the molecular and genetic mechanisms related to herbaceous peony.

Data availability statement

The datasets presented in this study can be found in online repositories. The names of the repository/repositories and accession number(s) can be found in the article/Supplementary Material.

Author contributions

XS, SD and XL designed the project. WC, QP, XL, SD and RF completed the callus induction and proliferation experiment. SD, RX and XL completed *Agrobacterium*-mediated transformation conditions screening experiment. XL and RF were involved in GUS staining experiment. This article was written by SD, XL and SG. All authors contributed to the article and approved the submitted version.

Funding

This work was supported by the National Natural Science Foundation of China (32071814 and 31470696).

Conflict of interest

The authors declare that the research was conducted in the absence of any commercial or financial relationships that could be construed as a potential conflict of interest.

Publisher's note

All claims expressed in this article are solely those of the authors and do not necessarily represent those of their affiliated organizations, or those of the publisher, the editors and the reviewers. Any product that may be evaluated in this article, or claim that may be made by its manufacturer, is not guaranteed or endorsed by the publisher.

References

Ahmed, M., Khan, N., Hafiz, I. A., Abbasi, N. A., and Anjum, M. A. (2015). Effect of various factors on the efficiency of *Agrobacterium*-mediated transformation of grape (*Vitis vinifera* l.). *Vegetos* 28, 171. doi: 10.5958/2229-4473.2015.00024.5

An, J. P., Li, R., Qu, F. J., You, C. X., Wang, X. F., and Hao, Y. J. (2018). An apple NAC transcription factor negatively regulates cold tolerance *via* CBF-dependent pathway. *J. Plant Physiol.* 221, 74–80. doi: 10.1016/j.jplph.2017.12.009

Bai, S. L., Tao, R. W., Tang, Y. X., Yin, L., Ma, Y. J., Ni, J. B., et al. (2019). BBX16, a b-box protein, positively regulates light-induced anthocyanin accumulation by activating MYB10 in red pear. *Plant Biotechnol. J.* 17, 1985–1997. doi: 10.1111/pbi.13114

Bai, S. L., Tao, R. Y., Yin, L., Ni, J. B., Yang, Q. S., Yan, X. H., et al. (2019). Two b-box proteins, PpBBX18 and PpBBX21, antagonistically regulate anthocyanin biosynthesis *via* competitive association with *Pyrus pyrifolia* elongated hypocotyl 5 in the peel of pear fruit. *Plant J.* 100, 1208–1233. doi: 10.1111/tpj.14510

Chakraborty, N., Chakraborty, P., Sen, M., and Bandopadhyay, R. (2020). Choice of explant for plant genetic transformation. *Methods Mol. Biol.* 2124, 107–123. doi: 10.1007/978-1-0716-0356-7_5. Springer Press.

Chen, Y., Rivlin, A., Lange, A., Ye, X. D., Vaghchhipawala, Z., Eisinger, E., et al. (2014). High throughput *Agrobacterium* tumefaciens-mediated germline transformation of mechanically isolated meristem explants of cotton (*Gossypium hirsutum* l.). *Plant Cell Rep.* 33, 153–164. doi: 10.1007/s00299-013-1519-x

Chetty, V. J., Ceballos, N., Garcia, D., Narvaez-Vasquez, J., Lopez, W., and Orozco-Cardenas, M. L. (2013). Evaluation of four *Agrobacterium* tumefaciens strains for the genetic transformation of tomato (*Solanum lycopersicum* l.) cultivar micro-tom. *Plant Cell Rep.* 32, 239–247. doi: 10.1007/s00299-012-1358-1

Din, A. J. M., Ahmad, F. I., Wagiran, A., Abd Samad, A., Rahmat, Z., and Sarmidi, M. R. (2016). Improvement of efficient *in vitro* regeneration potential of mature callus induced from Malaysian upland rice seed (*Oryza sativa* cv. panderas). *Saudi J. Biol. Sci.* 23, S69–S77. doi: 10.1016/j.sjbs.2015.10.022

Freiman, A., Shlizerman, L., Golobovitch, S., Yablovitz, Z., Korchinsky, R., Cohen, Y., et al. (2012). Development of a transgenic early flowering pear (*Pyrus communis* l.) genotype by RNAi silencing of PcTFL1-1 and PcTFL1-2. *Planta* 235, 1239–1251. doi: 10.1007/s00425-011-1571-0

Gao, J., Xue, J. Q., Xue, Y. Q., Liu, R., Ren, X. X., Wang, S. L., et al. (2020). Transcriptome sequencing and identification of key callus browning-related genes from petiole callus of tree peony (*Paeonia suffruticosa* cv. kao) cultured on media with three browning inhibitors. *Plant Physiol. Biochem.* 149, 36–49. doi: 10.1016/j.plaphy.2020.01.029

Georgiev, V., Slavov, A., Vasileva, I., and Pavlov, A. (2018). Plant cell culture as emerging technology for production of active cosmetic ingredients. *Eng. Life Sci.* 18, 779–798. doi: 10.1002/elsc.201800066

Guo, G., and Jeong, B.R. (2021). Explant, medium, and plant growth regulator (PGR) affect induction and proliferation of callus in *Abies koreana*. *Forests* 12, 10. doi: 10.3390/f12101388

Hu, S., Ma, Y. Y., Jiang, H. L., Feng, D. J., Yu, W., Dai, D. M., et al. (2015). Production of paeoniflorin and albiflorin by callus tissue culture of *Paeonia lactiflora* pall. *Chin. J. Chem. Eng.* 23, 451–455. doi: 10.1016/j.cjche.2014.06.036

Jana, S., Sivanesan, I., Lim, M. Y., and Jeong, B. R. (2013). *In vitro* zygotic embryo germination and somatic embryogenesis through cotyledonary explants of *Paeonia lactiflora* pall. *Flower Res. J.* 21, 17–22. doi: 10.11623/frj.2013.21.1.2

Jefferson, R. A. (1987). Assaying chimeric genes in plants: The GUS gene fusion system. *Plant Mol. Biol. Rep.* 5, 387–405. doi: 10.1007/bf02667740

Kotb, O. M., Abd El-Latif, F. M., Atawia, A. R., Saleh, S. S., and El-Gioushy, S. F. (2020). *In vitro* propagation and callus induction of pear (*Pyrus communis*) cv. *'Le-conte'*. *Asian J. Biotechnol. Genet. Eng.* 3, 1–10. doi: 10.3390/agronomy12102531

Li, X. T., Fei, R. W., Chen, Z. J., Fan, C. Z., and Sun, X. M. (2020). Plant hormonal changes and differential expression profiling reveal seed dormancy removal process in double dormant plant-herbaceous peony. *PLoS One* 15, e0231117. doi: 10.1371/journal.pone.0231117

Liu, Y. R., Cen, H. F., Yan, J. P., Zhang, Y. W., and Zhang, W. J. (2015). Inside out: high-efficiency plant regeneration and *Agrobacterium*-mediated transformation of upland and lowland switchgrass cultivars. *Plant Cell Rep.* 34, 1099–1108. doi: 10.1007/s00299-015-1769-x

Liu, C. Y., Jiao, S. Q., Zhang, Q., Yao, P. Q., Xie, L. H., Wang, Z., et al. (2022). Transcriptome profiling provides preliminary molecular insights into adventitious bud formation in herbaceous peony (*Paeonia* x 'Coral charm'). *J. Horticult. Sci. Biotechnol.* 97, 476–486. doi: 10.1080/14620316.2021.2025156

Liu, G. Q., Yuan, Y., Jiang, H., Bao, Y., Ning, G. G., Zhao, L. J., et al. (2021). *Agrobacterium tumefaciens*-mediated transformation of modern rose (*Rosa hybrida*) using leaf-derived embryogenic callus. *Hortic. Plant J.* 7, 359–366. doi: 10.1016/j.hpj.2021.02.001

Lu, J., Sun, M. H., Ma, Q. J., Kang, H., Liu, Y. J., Hao, Y. J., et al. (2019). MdSWEET17, a sugar transporter in apple, enhances drought tolerance in tomato. *J. Integr. Agric.* 18, 2041–2051. doi: 10.1016/s2095-3119(19)62695-x

Lv, Y. D., Zhang, M. L., Wu, T., Wu, T. L., and Zhong, Y. (2019). The infiltration efficiency of *Agrobacterium*-mediated transient transformation in four apple cultivars. *Sci. Hortic.* 256, 108597. doi: 10.1016/j.scienta.2019.108597

Matsuda, N., Gao, M., Kanji, I., Tadashi, T., and Nishimura, K. (2005). Development of an *Agrobacterium*-mediated transformation method for pear (*Pyrus communis* l.) with leaf-section and axillary shoot-meristem explants. *Plant Cell Rep.* 24, 45–51. doi: 10.1007/s00299-005-0924-1

Mayavan, S., Subramanyam, K., Arun, M., Rajesh, M., Dev, G., Sivanandhan, G., et al. (2013). *Agrobacterium* tumefaciens-mediated in planta seed transformation strategy in sugarcane. *Plant Cell Rep.* 32, 1557–1574. doi: 10.1007/s00299-013-1467-5

Ni, J. B., Bai, S. L., Zhao, Y., Qian, M. J., Tao, R. Y., Yin, L., et al. (2018). Ethylene response factors Pp4ERF24 and Pp12ERF96 regulate blue light-induced anthocyanin biosynthesis in 'Red zaosu' pear fruits by interacting with MYB114. *Plant Mol.Biol.* 99, 67–78. doi: 10.1007/s11103-018-0802-1

Orlikowska, T., Marasek, A., and Kucharska, D. (1998). Regeneration of *Paeonia mloksewitschii* lom. and *Paeonia ten*uifolia lom. *in vitro* from different explants. *Acta Soc Bot. Pol.* 67, 223–227. doi: 10.5586/asbp.1998.026

Osakabe, Y., Liang, Z., Ren, C., Nishitani, C., Osakabe, K., Wada, M., et al. (2018). CRISPR-Cas9-mediated genome editing in apple and grapevine. *Nat. Protoc.* 13, 2844–2863. doi: 10.1038/s41596-018-0067-9

Palla, K. J., and Pijut, P. M. (2014). *Agrobacterium*-mediated genetic transformation of *Fraxinus americana* hypocotyls. *Plant Cell Tissue Organ Cult.* 120, 631–641. doi: 10.1007/s11240-014-0630-1

Qi, C. H., Zhao, X. Y., Jiang, H., Zheng, P. F., Liu, H. T., Li, Y. Y., et al. (2018). Isolation and functional identification of an apple MdCER1 gene. *Plant Cell Tissue Organ Cult.* 136, 1–13. doi: 10.1007/s11240-018-1504-8

Rajeevkumar, S., Anunanthini, P., and Sathishkumar, R. (2015). Epigenetic silencing in transgenic plants. *Front. Plant Sci.* 6. doi: 10.3389/fpls.2015.00693

Roy, A. R., Deka, B. C., Sajeev, S., and Pattanayak, A. (2012). TDZ induced micropropagation in *Cymbidium giganteum* wall. ex lindl. and assessment of genetic variation in the regenerated plants. *Plant Growth Regul.* 68, 435–445. doi: 10.1007/s10725-012-9732-0

Sedaghati, B., Haddad, R., and Bandehpour, M. (2018). Efficient plant regeneration and *Agrobacterium*-mediated transformation *via* somatic embryogenesis in purslane (*Portulaca oleracea* l.): an important medicinal plant. *Plant Cell Tissue Organ Cult.* 136, 231–245. doi: 10.1007/s11240-018-1509-3

Shen, M. M., Tang, Z. J., Teixeira, da Silva, J. A., and Yu, X. N. (2014). Induction and proliferation of axillary shoots from *in vitro* culture of *Paeonia lactiflora* pall. mature zygotic embryos. *N. Z. J. Crop Hortic. Sci.* 43, 42–52. doi: 10.1080/01140671.2014.944548

Shen, M. M., Wang, Q., Yu, X. N., and da Silva, J. A. T. (2012). Micropropagation of herbaceous peony (*Paeonia lactiflora* pall.). *Sci. Hortic.* 148, 30–38. doi: 10.1016/j.scienta.2012.09.017

Singh, P., Khan, S., Kumar, S., and Rahman, L. (2016). Establishment of an efficient *Agrobacterium*-mediated genetic transformation system in *Pelargonium graveolens*: an important aromatic plant. *Plant Cell Tissue Organ Cult.* 129, 35–44. doi: 10.1007/s11240-016-1153-8

Singh, R., Rai, M. K., and Kumari, N. (2015). Somatic embryogenesis and plant regeneration in *Sapindus mukorossi* gaertn. from leaf-derived callus induced with 6-benzylaminopurine. *Appl. Biochem. Biotechnol.* 177, 498–510. doi: 10.1007/s12010-015-1758-0

Sivanesan, I., Muthu, M., Gopal, J., Tasneem, S., Kim, D. H., and Oh, J. W. (2021). A fumigation-based surface sterilization approach for plant tissue culture. *Int. J. Environ. Res. Public Health* 18, 5. doi: 10.3390/ijerph18052282

Sun, Z. L., Li, X., Zhou, W., Yan, J., Gao, Y., Li, X. W., et al. (2019). *Agrobacterium*-mediated genetic transformation of Chinese chestnut (*Castanea mollissima* blume). *Plant Cell Tissue Organ Cult.* 140, 95–103. doi: 10.1007/s11240-019-01713-4

Sun, M., Wang, Y. Z., Yang, Y., Lv, M. W., Li, S. S., da Silva, J. A. T., et al. (2021). Analysis of chemical components in the roots of eight intersubgeneric hybrids of *Paeonia*. *Chem. Biodivers.* 18, 2. doi: 10.1002/cbdv.202000848

Tian, D., Tilt, K. M., Dane, F., Woods, F. M., and Sibley, J. L. (2010). Comparison of shoot induction ability of different explants in herbaceous peony (*Paeonia lactiflora* pall.). *Sci. Hortic.* 123, 385–389. doi: 10.1016/j.scienta.2009.10.007

Wang, J. F., Li, Q., and Meng, H. (2010). Induction and regeneration of callus tissues in five peony cultivars. *J. Beijing Forestry Univ.* 32, 213–216. doi: 10.13332/j.1000-1522.2010.03.009

Wang, F. P., Wang, X. F., Zhang, J., Ma, F., and Hao, Y. J. (2018). MdMYB58 modulates fe homeostasis by directly binding to the MdMATE43 promoter in plants. *Plant Cell Physiol.* 59, 2476–2489. doi: 10.1093/pcp/pcy168

Wang, Q., Fan, Y., da Silva, J. A. T., and Yu, X. N. (2021a). Transcriptomics analysis of *Paeonia lactiflora* pall. in response to drought stress by high-throughput sequencing. *J. Horticult. Sci. Biotechnol.* 96, 479–493. doi: 10.1080/14620316.2021.1886000

Wang, X. H., Zhou, F. L., Liu, J. L., Liu, W. Q., Zhang, S. L., and Li, D. L. (2021b). Establishment of efficient callus genetic transformation system for *Pyrus armeniacaefolia*. *Sci. Hortic.* 289, 110429. doi: 10.1016/j.scienta.2021.110429

Wu, J. D., Jiang, Y. L., Liang, Y. N., Chen, L., Chen, W. J., and Cheng, B. J. (2019). Expression of the maize MYB transcription factor ZmMYB3R enhances drought and salt stress tolerance in transgenic plants. *Plant Physiol. Biochem.* 137, 179–188. doi: 10.1016/j.plaphy.2019.02.010

Wu, J., Liu, C., Seng, S. S., Khan, M., Sui, J. J., Gong, B. H., et al. (2015). Somatic embryogenesis and agrobacterium-mediated transformation of *Gladiolus hybridus* cv. 'Advance red'. *Plant Cell Tissue Organ Cult.* 120, 717–728. doi: 10.1007/s11240-014-0639-5

Wu, R. G., Wang, Y., Wu, T., Xu, X. F., and Han, Z. H. (2017). Functional characterisation of MdMYB44 as a negative regulator in the response to cold and salt stress in apple calli. j. pomol. *J. Horticult. Sci. Biotechnol.* 93, 347–355. doi: 10.1080/14620316.2017.1373038

Xue, J. Q., Tang, Y., Wang, S. L., Yang, R. W., Xue, Y. Q., Wu, C. H., et al. (2018). Assessment of vase quality and transcriptional regulation of sucrose transporter and invertase genes in cut peony (*Paeonia lactiflora* 'Yang fei chu yu') treated by exogenous sucrose. *Postharvest Biol. Technol.* 143, 92–101. doi: 10.1016/j.postharvbio.2018.04.014

Xu, J. D., Wang, ,. X., Cao, H., Xu, H. D., Xu, Q., and Deng, X. X. (2017). Dynamic changes in methylome and transcriptome patterns in response to methyltransferase inhibitor 5-azacytidine treatment in citrus. *DNA Res.* 24, 509–522. doi: 10.1093/dnares/dsx021

Xu, K., Zhang, X. M., Fan, C. M., Chen, F. L., Zhu, J. L., Zhang, S. L., et al. (2017). A callus transformation system for gene functional studies in soybean. *J. Integr. Agric.* 16, 1913–1922. doi: 10.1016/S2095-3119(16)61621-0

Yang, Y. J., Wang, D. F., Wang, C. S., Wang, X. H., Li, J. N., and Wang, R. (2017). Construction of high efficiency regeneration and transformation systems of *Pyrus ussuriensis* maxim. *Plant Cell Tissue Organ Cult.* 131, 139–150. doi: 10.1007/s11240-017-1271-y

Yan, R., Wang, Z. P., Ren, Y. M., Li, H. Y., Liu, N., and Sun, H. M. (2019). Establishment of efficient genetic transformation systems and application of CRISPR/Cas9 genome editing technology in *Lilium pumilum* DC. fisch. and *Lilium longiflorum* white heaven. *Int. J. Mol. Sci.* 20, 12. doi: 10.3390/ijms20122920

Zhang, R. L., Wang, X. B., Shi, X. H., Shao, L. M., Xu, T., Xia, Y. P., et al. (2021). Chilling requirement validation and physiological and molecular responses of the bud endodormancy release in *Paeonia lactiflora* 'Meiju'. *Int. J. Mol. Sci.* 22, 16. doi: 10.3390/ijms22168382

Zhao, D. Q., Xia, X., Tang, Y., and Tao, J. (2019a). Microstructural and lignin characteristics in herbaceous peony cultivars with different stem strengths. *Postharvest Biol. Technol.* 159, 111043. doi: 10.1016/j.postharvbio.2019.111043

Zhao, X. Y., Qi, C. H., Jiang, H., Zheng, P. F., Zhong, M. S., Zhao, Q., et al. (2019b). Functional identification of apple on MdHIR4 in biotic stress. *Plant Sci.* 283, 396–406. doi: 10.1016/j.plantsci.2018.10.023

Zhao, D. Q., Xue, Y. F., Shi, M., and Tao, J. (2017). Rescue and *in vitro* culture of herbaceous peony immature embryos by organogenesis. *Sci. Hortic.* 217, 123–129. doi: 10.1016/j.scienta.2017.01.040

frontiers | Frontiers in Plant Science

TYPE Original Research
PUBLISHED 06 January 2023
DOI 10.3389/fpls.2022.1072717

OPEN ACCESS

EDITED BY
Shunli Wang,
Chinese Academy of Agricultural Sciences (CAAS), China

REVIEWED BY
Md Abdur Rahim,
Sher-e-Bangla Agricultural University, Bangladesh
Jason Zurn,
Kansas State University, United States

*CORRESPONDENCE
Zhanao Deng
zdeng@ufl.edu

SPECIALTY SECTION
This article was submitted to Plant Breeding, a section of the journal Frontiers in Plant Science

RECEIVED 17 October 2022
ACCEPTED 09 December 2022
PUBLISHED 06 January 2023

CITATION
Bhattarai K, Sharma S, Verma S, Peres NA, Xiao S, Clark DG and Deng Z (2023) Construction of a genome-wide genetic linkage map and identification of quantitative trait loci for powdery mildew resistance in *Gerbera* daisy. *Front. Plant Sci.* 13:1072717. doi: 10.3389/fpls.2022.1072717

Construction of a genome-wide genetic linkage map and identification of quantitative trait loci for powdery mildew resistance in *Gerbera* daisy

Krishna Bhattarai[1], Sadikshya Sharma[2], Sujeet Verma[2], Natalia A. Peres[3], Shunyuan Xiao[4], David G. Clark[5] and Zhanao Deng[1]*

[1]Department of Environmental Horticulture, Gulf Coast Research and Education Center, University of Florida, Institute of Food and Agricultural Sciences (IFAS), Wimauma, FL, United States, [2]Department of Horticultural Science, Gulf Coast Research and Education Center, University of Florida, Wimauma, FL, United States, [3]Department of Plant Pathology, Gulf Coast Research and Education Center, University of Florida, IFAS, Wimauma, FL, United States, [4]University of Maryland, Institute for Bioscience and Biotechnology Research, University of Maryland College Park, Rockville, MD, United States, [5]Department of Environmental Horticulture, University of Florida, IFAS, Gainesville, FL, United States

Powdery mildew (PM) is a common fungal disease in many important crops. The PM caused by *Podosphaera xanthii* has been the most challenging problem in commercial *Gerbera* (*Gerbera hybrida*) production globally, often leading to severe losses of crop yield and quality. A small number of PM-resistant breeding lines and cultivars have been reported in *Gerbera*, but the underlying genetics for PM resistance in *Gerbera* is largely unknown. Scarcity of genomic resources such as genetic linkage maps and molecular markers has severely hindered the effort to understand the genetic basis and locate loci controlling PM resistance in *Gerbera*. This study aimed to construct a genome-wide genetic linkage map, identify quantitative trait loci (QTL), and molecular markers for PM resistance in *Gerbera*. A segregating mapping population was developed by crossing PM-resistant and -susceptible *Gerbera* breeding lines, genotyped by sequencing, and phenotyped for PM resistance. A genome-wide genetic linkage map constructed with 791 single polymorphic site (SNP) markers spans 1912.30 cM across 27 linkage groups (LG) and reaches a density of 1 marker per 2.42 cM. One major consistent QTL was discovered in LG16, explaining more than 16.6% of the phenotypic variance for PM resistance. The QTL was tagged with two flanking SNP markers. The availability of this genetic linkage map will be very useful for locating and tagging QTLs for other important traits in *Gerbera*, and the newly discovered QTL and SNP markers will enable development of molecular markers for improving *Gerbera* for resistance to PM.

KEYWORDS

***Gerbera (Gerbera hybrida)*, powdery mildew resistance, genetic linkage map, QTL, disease resistance QTL, genotyping by sequecncing, single nucleotide polymorphism**

1 Introduction

Gerbera daisy (*Gerbera hybrida*) ($2n = 2\times = 50$) is commonly grown in many countries as cut flowers, garden flowers, and flowering potted plants. The sales value of cut *Gerbera*s sold by Royal FloraHolland in 2020 alone was €130 million (~$147 million) (https://www.statista.com/statistics/829413/sales-value-of-cut-flowers-sold-by-royal-floraholland-by-type/). Cut *Gerbera*s in the U.S. generated a wholesale value of $32 million in 2015 (USDA, 2016). The continuous introduction of new *Gerbera* cultivars with improved and novel traits is important for the global floral industry. Development of new cultivars in *Gerbera* has predominantly relied on conventional breeding (Deng and Bhattarai, 2018). Increased breeding efficiency is much needed to meet the demands of the floral industry and consumers of new *Gerbera* cultivars with better disease resistance.

There have been few efforts to develop genomic resources in *Gerbera*, including generation of expressed sequence tags, identification of single nucleotide polymorphisms (SNPs), genetic mapping of quantitative trait loci (QTLs), and simple sequence repeats (SSRs) (Gong and Deng, 2010; de Pinho Benemann et al., 2012; Gong and Deng, 2012; Song and Deng, 2013; Fu et al., 2016; Fu et al., 2017). With the advent of next generation sequencing (NGS) and genotyping-by-sequencing (GBS), large numbers of polymorphic sites, such as SNPs, can be readily identified, and construction of genetic linkage maps has become easier in plants for which reference genomes are not available (Elshire et al., 2011; Poland et al., 2012). SNPs are desirable among molecular markers because of their large numbers, ubiquitous distribution, biallelic nature, and high heritability (The International SNP Map Working Group, 2001). GBS is a genome complexity reduction approach that allows sequencing, discovery, and genotyping of thousands of SNPs using restriction enzyme-digested fragments from relatively small amounts of genomic DNA (Ansorge, 2009; Gore et al., 2009). Given the low cost of the technology, GBS has been widely used in several ornamental crops including rose, chrysanthemum, and hydrangea (Horst, 1990; Heo et al., 2017; Song et al., 2020; Wu and Alexander, 2020). In *Gerbera*, genetic analysis had not been done before using genome-wide SNPs and NGS technology. Previously, a linkage map was constructed using SNPs identified from ESTs of *Gerbera* lines segregating for *Botrytis* resistance (Fu et al., 2017). High-density genetic linkage maps are important for plant breeding and genetic research, particularly in plant species for which there are no well annotated reference genomes available. High-density linkage maps can be useful for identifying genes of interest, associating molecular markers with important traits, locating QTLs, and molecular cloning of valuable genes for breeding and genetic studies.

Powdery mildew (PM) is one of the most devastating pathogens infecting many row crops, vegetables, fruits, and ornamental/specialty crops worldwide. Numerous ornamental crops including *Gerbera*, rose, hydrangea, dahlia, and poinsettia can be severely infected by PM in the absence of resistant cultivars (Price, 1970; Benson et al., 2002; Braun et al., 2002; Deng and Bhattarai, 2018; Li et al., 2018). PM, caused by *Podosphaera xanthii* (syn. *Sphaerotheca fusca*), is one of the most challenging diseases in *Gerbera* production (Hausbeck, 2004; Channel, 2005; Granke et al., 2012). Negative impacts of PM in *Gerbera* are observed when the white powder-like spores and mycelia on the flower and plant canopy surfaces develop and severely reduce the aesthetic value. Reduction in visual appeal can result in significant losses to both *Gerbera* nurseries and the cutflower industry. In addition, reduced flower production and stunted plant growth are also caused by PM in controlled and field growing conditions. Various management practices, including the use of fungicides (e.g., azoxystrobin, myclobutanil, and pyraclostrobin), biofungicides (e.g., K-Phite, Millstop, and Tricon), treating with acidic electrolyzed oxidizing water, and burning elemental sulfur have offered preventative or limited post-infection control (Mueller et al., 2003).

Host resistance is considered to be one of the most effective, environmentally friendly and cost-effective methods to control PM and minimize crop losses in *Gerbera*. Developing PM-resistant *Gerbera* cultivars could offer a long-term solution to mitigate the disease, reduce the use of fungicides, and lower costs in *Gerbera* production. A better understanding of the genetics underlying PM resistance in *Gerbera* will facilitate the development of new PM-resistant cultivars. The main objectives of this study were to i) construct a genome-wide genetic linkage map using a biparental segregating mapping population and high-quality SNPs discovered from genotyping by sequencing and ii) identify QTLs and markers for PM resistance in *Gerbera*. This study is the first instance in *Gerbera* where GBS was used to discover SNPs and construct genetic linkage maps. Thus, the results from this study fill a major knowledge gap in *Gerbera* genetics and will likely advance PM resistance breeding efforts in *Gerbera*.

2 Results

2.1 Restriction enzyme combination and sequencing depth on SNP discovery

Two GBS experiments were conducted to select restriction enzymes (REs) and determine the sequencing depth for discovering SNPs in *Gerbera*. These experiments consisted of both parental lines, one pool of PM-resistant progenies, and one pool of PM-susceptible progenies. The number of loci and the total number of SNPs discovered in the two GBS experiments are shown in Figure 1 and Supplementary Table 1. Digestion of genomic DNA with *Bam*HI and *Nsi*I produced 7,029 SNPs when sequenced at 2 million reads/sample as compared to 4,059 SNPs

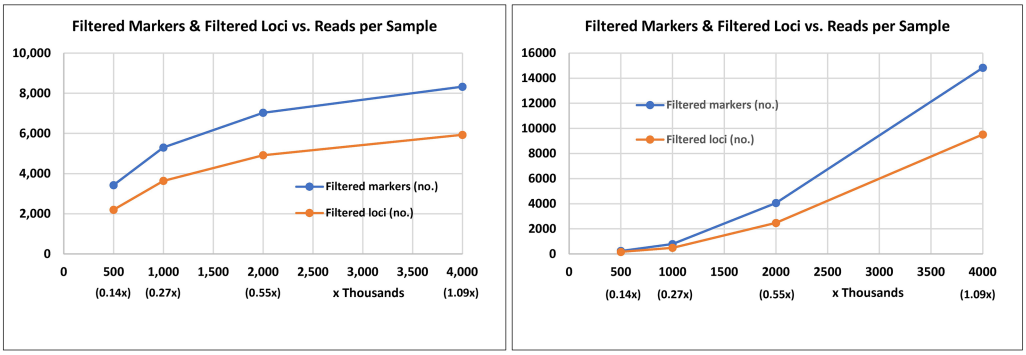

FIGURE 1
Marker and locus discovery rate from genotyping by sequence after digestion of *Gerbera* genomic DNA with two combinations of restriction enzymes and sequencing at different read depths (number of reads per sample). The combination of *Bam*HI and *Nsi* was used in the left chart and the combination of *Btg*I and *Taq*I in the right chart. Genomic DNA digestion, sequencing library preparation, and genotyping by sequencing were completed at the University of Minnesota Genomics Center.

when sequenced at 2 million reads/sample using *Btg*I and *Taq*I. Although, digestion of *Gerbera* genomic DNA with *Btg*I and *Taq*I prior to GBS generated a greater number of SNPs (14,826) when compared to digestion with *Bam*HI and *Nsi*I, which generated 8,327 SNPs when each sample was sequenced with 4 million reads, the rate of increment of SNP discovery declined as the reads per sample increased from 2 million to 4 million per sample (Figure 1). Digestion with *Bam*HI and *Nsi*I and sequencing rate of 2 million reads per sample seemed adequate for genotyping the *Gerbera* population in this study.

2.2 Linkage map construction

In total, 88 segregating individuals were genotyped-by-sequencing using the *Bam*HI and *Nsi*I for genomic DNA digestion. Three individuals were removed from further analyses because their GBS data failed to meet the SNP filtering criteria. In total, 3,541 SNPs and the genotyping data from 85 progenies were used in JoinMap 4.0 (Van Ooijen, 2006) for the linkage map construction. SNPs that showed recombination frequencies (> 0.4), distorted segregation ratios ($\chi^2 > 11.31$; $p < 0.0001$), or high nearest-neighbor stress values (> 10 cM) were excluded from use for the map construction. Out of 3,541 SNPs, 791 SNPs were mapped in the linkage map. Among 791 SNPs, there were 277 (35%) SNPs that were heterozygous in the maternal parent and homozygous in the paternal parent and segregated in the expected ratio of 1:1 'lm × ll', 439 (55%) SNPs heterozygous in the paternal parent and homozygous in the maternal parent and segregated in the expected ratio of 1:1 'nn × np', and 75 (9%) SNPs were heterozygous in both parents and segregated in the expected ratio of 1:2:1 'hk × hk', respectively. These data indicated that 06-245-03 carried a greater number of heterozygous loci compared to UFGE 4033. In total, 791 SNP markers were mapped to 27 linkage groups (LGs) (Figure 2). The description of LGs including distance and number of SNPs are shown in Table 1. The overall average length of the LGs was 70.83 cM. The composite genetic linkage map spans 1912.30 cM with an average of 2.42 cM between SNP markers. The largest LG was LG04 spanning 124.4 cM, and the smallest was LG14 with a genetic distance of 18.3 cM. LG01 contains the largest number of SNPs (62), whereas LG15 and LG27 contain the smallest number of SNPs (6). There were 12 gaps in the linkage groups that each span more than 15 cM, with an average genetic distance of 15.17 cM between two adjacent markers. These gaps are present in 12 linkage groups (LG02, LG04, LG08, LG12, LG13, LG15, LG16, LG18, LG20, LG21, LG23, and LG27). The largest gap is in LG18, which extends 27.54 cM (Table 1).

2.3 Phenotyping and segregation of PM resistance

All progenies in the mapping population (and both parents) were phenotyped for PM resistance inside a greenhouse over two years (2018-2019). Each progeny was asexually propagated to obtain four clonal plants, which served as four biological replicates. Visual score rating was performed by evaluating the presence of PM spores and mycelial growth on the plant surfaces. Each disease evaluation was performed every seven days for four consecutive weeks. Area under disease progress curve (AUDPC) scores for each year for every individual were calculated separately. No significant block (or replicate) effect was observed, therefore the average of all evaluations within a year was calculated and used for QTL mapping (Supplementary Table 2). Histograms of the mapping population with the frequency of individuals in each AUDPC category for 2018 and 2019 are shown in Figure 3. The AUDPC score for

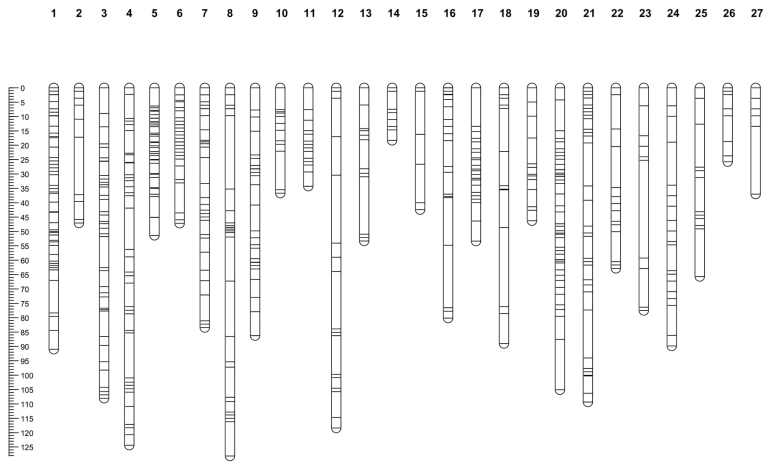

FIGURE 2
Linkage map of *Gerbera hybrida* containing 27 linkage groups developed by using SNPs discovered from genotyping by sequencing. The mapping F_1 population consisted of 88 individuals developed by crossing two breeding lines UFGE 4033 and 06-245-03. The scale plate on the left displays genetic distance in centiMorgan (cM) that was calculated using the Kosambi mapping function.

individuals ranged from 11.17 to 21.63 and averaged 16.00 in 2018; the AUDPC score for individuals ranged from 3.50 to 13.25 and averaged 6.90 in 2019. The AUDPC scores for the PM-resistant parent UFGE 4033 in 2018 and 2019 were 11.17 and 3.23, respectively, whereas the AUDPC scores for the PM-susceptible parent 06-245-03 breeding line in 2018 and 2019 were 20.36 and 10.18, respectively. Based on the frequency distribution of the disease severity in the mapping population, the histogram showed an approximately normal distribution, and therefore, no data transformation was performed prior to QTL analysis. The correlation coefficient of the AUDPC scores of the mapping population in 2018 and 2019 was 0.60.

2.4 QTL analysis for PM resistance

QTL analysis was performed for the PM AUDPC scores for 2018 and 2019 separately. The newly constructed linkage map containing 791 SNPs and the yearly AUDPC values from individuals in the mapping population calculated for each season were used in the MapQTL program for QTL analysis. Initially, interval mapping was performed and the LOD score was determined by permutation 1,000 tests. For year-wise QTL analysis, a LOD score significant at the level of $p < 0.05$ was used to determine the significance of the QTLs identified. MQM analysis was performed by assigning the significant markers in the proximity of the identified locus. Based on the phenotypic PM AUDPC values in 2018, one QTL was identified in LG16 and the associated marker, Gh-13_8125127, located at 15.98 cM with a LOD of 3.35 (Table 2; Figure 4). This QTL explained 16.6% of the phenotypic variation in 2018. Based on the AUDPC values in 2019, the same procedure identified one QTL in the same linkage group, LG16, and the marker associated with the locus is Gh-4_18873493 located at 27.41 cM. The locus was significant with a LOD score of 4.83. This locus explained 20.4% of the phenotypic variance in 2019 (Table 2). This locus was identified in both years and hence was considered consistent.

3 Discussion

In this study, GBS was used to identify SNPs using a biparental population developed by crossing two *Gerbera* breeding lines. Two small pooled GBS experiments conducted on parental lines and resistant and susceptible pools confirmed the successful use of sequencing depth of 2 million reads per sample and selection of *Bam*HI and *Nsi*I REs for population genotyping and obtaining required number of SNPs for linkage mapping and QTL analysis. In the NGS-era, SNP markers have been widely used for linkage map development because of their abundance and distribution throughout plant genomes (Pootakham et al., 2015; Verma et al., 2015; Yang et al., 2017). GBS facilitates the discovery and genotyping of large numbers of novel SNPs distributed from telomere to telomere in multiple samples simultaneously. Identification of large number of SNPs increases the flexibility of retaining a higher density of SNPs per cM, even after removing SNPs that do not pass all filtering steps and fit in the linkage maps. GBS has been used to construct high-density linkage maps in a wide range of herbs, trees, vegetables, fruits, and ornamental crops including chickpea, rubber tree, pea, maize, sweet cherry, wheat, rose, and sunflower (Leonforte et al., 2013; Guajardo et al., 2015; Li et al., 2015; Pootakham et al.,

TABLE 1 Description of *Gerbera* genetic linkage groups constructed using SNPs discovered by genotyping by sequencing of a biparental mapping population (F_1).

Linkage Group	Number of markers mapped	Length (cM)	Marker density (markers per cM)	Largest gaps between markers (cM)
LG01	62	91.00	0.68	11.32
LG02	13	47.10	0.28	19.98
LG03	60	108.10	0.56	10.82
LG04	59	124.40	0.47	15.68
LG05	55	51.40	1.07	7.21
LG06	38	47.20	0.81	10.43
LG07	42	83.50	0.50	9.00
LG08	37	128.10	0.29	25.54
LG09	39	86.30	0.45	8.33
LG10	20	36.70	0.54	13.41
LG11	18	34.20	0.53	7.11
LG12	22	118.40	0.19	19.80
LG13	19	53.30	0.36	19.98
LG14	13	18.30	0.71	5.91
LG15	6	42.40	0.14	15.00
LG16	38	80.20	0.47	21.77
LG17	31	53.40	0.58	13.42
LG18	21	89.00	0.24	27.54
LG19	17	46.20	0.37	5.98
LG20	56	105.10	0.53	17.50
LG21	43	109.40	0.39	16.68
LG22	19	62.90	0.30	14.29
LG23	10	77.50	0.13	34.10
LG24	26	89.80	0.29	13.30
LG25	13	65.70	0.20	16.60
LG26	8	25.70	0.31	9.00
LG27	6	37.00	0.16	19.80
Average		70.83	0.41	15.17
Total	791	1912.30		

2015; Verma et al., 2015; Celik et al., 2016; Su et al., 2017; Li et al., 2019). In this study, we show that GBS can be used in *Gerbera* to identify SNPs and perform linkage mapping.

Construction of genetic linkage maps has been reported in few ornamental crops including rose, carnation, sunflower, tulip and lotus (Debener and Mattiesch, 1999; Hayashi et al., 2001; Han et al., 2002; Yu et al., 2003; Yagi et al., 2013; Tang et al., 2015). The large genome size, large number of chromosomes ($2n = 50$), and limited availability of molecular markers have hindered the construction of linkage map in *Gerbera*. In this study, we constructed a genetic linkage map by using GBS-generated SNPs and a F_1 biparental population. In outcrossing ornamental crops, most studies have used F_1 populations to construct linkage maps (Debener and Mattiesch, 1999; Rajapakse et al., 2001; Han et al., 2002; Shahin et al., 2011; Zhang et al., 2015; Fu et al., 2016). Use of segregating F_1 populations was due to occurrence of severe inbreeding depression and no seed formation or seed decline as homozygosity increases with the advancement of generations *via* selfing. Prior to this study,

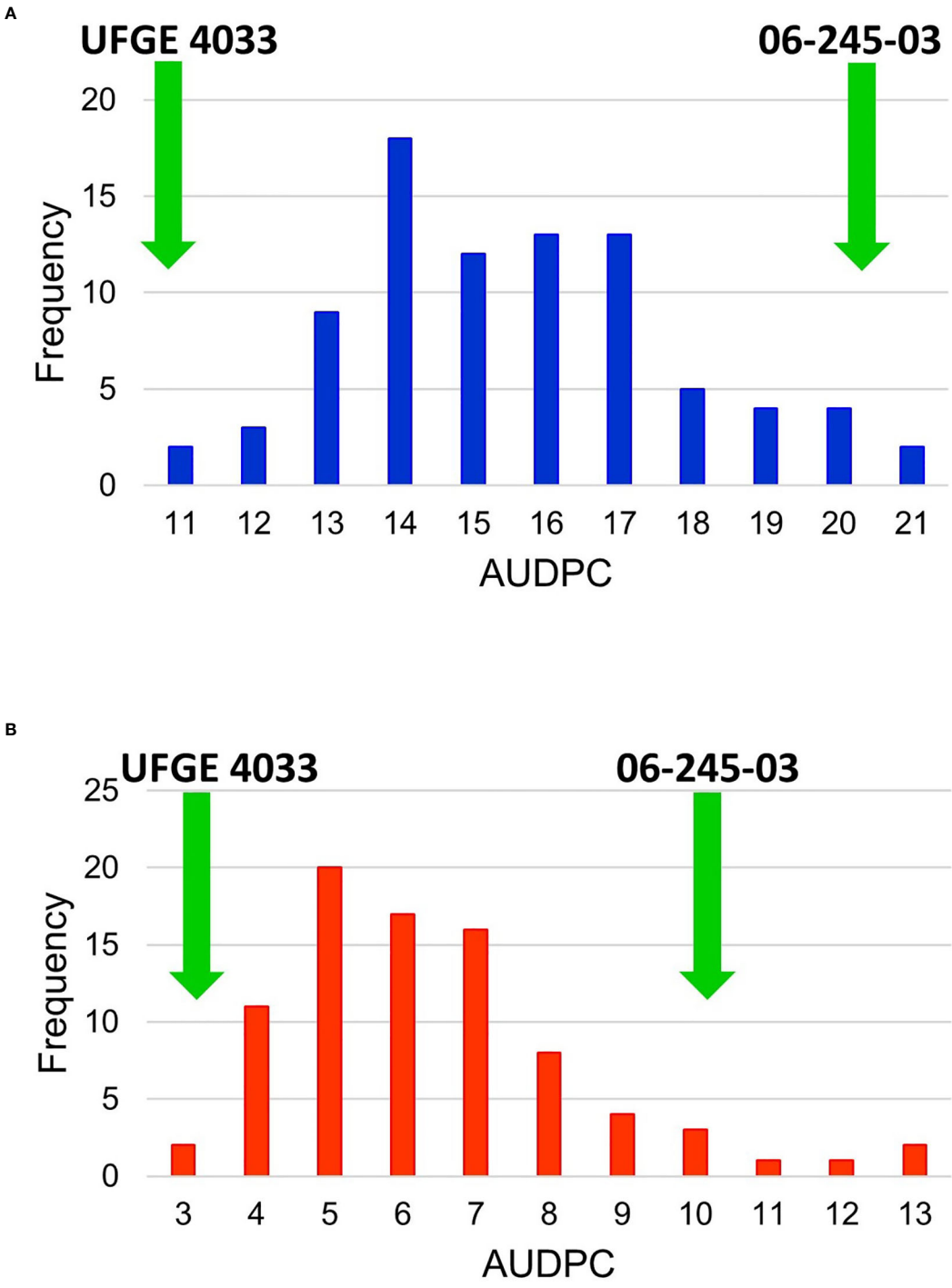

FIGURE 3
Frequency histogram of the Area Under Disease Progress Curve (AUDPC) values of an F_1 segregating population in **(A)** year 2018 and **(B)** 2019 for powdery mildew. The segregating population was developed by crossing *Gerbera* breeding lines 06-245-03 and UFGE 4033. The green arrows indicate the scores of resistant (UFGE 4033) and susceptible (06-245-03) parents used in developing the mapping population.

TABLE 2 QTLs identified by using the linkage map and *Gerbera* powdery mildew resistance phenotyping data from 2018 and 2019.

Year	Linkage group	Position(cM from the end)	Locus	QTL interval (cM)	LOD	% phenotypic variance
2018	LG16	15.99	Gh-13_8125127	4.94	3.35	16.6
2019	LG16	27.41	Gh-4_18873493	11.00	4.83	20.4

one linkage map was available in *Gerbera* which was developed based on markers discovered from ESTs and an F_1 population (Fu et al., 2016). As the first GBS study in *Gerbera*, we observed interesting phenomena in this species. Out of the high-quality SNPs from GBS, only 22.3% of them could be mapped to the linkage groups. Many SNPs showed significant segregation distortion ratios, unexpected high recombination frequencies, or high nearest-neighbor stress values. These phenomena might have resulted from *Gerbera*'s highly heterozygous, complex genome and/or the lack of high-quality reference genome for reliable variant calls. Although the cause(s) for this high portion (nearly 78%) of unmappable SNPs remain(s) to be understood, it does suggest the need for discovery of a lot of more SNPs for genetic mapping in *Gerbera*.

Our new *Gerbera* linkage map has an average distance of 2.42 cM between markers. Compared to the previous *Gerbera* linkage map, this linkage map has a better genome coverage, fewer gaps (12) that are > 15 cM, a higher marker density, and a larger number of SNPs. These improvements are due to the use of genome-wide high-quality SNPs. Due to the increased coverage of the genome by the linkage map constructed in this study, it could be useful to perform QTL studies, develop molecular markers and assemble chromosomes during genome assembly and construction of physical maps. The current linkage map consisted of 27 LGs, which was two more than the expected 25 chromosomal level-LGs given that *Gerbera* is a diploid with $2n = 50$ chromosomes. This result suggests the presence of two large gaps each of which is bigger than 15 cM in one or two of the LGs obtained in this study, accounting for the two extra LGs. Gaps present in the current linkage map could be potentially minimized by increasing the genome coverage during sequencing leading to increased SNPs discovery. Another strategy for gap reduction could be use of larger mapping populations, multiple crossing families and higher marker densities to capture more recombination events to merge the broken linkage groups.

In this study, we relied on the naturally available PM conidia in the environment (greenhouse) as inoculum to infect the F_1 mapping population. In Florida's warm and humid climate, PM can survive as mycelium and conidia, reproduce asexually and continuously cause disease as *Gerbera* can be grown year-round in both landscape and greenhouse conditions. Indeed, PM infection was observed year-round on the *Gerbera* plants in our greenhouse previously and during this study. Prior to this study, Kloos et al. (2005) assessed PM incidences and severity on *Gerbera* based on natural inoculation in the greenhouse and field studies (Kloos et al., 2005). The disease severity distribution under the two inoculation schemes was similar (Song and Deng, 2013). The fact that our PM phenotypic data from 2018 and 2019 allowed us to independently map two QTLs in the same

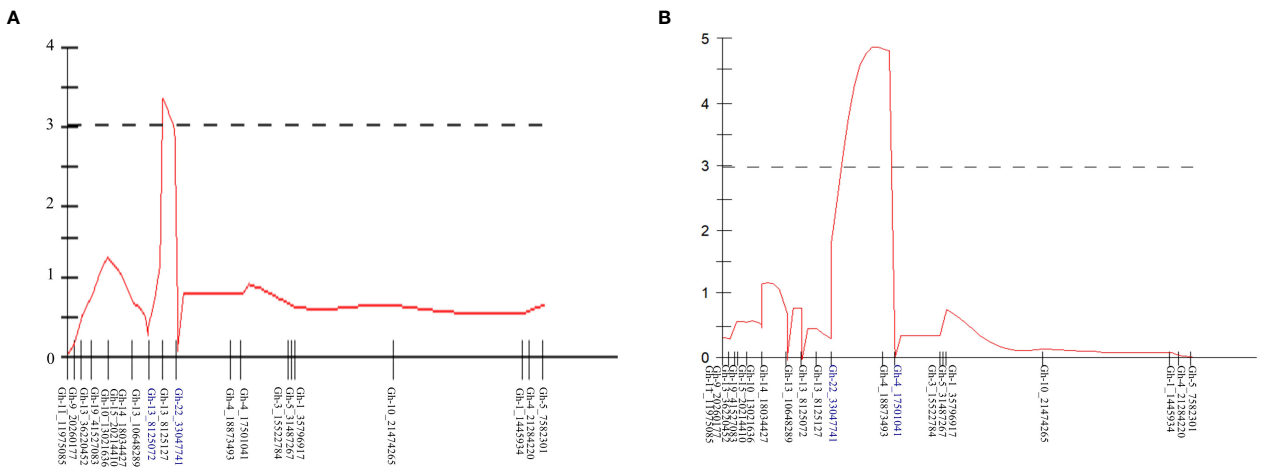

FIGURE 4
QTLs for powdery mildew (PM) resistance identified in **(A)** 2018 and **(B)** 2019 using the phenotypic PM scores and linkage map developed using F_1 segregating mapping population by crossing *Gerbera* breeding lines UFGE 4033 (resistant to PM) and o6-245-03 (susceptible to PM).

linkage group (LG16; despite being ~11cM apart) attested the adequacy of natural PM infection of the F_1 population in our greenhouse. However, inoculation of *Gerbera* plants with a pure PM isolate, when available in the future, should further increase the accuracy of phenotyping results, which in turn should increase the accuracy of the map location of the QTL contributing to PM resistance in UFGE 4033.

The PM fungal development in resistant and susceptible *Gerbera* has been previously studied (Song and Deng, 2013). When the conidia land and establish on the leaf surfaces, they germinate in both resistant and susceptible *Gerbera* lines. However, hyphal branching was observed in the susceptible lines whereas it was significantly reduced in the resistant lines at 72 hours post inoculation (Song and Deng, 2013). Similar reduction of haustorial and hyphal growths have been observed on the leaf surface of PM resistant line in cucumber, PI197088-1 (Hausbeck et al., 2002). Previous genetic studies suggested that PM resistance in *Gerbera* may be attributed to a single gene and/or QTL (Kloos et al., 2005). Kloos et al. reported that although a single dominant gene *Pmr1* (powdery mildew resistance 1) was shown to confer the resistance in *Gerbera*, *Pmr1*-controlled resistance appeared to be partially relied on other unidentified genes that may modify the effect of *Pmr1* (Kloos et al., 2005). Multiple PM resistance mechanisms in cucumber are known to confer the resistance including recessive genes showing *R*-gene like response including HR-like spots (Sakata et al., 2006), accumulation of serine/threonine-protein kinase receptor (RPK2) (Zhang et al., 2021) or loss of function of *CsMLO1* susceptibility gene (Nie et al., 2015). However, the molecular mechanisms underlying the resistance in both *Gerbera* and cucumber remain to be completely understood. Our previous study by Song and Deng using a limited number of markers designed from ESTs suggested that the PM resistance in *Gerbera* to be a quantitative trait controlled by one or more major genes (Song and Deng, 2013). In that study using UFGE 4033 and a PM-susceptible line Sunburst Snow White, two QTLs, resistance to *Podosphaera xanthii* 1 (*Rpx1*) and *Rpx2* were identified in UFGE 4033 to confer resistance to PM (Song and Deng, 2013). These QTLs contributed more than 71% of the resistance and *Rpx1* alone explained 56.5% PM resistance (Song and Deng, 2013). However, this study only included 17 EST-SSR markers and the QTLs could not be assigned to specific linkage group or chromosome. In the present study, we used genome-wide distributed SNPs which, theoretically, offers comprehensive search and analysis of QTLs present in *Gerbera* for PM resistance. Interestingly, we identified a QTL locus on LG16 using both the 2018 and 2019 phenotypic data spanning 4.95 cM and 11.00 cM and explaining 16.6% and 20.4% of phenotypic variance, respectively. This locus was tentatively named as *Gerbera hybrida* powdery mildew resistance locus 1 (*GhPMR1*). Some of the linked SNPs have been converted into high-resolution melting curve (HRM) markers (Supplementary Figure 1). They are or will be used for fingerprinting *Gerbera* lines and selecting proper F_1 individuals to create new segregating populations for identifying additional PM resistance QTLs.

Disease severity in year 2018 was higher compared to that in year 2019. High disease pressure in year 2018 could have revealed a locus with a sharper LOD peak whereas low disease pressure in year 2019 might have ensured more accurate determination of the disease infection phenotypes of the F_1 population, resulting in a more confined map location of the QTL. Disease distribution in the mapping population and phenotypic variance explained by *GhPMR1* demonstrate that PM resistance in *Gerbera* is controlled by more than one locus. As observed in other flowers or closely related species including sunflower, lettuce, and rose, PM resistance in *Gerbera* is very likely controlled by multiple loci. Low phenotypic variance (16.6% and 20.4% in 2018 and 2019, respectively) explained by the identified QTL could be attributed to the relatively small mapping population size (88 individuals) as compared to a rather large number of linkage groups (25) of *Gerbera*. The small population size also severely limited the resolution of the genetic map. Development of larger mapping populations could increase the recombination events and identification of additional SNPs for filling the gaps in the linkage map. Increased recombination events and SNPs could increase the marker density and the resolution in the genetic map, which in turn should increase the probability of identifying other QTLs and explaining more phenotypic variance for PM resistance. Availability of a high-quality reference genome in future could facilitate the identification of potentially all genomic regions contributing to PM resistance in *Gerbera*.

In summary, this study has used genome-wide SNPs for the first time to construct a genome-wide genetic linkage map and identified a major QTL for PM resistance in *Gerbera*. These results will be useful for developing molecular markers for marker-assisted selection of *Gerbera* for PM resistance, tagging other traits important in *Gerbera*, and identifying the genes present in the QTL regions that control PM resistance in *Gerbera*.

4 Materials and methods

4.1 Plant materials

A segregating F_1 population comprising of 88 individuals was developed by crossing two *Gerbera* breeding lines exhibiting PM resistance (UFGE 4033) and susceptibility (06-245-03) as reported in the previous study (Bhattarai et al., 2020). UFGE 4033 was developed at the University of Florida and is resistant to PM (Deng and Harbaugh, 2013; Song and Deng, 2013). UFGE 4033 is characterized by shiny large green leaves, long peduncles, semi-double flower, soft-white ray-florets, and light green disc florets, and it can be grown for both pot and cut flower production. UFGE 4033 consistently showed resistance to PM

in both fields and greenhouse screening studies and in the current study (Gong and Deng, 2010; Song and Deng, 2013; Bhattarai et al., 2020). UFGE 4033 has been used in *Gerbera* breeding programs as a source of PM resistance in developing new cultivars (Deng and Bhattarai, 2018). UFGE 4033 originated from a cross between breeding line UFGE 31-19 (PM-resistant) and UFGE 35-4 (PM-susceptible). Hence, the PM resistance in UFGE 4033 was expected to be heterozygous. Contrastingly, 06-245-03 has dark green leaves, short peduncles, simple flowers, dark-brown disc center, and dark red ray florets, and it is primarily grown for pot plant production. Previously, breeding line 06-245-03 was identified as being highly susceptible to PM (Bhattarai et al., 2020).

Artificial crossing between the two breeding lines was done in a greenhouse at the Gulf Coast Research and Education Center in Wimauma, FL, USA from October 2015 to March 2016. Seeds developed from the crosses were sown in September 2016 in plastic 72-cell trays and were kept in a growth room at 25°C with 16/8-hour day-night light conditions. Seedlings were grown for a month until they had three to four true-leaves and then transferred to four-inch plastic containers filled with a soilless potting mixture Faffard® 3B (50% Canadian peat and 50% of the mixture of vermiculite, pine bark and perlite) (Agawam, MA, USA). Seedlings (progeny) were later individually transferred to 3.79-L plastic containers and grown in these containers for six months to develop enough crowns for multiplication. The crown of each plant was divided into four parts of similar sizes and grown individually as four replicates for the progeny for subsequent studies. Subsequently, the clonally propagated plants were grown in two-gallon plastic containers in a greenhouse from 2017 to 2019. As expected, the progeny of this population segregated for PM resistance as well as for various other traits including plant height, peduncle length, flower color, and leaf color (data not shown).

4.2 Genotyping by sequencing

Genotyping by sequencing was conducted in two phases. In the first phase, the genomic DNA of two *Gerbera* parents (UFGE 4033 and 06-245-03) in two replicates (four samples total), one pool of PM-resistant individuals, and one pool of PM-susceptible individuals were digested with one of the two combinations of restriction enzymes (*Bam*HI and *Nsi*I, or *Btg*I and *Taq*I) prior to sequencing to evaluate the effect of restriction enzyme combinations on SNP marker discovery. The resistant pool consisted of 10 F_1 individuals Gh-213, Gh-77, Gh-243, Gh-3, Gh-202, Gh-288, Gh-281, Gh-191, Gh-256, and Gh-212. The susceptible pool consisted of 13 F_1 individuals Gh-21, Gh-27, Gh-306, Gh-303, Gh-47, Gh-234, Gh-50, Gh-302, Gh-37, Gh-308, Gh-19, Gh-2, and Gh-42. In the second phase, all F_1 progenies of the mapping population and their two parents were subjected to GBS with *Bam*HI and *Nsi*I as the restriction enzymes for genomic DNA digestion.

Genomic DNA was extracted from young, unopened leaves using a DNeasy Plant Mini Kit (Qiagen, Hilden, Germany) following the manufacturer's protocol. DNA concentrations were determined on a Nanodrop 8000 spectrophotometer (Fisher Scientific, Waltham, MA, USA) and a Qubit 4 fluorometer (Thermo Fisher Scientific, Waltham, MA, USA) using the Quant-iT™ PicoGreen® (Thermo Fisher Scientific). DNA preparations with the concentration >10 ng/μL and a minimum quantity of 200 ng were used for GBS library preparation.

Library preparation and sequencing for GBS were conducted at the University of Minnesota Genomics Center (Minneapolis, MN). Briefly, genomic DNA was digested with a combination of two restriction enzymes, followed by ligation of adapters consisting of barcode sequences and Illumina sequencing primers. The ligated DNA fragments from all samples were pooled, PCR-amplified, and sequenced in one Flowcell on a NextSeq 500 sequencer (Illumina, San Diego, CA, USA). Sequencing was performed using the single end chemistry with a read length of 150 bases.

4.3 Variant calling and SNP analysis

Raw sequencing data were converted to de-multiplexed Fastq files using the Illumina bcl2fastq software. Adapters at the beginning and the end of the raw reads were removed using Trimmomatic (Bolger et al., 2014). The resultant Fastq files were aligned to a draft partial *Gerbera* genome sequence (developed using the Illumina and PacBio sequencing approaches for the program's internal use) (Bhattarai and Deng, unpublished data) using the Burrows-Wheeler Alignment tool (Li, 2013). Freebayes was used to jointly call variants across all samples simultaneously (Garrison and Marth, 2012). The raw VCF file generated by Freebayes was filtered using the VCFtools to remove variants with the minor allele frequency < 1%, variants with genotype rates < 95%, and samples with genotype rates of < 50% (Danecek et al., 2011).

4.4 Linkage map construction

A linkage map was constructed using SNPs discovered from the mapping population. SNPs identified from the variant calling procedure were filtered to select high-quality SNPs. SNPs that were not called and absent in more than 8 individuals (10% of the population) were removed from further analysis. Individuals missing more than 2% genotypic data were excluded. Chi-square tests were performed to detect potential segregation distortion for each SNP, and those SNPs with $\chi^2 > 11.31$ ($p < 0.0001$) were discarded. Additional SNPs were excluded due to unexpected high recombination frequencies (> 0.40) or high nearest-neighbor stress values (> 10 cM). The *Gerbera* segregating population type was coded as cross pollinated (CP), and the genotype for SNPs were coded "hk × hk" when both parents were heterozygous, "nn × np" when parent 1 (P_1) was

homozygous and P_2 was heterozygous, and "lm × ll" when P_1 was heterozygous and P_2 was homozygous for the given locus. Linkage groups (LGs) were constructed using the JOINMAP® 4.1 program with the following parameters: A minimum logarithm of odds (LOD) score of 5, a maximum recombination frequency of 0.40, and goodness-of-fit jump at 5 (Van Ooijen, 2006). The maximum likelihood algorithm and the Kosambi mapping function with 3 reiterations were selected for construction of the linkage map. The linkage groups were drawn using MapChart (Voorrips, 2002).

4.5 Phenotyping PM resistance

Individuals of the segregating population and its parents were evaluated for PM resistance in a greenhouse. All plants were arranged in four blocks on metal benches. Each block contained one replicate of all individuals and the parents randomly placed on the metal benches. The individuals were exposed to natural PM infection in the greenhouse. The greenhouse had been used to grow *Gerbera* plants for more than 10 years, and severe PM was observed in the greenhouse during this period. To promote PM development in the greenhouse, two highly susceptible commercial cultivars, Tangerine Dark Eye and Yellow Dark Eye, were grown and placed among the *Gerbera* individuals. PM disease scoring began 30 to 45 days after moving *Gerbera* plants into the greenhouse or repotting of the plants. Uniform distribution of the inoculum in the whole greenhouse was maintained by running circulation fans within the greenhouse. These actively growing foliar parts had equal chances for freely spreading PM spores to land and germinate on the foliar leaf surfaces. All individuals were phenotyped over two years in 2018 and 2019 to capture the variation caused due to difference in growing conditions. PM severity was rated using a scale of 1 to 10 as described previously with minor modifications: 1 = no disease, 2 = trace to 10%, 3 = 10 to 20%, 4 = 20 to 30%, 5 = 30 to 40%, 6 = 40 to 50%, 7 = 50 to 60%, 8 = 60 to 70%, 9 = 70 to 80%, and 10 = 80 to 100% (Hausbeck et al., 2002). The disease severity data were recorded for four weeks and following a weekly disease rating procedure. The means of the four replications were calculated and used for Area Under Disease Progress Curve (AUDPC) calculation as described previously (Jeger and Viljanen-Rollinson, 2001). AUDPC scores for each individual and for each season were used in QTL analysis.

4.6 Quantitative trait loci analysis

QTL mapping was performed by analyzing genotyping data of the mapped SNPs, and the disease severity of the mapping population using mapQTL® 6 (Van Ooijen, 2009). Putative QTL regions associated with PM resistance were detected in the LGs using interval mapping. After performing interval mapping, MQM was performed by assigning the closest markers as co-factors. Determination of LOD score threshold was performed by 1,000 permutation tests corresponding to a genome-wide confidence level of $P < 0.05$. The software also estimated the percentage of phenotypic variance and additive effect explained by a QTL for a trait. QTL analysis was performed for 2018 and 2019 individually and the loci appearing in both years were considered consistent.

5 Conclusion

A genome-wide genetic linkage map was constructed for *Gerbera* using SNPs discovered by GBS. The linkage map contained 791 SNPs distributed across 27 LGs and spanning 1912.30 cM. A QTL, *GPhMR1* conferring resistance to PM, was discovered in LG16. *GPhMR1* explained more than 16.6% phenotypic variance for PM resistance. The locus was tagged with two markers Gh-13_8125127 and Gh-4_18873493 located at 15.987 cM and 27.410 cM, respectively. This locus and the SNP markers will be useful for breeding *Gerbera* for PM resistance in future. Similarly, the genetic linkage map developed could be utilized in studying genetic architecture of other traits, identification of novel QTLs, and developing molecular markers associated with those traits in *Gerbera*, one of the top cut flowers in the world.

Data availability statement

The Gerbera genotyping by sequencing data presented in the study are deposited in the NCBI BioProject: PRJNA902916, https://www.ncbi.nlm.nih.gov/bioproject/PRJNA902916.

Author contributions

ZD designed and supervised the project, secured the funding, and critically revised the manuscript; KB performed the experiments, analyzed data, and wrote the manuscript; SS assisted in population development, plant propagation, and disease phenotyping; SV guided the linkage mapping analysis; NP, SX, and DC provided essential guidance to the study and provided essential comments and critically revised the manuscript. All authors contributed to the article and approved the submitted version.

Funding

Funding for this project, including assistantship to KB, was provided by the University of Florida/IFAS Plant Breeding Graduate Initiative (PBGI). Additional funding was provided by the USDA Hatch project FLA-GCC-005507.

Acknowledgments

We thank University of Minnesota Genomics Center for performing the genotyping by sequencing experiments and the lab members of the Ornamental Plant Breeding and Genetics Program at Gulf Coast Research and Education Center for their help managing and caring *Gerbera* plants in the growth rooms and greenhouses.

Conflict of interest

The authors declare that the research was conducted in the absence of any commercial or financial relationships that could be construed as a potential conflict of interest.

Publisher's note

All claims expressed in this article are solely those of the authors and do not necessarily represent those of their affiliated organizations, or those of the publisher, the editors and the reviewers. Any product that may be evaluated in this article, or claim that may be made by its manufacturer, is not guaranteed or endorsed by the publisher.

Supplementary material

The Supplementary Material for this article can be found online at: https://www.frontiersin.org/articles/10.3389/fpls.2022.1072717/full#supplementary-material

SUPPLEMENTARY FIGURE 1
Histogram of one high-resolution melting (HMR) curve marker developed from one of the SNPs that is linked to the major QTL *GhPMR1*. Two patterns, indicated by the red and blue melting curves, were evident among the *Gerbera* parental and F_1 individuals. This marker could clearly differentiate *Gerbera* individuals, but as the QTL *GhPMR1* explained only 16.6% or 20.4% of the phenotypic variance for PM resistance, this marker had only a limited diagnostic capability for PM resistance. Additional QTLs and SNP markers are needed for reliable selection of PM-resistant *Gerbera* breeding lines.

References

Ansorge, W. J. (2009). Next-generation DNA sequencing techniques. *New Biotech.* 25 (4), 195–203. doi: 10.1016/j.nbt.2008.12.009

Benson, D. M., Hall, J. L., Moorman, G. W., Daughtrey, M. L., Chase, A. R., and Lamour, K. H. (2002). The history and diseases of poinsettia, the Christmas flower. *Plant Health Prog.* 3 (1), 18. doi: 10.1094/PHP-2002-0212-01-RV

Bhattarai, K., Conesa, A., Xiao, S., Peres, N. A., Clark, D. G., Parajuli, S., et al. (2020). Sequencing and analysis of *Gerbera* daisy leaf transcriptomes reveal disease resistance and susceptibility genes differentially expressed and associated with powdery mildew resistance. *BMC Plant Biol.* 20 (1), 1–17. doi: 10.1186/s12870-020-02742-4

Bolger, A. M., Lohse, M., and Usadel, B. (2014). Trimmomatic: a flexible trimmer for illumina sequence data. *Bioinformatics* 30 (15), 2114–2120. doi: 10.1093/bioinformatics/btu170

Braun, U., Cook, R. T. A., Inman, A. J., and Shin, H. D.. (2002). "The taxonomy of powdery mildew fungi," in *The powdery mildew: A comprehensive treatise* (American Phytopathological Society, St. Paul, Minnesota, USA), 13–55.

Celik, I., Bodur, S., Frary, A., and Doganlar, S. (2016). Genome-wide SNP discovery and genetic linkage map construction in sunflower (*Helianthus annuus* l.) using a genotyping by sequencing (GBS) approach. *Mol. Breed.* 36 (9), 1, 133. doi: 10.1007/s11032-016-0558-8

Channel, C. (2005). *Gerbera* trials rate plants. *GM Pro* 25, 30–31.

Danecek, P., Auton, A., Abecasis, G., Albers, C. A., Banks, E., DePristo, M. A., et al. (2011). The variant call format and VCFtools. *Bioinformatics* 27 (15), 2156–2158. doi: 10.1093/bioinformatics/btr330

Debener, T., and Mattiesch, L. (1999). Construction of a genetic linkage map for roses using RAPD and AFLP markers. *Theor. Appl. Genet.* 99 (5), 891–899. doi: 10.1007/s001220051310

Deng, Z., and Bhattarai, K. (2018). "Gerbera," in *Ornamental crops* (Cham, Switzerland: Springer International Publishing AG), 407–438.

Deng, Z., and Harbaugh, B. K. (2013). UFGE 7031 and UFGE 7080 *Gerbera* cultivars. *HortScience* 48 (5), 659–663. doi: 10.21273/HORTSCI.48.5.659

de Pinho Benemann, D., Machado, L. N., Arge, L. W. P., Bianchi, V. J., de Oliveira, A. C., da Maia, L. C., et al. (2012). Identification, characterization and validation of SSR markers from the *Gerbera* EST database. *Plant Omics* 5 (2), 159–166.

Elshire, R. J., Glaubitz, J. C., Sun, Q., Poland, J. A., Kawamoto, K., Buckler, E. S., et al. (2011). A robust, simple genotyping-by-sequencing (GBS) approach for high diversity species. *PloS One* 6 (5), e19379. doi: 10.1371/journal.pone.0019379

Fu, Y., Esselink, G. D., Visser, R. G., van Tuyl, J. M., and Arens, P. (2016). Transcriptome analysis of *Gerbera hybrida* including in silico confirmation of defense genes found. *Front. Plant Sci.* 7, 247. doi: 10.3389/fpls.2016.00247

Fu, Y., Van Silfhout, A., Shahin, A., Egberts, R., Beers, M., van der Velde, A., et al. (2017). Genetic mapping and QTL analysis of botrytis resistance in *Gerbera hybrida*. *Mol. Breed.* 37 (2), 1–13. doi: 10.1007/s11032-016-0617-1

Garrison, E., and Marth, G. (2012). Haplotype-based variant detection from short-read sequencing. *arXiv*:1207.3907v2 [q-bio.GN]. doi: 10.48550/arXiv.1207.3907.

Gong, L., and Deng, Z. (2010). EST-SSR markers for *Gerbera* (*Gerbera hybrida*). *Mol. Breed.* 26 (1), 125–132. doi: 10.1007/s11032-009-9380-x

Gong, L., and Deng, Z. (2012). Selection and application of SSR markers for variety discrimination, genetic similarity and relation analysis in *Gerbera* (*Gerbera hybrida*). *Scientia Hortic.* 138, 120–127. doi: 10.1016/j.scienta.2012.02.020

Gore, M. A., Chia, J. M., Elshire, R. J., Sun, Q., Ersoz, E. S., Hurwitz, B. L., et al. (2009). A first-generation haplotype map of maize. *Science* 326 (5956), 1115–1117. doi: 10.1126/science.1177837

Granke, L. L., Crawford, L. E., and Hausbeck, M. K. (2012). Factors affecting airborne concentrations of *Podosphaera xanthii* conidia and severity of *Gerbera* powdery mildew. *HortScience* 47 (8), 1068–1072. doi: 10.21273/HORTSCI.47.8.1068

Guajardo, V., Solís, S., Sagredo, B., Gainza, F., Muñoz, C., Gasic, K., et al. (2015). Construction of high-density sweet cherry (Prunus avium l.) linkage maps using microsatellite markers and SNPs detected by genotyping-by-sequencing (GBS). *PloS One* 10 (5), e0127750. doi: 10.1371/journal.pone.0127750

Han, T. H., van Eck, H. J., De Jeu, M. J., and Jacobsen, E. (2002). Mapping of quantitative trait loci involved in ornamental traits in *Alstroemeria*. *HortScience* 37 (3), 585–592. doi: 10.21273/HORTSCI.37.3.585

Hausbeck, M. K. (2004). Take a long-range approach to powdery mildew resistance. *GMPro* 24, 68–69.

Hausbeck, M. K., Quackenbush, W. R., and Linderman, S. D. (2002). Evaluation of cultivars of African daisy for resistance to powdery mildew. *B&C Tests* 18, O0004.

Hayashi, M., Miyahara, A., Sato, S., Kato, T., Yoshikawa, M., Taketa, M., et al. (2001). Construction of a genetic linkage map of the model legume *Lotus japonicus* using an intraspecific F2 population. *DNA Res.* 8 (6), 301–310. doi: 10.1093/dnares/8.6.301

Heo, M. S., Han, K., Kwon, J. K., and Kang, B. C. (2017). Development of SNP markers using genotyping-by-sequencing for cultivar identification in rose (*Rosa hybrida*). *Horticult. Environ. Biotechnol.* 58 (3), 292–302. doi: 10.1007/s13580-017-0268-0

Horst, R. K. (1990). "Plant diseases and their pathogens," in *Westcott's plant disease handbook* (Springer Science+Business Media, New York, NY, USA), 86–515.

Jeger, M. J., and Viljanen-Rollinson, S. L. H. (2001). The use of the area under the disease-progress curve (AUDPC) to assess quantitative disease resistance in crop cultivars. *Theor. Appl. Genet.* 102 (1), 32–40. doi: 10.1007/s001220051615

Kloos, W. E., George, C. G., and Sorge, L. K. (2005). Inheritance of powdery mildew resistance and leaf macrohair density in *Gerbera hybrida*. *HortScience* 40 (5), 1246–1251. doi: 10.21273/HORTSCI.40.5.1246

Leonforte, A., Sudheesh, S., Cogan, N. O., Salisbury, P. A., Nicolas, M. E., Materne, M., et al. (2013). SNP marker discovery, linkage map construction and identification of QTLs for enhanced salinity tolerance in field pea (*Pisum sativum* l.). *BMC Plant Biol.* 13 (1), 1–14. doi: 10.1186/1471-2229-13-161

Li, H. (2013). Aligning sequence reads, clone sequences and assembly contigs with BWA-MEM. *arXiv*:1303.3997vs [q-bio.GN]. doi: 10.48550/arXiv.1303.3997.

Li, Y., Mmbaga, M. T., Zhou, B., Joshua, J., Rotich, E., and Parikh, L. (2018). "Diseases of hydrangea," in *Handbook of florists' crops diseases* (Springer International Publishing AG, Cham, Switzerland), 987–1006.

Li, H., Vikram, P., Singh, R. P., Kilian, A., Carling, J., Song, J., et al. (2015). A high density GBS map of bread wheat and its application for dissecting complex disease resistance traits. *BMC Genomics* 16 (1), 1–15. doi: 10.1186/s12864-015-1424-5

Li, S., Yang, G., Yang, S., Just, J., Yan, H., Zhou, N., et al. (2019). The development of a high-density genetic map significantly improves the quality of reference genome assemblies for rose. *Sci. Rep.* 9 (1), 1–13. doi: 10.1038/s41598-019-42428-y

Mueller, D. S., Hung, Y. C., Oetting, R. D., Van Iersel, M. W., and Buck, J. W. (2003). Evaluation of electrolyzed oxidizing water for management of powdery mildew on *Gerbera* daisy. *Plant Dis.* 87 (8), 965–969. doi: 10.1094/PDIS.2003.87.8.965

Nie, J., Wang, Y., He, H., Guo, C., Zhu, W., Pan, J., et al. (2015). Loss-of-function mutations in *CsMLO1* confer durable powdery mildew resistance in cucumber (*Cucumis sativus* l.). *Front. Plant Sci.* 6. doi: 10.3389/fpls.2015.01155

Poland, J. A., Brown, P. J., Sorrells, M. E., and Jannink, J. L. (2012). Development of high-density genetic maps for barley and wheat using a novel two-enzyme genotyping-by-sequencing approach. *PloS One* 7 (2), e32253. doi: 10.1371/journal.pone.0032253

Pootakham, W., Ruang-Areerate, P., Jomchai, N., Sonthirod, C., Sangsrakru, D., Yoocha, T., et al. (2015). Construction of a high-density integrated genetic linkage map of rubber tree (*Hevea brasiliensis*) using genotyping-by-sequencing (GBS). *Front. Plant Sci.* 6, 367. doi: 10.3389/fpls.2015.00367

Price, T. V. (1970). Epidemiology and control of powdery mildew (*Sphaerotheca pannosa*) on roses. *Ann. Appl. Biol.* 65 (2), 231–248. doi: 10.1111/j.1744-7348.1970.tb04583.x

Rajapakse, S., Byrne, D. H., Zhang, L., Anderson, N., Arumuganathan, K., and Ballard, R. E. (2001). Two genetic linkage maps of tetraploid roses. *Theor. Appl. Genet.* 103 (4), 575–583. doi: 10.1007/PL00002912

Sakata, Y., Kubo, N., Morishita, M., Kitadani, E., Sugiyama, M., and Hirai, M. (2006). QTL analysis of powdery mildew resistance in cucumber (*Cucumis sativus* l.). *Theor. Appl. Genet.* 112 (2), 243–250. doi: 10.1007/s00122-005-0121-1

Shahin, A., Arens, P., Van Heusden, A. W., van der Linden, G., Van Kaauwen, M., Khan, N., et al. (2011). Genetic mapping in lilium: mapping of major genes and quantitative trait loci for several ornamental traits and disease resistances. *Plant Breed.* 130 (3), 372–382. doi: 10.1111/j.1439-0523.2010.01812.x

Song, X., and Deng, Z. (2013). Powdery mildew resistance in *Gerbera*: mode of inheritance, quantitative trait locus identification, and resistance responses. *J. Am. Soc. Hortic. Sci.* 138 (6), 470–478. doi: 10.21273/JASHS.138.6.470

Song, X., Xu, Y., Gao, K., Fan, G., Zhang, F., Deng, C., et al. (2020). High-density genetic map construction and identification of loci controlling flower-type traits in chrysanthemum (*Chrysanthemum× morifolium* ramat.). *Horticult. Res.* 7, 108. doi: 10.1038/s41438-020-0333-1

Su, C., Wang, W., Gong, S., Zuo, J., Li, S., and Xu, S. (2017). High density linkage map construction and mapping of yield trait QTLs in maize (*Zea mays*) using the genotyping-by-sequencing (GBS) technology. *Front. Plant Sci.* 8, 706. doi: 10.3389/fpls.2017.00706

Tang, N., van der Lee, T., Shahin, A., Holdinga, M., Bijman, P., Caser, M., et al. (2015). Genetic mapping of resistance to *Fusarium oxysporum* f. sp. *tulipae* in tulip. *Mol. Breed.* 35 (5), 1–17. doi: 10.1007/s11032-015-0316-3

The International SNP Map Working Group (2001). A map of human genome sequence variation containing 1.42 million single nucleotide polymorphisms. *Nature* 409, 928–933. doi: 10.1038/35057149

United States Department of Agriculture (2016) *Floriculture crops 2009 summary national agricultural statistics service*. Available at: https://www.nass.usda.gov/.

Van Ooijen, J. W. (2006). *JoinMap 4: Software for the calculation of genetic linkage maps in experimental populations* B. V. Kyazma, Wageningen, Netherlands.

Van Ooijen, J. W. (2009). MapQTL(R) 6, Software for the mapping of quantitative trait loci in experimental populations of diploid species. B. V. Kyazma, Wageningen, Netherlands. Available at: https://www.kyazma.nl/index.php/MapQTL/.

Verma, S., Gupta, S., Bandhiwal, N., Kumar, T., Bharadwaj, C., and Bhatia, S. (2015). High-density linkage map construction and mapping of seed trait QTLs in chickpea (*Cicer arietinum* l.) using genotyping-by-Sequencing (GBS). *Sci. Rep.* 5, 17512. doi: 10.1038/srep17512

Voorrips, R. (2002). MapChart: software for the graphical presentation of linkage maps and QTLs. *J. Hered.* 93 (1), 77–78. doi: 10.1093/jhered/93.1.77

Wu, X., and Alexander, L. W. (2020). Genome-wide association studies for inflorescence type and remontancy in *Hydrangea macrophylla*. *Horticult. Res.* 7, 27. doi: 10.1038/s41438-020-0255-y

Yagi, M., Yamamoto, T., Isobe, S., Hirakawa, H., Tabata, S., Tanase, K., et al. (2013). Construction of a reference genetic linkage map for carnation (*Dianthus caryophyllus* l.). *BMC Genomics* 14 (1), 1–10. doi: 10.1186/1471-2164-14-734

Yang, Z., Chen, Z., Peng, Z., Yu, Y., Liao, M., and Wei, S. (2017). Development of a high-density linkage map and mapping of the three-pistil gene (*Pis1*) in wheat using GBS markers. *BMC Genomics* 18, 567. doi: 10.1186/s12864-017-3960-7

Yu, J. K., Tang, S., Slabaugh, M. B., Heesacker, A., Cole, G., Herring, M., et al. (2003). Towards a saturated molecular genetic linkage map for cultivated sunflower. *Crop Sci.* 43 (1), 367–387. doi: 10.2135/cropsci2003.3670

Zhang, C., Badri Anarjan, M., Win, K. T., Begum, S., and Lee, S. (2021). QTL-seq analysis of powdery mildew resistance in a Korean cucumber inbred line. *Theor. Appl. Genet.* 134 (2), 435–451. doi: 10.1007/s00122-020-03705-x

Zhang, J., Zhang, Q., Cheng, T., Yang, W., Pan, H., Zhong, J., et al. (2015). High-density genetic map construction and identification of a locus controlling weeping trait in an ornamental woody plant (*Prunus mume* sieb. et zucc). *DNA Res.* 22 (3), 183–191. doi: 10.1093/dnares/dsv003

Frontiers in
Plant Science

Cultivates the science of plant biology and its applications

The most cited plant science journal, which advances our understanding of plant biology for sustainable food security, functional ecosystems and human health.

Discover the latest Research Topics

See more →

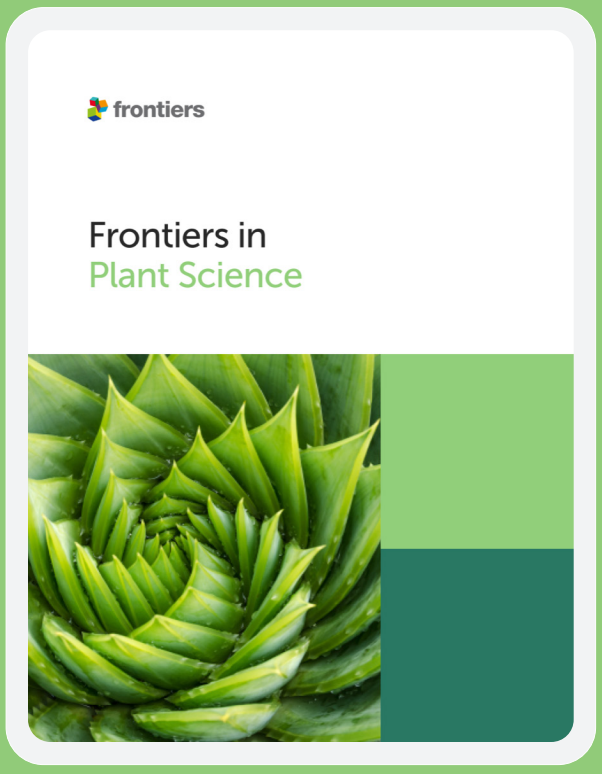

Frontiers

Avenue du Tribunal-Fédéral 34
1005 Lausanne, Switzerland
frontiersin.org

Contact us

+41 (0)21 510 17 00
frontiersin.org/about/contact